

# Stabilisation of heavier carbene analogues with bulky phosphides and related systems

by

Peter Evans

A thesis submitted in partial  
fulfilment of the requirements  
for the degree of

Doctor of Philosophy

Newcastle University

September 2018



## Abstract

An array of monodentate alkali metal phosphides was prepared, for use as precursors to diphosphatetrylenes. Treatment of (Dipp)<sub>2</sub>PH (**111**) with either *n*BuLi, PhCH<sub>2</sub>Na or PhCH<sub>2</sub>K in THF gives [(Dipp)<sub>2</sub>P]Li(THF)<sub>3</sub> (**128a**), {[(Dipp)<sub>2</sub>P]Na(THF)<sub>2</sub>}<sub>2</sub> (**129a**) and [(Dipp)<sub>2</sub>P]K(THF)<sub>4</sub> (**130a**), respectively; the alternative adduct [(Dipp)<sub>2</sub>P]Na(PMDETA) (**129c**) was prepared by the treatment of **129a** with PMDETA. Treatment of either (Dipp)(Mes)PH (**109**) or (Dipp){(Me<sub>3</sub>Si)<sub>2</sub>CH}PH (**113**) with *n*BuLi gives [(Dipp)(Mes)P]Li(THF)<sub>3</sub> (**131a**) and [(Dipp){(Me<sub>3</sub>Si)<sub>2</sub>CH}P]Li(THF)<sub>3</sub> (**134**), respectively. Treatment of (Mes)<sub>2</sub>PH (**108**) with *n*BuLi gives [(Mes)<sub>2</sub>P]Li(THF)<sub>3</sub> (**132a**) after recrystallization from *n*-hexane or the alternative solvate [(Mes)<sub>2</sub>P]<sub>2</sub>Li<sub>2</sub>(THF)<sub>2</sub>(OEt<sub>2</sub>) (**132b**) after recrystallization from Et<sub>2</sub>O. Exposure of compounds **128a**, **129a**, **130a**, **131a**, **132a** and **132b** to vacuum leads to the loss of coordinated solvent, yielding the alternative solvates [(Dipp)<sub>2</sub>P]Li(THF)<sub>2</sub> (**128b**), [(Dipp)<sub>2</sub>P]Na(THF)<sub>2</sub>]<sub>1.5</sub> (**129b**), [(Dipp)<sub>2</sub>P]K (**130b**), [(Dipp)(Mes)P]Li(THF)<sub>2</sub> (**131b**) and [(Mes)<sub>2</sub>P]Li(THF) (**132c**). Variable-temperature <sup>7</sup>Li and <sup>31</sup>P{<sup>1</sup>H} NMR spectroscopy indicates that **128b**, **129b**, **131b** and **134** are subject to a monomer-dimer equilibrium in solution, while **132c** is subject to a dynamic equilibrium between a dimer and cyclic trimer in solution.

An array of diphosphatetrylenes was prepared by reactions between two equivalents of the corresponding lithium phosphides discussed above and the group 14 dihalide. In the solid-state, compounds {(Dipp)<sub>2</sub>P}<sub>2</sub>Sn (**104Sn**), {(Tripp)<sub>2</sub>P}<sub>2</sub>Ge·(C<sub>7</sub>H<sub>14</sub>) (**145Ge**·(C<sub>7</sub>H<sub>14</sub>)) and [{(Me<sub>3</sub>Si)<sub>2</sub>CH}<sub>2</sub>P]<sub>2</sub>Sn (**148Sn**) are stabilised by  $\pi$  interactions from a planar phosphorus centre, while {(Tripp)<sub>2</sub>P}<sub>2</sub>Sn (**145Sn**), {(Dipp)(Mes)P}<sub>2</sub>Ge·(C<sub>6</sub>H<sub>14</sub>)<sub>0.5</sub> (**146Ge**·(C<sub>6</sub>H<sub>14</sub>)<sub>0.5</sub>), {(Dipp)(Mes)P}<sub>2</sub>Sn (**146Sn**) and [(Dipp){(Me<sub>3</sub>Si)<sub>2</sub>CH}P]<sub>2</sub>Sn (**147Sn**) adopt the alternative configuration with two pyramidal phosphorus centres, which stabilises the tetrel centre with up to two short Ge/Sn...C<sub>ipso</sub> contacts. Variable-temperature <sup>31</sup>P{<sup>1</sup>H} NMR spectroscopy indicates that **104Sn**, **145Ge** and **145Sn** are subject to a dynamic equilibria in solution, which interconverts between the planar and pyramidal centre and between two possible configurations.

The reaction between two equivalents of [(Mes)<sub>2</sub>P]K and GeCl<sub>2</sub>(1,4-dioxane) in THF initially gives a blue solution of the putative diphosphagermylene {(Mes)<sub>2</sub>P}<sub>2</sub>Ge (**160Ge**). However, this solution degrades after three days at room temperature to the diphosphine (Dipp)<sub>2</sub>P-P(Dipp)<sub>2</sub> (**150**) and the tetranuclear Ge(I) cluster [{(Mes)<sub>2</sub>P}Ge]<sub>4</sub> (**162**).

Treatment of  $\{(\text{Mes})_2\text{P}\}_2\text{SiHCl}$  (**174**) with either  $(\text{Me}_3\text{Si})_2\text{NLi}$  or  $\text{TMPLi}$  gives a mixture of unidentified products. The reaction between  $\{(\text{Mes})_2\text{P}\}_2\text{SiCl}_2$  (**175**) and lithium or potassium metal gives the corresponding alkali metal phosphide  $[(\text{Mes})_2\text{P}]_2\text{M}$  [ $\text{M} = \text{Li}, \text{K}$ ] as the major product, although a small number of crystals of the potassium triphosphasilanate  $[\{(\text{Mes})_2\text{P}\}_3\text{Si}]\text{K}(\text{THF})_3$  (**177**·THF) were isolated from the reaction with the potassium phosphide and characterised by X-ray crystallography. The reaction between four equivalents of  $[(\text{Mes})_2\text{P}]\text{Li}$  and  $\text{SiBr}_4$  in  $\text{Et}_2\text{O}$  gives the tetraphosphadisilene  $\{(\text{Mes})_2\text{P}\}_2\text{Si}=\text{Si}\{(\text{Mes})_2\text{P}\}_2$  (**181**).

The reaction between two equivalents of  $[(\text{Dipp})_2\text{P}]\text{K}$  and either  $\text{SiHCl}_3$  or  $\text{SiCl}_4$  gives  $\{(\text{Dipp})_2\text{P}\}_2\text{SiHCl}$  (**189**) or  $\{(\text{Dipp})_2\text{P}\}_2\text{SiCl}_2$  (**190**), respectively, as impure mixtures. Compound **189** proved to be inert towards a range of strong bases, while the reduction of **190** with lithium or potassium metal in THF gives  $(\text{Dipp})_2\text{P}-\text{P}(\text{Dipp})_2$  (**150**). Treatment of the base stabilised dichlorosilylene  $[\{\text{CH}_2\text{N}(\text{Dipp})\}_2\text{C}]\text{SiCl}_2$  (**191**) with two equivalents of  $[(\text{Dipp})_2\text{P}]\text{K}$  gives the phosphasilene  $\{(\text{Dipp})_2\text{P}\}\text{Si}(\text{Dipp})\{\text{P}(\text{Dipp})\}$  (**192**), rather than the corresponding diphosphasilylene, due to a 1,2-aryl migration.

The diphosphaarsenium cation  $[\{(\text{Dipp})_2\text{P}\}_2\text{As}][\text{Al}\{\text{OC}(\text{CF}_3)_3\}_4]$  (**208**) was prepared by the reaction between  $\{(\text{Dipp})_2\text{P}\}_2\text{AsCl}$  (**205**) and  $\text{Li}[\text{Al}\{\text{OC}(\text{CF}_3)_3\}_4]$  in fluorobenzene. In the solid-state, compound **208** is stabilised by a  $\pi$  interaction from a planar phosphorus centre, while in solution a dynamic equilibrium is in operations, which interconverts the planar and pyramidal phosphorus centres, similarly to the diphosphagermylenes **104Ge** and **145Ge**.

The reaction between  $\{(\text{Mes})_2\text{P}\}_2\text{PCl}$  (**213**) and  $\text{Na}[\text{B}\{3,5-(\text{CF}_3)_2\text{C}_6\text{H}_3\}_4]$  in fluorobenzene gives the cyclic diphosphaphosphonium salt  $[\{\mu-(\text{Mes})\text{P}\}_2\text{P}(\text{Mes})_2][\text{B}\{3,5-(\text{CF}_3)_2\text{C}_6\text{H}_3\}_4]$  (**216**). Compound **216** arises from a 1,2-aryl migration of the putative diphosphaphosphenium cation  $\{(\text{Mes})_2\text{P}\}_2\text{P}^+$ , followed by a cyclization.

The reaction between two equivalents of  $[(\text{Dipp})_2\text{As}]\text{Li}$  and  $\text{GeCl}_2(1,4\text{-dioxane})$  or  $\text{SnCl}_2$  gives  $\{(\text{Dipp})_2\text{As}\}_2\text{Ge}\cdot\text{C}_7\text{H}_8$  (**234Ge**) and  $\{(\text{Dipp})_2\text{As}\}_2\text{Sn}\cdot\text{C}_7\text{H}_8$  (**234Sn**), respectively. Compounds **234Ge** and **234Sn** each adopt a configuration with two pyramidal arsenic centres in the solid state and are stabilised by two short  $\text{Ge/Sn}\cdots\text{C}_{ipso}$  contacts.

A series of bidentate lithium phosphides were prepared, for use as potential precursors to *P*-heterocyclic tetrylenes. Treatment of  $\text{CH}_2(\text{PHDipp})_2$  (**246**) with two equivalents of *n*BuLi, followed by TMEDA gives  $[\text{CH}_2(\text{PLiDipp})_2](\text{TMEDA})_2$  (**257**). Treatment of  $\{\text{CH}_2\text{PHDipp}\}_2$  (**253**) with two equivalents of *n*BuLi gives the solvate



$\{\text{CH}_2(\text{PLiDipp})\}_2(\text{THF})(\text{OEt}_2)_{1.5}$  (**258b**), from this material the alternative solvate  $\{\text{CH}_2(\text{PLiDipp})\}_2(\text{THF})(\text{OEt}_2)$  (**258a**) was characterised by X-ray crystallography. Treatment of  $\text{DippPH}(\text{CH}_2)_n\text{PHDipp}$  [ $n = 3$  (**254**), 4 (**255**), 5 (**256**)] with two equivalents of  $n\text{BuLi}$  in THF gives  $[\text{CH}_2\{\text{CH}_2(\text{PLiDipp})\}_2(\text{THF})_4]$  (**259**),  $\{\text{CH}_2\text{CH}_2(\text{PLiDipp})\}_2(\text{THF})_6$  (**260**) and  $[\text{CH}_2\{\text{CH}_2\text{CH}_2\text{P}(\text{Dipp})\}_2]\text{Li}_2(\text{THF})_6(\text{C}_7\text{H}_8)$  (**261a**). Compound **261a** rapidly loses coordinated solvent on exposure to vacuum, yielding the alternative solvate  $[\text{CH}_2\{\text{CH}_2\text{CH}_2(\text{PLiDipp})\}_2](\text{THF})_{2.5}$  (**261b**). Compounds **258b**, **259**, **260** and **261b** exhibit complex variable-temperature  $^{31}\text{P}\{^1\text{H}\}$  and  $^7\text{Li}$  NMR behaviour indicating dynamic equilibria between monomeric and oligomeric species in solution.

The reaction between  $\{\text{CH}_2(\text{PLiDipp})\}_2$  and  $\text{SnCl}_2$  gives  $[\{\text{CH}_2(\text{PDipp})\}_2\text{Sn}]_2$  (*cis/trans*-**265**) as a mixture of *cis* and *trans* stereoisomers, while the reaction between  $[\text{CH}_2\{\text{CH}_2(\text{PLiDipp})\}_2]$  and  $\text{SnCl}_2$  gives the *cis* stereoisomer of  $[\text{CH}_2\{\text{CH}_2(\text{PDipp})\}_2\text{Sn}]_2$  (*cis*-**266c**). The solvates  $[\{\text{CH}_2(\text{PDipp})\}_2\text{Sn}]_2.\text{Et}_2\text{O}$  (*trans*-**265a**),  $[\text{CH}_2\{\text{CH}_2(\text{PDipp})\}_2\text{Sn}]_2.(\text{THF})_2$  (*cis*-**266b**) and  $[\text{CH}_2\{\text{CH}_2(\text{PDipp})\}_2\text{Sn}]_2.(\text{THF})_3$  (*cis*-**266c**) were characterised by X-ray crystallography.



## **Acknowledgements**

There are several people who I wish to thank for helping me produce this piece of work. In particular, I am very grateful to my supervisor Dr Keith Izod for his continued support and guidance in both the production of this thesis and in the laboratory over the past four years. I would also like to thank Dr. Corinne Wills and Professor William McFarlane for their guidance and expertise with NMR spectroscopy, and to Dr. Paul. G. Waddell for his patience and care with my samples for X-ray crystallography.

I would also like to thank members of the research group, past and present, for their help and advice in the laboratory. In particular, thanks to Dr. Claire Jones, Atheer Al-Rammahi and Dr. Casey Dixon.

Finally, I would like to say a huge thank you to my family and friends for their support over the past few years, in particular, to my parents Maureen and Paul, to whom I dedicate this thesis.



## Publications from this work

### Chapter 3

Desolvation and aggregation of sterically demanding alkali metal diarylphosphides. K. Izod, P. Evans, P. G. Waddell, *Dalton Trans.*, **2017**, 46, 13824.

### Chapter 4

Remote substituent effects on the structures and stabilities of P=E  $\pi$ -stabilized diphosphatetrylenes (R<sub>2</sub>R)<sub>2</sub>E (E = Ge, Sn). K. Izod, P. Evans, P. G. Waddell, M. R. Probert, *Inorg. Chem.* **2016**, 55, 10510.

### Chapter 6

A fully phosphane-substituted disilene. K. Izod, P. Evans, P. G. Waddell, *Angew. Chem. Int. Ed.* **2017**, 56, 5593.

### Chapter 10

A diarsagermylene and a diarsastaannylene stabilised by arene $\cdots$ Ge/Sn interactions. K. Izod, P. Evans, P. G. Waddell, *Chem. Comm.*, **2018**, 2526.

### Chapter 11 and 12

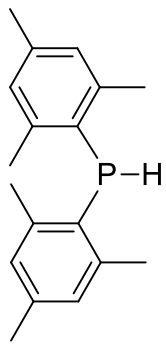
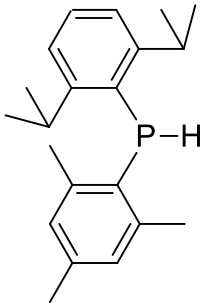
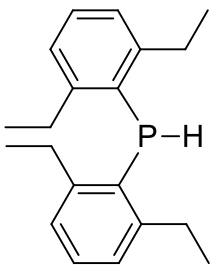
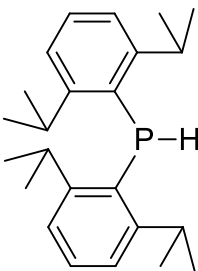
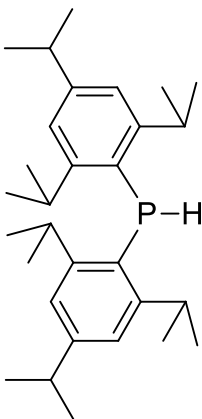
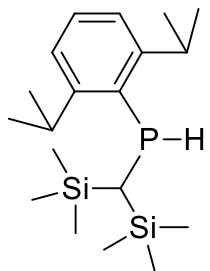
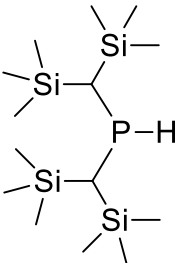
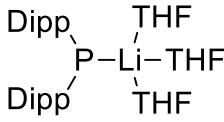
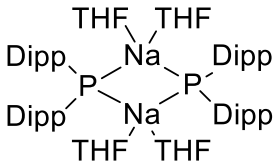
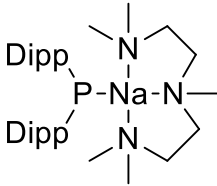
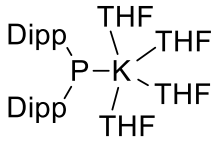
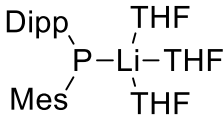
Influence of Chain Length on the Structures and Dynamic Behavior of Alkyl-Tethered  $\alpha,\omega$ -Diphosphide Complexes of Lithium and Their Use in the Synthesis of P-Heterocyclic Stannylenes, K. Izod, P. Evans, T. H. Downie, W. McFarlane, P. G. Waddell, *Inorg. Chem.*, **2018**, 57, 14733.

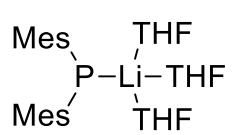
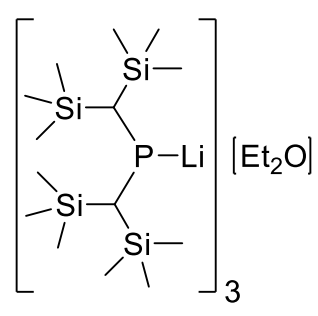
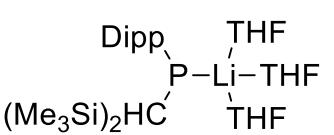
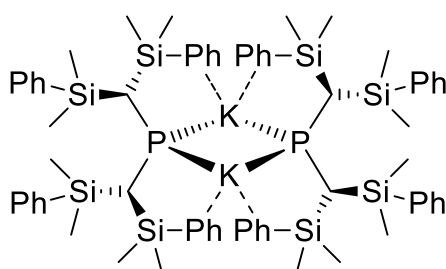
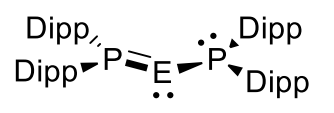
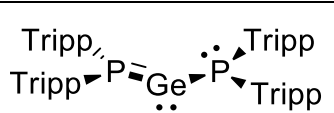
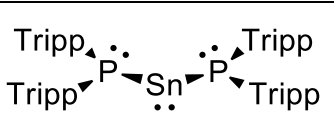
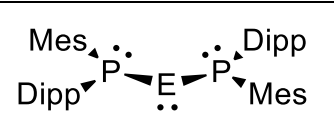
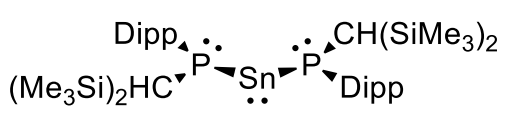
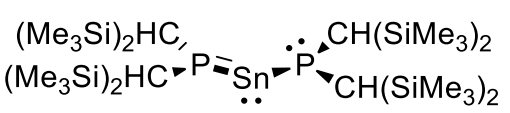
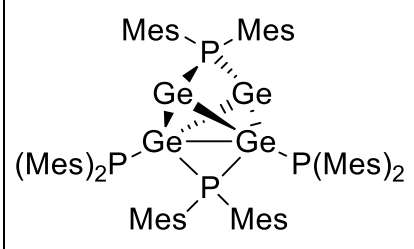
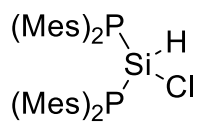
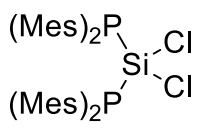
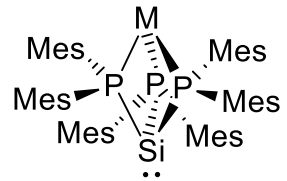
## List of Abbreviations

<b>Å</b>	angstrom	<b>Ppm</b>	parts per million
<b>br</b>	broad	<b>PMDETA</b>	<i>N,N,N',N'',N''</i> -
<b>Cp</b>	cyclopentadienyl		pentamethyldiethylenetriamine
<b>Cp*</b>	pentamethylcyclopentadienyl	<b>q</b>	quartet
<b>d</b>	doublet	<b>s</b>	singlet
<b>Dep</b>	2,6-di <i>iso</i> ethylphenyl	<b>t</b>	triplet
<b>Dipp</b>	2,6-di <i>iso</i> propylphenyl	<b>Tripp</b>	2,4,6-tri <i>iso</i> propylphenyl
<b>Hz</b>	hertz	<b>TMEDA</b>	<i>N,N,N',N'</i> -
<b>Mes</b>	2,4,6-trimethylphenyl		tetramethylethylenediamine
<b>Mes*</b>	2,4,6-tri <i>tert</i> butylphenyl		

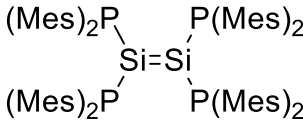
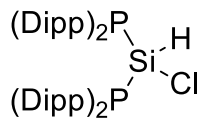
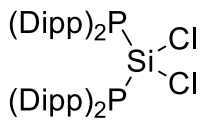
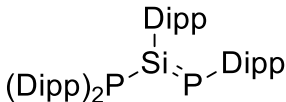
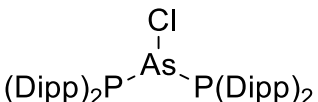
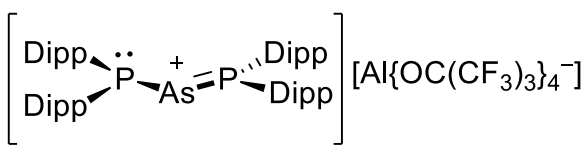
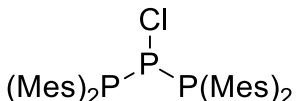
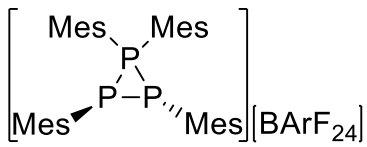
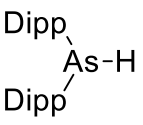
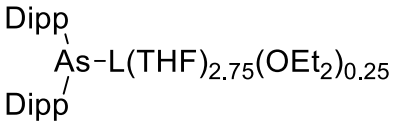
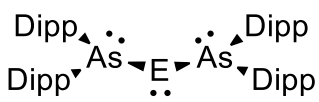
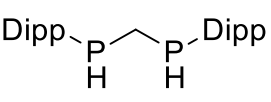
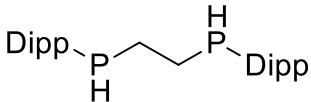
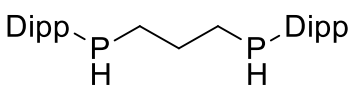
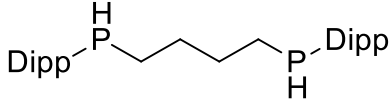
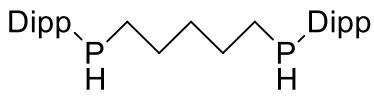
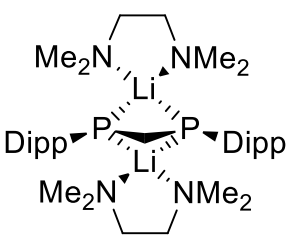
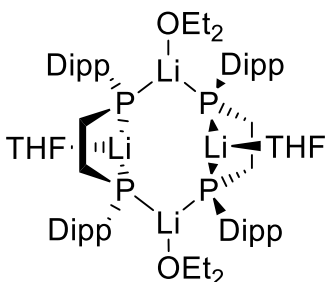
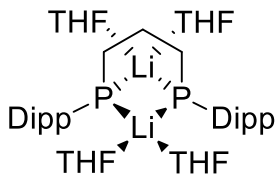


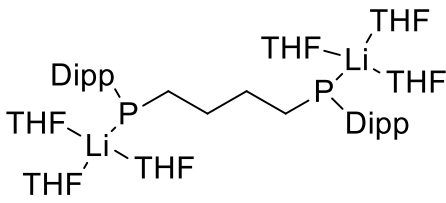
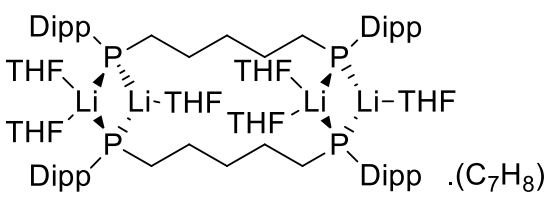
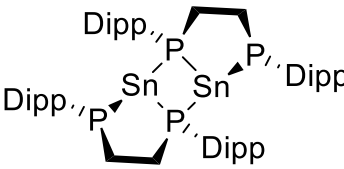
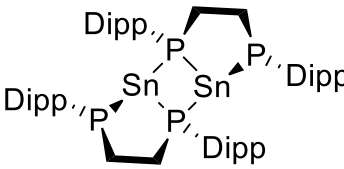
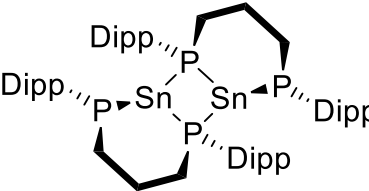
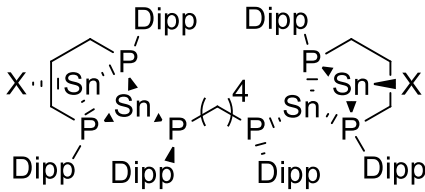
**Table of important compounds**

 <p><b>108</b></p>	 <p><b>109</b></p>	 <p><b>110</b></p>
 <p><b>111</b></p>	 <p><b>112</b></p>	 <p><b>113</b></p>
 <p><b>114</b></p>	 <p><b>128a</b></p>	 <p><b>129a</b></p>
 <p><b>129c</b></p>	 <p><b>130a</b></p>	 <p><b>131a</b></p>

 <p style="text-align: center;"><b>132a</b></p>	 <p style="text-align: center;"><b>139</b></p>	 <p style="text-align: center;"><b>134</b></p>
 <p style="text-align: center;"><b>144</b></p>		 <p style="text-align: center;">E = Ge (<b>104Ge</b>), Sn (<b>104Sn</b>)</p>
 <p style="text-align: center;"><b>145Ge</b></p>	 <p style="text-align: center;"><b>145Sn</b></p>	 <p style="text-align: center;">E = Ge (<b>146Ge</b>), Sn (<b>146Sn</b>)</p>
 <p style="text-align: center;"><b>147Sn</b></p>		 <p style="text-align: center;"><b>148Sn</b></p>
<p style="text-align: center;">(Dipp)<sub>2</sub>P–P(Dipp)<sub>2</sub></p> <p style="text-align: center;"><b>150</b></p>	<p style="text-align: center;">(Mes)<sub>2</sub>P–P(Mes)<sub>2</sub></p> <p style="text-align: center;"><b>161</b></p>	 <p style="text-align: center;"><b>162</b></p>
 <p style="text-align: center;"><b>174</b></p>	 <p style="text-align: center;"><b>175</b></p>	 <p style="text-align: center;">M = Li (<b>176</b>), K (<b>177</b>)</p>



 <p style="text-align: center;"><b>181</b></p>	 <p style="text-align: center;"><b>189</b></p>	 <p style="text-align: center;"><b>190</b></p>
 <p style="text-align: center;"><b>192</b></p>	 <p style="text-align: center;"><b>205</b></p>	
 <p style="text-align: center;"><b>208</b></p>	 <p style="text-align: center;"><b>213</b></p>	
 <p style="text-align: center;"><b>216</b></p>	 <p style="text-align: center;"><b>226</b></p>	 <p style="text-align: center;"><b>233</b></p>
 <p style="text-align: center;"><b>E = Ge (234Ge), Sn (234Sn)</b></p>	 <p style="text-align: center;"><b>246</b></p>	 <p style="text-align: center;"><b>253</b></p>
 <p style="text-align: center;"><b>254</b></p>	 <p style="text-align: center;"><b>255</b></p>	 <p style="text-align: center;"><b>256</b></p>
 <p style="text-align: center;"><b>257</b></p>	 <p style="text-align: center;"><b>258a</b></p>	 <p style="text-align: center;"><b>259</b></p>

 <p style="text-align: center;"><b>260</b></p>	 <p style="text-align: center;"><b>261a</b></p>	
 <p style="text-align: center;"><i>cis</i>-<b>265</b></p>	 <p style="text-align: center;"><i>trans</i>-<b>265</b></p>	 <p style="text-align: center;"><i>cis</i>-<b>266</b></p>
		
<p style="text-align: center;"><b>267</b></p>		

## Table of Contents

Abstract.....	i
Acknowledgements.....	v
Publications from this work.....	vii
List of Abbreviations.....	vii
Table of important compounds.....	ix
 Chapter 1. Introduction .....	 1
1.1 Introduction to low-oxidation state group 14 compounds .....	1
1.2 Ground state electronic configuration of tetrylenes.....	2
1.2.1 Inductive effects .....	3
1.2.2 Mesomeric effects.....	4
1.2.3 Kinetic stabilisation .....	5
1.3 Stabilisation by $\pi$ -interactions.....	6
1.4 Intramolecular stabilisation.....	6
1.5 Intermolecular base stabilisation.....	7
1.6 Synthetic approaches to tetrylenes.....	7
1.6.1 Synthesis of carbenes.....	7
1.6.2 Synthesis of silylenes.....	9
1.6.3 Synthesis of heavier tetrylenes .....	9
1.7 Reactivity .....	9
1.7.1 Dimerization .....	9
1.7.2 Small molecule activation .....	10
1.7.3 Transition metal complexes of tetrylenes .....	12
1.7.4 Stabilisation of reactive species.....	13
1.8 Stable tetrylenes .....	14
1.8.1 Diaminotetrylenes.....	14
1.8.2 Oxygen- and sulphur-substituted tetrylenes .....	15
1.8.3 Alkylaminotetrylenes.....	15
1.8.4 Dialkyltetrylenes.....	16
1.8.5 Diaryltetrylenes .....	17
1.8.6 Silyl- and phosphoniotetrylenes .....	18
1.8.7 Boryltetrylenes.....	18
1.8.8 Phosphatetrylenes .....	19
1.9 Conclusions and research proposal.....	27
1.10 References .....	28
Chapter 2. Experimental.....	32
2.1 General procedures .....	32
2.2 NMR spectroscopy.....	32
2.3 SSNMR spectroscopy .....	33
2.4 Crystal structure determinations .....	33
2.5 DFT Calculations .....	34
2.6 References.....	34
Chapter 3. Monodentate phosphine and phosphide synthesis.....	36
3.1 Introduction.....	36
3.2 Developing of an array of bulky phosphines .....	37
3.2.1 Synthesis of metalated precursors .....	38
3.2.2 Synthesis of phosphines.....	39
3.3 Structural investigation of (Dipp) <sub>2</sub> P ligand system .....	40
3.3.1 Solid-state structures of [(Dipp) <sub>2</sub> P]Li(THF) <sub>3</sub> ( <b>128a</b> ), {[(Dipp) <sub>2</sub> P]Na(THF) <sub>2</sub> } <sub>2</sub> ( <b>129a</b> ), [(Dipp) <sub>2</sub> P]Na(TMEDA) ( <b>129c</b> ), [(Dipp) <sub>2</sub> P]K(THF) <sub>4</sub> ( <b>130a</b> ).....	41

3.3.2	Solution behaviour of <b>128b</b> , <b>129b</b> , <b>129c</b> and <b>130b</b> .....	43
3.3.3	Dynamic behaviour of [(Dipp) <sub>2</sub> P]Li(THF) <sub>2</sub> ( <b>128b</b> ) .....	43
3.3.4	Dynamic behaviour of [(Dipp) <sub>2</sub> P]Na(THF) <sub>1.5</sub> ( <b>129b</b> ) .....	44
3.4	The effect of steric demand on the phosphorus centre in lithium phosphides .....	45
3.4.1	Solid-state structures of [(Dipp)(Mes)P]Li(THF) <sub>3</sub> ( <b>131a</b> ), [(Mes) <sub>2</sub> P]Li(THF) <sub>3</sub> ( <b>132a</b> ), [(Mes) <sub>2</sub> P] <sub>2</sub> Li <sub>2</sub> (THF) <sub>2</sub> (OEt <sub>2</sub> ) ( <b>132b</b> ) and [(Dipp){(Me <sub>3</sub> Si) <sub>2</sub> CH}P]Li(THF) <sub>3</sub> ( <b>134</b> ) .....	47
3.4.2	Solution-state NMR behaviour of [(Dipp)(Mes)P]Li(THF) <sub>2</sub> ( <b>131b</b> ).....	48
3.4.3	Solution-state NMR behaviour of [(Mes) <sub>2</sub> P]Li(THF) <sub>3</sub> ( <b>132c</b> ).....	50
3.4.4	Solution-state NMR behaviour of [(Dipp){(Me <sub>3</sub> Si) <sub>2</sub> CH}P]Li(THF) <sub>3</sub> ( <b>134</b> ) .....	51
3.5	Attempted synthesis of dialkylphosphides .....	53
3.6	Conclusions .....	56
3.7	Experimental .....	57
3.7.1	Modified synthesis of DippBr ( <b>118</b> ) <sup>[9]</sup> .....	57
3.7.2	Modified synthesis of DippLi(OEt <sub>2</sub> ) ( <b>119</b> ) <sup>[10]</sup> .....	57
3.7.3	Modified synthesis of (Dipp) <sub>2</sub> PH ( <b>111</b> ) <sup>[11]</sup> .....	58
3.7.4	Synthesis of DepBr ( <b>116</b> ).....	58
3.7.5	Synthesis of DepMgBr ( <b>117</b> ) .....	58
3.7.6	Synthesis of (Dep) <sub>2</sub> PH ( <b>110</b> ).....	59
3.7.7	Modified synthesis of TrippBr ( <b>120</b> ) <sup>[10]</sup> .....	59
3.7.8	Modified synthesis of TrippLi(OEt <sub>2</sub> ) ( <b>121</b> ) <sup>[10]</sup> .....	60
3.7.9	Modified synthesis of (Tripp) <sub>2</sub> PH ( <b>112</b> ) <sup>[7a]</sup> .....	60
3.7.10	Modified synthesis of (Mes) <sub>2</sub> PH ( <b>108</b> ) <sup>[7b]</sup> .....	60
3.7.11	Synthesis of {(Me <sub>3</sub> Si) <sub>2</sub> CH} <sub>2</sub> PCl ( <b>140</b> ) <sup>[17]</sup> .....	61
3.7.12	Synthesis of {(Me <sub>3</sub> Si)CH} <sub>2</sub> PH ( <b>114</b> ) <sup>[7c]</sup> .....	61
3.7.13	Synthesis of (Dipp)(Mes)PH ( <b>109</b> ) .....	62
3.7.14	Synthesis of {(Me <sub>3</sub> Si) <sub>2</sub> CH}PCl <sub>2</sub> ( <b>127</b> ) <sup>[17]</sup> .....	62
3.7.15	Synthesis of (Dipp){(Me <sub>3</sub> Si) <sub>2</sub> CH}PH ( <b>113</b> ) .....	63
3.7.16	Synthesis of [(Dipp) <sub>2</sub> P]Li(THF) <sub>2</sub> ( <b>128b</b> ) .....	63
3.7.17	Synthesis of [(Dipp) <sub>2</sub> P]Na(THF) <sub>1.5</sub> ( <b>129b</b> ) .....	64
3.7.18	Synthesis of [(Dipp) <sub>2</sub> P]Na(PMDETA) ( <b>129c</b> ).....	64
3.7.19	Synthesis of [(Dipp) <sub>2</sub> P]K ( <b>130b</b> ) .....	65
3.7.20	Synthesis of [(Mes) <sub>2</sub> P]Li(THF) ( <b>132c</b> ) .....	65
3.7.21	Synthesis of [(Dipp)(Mes)P]Li(THF) <sub>2</sub> ( <b>131b</b> ) .....	66
3.7.22	Synthesis of [(Dipp){(Me <sub>3</sub> Si) <sub>2</sub> CH}P]Li(THF) <sub>3</sub> ( <b>134</b> ).....	66
3.7.23	Synthesis of (Me <sub>2</sub> PhSi) <sub>2</sub> CHLi ( <b>125</b> ) <sup>[11b]</sup> .....	67
3.7.24	Synthesis of {(Me <sub>2</sub> PhSi) <sub>2</sub> CH} <sub>2</sub> PCl ( <b>143</b> ) .....	67
3.7.25	Synthesis of [(Me <sub>3</sub> Si) <sub>2</sub> CH] <sub>2</sub> P]Li <sub>3</sub> (OEt <sub>2</sub> ) ( <b>139</b> ).....	68
3.7.26	Synthesis of [(Me <sub>3</sub> Si) <sub>2</sub> CH] <sub>2</sub> P]K ( <b>141</b> ) .....	68
3.7.27	Synthesis of [Li(μ-P{CH(SiMe <sub>3</sub> ) <sub>2</sub> })][K(μ-P{CH(SiMe <sub>3</sub> ) <sub>2</sub> })] ( <b>142</b> ).....	68
3.8	References .....	69
Chapter 4.	Synthesis of diphosphatetrylenes .....	71
4.1	Introduction .....	71
4.2	Synthesis of {(Dipp) <sub>2</sub> P} <sub>2</sub> Sn ( <b>104Sn</b> ), {(Tripp) <sub>2</sub> P} <sub>2</sub> Ge ( <b>145Ge</b> ), {(Tripp) <sub>2</sub> P} <sub>2</sub> Sn ( <b>145Sn</b> ), {(Dipp)(Mes)P} <sub>2</sub> Ge.( <i>n</i> -hexane) <sub>0.5</sub> ( <b>146Ge</b> .(C <sub>6</sub> H <sub>14</sub> ) <sub>0.5</sub> ), {(Dipp)(Mes)P} <sub>2</sub> Sn ( <b>146Sn</b> ) and [(Dipp){(Me <sub>3</sub> Si) <sub>2</sub> CH}P] <sub>2</sub> Sn ( <b>147Sn</b> ) .....	72
4.3	Attempted synthesis of {(Dipp) <sub>2</sub> P} <sub>2</sub> Pb ( <b>104Pb</b> ) and solid-state structure of (Dipp) <sub>2</sub> P-P(Dipp) <sub>2</sub> ( <b>150</b> ).....	73
4.4	Solid-state structure of {(Dipp) <sub>2</sub> P} <sub>2</sub> Sn ( <b>104Sn</b> ).....	75
4.5	Solid-state structure of {(Tripp) <sub>2</sub> P} <sub>2</sub> Ge.(C <sub>7</sub> H <sub>14</sub> ) ( <b>145Ge</b> ·C <sub>7</sub> H <sub>14</sub> ).....	75
4.6	Solid-state structure of {(Tripp) <sub>2</sub> P} <sub>2</sub> Sn ( <b>145Sn</b> ).....	76

4.6.1	Solid state structures of $\{(\text{Dipp})(\text{Mes})\text{P}\}_2\text{Ge}\cdot(n\text{-hexane})_{0.5}$ ( <b>146Ge</b> $\cdot(\text{C}_6\text{H}_{14})_{0.5}$ ) and $\{(\text{Dipp})(\text{Mes})\text{P}\}_2\text{Sn}$ ( <b>146Sn</b> )	78
4.6.2	Solid-state structure of $[(\text{Dipp})\{(\text{Me}_3\text{Si})_2\text{CH}\}\text{P}]_2\text{Sn}$ ( <b>147Sn</b> )	79
4.6.3	Isolation of $[(\text{Me}_3\text{Si})_2\text{CH}]_2\text{P}]_2\text{Sn}$ ( <b>148Sn</b> )	80
4.7	Conclusion of solid-state structures	81
4.8	NMR spectra of diphosphatetrylenes	81
4.8.1	Dynamic behaviour of $\{(\text{Tripp})_2\text{P}\}_2\text{Ge}$ ( <b>145Ge</b> )	82
4.8.2	Dynamic behaviour and SSNMR of $\{(\text{Dipp})_2\text{P}\}_2\text{Sn}$ ( <b>104Sn</b> ) and $\{(\text{Tripp})_2\text{P}\}_2\text{Sn}$ ( <b>145Sn</b> )	84
4.8.3	Dynamic behaviour of $\{(\text{Dipp})(\text{Mes})\text{P}\}_2\text{Ge}\cdot(n\text{-hexane})_{0.5}$ ( <b>146Ge</b> $\cdot(\text{C}_6\text{H}_{14})_{0.5}$ )	88
4.8.4	Dynamic behaviour of $\{(\text{Dipp})(\text{Mes})\text{P}\}_2\text{Sn}$ ( <b>146Sn</b> )	89
4.9	Crystal colouration, thermochromism and UV-visible spectra	92
4.10	Conclusions from UV-visible spectra	95
4.11	DFT calculations	96
4.12	Conclusion of DFT calculations	105
4.13	Overall conclusions	106
4.14	Experimental	107
4.14.1	Synthesis of $\{(\text{Dipp})_2\text{P}\}_2\text{Ge}$ ( <b>104Ge</b> )	107
4.14.2	Synthesis of $\{(\text{Dipp})_2\text{P}\}_2\text{Sn}$ ( <b>104Sn</b> )	107
4.14.3	Synthesis of $\{(\text{Tripp})_2\text{P}\}_2\text{Ge}$ ( <b>145Ge</b> )	108
4.14.4	Synthesis of $\{(\text{Tripp})_2\text{P}\}_2\text{Sn}$ ( <b>145Sn</b> )	108
4.14.5	Synthesis of $(\text{Dipp})_2\text{P}-\text{P}(\text{Dipp})_2$ ( <b>150</b> )	109
4.14.6	Synthesis of $\{(\text{Dipp})(\text{Mes})\text{P}\}_2\text{Ge}\cdot(n\text{-hexane})_{0.5}$ ( <b>146</b> $\cdot(\text{C}_6\text{H}_{14})_{0.5}$ )	109
4.14.7	Synthesis of $\{(\text{Dipp})(\text{Mes})\text{P}\}_2\text{Sn}$ ( <b>146Sn</b> )	110
4.14.8	Synthesis of $[(\text{Dipp})\{(\text{Me}_3\text{Si})_2\text{CH}\}\text{P}]_2\text{Sn}$ ( <b>147Sn</b> )	111
4.15	References	111
Chapter 5.	Isolation of an unusual Ge(I) cluster	113
5.1	Introduction	113
5.2	Attempted synthesis of $\{(\text{Mes})_2\text{P}\}_2\text{Ge}$ ( <b>160Ge</b> )	113
5.3	Solid-state structure of $[\{(\text{Mes})_2\text{P}\}\text{Ge}]_4(\text{C}_7\text{H}_{14})_5$ ( <b>162</b> $\cdot(\text{C}_7\text{H}_{14})$ )	114
5.4	Proposed formation of $[\{(\text{Mes})_2\text{P}\}\text{Ge}]_4$ ( <b>162</b> )	116
5.5	Attempted synthesis of $\{(\text{Mes})_2\text{P}\}_2\text{Sn}$ ( <b>160Sn</b> )	117
5.6	Conclusions and future work	117
5.7	Experimental	118
5.7.1	Attempted synthesis of $\{(\text{Mes})_2\text{P}\}_2\text{Ge}$ ( <b>160Ge</b> )	118
5.7.2	Attempted synthesis of $\{(\text{Mes})_2\text{P}\}_2\text{Sn}$ ( <b>160Sn</b> )	118
5.8	References	119
Chapter 6.	A fully phosphide-substituted disilene	120
6.1	Introduction	120
6.2	Synthesis of Si(IV) precursors $\{(\text{Mes})_2\text{P}\}_2\text{SiHCl}$ ( <b>174</b> ) and $\{(\text{Mes})_2\text{P}\}_2\text{SiCl}_2$ ( <b>175</b> )	120
6.3	Attempted dehydrochlorination of $\{(\text{Mes})_2\text{P}\}_2\text{SiHCl}$ ( <b>174</b> )	121
6.4	Attempted reduction of $\{(\text{Mes})_2\text{P}\}_2\text{SiCl}_2$ ( <b>175</b> )	121
6.5	Synthesis of $\{(\text{Mes})_2\text{P}\}_2\text{Si}=\text{Si}\{\text{P}(\text{Mes})_2\}_2$ ( <b>181</b> )	123
6.6	Solid-state structure of $\{(\text{Mes})_2\text{P}\}_2\text{Si}=\text{Si}\{\text{P}(\text{Mes})_2\}_2$ ( <b>181</b> )	125
6.7	CP-MAS NMR spectra of $\{(\text{Mes})_2\text{P}\}_2\text{Si}=\text{Si}\{\text{P}(\text{Mes})_2\}_2$ ( <b>181</b> )	126
6.8	DFT calculations	127
6.9	Synthesis of $[\{(\text{Mes})_2\text{P}\}_3\text{Si}]\text{Li}(\text{THF})$ ( <b>176(THF)</b> )	130
6.10	Conclusions	131
6.11	Experimental	131
6.11.1	Synthesis of $\{(\text{Mes})_2\text{P}\}_2\text{SiHCl}$ ( <b>174</b> )	131

6.11.2	Synthesis of $\{(\text{Mes})_2\text{P}\}_2\text{SiCl}_2$ ( <b>175</b> )	132
6.11.3	Synthesis of $\{(\text{Mes})_2\text{P}\}_2\text{Si}=\text{Si}\{\text{P}(\text{Mes})_2\}_2$ ( <b>181</b> )	133
6.11.4	Synthesis of $[(\text{Mes}_2\text{P})_3\text{Si}]\text{Li}(\text{THF})$ ( <b>176</b> ·( <b>THF</b> ))	133
6.12	References	134
Chapter 7.	Rearrangement of a transient diphosphasilene	135
7.1	Introduction	135
7.2	Synthesis of Si(IV) precursors $\{(\text{Dipp})_2\text{P}\}_2\text{SiHCl}_3$ ( <b>189</b> ) and $\{(\text{Dipp})_2\text{P}\}_2\text{SiCl}_2$ ( <b>190</b> )	135
7.3	Attempted dehydrochlorination of <b>189</b> and reduction of <b>190</b>	136
7.4	Attempted reaction between $\text{SiBr}_4$ and $[(\text{Dipp})_2\text{P}]\text{Li}$	137
7.5	Synthesis of the phosphasilene $\{(\text{Dipp})_2\text{P}\}\text{Si}(\text{Dipp})\{\text{P}(\text{Dipp})\}$ ( <b>192</b> )	138
7.6	Solid-state structure of $\{(\text{Dipp})_2\text{P}\}\text{Si}(\text{Dipp})\{\text{P}(\text{Dipp})\}$ ( <b>192</b> )	138
7.7	DFT calculations	139
7.8	Conclusions	141
7.9	Experimental	142
7.9.1	Attempted synthesis of $\{(\text{Dipp})_2\text{P}\}_2\text{SiHCl}$ ( <b>189</b> )	142
7.9.2	Attempted synthesis of $\{(\text{Dipp})_2\text{P}\}_2\text{SiCl}_2$ ( <b>190</b> )	142
7.10	Synthesis of $\{(\text{Dipp})_2\text{P}\}\text{Si}(\text{Dipp})\{\text{P}(\text{Dipp})\}$ ( <b>192</b> )	142
7.11	References	143
Chapter 8.	A diphospharsenium cation stabilised a planar phosphorus	144
8.1	Introduction to pnictenium cations	144
8.1.1	Phosphorus-substituted pnictenium cations	145
8.1.2	Heavier acyclic pnictenium cations	145
8.1.3	Proposed diphosphapnictenium cation	146
8.2	Synthesis of $\{(\text{Dipp})_2\text{P}\}_2\text{AsCl}$	146
8.3	Synthesis of $[\{(\text{Dipp})_2\text{P}\}_2\text{As}][\text{Al}\{\text{OC}(\text{CF}_3)_3\}(\text{PhMe})_{0.5}]$	147
8.4	Solid-state structure of $[\{(\text{Dipp})_2\text{P}\}_2\text{As}][\text{Al}\{\text{OC}(\text{CF}_3)_3\}(\text{PhMe})_{1.5}]$ ( <b>208</b> )	148
8.5	Variable-temperature $^{31}\text{P}\{^1\text{H}\}$ and solid-state CP-MAS $^{31}\text{P}\{^1\text{H}\}$ NMR spectra of $[\{(\text{Dipp})_2\text{P}\}_2\text{As}][\text{Al}\{\text{OC}(\text{CF}_3)_3\}(\text{PhMe})_{0.5}]$ ( <b>208a</b> )	150
8.6	DFT calculations	152
8.7	Conclusions	154
8.8	Experimental	154
8.8.1	Synthesis of $\{(\text{Dipp})_2\text{P}\}_2\text{AsCl}$ ( <b>205</b> )	154
8.8.2	Synthesis of $[\{(\text{Dipp})_2\text{P}\}_2\text{As}][\text{Al}\{\text{OC}(\text{CF}_3)_3\}_4](\text{PhMe})_{0.5}$ ( <b>208a</b> )	154
8.9	References	155
Chapter 9.	Attempted synthesis of a phosphonium cation	157
9.1	Attempted synthesis of $\{(\text{Dipp})_2\text{P}\}_2\text{PCl}$ ( <b>212</b> )	157
9.2	Synthesis of $\{(\text{Mes})_2\text{P}\}_2\text{PCl}$ ( <b>213</b> )	157
9.3	Solid-state structure of $\{(\text{Mes})_2\text{P}\}_2\text{PCl}$ ( <b>213</b> )	158
9.4	Chloride abstraction from $\{(\text{Mes})_2\text{P}\}_2\text{PCl}$ ( <b>213</b> )	158
9.5	Solid-state structure of $[\{\mu-(\text{Mes})\text{P}\}_2\text{P}(\text{Mes})_2][\text{BArF}_{24}]\cdot(\text{C}_7\text{H}_{14})$ ( <b>216</b> )·( <b>C<sub>7</sub>H<sub>14</sub></b> )	159
9.6	Proposed mechanisms for the formation of $[\{\mu-(\text{Mes})\text{P}\}_2\text{P}(\text{Mes})_2][\text{BArF}_{24}]$ ( <b>216</b> )	160
9.7	Conclusions	162
9.8	Experimental	163
9.8.1	Synthesis of $\{(\text{Mes})_2\text{P}\}_2\text{PCl}$ ( <b>213</b> )	163
9.9	Synthesis of $[\{\mu-(\text{Mes})\text{P}\}_2\text{P}(\text{Mes})_2][\text{BArF}_{24}]\cdot(\text{C}_7\text{H}_{14})$ ( <b>216</b> )·( <b>C<sub>7</sub>H<sub>14</sub></b> )	163
9.10	References	164
Chapter 10.	Diarsatetrylenes	165
10.1	Background	165
10.2	Synthesis of $(\text{Dipp})_2\text{AsH}$	166
10.3	Synthesis and solid-state structure of $[(\text{Dipp})_2\text{As}]\text{Li}(\text{THF})_{2.5}(\text{OEt}_2)_{0.25}$	166

10.4	Synthesis of $\{(Dipp)_2As\}_2Ge \cdot PhMe$ ( <b>234Ge</b> ) and $\{(Dipp)_2As\}_2Sn \cdot PhMe$ ( <b>234Sn</b> )	167
10.5	Solid-state structures of $\{(Dipp)_2As\}_2E \cdot PhMe$ [ $E = Ge$ ( <b>234Ge</b> ), $Sn$ ( <b>234Sn</b> )] ..	168
10.6	NMR spectra of $\{(Dipp)_2As\}_2E \cdot PhMe$ [ $E = Ge$ ( <b>234Ge</b> ), $Sn$ ( <b>234Sn</b> )].....	169
10.7	DFT calculations .....	171
10.8	Conclusions .....	173
10.9	Experimental .....	173
10.9.1	Synthesis of $(iPr_2N)AsCl_2$ ( <b>230</b> ) .....	173
10.9.2	Synthesis of $(Dipp)_2As(NiPr_2)$ ( <b>231</b> ) .....	174
10.9.3	Synthesis of $(Dipp)_2AsCl$ ( <b>232</b> ).....	174
10.9.4	Synthesis of $(Dipp)_2AsH$ ( <b>226</b> ).....	175
10.9.5	Synthesis of $(Dipp)_2AsLi(THF)_{2.5}(OEt_2)_{0.5}$ ( <b>233</b> ).....	175
10.9.6	Synthesis of $\{(Dipp)_2As\}_2Ge \cdot C_7H_8$ ( <b>234Ge</b> ).....	175
10.10	Synthesis of $\{(Dipp)_2As\}_2Sn \cdot C_7H_8$ ( <b>234Sn</b> ) .....	176
10.11	References .....	177
Chapter 11.	Synthesis of diphosphines and dilithium diphosphides .....	178
11.1	Introduction .....	178
11.1.1	Proposed synthetic strategy to alkyl-bridged diphosphines .....	179
11.2	Synthesis of $DippPH_2$ ( <b>243</b> ) .....	180
11.3	Synthesis of $CH_2(PHDipp)_2$ ( <b>246</b> ).....	180
11.4	Synthesis of $\{CH_2(PHDipp)\}_2$ ( <b>253</b> ).....	181
11.5	Synthesis of $CH_2\{CH_2(PHDipp)\}_2$ , ( <b>254</b> ) $\{CH_2CH_2(PHDipp)\}_2$ ( <b>255</b> ) and $CH_2\{CH_2CH_2(PHDipp)\}_2$ ( <b>256</b> ).....	182
11.6	Synthesis and solid-state structures of $[CH_2(PLiDipp)_2](TMEDA)_2$ ( <b>257</b> ), $\{CH_2(PLiDipp)\}_2(THF)(OEt_2)_{1.5}$ ( <b>258a</b> ), $[CH_2\{CH_2(PLiDipp)\}_2(THF)_4$ ( <b>259</b> ), $\{CH_2CH_2(PLiDipp)\}_2(THF)_6$ ( <b>260</b> ) and $[CH_2\{CH_2CH_2P(Dipp)\}_2]Li_2(THF)_6(C_7H_8)$ ( <b>261a</b> )	183
11.7	Solution behaviour of dilithium diphosphides <b>257</b> , <b>258b</b> , <b>259</b> , <b>260</b> and <b>261b</b> ....	187
11.7.1	NMR spectra of $[CH_2(PLiDipp)_2](TMEDA)_2$ ( <b>257</b> ),.....	187
11.7.2	Dynamic behaviour of $\{CH_2(PLiDipp)\}_2(THF)(OEt_2)_{1.5}$ ( <b>258b</b> ) .....	187
11.7.3	Dynamic behaviour of $[CH_2\{CH_2(PLiDipp)\}_2](THF)_4$ ( <b>259</b> ),.....	189
11.7.4	Dynamic behaviour of $\{CH_2CH_2(PLiDipp)\}_2(THF)_6$ ( <b>260</b> ) .....	190
11.7.5	Dynamic behaviour of $[CH_2\{CH_2CH_2(PLiDipp)\}_2](THF)_{2.5}$ ( <b>261b</b> ) .....	192
11.8	Conclusions .....	193
11.9	Experimental .....	193
11.9.1	Synthesis of $DippPH_2$ ( <b>243</b> ).....	193
11.9.2	Synthesis of $CH_2(PHDipp)_2$ ( <b>246</b> ) .....	194
11.9.3	Synthesis of $[CH_2(PLiDipp)_2](TMEDA)_2$ ( <b>257</b> ).....	195
11.9.4	Synthesis of $(Dipp)(iPr_2N)PH$ ( <b>250</b> ).....	195
11.9.5	Synthesis of $\{CH_2(PHDipp)\}_2$ ( <b>253</b> ) .....	196
11.9.6	Synthesis of $\{CH_2(PLiDipp)\}_2(THF)(OEt_2)_{1.5}$ ( <b>258b</b> ) .....	197
11.9.7	Synthesis of $CH_2\{CH_2(PHDipp)\}_2$ ( <b>254</b> ) .....	197
11.9.8	Synthesis of $[CH_2\{CH_2(PLiDipp)\}_2](THF)_4$ ( <b>259</b> ) .....	198
11.9.9	Synthesis of $\{CH_2CH_2(PHDipp)\}_2$ ( <b>255</b> ) .....	198
11.9.10	Synthesis of $\{CH_2CH_2(PLiDipp)\}_2(THF)_6$ ( <b>260</b> ) .....	199
11.9.11	Synthesis of $CH_2\{CH_2CH_2(PHDipp)\}_2$ ( <b>256</b> ) .....	199
11.9.12	Synthesis of $[CH_2\{CH_2CH_2P(Dipp)\}_2]Li_2(THF)_6(C_7H_8)$ ( <b>261b</b> ).....	200
11.10	References .....	200
Chapter 12.	<i>P</i> -Heterocyclic stannylenes.....	202
12.1	Synthesis of the <i>P</i> -Heterocyclic stannylenes .....	202

12.2	Solid-state structures of $[\{\text{CH}_2(\text{PDipp})\}_2\text{Sn}]_2\cdot\text{Et}_2\text{O}$ ( <i>trans</i> - <b>265a</b> ), $[\text{CH}_2\{\text{CH}_2(\text{PDipp})\}_2\text{Sn}]_2(\text{THF})_2$ ( <i>cis</i> - <b>266b</b> ) and $[\{\text{CH}_2\{\text{CH}_2(\text{PDipp})\}_2\text{SnX}\}\text{Sn}]_2\{(\text{PDipp})\text{CH}_2\}_2\text{CH}_2$ [ $\text{X} = \text{Cl}/\text{Br}$ ] ( <b>267</b> ).....	204
12.3	NMR spectra of $[\{\text{CH}_2(\text{PDipp})\}_2\text{Sn}]_2$ ( <i>cis/trans</i> - <b>265b</b> ) and $[\text{CH}_2\{\text{CH}_2(\text{PDipp})\}_2\text{Sn}]_2(n\text{-hexane})(\text{THF})_{0.5}$ ( <i>cis</i> - <b>266c</b> ).....	207
12.4	Conclusions.....	210
12.5	Experimental.....	211
12.5.1	Synthesis of $[\{\text{CH}_2(\text{PDipp})\}_2\text{Sn}]_2$ ( <i>cis/trans</i> - <b>265b</b> ) .....	211
12.5.2	Synthesis of $[\text{CH}_2\{\text{CH}_2(\text{PDipp})\}_2\text{Sn}]_2(n\text{-hexane})(\text{THF})_{0.5}$ ( <b>266c</b> ) .....	212
12.6	References.....	213
Chapter 13.	Conclusions .....	214
13.1	Solid-state and solution behaviour of alkali metal phosphides .....	214
13.2	Effect of modifying the steric demands of the phosphide ligands on the structure of diphosphatetrylenes .....	215
13.3	Effect of modifying the tetrel/pnictogen centre ( $\text{R}_2\text{E}$ ; $\text{E} = \text{Ge}, \text{Sn}, \text{As}, \text{Si}, \text{P}$ ) .....	217
13.4	Effect of modifying the pnictogen of the ligand system.....	218
13.5	Possible future work .....	219
Chapter 14.	Appendix (on attached CD).....	220



## Chapter 1. Introduction

### 1.1 Introduction to low-oxidation state group 14 compounds

The transition from the observation of fleeting intermediates of low oxidation state group 14 compounds, such as  $\text{CCl}_2$  (prepared by reacting chloroform with a strong base),<sup>[1]</sup> to the isolation of persistent species is due to advances in ligand development. In 1956, Fischer prepared the first example of a monomeric group 14 compound in the +2 oxidation state, bis(cyclopentadienyl)tin ( $\text{Cp}_2\text{Sn}$ , **1**),<sup>[2]</sup> which was later characterised by X-ray crystallography by Atwood.<sup>[3]</sup> There are now examples of metallocenes for all the group 14 elements:  $\text{Cp}_2\text{Pb}$  (**2**)<sup>[4]</sup>,  $\text{GeCp}^*_2$  (**3**)<sup>[5]</sup> and  $\text{SiCp}^*_2$  (**4**)<sup>[6]</sup>, with the exception of carbon. The lighter metallocenes **3** and **4** utilise the larger pentamethylcyclopentadienyl ligand ( $\text{Cp}^*$ ) for greater stabilisation. The metallocenes **1-3** have a bent geometry, with respect to the cyclopentadienyl rings, in the solid-state, while **4** crystallises with one bent and one linear metallocene in the asymmetric unit, as shown in Figure 1.

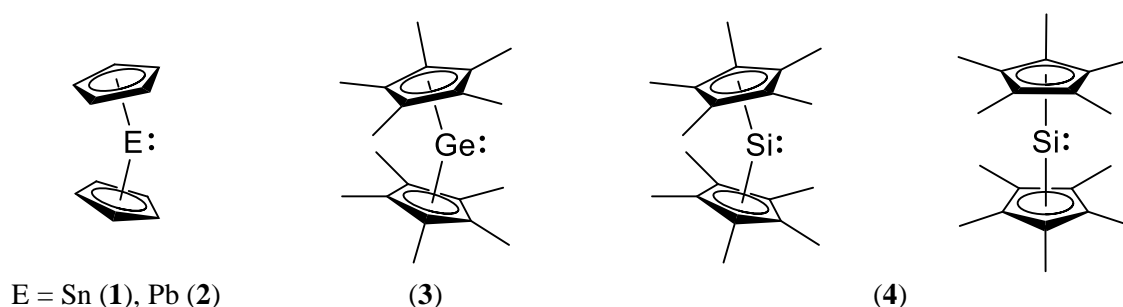


Figure 1: Geometries of the group 14 metallocenes

The first true two-coordinate group 14 compounds in the +2 oxidation state, also known as tetrylenes ( $\text{R}_2\text{E}$ ;  $\text{E} = \text{C}, \text{Si}, \text{Ge}, \text{Sn}, \text{Pb}$ ), were prepared by Lappert in 1974. These initial tetrylenes [ $\{(\text{Me}_3\text{Si})(\text{R})\text{N}\}_2\text{E}$  (**5**);  $\text{E} = \text{Ge}, \text{Sn}, \text{Pb}$ ;  $\text{R} = \text{SiMe}_3, t\text{Bu}$ ] featured bulky amino substituents.<sup>[7]</sup> It was not until 1992 that the first stable, crystalline carbene ( $\text{R}_2\text{C}$ ) was reported by Arduengo (**6**), which is an example of an *N*-heterocyclic carbene (NHC).<sup>[8]</sup>

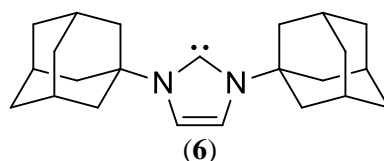


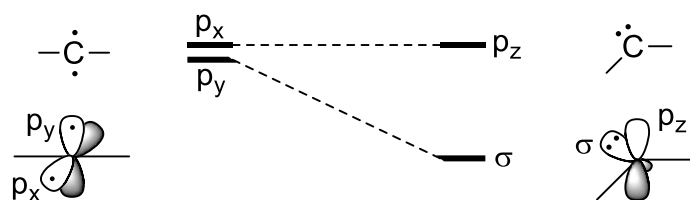
Figure 2: The first stable, crystalline carbene

The isolation of **6** demonstrated the accessibility and stability of the +2 oxidation of carbon through careful ligand design and sparked the development of tetrylene chemistry. Carbenes have been developed into indispensable reagents for catalysis, either as ligands for

transition metal complexes or as organocatalysts themselves.<sup>[9]</sup> Following the initial advancements in ligand systems, which allowed for the isolation of a plethora of persistent tetrylenes, the current research focus is modification of the electronic properties at the low oxidation state group 14 (tetrel) centre to heighten and tune their reactivity towards small molecules (see below).<sup>[10]</sup>

## 1.2 Ground state electronic configuration of tetrylenes

A major factor determining the reactivity, and stability, of a tetrylene is the electronic configuration of the tetrel centre, which will first be explored in the lightest and simplest example of a tetrylene, a carbene ( $\text{CR}_2$ ). The two non-bonding electrons can adopt a spin-paired or spin-parallel configuration, which represent the singlet and triplet state respectively. A linear carbene features a  $\text{sp}$  hybridised carbenic carbon with two degenerate orbitals ( $p_x$  and  $p_y$ ) that favour the triplet state. In contrast, a bent carbene features a  $\text{sp}^2$  hybridised carbenic centre in which the multiplicity is determined by the relative energy between the non-degenerate  $\sigma$  and  $p_z$  orbitals (Fig. 3). A large  $\sigma$ - $p_z$  separation favours the singlet state, whereas a small separation favours the triplet state. The substituents on a carbene perturb the orbital energies and play an important role in stabilising the singlet state.



**Figure 3:** Energy level diagram and frontier orbitals of bent (right) and linear (left) carbenes

The constitution of the orbitals at the low oxidation state group 14 (tetrel) centre of the heavier analogues of carbenes ( $\text{ER}_2$ ; E = Si, Ge, Sn, Pb) differs slightly as the affinity for orbital hybridisation decreases with increasing principal quantum number, due to the Inert Pair effect. For the heavier elements, the bonding orbitals have greater p-orbital character and the  $\sigma$ -orbital has greater s-orbital character, while leaving the vacant  $p_z$  orbital unchanged. This results in decreased R-E-R angles and reduced nucleophilicity of the lone pair in a singlet tetrylene, respectively (Fig. 4). These effects are most pronounced in plumbylenes ( $\text{PbR}_2$ ) as the orbitals at the lead centre are effectively unhybridized and bonds are formed to the substituents through the  $p_x$  and  $p_y$  orbitals. Therefore, plumbylenes typically feature R-Pb-R angles close to  $90^\circ$  and a  $\sigma$  orbital that is essentially an s orbital, which contrasts with the R-C-R angle of  $120^\circ$  in an idealised bent carbene with a nucleophilic,  $\text{sp}^2$ -hybridised  $\sigma$  orbital. The variation of the frontier molecular orbitals from  $\text{sp}^2$ -hybridised in carbenes to essentially

atomic orbitals in plumbylenes may be utilised to tune the reactivity of a tetrylene by varying the group 14 element.

In addition, the increased s-orbital character of the  $\sigma$ -orbital for the heavier tetrylenes destabilises the triplet state, as the  $\sigma$ - $p_z$  energy gap is increased. Consequently, the chemistry of the heavier tetrylenes is dominated by the singlet state, with only a single example of a persistent triplet heavier tetrylene reported.<sup>[11]</sup>

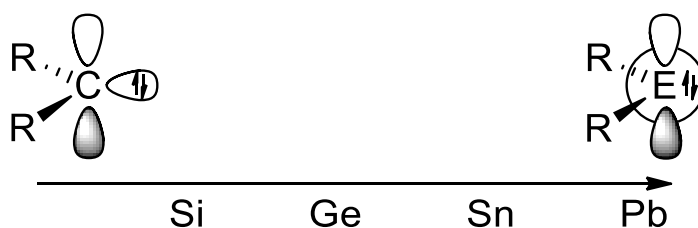


Figure 4: Orbital variance for singlet tetrylenes

### 1.2.1 Inductive effects

The relative energies of the  $\sigma$  and  $p_z$  orbitals of the tetrel centre are perturbed by the inductive nature of the substituents. For example, in a carbene, an electronegative substituent (Z) withdraws electron density through the  $\sigma$ -bond and, in doing so, increases the p-orbital character of the Z-C bond (Bent's rule).<sup>[12]</sup> The resulting increased s-orbital character of the  $\sigma$ -orbital lowers its energy relative to the  $p_z$ -orbital, and so stabilises the singlet state. (Fig. 5a). Conversely, an electropositive substituent stabilises the triplet state by reducing the  $\sigma$ - $p_z$  energy gap by increasing the p-orbital character of the  $\sigma$ -orbital (Fig. 5b).

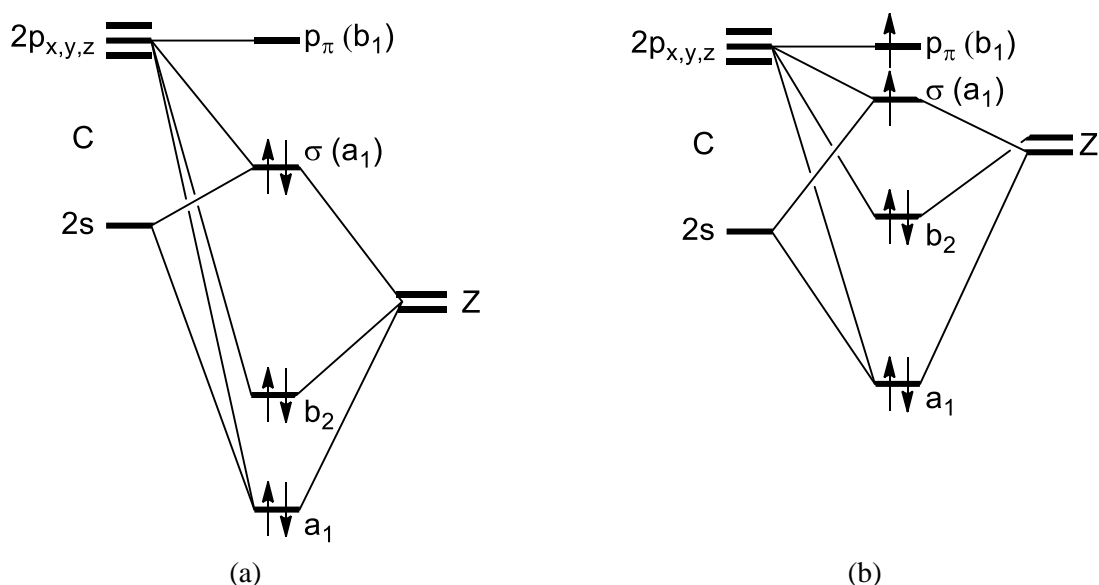


Figure 5: Inductive effects of (a)  $\sigma$ -electron-withdrawing substituents and (b)  $\sigma$ -electron-donating substituents on the relative energies of the orbitals in a carbene [Z =  $\sigma$ -electron-withdrawing substituent]

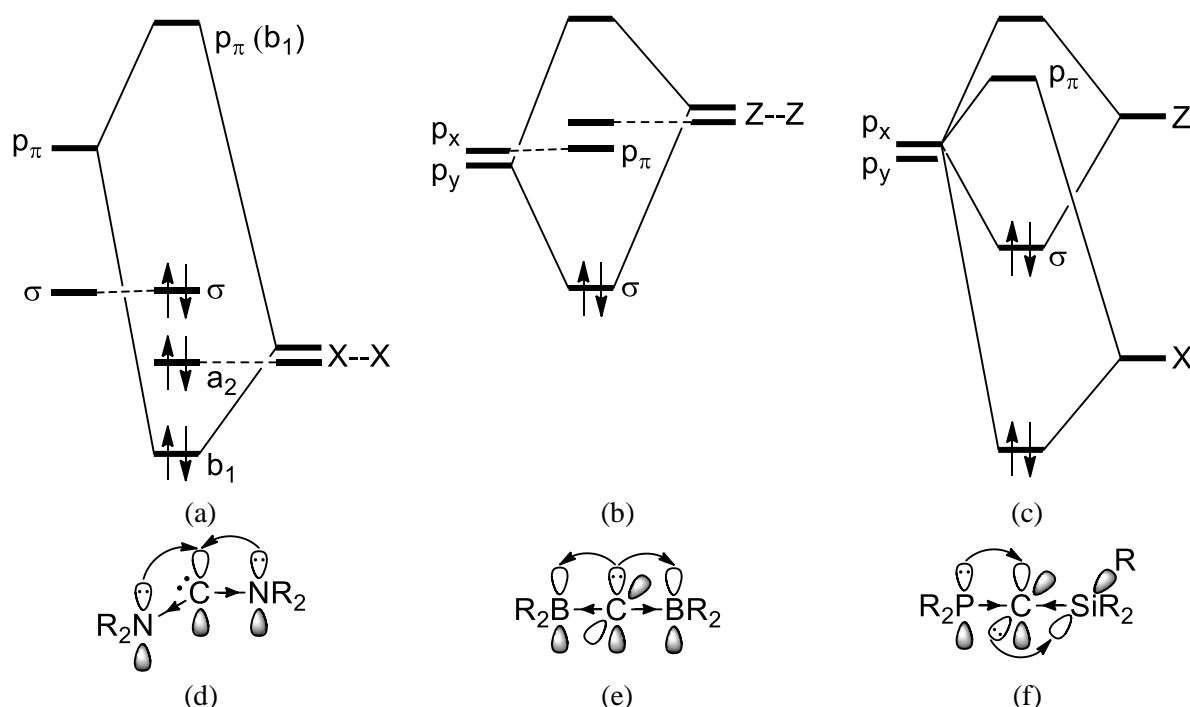
### 1.2.2 Mesomeric effects

The mesomeric effect of a substituent is typically a stronger influence on the multiplicity of a tetrylene than the substituents' inductive effects. Substituents that interact with the tetrel centre through  $\pi$  interactions can be considered as  $\pi$ -electron-donating groups (e.g. F, Cl, Br, I, OR, NR<sub>2</sub>, PR<sub>2</sub>) or  $\pi$ -electron-withdrawing groups (e.g. COR, CN, CF<sub>3</sub>, BR<sub>2</sub>, SiR<sub>3</sub>, PR<sub>3</sub><sup>+</sup>). Through the perturbation of the orbitals at the tetrel centre and their relative energies, the multiplicity and geometry of a tetrylene is strongly influenced by the combination of  $\pi$ -electron-donating (X) or  $\pi$ -electron-withdrawing (Z) substituents.

Carbenes featuring two  $\pi$ -electron-donating substituents, a (X,X)-carbene, such as a diaminocarbene (R<sub>2</sub>N)<sub>2</sub>C:, are predicted to be singlet carbenes with a bent geometry.<sup>[13]</sup> The interaction between the p<sub>z</sub> orbital at the carbenic carbon with the two lone pairs of the substituents raises the relative energy of the vacant p<sub>π</sub> orbital, while leaving the energy of the  $\sigma$ -orbital unchanged (Fig. 6a). This increases the  $\sigma$ -p<sub>π</sub> gap and so favours the singlet state. In addition, the “push-push”  $\pi$ -electron-donating interactions and “pull-pull”  $\sigma$ -electron-withdrawing interactions in a diaminocarbene synergistically stabilise the carbene (Fig. 6d).

In contrast, carbenes with two  $\pi$ -electron-withdrawing substituents are predicted to be linear.<sup>[13]</sup> The degeneracy of the p<sub>x</sub> and p<sub>y</sub> orbitals is broken by the interaction of the carbene lone pair through the p<sub>y</sub> orbital with the vacant orbitals on the substituents (Fig. 6b). One such example of a (Z,Z)-carbene is a diborylcarbene; these are typically transient species (Fig. 6e).

The  $\pi$ -electron-donating and  $\pi$ -electron-withdrawing substituents in a (X,Z)-carbene interact with separate p-orbitals at a pseudo-linear carbene centre, which stabilises the  $\sigma$  orbital and destabilises the p<sub>π</sub> orbital (Fig. 6c). For example, in a (phospha)(silyl)carbene the lone pair on the phosphorus donates electron density into the vacant p<sub>z</sub> orbital at the carbenic carbon, while the silyl group withdraws electron density through negative hyperconjugation between the carbenic carbon lone pair and a vacant Si-R  $\sigma^*$  orbital (Fig. 6f).



**Figure 6:** Orbital diagrams showing the influence of mesomeric effects [ $X = \pi$ -electron-donating substituent,  $Z = \pi$ -electron-withdrawing substituent]

### 1.2.3 Kinetic stabilisation

The ambiphilic nature of the frontier molecular orbitals in a tetrylene, which has a vacant  $p_z$  orbital and a lone pair at the tetrel centre, makes them susceptible to dimerization and nucleophilic or electrophilic attack. Dimerization may be kinetically suppressed by the placement of sterically encumbering substituents adjacent to the tetrel centre. Substituents with a higher degree of substitution are able to provide greater steric crowding at the tetrel centre (e.g.  $O < N < C$ ). For the heavier tetrylenes, bulkier substituents may be required to prevent dimerization than for carbenes, due to the increased size of the tetrel atom and the increased E-R bond length from the poorer orbital overlap caused by the larger, more diffuse orbitals.

In systems where the substituents afford no electronic stabilisation towards the tetrel centre (by inductive or mesomeric effects), sterically demanding substituents may favour the triplet state as the tetrylene approaches a linear geometry, which reduces the  $\sigma$ - $p_z$  gap.<sup>[14]</sup> For example, dimethylcarbene is a singlet with a bent geometry ( $111^\circ$ )<sup>[15]</sup> while di(*t*-butyl)-<sup>[16]</sup> and diadamantylcarbenes<sup>[17]</sup> are triplets, although all three compounds are transient species.

### 1.3 Stabilisation by $\pi$ -interactions

The majority of stable tetrylenes feature at least one heteroatom (e.g.  $\text{NR}_2$ ,  $\text{PR}_2$ ,  $\text{OR}$ ) adjacent to the tetrel centre, which alleviates the electron-deficiency of the tetrel centre by  $p\pi$ - $p\pi$  interactions. In addition, these  $\pi$  interactions stabilise the singlet state over the triplet state by populating the  $p_z$  orbital increasing the E-heteroatom bond-order. The stability of tetrylenes featuring heteroatoms can be increased by (a) the addition of a second adjacent heteroatom; (b) constraining the system into ring to restrict E-R bond rotation; and (c) the introduction of conjugation or aromaticity into the cyclic backbone (as illustrated in Figure 7 with the prototypical analogues of a stannylene shown directly below). Amino groups are used ubiquitously as substituents for tetrylenes as they provide significant stabilisation through  $p\pi$ - $p\pi$  interactions from a planar nitrogen centre and synergistic inductive effects.

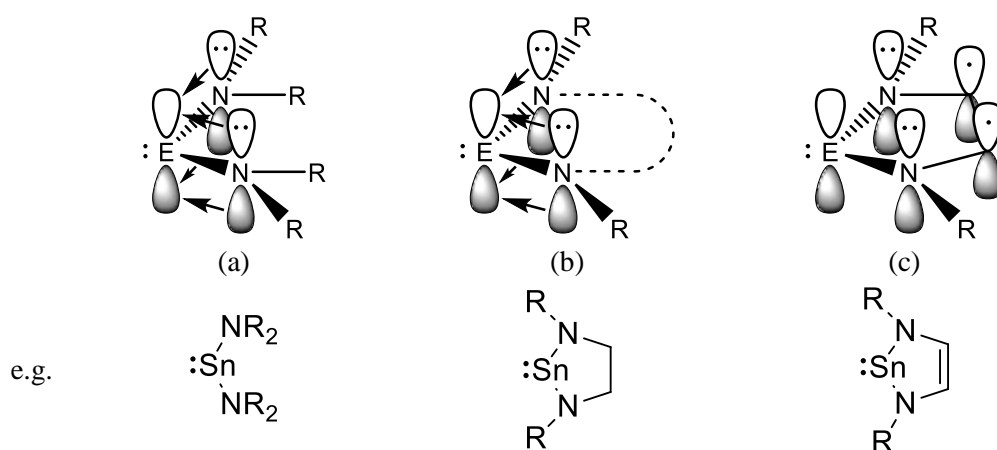


Figure 7: Stabilisation of tetrylenes by  $\pi$  interactions

### 1.4 Intramolecular stabilisation

Tetrylenes may also be stabilised by heteroatoms that are located more remotely to the tetrel centre. For example, in the solid-state, the diarylgermylene **7** is stabilised by four short  $\text{Ge}\cdots\text{F}$  contacts from the *ortho*-trifluoromethyl groups,<sup>[18]</sup> while the dialkylstannylene **8** is stabilised by the two pendant pyridyl groups.<sup>[19]</sup> The interactions from pendant Lewis bases may be static or fluxional in solution (see Section 1.5).

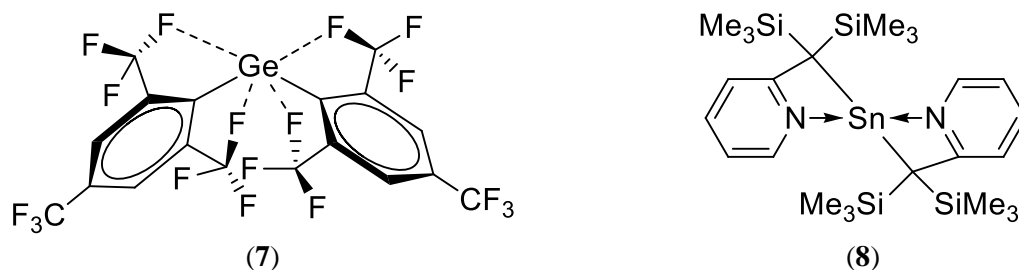


Figure 8: Examples of tetrylenes featuring short heteroatom $\cdots$ E contacts and intramolecular base stabilisation

## 1.5 Intermolecular base stabilisation

The synthesis of tetrylenes in the presence of strong Lewis bases is often used to trap reactive tetrylenes. Although the resulting tetrylene complex has an electron-precise tetrel centre, the isolation of such complexes provides invaluable data for inherently unstable free tetrylenes. This strategy was used for the isolation of the disilylstannylene complex **9**<sup>[20]</sup> and the initial isolation of the germanium (II) hydride complex **10**-DMAP,<sup>[21]</sup> which was later shown to have catalytic activity for the hydroboration of carbonyl compounds as the free germanium (II) hydride (See section 1.7.2).

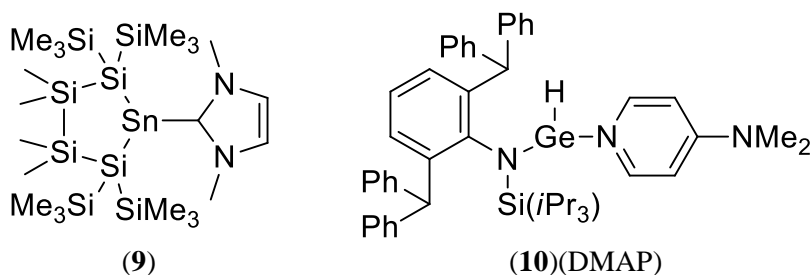


Figure 9: Selected examples of intermolecularly Lewis base-stabilised tetrylenes

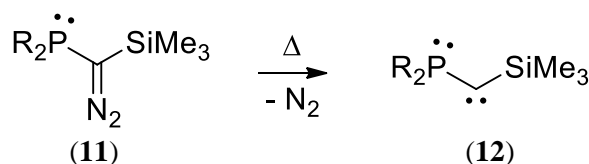
## 1.6 Synthetic approaches to tetrylenes

The synthetic approaches for preparing carbenes and silylenes differ substantially compared to those for the heavier tetrylenes because of the absence of C(II) precursors and the limited supply of synthetically accessible Si(II) precursors. Therefore, carbenes and silylenes are almost exclusively prepared from precursors in the +4 oxidation state. In contrast, the +2 oxidation state is inherently more stable for the heavier elements (Ge, Sn, Pb) and so germylenes ( $R_2Ge:$ ), stannylenes ( $R_2Sn:$ ) and plumbylenes may be prepared from a range of precursors in this oxidation state.

### 1.6.1 Synthesis of carbenes

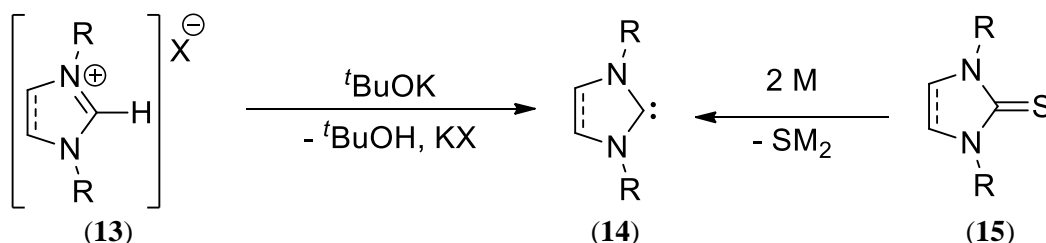
Carbenes have the most diverse range of synthetic approaches out of all the tetrylenes because of the synthetic versatility of carbon. One of the earliest approaches to synthesising carbenes is the photolysis or thermolysis of diazo precursors ( $R_2C=N=N$ ), which eliminates  $N_2$  as the side-product. Flash photolysis is an invaluable technique for the *in-situ* generation and analysis of transient triplet carbenes as it can be performed at low temperature. However, some carbenes require rather specific reaction conditions to be prepared from the diazo precursors or by-products are preferentially generated. For example, the first persistent carbene ( $iPr_2N$ )<sub>2</sub>PCSiMe<sub>3</sub> (**12**) was prepared by flash thermolysis of neat **11** at 250 °C under

vacuum (Scheme 1).<sup>[22]</sup> Photolysis of **11** in various solvents gave mixtures of by-products. Similar methods have been used to prepare a range of (phospha)(silyl)carbenes.<sup>[23]</sup>



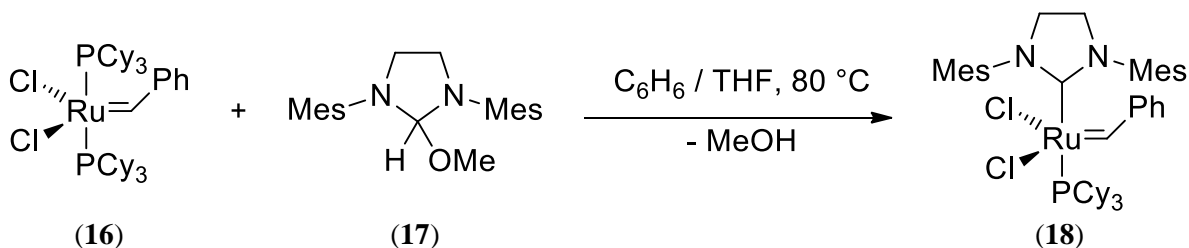
**Scheme 1:** Synthesis of **12** by flash thermolysis (R = NiPr<sub>2</sub>)

Perhaps the most prominent class of carbene is the *N*-heterocyclic carbene (NHC). The success of NHCs may be partially attributed to their ease of synthesis and functionalization, which is achieved from their cyclic iminium precursors (**13**). Such precursors can be deprotonated with strong bases (e.g. *t*BuOK, NaH, KH or *n*BuLi) in near quantitative yields to give the respective NHC after simple purification (Scheme 2). An alternative route to NHCs is the reduction of thiourea precursors with an alkali metal, although this route requires the destruction of the resulting alkali metal sulphide side-product (Scheme 2).<sup>[24]</sup>



**Scheme 2:** Synthesis of NHCs by deprotonation and reduction [M = Li, Na, K; X = Cl, Br]

Another method for preparing NHCs is the thermal elimination of an alcohol or chloroform. This approach offers the advantage that a transition-metal NHC complex can be generated without first isolating the free carbene. The Grubbs 2<sup>nd</sup> generation catalyst (**18**) is prepared by the thermal deprotection of **17** in the presence of the Grubbs 1<sup>st</sup> generation catalyst (**16**) (Scheme 3). The intermediate carbene rapidly displaces the less nucleophilic PCy<sub>3</sub> ligand to give **18**, which is a more air- and moisture-tolerant complex than **16**, by an *in-situ* reaction.<sup>[25]</sup>

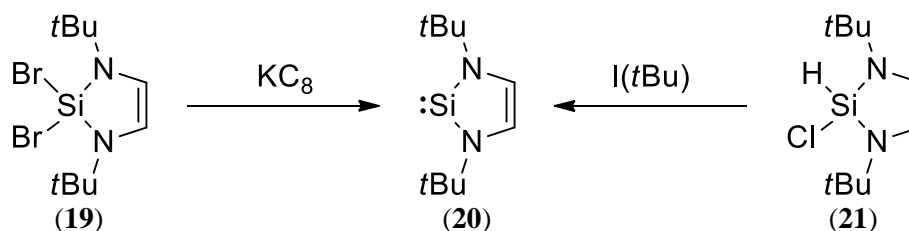


**Scheme 3:** Synthesis of Grubbs 2<sup>nd</sup> generation catalysts (Mes = 2,4,6-Me<sub>3</sub>C<sub>6</sub>H<sub>2</sub>)



## 1.6.2 Synthesis of silylenes

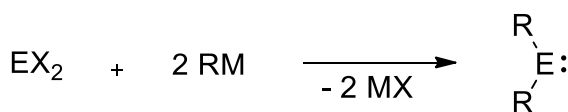
The low affinity for silicon to form double bonds, compared to carbon, limits the range of suitable precursors for silylenes. The two main synthetic approaches for preparing silylenes are the reduction of dihalosilanes ( $\text{SiX}_2\text{R}_2$ ;  $\text{X} = \text{Cl}, \text{Br}$ ) with alkali metals and the dehydrochlorination of chlorosilanes ( $\text{HSiClR}_2$ , **20**) with strong, non-nucleophilic bases. For example, compound **20** was first prepared by West through the reduction of **19** with potassium graphite<sup>[26]</sup> and later by Cui and co-workers through the dehydrochlorination of **21** with a bulky NHC (Scheme 4).<sup>[27]</sup>



**Scheme 4:** Synthetic routes to silylenes [ $\text{I}(t\text{Bu}) = \text{C}\{\text{N}(t\text{Bu})\text{CH}\}_2$ ]

## 1.6.3 Synthesis of heavier tetrylenes

The access to precursors in the +2 oxidation state (e.g.  $\text{EX}_2$ ,  $\text{E} = \text{Ge}, \text{Sn}, \text{Pb}$ ;  $\text{X} = \text{Cl}, \text{Br}, \text{I}, \text{Cp}, \text{NR}_2, \text{OR}$ ) allows for the synthesis of the heavier tetrylenes more directly by a metathesis reaction with two equivalents of the corresponding metalated precursor (Scheme 5). In cases where the tetrel centre is reduced by the metalated precursors the dicyclopentadienyl precursors ( $\text{ECp}_2$ ,  $\text{E} = \text{Sn}, \text{Pb}$ ) have proven to be invaluable.<sup>[28]</sup>



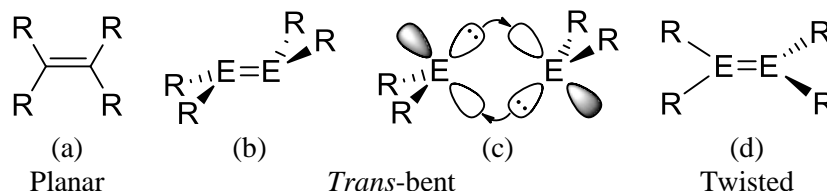
**Scheme 5:** Synthesis of heavier tetrylenes by salt metathesis

## 1.7 Reactivity

### 1.7.1 Dimerization

As previously mentioned in Section 1.2.3, tetrylenes with insufficient kinetic or thermodynamic stabilisation may dimerize through the ambiphilic tetrel centre. The geometry of the resulting dimer is dependent on the tetrel element. Carbenes dimerize to give planar, electron-rich alkenes (Fig. 10a), while the bonding of the heavier ditetrylenes ( $\text{R}_2\text{E}=\text{ER}_2$ ;  $\text{E} = \text{Si}, \text{Ge}, \text{Sn}, \text{Pb}$ ) is more complex and varied. While some disilenes ( $\text{R}_2\text{Si}=\text{SiR}_2$ ) may also exhibit a planar geometry, the formation of E-E  $\pi$  bonds is less favourable for the heavier

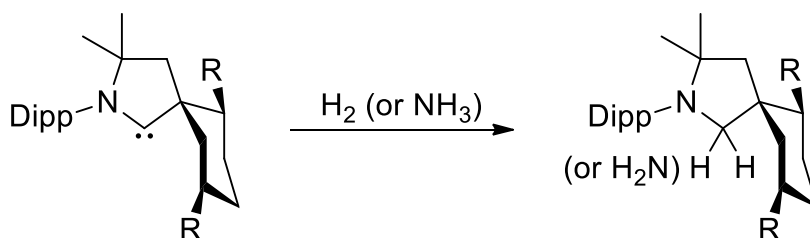
tetrel centres because of the reduced affinity for hybridisation and the larger, more diffuse orbital of these elements. Therefore, the heavier ditetrylenes ( $R_2E=ER_2$ ; E = Si, Ge, Sn, Pb) typically have either a *trans*-bent (Fig. 10b) or twisted geometry (Fig. 10d). The bonding in a *trans*-bent structure may be interpreted as a double donor-acceptor bond (Fig. 10c). Furthermore, recent work by Power indicates that dispersion forces may provide significant stabilisation in heavier tetrylenes with sterically demanding substituents.<sup>[29]</sup>



**Figure 10:** Geometry of tetrylene dimers

### 1.7.2 Small molecule activation

There is growing interest in the activation of small molecules (such as  $H_2$ , CO,  $CO_2$  and (un)saturated hydrocarbons) by main group compounds, with the ambition of eventually developing main group catalysts to rival transition metal complexes. Tetrylenes are proving to be a promising class of reactive compounds, with the first activation of  $H_2$  by a tetrylene reported in 2007 by Bertrand (Scheme 6).<sup>[30]</sup>



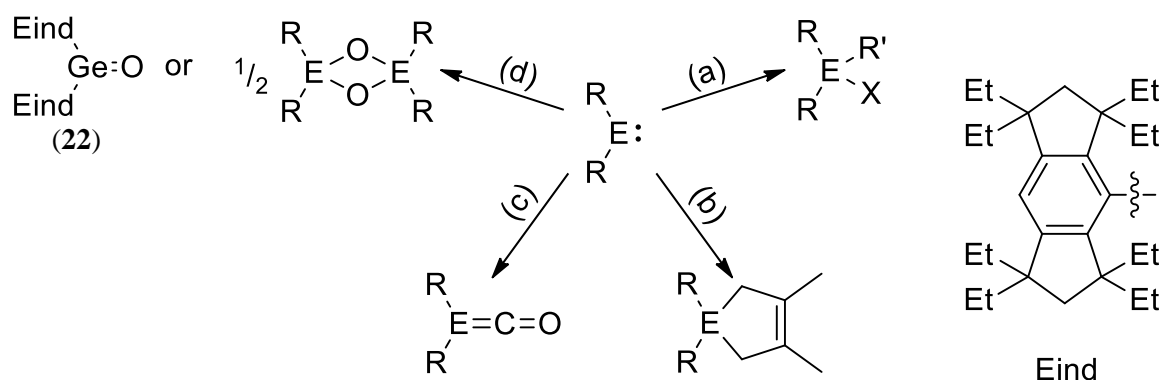
**Scheme 6:** Activation of hydrogen and ammonia by an (alkyl)(amino)carbene

It is proposed that the activation of  $H_2$  by a tetrylene occurs by the synergistic donation of the tetrel lone pair (the HOMO  $\sigma(a_1)$  orbital) into the  $\sigma^*$  orbital on  $H_2$  while withdrawing electron density from the  $H_2$   $\sigma$  orbital into the vacant  $p_z$  orbital at the tetrel centre (Fig. 11a).<sup>[30]</sup> This process is analogous to the activation of  $H_2$  at a transition metal complex through the d orbitals (Fig. 11b). Therefore, tetrylenes are often referred to as transition metal mimics with respect to their reactivity.<sup>[30-31]</sup> The reactivity of a tetrylene is proposed to correlate to the HOMO-LUMO and singlet-triplet separations, with small values giving lower activation energies.<sup>[31]</sup> It is worth noting that NHCs do not exhibit reactivity toward  $H_2$  because the significant  $N \rightarrow C$   $\pi$  interactions partially populate the  $p_z$  orbital, which quenches the synergistic mechanism.



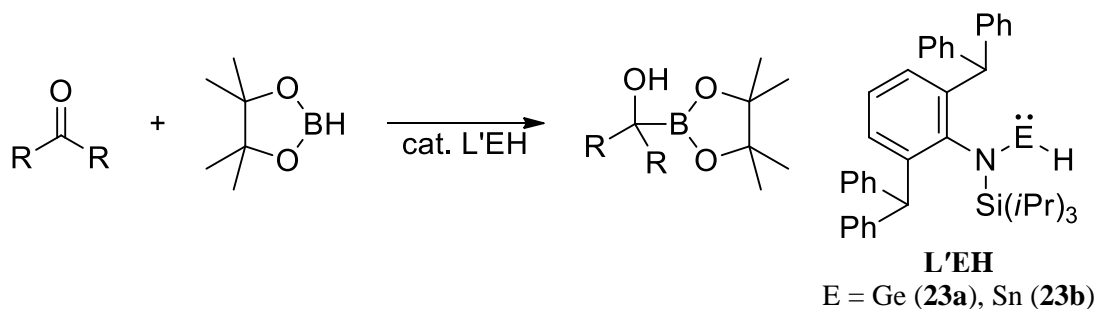
**Figure 11:** (a) the interaction of H<sub>2</sub> with the  $\sigma(a_1)$  (HOMO) and  $p_z$  (LUMO) frontier orbitals of R<sub>2</sub>E (E = C-Pb) and (b) the interaction of H<sub>2</sub> with the frontier d orbitals in a transition metal complex (M is a transition metal)

In addition to the activation of H<sub>2</sub> or NH<sub>3</sub>, as shown in Scheme 6, tetrylenes may also undergo, but are not limited to, (a) oxidative-addition reactions with alkyl halides; (b) cycloadditions with dienes; and (c) complexation of CO to give ketenes and their heavier analogues (Fig. 12). The oxidation of the tetrel centre may give oxygen-bridged dimers or, in the oxidation of the sterically encumbered germylene (Eind)<sub>2</sub>Ge with Me<sub>3</sub>NO, the germanone (Eind)<sub>2</sub>Ge=O (**22**), which is the first example of a heavier ketone analogue (Fig. 12d).<sup>[32]</sup>



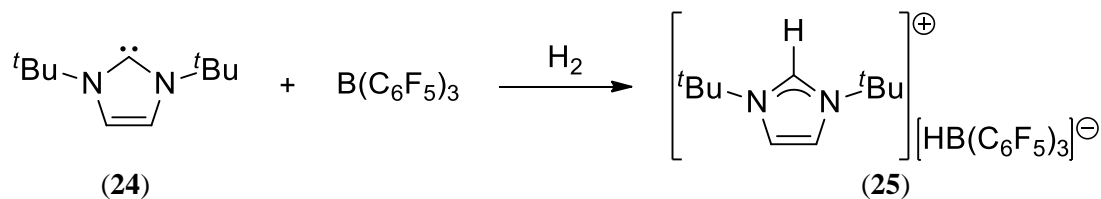
**Figure 12:** Typical reactivity of a tetrylene (R<sub>2</sub>E) with (a) alkyl halides (R'-X), (b) 2,3-dimethyl-1,3-butadiene, (c) CO and (d) TEMPO, Me<sub>3</sub>NO or N<sub>2</sub>O

Examples of reversible reactions of tetrylenes with small molecules are limited and reactions using heavier tetrylenes as catalysts are scarce. One such example is the hydroboration of carbonyl compounds using the germanium(II) and tin(II) hydride complexes (*i*Pr<sub>3</sub>Si){2,6-(Ph<sub>2</sub>CH)<sub>2</sub>-4-*i*Pr-C<sub>6</sub>H<sub>2</sub>}NEH [E = Ge (**23a**), Sn (**23b**)] developed by Jones and co-workers (Scheme 7).<sup>[33]</sup>



**Scheme 7:** Example of a catalytic reaction using a tetrylene

As previously mentioned, tetrylenes that are stabilised by significant  $\pi$ -interactions typically do not exhibit reactivity towards small molecules through the pathways described above, although they may still exhibit small molecule activation through alternative pathways. NHCs and related carbenes have been extensively studied as organocatalysts because of their strong nucleophilic character and potential for functionalization, which allows for tuning of the catalyst and direct introduction of chirality for asymmetric reactions.<sup>[9]</sup> Another type of reactivity of NHCs is their use in Frustrated Lewis Pairs (FLPs), in which  $H_2$  can be activated (Scheme 8).<sup>[34]</sup>

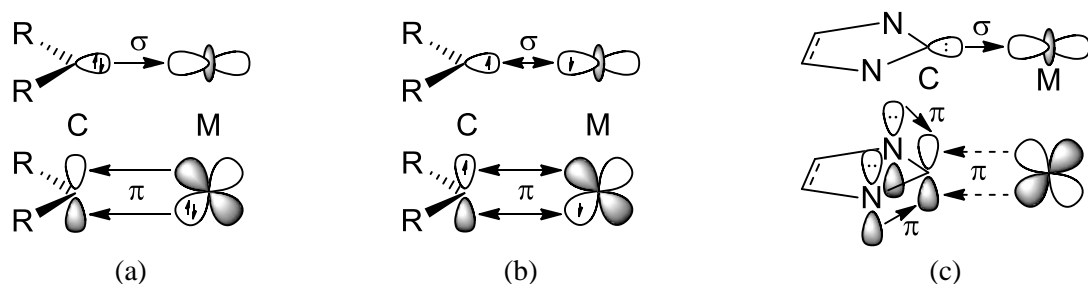


**Scheme 8:** Activation of  $H_2$  using a carbene in a FLP

### 1.7.3 Transition metal complexes of tetrylenes

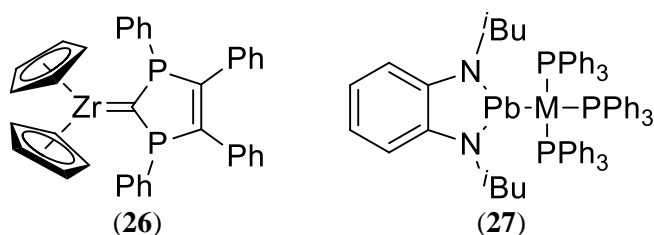
The initial research into carbenes involved trapping the unstabilized, and so reactive, species as transition metal complexes, which are classically divided into two classes, Fischer- and Schrock-type carbene complexes, depending on the nature of the carbene-metal bond. A Fischer-type carbene complex has a donor-acceptor bond from the donation of the carbene  $\sigma$  lone pair into the metals d-orbital and the backbonding from a metal d-orbital into the carbene  $p_z$  orbital (Fig. 13a). In contrast, the bonding in a Schrock-type carbene complex results from a covalent bond between a triplet carbene and a triplet metal centre (Fig. 13b).

Although the bonding in a NHC-transition-metal complex is similar to that of a Fischer-type carbene complex, the  $\pi$ -interactions from the two adjacent nitrogen atoms on the carbenic carbon inhibit backbonding from the metal (Fig. 13c). The strong  $\sigma$ -donating and weak  $\pi$ -acceptor ability of NHCs contrasts that of typical phosphines, which are usually weaker  $\sigma$ -donors and better  $\pi$ -acceptors, and makes NHCs attractive spectator ligands for transition-metal complexes.



**Figure 13:** The interactions between a carbene and transition-metal centre in (a) a Fischer-type carbene complex; (b) a Schrock-type carbene complex; and (c) a NHC-complex

The affinity for carbenes to form strong complexes with transition metals can be used to simplify the synthesis of such complexes by generating the carbenes *in-situ*, as seen in Scheme 3 for the Grubbs 2<sup>nd</sup> generation catalyst **18**, or to trap unstable, short-lived carbenes. This strategy was employed for the synthesis of the zirconocene complex **26** as the free *P*-heterocyclic carbene cannot be isolated because of its inherent instability (see later).<sup>[35]</sup>

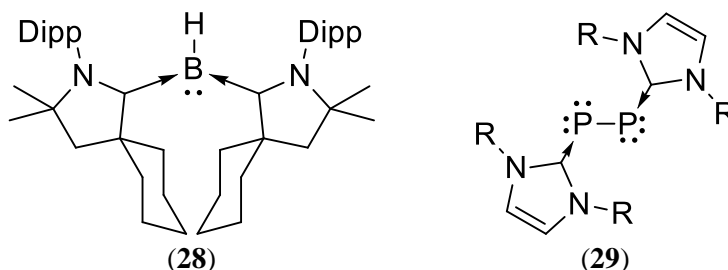


**Figure 14:** Transition metal complexes of tetrylenes [M = Pd, Pt]

For transition-metal complexes of the heavier tetrylenes, the nature of the tetrel-metal bond differs to that of carbenes. The reduced nucleophilicity of the lone pair at the heavier tetrel centres leads to heavier tetrylenes being poorer  $\sigma$ -donors than carbenes, while the reduced orbital overlap of the heavier tetrel centres with the substituents increases their  $\pi$ -acceptor ability. This allows for the subtle tunability of the electronics at the metal centres in such complexes by alteration of the tetrel centre. However, the combination of the decreased  $\sigma$ -donating and increased  $\pi$ -accepting ability of the heavier tetrylenes may lead to different bonding modes. For example, the transition-metal-plumbylene complexes **27** have an unusual bonding mode, in which the *N*-heterocyclic lead centre acts as an acceptor from the transition metal d-orbitals, which contrasts with the behaviour of NHC complexes.<sup>[36]</sup>

#### 1.7.4 Stabilisation of reactive species

In addition to stabilising metal centres, carbenes have been used to stabilise low oxidation state main group compounds and unusual allotropes, such as **28**<sup>[37]</sup> and **29**<sup>[38]</sup>, respectively. The tunability of the nucleophilicity and sterics at the carbenic carbon has made carbenes invaluable tools in the isolation of reactive electron-deficient species, which otherwise have proven to be inaccessible.



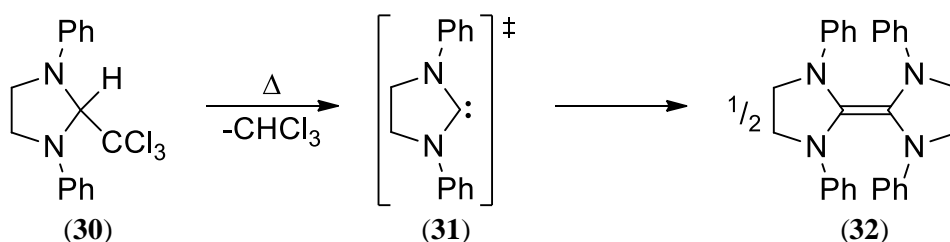
**Figure 15:** Carbene-stabilised low oxidation state species (R = Dipp, Mes)

## 1.8 Stable tetrylenes

Since most stable tetrylenes feature at least one adjacent heteroatom, this section will focus on stable, two-coordinate tetrylenes featuring heteroatom substituents and their stabilisation modes. In cases where the geometry of the heteroatom is critical, emphasis will be placed on compounds with X-ray crystallographically authenticated structures.

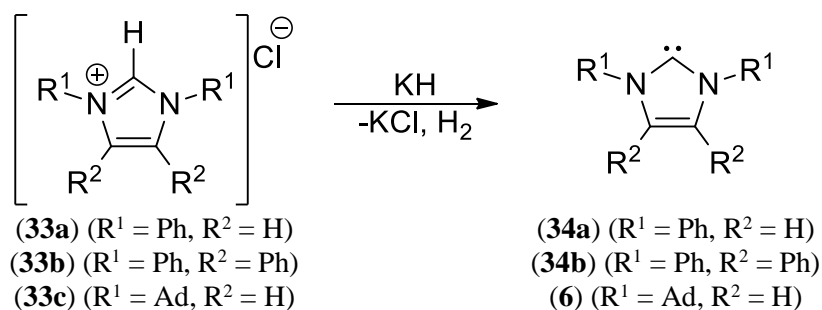
### 1.8.1 Diaminotetrylenes

Amino substituents are the most common class of ligands for tetrylenes as the low planarization energy of nitrogen allows up to two amino substituents to stabilise the tetrel centre by efficient  $\pi\text{-}\pi$  interactions. The increased stability of carbenes featuring amino substituents was realised by in the 1960's Wanzlick who, in an attempt to prepare the carbene **31**, isolated the electron-rich alkene **32** by the thermal deprotection of **30** (Scheme 9).<sup>[39]</sup>



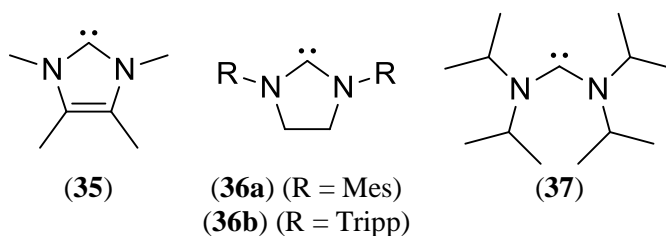
Scheme 9: Synthesis of Wanzlick's electron-rich carbene

Wanzlick further developed the diamino ligand system by using the imidazolium precursors **33a** and **33b** to introduce aromaticity in the corresponding carbenes **34a** and **34b**, which were not isolated directly.<sup>[40]</sup> It was not until two decades later, by following this same principle, that Arduengo isolated the first stable, crystalline carbene **6** in 1991 (Scheme 10).<sup>[8]</sup>



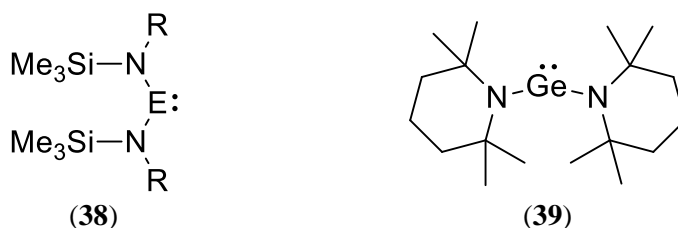
Scheme 10: Synthesis of the first NHCs by Wanzlick and Arduengo

Shortly after the isolation of **6**, the unhindered NHC **35** was reported by Arduengo, which demonstrates the remarkable electronic stability provided by the aromatic *N*-heterocyclic ligand system (Fig. 16).<sup>[41]</sup> Furthermore, through the use of bulky substituents, a range of NHCs featuring “saturated” backbones have been isolated, such **36a**<sup>[42]</sup> and **36b**<sup>[43]</sup>, and the acyclic diaminocarbene **37**<sup>[44]</sup>.



**Figure 16:** Selected diaminocabenenes

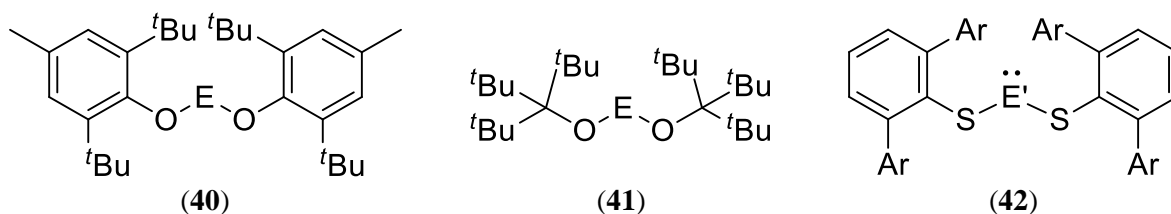
Prior to the isolation of the first stable, crystalline carbene **6**, the chemistry of the heavier diaminotetrylenes  $[(R_2N)_2E]$ ;  $E = Ge, Sn, Pb$ ] was established by Lappert in the 1970s using bulky amides as ligands.<sup>[7, 45]</sup> The first examples of monomeric diamidotetrylenes  $\{(Me_3Si)(R)N\}_2E$  (**38**) were reported in 1974, and were shown to be monomeric in solution by cryoscopy.<sup>[7]</sup> Compound **39** was the first example of an X-ray crystallographically characterised, monomeric diaminotetrylene.<sup>[46]</sup>



**Figure 17:** Selected acyclic diaminotetrylenes ( $E = Ge, Sn, Pb$ ;  $R = SiMe_3, CMe_3$ )

### 1.8.2 Oxygen- and sulphur-substituted tetrylenes

Although oxygen and sulphur substituents provide significant electronic stabilisation to tetrel centres through  $\pi$ -interactions from the lone pairs on the chalcogen atom, the low coordination number limits the steric encumbrance that can be installed on these substituents, compared to amino and alkyl substituents. Therefore, very bulky groups are used in these substituents to kinetically stabilise the corresponding tetrylenes, such as the bulky alkyl and aryl groups featured in **40**<sup>[47]</sup>, **41**<sup>[48]</sup> and **42**<sup>[29a]</sup>.

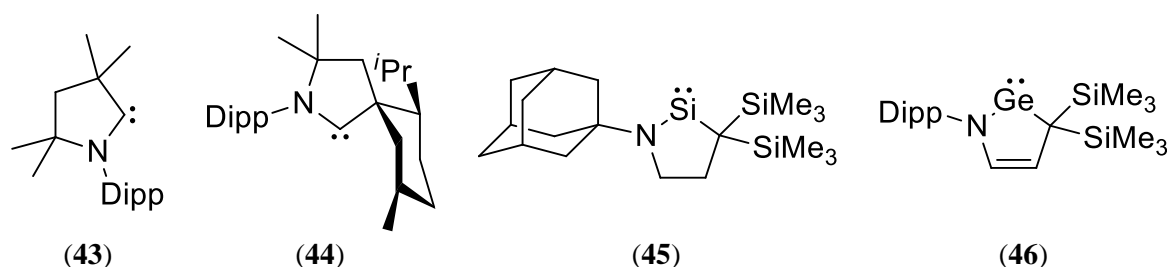


**Figure 18:** Selected dioxo- and dithiotetrylenes [ $E = Ge, Sn$ ;  $E' = Si, Ge, Sn, Pb$ ;  $Ar = Dipp, Tripp, Mes$ ]

### 1.8.3 Alkylaminotetrylenes

Cyclic(alkyl)(amino)carbenes (cAACs) are a recent development in carbene chemistry, with the first examples (**43** and **44**) reported in 2005 by Bertrand.<sup>[49]</sup> While cAACs are closely related to NHCs, the exchange of an amino group for an alkyl group results in a

more reactive carbene. The alkyl-substituents no longer provide any  $\pi$  interactions and inductively destabilise the carbenic carbon, compared to an amino substituent, resulting in a more electro- and nucleophilic carbene with a reduced singlet/triplet separation. This makes cAACs potential candidates for small molecule activation. In addition, the increased substitution of the alkyl carbon allows for increased steric crowding at the carbenic carbon, compared to an amino substituent, and direct introduction of chirality, as seen in **44**. Compounds **45**<sup>[50]</sup> and **46**<sup>[51]</sup> are the only examples of heavier cyclic(alkyl)(amino)tetrylenes (cAATs) that have been characterised by X-ray crystallography.

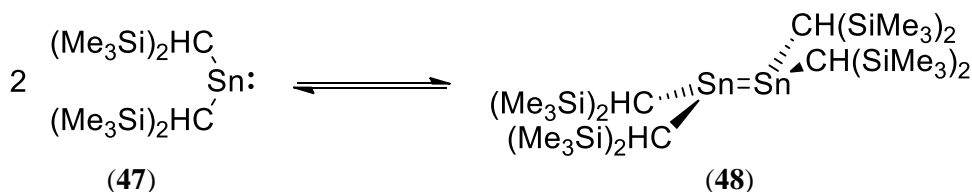


**Figure 19:** Cyclic(alkyl)(amino)carbenes and -tetrylenes

#### 1.8.4 Dialkyltetrylenes

Tetrylenes featuring two alkyl substituents exhibit greater reactivity at the tetrel centres compared to NHCs and cAACs. The  $\sigma$ -electron donating alkyl substituents inductively stabilise the triplet state (see Section 1.2.1) and typically provide no electronic donation into the  $p_z$ -orbital. As a result, no persistent dialkylcarbenes have been reported, as the triplet state is favoured in these systems. However, due to the increased  $\sigma$ - $p_z$  separation in heavier tetrylenes, a limited number of heavier dialkyltetrylenes have been characterised.

In 1973, the synthesis of the first two-coordinate tetrylene,  $\{(\text{Me}_3\text{Si})_2\text{CH}\}_2\text{Sn}$  (**47**),<sup>[52]</sup> was reported by Lappert and subsequently the same group reported the solid-state structure of dimeric  $[(\text{Me}_3\text{Si})_2\text{CH}]_2\text{Sn}_2$  (**48**).<sup>[53]</sup> NMR studies have shown that the dialkylstannylene **47** and distannene **48** are in dynamic equilibrium in solution (Scheme 11), with the monomeric species **47** being favoured at low concentrations and high temperatures.<sup>[54]</sup>

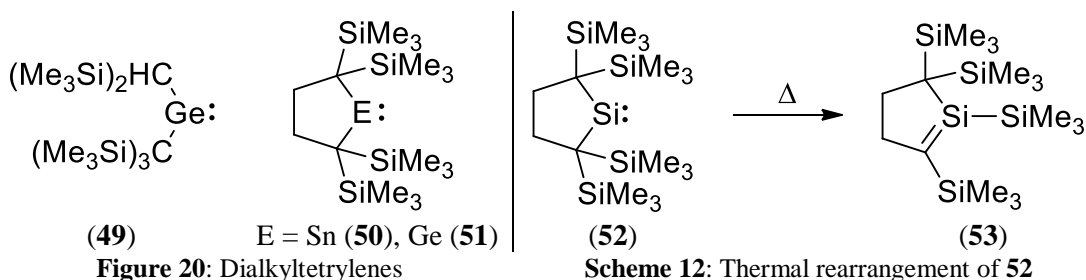


**Scheme 11**

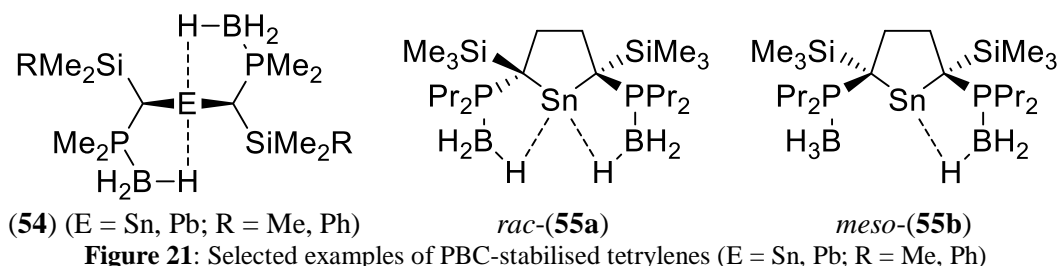
It was not until nearly two decades later that the first X-ray crystallographically authenticated dialkyltetrylene,  $\{(\text{Me}_3\text{Si})_3\text{C}\}\text{Ge}\{\text{CH}(\text{SiMe}_3)_2\}$  (**49**), was reported by Jutzi,



featuring the more sterically encumbering  $(\text{Me}_3\text{Si})_3\text{C}$  substituent (Fig. 20). The array of cyclic dialkyltetrylenes **50**,<sup>[55]</sup> **51**<sup>[56]</sup> and **52**<sup>[50]</sup> were prepared by Kira and co-workers. While compounds **50** and **51** are thermally stable, the silylene **52** undergoes a thermal 1,2-trimethylsilyl migration to give compound **53** (Scheme 12).<sup>[50]</sup>



The use of phosphine-borane stabilised carbanions (PBCs) as ligands for tetrylenes was pioneered by the Izod group. Phosphine-boranes are isoelectronic analogues of silyl groups; however, the more electronegative phosphorus and polarised P-C bond provide a greater degree of stabilisation towards carbanions compared to their silyl analogues. Unlike conventional alkyl substituents, PBCs stabilise the tetrel centre by agostic-type interactions from the borane group, as shown in Fig. 21.<sup>[57]</sup> The increased stability afforded by PBCs is highlighted in **54** (when  $\text{R} = \text{Me}$ ), which is isoelectronic and essentially isostructural with Lapperts' dialkylstannylene **47**. However, compound **54** is monomeric in the solid-state and in solution. The introduction of chirality at the two carbon centres adjacent to the tetrel centre leads to the formation of diastereomers, which may be stabilised by a differing number of agostic-type interactions as observed in *rac*-**55a** and *meso*-**55b**.<sup>[28]</sup>



### 1.8.5 Diaryltetrylenes

The functionalization of an aryl substituent influences its stabilisation mode. In compound **56**, which was the first example of a crystalline diaryltetrylene without donor interactions, the aryl groups provide kinetic stabilisation and act as “spectator” ligands.<sup>[58]</sup> Electron-withdrawing aryl substituents such as  $\text{C}_6\text{F}_5$ , 2,6- $(\text{CF}_3)_2\text{C}_6\text{H}_3$  and 2,4,6- $(\text{CF}_3)_3\text{C}_6\text{H}_2$  inductively stabilised the tetrel centre and may act as strong  $\pi$ -acceptors. The considerable steric crowding of terphenyl substituents has extensively been utilised by Power to stabilise a

wide range of organometallic compounds, such as the first examples of stable tetrylene hydrides, **57** and **58**.<sup>[59]</sup>

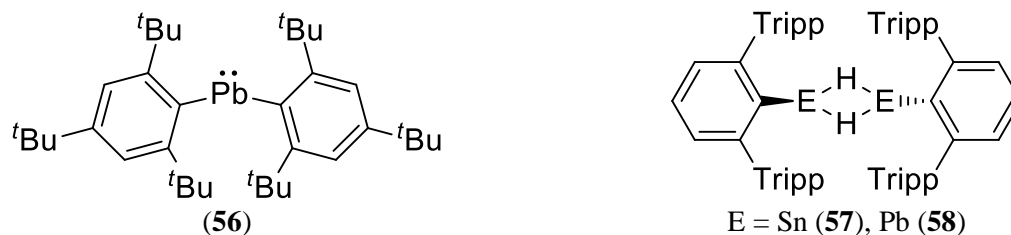


Figure 22: Selected aryltetrylenes

### 1.8.6 Silyl- and phosphoniotetrylenes

Silyl substituents and their cationic analogues, phosphonio substituents, withdraw electron density from the tetrel centre by negative hyperconjugation. The stabilisation mode of these substituents is dependent on the  $\pi$ -interactions in the system. For example, in the bis(silyl)tetrylenes  $\{(\text{Me}_3\text{Si})_3\text{Si}\}_2\text{E}$  ( $\text{E} = \text{Sn}, \text{Pb}$ ) **59** and the (aryl)(phosphonio)stannylene **60** the silyl and phosphonio groups act as spectator ligands. However, in heteroleptic systems with  $\pi$ -donating substituents, such as the (amido)(silyl)silylene **61**, silyl and phosphonio groups act as strong  $\pi$ -acceptors to give “push-pull”  $\pi$ -stabilised systems (see below for further detail).<sup>[60]</sup>

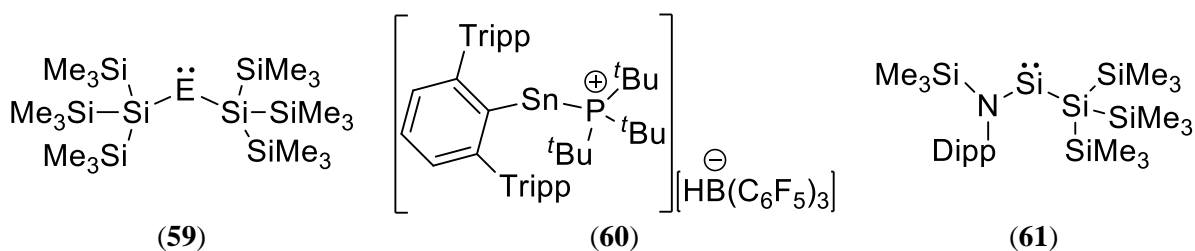
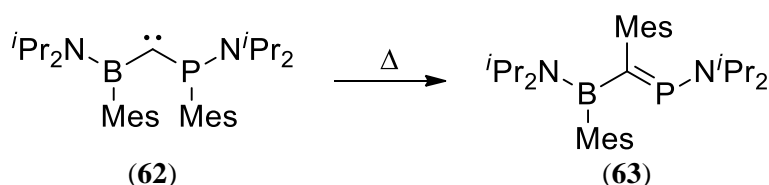


Figure 23: Selected silyl- and phosphoniotetrylenes

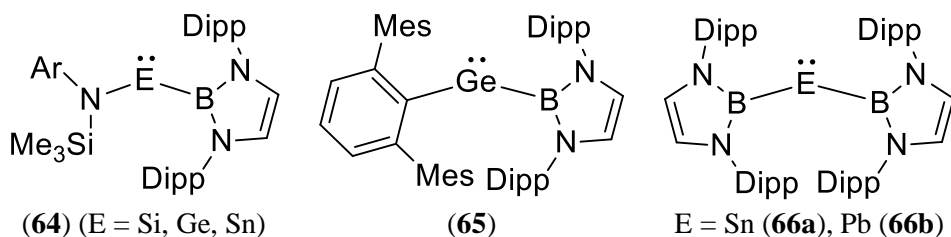
### 1.8.7 Boryltetrylenes

One of the most recent developments in tetrylene ligand systems is the isolation of stable boryl-substituted tetrylenes, of which the “push-pull” (boryl)(phospha)carbene **62** reported by Baceiredo in 2010 was the first example (Scheme 24).<sup>[61]</sup> The stability of **62** may be attributed to the amino group reducing the electrophilicity of the boryl substituent through  $\pi$ -interactions. However, in solution, compound **62** undergoes a thermal migration of a mesityl group from the phosphide substituent to give **63**, which is reminiscent of the rearrangement observed for the dialkylsilylene **52**.



**Figure 24:** Thermal rearrangement of **62**

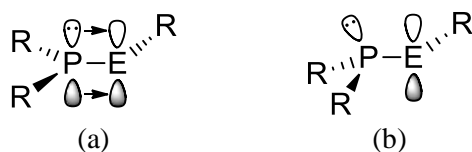
Subsequently, Aldridge has employed *N*-heterocyclic ligands on the boryl substituents to synthesise the heavier (amido)(boryl)tetrylenes **64**<sup>[62]</sup>, the (aryl)(boryl)germylene **65**<sup>[63]</sup> and the bis(boryl)tetrylenes **66a** and **66b**<sup>[64]</sup> (Fig. 25). These boryl-substituted tetrylenes have been shown to have a small singlet/triplet separation, which has been correlated with their increased reactivity towards small molecules, compared to *N*-heterocyclic tetrylenes.



**Figure 25:** Boryltetrylenes

### 1.8.8 Phosphatetrylenes

There are significantly fewer examples of tetrylenes featuring phosphide substituents than their lighter analogues, amides, although phosphides offer a wide range of structural diversity and diagnostic NMR data (<sup>31</sup>P = 100% abundance, *I* = 1/2). A major factor for the low usage of phosphide substituents in these systems is the high energy barrier of planarization of phosphorus, compared to nitrogen. Whereas the nitrogen centres in amino substituents readily adopt a trigonal planar geometry that provides efficient pπ-pπ interactions to the tetrel centre, this geometry is unusual for phosphorus (Fig. 26a). Consequently, phosphorus centres adjacent to the tetrel centre typically adopt a trigonal pyramidal geometry, which does not provide efficient orbital overlap with the p<sub>z</sub> orbital at the tetrel centre (Fig. 26b).



**Figure 26:** Stabilisation modes of phosphide ligands

Although there is significant precedent for planar, three-coordinate phosphorus centres in transition metal complexes,<sup>[65]</sup> there are few examples of main-group compounds with a truly planar, three-coordinate phosphorus.<sup>[66]</sup> The energy barrier for the planarization of

phosphorus can be reduced by: (a) the incorporation of the phosphorus centre into a ring;<sup>[66a]</sup> (b) the use of bulky substituents;<sup>[66e]</sup> and (c) the presence of electropositive substituents adjacent to phosphorus.<sup>[67]</sup> These strategies were employed in the compounds **67**<sup>[66a]</sup>, **68**<sup>[66b]</sup> and **69**<sup>[66e]</sup>, respectively, to give planar phosphorus centres.

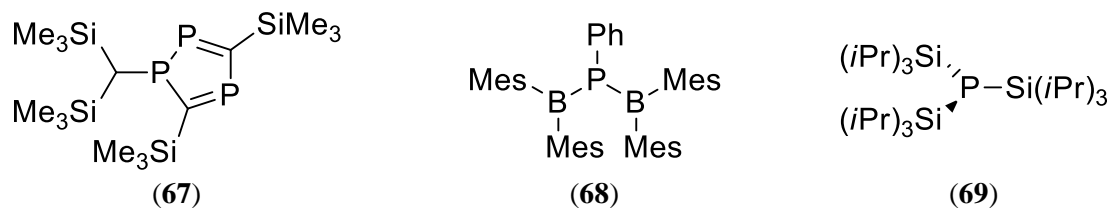


Figure 27: Selected examples of main group compounds containing a planar three-coordinate phosphorus centre

It has been predicted that a planar phosphorus centre has almost identical  $\pi$ -donor capacity to that of nitrogen, if the energy of planarization is neglected.<sup>[68]</sup> Therefore, with careful ligand design, a significant reduction in the energy barrier of planarization of a phosphorus centre adjacent to a tetrel centre should result in a tetrylene stabilised by efficient  $p\pi$ - $p\pi$  interactions from planar phosphorus.

Examples of compounds containing  $P=E$  ( $E = \text{Si, Ge, Sn}$ ) double bonds are mostly limited to phosphasilenes ( $R_2\text{Si}=\text{PR}'$ ) and their heavier analogues ( $R_2E=\text{PR}'$ ;  $E = \text{Ge and Sn}$ ), in which the  $P=E$  double bond is between a two-coordinate phosphorus (phosphinidene) and a group 14 centre in the +4 oxidation state. Recently, Baceiredo has report the isolation of the  $P,N$ -heterocyclic germylene **70**, which exhibits the first example of  $\pi$ -interactions from a phosphinidine ligand to a heavier group 14 centre in the +2 oxidation state.

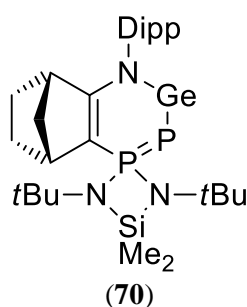
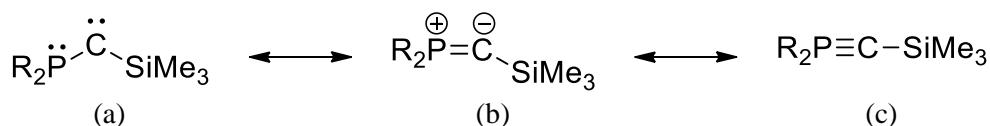


Figure 28:  $P,N$ -heterocyclic germylene **70**

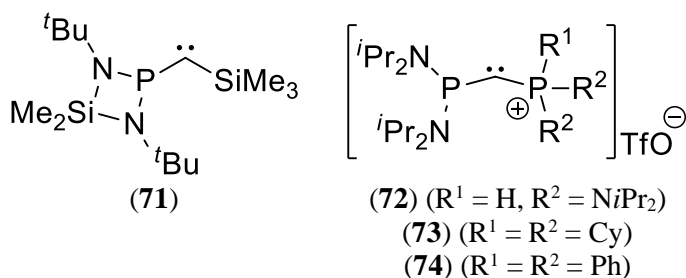
In 1988, Bertrand reported the isolation of the first stable carbene  $(i\text{Pr}_2\text{N})_2\text{PCSiMe}_3$  (**12**).<sup>[22]</sup> However, the bonding in such (phospha)(silyl)carbenes is ambiguous without characterisation by X-ray crystallography as the “push-pull” carbenes may be interpreted as  $\lambda^3$ -phosphacarbenes (Fig. 29a) or  $\lambda^5$ -phosphaacetylenes (Fig. 29c), although **12** has been reported to exhibit carbene-type reactivity. The phosphide substituents in (phospha)(silyl)carbenes and their cationic analogues, (phospha)(phosphonio)carbenes, all

feature two amido groups that stabilise the ylide-like resonance form (Fig. 29b), with the exception of (TMP)(Ph)PCSiMe<sub>3</sub> (TMP = 2,2,6,6-tetramethylpiperidyl).<sup>[22-23, 69]</sup>



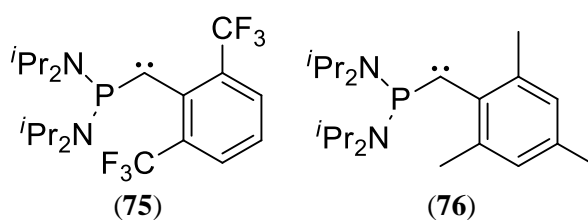
**Figure 29:** Potential bonding modes of (phospha)(silyl)carbenes

There are only four examples of such systems that have been characterised by X-ray crystallography; compounds **71**,<sup>[69d]</sup> **72**,<sup>[69b]</sup> **73**,<sup>[69f]</sup> and **74**<sup>[69f]</sup> all feature a planar phosphorus centre that stabilises the carbenic carbon by p $\pi$ -p $\pi$  interactions (Fig. 30). The large P-C-Si/P angles in **71** and **72** [152.6(3) and 164.1(4) $^\circ$ , respectively] suggest these compounds have significant  $\lambda^5$ -phosphaacetylene character, while the P-C-P angles in **73** and **74** [129.3 and 129.14 $^\circ$ , respectively] are typical for acyclic carbenes; for example, the N-C-N angle in (iPr<sub>2</sub>N)<sub>2</sub>C (**37**) is 121.0(5) $^\circ$ .<sup>[44]</sup>



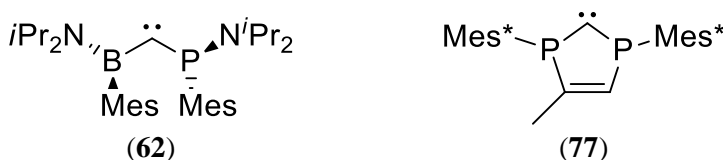
**Figure 30:** (phospha)(silyl)- and (phospha)(phosphonio)carbenes

Although both (phospha)(aryl)carbenes **75**<sup>[70]</sup> and **76**<sup>[71]</sup> are stabilised by  $\pi$ -interactions from a planar phosphorus centre, they have differing interactions from the aryl substituents (Fig. 31). In compound **75**, the electron-withdrawing aryl group lies in-plane with the carbene lone pair and acts as a  $\pi$ -acceptor ligand. This “push-pull” stabilised carbene has a large P-C-C angle of 162.1(0.3) $^\circ$ , which is similar to the respective angles in **71** and **72**, suggesting significant  $\lambda^5$ -phosphaacetylene character. In contrast, the plane of the mesityl group in **76** lies orthogonal to the carbene lone pair and so acts as a spectator ligand. The P-C-C angle in **76** of 120.09(123) $^\circ$  is significantly more acute than in **75** and is typical for that for an acyclic carbene (see above).<sup>[44]</sup>



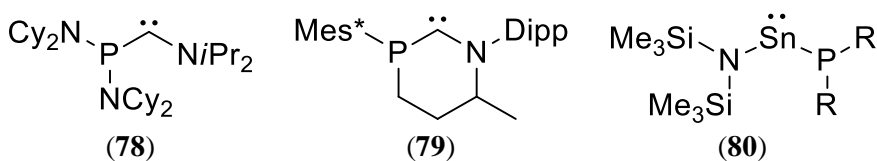
**Figure 31:** (phospha)(aryl)carbenes

The (boryl)(phospha)carbene **62** has an unusual geometry in the solid-state, in which the vacant orbital and lone pair of the boron and phosphorus centres, respectively, are orthogonal to the  $p_z$ -orbital at the carbenic carbon centre. (Fig. 32). Consistent with the large P-C-B angle of  $151.6(13)^\circ$ , NBO analysis of this compound shows a  $P\equiv C$  triple bond. The  $P$ -heterocyclic carbene **77** reported by Bertrand is the only tetrylene featuring two near-planar phosphorus centres, which provide significant simultaneous  $\pi$ -interactions towards the carbenic carbon (Fig. 32)..<sup>[72]</sup>



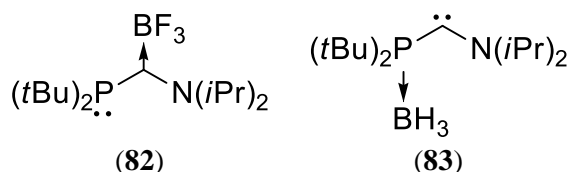
**Figure 32:** Phosphacarbenes with unusual structures [Mes\* = 2,4,6-*t*Bu<sub>3</sub>C<sub>6</sub>H<sub>3</sub>]

In contrast to the planar phosphorus centres observed in the phosphacarbenes **62** and **71-77**, the (phospha)(amino)carbenes **78**<sup>[69g]</sup> and **79**<sup>[73]</sup> and the (phospha)(amino)stannylene **80**<sup>[74]</sup> have pyramidal phosphorus centres (Fig. 33). The nitrogen centres in these compounds have a lower energy barrier of planarization than the phosphorus centres; therefore, the nitrogen atoms preferentially planarize to stabilise the tetrel centres by  $\pi$ -interactions.



**Figure 33:** R = (*o*-CH<sub>3</sub>-C<sub>2</sub>B<sub>10</sub>H<sub>10</sub>)

While phosphide substituents with a pyramidal geometry act as “spectator” ligands, phosphacarbenes may exhibit regioselective reactivity through the lone pair at the carbenic carbon or phosphorus centre. For example, the (phospha)(amino)carbene (*t*Bu)<sub>2</sub>PCN(*i*Pr)<sub>2</sub> (**81**) has been shown to complex with BF<sub>3</sub> through the carbenic carbon or with BH<sub>3</sub> through the phosphorus centre to form complexes **82** or **83**, respectively (Fig. 34).<sup>[69g]</sup> The regioselectivity of **81** demonstrates the relative hardness of the phosphorus (soft) and carbenic carbon (hard) centres.



**Figure 34:** Borane complexes of **81**

Transition-metal complexes of phosphacarbene exhibit similar regioselectivity. The complexes **26**,<sup>[35]</sup> **85**<sup>[75]</sup> and **86** bond to the metal centres through the carbenic carbon, while each phosphacarbene molecule in the cationic complex **87** binds through the carbenic carbon and phosphorus centre to the rhodium centre.<sup>[76]</sup>

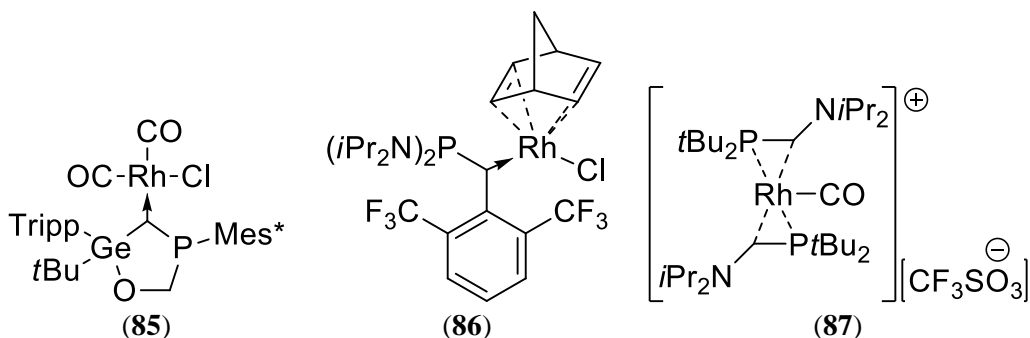


Figure 35: Phosphatetrylene transition metal complexes

Furthermore, the dimerization of phosphacarbene through the phosphorus centres to give head-to-tail dimers, such as the 1,3-diphosphete **88**,<sup>[23]</sup> contrasts with the dimerization of most heteroatom-substituted carbenes to form alkenes (Fig. 36). The heavier diphosphatetrylenes are more susceptible to give dimers of the form **89**, compared to carbenes, because of their more exposed and electrophilic tetrel centre.<sup>[77]</sup> Another complication when synthesising heavier phosphatetrylenes through precursors in the +2 oxidation state is that the use of moderately bulky phosphides may result in the formation of electron-precise trisubstituted compounds, such as the lithium ‘ate’ complex **90**.<sup>[78]</sup>

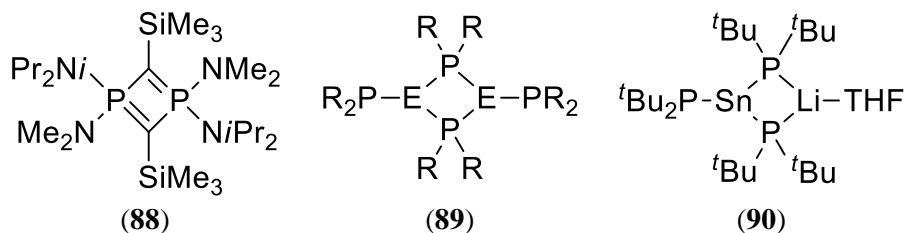


Figure 36

The dimerization of the diphosphastannylenes {(Ph<sub>3</sub>Si)<sub>2</sub>P}<sub>2</sub>Sn (**91**)<sup>[79]</sup> and {(Ph)(2,6-Mes<sub>2</sub>-C<sub>6</sub>H<sub>3</sub>)P}<sub>2</sub>Sn (**92**)<sup>[80]</sup> is prevented by the very sterically bulky substituents (Fig. 37). Although these compounds were not characterised by X-ray crystallography, compound **91** was shown to be monomeric in solution by cryoscopy while **92** exhibits a triplet in the <sup>119</sup>Sn spectrum, consistent with a monomeric diphosphastannylene.

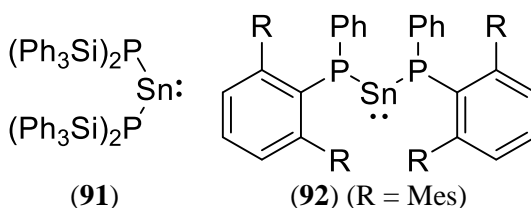
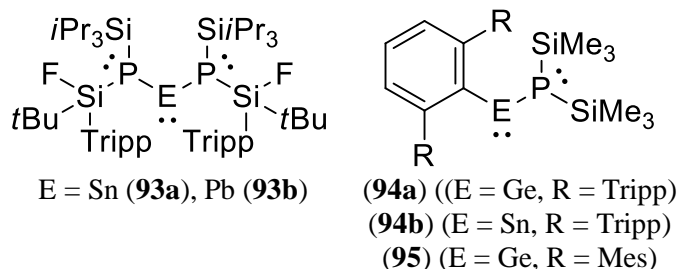


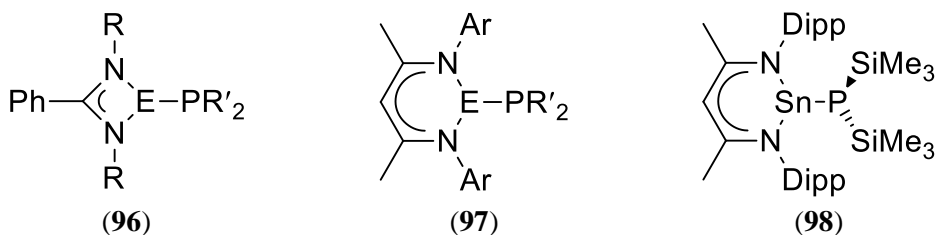
Figure 37: Monomeric diphosphatetrylenes

The first examples of heavier phosphatetrylenes that were characterised by X-ray crystallography, [ $\{i\text{Pr}_3\text{Si}\}\{(\text{F})(t\text{Bu})(\text{Tripp})\text{Si}\}\text{P}\}_2\text{E}$ , E = Sn (**93a**), Pb (**93b**), were reported by Driess in 1995.<sup>[81]</sup> In the solid-state, these compounds each have two pyramidal phosphorus centres and so act as “spectator” ligands. The (phospha)(terphenyl)tetrylenes **94a**, **94b**<sup>[82]</sup> and **95**<sup>[63]</sup>, reported by Scheer and Aldridge, also feature a pyramidal phosphorus centres on the phosphide substituents.



**Figure 38:** Phosphatetrylenes

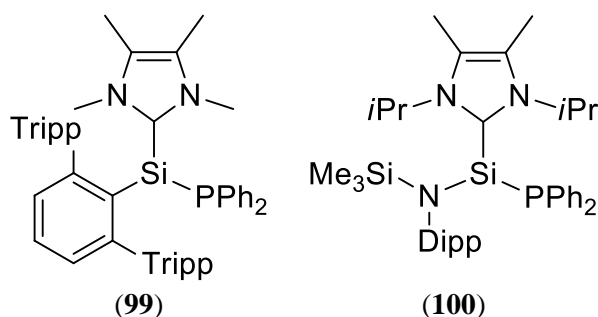
Access to stable chlorotetrylenes with amidinate and  $\beta$ -diketiminato substituents has facilitated the synthesis of a range of heteroleptic tetrylenes, (eg. **96**<sup>[83]</sup> and **97**<sup>[84]</sup>). These bidentate nitrogen ligands electronically saturate the tetrel centres by donation of electron density into the tetrel  $p_z$  orbital, to give electron-precise systems. Consequently, these phosphatetrylenes have pyramidal phosphorus centres in the solid-state, with the exception of **98**, in which the planar phosphorus centre lies orthogonal to the  $\beta$ -diketiminato substituent and  $p_z$  orbital on the tin centre and, therefore, does not exhibit P=E  $\pi$ -interactions.<sup>[83c, 84]</sup>



**Figure 39:** Ar = Dipp, Tripp; R = *t*Bu, SiMe<sub>3</sub>; R' = H, *i*Pr, Ph, Cy, SiMe<sub>3</sub>, 2-thienyl, 1,3-P<sub>2</sub>C<sub>3</sub>*t*Bu<sub>3</sub>

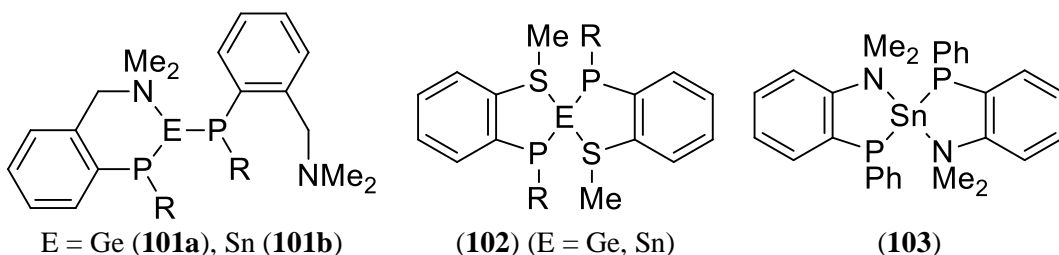
The NHC-phosphasilylene complexes **99**<sup>[85]</sup> and **100**<sup>[86]</sup> are the only reported examples of silylenes featuring phosphide substituents (Fig. 40). These complexes feature pyramidal phosphorus centres and an electron-precise silicon centre.





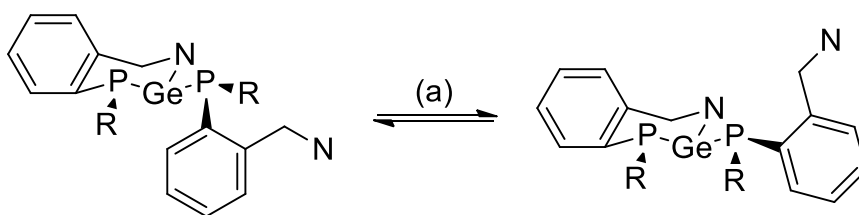
**Figure 40:** NHC-complexes of phosphasilylenes

A similar strategy for increasing the stability of phosphatetrylenes is the use of pendant Lewis bases (e.g.  $\text{NMe}_2$ ,  $\text{SMe}$ ), which was first explored by the Izod group. The formation of a single intramolecular ring gives an electron-precise tetrel centre, while the formation of two intramolecular rings gives a hypervalent tetrel centre (Fig 41). Compounds **101a**<sup>[87]</sup>, **101b**<sup>[88]</sup> and **102**<sup>[89]</sup> exhibit complex dynamic behaviour in solution, while the less sterically hindered derivative **103** maintains its solid-state structure in solution.



**Figure 41:** Intramolecularly bases-stabilised phosphatetrylenes [ $\text{R} = \text{CH}(\text{SiMe}_3)_2$ ]

Compound **101a** exhibits variable-temperature  $^{31}\text{P}\{^1\text{H}\}$  NMR behaviour consistent with (a) inversion at the terminal phosphorus centre (Scheme 13), (b) inversion at germanium via Ge-N cleavage/ Ge-P rotation/ Ge-N re-coordination, (c) inversion at germanium and simultaneous exchange of the terminal and chelating phosphorus atoms and (d) exchange of the chelating and terminal phosphorus atoms without inversion at germanium or phosphorus. DFT calculations on a simplified model of **101a**, in which the  $\text{CH}(\text{SiMe}_3)_2$  groups were replaced with methyl groups, revealed a moderate energy barrier to inversion of the terminal phosphorus centre ( $21.0 \text{ kcal mol}^{-1}$ ); this is likely to be an underestimate of the true value because of the reduced sterics of the system.<sup>[87]</sup>



**Scheme 13:** Inversion of the terminal phosphorus centre of **101a**

Recently, the Izod group isolated the first diphosphagermylene  $\{(\text{Dipp})_2\text{P}\}_2\text{Ge}$  (**104Ge**) stabilised by efficient  $\text{p}\pi\text{-p}\pi$  interactions from a planar phosphorus. In the solid state, compound **104Ge** has one planar and one pyramidal phosphorus centre [ $\text{Dipp} = 2,6\text{-iPr}_2\text{C}_6\text{H}_3$ ]. The  $\text{P}_{\text{plan}}\text{-Ge}$  distance is 6% shorter than the  $\text{P}_{\text{pyr}}\text{-Ge}$  distance. The  $\pi$  interactions were further confirmed by DFT calculations, which show the HOMO-1 and LUMO+1 correspond to the  $\pi$  and  $\pi^*$  orbitals, respectively (Fig. 42).

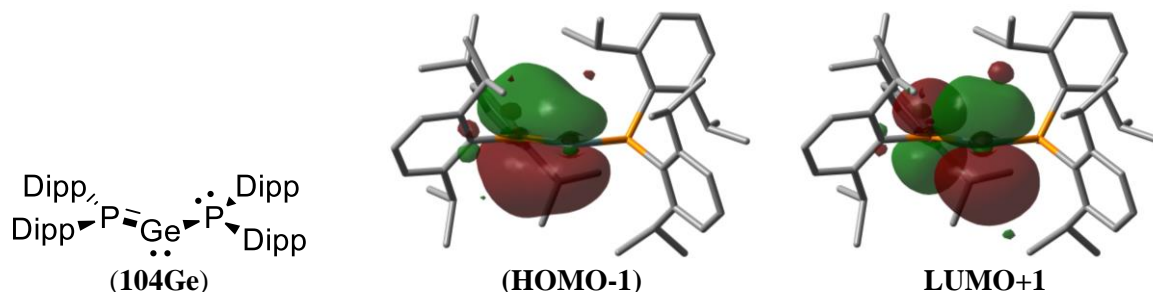


Figure 42: Molecular orbitals of **104Ge**

Compound **104Ge** exhibits complex variable-temperature  $^{31}\text{P}\{^1\text{H}\}$  NMR behaviour; at 25 °C a single broad signal is exhibited, which decoalesces as the temperature is reduced, until, at the -95 °C, the spectrum consists of the signals **A-D** (Fig. 43). The peaks **A** and **D** are associated with the planar and pyramidal phosphorus centres, respectively, in the solid-state structure, while the identity of the species corresponding to the peaks **A** and **C** are less clear, but are thought to be configurations of **104Ge** with two pyramidal phosphorus centres.<sup>[90]</sup>

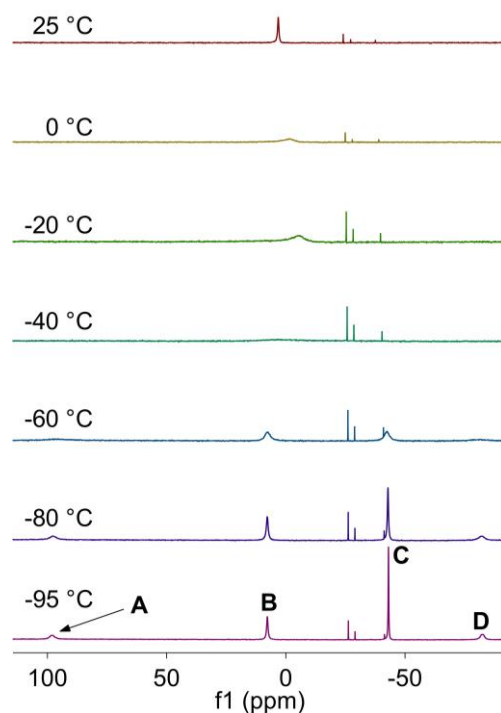


Figure 43: Variable-temperature  $^{31}\text{P}\{^1\text{H}\}$  NMR spectra of **104Ge**

## 1.9 Conclusions and research proposal

We have discussed how a tetrylenes' stability and reactivity towards small molecules correlates with the electronic properties of its tetrel centre and how these are influenced by the substituents. In summary, the  $\pi$  interactions from heteroatom substituents provide significant stabilisation towards the tetrel centre but inhibit various reaction pathways (see above). Since the phosphorus centres in phosphide substituents can adopt either a pyramidal or a planar geometry, resulting in the phosphides acting as spectator or  $\pi$ -donating ligands, respectively, we propose diphosphatetrylenes are candidates for small molecule activation. While the geometry of the phosphide ligand is typically static in phosphide-substituted tetrylenes, a dynamic equilibrium between the pyramidal and planar configurations of the phosphide ligands is observed in compound **104Ge**. This may allow access to the transition metal-like reactivity of the pyramidal configuration, while stability is provided by the planar configuration, which may also offer interesting reactivity through the P=Ge bond.

In order to first explore the nature of the P=E bond in tetrylene systems, we aimed to prepare a range of bulky phosphides with varying steric bulk. These would then be used as ligands to prepare a series of diphosphatetrylenes  $[(R_2P)_2E]$ ; E = Si, Ge, Sn, Pb] in order to investigate the influence of the steric encumbrance of the phosphide ligands and electronics of the tetrel centre on the energy barrier of planarization for the phosphorus centres and the bonding in these compounds. In addition, we aimed to prepare the corresponding two-coordinate pnictide cations  $[(R_2P)_2E']^+$ ; E' = P, As), which are isoelectronic with tetrylenes, to investigate how the positive charge at the two-coordinate pnictogen atoms effects the bonding of the phosphide ligands. The thesis herein describes the results of these studies.



**Figure 44:** Proposed isoelectronic analogues of **104Ge** (E = Si, Sn, Pb; E' = P, As; Y = non-coordinating anion)

## 1.10 References

- [1] (a) J. Hine, *J. Am. Chem. Soc.*, **1950**, 72, 2438-2445; (b) W. von E. Doering, A. K. Hoffmann, *J. Am. Chem. Soc.*, **1954**, 76, 6162-6165.
- [2] V. E. O. Fischer, H. Gruber, *Z. Naturforsch., B*, **1956**, 11, 423-424.
- [3] J. L. Atwood, W. E. Hunter, A. H. Cowley, R. A. Jones, C. A. Stewart, *J. Chem. Soc., Chem. Commun.*, **1981**, 925.
- [4] E. O. Fischer, H. Grubert, *Z. Anorg. Allg. Chem.*, **1956**, 286, 237-242.
- [5] A. Schöpper, W. Saak, M. Weidenbruch, *J. Organomet. Chem.*, **2006**, 691, 809-810.
- [6] P. Jutzi, D. Kanne, C. Krüger, *Angew. Chem. Int. Ed.*, **1986**, 25, 164-164.
- [7] D. H. Harris, M. F. Lappert, *J. Chem. Soc., Chem. Commun.*, **1974**, 895-896.
- [8] A. J. Arduengo, R. L. Harlow, M. Kline, *J. Am. Chem. Soc.*, **1991**, 113, 361-363.
- [9] (a) D. Enders, O. Niemeier, A. Henseler, *Chem. Rev.*, **2007**, 107, 5606-5655; (b) D. M. Flanigan, F. Romanov-Michailidis, N. A. White, T. Rovis, *Chem. Rev.*, **2015**, 115, 9307-9387; (c) X. Bugaut, F. Glorius, *Chem. Soc. Rev.*, **2012**, 41, 3511-3522.
- [10] T. Chu, G. I. Nikonov, *Chem. Rev.*, **2018**, 118, 3608-3680.
- [11] A. Sekiguchi, T. Tanaka, M. Ichinohe, K. Akiyama, S. Tero-Kubota, *J. Am. Chem. Soc.*, **2003**, 125, 4962-4963.
- [12] H. A. Bent, *J. Chem. Phys.*, **1960**, 33, 1260-1261.
- [13] (a) W. W. Schoeller, *J. Chem. Soc., Chem. Commun.*, **1980**, 124; (b) L. Pauling, *J. Chem. Soc., Chem. Commun.*, **1980**, 688; (c) K. K. Irikura, W. A. Goddard, J. L. Beauchamp, *J. Am. Chem. Soc.*, **1992**, 114, 48-51.
- [14] B. C. Gilbert, D. Griller, A. S. Nazran, *J. Org. Chem.*, **1985**, 50, 4738-4742.
- [15] (a) D. A. Modarelli, S. Morgan, M. S. Platz, *J. Am. Chem. Soc.*, **1992**, 114, 7034-7041; (b) C. A. Richards, S.-J. Kim, Y. Yamaguchi, H. F. Schaefer, *J. Am. Chem. Soc.*, **1995**, 117, 10104-10107.
- [16] J. E. Gano, R. H. Wettach, M. S. Platz, V. P. Senthilnathan, *J. Am. Chem. Soc.*, **1982**, 104, 2326-2327.
- [17] D. R. Myers, V. P. Senthilnathan, M. S. Platz, M. Jones, *J. Am. Chem. Soc.*, **1986**, 108, 4232-4233.
- [18] J. E. Bender, M. M. Banaszak Holl, J. W. Kampf, *Organometallics*, **1997**, 16, 2743-2745.
- [19] L. M. Engelhardt, B. S. Jolly, M. F. Lappert, C. L. Raston, A. H. White, *J. Chem. Soc., Chem. Commun.*, **1988**, 0, 336-338.
- [20] M. Walewska, J. Hlina, W. Gaderbauer, H. Wagner, J. Baumgartner, C. Marschner, *Z. Anorg. Allg. Chem.*, **2016**, 642, 1304-1313.
- [21] T. J. Hadlington, M. Hermann, J. Li, G. Frenking, C. Jones, *Angew. Chem. Int. Ed. Engl.*, **2013**, 52, 10199-10203.
- [22] A. Igau, H. Grutzmacher, A. Baceiredo, G. Bertrand, *J. Am. Chem. Soc.*, **1988**, 110, 6463-6466.
- [23] G. R. Gillette, A. Baceiredo, G. Bertrand, *Angew. Chem. Int. Ed.*, **1990**, 29, 1429-1431.
- [24] N. Kuhn, T. Kratz, *Synthesis*, **1993**, 1993, 561-562.
- [25] M. Scholl, S. Ding, C. W. Lee, R. H. Grubbs, *Org. Lett.*, **1999**, 1, 953-956.
- [26] M. Denk, R. Lennon, R. Hayashi, R. West, A. V. Belyakov, H. P. Verne, A. Haaland, M. Wagner, N. Metzler, *J. Am. Chem. Soc.*, **1994**, 116, 2691-2692.
- [27] H. Cui, Y. Shao, X. Li, L. Kong, C. Cui, *Organometallics*, **2009**, 28, 5191-5195.
- [28] K. Izod, W. McFarlane, C. Wills, W. Clegg, R. W. Harrington, *Organometallics*, **2008**, 27, 4386-4394.

- [29] (a) B. D. Reken, T. M. Brown, J. C. Fetting, F. Lips, H. M. Tuononen, R. H. Herber, P. P. Power, *J. Am. Chem. Soc.*, **2013**, *135*, 10134-10148; (b) J.-D. Guo, D. J. Liptrot, S. Nagase, P. P. Power, *Chem. Sci.*, **2015**, *6*, 6235-6244.
- [30] G. D. Frey, V. Lavallo, B. Donnadieu, W. W. Schoeller, G. Bertrand, *Science*, **2007**, *316*, 439-441.
- [31] D. Martin, M. Soleilhavoup, G. Bertrand, *Chem. Sci.*, **2011**, *2*, 389-399.
- [32] L. Li, T. Fukawa, T. Matsuo, D. Hashizume, H. Fueno, K. Tanaka, K. Tamao, *Nature chemistry*, **2012**, *4*, 361-365.
- [33] T. J. Hadlington, M. Hermann, G. Frenking, C. Jones, *J. Am. Chem. Soc.*, **2014**, *136*, 3028-3031.
- [34] P. A. Chase, D. W. Stephan, *Angew. Chem. Int. Ed. Engl.*, **2008**, *47*, 7433-7437.
- [35] T. Cantat, N. Mezailes, N. Maigrot, L. Ricard, P. Le Floch, *Chem. Commun.*, **2004**, 1274-1275.
- [36] D. Heitmann, T. Pape, A. Hepp, C. Muck-Lichtenfeld, S. Grimme, F. E. Hahn, *J. Am. Chem. Soc.*, **2011**, *133*, 11118-11120.
- [37] R. Kinjo, B. Donnadieu, M. A. Celik, G. Frenking, G. Bertrand, *Science*, **2011**, *333*, 610-613.
- [38] Y. Wang, Y. Xie, P. Wei, R. B. King, H. F. Schaefer, 3rd, P. Schleyer, G. H. Robinson, *J. Am. Chem. Soc.*, **2008**, *130*, 14970-14971.
- [39] H. W. Wanzlick, H. J. Kleiner, *Angew. Chem.*, **1961**, *73*, 493-493.
- [40] H.-J. Schönherr, H.-W. Wanzlick, *Chem. Ber.*, **1970**, *103*, 1037-1046.
- [41] A. J. Arduengo, H. V. R. Dias, R. L. Harlow, M. Kline, *J. Am. Chem. Soc.*, **1992**, *114*, 5530-5534.
- [42] A. J. Arduengo, J. R. Goerlich, W. J. Marshall, *J. Am. Chem. Soc.*, **1995**, *117*, 11027-11028.
- [43] A. J. Arduengo, R. Krafczyk, R. Schmutzler, H. A. Craig, J. R. Goerlich, W. J. Marshall, M. Unverzagt, *Tetrahedron*, **1999**, *55*, 14523-14534.
- [44] R. W. Alder, P. R. Allen, M. Murray, A. G. Orpen, *Angew. Chem. Int. Ed.*, **1996**, *35*, 1121-1123.
- [45] M. J. S. Gynane, D. H. Harris, M. F. Lappert, P. P. Power, P. Rivière, M. Rivière-Baudet, *J. Chem. Soc., Dalton Trans.*, **1977**, 2004-2009.
- [46] M. F. Lappert, M. J. Slade, J. L. Atwood, M. J. Zaworotko, *J. Chem. Soc., Chem. Commun.*, **1980**, 621.
- [47] B. Cetinkaya, I. Gumrukcu, M. F. Lappert, J. L. Atwood, R. D. Rogers, M. J. Zaworotko, *J. Am. Chem. Soc.*, **1980**, *102*, 2088-2089.
- [48] T. Fjeldberg, P. B. Hitchcock, M. F. Lappert, S. J. Smith, A. J. Thorne, *J. Chem. Soc., Chem. Commun.*, **1985**, 939.
- [49] V. Lavallo, Y. Canac, C. Prasang, B. Donnadieu, G. Bertrand, *Angew. Chem. Int. Ed. Engl.*, **2005**, *44*, 5705-5709.
- [50] M. Kira, S. Ishida, T. Iwamoto, C. Kabuto, *J. Am. Chem. Soc.*, **1999**, *121*, 9722-9723.
- [51] L. Wang, Y. S. Lim, Y. Li, R. Ganguly, R. Kinjo, *Molecules*, **2016**, *21*.
- [52] P. J. Davidson, M. F. Lappert, *J. Chem. Soc., Chem. Commun.*, **1973**, 317a.
- [53] D. E. Goldberg, D. H. Harris, M. F. Lappert, K. M. Thomas, *J. Chem. Soc., Chem. Commun.*, **1976**, 261.
- [54] K. W. Zilm, G. A. Lawless, R. M. Merrill, J. M. Millar, G. G. Webb, *J. Am. Chem. Soc.*, **1987**, *109*, 7236-7238.
- [55] M. Kira, R. Yauchibara, R. Hirano, C. Kabuto, H. Sakurai, *J. Am. Chem. Soc.*, **1991**, *113*, 7785-7787.
- [56] M. Kira, S. Ishida, T. Iwamoto, M. Ichinohe, C. Kabuto, L. Ignatovich, H. Sakurai, *Chem. Lett.*, **1999**, *28*, 263-264.

- [57] K. Izod, C. Wills, W. Clegg, R. W. Harrington, *Organometallics*, **2009**, 28, 5661-5668.
- [58] M. Weidenbruch, J. Schlaefke, A. Schäfer, K. Peters, H. G. von Schnering, H. Marsmann, *Angew. Chem. Int. Ed.*, **1994**, 33, 1846-1848.
- [59] B. E. Eichler, P. P. Power, *J. Am. Chem. Soc.*, **2000**, 122, 8785-8786.
- [60] A. V. Protchenko, A. D. Schwarz, M. P. Blake, C. Jones, N. Kaltsoyannis, P. Mountford, S. Aldridge, *Angew. Chem. Int. Ed. Engl.*, **2013**, 52, 568-571.
- [61] F. Lavigne, E. Maerten, G. Alcaraz, N. Saffon-Merceron, C. Acosta-Silva, V. Branchadell, A. Baceiredo, *J. Am. Chem. Soc.*, **2010**, 132, 8864-8865.
- [62] A. V. Protchenko, K. H. Birjkumar, D. Dange, A. D. Schwarz, D. Vidovic, C. Jones, N. Kaltsoyannis, P. Mountford, S. Aldridge, *J. Am. Chem. Soc.*, **2012**, 134, 6500-6503.
- [63] M. Usher, A. V. Protchenko, A. Rit, J. Campos, E. L. Kolychev, R. Tirfoin, S. Aldridge, *Chem. Eur. J.*, **2016**, 22, 11685-11698.
- [64] A. V. Protchenko, D. Dange, A. D. Schwarz, C. Y. Tang, N. Phillips, P. Mountford, C. Jones, S. Aldridge, *Chem. Commun.*, **2014**, 50, 3841-3844.
- [65] L. Rosenberg, *Coord. Chem. Rev.*, **2012**, 256, 606-626.
- [66] (a) F. G. N. Cloke, P. B. Hitchcock, P. Hunnable, J. F. Nixon, L. Nyulászi, E. Niecke, V. Thelen, *Angew. Chem. Int. Ed.*, **1998**, 37, 1083-1086; (b) R. A. Bartlett, H. V. R. Dias, P. P. Power, *Inorg. Chem.*, **1988**, 27, 3919-3922; (c) S. J. Geier, T. M. Gilbert, D. W. Stephan, *J. Am. Chem. Soc.*, **2008**, 130, 12632-12633; (d) D. C. Pestana, P. P. Power, *J. Am. Chem. Soc.*, **1991**, 113, 8426-8437; (e) M. Driess, K. Merz, C. Monsé, *Z. Anorg. Allg. Chem.*, **2000**, 626, 2264-2268; (f) G. Fritz, E. Matern, H. Krautscheid, R. Ahlrichs, J. W. Olkowska, J. Pikies, *Z. Anorg. Allg. Chem.*, **1999**, 625, 1604-1607.
- [67] (a) K. Mislow, R. D. Baechler, *J. Am. Chem. Soc.*, **1971**, 93, 773-774; (b) K. Izod, E. R. Clark, J. Stewart, *Inorg. Chem.*, **2011**, 50, 3651-3661; (c) R. D. Baechler, J. D. Andose, J. Stackhouse, K. Mislow, *J. Am. Chem. Soc.*, **1972**, 94, 8060-8065; (d) D. A. Dixon, A. J. Arduengo, *J. Am. Chem. Soc.*, **1987**, 109, 338-341.
- [68] (a) J. Kapp, C. Schade, A. M. El-Nahas, P. v. R. Schleyer, *Angew. Chem.*, **1996**, 108, 2373-2376; (b) J. Kapp, C. Schade, A. M. El-Nahasa, P. von Ragué Schleyer, *Angew. Chem. Int. Ed.*, **1996**, 35, 2236-2238.
- [69] (a) A. Igau, A. Baceiredo, G. Trinquier, G. Bertrand, *Angew. Chem. Int. Ed.*, **1989**, 28, 621-622; (b) M. Soleilhavoup, A. Baceiredo, O. Treutler, R. Ahlrichs, M. Nieger, G. Bertrand, *J. Am. Chem. Soc.*, **1992**, 114, 10959-10961; (c) G. Alcaraz, R. Reed, A. Baceiredo, G. Bertrand, *J. Chem. Soc., Chem. Commun.*, **1993**, 1354-1355; (d) T. Kato, H. Gornitzka, A. Baceiredo, A. Savin, G. Bertrand, *J. Am. Chem. Soc.*, **2000**, 122, 998-999; (e) J. Krysiak, C. Lyon, A. Baceiredo, H. Gornitzka, M. Mikolajczyk, G. Bertrand, *Chem. Eur. J.*, **2004**, 10, 1982-1986; (f) S. Conejero, Y. Canac, F. S. Tham, G. Bertrand, *Angew. Chem. Int. Ed. Engl.*, **2004**, 43, 4089-4093; (g) N. Merceron, K. Miqueu, A. Baceiredo, G. Bertrand, *J. Am. Chem. Soc.*, **2002**, 124, 6806-6807.
- [70] C. Buron, *Science*, **2000**, 288, 834-836.
- [71] E. Despagne, H. Gornitzka, A. B. Rozhenko, W. W. Schoeller, D. Bourissou, G. Bertrand, *Angew. Chem. Int. Ed.*, **2002**, 41, 2835-2837.
- [72] D. Martin, A. Baceiredo, H. Gornitzka, W. W. Schoeller, G. Bertrand, *Angew. Chem. Int. Ed. Engl.*, **2005**, 44, 1700-1703.
- [73] G. D. Frey, M. Song, J. B. Bourg, B. Donnadieu, M. Soleilhavoup, G. Bertrand, *Chem. Commun.*, **2008**, 4711-4713.
- [74] T. Řezníček, L. Dostál, A. Růžicka, R. Jambor, *Eur. J. Inorg. Chem.*, **2012**, 2012, 2983-2987.

- [75] D. Ghereg, S. Ladeira, N. Saffon, J. Escudie, H. Gornitzka, *Angew. Chem. Int. Ed. Engl.*, **2011**, *50*, 7607-7610.
- [76] N. Merceron-Saffon, H. Gornitzka, A. Baceiredo, G. Bertrand, *J. Organomet. Chem.*, **2004**, *689*, 1431-1435.
- [77] (a) K. Izod, J. Stewart, E. R. Clark, W. Clegg, R. W. Harrington, *Inorg. Chem.*, **2010**, *49*, 4698-4707; (b) C. Druckenbrodt, W. W. du Mont, F. Ruthe, P. G. Jones, *Z. Anorg. Allg. Chem.*, **1998**, *624*, 590-594; (c) S. C. Goel, M. Y. Chiang, D. J. Rauscher, W. E. Buhro, *J. Am. Chem. Soc.*, **1993**, *115*, 160-169; (d) A. H. Cowley, D. M. Giolando, R. A. Jones, C. M. Nunn, J. M. Power, W.-W. du Mont, *Polyhedron*, **1988**, *7*, 1317-1319; (e) A. H. Cowley, D. M. Giolando, R. A. Jones, C. M. Nunn, J. M. Power, *Polyhedron*, **1988**, *7*, 1909-1910.
- [78] A. M. Arif, A. H. Cowley, R. A. Jones, J. M. Power, *J. Chem. Soc., Chem. Commun.*, **1986**, 1446.
- [79] M. A. Matchett, M. Y. Chiang, W. E. Buhro, *Inorg. Chem.*, **1994**, *33*, 1109-1114.
- [80] E. Rivard, A. D. Sutton, J. C. Fettingner, P. P. Power, *Inorg. Chim. Acta*, **2007**, *360*, 1278-1286.
- [81] M. Driess, R. Janoschek, H. Pritzkow, S. Rell, U. Winkler, *Angew. Chem. Int. Ed.*, **1995**, *34*, 1614-1616.
- [82] B. P. Johnson, S. Almstätter, F. Dielmann, M. Bodensteiner, M. Scheer, *Z. Anorg. Allg. Chem.*, **2010**, *636*, 1275-1285.
- [83] (a) S. Yao, S. Block, M. Brym, M. Driess, *Chem. Commun.*, **2007**, 3844; (b) S. Yao, M. Brym, K. Merz, M. Driess, *Organometallics*, **2008**, *27*, 3601-3607; (c) E. C. Tam, N. A. Maynard, D. C. Apperley, J. D. Smith, M. P. Coles, J. R. Fulton, *Inorg. Chem.*, **2012**, *51*, 9403-9415; (d) Y. Yang, N. Zhao, Y. Wu, H. Zhu, H. W. Roesky, *Inorg. Chem.*, **2012**, *51*, 2425-2431.
- [84] (a) M. Brym, M. D. Francis, G. Jin, C. Jones, D. P. Mills, A. Stasch, *Organometallics*, **2006**, *25*, 4799-4807; (b) C. W. So, H. W. Roesky, P. M. Gurubasavaraj, R. B. Oswald, M. T. Gamer, P. G. Jones, S. Blaurock, *J. Am. Chem. Soc.*, **2007**, *129*, 12049-12054.
- [85] K. Hansen, T. Szilvasi, B. Blom, E. Irran, M. Driess, *Chem. Eur. J.*, **2015**, *21*, 18930-18933.
- [86] H. Cui, J. Zhang, Y. Tao, C. Cui, *Inorg. Chem.*, **2016**, *55*, 46-50.
- [87] K. Izod, W. McFarlane, B. Allen, W. Clegg, R. W. Harrington, *Organometallics*, **2005**, *24*, 2157-2167.
- [88] K. Izod, J. Stewart, E. R. Clark, W. McFarlane, B. Allen, W. Clegg, R. W. Harrington, *Organometallics*, **2009**, *28*, 3327-3337.
- [89] K. Izod, E. R. Clark, W. Clegg, R. W. Harrington, *Organometallics*, **2012**, *31*, 246-255.
- [90] K. Izod, D. G. Rayner, S. M. El-Hamruni, R. W. Harrington, U. Baisch, *Angew. Chem. Int. Ed. Engl.*, **2014**, *53*, 3636-3640.

## Chapter 2. Experimental

### 2.1 General procedures

All manipulations were carried out using standard Schlenk techniques under an atmosphere of nitrogen/argon or in a nitrogen filled dry-box. Diethyl ether, tetrahydrofuran, petroleum ether (40-60 °C), toluene, *n*-hexane and methylcyclohexane were pre-dried with sodium wire and distilled from sodium, potassium or sodium/potassium alloy, depending on the boiling point. Dichloromethane, fluorobenzene and hexamethyldisiloxane were distilled from CaH<sub>2</sub>. THF, DCM, fluorobenzene and hexamethyldisiloxane were stored over activated 4 Å molecular sieves; all other solvents were stored over a potassium mirror. Deuterated chloroform and DCM were distilled from CaH<sub>2</sub> while deuterated THF, benzene and toluene were distilled from potassium. All the deuterated solvents were deoxygenated by three freeze-pump-thaw cycles and were stored over activated 4 Å molecular sieves.

*n*-Butyllithium was obtained from Sigma Aldrich as a 2.5 M solution in hexanes and the exact concentration was determined by titration against a 1.0 M hydrochloric acid solution using phenolphthalein as indicator. Mesityl magnesium bromide was obtained from Aldrich as a 1.0 M solution in diethyl ether and was used as supplied. *t*-BuOK and *t*-BuONa were heated at 100 °C under vacuum (0.01 Torr) prior to use. SnCl<sub>2</sub> was dried by stirring with trimethylchlorosilane overnight and then impurities were removed under vacuum (0.01 Torr) at room temperature. TMEDA was distilled from CaH<sub>2</sub> and was stored over activated 4 Å molecular sieves. All other chemicals were used as supplied by the manufacturers.

The compounds PhCH<sub>2</sub>K,<sup>[1]</sup> PhCH<sub>2</sub>Na,<sup>[2]</sup> (2,4,6-Me<sub>3</sub>C<sub>6</sub>H<sub>2</sub>)PCl<sub>2</sub>,<sup>[3]</sup> (Me<sub>3</sub>Si)<sub>2</sub>CHBr,<sup>[4]</sup> (Me<sub>2</sub>Ph)<sub>2</sub>CHBr,<sup>[5]</sup> Cl<sub>2</sub>PCH<sub>2</sub>PCl<sub>2</sub>,<sup>[6]</sup> Na[B{3,5-(CF<sub>3</sub>)<sub>2</sub>C<sub>6</sub>H<sub>3</sub>}<sub>4</sub>]<sup>[7]</sup> and Li[Al{OC(CF<sub>3</sub>)<sub>3</sub>}<sub>4</sub>]<sup>[8]</sup> were prepared by previously reported procedures.

### 2.2 NMR spectroscopy

All NMR spectra were recorded at room temperature, unless otherwise stated, on a Bruker Avance III 300, Bruker Avance II 400 or Bruker Avance III HD 500 spectrometer. The chemical shifts are quoted in ppm relative to the references shown in the table below along with the operating frequency of the measured nuclei on each spectrometer.



Isotope	Spectrometer frequency (MHz)			Reference
	Bruker Avance III 300	Bruker Avance II 400	Bruker Avance III HD 500	
$^1\text{H}$	300.13	399.78	500.15	$\text{Me}_4\text{Si}$ , $\text{CDCl}_3$ , 1 %
$^{13}\text{C}$	75.48	100.50	125.78	$\text{Me}_4\text{Si}$ , $\text{CDCl}_3$ , 1 %
$^7\text{Li}$	116.64	155.37	194.38	$\text{LiCl}$ , $\text{D}_2\text{O}$ , 9.7 M
$^{19}\text{F}$	282.39	376.14	470.58	$\text{CCl}_3\text{F}$ , neat
$^{29}\text{Si}$	59.63	79.43	99.37	$\text{Me}_4\text{Si}$ , $\text{CDCl}_3$ , 1 %
$^{31}\text{P}$	121.49	161.83	202.46	$\text{H}_3\text{PO}_4$ , 85 %
$^{119}\text{Sn}$	111.97	149.15	186.60	$\text{Me}_4\text{Sn}$ , neat, $\text{C}_6\text{D}_6$

## 2.3 SSNMR spectroscopy

Solid-state  $^{31}\text{P}\{^1\text{H}\}$  NMR spectra were recorded at 161.99 MHz using a Bruker Avance III 400 MHz spectrometer and a 4 mm (rotor o.d.) MAS probe. Spectra were obtained using cross-polarization with a 1 s recycle delay and a 1 ms contact time at ambient probe temperature ( $\sim 25^\circ\text{C}$ ) and at a sample spin rate of either 10 or 12 kHz. Spectral referencing was with respect to an external sample of 85%  $\text{H}_3\text{PO}_4$  (carried out by setting the signal from brushite to 1.0 ppm). Elemental analysis

Elemental analysis was obtained from the Elemental Analysis Service of London Metropolitan University. Unfortunately, most of the compounds presented in this thesis were too air sensitive for reproducible elemental analyses.

## 2.4 Crystal structure determinations

Measurements were made on a Xcalibur, Atlas, Gemini ultra diffractometer using an Enhance Ultra X-ray source ( $\lambda_{\text{Cu K}\alpha} = 1.54184 \text{ \AA}$ ) or a fine-focus sealed X-ray tube ( $\lambda_{\text{Mo K}\alpha} = 0.71073 \text{ \AA}$ ). Using an Oxford Cryosystems CryostreamPlus open-flow  $\text{N}_2$  cooling device, data for all structures were collected at 150 K, with the exception of **234Ge**, **261a** and *cis*-**266b**, which were collected at 190 K, 210 K and 200 K, respectively. Cell refinement, data collection and data reduction were undertaken by using *CrysAlisPro*.<sup>[9]</sup> The intensities were corrected semi-empirically using spherical harmonics or analytically using a multifaceted crystal model based on expressions derived by Clark and Reid.<sup>[10]</sup> The structures were solved using SHELXT<sup>[11]</sup> and refined by SHELXL<sup>[12]</sup> through the Olex2 interface.<sup>[13]</sup> H atoms were positioned with idealized geometry with the exception of  $(\text{Dipp})_2\text{PH}$  (**111**) for which the H atoms were located using peaks in the Fourier difference map. Displacement parameters for all H atoms were constrained using a riding model. Further details of each structure, such as minor disorder, can be found in the attached appendix while major disorder is discussed in the relevant section.

## 2.5 DFT Calculations

Geometry optimizations were performed with the Gaussian09 suite of programs (revision E.01).<sup>[14]</sup> The pure B97D functional,<sup>[15]</sup> which includes a correction for dispersion effects, was employed throughout; the 6-311G(2d,p) all-electron basis set<sup>[15]</sup> was used on all atoms except Sn, for which the relativistic LANL2DZ basis set<sup>[16]</sup> was used (default parameters were used throughout). The identities of minima were confirmed by the absence of imaginary vibrational frequencies in each case. Automatic density fitting was employed for all geometry optimizations and frequency calculations. NMR shielding tensors were calculated using the GIAO method<sup>[17]</sup> at the B97D/LANL2DZ,6-311++G(2d,p)//LANL2DZ,6-311G(2d,p) level of theory, and chemical shifts are quoted in ppm relative to H<sub>3</sub>PO<sub>4</sub> (based on PMe<sub>3</sub> at –61 ppm calculated at the same level of theory); TD-DFT calculations were carried out at the B97D/LANL2DZ,6-311G(2d,p) level of theory with solvation by toluene using the IEF polarizable continuum model implemented in Gaussian09.<sup>[18]</sup> NBO analyses were performed using the NBO 3.1 module of Gaussian09.<sup>[19]</sup> Where appropriate, energies were correct for Basis Set Superposition Error using Boys and Bernadi's Counterpoise method.<sup>[20]</sup>

## 2.6 References

- [1] L. Lochmann, J. Trekoval, *J. Organomet. Chem.*, **1987**, 326, 1-7.
- [2] S. Corbelin, N. P. Lorenzen, J. Kopf, E. Weiss, *J. Organomet. Chem.*, **1991**, 415, 293-313.
- [3] S. T. Liddle, K. Izod, *Organometallics*, **2004**, 23, 5550-5559.
- [4] N. Wiberg, G. Wagner, G. Müller, J. Riede, *J. Organomet. Chem.*, **1984**, 271, 381-391.
- [5] C. Eaborn, W. Clegg, P. B. Hitchcock, M. Hopman, K. Izod, P. N. O'Shaughnessy, J. D. Smith, *Organometallics*, **1997**, 16, 4728-4736.
- [6] S. Hietkamp, H. Sommer, O. Stelzer, A. L. Balch, J. C. Linehan, D. E. Oram, **1989**, 25, 120-122.
- [7] S. R. Bahr, P. Boudjouk, *J. Org. Chem.*, **1992**, 57, 5545-5547.
- [8] I. Krossing, *Chem. Eur. J.*, **2001**, 7, 490-502.
- [9] *CrysAlisPro*, version 1.171.36, Agilent Technologies, Oxfordshire, U.K., **2014**.
- [10] R. C. Clark, J. S. Reid, *Acta Crystallogr. A*, **1995**, 51, 887-897.
- [11] G. M. Sheldrick, *Acta Crystallogr. A*, **2015**, 71, 3-8.
- [12] G. M. Sheldrick, *Acta Crystallogr. A*, **2008**, 64, 112-122.
- [13] O. V. Dolomanov, L. J. Bourhis, R. J. Gildea, J. A. K. Howard, H. Puschmann, *J. Appl. Crystallogr.*, **2009**, 42, 339-341.
- [14] M. J. T. Frisch, G. W.; Schlegel, H. B.; Scuseria, G. E.; Robb, M. A.; Cheeseman, J. R.; Scalmani, G.; Barone, V.; Mennucci, B.; Petersson, G. A.; Nakatsuji, H.; Caricato, M.; Li, X.; Hratchian, H. P.; Izmaylov, A. F.; Bloino, J.; Zheng, G.; Sonnenberg, J. L.; Hada, M.; Ehara, M.; Toyota, K.; Fukuda, R.; Hasegawa, J.; Ishida, M.; Nakajima, T.; Honda, Y.; Kitao, O.; Nakai, H.; Vreven, T.; Montgomery, J. A., Jr.; Peralta, J. E.; Ogliaro, F.; Bearpark, M.; Heyd, J. J.; Brothers, E.; Kudin, K. N.; Staroverov, V. N.;

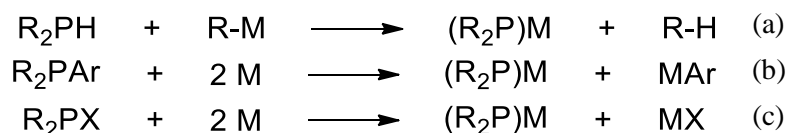
- Kobayashi, R.; Normand, J.; Raghavachari, K.; Rendell, A.; Burant, J. C.; Iyengar, S. S.; Tomasi, J.; Cossi, M.; Rega, N.; Millam, J. M.; Klene, M.; Knox, J. E.; Cross, J. B.; Bakken, V.; Adamo, C.; Jaramillo, J.; Gomperts, R.; Stratmann, R. E.; Yazyev, O.; Austin, A. J.; Cammi, R.; Pomelli, C.; Ochterski, J. W.; Martin, R. L.; Morokuma, K.; Zakrzewski, V. G.; Voth, G. A.; Salvador, P.; Dannenberg, J. J.; Dapprich, S.; Daniels, A. D.; Farkas, Ö.; Foresman, J. B.; Ortiz, J. V.; Cioslowski, J.; Fox, D. J., *Gaussian09, revision E.01*, Gaussian, Inc., Wallingford, CT, **2009**.
- [15] (a) S. Grimme, *J. Comput. Chem.*, **2006**, *27*, 1787-1799; (b) R. Krishnan, J. S. Binkley, R. Seeger, J. A. Pople, *J. Chem. Phys.*, **1980**, *72*, 650-654; (c) L. A. Curtiss, M. P. McGrath, J. P. Blaudeau, N. E. Davis, R. C. Binning, L. Radom, *J. Chem. Phys.*, **1995**, *103*, 6104-6113; (d) T. Clark, J. Chandrasekhar, G. n. W. Spitznagel, P. V. R. Schleyer, *J. Comput. Chem.*, **1983**, *4*, 294-301; (e) A. D. McLean, G. S. Chandler, *J. Chem. Phys.*, **1980**, *72*, 5639-5648; (f) R. C. Binning, L. A. Curtiss, *J. Comput. Chem.*, **1990**, *11*, 1206-1216.
- [16] (a) P. J. Hay, W. R. Wadt, *J. Chem. Phys.*, **1985**, *82*, 299-310; (b) W. R. Wadt, P. J. Hay, *J. Chem. Phys.*, **1985**, *82*, 284-298; (c) P. J. Hay, W. R. Wadt, *J. Chem. Phys.*, **1985**, *82*, 270-283.
- [17] (a) J. R. Cheeseman, G. W. Trucks, T. A. Keith, M. J. Frisch, *J. Chem. Phys.*, **1996**, *104*, 5497-5509; (b) K. Wolinski, J. F. Hinton, P. Pulay, *J. Am. Chem. Soc.*, **1990**, *112*, 8251-8260; (c) R. McWeeny, *Physical Review*, **1962**, *126*, 1028-1034; (d) R. Ditchfield, *Mol. Phys.*, **1974**, *27*, 789-807.
- [18] J. Tomasi, B. Mennucci, R. Cammi, *Chem. Rev.*, **2005**, *105*, 2999-3093.
- [19] E. D. R. Glendening, A. E.; Carpenter, J. E.; Weinhold, F., *NBO, version 3.1*.
- [20] (a) S. F. Boys, F. Bernardi, *Mol. Phys.*, **2006**, *19*, 553-566; (b) S. Simon, M. Duran, J. J. Dannenberg, *J. Chem. Phys.*, **1996**, *105*, 11024-11031.

## Chapter 3. Monodentate phosphine and phosphide synthesis

### 3.1 Introduction

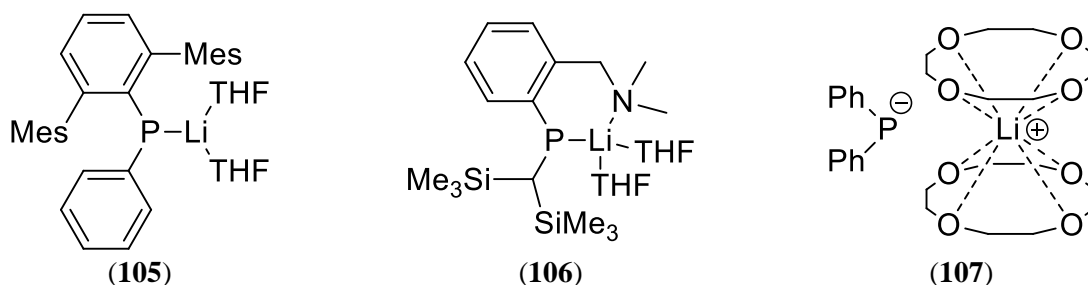
In the previous chapter, we have discussed the importance of ligand design to the stability, structures and stabilisation modes of phosphatetrylenes. Given the success of the (Dipp)<sub>2</sub>P ligand system in diphosphagermylene {(Dipp)<sub>2</sub>P}<sub>2</sub>Ge (**104Ge**), which is stabilised by a planar phosphorus centre, we sought to develop an array of phosphides with bulky aryl and alkyl substituents as ligands for tetrylenes.<sup>[1]</sup> The varying steric and electronic properties of these ligands will allow us to study their influence on the energy barrier to planarization of the phosphorus centres in the corresponding diphosphatetrylenes.

A convenient route to synthesising heavier diphosphatetrylenes is the metathesis reaction between two equivalents of the corresponding alkali metal phosphide and the group 14 dihalide. Alkali metal phosphides are routinely used as transfer reagents in the synthesis of phosphorus-substituted main group, transitional metal and f-block compounds. Secondary alkali metal phosphides may be prepared by a variety of methods such as: (a) the deprotonation of a secondary phosphine; (b) cleavage of a P-C bond of a tertiary arylphosphine; and (c) direct metalation of a halophosphine with an alkali metal (Scheme 14). Since the deprotonation of phosphines is typically quantitative, we chose to prepare secondary phosphines as pro-ligands as this offers the flexibility to use isolated or *in-situ* generated alkali metal phosphides as the transfer reagents.



**Scheme 14:** Selected synthetic routes to alkali metal phosphides

In the solid-state, alkali metal phosphides exhibit a variety of structural motifs such as monomers, dimers, higher oligomers, polymers, ladders, 2-dimensional sheets and 3-dimensional networks.<sup>[2]</sup> Their structures are highly dependent on the size and polarizability of the metal cation, the sterics of the phosphide ligand and the presence of co-ligands such as THF, TMEDA and PMDETA [TMEDA = *N,N,N',N'*-tetramethylethane-1,2-diamine, PMDETA = *N,N,N',N'',N''*-pentamethyldiethylenetriamine].<sup>[2a]</sup> Monomeric structures are favoured by bulky substituents (**105**),<sup>[3]</sup> intra-molecular base stabilisation (**106**)<sup>[4]</sup> or the sequestration of the alkali metal ion using crown ethers or cryptands (**107**)<sup>[5]</sup> (Figure 45).

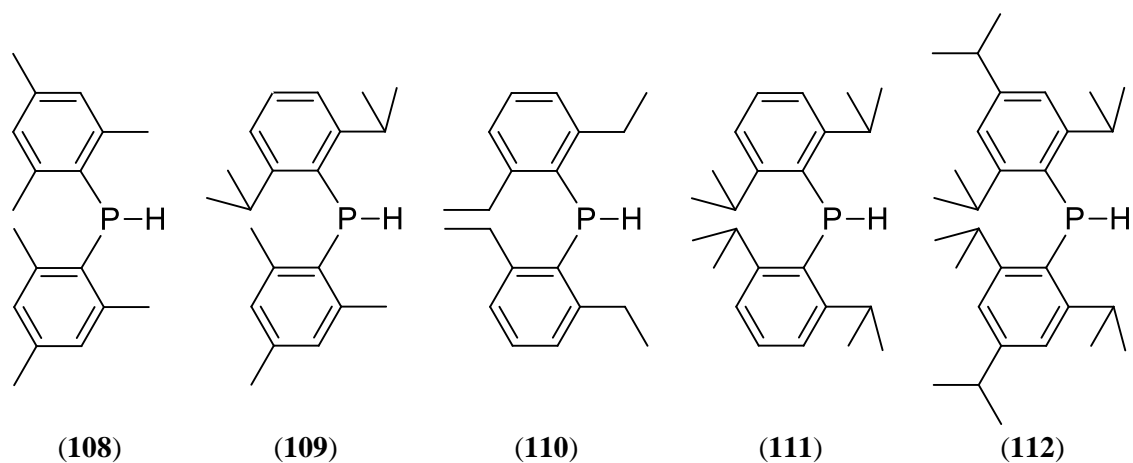


**Figure 45:** Selected examples of monomeric lithium phosphides

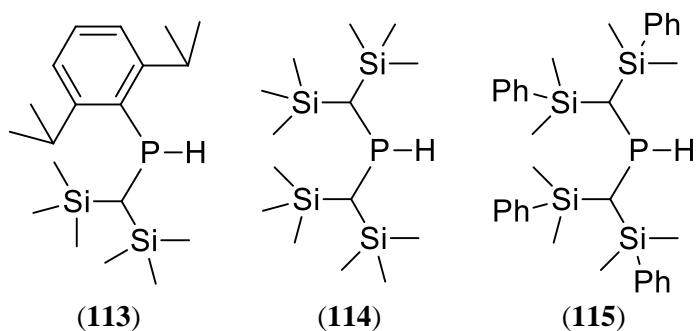
While the solid-state structures may be preserved in solution, there may also be complex dynamic equilibria between aggregates. For lithium phosphides,  $^7\text{Li}$  and  $^{31}\text{P}$  NMR spectroscopy may provide diagnostic data for identifying the molecular connectivity; monomeric lithium phosphides should exhibit a doublet in the  $^7\text{Li}$  NMR spectrum and an equal intensity triplet in the  $^{31}\text{P}$  NMR spectrum while higher aggregates typically exhibit a triplet and a septet in the  $^7\text{Li}$  and  $^{31}\text{P}$  NMR spectra, respectively. However, coupling between the nuclei may not be observed at room temperature because of rapid exchange processes but may be seen at lower temperatures where these processes are frozen out. Therefore, the variable-temperature NMR spectra of the lithium phosphides prepared in this chapter may be informative about the relative sterics of the ligands.

### 3.2 Developing of an array of bulky phosphines

The steric encumbrance at the phosphorus centre in the series of phosphines shown in Figure 46 was varied by altering the size of *ortho*-substituents of the phenyl rings from methyl to *iso*-propyl. Further increasing the steric properties of the *ortho*-substituents may not only hinder reactivity at the phosphorus centre but give inherently unstable phosphines; it has been reported previously that the attempted synthesis of  $(2,4,6\text{-}t\text{Bu}_3\text{C}_6\text{H}_2)_2\text{PH}$ , which features four *tert*-butyl *ortho*-substituents, instead gave  $(2,4,6\text{-}t\text{Bu}_3\text{C}_6\text{H}_2)(2,4\text{-}t\text{Bu}_2\text{C}_6\text{H}_3)\text{PH}$  by the elimination of isoprene.<sup>[6]</sup> The additional series of phosphines **113–115** features the flexible, bulky  $\text{CH}(\text{SiMe}_3)_2$  or  $\text{CH}(\text{SiMe}_2\text{Ph})_2$  substituents (Fig. 47). Whereas the steric modification of the *ortho*-alkyl substituents and varying substitution at the *para*-positions in **108–112** should have minimal perturbation of the electronics of the phosphorus centre, the alkyl substituents in **113–115** will have a more significant impact on the  $\sigma$ -electron donating character of the phosphines and corresponding phosphides. Although the phosphines **108**, **112** and **114** have previously been reported, the corresponding phosphides have not been used as ligands in tetraylenes.<sup>[7]</sup>



**Figure 46:** A series of diarylphosphines with increasing steric demands from left to right

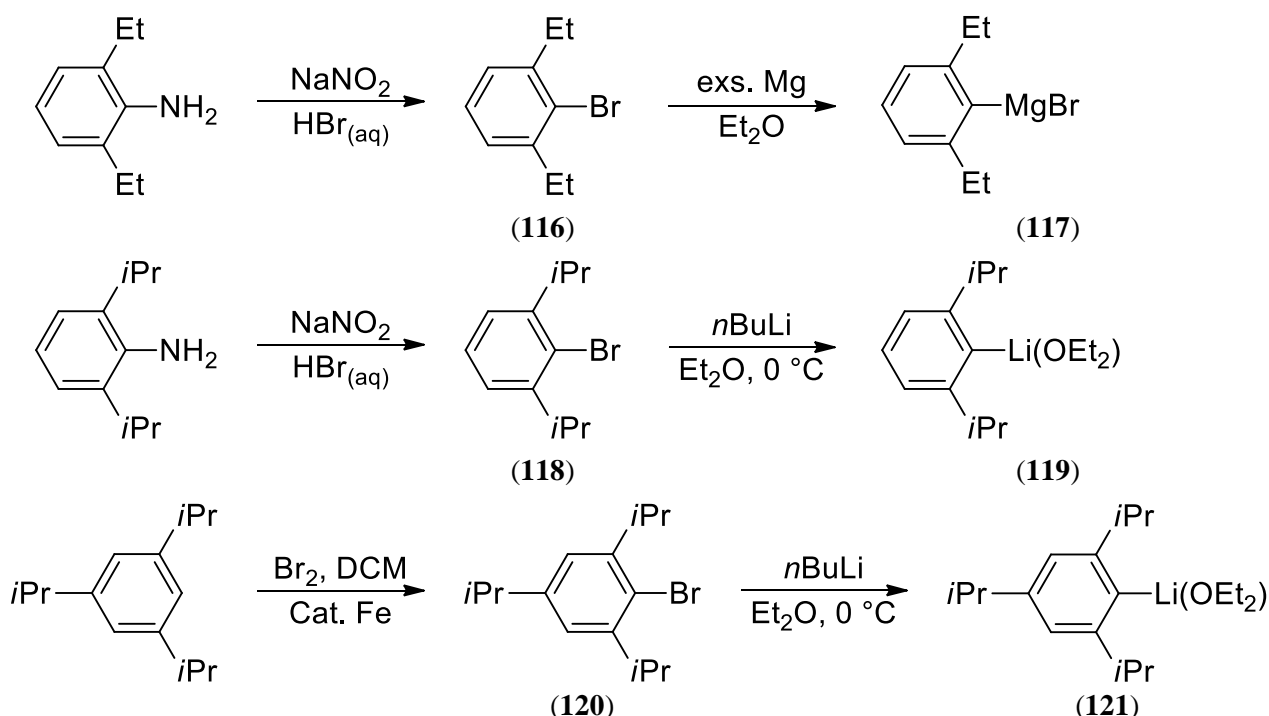


**Figure 47:** A series of phosphines with alkyl substituents

### 3.2.1 Synthesis of metalated precursors

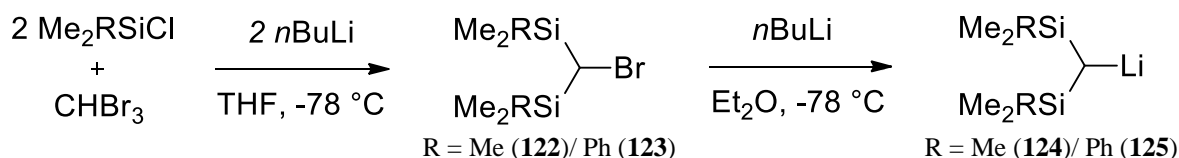
The aryl bromide precursors DepBr (**118**) and DippBr (**116**) were prepared from the respective anilines by a diazotisation reaction with sodium nitrite in concentrated hydrobromic acid [Dep = 2,6-Et<sub>2</sub>C<sub>6</sub>H<sub>3</sub>] (Scheme 15).<sup>[8]</sup> An electrophilic bromination of 2,4,6-triisopropylbenzene gave the more substituted aryl bromide TrippBr (**120**) [Tripp = 2,4,6-*i*PrC<sub>6</sub>H<sub>2</sub>].<sup>[9]</sup> The aryllithiums DippLi(OEt<sub>2</sub>) (**119**) and TrippLi(OEt<sub>2</sub>) (**121**) were prepared by a metal-halogen exchange of **118** or **120**, respectively, using *n*BuLi and isolated as clean, crystalline solids.<sup>[10]</sup> We attribute the comparatively low isolated yield of **121** (53%) to the increased solubility afforded by the *para*-isopropyl group.

It was not possible to isolate DepLi(OEt<sub>2</sub>)<sub>x</sub> cleanly as the crystals formed by storage at -78 °C had an extremely low melting point (approximately -70 °C). The use of DepLi prepared *in-situ* gave products that were contaminated with a significant amount of DepBr. However, the corresponding Grignard reagent, DepMgBr (**117**), proved to be a more successful transfer reagent as reactions with PCl<sub>3</sub> proceeded more cleanly and in good yield.



**Scheme 15:** Synthesis of aryl bromides and metalated precursors

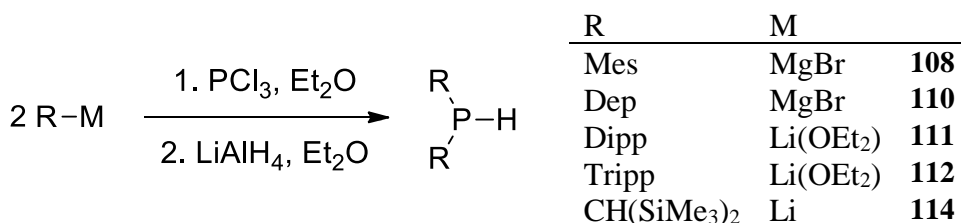
The bulky alkyl bromide precursors  $(\text{Me}_3\text{Si})_2\text{CHBr}$  **122** and  $(\text{Me}_2\text{PhSi})_2\text{CHBr}$  **123** were prepared by the addition of two equivalents of  $n\text{BuLi}$  to bromoform in the presence of the corresponding chlorosilane, at low temperature (Scheme 16).<sup>[11]</sup> Compounds **122** and **123** were metalated by a low temperature metal-halogen exchange with  $n\text{BuLi}$  to give the solvent-free alkyl lithiums  $(\text{Me}_3\text{Si})_2\text{CHLi}$  (**124**) and  $(\text{Me}_2\text{PhSi})_2\text{CHLi}$  (**125**) (Scheme 16).<sup>[11b, 12]</sup>



**Scheme 16:** Synthesis of  $(\text{Me}_2\text{RSi})_2\text{CHBr}$  and  $(\text{Me}_2\text{RSi})_2\text{CHLi}$

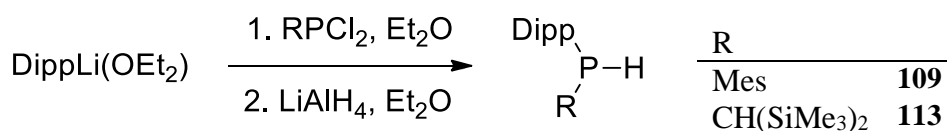
### 3.2.2 Synthesis of phosphines

The homoleptic phosphines were prepared by a metathesis reaction between two equivalents of the corresponding metalated alkyl or aryl precursors and  $\text{PCl}_3$ . The resulting secondary chlorophosphines were reacted *in situ* with  $\text{LiAlH}_4$ , with the exception of  $\{(\text{Me}_3\text{Si})_2\text{CH}\}_2\text{PCl}$  (**126**) that was first purified by distillation. Following an aqueous work-up, the secondary phosphines  $(\text{Mes})_2\text{PH}$  (**108**),  $(\text{Dep})_2\text{PH}$  (**110**),  $(\text{Dipp})_2\text{PH}$  (**111**),  $(\text{Tripp})_2\text{PH}$  (**112**) and  $\{(\text{Me}_3\text{Si})_2\text{CH}\}_2\text{PH}$  (**114**) were isolated with moderate to high yields (Scheme 17).



**Scheme 17:** Synthesis of homoleptic phosphines

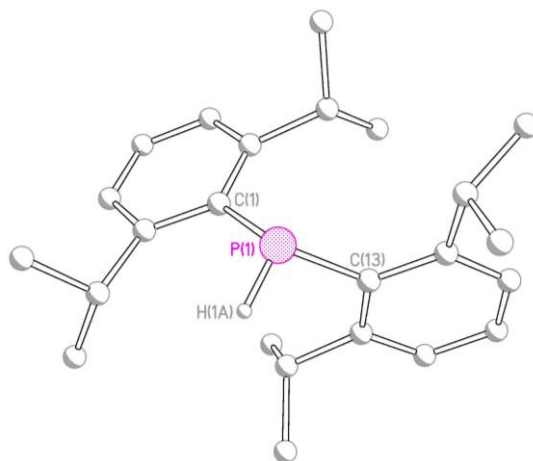
The heteroleptic phosphines were prepared in a similar method; (Mes)PCl<sub>2</sub> and {(Me<sub>3</sub>Si)<sub>2</sub>CH}PCl<sub>2</sub> (**127**) were reacted with one equivalent of DippLi(OEt)<sub>2</sub> and the resulting secondary chlorophosphines were reacted *in situ* with LiAlH<sub>4</sub>. Following an aqueous work up, the secondary phosphines (Dipp)(Mes)PH (**109**) and (Dipp){(Me<sub>3</sub>Si)<sub>2</sub>CH}PH (**113**) were isolated with good yields (Scheme 18).



**Scheme 18:** Synthesis of heteroleptic phosphines

### 3.3 Structural investigation of (Dipp)<sub>2</sub>P ligand system

We initially sought to investigate the effect of metal cation size on the aggregation of the alkali metal derivatives of the (Dipp)<sub>2</sub>P ligand. Single crystals of **111** were obtained by sublimation at 100 °C/ 10<sup>-3</sup> Torr and were characterised by X-ray crystallography (Fig. 48). The phosphorus-bound hydrogen and one isopropyl group were disordered over two positions. This structure served as a reference for the impact of metalation on the structure of the ligand framework.



**Figure 48:** Molecular structure of **111** with minor disorder components and C-bound H atoms omitted for clarity. Selected bond lengths (Å) and angles (°): P(1)–C(1) 1.8536(14), P(1)–C(13) 1.8527(15), C(1)–P(1)–C(13) 104.81(7).



Treatment of **111** with one equivalent of *n*BuLi, benzylsodium or benzylpotassium in THF gave the corresponding alkali metal complexes [(Dipp)<sub>2</sub>P]Li(THF)<sub>3</sub> (**128a**), {[(Dipp)<sub>2</sub>P]Na(THF)<sub>2</sub>}<sub>2</sub> (**129a**) and [(Dipp)<sub>2</sub>P]K(THF)<sub>4</sub> (**130a**) after crystallisation, respectively (Fig. 49). These complexes rapidly lose coordinated THF under vacuum to give the alternative solvates [(Dipp)<sub>2</sub>P]Li(THF)<sub>2</sub> (**128b**), [(Dipp)<sub>2</sub>P]Na(THF)<sub>1.5</sub> (**129b**) and the solvent-free complex [(Dipp)<sub>2</sub>P]K (**130b**), respectively. Single crystals of the adduct [(Dipp)<sub>2</sub>P]Na(TMEDA) (**129c**) were obtained by treatment of **111** with benzylsodium and PMDETA followed by crystallisation from *n*-hexane (Fig. 49).

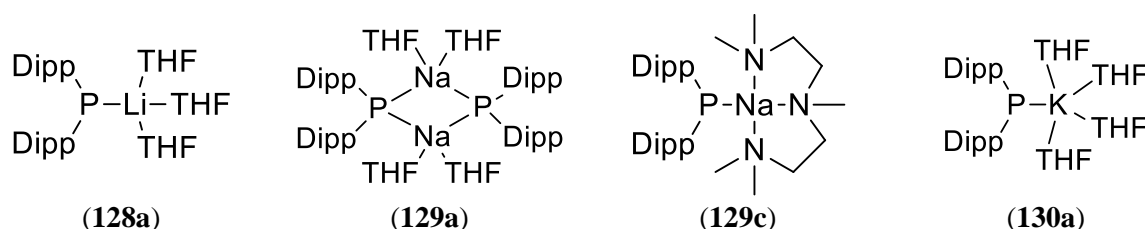


Figure 49: Alkali metal phosphides

### 3.3.1 Solid-state structures of [(Dipp)<sub>2</sub>P]Li(THF)<sub>3</sub> (**128a**), {[(Dipp)<sub>2</sub>P]Na(THF)<sub>2</sub>}<sub>2</sub> (**129a**), [(Dipp)<sub>2</sub>P]Na(TMEDA) (**129c**), [(Dipp)<sub>2</sub>P]K(THF)<sub>4</sub> (**130a**)

The molecular structures of **128a**, **129a**, **129c** and **130a** are shown in Figure 50, along with selected bond lengths and angles. Compound **129a** crystallises with two crystallographically independent molecules in the asymmetric unit that have almost identical conformations. The X-ray data for **130a** are of poor quality (R factor > 10), which may be due to the rapid loss of coordinated solvent. Compounds **128a** and **129c** have a similar structure that contains a metal ion coordinated by the phosphide ligand and the O or N atoms of the co-ligands, which results in the metal centre in **130a** having a distorted tetrahedral geometry, while the potassium centre in **130b** has a distorted trigonal bipyramidal geometry. In addition, there is one short Na...Me(N) contact in **129a** [Na(1)...C(32) 3.121(17) Å] and two short K...CH<sub>2</sub> contacts in **130a** [K(1)...C(29) 3.505(13), K(1)...C(37) 3.537(13) Å]. The P-M distances [2.482(3) (**128a**), 2.8745(12) (**129a**) and 3.221(2) Å (**130a**)] all lie at the shorter end of the range typical for such contacts.<sup>[2a]</sup> For example, the Li-P distances in [(Ph<sub>2</sub>P)Li(TMEDA)]<sub>2</sub> range from 2.574(19) to 2.629(20) Å,<sup>[13]</sup> while the Na-P distances in [(CyPH)Na(PMDETA)]<sub>2</sub> are 2.884(8) and 2.936(7) Å,<sup>[14]</sup> and the K-P distances in polymeric [(Mes\*PH)K]<sub>∞</sub> range from 3.181(2) to 3.357(2) Å.<sup>[15]</sup> The phosphorus centres in **128a** and **130a** have a planar geometry [sum of angles at P = 358.13(13) and 356.73(13)° (**128a**) and 359.97(20)° (**130a**)] while the phosphorus centre in **129a** has a pyramidal geometry [sum of angles at P = 322.73(17)°].

In contrast, compound **129c** crystallises as dimers with a planar  $\text{Na}_2\text{P}_2$  rhombus-shaped core. Each sodium ion is further coordinated by two molecules of THF in a distorted tetrahedral geometry. The Na-P distances [2.9246(8) and 3.0178(8) Å] are rather unsymmetrical, but are typical of Na-( $\mu$ -PR<sub>2</sub>) distances; for example, the Na-P distances in [EtSi{PNa(Si*i*Pr<sub>3</sub>)<sub>2</sub>}<sub>2</sub>]<sub>2</sub>·PhMe range from 2.778(2) to 3.3572(2) Å.

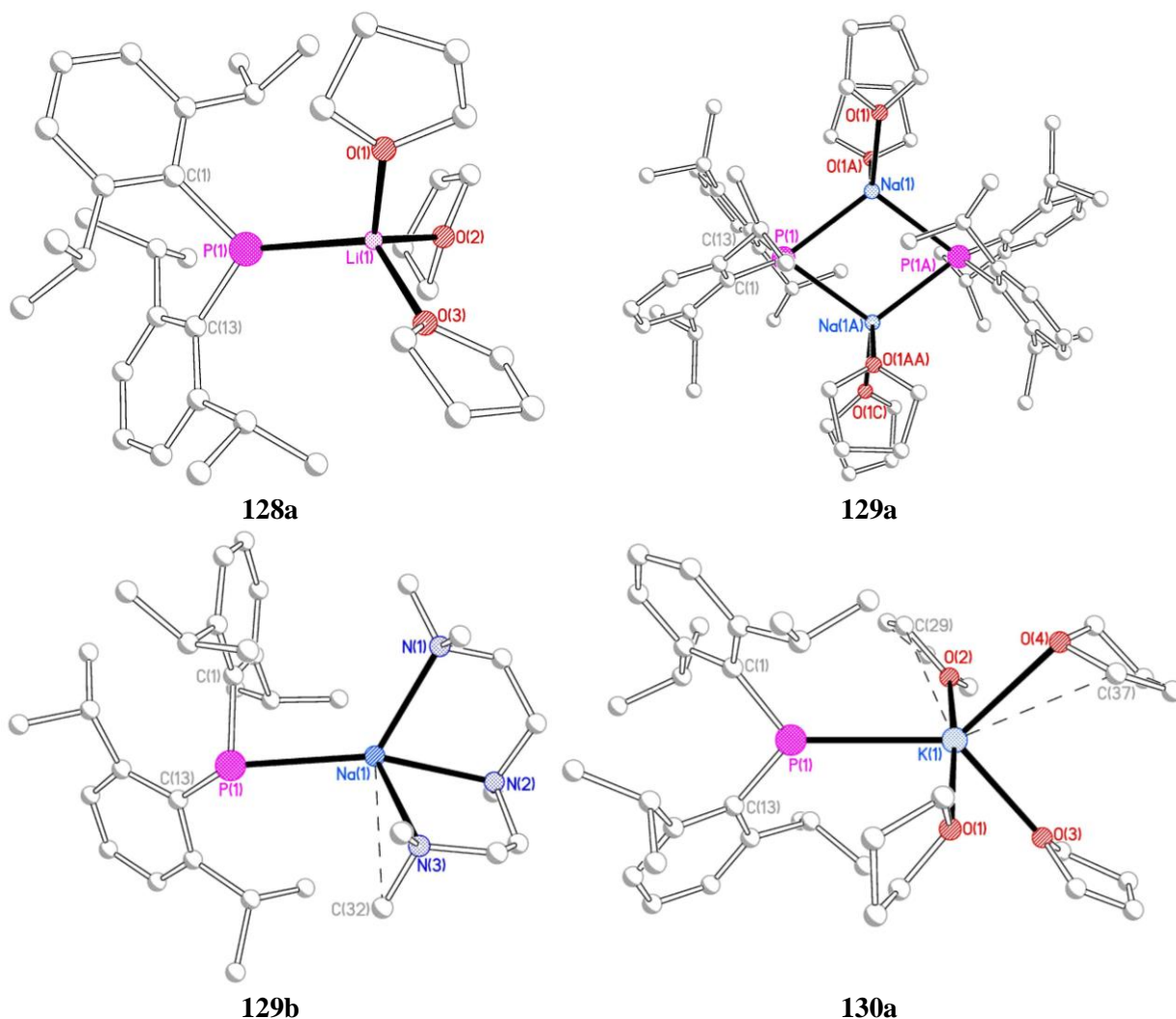


Figure 50: Molecular structures of **128a**, **129a**, **129b** and **130a** with H atoms and disorder components omitted for clarity. Selected bond lengths (Å) and angles (°):

**128a** (molecule 1) Li(1)–P(1) 2.482(3), Li(1)–O(1) 1.934(3), Li(1)–O(2) 1.948(3), Li(1)–O(3) 1.960(3), P(1)–C(1) 1.8474(15), P(1)–C(13) 1.8459(15), Li(1)–P(1)–C(1) 123.05(8), Li(1)–P(1)–C(13) 132.16(8), C(1)–P(1)–C(13) 102.92(6), (molecule 2) Li(2)–P(2) 2.498(3), Li(2)–O(4) 1.978(3), Li(2)–O(5) 1.934(3), Li(2)–O(6A) 1.922(18), P(2)–C(37) 1.8506(15), P(2)–C(49) 1.8467(15), Li(2)–P(2)–C(37) 129.85(8), Li(2)–P(2)–C(49) 124.14(8), C(37)–P(2)–C(49) 102.74(6);

**129a** Na(1)–P(1) 2.9246(8), Na(1)–P(1A) 3.0178(8), Na(1)–O(1) 2.3231(16), Na(1)–O(1A) 2.343(4), P(1)–C(1) 1.8672(17), P(1)–C(13) 1.8622(16), Na(1)–P(1)–Na(1A) 73.83(2), P(1)–Na(1)–P(1A) 106.17(2), C(1)–P(1)–C(13) 100.84(7);

**129b** Na(1)–P(1) 2.8745(12), Na(1)–N(1) 2.509(9), Na(1)–N(2) 2.525(10), Na(1)–N(3) 2.472(10), Na(1)···C(32) 3.121(17), P(1)–C(1) 1.856(3), P(1)–C(13) 1.847(3), Na(1)–P(1)–C(1) 85.70(8), Na(1)–P(1)–C(13) 132.75(9), C(1)–P(1)–C(13) 104.28(12);

**130a** K(1)–P(1) 3.221(2), K(1)–O(1) 2.696(7), K(1)–O(2) 2.698(7), K(1)–O(3) 2.706(5), K(1)–O(4) 2.817(6), K(1)···C(29) 3.505(13), K(1)···C(37) 3.537(13), P(1)–C(1) 1.844(3), P(1)–C(13) 1.841(3), K(1)–P(1)–C(1) 126.47(10), K(1)–P(1)–C(13) 130.00(10), C(1)–P(1)–C(13) 103.50(14).

Surprisingly, the metalation of **111** has little impact on the gross structure of the (Dipp)<sub>2</sub>P framework: the P-C distances in **111** [1.8536(14) and 1.8257(15) Å] are similar to the P-C distances in **128a**, **129a**, **129c** and **130a** [range 1.841(3)-1.8672(17) Å] and the corresponding C(1)-P(1)-C(13) angle in **111** [101.81(17)°] is similar to the corresponding angles in **128a**, **129a**, **129c** and **130a** [range 100.84(3)-104.28(12)°].

### 3.3.2 Solution behaviour of **128b**, **129b**, **129c** and **130b**

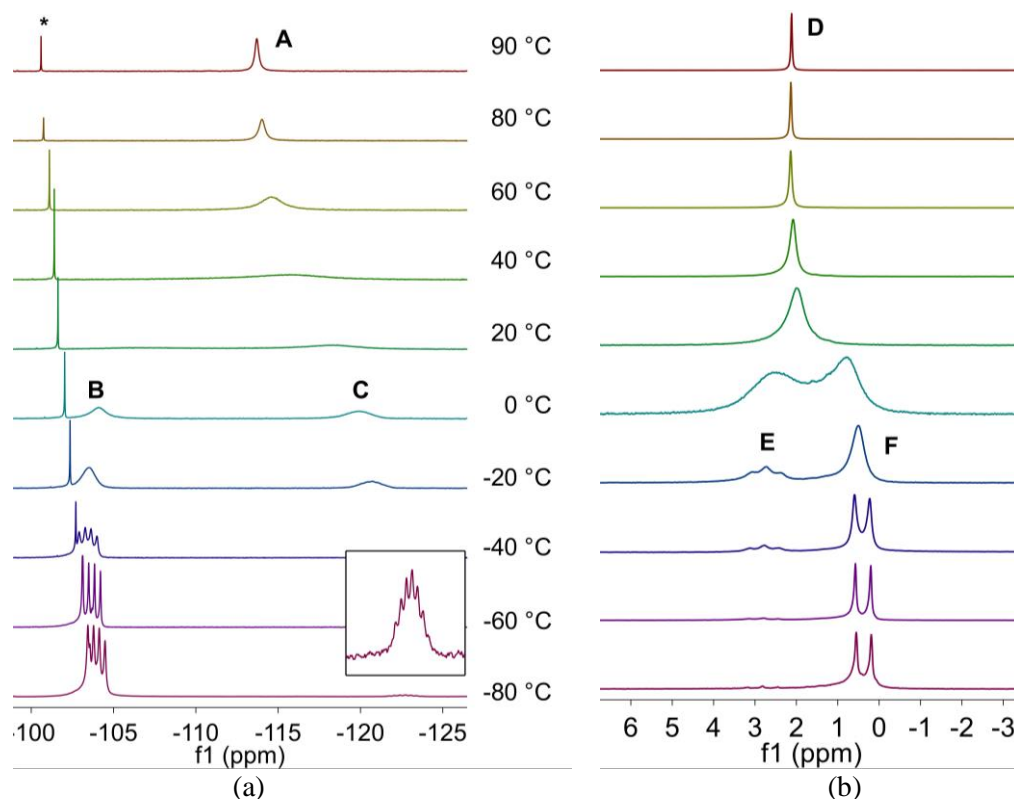
It was not possible to obtain NMR spectra of **128a**, **129a** and **130a** because of the rapid loss of coordinated solvent from the bulk material under vacuum. The <sup>1</sup>H, <sup>31</sup>P{<sup>1</sup>H} and <sup>7</sup>Li NMR spectra of **128b** and **129b** in toluene suggest that there is dynamic behaviour at room temperature while the corresponding NMR spectra of **129c** do not display any temperature-dependent behaviour. Compound **130b** has limited solubility in non-coordinating solvents so it was not possible to do a comparable variable-temperature NMR study and this compound did not display any evidence for dynamic behaviour in THF.

### 3.3.3 Dynamic behaviour of [(Dipp)<sub>2</sub>P]Li(THF)<sub>2</sub> (**128b**)

At 90 °C the <sup>31</sup>P{<sup>1</sup>H} NMR spectrum of **128b** in d<sub>8</sub>-toluene consists of a singlet at -113.7 ppm (**A**). As the temperature is reduced the signal broadens and decoalesces, at 0 °C, into two broad signals at -106.0 (**B**) and -118.3(**C**) ppm, respectively. As the temperature is reduced further, the signals sharpen and change in intensity, with peak **B** increasing in relative intensity at the expense of peak **C**. At -80 °C the signals are resolved into a 1:1:1:1 quartet (*J*<sub>PLi</sub> = 70.7 Hz) and a 1:2:3:4:3:2:1 septet (*J*<sub>PLi</sub> = 67.1 Hz) at -104.0 and -122.7 in a 1:0.05 ratio, respectively. Similarly, at 90 °C the <sup>7</sup>Li NMR spectrum of **128b** consists of a sharp singlet at 2.1 ppm (**D**). As the temperature is reduced, this signal broadens and decoalesces into two signals at 2.5 (**E**) and 0.8 ppm (**F**) ppm at 0 °C. These signals sharpen and resolve into a triplet and a doublet, respectively, as the temperature is reduced. At -80 °C the spectrum consists of a triplet (*J*<sub>PLi</sub> = 71.4 Hz) and a doublet (*J*<sub>PLi</sub> = 68.9 Hz) at 2.8 and 0.4 ppm in the approximate ratio of 0.08:1.

The variable temperature <sup>31</sup>P{<sup>1</sup>H} and <sup>7</sup>Li NMR spectra of **128b** are consistent with a dynamic equilibrium between monomeric **128b** and a dimeric species of the form (THF)<sub>n</sub>Li{μ-P(Dipp)<sub>2</sub>}<sub>2</sub>Li(THF)<sub>n</sub>. The exchange between these two species is rapid above room temperature. At lower temperatures, the dimer appears to be disfavoured and the monomer predominates. The loss of coordinated THF under vacuum of **128a** must be

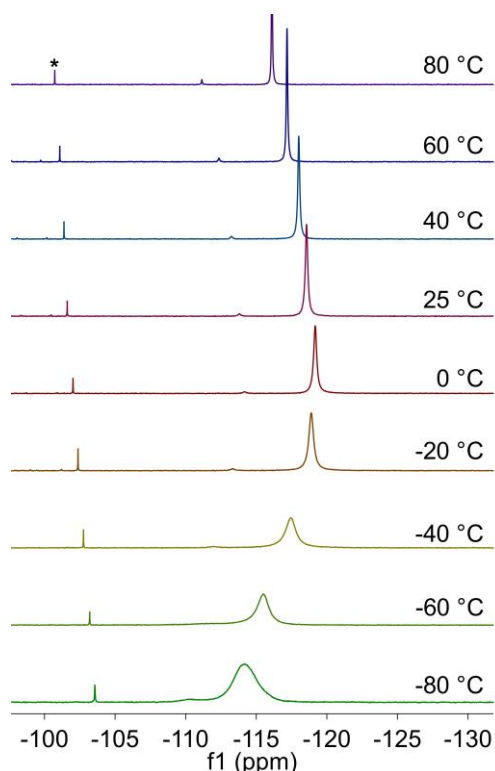
associated with the formation of a dimer as the resulting lithium ions would be three-coordinate as monomers. However, the (Dipp)<sub>2</sub>P ligand appears to have sufficient steric bulk to stabilise the monomeric species with a three-coordinate lithium ion. This behaviour is unusual as low temperatures typically favour the formation of higher aggregates. The time-averaged <sup>31</sup>P{<sup>1</sup>H} NMR spectrum of **128b** at 90 °C suggests equal proportions of monomer and dimer in equilibrium.



**Figure 51:** Variable-temperature <sup>31</sup>P{<sup>1</sup>H} and <sup>7</sup>Li NMR spectra of **128b** in d<sub>8</sub>-toluene (\* free phosphine **111**)

### 3.3.4 Dynamic behaviour of [(Dipp)<sub>2</sub>P]Na(THF)<sub>1.5</sub> (**129b**)

The variable-temperature <sup>31</sup>P{<sup>1</sup>H} spectra of **129b** exhibit behaviour consistent with one or more exchange process(es) occurring. At 80 °C the <sup>31</sup>P{<sup>1</sup>H} NMR spectrum of **129b** consists of a singlet at -116.1 ppm. As the temperature is reduced, the signal first moves to a slightly higher field, until, at 0 °C, this signal starts to broaden and move to low field. At -80 °C the spectrum consists of a broad singlet at -114.1 ppm (FWHM 420 Hz). These spectra are consistent with a dynamic equilibrium between a dimer with a structure similar to the solid-state structure of **129a** and a monomeric or higher oligomeric species.



**Figure 52:** Variable-temperature  $^{31}\text{P}\{^1\text{H}\}$  NMR spectra of **129b** in  $d_8$ -toluene (\* free phosphine **111**)

### 3.4 The effect of steric demand on the phosphorus centre in lithium phosphides

In addition, we sought to investigate the relationship between the sterics properties of the corresponding lithium phosphides of **108**, **109**, **110** and **113** and their aggregation behaviour. While comparison between the relative steric properties of the aryl substituents are straightforward, the steric comparison between Dipp and the flexible  $(\text{Me}_3\text{Si})\text{CH}$  group is more ambiguous. The comparison between the  $^{31}\text{P}\{^1\text{H}\}$  and  $^1\text{H}$  NMR spectra of **128a** and those of  $[(\text{Dipp})\{(\text{Me}_3\text{Si})_2\text{CH}\}\text{P}]\text{Li}$  may provide an insight as phosphides with reduced steric demands from the substituents have an increased tendency to form aggregates.

Treatment of **109** with  $n\text{BuLi}$  gave the corresponding lithium phosphide  $[(\text{Dipp})(\text{Mes})\text{P}]\text{Li}(\text{THF})_3$  (**131a**) after crystallisation. This compound rapidly loses solvent when exposed to vacuum to give the alternative solvate  $[(\text{Dipp})(\text{Mes})\text{P}]\text{Li}(\text{THF})_2$  (**131b**), as judged by  $^1\text{H}$  NMR spectroscopy. Similarly, treatment of **108** with  $n\text{BuLi}$  in THF gave  $[(\text{Mes})_2\text{P}]\text{Li}(\text{THF})_3$  (**132a**) or the dimer  $[(\text{Mes})_2\text{P}]_2\text{Li}_2(\text{THF})_2(\text{OEt}_2)$  (**132b**) after crystallisation from  $n$ -hexane or diethyl ether, respectively. The alternative solvate  $[(\text{Mes})_2\text{P}]_2\text{Li}_2(\text{OEt}_2)_2$  has previously been isolated by the deprotonation of **108** with  $n\text{BuLi}$  in  $\text{Et}_2\text{O}$ ; this compound is dimeric in the solid-state and in solution.<sup>[16]</sup> Compounds **132a** and **132b** rapidly lost solvent when exposed to vacuum to give the same alternative solvate  $[(\text{Mes})_2\text{P}]\text{Li}(\text{THF})$  (**132c**) as an orange powder. Treatment of **110** with  $n\text{BuLi}$  in THF gave

poor quality crystals of  $[(\text{Dep})_2\text{P}]\text{Li}(\text{THF})_3$  (**133**) after crystallisation from a mixture of  $\text{Et}_2\text{O}$  and THF. Unfortunately, no material for further analysis was obtained due to the very low melting point of these crystals (approximately  $-25\text{ }^\circ\text{C}$ ). Although the structure of this compound cannot be discussed in detail, the data were sufficiently good to establish connectivity of the compound, which is similar to that of **132a** and **132b**.

The initial reaction between **113** and  $n\text{BuLi}$  in THF at room temperature gave a pale yellow solution that contained a small amount (approx. 10%) of the corresponding phosphide,  $[(\text{Dipp})\{(\text{Me}_3\text{Si})_2\text{CH}\}\text{P}]\text{Li}$ , relative to the starting phosphine, as judged by  $^{31}\text{P}$  NMR spectroscopy. However, the addition of  $n\text{BuLi}$  to a solution of **113** in THF at  $-78\text{ }^\circ\text{C}$ , followed by allowing the resulting mixture to warm to room temperature gave a dark red solution, from which single crystals of  $[(\text{Dipp})\{(\text{Me}_3\text{Si})_2\text{CH}\}\text{P}]\text{Li}(\text{THF})_3$  (**134**) were obtained after crystallisation from a mixture of  $\text{Et}_2\text{O}$  and light petroleum; this compound was stable towards solvent loss under vacuum. We attribute the reactivity of **113** with  $n\text{BuLi}$  at room temperature to the formation of the phosphinyl radical  $(\text{Dipp})\{(\text{Me}_3\text{Si})_2\text{CH}\}\text{P}^\cdot$ , which subsequently acquires a hydrogen from the solvent to reform the starting phosphine **113**. The  $(\text{Me}_3\text{Si})_2\text{CH}$  group is known to stabilise  $P$ -centred radicals; the related phosphinyl radical  $\{(\text{Me}_3\text{Si})_2\text{CH}\}_2\text{P}^\cdot$  is persistent in solution.<sup>[17]</sup> At low temperatures, the formation of the radical may be suppressed and so the deprotonation predominates, to give the corresponding lithium phosphide  $[(\text{Dipp})\{(\text{Me}_3\text{Si})_2\text{CH}\}\text{P}]\text{Li}$ .

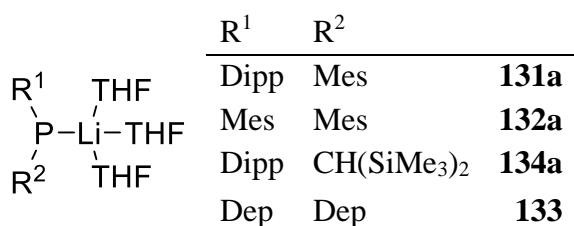


Figure 53

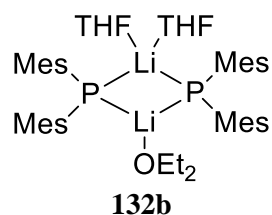


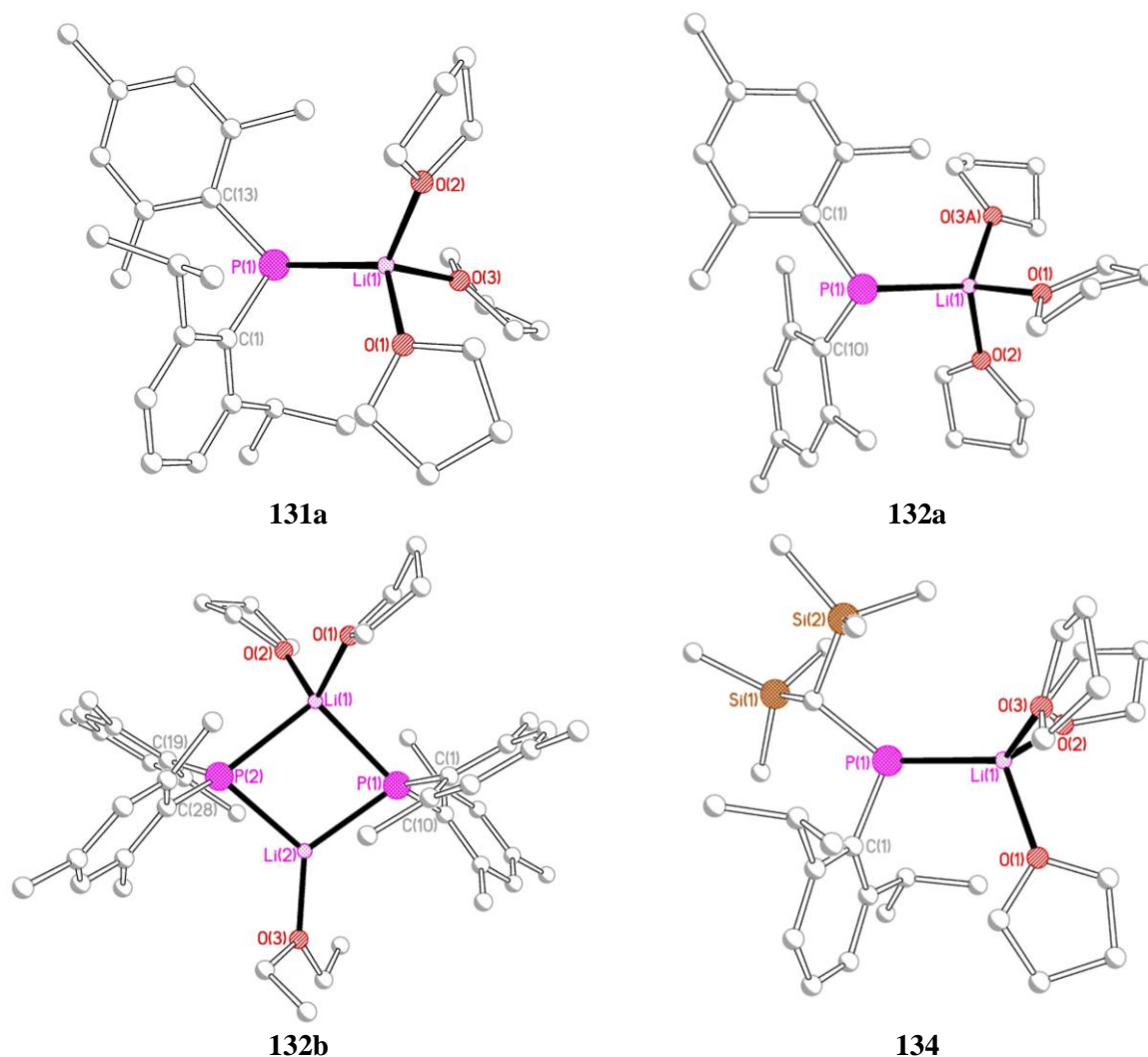
Figure 54

### 3.4.1 Solid-state structures of [(Dipp)(Mes)P]Li(THF)<sub>3</sub> (**131a**), [(Mes)<sub>2</sub>P]Li(THF)<sub>3</sub> (**132a**), [(Mes)<sub>2</sub>P]<sub>2</sub>Li<sub>2</sub>(THF)<sub>2</sub>(OEt<sub>2</sub>) (**132b**) and [(Dipp){(Me<sub>3</sub>Si)<sub>2</sub>CH}P]Li(THF)<sub>3</sub> (**134**)

The molecular structures of **131a**, **132a**, **132b** and **134** are shown in Figure 55, along with selected bond lengths and angles. Compounds **131a**, **132a** and **134** crystallise as discrete monomers in which the lithium ions are coordinated by the phosphide phosphorus atoms and the oxygen atoms of three THF molecules in a distorted tetrahedral geometry. The phosphorus centres in **131a**, **132a** and **134** all adopt a pyramidal geometry [sum of angles at P = 331.41(17) (**131a**), 330.58(17) (**132a**) and 337.03(18)° (**134**)]. Compound **134** is essentially isoskeletal with the less sterically hindered derivative [{(Me<sub>3</sub>Si)<sub>2</sub>CH}(Ph)P]Li(THF)<sub>3</sub> (**135**).<sup>[2k]</sup>

The P-Li distances in **131a**, **132a** and **134** [2.572(3), 2.552(3) and 2.563(3) Å, respectively] are similar to previously reported P-Li distances.<sup>[2a]</sup> Surprisingly, the P-Li distances for the essentially isostructural diarylphosphides **128a**, **131a** and **132a** do not correlate with the steric bulk of the phosphide ligands and decrease in the order **132a** > **131a** > **128a**. The shortest P-Li distance occurs in the complex with the most sterically demanding aryl substituents. The P-Li distance in **134** is slightly shorter than that of **132a**.

In contrast to **131a**, **132a** and **134**, **132b** crystallises as a phosphide-bridged dimer with an essentially planar P<sub>2</sub>Li<sub>2</sub> core. This structure is similar to that of **129a** although the lithium ions in **131a** are in distinct environments that are each coordinated by the two bridging phosphides: Li(1) is further coordinated by two molecules of THF in a distorted tetrahedral geometry, while Li(2) is coordinated to a single molecule of diethyl ether in a trigonal planar geometry. The Li(1)-P distances [2.609(4) and 2.684(4) Å] are significantly longer than the Li(2)-P distances [2.513(4) and 2.518(4) Å] and the P(1)-Li(2)-P(2) angle [97.46(12)°] is considerably smaller than the P(1)-Li(2)-P(2) angle [104.53(13)°], consistent with the lower coordination number at Li(2).



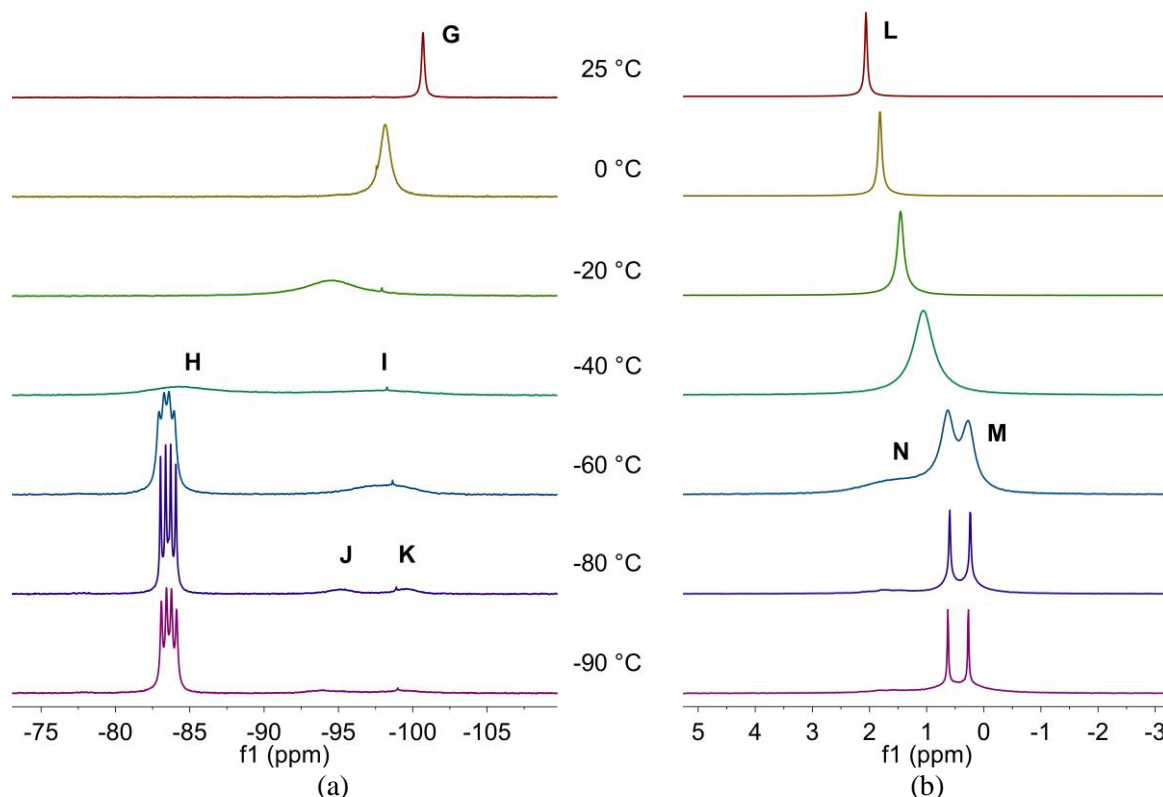
**Figure 55:** Molecular structures of **131a**, **132a**, **132b** and **134** with H atoms and disorder components omitted for clarity. Selected bond lengths (Å) and angles (°): **131a** Li(1)–P(1) 2.572(3), Li(1)–O(1) 1.963(4), Li(1)–O(2) 1.950(4), Li(1)–O(3) 1.999(4), P(1)–C(1) 1.854(2), P(1)–C(13) 1.832(2), Li(1)–P(1)–C(1) 99.42(10), Li(1)–P(1)–C(13) 127.65(10), C(1)–P(1)–C(13) 104.34(9); **132a** Li(1)–P(1) 2.552(3), Li(1)–O(1) 1.944(3), Li(1)–O(2) 1.954(4), Li(1)–O(3B) 1.944(10), P(1)–C(1) 1.8164(19), P(1)–C(10) 1.829(2), Li(1)–P(1)–C(1) 122.48(10), Li(1)–P(1)–C(10) 97.81(10), C(1)–P(1)–C(10) 110.29(9); **132b** Li(1)–P(1) 2.609(4), Li(1)–P(2) 2.684(4), Li(2)–P(1) 2.513(4), Li(2)–P(2) 2.518(4), P(1)–C(1) 1.8365(18), P(1)–C(10) 1.836(2), P(2)–C(19) 1.8391(19), P(2)–C(28) 1.840(2), P(1)–Li(1)–P(2) 97.46(12), P(1)–Li(2)–P(2) 104.53(13), Li(1)–P(1)–Li(2) 79.69(12), Li(1)–P(2)–Li(2) 78.18(12); **134** Li(1)–P(1) 2.563(3), Li(1)–O(1) 2.000(4), Li(1)–O(2) 1.982(4), Li(1)–O(3) 1.990(4), P(1)–C(1) 1.851(2), P(1)–C(13) 1.909(2), C(1)–P(1)–C(13) 105.24(10), C(1)–P(1)–Li(1) 103.86(11), (C13)–P(1)–Li(1) 127.93(11).

### 3.4.2 Solution-state NMR behaviour of [(Dipp)(Mes)P]Li(THF)<sub>2</sub> (**131b**)

At room temperature the  $^{31}\text{P}\{^1\text{H}\}$  NMR spectrum of **131b** in  $d_8$ -toluene consists of a singlet at -100.7 ppm (**G**). As the temperature is reduced, this peak broadens and moves downfield until, at -40 °C, it decoalesces into two broad signals at -97.5 ppm (**H**) and -88.4 ppm (**I**). At lower temperatures, peak **H** sharpens into a well-resolved quartet ( $J_{\text{PLi}} = 69.5$  Hz), while peak **I** decoalesces into two low intensity, broad signals at approximately -99 (**J**) and -94 ppm (**K**) (approximate ratio of **H**:**J**:**K** at -80 °C 12:1:1). The room temperature  $^7\text{Li}$  NMR

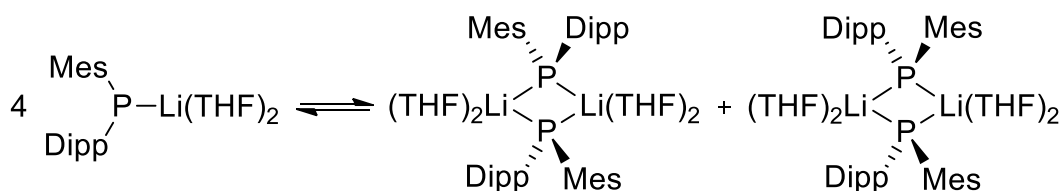


spectrum of **131b** at room temperature consists of a singlet at 2.1 ppm (**L**), which broadens and moves upfield as the temperature is reduced, until, at -60 °C, it decoalesces into a broad signal at approximately 1.2 ppm (**N**) and a broad doublet at 0.4 ppm (**M**). Below this temperature, peak **N** decreases in relative intensity and peak **M** sharpens, until, at -80 °C, the spectrum consists of an approximate triplet at 1.8 ppm (**N**,  $J_{\text{PLi}} = 48$  Hz) and a sharp doublet at 0.4 ppm (**M**,  $J_{\text{PLi}} = 69.5$  Hz).



**Figure 56:** Variable-temperature (a)  $^{31}\text{P}\{^1\text{H}\}$  and (b)  $^7\text{Li}$  NMR data of **131b** in  $d_8$ -toluene

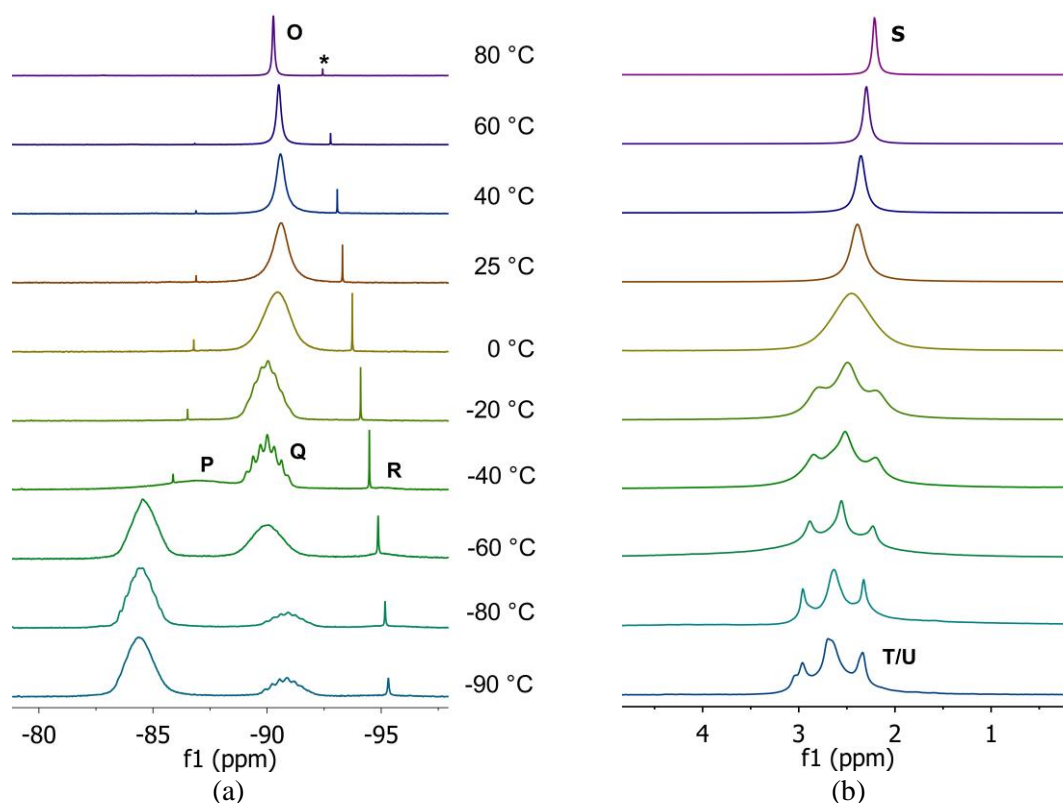
The variable-temperature  $^{31}\text{P}\{^1\text{H}\}$  and  $^7\text{Li}$  NMR spectra of **131b** are consistent with a dynamic equilibrium between monomeric (**H/M**) and dimeric (**J/K**, **N**) species in which the monomeric species is favoured at low temperatures (Scheme 19). We assign the two higher field signals **J** and **K** to the *cis* and *trans* isomers of the dimer, which appear to have equal probability. While this behaviour is similar to that observed for **128b**, the time-averaged room temperature  $^{31}\text{P}\{^1\text{H}\}$  NMR signal for **131b** lies to higher field than the arithmetical mean of the monomer and dimer signals and suggests that the dimeric form predominates at room temperature for this compound, even though this species is only observed in low concentrations at low temperatures.



**Scheme 19:** Dynamic behaviour exhibited by **131b** in solution

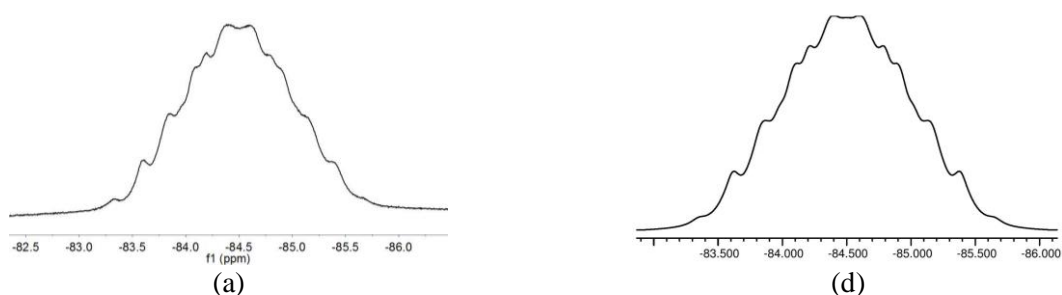
### 3.4.3 Solution-state NMR behaviour of $[(\text{Mes})_2\text{P}]\text{Li}(\text{THF})_3$ (**132c**)

At 80 °C the  $^{31}\text{P}\{^1\text{H}\}$  NMR spectrum of **132c** in  $d_8$ -toluene consists of a singlet (**O**) at -90.3 ppm. As the temperature is reduced, this peak broadens and moves to lower field. At -40 °C this peak decoalesces into a broad signal (**P**) at -86.9 ppm, a well-resolved septet (**Q**) at -90.0 ppm and a very low intensity broad signal (**R**) at approximately -95.5 ppm. As the temperature is further reduced, peak **P** moves to a lower field and resolves into a complex multiplet, while peak **Q** broadens and then sharpens again, and peak **R** decreases in intensity. At -80 °C the spectrum consists of a complex multiplet at -84.4 ppm and a broad septet at -91.0 ppm. At 80 °C the  $^7\text{Li}$  NMR spectrum consists of a singlet (**S**) at 2.2 ppm. As the temperature is reduced, this signal moves slightly downfield and decoalesces into a complex multiplet. At -80 °C the signal appears to consist of two overlapping signals (**T/U**).

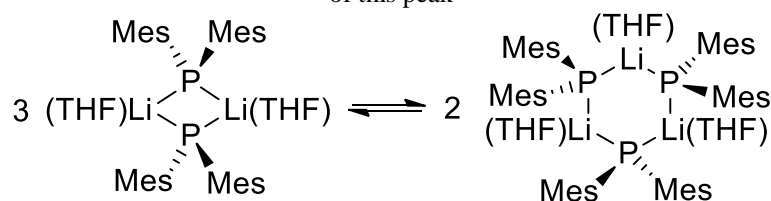


**Figure 57:** Variable-temperature (a)  $^{31}\text{P}\{^1\text{H}\}$  and (b)  $^7\text{Li}$  NMR data of **132c** in  $d_8$ -toluene (\* free phosphine 108); (c) expansion of the low field  $^{31}\text{P}\{^1\text{H}\}$  NMR signal at -80 °C and (d) simulation of this peak

While the low-field peak **P** observed in the  $^{31}\text{P}\{^1\text{H}\}$  NMR spectrum of **132c** at  $-80\text{ }^\circ\text{C}$  is inconsistent with a monomer or dimer it has a similar lineshape to the signal observed for the proposed trimer  $[(\text{PhPH})\text{Li}(\text{OEt}_2)]_n$  at  $-73\text{ }^\circ\text{C}$  in diethyl ether, which has calculated coupling constants of  $J_{\text{PLi}} = 39\text{ Hz}$ ,  $J_{\text{PP}} = 40\text{ Hz}$ .<sup>[18]</sup> A simulation of a cyclic trimer with  $^1J_{\text{PLi}} = 60\text{ Hz}$ ,  $^2J_{\text{PP}} = 46\text{ Hz}$  and  $^3J_{\text{PLi}} < 5\text{ Hz}$  is consistent with the observed peak **P** (Fig. 58). Although we cannot rule out higher oligomers, simulations based on tetrameric oligomers did not match the observed peak. Therefore, the variable-temperature  $^{31}\text{P}\{^1\text{H}\}$  and  $^7\text{Li}$  NMR spectra of **132c** are consistent with a dynamic equilibrium between a dimer, a cyclic trimer (Scheme 20) and a further unidentified species, which is present only in low concentration.



**Figure 58:** (a) A expansion of the low field  $^{31}\text{P}\{^1\text{H}\}$  NMR signal exhibited by **132c** at  $-80\text{ }^\circ\text{C}$  and (b) simulation of this peak



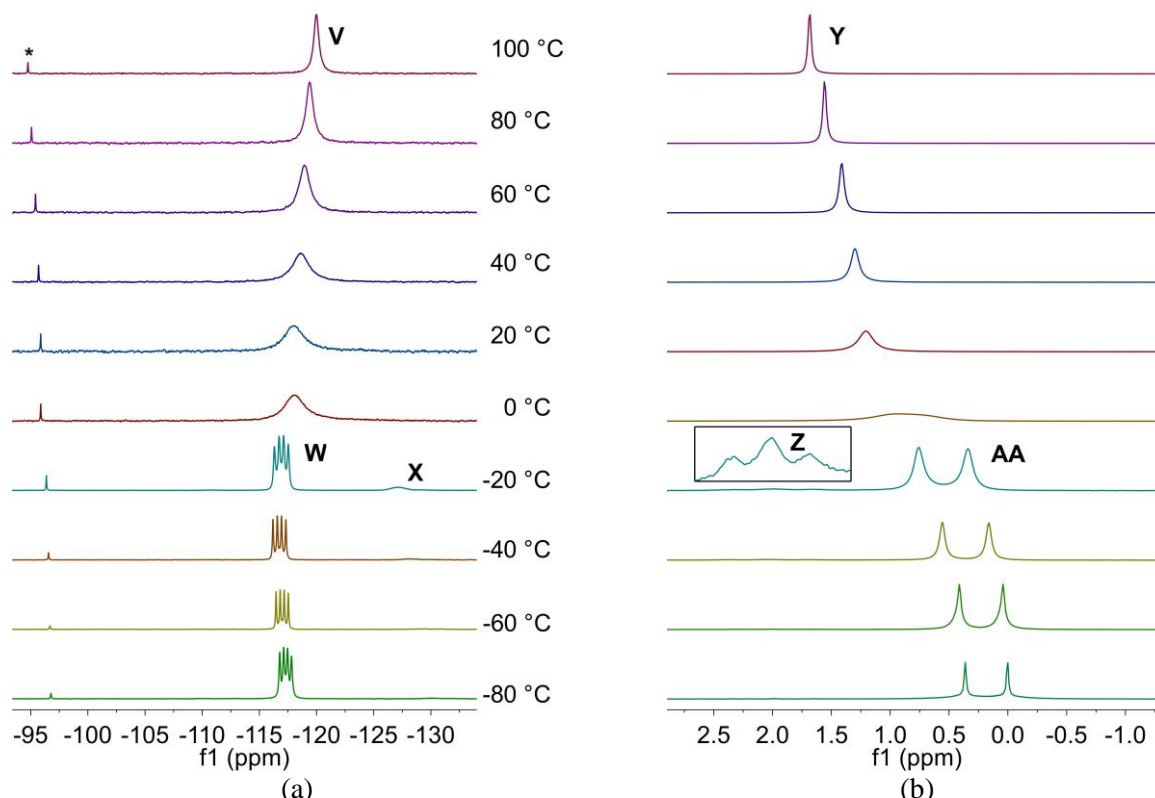
**Scheme 20:** Dynamic behaviour exhibited by **132c** in solution

There is a single example of a lithium phosphide with a crystallographically characterised cyclic trimeric structure: the sterically hindered tetrasilaphosphide  $[[i\text{Pr}_2\text{Si}]_4\text{P}]\text{Li}_3$  (**136**) adopts a triangle structure in the solid state.<sup>[19]</sup> Unfortunately, there are limited NMR data of **136** and the  $^{31}\text{P}\{^1\text{H}\}$  NMR spectrum consists of a broad singlet at room temperature, which prevents comparisons with our data.

### 3.4.4 Solution-state NMR behaviour of $[(\text{Dipp})\{(\text{Me}_3\text{Si})_2\text{CH}\}\text{P}]\text{Li}(\text{THF})_3$ (**134**)

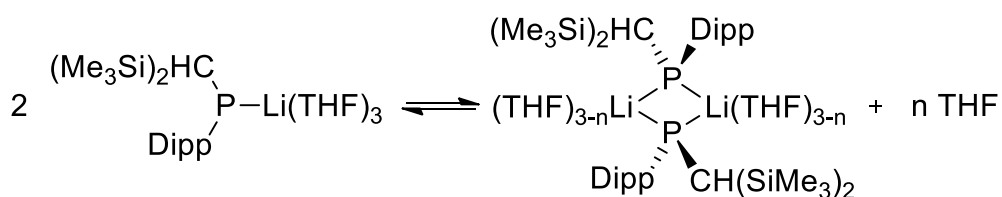
At  $100\text{ }^\circ\text{C}$  the  $^{31}\text{P}\{^1\text{H}\}$  NMR spectrum of **134** consists of a singlet at  $-120.0\text{ ppm}$  (**V**). As the temperature is reduced the signal broadens and moves slightly downfield. At  $-20\text{ }^\circ\text{C}$  the signal decoalesces into a well resolved 1:1:1:1 quartet ( $J_{\text{PLi}} = 81\text{ Hz}$ ) and a broad multiplet at  $116.9$  (**W**) and  $127.2\text{ ppm}$  (**X**), respectively, in an 11:1 ratio. As the temperature is reduced further, the lower field signal **W** moves slightly upfield and sharpens while the higher field signal **X** rapidly loses intensity. The  $^7\text{Li}$  NMR spectrum of **134** at  $100\text{ }^\circ\text{C}$  consists of a singlet

at 1.7 ppm (**Y**). As the temperature is reduced, this signal broadens to an extremely broad signal at 0 °C. At -20 °C, this signal decoalesces into a low intensity triplet (**Z**,  $J_{\text{PLi}} = 66.8$  Hz) and a well-resolved doublet (**AA**,  $J_{\text{PLi}} = 77.0$  Hz) at 2.0 and 0.25 ppm, respectively. At lower temperatures, peak **Z** vanishes in intensity.



**Figure 59:** Variable-temperature (a)  $^{31}\text{P}\{^1\text{H}\}$  and (b)  $^7\text{Li}$  NMR spectra of **134** in  $d_8$ -toluene (\* free phosphine **113**)

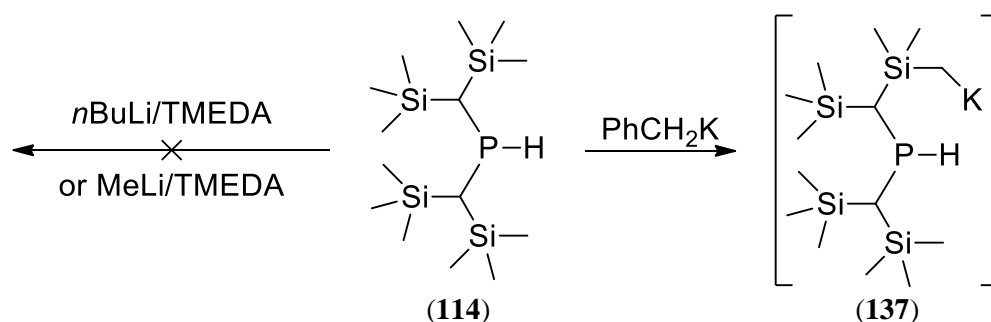
The variable temperature  $^{31}\text{P}\{^1\text{H}\}$  and  $^7\text{Li}$  NMR spectra of **134** are consistent with a dynamic equilibrium between monomeric **134** and dimeric species of the form  $(\text{THF})_{3-n}\text{Li}_2\{\mu\text{-P}(\text{Dipp})\{\text{CH}(\text{SiMe}_3)_2\}_2\text{Li}(\text{THF})_{3-n}\}$ , as shown in Scheme 21. In contrast to **131b**, only a single dimeric species is observed at low temperatures. We propose this species is the *trans* isomer, with respect to the  $\text{CH}(\text{SiMe}_3)_2$  or Dipp groups, as the bulky  $\text{CH}(\text{SiMe}_3)_2$  group may destabilise the *cis* isomer. This behaviour is similar to that observed for **128b** and **131b**. The time-averaged  $^{31}\text{P}\{^1\text{H}\}$  NMR signal of **134** at room temperature suggests the monomer is the predominant species at this temperature.



**Scheme 21:** Dynamic behaviour exhibited by **134** in solution

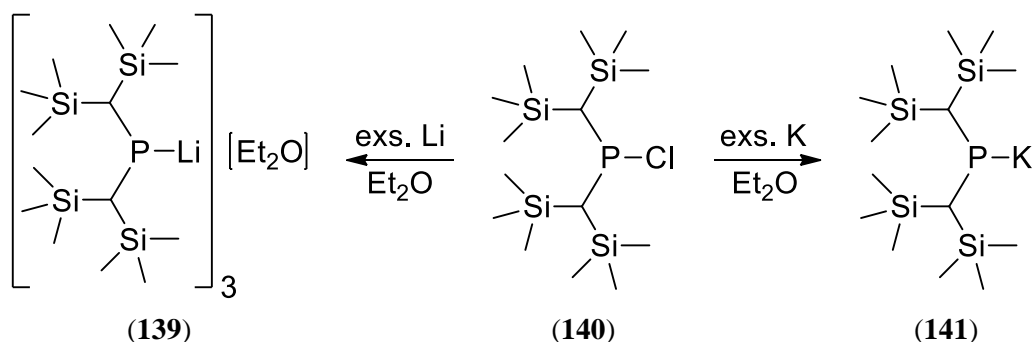
### 3.5 Attempted synthesis of dialkylphosphides

The synthesis of the dialkylphosphides  $\{(\text{Me}_3\text{Si})_2\text{CH}\}_2\text{PM}$  and  $\{(\text{Me}_2\text{Ph})_2\text{CH}\}_2\text{PM}$  proved to be more synthetically challenging than the diarylphosphides discussed previously. The phosphine **114** was inert towards deprotonation by  $n\text{BuLi/TMEDA}$  or  $\text{MeLi/TMEDA}$ , as judged by  $^{31}\text{P}$  NMR spectroscopy, which suggests the P-bound proton is too sterically encumbered by the alkyl ligands for the bases to access (Scheme 22). The addition of benzylpotassium to a solution of **114** in THF generated a pale yellow solution, which exhibited a single signal at -49.3 ppm (d,  $J_{\text{PH}} = 182$  Hz) in its  $^{31}\text{P}$  NMR spectrum. The large PH coupling of this new species suggests the P-H bond remains intact and that deprotonation may have occurred at a  $\text{SiMe}_3$  group, possibly forming the carbanion **137** (Scheme 22). Similar reactivity has been observed in the deprotonation of  $(\text{Me}_3\text{Si})_3\text{CH}$  with a series of alkylolithium reagents, where the size and basicity influenced the deprotonation site.<sup>[20]</sup> These results imply that deprotonation is not viable for the bulky alkylphosphines **114** and **115**.



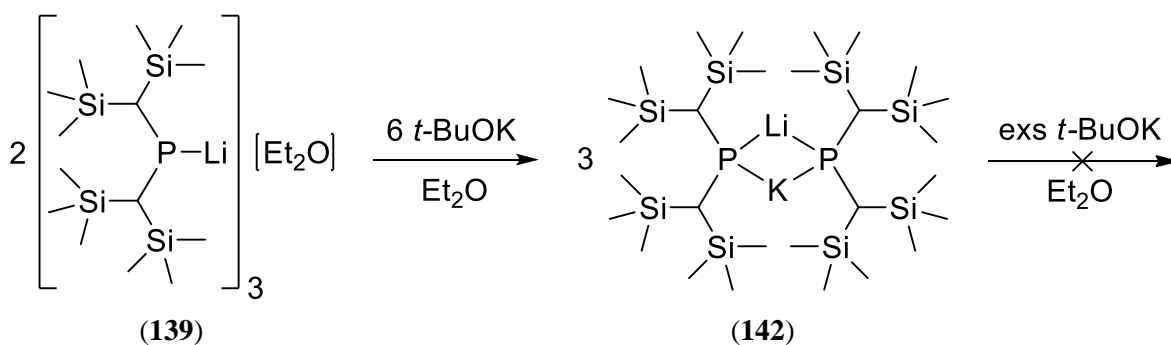
**Scheme 22:** Attempted deprotonation of **114** with strong bases

The lithium phosphide  $[\text{Li}(\mu\text{-P}\{\text{CH}(\text{SiMe}_3)_2\})_2]$  (**138**) has been previously prepared by the direct metalation of  $\{(\text{Me}_3\text{Si})_2\text{CH}\}_2\text{PCl}$  (**140**) with lithium in  $\text{Et}_2\text{O}$ . Compound **138** is dimeric in the solid-state and in solution, in which it exhibits a triplet and septet in the  $^{31}\text{P}\{^1\text{H}\}$  and  $^7\text{Li}$  NMR spectra, respectively. An attempt to replicate this reaction gave the solvate  $([\{(\text{Me}_3\text{Si})_2\text{CH}\}_2\text{P}]\text{Li})_3(\text{OEt}_2)$  (**139**) in low yield after crystallization from  $n$ -hexane (Scheme 23). Compound **139** exhibits broad signals in its  $^{31}\text{P}\{^1\text{H}\}$  and  $^7\text{Li}$  NMR spectra at -112.1 and 2.4 ppm, respectively. Preliminary reactions between **140** and an excess of potassium in  $\text{Et}_2\text{O}$  appear promising; the resulting green solution precipitates the desolvated potassium phosphide  $[\{(\text{Me}_3\text{Si})_2\text{CH}\}_2\text{P}]\text{K}$  (**141**) in good yield upon extraction into light petroleum (Scheme 23). Unfortunately, we have not been able to characterise **141** by X-ray crystallography.



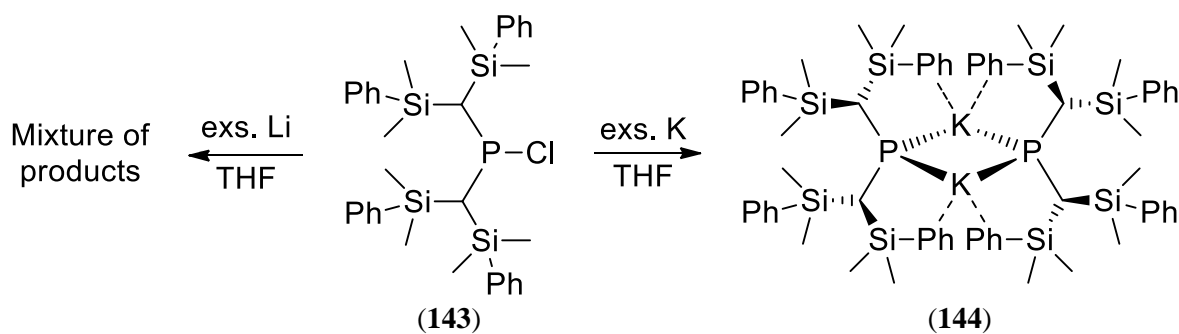
**Scheme 23:** Reactivity of **140** with lithium and potassium

It has previously been established that metathesis reactions between lithium phosphides and sodium or potassium *t*-BuOK yield the heavier alkali metal phosphides.<sup>[21]</sup> The reaction between **139** and six equivalents of *t*BuOK in Et<sub>2</sub>O gave the mixed alkali metal phosphide bridged-dimer [Li(μ-P{CH(SiMe<sub>3</sub>)<sub>2</sub>})][K(μ-P{CH(SiMe<sub>3</sub>)<sub>2</sub>})] (**142**) as a pale yellow powder (Scheme 24). Compound **142** exhibits a 1:1:1:1 quartet ( $J_{\text{PLi}} = 88$  Hz) and 1:2:1 triplet ( $J_{\text{PLi}} = 88$  Hz) in its <sup>31</sup>P{<sup>1</sup>H} and <sup>7</sup>Li NMR spectra, respectively. The reaction of **142** with an excess of *t*BuOK in Et<sub>2</sub>O showed no further reaction after several days by <sup>31</sup>P NMR spectroscopy.



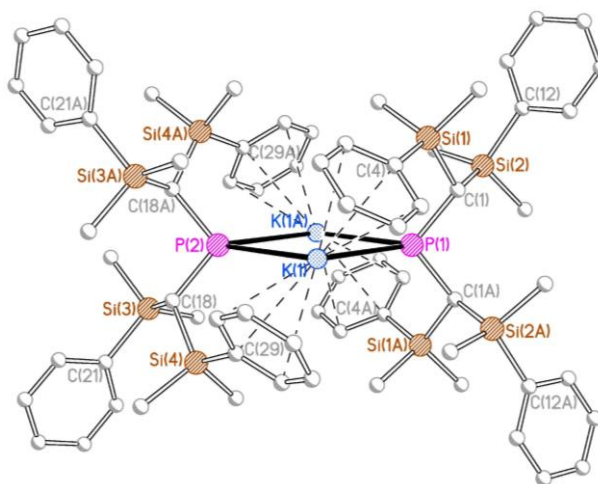
**Scheme 24:** Reactivity of **139** with *t*-BuOK

The reaction between {(Me<sub>2</sub>PhSi)}<sub>2</sub>CH)<sub>2</sub>PCl (**143**) and lithium in THF gave a dark red solution that contained multiple signals in the <sup>31</sup>P NMR spectrum of the crude reaction mixture. From this mixture, no products could be isolated. In a similar reaction, **143** was reacted with potassium in THF to give a dark brown mixture, which contained a single singlet at -91 ppm in its <sup>31</sup>P NMR spectrum. A dark green crystalline material precipitated when the reaction mixture was extracted into light petroleum but could not be identified by NMR spectroscopy. A small number of red crystals of [K[(μ-P{CH(SiMe<sub>2</sub>Ph)<sub>2</sub>})<sub>2</sub>]]<sub>2</sub>·(*n*-hexane) (**144**) were obtained by crystallization from *n*-hexane and characterised by X-ray crystallography.



**Scheme 25:** Reactivity of **143** with lithium and potassium

The molecular structure of **144** is shown in Figure 60, along with selected bond lengths and angles. Compound **144** crystallises as a phosphide-bridged dimer as an *n*-hexane solvate. The two potassium ions in the planar  $P_2K_2$  core are symmetrically equivalent and are each further coordinated by two  $\mu^3$ -phenyl rings. The P-K distances [3.2745(10) and 3.3525(10) Å] are quite unsymmetrical but are within the range of typical K-( $\mu$ -PR<sub>2</sub>) distances; for example, the P-K distances in  $K_2(PMDETA)_2(P_4Ph_4)$  range from 3.245(2) to 3.372(1) Å.<sup>[22]</sup> The K(1)-P-K(1A) bond angles [79.33(3) and 77.14(3)°] are similar for both phosphorus centres. It was not possible to obtain clean NMR spectra of **144** as the limited number of red crystals were contaminated by a thick, red oil.



**Figure 60:** Molecular structure of **144** with H atoms and molecule of solvation omitted for clarity. Selected bond lengths (Å) and angles (°): P(1)-K(1) 3.2745(10), P(2)-K(1) 3.3525(10), P(1)-C(1) 1.912(3), P(2)-C(18) 1.916(3), C(4)-K(1) 3.119(3), C(5)-K(1) 3.239(3), C(6)-K(1) 3.427(3), C(7)-K(1) 3.492(3), C(8)-K(1) 3.369(3), C(9)-K(1) 3.176(3), C(29)-K(1) 3.144(3), C(30)-K(1) 3.088(3), C(31)-K(1) 3.162(3), C(32)-K(1) 3.272(4), C(33)-K(1) 3.309(3), C(34)-K(1) 3.240, K(1A)-P(1)-K(1) 79.33(3), C(1A)-P(1)-(C) 104.02(17), C(1)-P(1)-K(1) 114.98(8), C(1)-P(1)-K(1A) 121.69(9), C(1A)-P(1)-K(1A) 114.98(8), C(1A)-P(1)-K(1) 121.69(8), K(1)-P(2)-K(1A) 77.14(3), C(18A)-P(2)-C(18) 101.29(17), C(18)-P(2)-K(1) 115.11(8), C(18)-P(2)-K(1A) 124.56(8), C(18A)-P(2)-K(1) 124.55(8), C(18A)-P(2)-K(1A) 115.11(8), P(1)-K(1)-P(2) 101.76(2).

### 3.6 Conclusions

An array of bulky phosphines **108-113** were prepared and the corresponding diarylphosphides and the (alkyl)(aryl) phosphide **134** are readily accessible and potentially useful transfer agents for the synthesis of phosphatetrylenes. In the solid state these compounds crystallise as either solvated monomers (**128a**, **129c**, **130a**, **131a**, **132a** and **134**) or phosphide-bridged dimers (**129a** and **132b**) that rapidly lose coordinated solvent, with the exception of **134**. Variable temperature  $^{31}\text{P}\{^1\text{H}\}$  and, where applicable,  $^7\text{Li}$  NMR spectra suggest these compounds are subject to dynamic processes in solution and that the species present are dependent on the sterics of the phosphorus substituents. For **128a**, **129b**, **131a** and **134** this dynamic behaviour may be attributed to a monomer-dimer equilibrium, where the monomer is favoured at low temperatures, whereas for **132c** there appears to be a dynamic equilibrium between a dimer and a cyclic trimer, where the trimer is favoured at low temperatures. In solution, the monomeric structures of **128b**, **129b**, **131b** and **134** are more stable than the dimeric structures at low temperatures, which contrasts the behaviour of less sterically hindered diarylphosphide complexes such as  $\text{Ph}_2\text{PLi}(\text{THF})_n$  and **132c** that favour dimeric, or higher oligomeric structures, at low temperatures.

The bulky dialkylphosphine **114** proved to be inert towards deprotonation at the phosphorus-bound hydrogen by a range of bases. The corresponding lithium phosphide **139** was accessed through direct metalation of **127** with lithium, although this is an alternative solvate to the literature procedure and was isolated in low yield. Preliminary reactions demonstrate the solvent-free potassium phosphide **141** can be accessed through a similar reaction with potassium. A crystal of the related potassium dialkylphosphide **144** was prepared by the direct metalation of **143** with potassium and was characterised by X-ray crystallography. In this structure, the phosphide ligands each provide two  $\mu^3$ -arene interactions to the potassium ions, which suggest this ligand may be useful at stabilising electron-deficient centres by these interactions.



### 3.7 Experimental

The compounds  $\text{PhCH}_2\text{K}$ ,<sup>[23]</sup>  $\text{PCH}_2\text{Na}$ ,<sup>[24]</sup>  $(\text{Mes})\text{PCl}_2$ ,<sup>[25]</sup>  $(\text{Me}_3\text{Si})_2\text{CHBr}$ <sup>[11a]</sup>,  $(\text{Me}_3\text{Si})_2\text{CHLi}$ ,<sup>[12]</sup>  $\{(\text{Me}_3\text{Si})_2\text{CH}\}_2\text{PCl}$ ,<sup>[17]</sup>  $\{(\text{Me}_3\text{Si})_2\text{CH}\}\text{PCl}_2$ ,<sup>[17]</sup>  $\{(\text{Me}_3\text{Si})_2\text{CH}\}_2\text{PH}$ <sup>[7c]</sup> and  $(\text{Me}_2\text{PhSi})_2\text{CHBr}$ <sup>[11b]</sup> were prepared by previously published procedures. The compounds  $\text{DippBr}$ ,<sup>[9]</sup>  $\text{TrippBr}$ ,<sup>[8]</sup>  $\text{DepBr}$ ,<sup>[9]</sup>  $\text{DippLi}(\text{OEt}_2)$ ,<sup>[10]</sup>  $\text{TrippLi}(\text{OEt}_2)$ ,<sup>[10]</sup>  $(\text{Me}_2\text{PhSi})_2\text{CHLi}$ ,<sup>[11b]</sup>  $(\text{Mes})_2\text{PH}$ ,<sup>[7b]</sup>  $(\text{Dipp})_2\text{PH}$ <sup>[1]</sup> and  $(\text{Tripp})_2\text{PH}$ <sup>[7a]</sup> were prepared by modifications of previously reported procedures.  $n\text{BuLi}$  in hexanes (2.5 M) and  $\text{MesMgBr}$  in  $\text{Et}_2\text{O}$  (1.0 M) were purchased from Sigma Aldrich.

#### 3.7.1 Modified synthesis of $\text{DippBr}$ (**118**)<sup>[9]</sup>

2,6-Diisopropylaniline (30 g, 169 mmol) was added to concentrated hydrobromic acid (48%, 150 ml) with vigorous stirring. The resulting pale yellow slurry was cooled to  $-50\text{ }^\circ\text{C}$  and  $\text{NaNO}_2$  (20 g, 289 mmol) was added in portions over 10 min. The resulting brown mixture was stirred for 1 h and pre-cooled ( $-50\text{ }^\circ\text{C}$ )  $\text{Et}_2\text{O}$  (150 ml) was added. The mixture was allowed to slowly warm to  $-15\text{ }^\circ\text{C}$  whereupon a brown gas evolved. Once the gas evolution stopped the now orange mixture was cooled to  $-50\text{ }^\circ\text{C}$  and  $\text{NaCO}_3$  (37 g, 349 mmol) and water (10 ml) was added. The mixture was allowed to warm to room temperature overnight. The product was extracted with  $\text{Et}_2\text{O}$  (2 x 150 ml). The combined organic layers were washed with saturated sodium metabisulphite solution (100 ml) and brine (100 ml) and dried with  $\text{MgSO}_4$ . The solvent was removed *in vacuo* to give a red oil. Distillation under reduced pressure gave the product as a pale yellow oil ( $65\text{ }^\circ\text{C}$ , 0.01 Torr). Yield: 33.2 g, 81%.

$^1\text{H}$  NMR [ $\text{CDCl}_3$ ]:  $\delta$  1.25 (d,  $J_{\text{HH}} = 6.9\text{ Hz}$ , 12H,  $\text{CHMe}_2$ ), 3.51 (sept,  $J_{\text{HH}} = 6.9\text{ Hz}$ , 2H,  $\text{CHMe}_2$ ), 7.13 (d,  $J_{\text{HH}} = 7.6\text{ Hz}$ , 2H, ArH), 7.25 (m, 1H, ArH).

#### 3.7.2 Modified synthesis of $\text{DippLi}(\text{OEt}_2)$ (**119**)<sup>[10]</sup>

A solution of  $n\text{BuLi}$  in hexanes (2.3 M, 33 ml, 75.9 mmol) was added, dropwise, to a cold ( $0\text{ }^\circ\text{C}$ ) solution of  $\text{DippBr}$  (**118**) (18.53 g, 76.8 mmol) in  $\text{Et}_2\text{O}$  (150 ml). The resulting solution was stirred at  $0\text{ }^\circ\text{C}$  for 1.5 h and the volume was reduced under vacuum to 50 ml. Storage of the solution at  $-78\text{ }^\circ\text{C}$  overnight resulted in the formation of large colourless crystals. The supernatant solution was removed by decantation and the crystals were washed with cold ( $-10\text{ }^\circ\text{C}$ ) light petroleum (2 x 10 ml). The residual solvent was removed under vacuum to give a white crystalline powder. Yield: 12.40 g, 67%.

### 3.7.3 Modified synthesis of (Dipp)<sub>2</sub>PH (111)<sup>[1]</sup>

To a cold (-78 °C) solution of PCl<sub>3</sub> (2.2 ml, 25.2 mmol) in Et<sub>2</sub>O (150 ml) was added, dropwise, a solution of DippLi(OEt<sub>2</sub>) (**119**) (12.40 g, 51.2 mmol) in Et<sub>2</sub>O (50 ml). The resulting mixture was allowed to warm to room temperature and was stirred for 1 h. The resulting pale yellow solution with pale solids was cooled to -78 °C and solid LiAlH<sub>4</sub> (0.971 g, 25.6 mmol) was added in portions. The resulting grey mixture was allowed to warm to room temperature and was stirred for 1 h. The mixture was cooled to 0 °C and degassed water (60 ml) was added gradually. The product was extracted into light petroleum (3 x 20 ml) and the combined organic phases were dried over 4 Å molecular sieves. The solution was filtered and the solvent was removed under vacuum to give a white crystalline solid. Yield: 8.30 g, 91%.

<sup>1</sup>H NMR [CDCl<sub>3</sub>]: δ 1.01 (d, *J*<sub>HH</sub> = 6.4 Hz, 12H, CHMeMe), 1.04 (d, *J*<sub>HH</sub> = 6.9 Hz, 12H, CHMeMe), 3.51 (m, 2H, CHMeMe), 5.47 (d, *J*<sub>PH</sub> = 232.6 Hz, 1H, PH), 7.08 (m, 2H, ArH), 7.24 (m, 1H, ArH). <sup>13</sup>C{<sup>1</sup>H} NMR [CDCl<sub>3</sub>]: δ 23.85 (CHMeMe), 24.26 (CHMeMe), 32.84 (d, *J*<sub>PH</sub> = 12.5 Hz, CHMeMe), 123.54, 128.83, 132.75 (Ar), 152.61 (d, *J*<sub>PC</sub> = 11.0 Hz, Ar). <sup>31</sup>P NMR [CDCl<sub>3</sub>]: δ 101.1 (d, *J*<sub>PH</sub> = 232.6 Hz).

### 3.7.4 Synthesis of DepBr (116)

DepBr was prepared by the same method as DippBr (**118**) using 2,6-diethylaniline (20.1 g, 135 mmol), concentrated hydrobromic acid (48%, 120 ml), NaNO<sub>2</sub> (16 g, 0.232 mmol) and Na<sub>2</sub>CO<sub>3</sub> (30 g, 283 mmol). Distillation under reduced pressure gave the product as a pale yellow oil (64 °C, 1.0 Torr). Yield: 17.01 g, 59%.

<sup>1</sup>H NMR [CDCl<sub>3</sub>]: δ 1.25 (t, *J*<sub>HH</sub> = 7.6 Hz, 6H, CH<sub>2</sub>CH<sub>3</sub>), 2.81 (q, *J*<sub>HH</sub> = 7.6 Hz, 4H, CH<sub>2</sub>CH<sub>3</sub>), 7.08 (q, *J*<sub>HH</sub> = 7.4 Hz, 2H, ArH), 7.18 (m, 1H, ArH).

### 3.7.5 Synthesis of DepMgBr (117)

To a slurry of magnesium turnings (2.443 g, 100.5 mmol) and a single crystal of iodine in Et<sub>2</sub>O (5 ml) was added a solution of DepBr (**116**) (10.71 g, 50.3 mmol) in Et<sub>2</sub>O (120 ml). The reaction initiated immediately and the solution of DepBr (**116**) was added at a rate to maintain constant reflux over 30 min. The mixture was then heated under reflux for 4 h and filtered to remove the excess magnesium. An aliquot of the filtrate was quenched with a

solution of hydrochloric acid (0.1 M, 10 ml) and titrated against a solution of NaOH (0.1M) to determine the Grignard solution had a concentration of 0.45 M.

### 3.7.6 Synthesis of (Dep)<sub>2</sub>PH (110)

To a cold (-78 °C) solution of PCl<sub>3</sub> (2.0 ml, 22.9 mmol) in Et<sub>2</sub>O (50 ml) was added a solution of DepMgBr (**117**) in Et<sub>2</sub>O (0.45 M, 100 ml, 45.0 mmol) and the mixture was allowed to warm to room temperature. After stirring for 1 h the mixture was cooled to -78 °C and solid LiAlH<sub>4</sub> (0.848 g, 22.3 mmol) was added in portions. The mixture was allowed to warm to room temperature and was stirred for 1 h. Degassed water (30 ml) was carefully added and the organic phase was extracted into light petroleum (3 x 20 ml) and dried over 4 Å molecular sieves. The dried solution was filtered and the solvent was removed *in vacuo* from the filtrate to give a white crystalline solid. Yield: 4.64 g, 69%.

<sup>1</sup>H NMR [CDCl<sub>3</sub>]: δ 1.06 (t, *J*<sub>HH</sub> = 7.5 Hz, 12H, CHHCH<sub>3</sub>), 2.64 (m, *J*<sub>HH</sub> = 7.2 Hz, 4H, CHHCH<sub>3</sub>), 2.81 (m, *J*<sub>HH</sub> = 7.2 Hz, 4H, CHHCH<sub>3</sub>), 5.40 (d, *J*<sub>PH</sub> = 234 Hz, 1H, PH), 7.04 (dd, *J*<sub>HH</sub> = 7.6 Hz, *J*<sub>PH</sub> = 2.6 Hz, 8H, m-ArH), 7.20 ppm (t, *J*<sub>HH</sub> = 7.6 Hz, 4H, p-ArH). <sup>13</sup>C{<sup>1</sup>H} NMR [CDCl<sub>3</sub>]: δ 15.64 (CH<sub>2</sub>CH<sub>3</sub>), 29.33 (CH<sub>2</sub>CH<sub>3</sub>), 126.58 (d, *J*<sub>PC</sub> = 2.9 Hz, m-ArH), 128.71 (p-ArH), 132.91 (d, *J*<sub>PC</sub> = 19.1 Hz, Ar), 148.57 ppm (d, *J*<sub>PC</sub> = 11.6 Hz, Ar). <sup>31</sup>P NMR [CDCl<sub>3</sub>]: δ -98.84 (d, *J*<sub>PH</sub> = 234 Hz).

### 3.7.7 Modified synthesis of TrippBr (120)<sup>[10]</sup>

A solution of bromine (40.37 g, 253 mmol) in DCM (30 ml) was added, dropwise, to a mixture of 1,3,5-triisopropylbenzene (51.78 g, 253 mmol) and iron filling (2.07 g, 37 mmol) in DCM (30 ml) over 2 h. The resulting mixture was stirred overnight and washed with water (2 x 10 ml), a solution of 20% NaOH in water (2 x 50 ml) and water (100 ml). The volume of organic phase was reduced to 100 ml and a solution of concentrated NaOEt in ethanol, which was prepared from sodium (5.0 g) and ethanol (100 ml), was added. The mixture was left to stand overnight. The resulting yellow solution with pale solids was diluted with water (50 ml) and the product was extracted into DCM (3 x 50 ml). The combined organic layers were washed with water (2 x 100 ml) and brine (100 ml) and dried over CaCl<sub>2</sub>. The solvent was removed *in vacuo* to give a clear yellow oil and the product was isolated by distillation under reduced pressure to give a clear colourless oil (110 °C, 0.01 Torr). Yield: 56.17 g, 78%.

<sup>1</sup>H NMR [CDCl<sub>3</sub>]: δ 1.27 (d, *J*<sub>HH</sub> = 6.9 Hz, 18H, o-CHMe<sub>2</sub> + p-CHMe<sub>2</sub>), 2.89 (sept, *J*<sub>HH</sub> = 6.9 Hz, 1H, p-CHMe<sub>2</sub>), 3.51 (sept, *J*<sub>HH</sub> = 6.9 Hz, 2H, o-CHMe<sub>2</sub>), 7.01 (s, 2H, ArH).

### 3.7.8 Modified synthesis of TrippLi(OEt<sub>2</sub>) (**121**)<sup>[10]</sup>

To a cold (0 °C) solution of TrippBr (**120**) (10.62 g, 37.5 mmol) in Et<sub>2</sub>O (100 ml) was added, dropwise, a solution of *n*BuLi in hexanes. The resulting solution was stirred at 0 °C for 3 h and reduced in volume to 30 ml. Storage at -78 °C resulted in the formation of large colourless crystals. The supernatant solution was removed by filtration and the crystals were washed with cold (-78 °C) light petroleum (2 x 10 ml) and the residual solvent was removed under vacuum to give a white crystalline solid. Yield: 5.67 g, 53%.

### 3.7.9 Modified synthesis of (Tripp)<sub>2</sub>PH (**112**)<sup>[7a]</sup>

To a cold (0 °C) solution of TrippLi(OEt<sub>2</sub>) (**121**) (5.67 g, 19.9 mmol) in Et<sub>2</sub>O (40 ml) was added, dropwise, PCl<sub>3</sub> (0.9 mL, 10 mmol). This mixture was allowed to warm to room temperature and was stirred for 1 h. To the resulting mixture with pale solids, solid LiAlH<sub>4</sub> (0.378 g, 10.0 mmol) was added in portions. The resulting mixture was stirred for 1 h and then degassed water (30 ml) was added slowly. The organic phase was extracted into Et<sub>2</sub>O (3 x 20 ml) and dried over activated 4 Å molecular sieves. The solution was filtered, and the solvent was removed *in vacuo* from the filtrate to give a viscous pale-yellow oil (4.28 g, 9.75 mmol). Recrystallization from isopropyl alcohol (30 ml) at -78 °C gave (Tripp)<sub>2</sub>PH as a white crystalline solid. Yield: 2.19 g, 50%.

<sup>1</sup>H NMR [CDCl<sub>3</sub>]: δ 0.99 (d, *J*<sub>HH</sub> = 6.9 Hz, 12H, o-CHMeMe), 1.03 (d, *J*<sub>HH</sub> = 6.9 Hz, 12H, o-CHMeMe), 1.20 (d, *J*<sub>HH</sub> = 6.9 Hz, 12H, p-CHMe<sub>2</sub>), 2.82 (sept, *J*<sub>HH</sub> = 6.9 Hz, 2H, p-CHMe<sub>2</sub>), 3.49 (m, 4H, o-CHMeMe), 5.42 (d, *J*<sub>PH</sub> = 231.7 Hz, 1H, PH), 6.93 (d, *J*<sub>PH</sub> = 2.4 Hz, 4H, ArH). <sup>13</sup>C{<sup>1</sup>H} NMR [CDCl<sub>3</sub>]: δ 24.14 (o-CHMeMe), 24.27 (p-CHMeMe), 24.30 (p-CHMeMe), 24.54 (o-CHMeMe), 33.08 (d, *J*<sub>PC</sub> = 12.8 Hz, o-CHMeMe), 34.54 (p-CHMeMe), 121.84 (d, *J*<sub>PC</sub> = 2.8 Hz, Ar), 130.23 (d, *J*<sub>PC</sub> = 16.5 Hz, Ar), 149.40 (Ar), 152.65 (d, *J*<sub>PC</sub> = 10.9 Hz, Ar). <sup>31</sup>P NMR [CDCl<sub>3</sub>]: δ -102.6 (d, *J*<sub>PH</sub> = 231.7 Hz).

### 3.7.10 Modified synthesis of (Mes)<sub>2</sub>PH (**108**)<sup>[7b]</sup>

To a cold (-78 °C) solution of PCl<sub>3</sub> (4.4 ml, 50 mmol) in Et<sub>2</sub>O (200 ml) was added, dropwise, a solution of MesMgBr in Et<sub>2</sub>O (1 M, 100 ml, 100 ml) with vigorous stirring. The resulting slurry was allowed to warm to room temperature and was stirred for 1h. The resulting orange solution with pale solids was cooled to -78 °C and solid LiAlH<sub>4</sub> (1.898 g, 50 mmol) was added in portions. The resulting mixture was allowed to warm to room temperature and was stirred for 1 h. The mixture was cooled to 0 °C and degassed water (150

ml) was added gradually. The organic phase was separated and the product was further extracted into light petroleum (3 x 100 ml). The combined organic phases were dried over 4 Å molecular sieves overnight. The solution was filtered and the solvent was removed under vacuum. Impurities were removed by heating the resulting sticky solid until molten (~80 °C) under vacuum from the filtrate. This purification procedure was repeated two more times to yield a pale yellow crystalline solid. Yield: 11.55 g, 85%.

$^1\text{H}$  NMR [ $\text{CDCl}_3$ ]:  $\delta$  2.27 (s, 6H, *p*-Me), 2.29 (s, 12H, *o*-Me), 3.63 (d,  $J_{\text{PH}} = 233$  Hz, PH), 6.85 (d,  $J_{\text{PH}} = 1.8$  Hz, ArH).  $^{13}\text{C}\{^1\text{H}\}$  NMR [ $\text{CDCl}_3$ ]:  $\delta$  21.08 (*p*-Me), 22.85, 22.95 (*o*-Me), 129.18 (d,  $J_{\text{PC}} = 3.1$  Hz, ArH), 129.40 (d,  $J_{\text{PC}} = 16.1$  Hz, Ar), 138.90 (Ar), 142.33 (d,  $J_{\text{PC}} = 12.2$  Hz, Ar).  $^{31}\text{P}$  NMR [ $\text{CDCl}_3$ ]:  $\delta$  93.08 (d,  $J_{\text{PH}} = 233$  Hz).

### 3.7.11 Synthesis of $\{(\text{Me}_3\text{Si})_2\text{CH}\}_2\text{PCl}$ (**140**)<sup>[17]</sup>

To a cold (78 °C) solution of  $(\text{Me}_3\text{Si})_2\text{CHBr}^{[11a]}$  (**122**) (11.94 g, 50.3 mmol) in  $\text{Et}_2\text{O}$  (25 ml) was added, dropwise, a solution of *n*BuLi in hexanes (2.47 M, 20 ml, 49.4 mmol). The resulting mixture was stirred for 1 h at -78 °C and the solvent was removed *in vacuo* while the mixture was still cold. The resulting solid was heated (~150 °C) under vacuum to give an oil that solidified upon further heating to give  $(\text{Me}_3\text{Si})_2\text{CHLi}$  (**124**) as a pale yellow powder. This solid was dissolved in  $\text{Et}_2\text{O}$  (20 ml) and added, dropwise, to a cold (-78 °C) solution of  $\text{PCl}_3$  (2.2 ml, 25.2 mmol) in  $\text{Et}_2\text{O}$  (20 ml). The resulting solution was allowed to slowly warm to room temperature and was stirred overnight. The resulting pale yellow solution with pale solids was filtered and the solvent was removed from the filtrate *in vacuo* to give a pale yellow solid. Volatile impurities were removed by distillation under reduced pressure (oil bath temperature 100 °C, 0.01 Torr) to give the product as a pale yellow solid upon cooling. Yield: 6.68 g, 69%.

$^1\text{H}$  NMR [ $\text{CDCl}_3$ ]:  $\delta$  0.20 (br. s, 18H,  $\text{CH}(\text{SiMe}_3)(\text{SiMe}_3)$ ), 0.25 (br. s, 18H,  $\text{CH}(\text{SiMe}_3)(\text{SiMe}_3)$ ), 1.13 (br. s, 2H,  $\text{CH}(\text{SiMe}_3)(\text{SiMe}_3)$ ).  $^{31}\text{P}\{^1\text{H}\}$  NMR [ $\text{CDCl}_3$ ]:  $\delta$  156.

### 3.7.12 Synthesis of $\{(\text{Me}_3\text{Si})\text{CH}\}_2\text{PH}$ (**114**)<sup>[7c]</sup>

To a solution of  $\{(\text{Me}_3\text{Si})\text{CH}\}_2\text{PCl}$  (**140**) (2.79 g, 7.24 mmol) in  $\text{Et}_2\text{O}$  (40 ml) was added solid  $\text{LiAlH}_4$  (0.275 g, 7.24 mmol) in portions. The resulting mixture was stirred for 2 h and cooled to 0 °C. Degassed water (30 ml) was added slowly added. The product was extracted into light petroleum (3 x 15 ml) and the combined organic layers were dried over 4 Å molecular sieves overnight. The solution was filtered and the solvent was removed from the

filtrate *in vacuo* to give a clear colourless oil. Volatile impurities were removed by distillation under reduced pressure (oil bath temperature 100 °C, 0.01 Torr) to give the product as a colourless oil upon cooling. Yield: 1.78 g, 70%.

$^1\text{H}$  NMR [ $\text{CDCl}_3$ ]:  $\delta$  0.13 (s, 36H,  $\text{SiMe}_3$ ), 0.25 (d,  $J_{\text{PH}} = 6.5$  Hz, 2H, CH), 3.54 (dt,  $J_{\text{PH}} = 200$  Hz,  $J_{\text{HH}} = 6.5$  Hz, 1H, PH).  $^{31}\text{P}$  NMR [ $\text{CDCl}_3$ ]:  $\delta$  -72.0 (d,  $J_{\text{PH}} = 200$  Hz).

### 3.7.13 Synthesis of (Dipp)(Mes)PH (109)

To a cold (-78 °C) solution of  $\text{MesPCl}_2$ <sup>[25]</sup> (2.99 g, 13.5 mmol) in  $\text{Et}_2\text{O}$  (50 ml) was added a solution of  $\text{DippLi}(\text{Et}_2\text{O})$  (3.279 g, 13.5 mmol) in  $\text{Et}_2\text{O}$  (20 ml). The resulting yellow solution was warmed to room temperature and was stirred for 1 h. The mixture was cooled to -78 °C and solid  $\text{LiAlH}_4$  (0.511 g, 13.5 mmol) was added in portions. The mixture was warmed to room temperature and was stirred for 1 h. Degassed water (40 ml) was added slowly. The product was extracted into light petroleum (4 x 20 ml) and dried over 4 Å molecular sieves. The solution was then filtered and the solvent was removed under vacuum to yield a pale yellow solid. Yield: 3.29 g, 78%.

$^1\text{H}$  NMR [ $\text{CDCl}_3$ ]:  $\delta$  1.03 (d,  $J_{\text{HH}} = 6.8$  Hz,  $\text{CHMeMe}$ , 6H), 1.09 (d,  $J_{\text{HH}} = 6.8$  Hz,  $\text{CHMeMe}$ , 6H), 2.22 (s, o-Me, 6H), 2.23 (s, p-Me, 3H), 3.59 (m,  $\text{CHMeMe}$ , 2H), 5.34 (d,  $J_{\text{PH}} = 233$  Hz, PH, 1H), 6.80 (m, ArH, 2H), 7.11 (d,  $J_{\text{HH}} = 7.7$  Hz, ArH, 1H), 7.12 (d,  $J_{\text{HH}} = 7.7$  Hz, ArH, 1H), 7.30 (t,  $J_{\text{HH}} = 7.7$  Hz, ArH, 1H).  $^{13}\text{C}\{^1\text{H}\}$  NMR [ $\text{CDCl}_3$ ]:  $\delta$  21.05 (o-Me), 23.46 (d,  $J_{\text{PC}} = 9.7$  Hz, p-Me), 23.86 ( $\text{CHMeMe}$ ), 24.52 ( $\text{CHMeMe}$ ), 32.84 (d,  $J_{\text{PC}} = 13.5$  Hz,  $\text{CHMeMe}$ ), 123.40 (d,  $J_{\text{PC}} = 3.4$  Hz, ArH), 129.25 (ArH), 129.28 (m, ArH), 130.47 (d,  $J_{\text{PC}} = 16.9$  Hz, Ar), 131.54 (d,  $J_{\text{PC}} = 16.9$  Hz, Ar), 137.46 (Ar), 141.08 (d,  $J_{\text{PC}} = 11.8$  Hz, Ar), 153.83 (d,  $J_{\text{PC}} = 11.2$  Hz, Ar).  $^{31}\text{P}$  [ $\text{CDCl}_3$ ]:  $\delta$  -96.9 (d,  $J_{\text{PH}} = 233$  Hz)

### 3.7.14 Synthesis of $\{(\text{Me}_3\text{Si})_2\text{CH}\}\text{PCl}_2$ (127)<sup>[17]</sup>

A solution of  $(\text{Me}_3\text{Si})_2\text{CHLi}$  (**124**) (11.42 g, 68.7 mmol), prepared in the same method used in the synthesis of  $\{(\text{Me}_3\text{Si})_2\text{CH}\}_2\text{PCl}$  (**140**), in  $\text{Et}_2\text{O}$  (60 ml) was added, dropwise, to a solution of  $\text{PCl}_3$  (6.6 ml, 75.6 mmol) in  $\text{Et}_2\text{O}$  (30 ml). The resulting yellow solution was allowed to warm slowly to room temperature overnight. The yellow mixture with pale solids was filtered and the solvent was removed *in vacuo* to give a pale yellow oil. Distillation under reduced pressure (70 °C, 0.01 Torr) gave the product as a colourless oil. Yield: 10.09 g, 56%.

$^1\text{H}$  NMR [ $\text{CDCl}_3$ ]:  $\delta$  0.29 (d,  $J_{\text{PH}} = 1.16$  Hz, 18H,  $\text{SiMe}_3$ ), 1.29 (d,  $J_{\text{PH}} = 13.4$  Hz, CH).  
 $^{31}\text{P}\{^1\text{H}\}$  NMR [ $\text{CDCl}_3$ ]:  $\delta$  225.5.

### 3.7.15 Synthesis of (Dipp){(Me<sub>3</sub>Si)<sub>2</sub>CH}PH (113)

To a cold (-10 °C) solution of {(Me<sub>3</sub>Si)<sub>2</sub>CH}PCl<sub>2</sub> (**127**) (3.08 g, 11.8 mmol) in Et<sub>2</sub>O (50 ml) was added, dropwise, a solution of DippLi(OEt<sub>2</sub>) (**119**) (2.854 g, 11.8 mmol) in Et<sub>2</sub>O (20 ml). The resulting pale yellow solution with pale solids was allowed to warm to room temperature and was stirred for 1 h. The mixture was cooled to 0 °C and solid LiAlH<sub>4</sub> (0.444 g, 11.7 mmol) was added in portions. The mixture was allowed to warm to room temperature and was stirred for 1 h. The mixture was cooled to 0 °C and degassed water (50 ml) was added slowly. The product was extracted into light petroleum (3 x 15 ml) and the combined organic phases were dried over 4 Å molecular sieves. The solution was filtered and the solvent was removed from the filtrate under vacuum to give a pale yellow oil. Impurities were removed by vacuum distillation (100 °C/ 1 x 10<sup>-3</sup> Torr) to leave behind the product as a pale yellow oil. Yield: 3.33 g, 80%.

$^1\text{H}$  NMR [ $\text{CDCl}_3$ ]:  $\delta$  -0.02 (s, 9H, CH(SiMe<sub>3</sub>)(SiMe<sub>3</sub>)), 0.11 (s, 9H, CH(SiMe<sub>3</sub>)(SiMe<sub>3</sub>)), 0.60 (d,  $J_{\text{HH}} = 5.8$  Hz, 1H, CH(SiMe<sub>3</sub>)(SiMe<sub>3</sub>)), 1.25 (d,  $J_{\text{HH}} = 6.8$  Hz, 6H, CHMeMe), 1.26 (d,  $J_{\text{HH}} = 6.8$  Hz, 6H, CHMeMe), 3.76 (m, 2H, CHMeMe), 4.40 (dd,  $J_{\text{PH}} = 220$  Hz,  $J_{\text{HH}} = 5.8$  Hz, 1H, PH), 7.11 (d,  $J_{\text{HH}} = 7.6$  Hz, 1H, ArH), 7.12 (d,  $J_{\text{HH}} = 7.6$  Hz, 1H, ArH), 7.29 (t,  $J_{\text{HH}} = 7.6$  Hz, 1H, ArH).  $^{13}\text{C}\{^1\text{H}\}$  NMR [ $\text{CDCl}_3$ ]:  $\delta$  1.00 (d,  $J_{\text{PC}} = 3.6$  Hz, CH(SiMe<sub>3</sub>)(SiMe<sub>3</sub>)), 1.30 (d,  $J_{\text{PC}} = 6.2$  Hz, CH(SiMe<sub>3</sub>)(SiMe<sub>3</sub>)), 9.20 (d,  $J_{\text{PC}} = 47.2$ , CH(SiMe<sub>3</sub>)(SiMe<sub>3</sub>)), 24.18 (CHMeMe), 25.27 (CHMeMe), 32.72 (d,  $J_{\text{PC}} = 14.4$ , CHMeMe), 123.30 (d,  $J_{\text{PC}} = 3.1$  Hz, ArH), 129.39 (s, ArH), 133.38 (d,  $J_{\text{PC}} = 24.0$  Hz, Ar), 153.72 (d,  $J_{\text{PC}} = 11.6$  Hz, Ar).  $^{31}\text{P}$  NMR [ $\text{CDCl}_3$ ]:  $\delta$  -96.0 (d,  $J_{\text{PH}} = 220$  Hz).

### 3.7.16 Synthesis of [(Dipp)<sub>2</sub>P]Li(THF)<sub>2</sub> (128b)

To a solution of Dipp<sub>2</sub>PH (**111**) (0.695 g, 1.97 mmol) in THF (10 ml) was added a solution of *n*BuLi in hexanes (2.3 M, 0.85 ml, 2.0 mmol). The resulting red solution was stirred for 1 h. The solvent was removed *in vacuo* and the orange solid was dissolved in Et<sub>2</sub>O (5 ml). Storage of this solution at -25 °C for 2 days resulted in the formation of large yellow crystals of [(Dipp)<sub>2</sub>P]Li(THF)<sub>3</sub> (**128a**). These crystals were washed with cold (-10 °C) light petroleum (2 x 5 ml) and residual solvent was removed *in vacuo* to give the alternate solvate [(Dipp)<sub>2</sub>P]Li(THF)<sub>2</sub> (**128b**) as a yellow powder. Yield: 0.79 g, 80 %.

$^1\text{H}$  NMR [ $d_8$ -toluene, 363 K]:  $\delta$  0.99 (d,  $J_{\text{HH}} = 6.9$  Hz, 24H,  $\text{CHMe}_2$ ), 1.46 (m, 8H, THF), 3.57 (m, 8H, THF), 4.17 (m, 4H,  $\text{CHMe}_2$ ), 6.97 (d,  $J_{\text{HH}} = 7.7$  Hz, 4H, ArH), 7.04 (m, 2H, ArH).  $^{13}\text{C}\{^1\text{H}\}$  NMR [ $d_8$ -toluene, 363 K]:  $\delta$  25.00 ( $\text{CHMe}_2$ ), 25.88 (THF), 33.92 ( $\text{CHMe}_2$ ), 68.61 (THF), 123.29 (ArH), 125.47 (ArH, obscured by solvent peak), 147.00 (br. d,  $J_{\text{PC}} = 23.1$  Hz, Ar), 152.85 (d,  $J_{\text{PC}} = 6.2$  Hz, Ar).  $^7\text{Li}$  NMR [ $d_8$ -toluene, 363 K]:  $\delta$  2.2 (s).  $^{31}\text{P}$  NMR [ $d_8$ -toluene, 363 K]:  $\delta$  -114.4.

### 3.7.17 Synthesis of $[(\text{Dipp})_2\text{P}]\text{Na}(\text{THF})_{1.5}$ (**129b**)

To a solution of  $\text{Dipp}_2\text{PH}$  (**111**) (0.81 g, 2.28 mmol) in THF (15 ml) was added a solution of benzylnsodium (0.261 g, 2.28 mmol) in THF (10 ml). The resulting orange solution was stirred for 30 min and the solvent was removed *in vacuo* to give a sticky yellow solid. Light petroleum (15 ml) was added to give an orange solution that spontaneously formed yellow crystals of  $\{[(\text{Dipp})_2\text{P}]\text{Na}(\text{THF})_2\}_2$  (**129a**). Further crystalline material was obtained by cooling the mixture to  $-25\text{ }^\circ\text{C}$  for 12 h. The supernatant solution was removed by filtration and the crystals were washed with cold ( $-10\text{ }^\circ\text{C}$ ) light petroleum. The residual solvent was removed under vacuum to give the alternative solvate  $[(\text{Dipp})_2\text{P}]\text{Na}(\text{THF})_{1.5}$  (**129b**) as a yellow powder. Yield of **129b**: 0.89 g, 81%.

$^1\text{H}$  NMR [ $d_8$ -toluene]:  $\delta$  1.04 (d,  $J_{\text{HH}} = 6.9$  Hz, 24H,  $\text{CHMe}_2$ ), 1.38 (m, 6H, THF), 3.50 (m, 6H, THF), 4.24 (m, 4H,  $\text{CHMe}_2$ ), 7.03 (d,  $J_{\text{HH}} = 7.6$  Hz, 4H, ArH), 7.11 (m, 2H, ArH).  $^{13}\text{C}\{^1\text{H}\}$  NMR [ $d_8$ -toluene]:  $\delta$  24.54 ( $\text{CHMe}_2$ ), 25.60 (THF), 33.57 (d,  $J_{\text{PC}} = 11.7$  Hz,  $\text{CHMe}_2$ ), 68.19 (THF), 122.95, 124.92 (ArH), 147.84 (d,  $J_{\text{PC}} = 33.5$  Hz, Ar), 151.98 (d,  $J_{\text{PC}} = 4.8$  Hz, Ar).  $^{31}\text{P}\{^1\text{H}\}$  NMR [ $d_8$ -toluene]:  $\delta$  -118.6.

### 3.7.18 Synthesis of $[(\text{Dipp})_2\text{P}]\text{Na}(\text{PMDETA})$ (**129c**)

$(\text{Dipp})_2\text{PH}$  (**111**) (0.596 g, 1.68 mmol) and benzylnsodium (0.194 g, 1.70 mmol) were dissolved in THF (10 ml) and this mixture was stirred for 1 h to give a red solution. The solvent was removed *in vacuo*. To the resulting orange solid was added *n*-hexane (10 ml) and PMDETA (0.35 ml, 1.70 mmol) to give a red solution that deposited yellow crystalline material of  $[(\text{Dipp})_2\text{P}]\text{Na}(\text{PMDETA})$  (**129c**) on standing. The mixture was cooled to  $-25\text{ }^\circ\text{C}$  for 2 h, the supernatant was removed, the yellow crystalline material of **129c** was washed with cold ( $-10\text{ }^\circ\text{C}$ ) light petroleum (2 x 5 ml) and residual solvent was removed *in vacuo*. Yield: 0.60 g, 65%.



$^1\text{H}$  NMR [ $d_8$ -toluene]:  $\delta$  1.21 (d,  $J_{\text{HH}} = 7.0$  Hz, 24H,  $\text{CHMe}_2$ ), 1.67 (br. s, 8H,  $\text{NCH}_2\text{CH}_2\text{N}$ ), 1.79 (s, 12H,  $\text{NMe}_2$ ), 1.81 (s, 3H,  $\text{NMe}$ ), 4.68 (m, 4H,  $\text{CHMe}_2$ ), 7.10 (s, 6H, ArH).  $^{13}\text{C}\{^1\text{H}\}$  NMR [ $d_8$ -toluene]:  $\delta$  24.93 ( $\text{CHMe}_2$ ), 33.18 ( $\text{CHMe}_2$ ), 43.30 ( $\text{NMe}$ ), 45.28 ( $\text{NMe}_2$ ), 54.03 ( $\text{NCH}_2\text{CH}_2\text{N}$ ), 56.97 ( $\text{NCH}_2\text{CH}_2\text{N}$ ), 122.42, 123.20 (ArH), 151.88 (d,  $J_{\text{PC}} = 7.3$  Hz, Ar), 152.92 (d,  $J_{\text{PC}} = 49.3$  Hz, Ar).  $^{31}\text{P}\{^1\text{H}\}$  NMR [ $d_8$ -toluene]:  $\delta$  -106.7.

### 3.7.19 Synthesis of [(Dipp) $_2$ P]K (130b)

To a mixture of (Dipp) $_2$ PH (**111**) (1.06 g, 2.99 mmol) and benzylpotassium (0.391 g, 3.00 mmol) was added THF (15 ml) and the resulting red solution was stirred for 1 h. The solution was reduced in volume to 3 ml *in vacuo* and light petroleum (25 ml) was added, generating an orange precipitate. The solid was isolated by filtration, washed with light petroleum (2 x 5 ml) and dried *in vacuo*. Yield: 0.99 g, 84%.

$^1\text{H}$  NMR [ $d_8$ -toluene/ $d_8$ -THF]:  $\delta$  1.11 (d,  $J_{\text{HH}} = 7.0$  Hz, 24H,  $\text{CHMe}_2$ ), 4.59 (m, 4H,  $\text{CHMe}_2$ ), 6.92-6.96 (m, 6H, ArH).  $^{13}\text{C}\{^1\text{H}\}$  NMR [ $d_8$ -toluene/ $d_8$ -THF]:  $\delta$  24.81 ( $\text{CHMe}_2$ ), 33.09 (d,  $J_{\text{PC}} = 13.7$  Hz,  $\text{CHMe}_2$ ), 122.27, 122.50 (ArH), 151.93 (d,  $J_{\text{PC}} = 8.2$  Hz, Ar), 154.68 (d,  $J_{\text{PC}} = 55.8$  Hz, Ar).  $^{31}\text{P}\{^1\text{H}\}$  NMR [ $d_8$ -toluene/ $d_8$ -THF]:  $\delta$  -92.3.

Crystals of the solvate [(Dipp) $_2$ P]K(THF) $_4$  (**130a**) suitable for characterisation by single crystal X-ray diffraction were obtained by recrystallization of [(Dipp) $_2$ P]K (**130b**) from an Et $_2$ O/THF mixture at -25 °C. These crystals rapidly lose THF under vacuum to give the solvent-free complex [(Dipp) $_2$ P]K (**130b**).

### 3.7.20 Synthesis of [(Mes) $_2$ P]Li(THF) (132c)

A solution of *n*BuLi in hexanes (2.3 M, 1.2 ml, 2.76 mmol) was added to a solution of (Mes) $_2$ PH (**108**) (0.76 g, 2.81 mmol) in THF (10 ml). The resulting dark red solution was stirred for 1 h then the solvent was removed *in vacuo*. The resulting sticky orange solid was dissolved in *n*-hexane (5 ml). Orange crystalline material was deposited on standing and the mixture was stored at -25 °C overnight. The supernatant was removed by filtration and the orange crystals were washed with cold (-10 °C) light petroleum (2 x 3 ml) and the residual solvent was removed under vacuum. Yield: 0.79 g, 81%.

$^1\text{H}$  NMR [ $\text{C}_6\text{D}_6$ ]:  $\delta$  1.05 (m, 4H, THF), 2.24 (s, 6H, *p*-Me), 2.41 (s, 12H, *o*-Me), 3.27 (m, 4H, THF), 6.92 (s, 4H, ArH).  $^{13}\text{C}\{^1\text{H}\}$  NMR [ $\text{C}_6\text{D}_6$ ]:  $\delta$  21.14 (*p*-Me), 25.18 (THF), 25.20

(*o*-Me), 68.68 (THF), 128.72 (ArH), 132.22, 140.54, 142.45 (Ar).  $^7\text{Li}\{^1\text{H}\}$  NMR [ $\text{C}_6\text{D}_6$ ]:  $\delta$  2.4 (br. s).  $^{31}\text{P}\{^1\text{H}\}$  NMR [ $\text{C}_6\text{D}_6$ ]:  $\delta$  -90.4 (br. s).

### 3.7.21 Synthesis of [(Dipp)(Mes)P]Li(THF)<sub>2</sub> (131b)

To a solution of (Dipp)(Mes)PH (**109**) (0.55 g, 1.76 mmol) in THF (10 ml) was added a solution of *n*BuLi in hexanes (2.3 M, 0.8 ml, 1.84 mmol). The resulting red solution was stirred for 1 h and the solvent was removed *in vacuo*. The resulting sticky orange solid was crystallized from cold (-25 °C) Et<sub>2</sub>O (10 ml) to give large orange crystals of [(Dipp)(Mes)P]Li(THF)<sub>3</sub> (**131a**). The crystals were isolated by filtration, washed with cold (0 °C) light petroleum (2 x 5 ml) and residual solvent was removed under vacuum to give the alternative solvate [(Dipp)(Mes)P]Li(THF)<sub>2</sub> (**131b**) as a yellow powder. Yield: 0.60 g, 74%.

$^1\text{H}$  NMR [*d*<sub>8</sub>-toluene, 298K]: 1.11 (d,  $J_{\text{HH}} = 6.9$  Hz, 12H, CHMe<sub>2</sub>), 1.37 (m, 8H, THF), 2.20 (s, 3H, *p*-Me), 2.34 (s, 6H, *o*-Me), 3.49 (m, 8H, THF), 4.19 (m, 2H, CHMe<sub>2</sub>), 6.81 (s, 2H, ArH), 7.08 (d,  $J_{\text{HH}} = 7.6$  Hz, 2H, ArH), 7.14 (m, 1H, ArH).  $^{13}\text{C}\{^1\text{H}\}$  NMR [*d*<sub>8</sub>-toluene, 298K]: 20.67 (*p*-Me), 24.36 (CHMe<sub>2</sub>), 24.94 (d,  $J_{\text{PC}} = 10.7$  Hz, *o*-Me), 25.23 (THF), 33.27 (d,  $J_{\text{PC}} = 12.3$  Hz, CHMe<sub>2</sub>), 67.84 (THF), 122.30, 124.79, 128.39 (ArH), 131.39 (Ar), 140.38 (d,  $J_{\text{PC}} = 8.3$  Hz, Ar), 144.39 (d,  $J_{\text{PC}} = 25.5$  Hz, Ar), 144.82 (d,  $J_{\text{PC}} = 22.5$ , Ar), 151.94 (d,  $J_{\text{PC}} = 6.2$  Hz, Ar).  $^7\text{Li}$  NMR [*d*<sub>8</sub>-toluene, 298K]: 2.1 (s).  $^{31}\text{P}\{^1\text{H}\}$  NMR [*d*<sub>8</sub>-toluene, 298K]: -100.7 (br. s).

### 3.7.22 Synthesis of [(Dipp){(Me<sub>3</sub>Si)<sub>2</sub>CH}P]Li(THF)<sub>3</sub> (134)

To a cold (-78 °C) solution of (Dipp){(Me<sub>3</sub>Si)<sub>2</sub>CH}PH (**113**) (0.75 g, 2.13 mmol) in THF (10 ml) was added a solution of *n*BuLi in hexanes (2.3 M, 0.9 ml, 2.07 mmol). The resulting pale orange solution was allowed to warm to room temperature. The resulting red solution was stirred for 30 min and the solvent was removed *in vacuo*. The sticky orange solid was dissolved in a mixture of Et<sub>2</sub>O (5 ml) and light petroleum (5 ml) to give an orange solution. Storage at -25 °C overnight formed large orange crystals of [(Dipp){(Me<sub>3</sub>Si)<sub>2</sub>CH}P]Li(THF)<sub>3</sub> (134). The supernatant solution was removed by filtration and the orange crystals were washed with cold (0 °C) light petroleum (10 ml). The residual solvent was removed under vacuum to give 134 as an orange crystalline solid. Yield: 0.50 g, 41%.

$^1\text{H}$  NMR [*d*<sub>8</sub>-toluene, 253 K]:  $\delta$  0.42 (s, 18H, CH(SiMe<sub>3</sub>)<sub>2</sub>), 0.93 (s, 1H, CH(SiMe<sub>3</sub>)<sub>2</sub>), 1.32 (m, 12H, THF), 1.48 (d,  $J_{\text{HH}} = 6.6$  Hz, 12H, CHMe<sub>2</sub>), 3.36 (br. m, 12H, THF), 4.94 (br. s,

2H,  $CHMe_2$ ), 7.18 (m, 3H, ArH).  $^{13}C\{^1H\}$  NMR [ $d_8$ -toluene, 253 K]:  $\delta$  1.87 (d,  $J_{PC} = 5.4$  Hz,  $CH(SiMe_3)_2$ ), 8.08 ( $J_{PC} = 66.3$  Hz,  $CH(SiMe_3)_2$ ), 25.29 (THF), 25.58 ( $CHMe_2$ ), 68.12 (THF), 122.03, 122.95 (ArH), 152.39 (Ar), 153.63 (d,  $J_{PC} = 57.5$  Hz, Ar).  $^7Li$  NMR [ $d_8$ -toluene, 253 K]: 2.0 (t,  $J_{LiP} = 66.8$  Hz), 0.54 (d,  $J_{LiP} = 82.4$  Hz, 11) in a 1:10 ratio.  $^{31}P\{^1H\}$  NMR [ $d_8$ -toluene, 253 K]: -100.7 (q,  $J_{LiP} = 82.4$  Hz), -127.2 (br. s) in a 11:1 ratio.

### 3.7.23 Synthesis of $(Me_2PhSi)_2CHLi$ (**125**)<sup>[11b]</sup>

To a cold (-78 °C) solution of  $(Me_2PhSi)_2SiHBr$  (**123**) (6.60 g, 18.2 mmol) in  $Et_2O$  (15 ml) was added, dropwise, a solution of  $nBuLi$  in hexanes (7.4 ml, mmol). The mixture was stirred for 2 h at -78 °C and the solvent was removed *in vacuo* while the solution was still cold. The resulting yellow oil was heated while under vacuum to remove volatile impurities and allowed to cool. To the resulting yellow solid was added *n*-hexane (20 ml) and the mixture was agitated to form a yellow solution with a white solid. The supernatant solution was removed by filtration and residual solvent was removed under vacuum from the remaining solid to give  $(Me_2PhSi)_2CHLi$  (**125**) as a white powder (2.21 g, 42%). The volume of the filtrate was reduced to 10 ml and stored at -25 °C overnight. The supernatant solution was removed by filtration and the residual solvent was removed from remaining solid under vacuum to give a second crop of **125** as a pale yellow powder (1.80 g, 34%). Combined yield: 4.01 g, 76%.

### 3.7.24 Synthesis of $\{(Me_2PhSi)_2CH\}_2PCl$ (**143**)

To a cold (-78 °C) solution of  $PCl_3$  (0.6 ml, 6.88 mmol) in  $Et_2O$  (20 ml) was added, dropwise, a solution of  $(Me_2PhSi)_2CHLi$  (**125**) (4.01 g, 13.80 mmol) in  $Et_2O$  (30 ml). The resulting mixture was allowed to warm to room temperature and was stirred for 2 h. The resulting pale yellow solution with pale solids was filtered and the solvent was removed *in vacuo* from the filtrate. The resulting yellow powder was extracted into *n*-hexane (15 ml) and stored at -25 °C overnight. The supernatant solution was removed by filtration and the remaining solid was washed with cold (-10 °C) light petroleum (10 ml) and residual solvent was removed under vacuum to give the product as a white powder. Yield: 2.38 g, 54%.

$^1H\{^{31}P\}$  NMR [ $d_8$ -toluene, 233 K]:  $\delta$  -0.58 (s, 3H, Me), -0.15 (s, 3H, Me), 0.23 (s, 3H, Me), 0.56 (s, 3H, Me), 0.62 (s, 6H, 2 Me), 0.67 (s, 1H, CH), 0.70 (s, 3H, Me), 0.72 (s, 3H, Me), 2.20 (s, 1H, CH), 7.17-7.26 (m, 16H, ArH), 7.47-7.51 (m, 4H, ArH).  $^{13}C\{^1H\}$  NMR [ $d_8$ -toluene, 233 K]: -2.10 (Me), -1.20 (2 Me), -0.45 (d,  $J_{PC} = 8.0$  Hz, Me), 0.38 (Me), 0.75 (d,  $J_{PC}$

= 16.9 Hz, Me), 3.32 (Me), 4.43 (Me), 18.03 (d,  $J_{PC}$  = 66.0 Hz, CH), 20.57 (d,  $J_{PC}$  = 84.9 Hz, CH), 129.75, 134.10, 134.72, 134.85 (ArH), 135.72 (d,  $J_{PC}$  = 4.5 Hz, ArH), 127.72, 127.88, 128.32, 129.08, 129.20, 129.77, 134.10, 134.72, 134.85 (Ar), 135.77 (d,  $J_{PC}$  = 4.0 Hz, Ar).  $^{31}\text{P}\{^1\text{H}\}$  NMR [ $d_8$ -toluene, 233 K]:  $\delta$  154.1 (s).

### 3.7.25 Synthesis of $[(\text{Me}_3\text{Si})_2\text{CH}]_2\text{P}(\text{Li})_3(\text{OEt}_2)$ (**139**)

To a solution of  $\{(\text{Me}_3\text{Si})_2\text{CH}\}_2\text{PCl}$  (**140**) (5.46 g, 14.2 mmol) in  $\text{Et}_2\text{O}$  (40 ml) was added Li shot (0.296 g, 42.5 mmol). The mixture was sonicated for 30 min and stirred overnight. The resulting red solution with pale solids was filtered and the solvent was removed *in vacuo*. The resulting sticky yellow solid was dissolved in *n*-hexane (15 ml). Storage at  $-25\text{ }^\circ\text{C}$  overnight formed large yellow crystals. The supernatant solution was removed by filtration and the crystals were washed with cold ( $-10\text{ }^\circ\text{C}$ ) light petroleum and the residual solvent was removed under vacuum to give  $[(\text{Me}_3\text{Si})_2\text{CH}]_2\text{P}(\text{Li})_3(\text{OEt}_2)$  (**139**) as a yellow crystalline solid. Yield: 2.04 g, 38%.

$^1\text{H}$  NMR [ $\text{C}_6\text{D}_6$ ]:  $\delta$  0.29 (s, 108H,  $\text{SiMe}_3$ ), 0.32 (s, 12H, CH), 1.00 (t,  $J_{\text{HH}}$  = 7.0 Hz, 6H,  $\text{OCH}_2\text{CH}_3$ ), 3.33 (q,  $J_{\text{HH}}$  = 7.0 Hz, 4H,  $\text{OCH}_2\text{CH}_3$ ).  $^{13}\text{C}\{^1\text{H}\}$  NMR [ $\text{C}_6\text{D}_6$ ]:  $\delta$  2.85 ( $\text{SiMe}_3$ ), 8.43 (br. s, CH), 14.79 ( $\text{OCH}_2\text{CH}_3$ ), 63.35 ( $\text{OCH}_2\text{CH}_3$ ).  $^7\text{Li}$  NMR [ $\text{C}_6\text{D}_6$ ]:  $\delta$  2.4 (br. s).  $^{31}\text{P}\{^1\text{H}\}$  NMR [ $\text{C}_6\text{D}_6$ ]:  $\delta$  -112.1 (br. s).

### 3.7.26 Synthesis of $[(\text{Me}_3\text{Si})_2\text{CH}]_2\text{P}(\text{K})$ (**141**)

A solution of  $\{(\text{Me}_3\text{Si})_2\text{CH}\}_2\text{PCl}$  (**140**) (0.78 g, 2.02 mmol) in  $\text{Et}_2\text{O}$  (25 ml) was added to a flask containing a potassium mirror (0.265 g, 6.78 mmol) and the resulting mixture was sonicated for 90 min. The resulting orange mixture was further stirred for 4 days to give a dark green mixture with pale solids. The mixture was filtered and solvent was removed *in vacuo* from the filtrate. The resulting sticky green solid was washed with *n*-hexane (15 ml) and the residual solvent was removed under vacuum to give (**141**) as a pale green powder. Yield: 0.451 g, 57%.

$^{31}\text{P}\{^1\text{H}\}$  NMR ( $\text{C}_6\text{D}_6$ ): -96.7 (s).

### 3.7.27 Synthesis of $[\text{Li}(\mu\text{-P}\{\text{CH}(\text{SiMe}_3)_2\})][\text{K}(\mu\text{-P}\{\text{CH}(\text{SiMe}_3)_2\})]$ (**142**)

To a mixture of  $[(\text{Me}_3\text{Si})_2\text{CH}]_2\text{P}(\text{Li})_3(\text{OEt}_2)$  (**139**) (0.785 g, 0.69 mmol) and *t*-BuOK (0.112 g, 1.00 mmol) was added  $\text{Et}_2\text{O}$  (10 ml). The resulting mixture was stirred for 1 h and the solvent was removed *in vacuo*. The resulting pale yellow solid was washed with light

petroleum (3 x 10 ml) and the residual solvent was removed under vacuum. Yield: 0.50 g, 67%.

$^1\text{H}$  NMR [ $\text{C}_6\text{D}_6$ ]:  $\delta$  0.17 (s, 4H, CH), 0.29 (s, 72H,  $\text{SiMe}_3$ ).  $^{13}\text{C}\{^1\text{H}\}$  NMR [ $\text{C}_6\text{D}_6$ ]:  $\delta$  3.10 ( $\text{SiMe}_3$ ), 9.89 (br. m, CH).  $^{31}\text{P}\{^1\text{H}\}$  NMR [ $\text{C}_6\text{D}_6$ ]:  $\delta$  -104.8 (q,  $J_{\text{PLi}} = 88$  Hz).  $^7\text{Li}$  NMR [ $\text{C}_6\text{D}_6$ ]: 3.4 (t,  $J_{\text{PLi}} = 88\text{Hz}$ ).

### 3.8 References

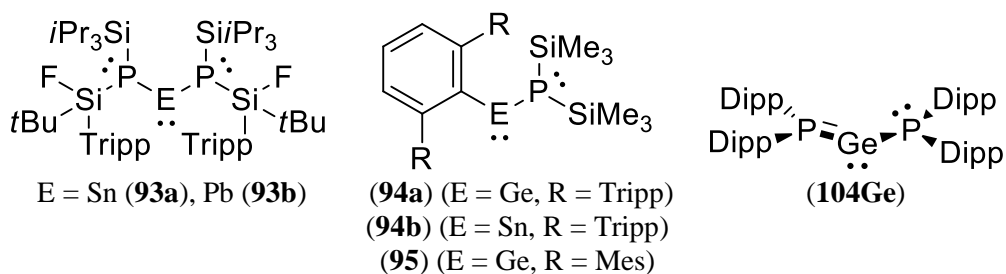
- [1] K. Izod, D. G. Rayner, S. M. El-Hamruni, R. W. Harrington, U. Baisch, *Angew. Chem. Int. Ed. Engl.*, **2014**, 53, 3636-3640.
- [2] (a) K. Izod, *Adv. Inorg. Chem.*, **2000**, 50, 33-107; (b) M. Westerhausen, T. Rotter, H. Górls, C. Birg, M. Warchold, H. Noth, *Z. Naturforsch., B*, **2005**, 60, 766-770; (c) C. von Hänisch, S. Traut, S. Stahl, *Z. Anorg. Allg. Chem.*, **2007**, 633, 2199-2204; (d) M. Driess, H. Pritzkow, *Z. Anorg. Allg. Chem.*, **1996**, 622, 1524-1530; (e) R. A. Jones, A. L. Stuart, T. C. Wright, *J. Am. Chem. Soc.*, **1983**, 105, 7459-7460; (f) P. B. Hitchcock, M. F. Lappert, P. P. Power, S. J. Smith, *J. Chem. Soc., Chem. Commun.*, **1984**, 1669-1670; (g) E. Hey-Hawkins, E. Sattler, *J. Chem. Soc., Chem. Commun.*, **1992**, 775-776; (h) G. W. Rabe, S. Kheradmandan, G. P. A. Yap, *Inorg. Chem.*, **1998**, 37, 6541-6543; (i) R. A. Bartlett, M. M. Olmstead, P. P. Power, *Inorg. Chem.*, **1986**, 25, 1243-1247; (j) I. Jevtovikj, R. Herrero, S. Gomez-Ruiz, P. Lonneck, E. Hey-Hawkins, *Inorg. Chem.*, **2013**, 52, 4488-4493; (k) K. Izod, J. Stewart, E. R. Clark, W. Clegg, R. W. Harrington, *Inorg. Chem.*, **2010**, 49, 4698-4707; (l) F. Dornhaus, M. Bolte, H.-W. Lerner, M. Wagner, *Eur. J. Inorg. Chem.*, **2006**, 2006, 1777-1785; (m) R. Edge, R. J. Less, V. Naseri, E. J. McInnes, R. E. Mulvey, D. S. Wright, *Dalton Trans*, **2008**, 6454-6460; (n) G. W. Rabe, S. Kheradmandan, L. M. Liable-Sands, I. A. Guzei, A. L. Rheingold, *Angew. Chem. Int. Ed.*, **1998**, 37, 1404-1407; (o) G. W. Rabe, J. Riede, A. Schier, *Acta Crystallogr. C*, **1996**, 52, 1350-1352.
- [3] E. Rivard, A. D. Sutton, J. C. Fetting, P. P. Power, *Inorg. Chim. Acta*, **2007**, 360, 1278-1286.
- [4] K. Izod, P. O'Shaughnessy, W. Clegg, *Organometallics*, **2002**, 21, 641-646.
- [5] H. Hope, M. M. Olmstead, P. P. Power, X. Xiaojie, *J. Am. Chem. Soc.*, **1984**, 106, 819-821.
- [6] C. G. Fleming, A. M. Slawin, K. S. Athukorala Arachchige, R. Randall, M. Buhl, P. Kilian, *Dalton Trans*, **2013**, 42, 1437-1450.
- [7] (a) D. J. Brauer, F. Bitterer, F. Dörrenbach, G. Heßler, O. Stelzer, C. Krüger, F. Lutz, *Z. Naturforsch., B*, **1996**, 51; (b) R. A. Bartlett, M. M. Olmstead, P. P. Power, G. A. Sigel, *Inorg. Chem.*, **1987**, 26, 1941-1946; (c) A. H. Cowley, R. A. Kemp, *Inorg. Chem.*, **1983**, 22, 547-550.
- [8] M. W. Wallasch, D. Weismann, C. Riehn, S. Ambrus, G. Wolmershäuser, A. Lagutschenkov, G. Niedner-Schatteburg, H. Sitzmann, *Organometallics*, **2010**, 29, 806-813.
- [9] G. M. Whitesides, M. Eisenhut, W. M. Bunting, *J. Am. Chem. Soc.*, **1974**, 96, 5398-5407.
- [10] R. A. Bartlett, H. V. R. Dias, P. P. Power, *J. Organomet. Chem.*, **1988**, 341, 1-9.
- [11] (a) N. Wiberg, G. Wagner, G. Müller, J. Riede, *J. Organomet. Chem.*, **1984**, 271, 381-391; (b) C. Eaborn, W. Clegg, P. B. Hitchcock, M. Hopman, K. Izod, P. N. O'Shaughnessy, J. D. Smith, *Organometallics*, **1997**, 16, 4728-4736.

- [12] J. L. Atwood, T. Fjeldberg, M. F. Lappert, N. T. Luong-Thi, R. Shakir, A. J. Thorne, *J. Chem. Soc., Chem. Commun.*, **1984**, 0, 1163-1165.
- [13] E. Hey, C. L. Raston, B. W. Skelton, A. H. White, *J. Organomet. Chem.*, **1989**, 362, 1-10.
- [14] M. Driess, G. Huttner, N. Knopf, H. Pritzkow, L. Zsolnai, *Angew. Chem. Int. Ed.*, **1995**, 34, 316-318.
- [15] G. W. Rabe, G. P. A. Yap, A. L. Rheingold, *Inorg. Chem.*, **1997**, 36, 1990-1991.
- [16] W.-W. du Mont, H.-J. Kroth, *Angew. Chem. Int. Ed.*, **1977**, 16, 792-793.
- [17] M. J. S. Gynane, A. Hudson, M. F. Lappert, P. P. Power, H. Goldwhite, *J. Chem. Soc., Dalton Trans.*, **1980**, 2428-2433.
- [18] I. J. Colquhoun, H. C. E. McFarlane, W. McFarlane, *Phosphorous Sulfur*, **1983**, 18, 61-64.
- [19] S. Traut, C. von Hänisch, H.-J. Kathagen, *Eur. J. Inorg. Chem.*, **2009**, 2009, 777-783.
- [20] O. W. Steward, J. S. Johnson, *J. Organomet. Chem.*, **1973**, 55, 209-213.
- [21] W. Clegg, S. Doherty, K. Izod, H. Kagerer, P. O'Shaughnessy, J. M. Sheffield, *J. Chem. Soc., Dalton Trans.*, **1999**, 1825-1830.
- [22] R. Wolf, E. Hey-Hawkins, *Z. Anorg. Allg. Chem.*, **2006**, 632, 727-734.
- [23] L. Lochmann, J. Trekoval, *J. Organomet. Chem.*, **1987**, 326, 1-7.
- [24] S. Corbelin, N. P. Lorenzen, J. Kopf, E. Weiss, *J. Organomet. Chem.*, **1991**, 415, 293-313.
- [25] S. T. Liddle, K. Izod, *Organometallics*, **2004**, 23, 5550-5559.

## Chapter 4. Synthesis of diphosphatetrylenes

### 4.1 Introduction

As previously mentioned in Section 1.8.8, there are only a small number of reported monomeric phosphatetrylenes, which contrasts the abundance of their lighter analogues aminotetrylenes. The low usage of phosphide ligands in tetrylenes is mostly associated with the higher energy of planarization of phosphorus, compared to nitrogen. Consequently, phosphorus centres adjacent to tetrel centres typically adopt a pyramidal geometry, which cannot provide efficient orbital overlap with the vacant  $p_z$  orbital at the tetrel centre and offer the potential for the formulation of head-to-tail dimers. The phosphorus centres in compounds **93a/b**, **94a/b** and **95** adopt a pyramidal geometry in the solid-state and are kinetically stabilised by the bulky substituents. However, the recently reported diphosphatetrylene **104Ge** is stabilised by efficient  $p\pi$ - $p\pi$  interactions from planar phosphorus.<sup>[1]</sup> Such interactions are very rare for main group compounds.

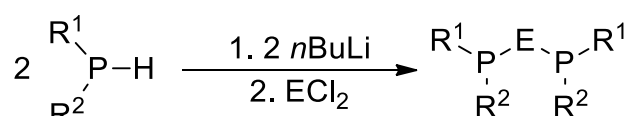


**Figure 61:** Previous monomeric heavier phosphatetrylenes

We sought to expand the number of tetrylenes stabilised by  $p\pi$ - $p\pi$  interactions from a planar phosphorus centre from the sole example of  $\{(Dipp)_2P\}_2Ge$  (**104Ge**)<sup>[1]</sup> by synthesising the heavier analogues,  $\{(Dipp)_2P\}_2E$  [E = Sn (**104Sn**), Pb (**104Pb**)], and using the bulky alkali metal phosphides prepared in Chapter 3 to synthesis an array of diphosphatetrylenes. The varying steric bulk of the pro-ligands **108-111** may allow for the determination of the minimum steric encumbrance required to planarize the phosphorus centre in the corresponding diphosphatetrylenes. In addition, the different electronics of the phosphorus centres in the pro-ligands **111**, **113** and **114** may influence the geometry and electronics of the corresponding diphosphatetrylenes.

## 4.2 Synthesis of {(Dipp)<sub>2</sub>P}<sub>2</sub>Sn (104Sn), {(Tripp)<sub>2</sub>P}<sub>2</sub>Ge (145Ge), {(Tripp)<sub>2</sub>P}<sub>2</sub>Sn (145Sn), {(Dipp)(Mes)P}<sub>2</sub>Ge.(*n*-hexane)<sub>0.5</sub> (146Ge.(C<sub>6</sub>H<sub>14</sub>)<sub>0.5</sub>), {(Dipp)(Mes)P}<sub>2</sub>Sn (146Sn) and [(Dipp){(Me<sub>3</sub>Si)<sub>2</sub>CH}P]<sub>2</sub>Sn (147Sn)

The diphosphatetrylenes shown in Tables 1 and 2 were prepared by the addition of two equivalents of the corresponding *in-situ* generated lithium phosphide, with the exception of **148Ge** and **148Sn** where [(Me<sub>3</sub>Si)<sub>2</sub>CH]<sub>2</sub>P]Li(OEt)<sub>2</sub> (139) was used, to GeCl<sub>2</sub>(1,4-dioxane) at room temperature or SnCl<sub>2</sub> at -78 °C, as shown in Scheme 26. Although these metathesis reactions appear to give the diphosphatetrylenes quantitatively, as judged by <sup>31</sup>P NMR spectroscopy, the isolated yields were rather low, which we attribute to the high solubility of the products even in non-polar solvents. The compounds presented in Table 1 were characterised by X-ray crystallography.



**Scheme 26:** General procedure for the synthesis of diphosphatetrylenes

E	R <sup>1</sup>	R <sup>2</sup>	Compound	Crystal colour	Solution colour	Yield (%)
Ge	Dipp	Dipp	<b>104Ge</b>	Red	Dark red	34
Sn	Dipp	Dipp	<b>104Sn</b>	Dark purple	Dark purple	39
Ge	Tripp	Tripp	<b>145Ge</b> ·C <sub>7</sub> H <sub>14</sub>	Red	Dark red	31
Sn	Tripp	Tripp	<b>145Sn</b>	Yellow	Dark purple	29
Ge	Dipp	Mes	<b>146Ge</b> ·(C <sub>6</sub> H <sub>14</sub> ) <sub>0.5</sub>	Red	Red	35
Sn	Dipp	Mes	<b>146Sn</b>	Purple	Dark purple	27
Sn	Dipp	CH(SiMe <sub>3</sub> ) <sub>2</sub>	<b>147Sn</b>	Dark green	Dark green	35
Sn	CH(SiMe <sub>3</sub> ) <sub>2</sub>	CH(SiMe <sub>3</sub> ) <sub>2</sub>	<b>148Sn</b>	Dark red	Red	-

**Table 1:** Colour and yield of X-ray crystallographically characterised diphosphatetrylenes

Unfortunately, we were unable to isolate material suitable for characterisation by X-ray crystallography or NMR spectroscopy for the tetrylenes **147Ge**, **147Sn**, **149Ge** and **149Sn**. The <sup>31</sup>P chemical shifts of these compounds observed in the crude reaction mixtures are shown in Table 2, along with the observed <sup>31</sup>P-Sn coupling constant for **149Sn**. The unexpected reactions of [(Mes)<sub>2</sub>P]Li with either GeCl<sub>2</sub>(1,4-dioxane) or SnCl<sub>2</sub> is reported in Chapter 5.

E	R <sup>1</sup>	R <sup>2</sup>	Compound	Solution colour	<sup>31</sup> P chemical shift (ppm)	J <sub>PSn</sub> (Hz)
Ge	Dipp	CH(SiMe <sub>3</sub> ) <sub>2</sub>	<b>147Ge</b>	Red	23.9	-
Ge	CH(SiMe <sub>3</sub> ) <sub>2</sub>	CH(SiMe <sub>3</sub> ) <sub>2</sub>	<b>148Ge</b>	Red	49.9	-
Ge	Dep	Dep	<b>149Ge</b>	Purple	-9.0	-
Sn	Dep	Dep	<b>149Sn</b>	Purple	-48.9	1290

**Table 2:** Colour and <sup>31</sup>P{<sup>1</sup>H} NMR shifts of diphosphatetrylenes that were not structurally characterised



The diphosphagermylenes **104Ge**, **145Ge** and **146Ge** appear to be stable in toluene solution over several days, as judged by  $^{31}\text{P}$  NMR spectroscopy. In contrast, the diphosphastannylenes **104Sn**, **145Sn**, **146Sn**, **147Sn**, and **148Sn** decompose after a day in solution to metallic tin and the corresponding diphosphine or phosphinyl radical (see below). Decomposition is accelerated on exposure to ambient light or elevated temperatures (above 50 °C) and complete decomposition is observed in less than 30 min under these conditions.

The synthesis of  $[\{(\text{Me}_3\text{Si})_2\text{CH}\}_2\text{P}]_2\text{Sn}$  (**148Sn**) was originally attempted by Lappert in 1984 by the reaction between  $[\text{Li}(\mu\text{-P}\{\text{CH}(\text{SiMe}_3)_2\})_2]$  (**138**) and  $\text{SnCl}_2$  in  $\text{Et}_2\text{O}$ , which yielded metallic tin and the corresponding phosphinyl radical  $\{(\text{Me}_3\text{Si})_2\text{CH}\}_2\text{P}^\cdot$ .<sup>[2]</sup> However, by slight modification of the reaction conditions, we were able to synthesise and structurally characterise **148Sn**, albeit in low yield (see below).

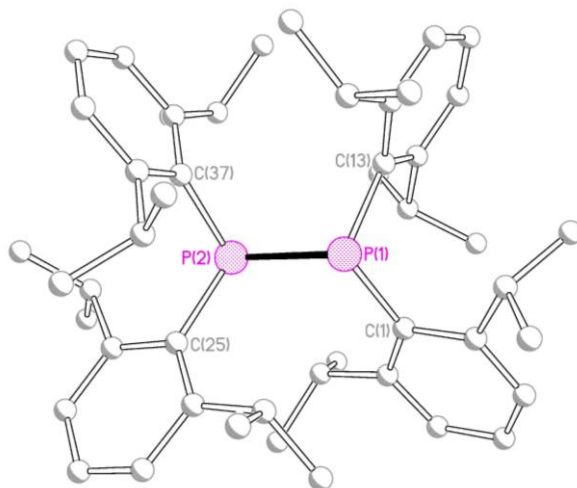
The initial reaction between the lithium phosphides and  $\text{SnCl}_2$  gave pale yellow to red solutions, which contrast the initial dark red to purple solutions formed in the corresponding reactions with  $\text{GeCl}_2(1,4\text{-dioxane})$ . We attribute the pale colours of the diphosphastannylenes to the initial formation of ate complexes of the form  $(\text{R}_2\text{P})_2\text{SnClLi}(\text{THF})_n$ , which would be electron precise and in which P-Sn  $p\pi\text{-}p\pi$  interactions would be absent. These ate complexes degrade in non-donor solvents to give  $\text{LiCl}$  and deeply coloured solutions associated with  $\text{P}=\text{E}$   $\pi\text{-}\pi^*$  transitions. The formation of similar ate complexes during the synthesis of the germylenes may be disfavoured because of the smaller size of the  $\text{Ge}(\text{II})$  atom and the consequently increased steric hindrance about these centres.

#### 4.3 Attempted synthesis of $\{(\text{Dipp})_2\text{P}\}_2\text{Pb}$ (**104Pb**) and solid-state structure of $(\text{Dipp})_2\text{P-P}(\text{Dipp})_2$ (**150**)

The inherently weak P-Pb bond in phosphaplumbylenes, resulting from the poor orbital overlap, makes these compounds more challenging to synthesise and isolate than the corresponding phosphagermylenes and -stannylenes. As a result, compound **93b** is the only reported example of a monomeric phosphaplumbylene.<sup>[3]</sup> Our attempt to expand the range of such compounds, by the reaction between two equivalents of *in-situ* generated  $[(\text{Dipp})_2\text{P}]\text{Li}$  and  $\text{PbI}_2$ , initially looked promising the very dark purple colour of the cold reaction solution suggested the presence of  $\pi\text{-}\pi^*$  transitions. However, this solution degraded to a pale yellow solution with a large amount of black solid, which we assume to be metallic lead, upon gradual warming to room temperature, even in the complete absence of light. The  $^{31}\text{P}\{^1\text{H}\}$  NMR spectrum of the resulting pale yellow solution exhibited a single peak at -38 ppm,

which we attribute to the diphosphine  $(\text{Dipp})_2\text{P}-\text{P}(\text{Dipp})_2$  (**150**), arising from the over-reduction or reductive-elimination of the lead centre. Attempts to prevent these decomposition pathways by substituting  $\text{PbI}_2$  for  $\text{PbCl}_2$  in the reaction or by only allowing the reaction mixture to warm to  $-10\text{ }^\circ\text{C}$ , were unsuccessful. From these results, we inferred that the putative diphosphaplumbylene  $\{(\text{Dipp})_2\text{P}\}_2\text{Pb}$  (**104Pb**) was too thermally unstable to isolate.

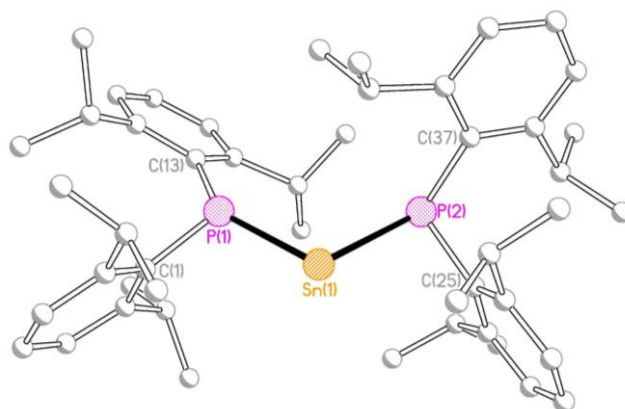
However, the reaction between two equivalents of  $[(\text{Dipp})_2\text{P}]\text{Li}$  and  $\text{PbI}_2$  at room temperature allowed us to deliberately isolate a clean sample of **150** in moderate yield. Single crystals of **150** suitable for characterisation by X-ray crystallography were previously obtained from a partially decomposed sample of **104Sn**. The structure of **150** is shown in Figure 62, along with selected bond lengths and angles. Compound **150** is isoskeletal with the more highly substituted analogue  $(\text{Tripp})_2\text{P}-\text{P}(\text{Tripp})_2$  (**151**).<sup>[4]</sup> While the P-P distance in **150** is slightly longer than the respective distance in the less bulky derivative  $\text{Ph}_2\text{P}-\text{PPh}_2$  (**152**),<sup>[5]</sup> it is significantly shorter than the respective distance in  $\{(\text{Me}_3\text{Si})_2\text{CH}\}_2\text{P}-\text{P}\{\text{CH}(\text{SiMe}_3)_2\}_2$  (**153**)<sup>[6]</sup> [P-P distance = 2.2250(5) (**150**), 2.217(1) (**152**), 2.3103(7) (**153**)].



**Figure 62:** Molecular structure of **150** with H atoms and minor disorder component omitted for clarity. Selected bond lengths (Å) and angles (°): P(1)-P(2) 2.2250(5), P(1)-C(1) 1.8752(15), P(1)-C(13) 1.8762(15), P(2)-C(25) 1.8810(14), P(2)-C(37) 1.8683(14), C(1)-P(1)-P(2) 109.90(5), C(1)-P(1)-C(13) 105.14(6), C(13)-P(1)-P(2) 103.90(4), C(25)-P(2)-P(1) 110.45(5), C(37)-P(2)-P(1) 102.69(4), C(37)-P(2)-C(25) 105.16(6).

#### 4.4 Solid-state structure of {(Dipp)<sub>2</sub>P}<sub>2</sub>Sn (104Sn)

Compound **104Sn** crystallises as discrete monomers that are isostructural and isomorphous with **104Ge**, with a V-shaped P-Sn-P core [P-Sn-P 106.20(3)°] and with one nearly planar and one pyramidal phosphorus centre [sum of angles at P(1) 355.53° and 311.58°] (Fig. 63). The slightly more pyramidal nature of P(1) in **104Sn** compared to **104Ge** is attributed to the reduced orbital overlap of the lone pair on the planar phosphorus with the 5p orbital at the tin centre compared to the 4p orbital at the germanium. The Sn(1)-P(2) distance [2.5757(7) Å] in **104Sn** is very similar to the average for the Sn-P bonds in [(*i*Pr<sub>3</sub>Si){(F)(*t*Bu)(Tripp)Si}P]<sub>2</sub>Sn (**93a**) of 2.567(1) Å.<sup>[3]</sup> However, no Sn=P double bonds have been authenticated by X-ray crystallography; the phosphastannanes {(Me<sub>3</sub>Si)<sub>2</sub>CH}<sub>2</sub>Sn=P(Mes\*) (**154**) and (Tripp)<sub>2</sub>Sn=P(Mes\*) (**155**) have been characterised by NMR spectroscopy.<sup>[7]</sup> The Sn(1)-P(1) distance [2.4458(8) Å] in **104Sn** is 5.0% shorter than the Sn(1)-P(2) distance, consistent with Sn=P multiple bond character.

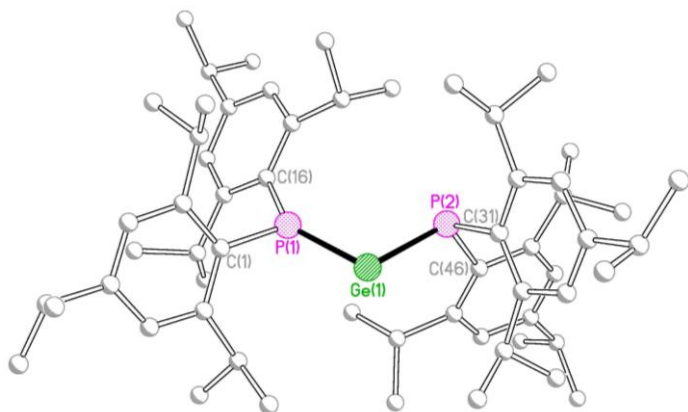


**Figure 63:** Molecular structure of **104Sn** with hydrogen atoms omitted for clarity. Selected bond lengths (Å) and angles (°): Sn(1)-P(1) 2.4458(8), Sn(1)-P(2) 2.5757(7), P(1)-C(1) 1.843(3), P(1)-C(13) 1.846(3), P(2)-C(25) 1.860(3), P(2)-C(37) 1.860(3), P(1)-Sn(1)-P(2) 106.20(3), C(1)-P(1)-Sn(1) 106.88(9), C(1)-P(1)-C(13) 105.21(12), C(13)-P(1)-Sn(1) 143.44(9), C(25)-P(2)-Sn(1) 88.59(8), C(25)-P(2)-C(37) 103.22(12), C(37)-P(2)-Sn(1) 119.77(9).

#### 4.5 Solid-state structure of {(Tripp)<sub>2</sub>P}<sub>2</sub>Ge·(C<sub>7</sub>H<sub>14</sub>) (145Ge·C<sub>7</sub>H<sub>14</sub>)

Compound **145Ge**·C<sub>7</sub>H<sub>14</sub> crystallises as a methylcyclohexane solvate that has an analogous structure to **104Ge**, with one planar and one pyramidal phosphorus centre [sum of angles at P(1) 360.0° and P(2) 311.5°] and a V-shaped P-Ge-P core [P-Ge-P 103.98(8)°] (Fig. 64). The solvent of crystallisation is only very weakly held and is rapidly lost under vacuum to give an amorphous pale red solid with elemental analysis and NMR spectra corresponding to the solvent-free {(Tripp)<sub>2</sub>P}<sub>2</sub>Ge (**145Ge**). While the Ge-P(2) distance (2.367(9) Å) in **145Ge**·C<sub>7</sub>H<sub>14</sub> is typical for Ge(II)-P distances, the Ge(1)-P(1) distance (2.231(2) Å) is

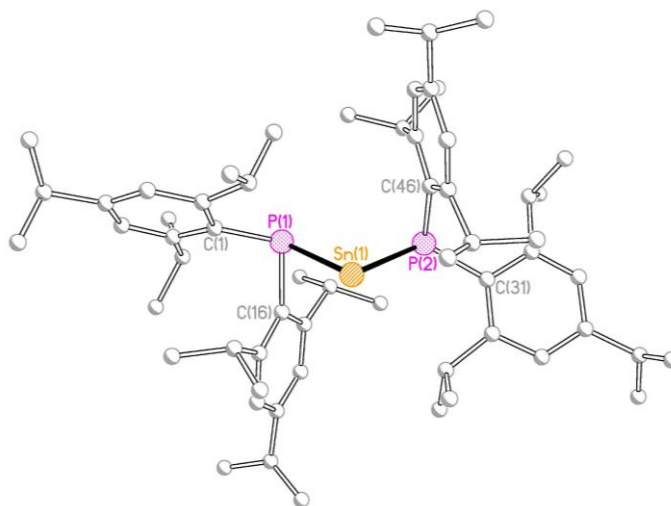
approximately 5% shorter, consistent with the multiple bond character of the Ge(1)-P(1) bond. For example, the Ge-P distance in the  $\beta$ -diketiminato-supported germanium phosphide complex **98**, which has an electron-precise germanium centre, is 2.3912(8) Å.<sup>[8]</sup> The (aryl)(phospha)germylene {2,6-(Tripp)<sub>2</sub>C<sub>6</sub>H<sub>3</sub>}Ge{P(SiMe<sub>3</sub>)<sub>2</sub>} has a relatively short Ge-P distance of 2.291(4) Å, although the phosphorus centre adopts a pyramidal geometry and, therefore, cannot possess significant  $\pi$ -interactions from this centre.<sup>[9]</sup> The Ge(1)-P(1) bond in **145Ge**·C<sub>7</sub>H<sub>14</sub> is slightly longer than the corresponding distances in the phosphagermenes (Mes)<sub>2</sub>Ge=P(Mes\*)<sup>[10]</sup> and (tBu<sub>2</sub>MeSi)<sub>2</sub>Ge=(Mes\*)<sup>[11]</sup> of 2.138(3) and 2.1748(14) Å, respectively, although these compounds involve Ge(IV)=P double bonds.



**Figure 64:** Molecular structure of **145Ge**·C<sub>7</sub>H<sub>14</sub> with the molecule of solvation and hydrogen atoms omitted for clarity. Selected bond lengths (Å) and angles (°): Ge(1)-P(1) 2.231(2), Ge(1)-P(2) 2.367(2), P(1)-C(1) 1.815(8), P(1)-C(16) 1.834(8), P(2)-C(31) 1.868(8), P(2)-C(46) 1.856(8), P(1)-Ge(1)-P(2) 103.98(8), C(1)-P(1)-C(16) 108.9(3), C(1)-P(1)-Ge(1) 107.8(3), C(16)-P(1)-Ge(1) 143.3(3), C(31)-P(2)-C(46) 104.6(3), C(31)-P(2)-Ge(1) 89.2(2), C(46)-P(2)-Ge(1) 117.7(3).

#### 4.6 Solid-state structure of {(Tripp)<sub>2</sub>P}<sub>2</sub>Sn (**145Sn**)

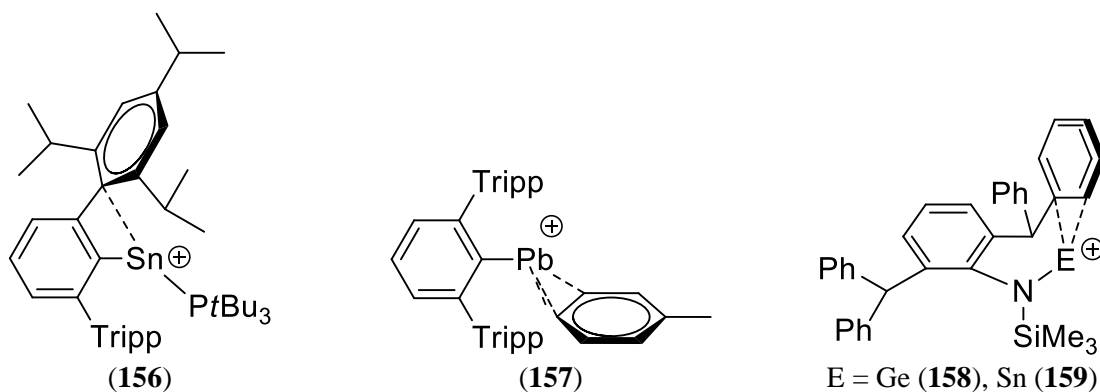
The pale yellow crystals of **145Sn** contrast with the dark purple crystals of **104Sn** (Table 1), suggesting an absence of  $\pi$ - $\pi^*$  interactions in **145Sn** that was confirmed by X-ray crystallography. Compound **145Sn** crystallises as discrete monomers with a V-shaped geometry and has two pyramidal phosphorus centres [sum of angles at P(1) 308.62° and P(2) 299.74°] in which the ligands adopt a *syn, syn* conformation (Fig. 65). The Sn-P distances [2.5836(6) and 2.5673(7) Å] are rather similar and are typical of P-Sn<sup>II</sup> distances.<sup>[3, 12]</sup> The P-Sn-P angle in **145Sn** is close to 90° and significantly more acute than the corresponding angle in **104Sn** [P(1)-Sn(1)-P(2) 89.62(2)° (**145Sn**) and 106.20(3)° (**104Sn**)].



**Figure 65:** Molecular structure of **145Sn** with hydrogen atoms omitted for clarity. Selected bond lengths (Å) and angles (°): Sn(1)-P(1) 2.5836(6), Sn(1)-P(2) 2.5673(7), P(1)-C(1) 1.862(2), P(1)-C(16) 1.870(2), P(2)-C(31) 1.856(2), P(2)-C(46) 1.876(2), P(1)-Sn(1)-P(2) 89.62(2), C(1)-P(1)-Sn(1) 114.93(7), C(1)-P(1)-C(16) 106.32(10), C(16)-P(1)-Sn(1) 82.37(7), C(31)-P(2)-Sn(1) 116.19(8), C(31)-P(2)-C(46) 104.35(11), C(46)-P(2)-Sn(1) 79.20(8).

The pyramidal phosphorus centres in **145Sn** prevent stabilisation of the tin centre by P-Sn  $\pi$ -interactions, which are observed in **104Sn**. However, one Tripp group from each phosphide ligand lies axial to the P-Sn-P core with rather acute and unsymmetrical  $C_{ipso}$ -P-Sn bond angles [C(16)-P(1)-Sn(1) 89.62(2)° and C(46)-P(2)-Sn(1) 79.20(8)°]. Along with these acute angles, the *ipso*-carbons of the phenyl rings lie in close proximity to the tin centre [Sn(1)⋯ $C_{ipso}$ (16) 2.9813(1) Å; Sn(1)⋯ $C_{ipso}$ (46) 2.882(2) Å]. These distances are well within the sums of the van der Waals radii of Sn and C (3.87 Å), suggesting there is significant interaction between the electron density at the *ipso*-carbons and the vacant p-orbital at the tin centre, with the latter distance corresponding to a slightly stronger interaction. The arene interactions were further confirmed by DFT calculations (see below).

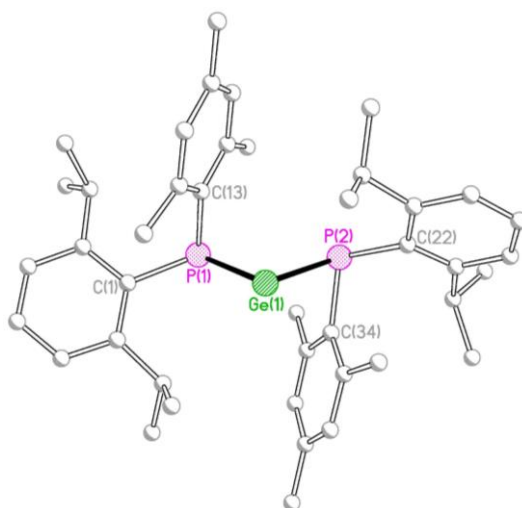
Group 14 element⋯arene interactions have previously been observed in a small number of cationic species, such as silylium cations ( $SiR_3^+$ ).<sup>[13]</sup> Very few of these compounds contain a group 14 element in the +2 oxidation state (e.g., **157-159**; Fig. 66).<sup>[14]</sup> The short Sn⋯ $C_{ipso}$  distance of 2.882(2) Å in **145Sn** is similar to the distances in **159** [Sn⋯ $C_{ipso}$  2.821(2) and 2.827(2) Å],<sup>[14i]</sup> while the longer Sn⋯C contacts in **157** of 3.27 and 3.35 Å suggest weaker interactions in this case.<sup>[14g]</sup>



**Figure 66:** Previous examples of arene...E interactions in group 14 systems.

#### 4.6.1 Solid state structures of $\{(\text{Dipp})(\text{Mes})\text{P}\}_2\text{Ge}\cdot(n\text{-hexane})_{0.5}$ (**146Ge** $\cdot(\text{C}_6\text{H}_{14})_{0.5}$ ) and $\{(\text{Dipp})(\text{Mes})\text{P}\}_2\text{Sn}$ (**146Sn**)

X-ray crystallography revealed that **146Ge** $\cdot(\text{C}_6\text{H}_{14})_{0.5}$  and **146Sn** are isostructural (although **146Ge** $\cdot(\text{C}_6\text{H}_{14})_{0.5}$  crystallises as an *n*-hexane hemisolvate); each has a V-shaped geometry with two pyramidal phosphorus centres [sum of angles at P for **146Ge** $\cdot(\text{C}_6\text{H}_{14})_{0.5}$  = 294.95° and 290.80°; **146Sn** = 292.59° and 291.38°] (Fig. 67). The P-E-P angles are close to 90° [P-Ge-P 91.873(13)°, P-Sn-P 91.994(12)°], which is significantly more acute in **146Ge** $\cdot(\text{C}_6\text{H}_{14})_{0.5}$  than the respective angles in **104Ge** and **145Ge** [107.40(4) and 103.98(8)°, respectively]. While the structures of **146Ge** $\cdot(\text{C}_6\text{H}_{14})_{0.5}$  and **146Sn** are similar to that of **145Sn**, with the mesityl groups lying in the axial position, the  $C_{\text{ipso}}$ -Sn distances in **146Sn** are shorter [Sn... $C_{\text{ipso}}$  2.855(2) and 2.7315(14) Å]. The  $C_{\text{ipso}}$ -Ge distances in **146Ge** $\cdot(\text{C}_6\text{H}_{14})_{0.5}$  [Ge... $C_{\text{ipso}}$  2.7008(14) and 2.5736(14) Å] are significantly shorter again, even with slightly smaller sum of the van der Waal radii of Ge and C (3.81 Å) taken into account. These short contacts are also associated with acute  $C_{\text{ipso}}$ -P-E angles [**146Ge** $\cdot(\text{C}_6\text{H}_{14})_{0.5}$  77.60(5) and 73.13(5)°; **146Sn** 78.02(6) and 73.80(4)°]. However, the asymmetry of these interactions was not reproduced by DFT calculations (see below), suggesting the asymmetry may be a result of crystal packing.



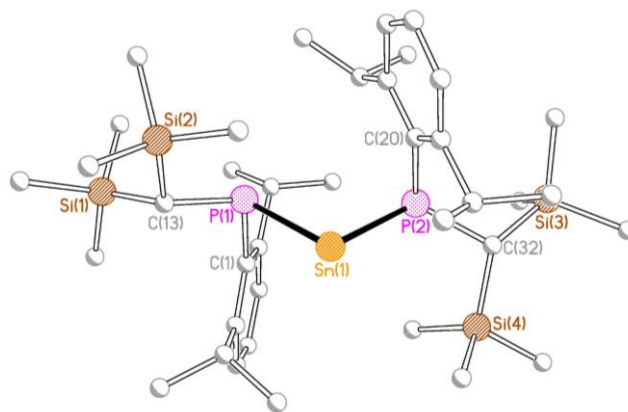
**Figure 67:** Molecular structure of **146Ge**·( $\text{C}_6\text{H}_{14}$ )<sub>0.5</sub> with the molecule of solvation and hydrogen atoms omitted for clarity [compound **146Sn** is isostructural]. Selected bond lengths (Å) and angles (°):

**146Ge**·( $\text{C}_6\text{H}_{14}$ )<sub>0.5</sub> Ge(1)-P(1) 2.3977(4), Ge(1)-P(2) 2.3978(4), P(1)-C(1) 1.8588(14), P(1)-C(13) 1.8600(14), P(2)-C(22) 1.8573(14), P(2)-C(34) 1.8613(14), P(1)-Ge(1)-P(2) 91.873(13), C(1)-P(1)-Ge(1) 113.28(5), C(1)-P(1)-C(13) 104.06(6), C(13)-P(1)-Ge(1) 77.61(4), C(22)-P(2)-Ge(1) 111.18(5), C(22)-P(2)-C(34) 106.50(6), C(34)-P(2)-Ge(1) 73.12(4);

**146Sn** Sn(1)-P(1) 2.5882(4), Sn(1)-P(2) 2.5847(4), P(1)-C(1) 1.8520(15), P(1)-C(13) 1.8570(15), P(2)-C(22) 1.8515(15), P(2)-C(34) 1.8610(15), P(2)-Sn(1)-P(1) 91.994(12), C(1)-P(1)-Sn(1) 108.99(5), C(1)-P(1)-C(13) 105.58(7), C(13)-P(1)-Sn(1) 78.02(5), C(22)-P(2)-Sn(1) 110.04(5), C(22)-P(2)-C(34) 107.53(7), C(34)-P(2)-Sn(1) 73.81(5).

#### 4.6.2 Solid-state structure of [(Dipp){( $\text{Me}_3\text{Si}$ )<sub>2</sub>CH}P]<sub>2</sub>Sn (**147Sn**)

The intense colour of the isolated crystals of **147Sn** initially suggested P-Sn  $\text{p}\pi\text{-p}\pi$  interactions were present based on comparison to the colours of the crystals of **104Ge**, **104Sn** and **145Ge** (Table 1). Surprisingly, X-ray crystallography reveals that **147Sn** has a similar structure to **146Ge**·( $\text{C}_6\text{H}_{14}$ )<sub>0.5</sub>, **145Sn** and **146Sn** with a V-shaped P-Sn-P core [P-Sn-P 91.548(16)°] and two pyramidal phosphorus centres [sum of angles at P(1) = 310.63° and P(2) = 302.50°] (Fig. 68). The P-Sn-P angle is slightly larger than in the previous stannylenes **145Sn** and **146Sn**, while the Sn-P distances are very similar to each other [2.5726(5) and 2.5810(5) Å]. The two Dipp groups lie axial to the P-Sn-P core and have considerably different short  $C_{\text{ipso}}$ -Sn distances [Sn $\cdots$ C(1) 3.3245(16) and Sn $\cdots$ C(20) 2.877(2) Å]. The asymmetry in these short contacts is reflected in the  $C_{\text{ipso}}$ -P-Sn angles [C(1)-P(1)-Sn(1) 95.56(6) and C(20)-P(2)-Sn(1) 78.75(6)°, respectively] and is reproduced by DFT calculations (see below).



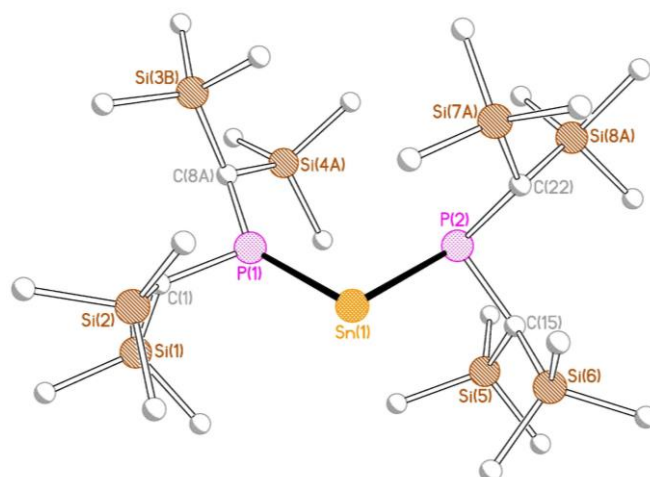
**Figure 68:** Molecular structure of **147Sn** with hydrogen atoms omitted for clarity. Selected bond lengths (Å) and angles (°): Sn(1)-P(1) 2.5726(5), Sn(1)-P(2) 2.5810(5), P(1)-C(1) 1.8711(19), P(1)-C(13) 1.8778(18), P(2)-C(20) 1.8716(19), P(2)-C(32) 1.8792(18), P(1)-Sn(1)-P(2) 91.548(15), C(1)-P(1)-Sn(1) 95.56(6), C(1)-P(1)-C(13) 106.56(8), C(13)-P(1)-Sn(1) 108.51(6), C(20)-P(2)-Sn(1) 78.75(6), C(20)-P(2)-C(32) 109.45(8), C(32)-P(2)-Sn(1) 114.30(6).

#### 4.6.3 Isolation of $[\{(\text{Me}_3\text{Si})_2\text{CH}\}_2\text{P}]_2\text{Sn}$ (**148Sn**)

The reaction between two equivalents of  $[\{(\text{Me}_3\text{Si})_2\text{CH}\}_2\text{P}]\text{Li}(\text{OEt}_2)_{0.33}$  (**139**) and one equivalent of  $\text{SnCl}_2$  in THF gave a pale yellow solution with a large amount of black solids, which we assume is metallic tin. After removal of the metallic tin and LiCl side-product by extraction of the product into toluene and filtration, the solvent was removed from the red filtrate to give a sticky orange solid, in which a small number of dark red crystals formed, that were shown by X-ray crystallography to be  $[\{(\text{Me}_3\text{Si})_2\text{CH}\}_2\text{P}]_2\text{Sn}$  (**148Sn**).

Compound **148Sn** crystallises with minor disorder of four trimethyl silyl groups and one methine group (Fig. 69). The structure of this compound is similar to those of **104Ge**, **104Sn** and **145Sn**, with a V-shaped P-Sn-P core  $[101.614(18)^\circ]$  and one planar and one pyramidal phosphorus centre [sum of angles at P(1)  $359.52/358.34^\circ$  and P(2)  $311.98^\circ$ ] (Fig. X). The P(1)-Sn(1) distance of  $2.4287(5)$  Å is approximately 7% shorter than the P(2)-Sn(1) distance, which is a larger difference in P-Sn distances than we observe in **104Sn**. In addition, the degree of planarity at P(1) is greater in **148Sn** than in **104Sn**.





**Figure 69:** Molecular structure of **148Sn** with minor disorder components and hydrogen atoms omitted for clarity. Selected bond lengths (Å) and angles (°): Sn(1)-P(1) 2.4287(5), Sn(1)-P(2) 2.6226(5), P(1)-C(1) 1.854(2), P(1)-C(8B) 1.844(7), P(1)-C(8A) 1.866(6), P(2)-C(15) 1.894(2), P(2)-C(22) 1.891(2), P(1)-Sn(1)-P(2) 101.614(18), C(1)-P(1)-Sn(1) 114.34(7), C(1)-P(1)-C(8A) 101.7(2), C(8B)-P(1)-Sn(1) 125.8(2), C(8B)-P(1)-C(1) 118.2(2), C(8A)-P(1)-Sn(1) 143.48(19), C(15)-P(2)-Sn(1) 97.80(6), C(22)-P(2)-Sn(1) 113.19(8), C(22)-P(2)-C(15) 100.99(11).

#### 4.7 Conclusion of solid-state structures

The diphosphatetrylenes characterised above crystallise with either a configuration with two pyramidal phosphorus centres or one planar and one pyramidal phosphorus centre. In addition to compound **104Ge**, compounds **104Sn**, **145Ge** and **148Sn** are rare examples of tetrylenes stabilised by  $p\pi$ - $p\pi$  interactions from planar phosphorus. The diphosphastannylenes **104Sn** and **148Sn** are the first X-ray crystallographically authenticated examples of Sn=P double bonds. Compounds **145Sn**, **146Ge**·(C<sub>6</sub>H<sub>14</sub>)<sub>0.5</sub> and **146Sn** adopt the alternative configuration with two pyramidal phosphorus centres, which prevents efficient overlap between the lone pairs on the phosphorus centres and the  $p_z$  orbital at the tetrel centre. However, these diphosphatetrylenes exhibit short  $C_{ipso}$ -P-Ge/Sn contacts that suggest stabilising arene interactions, which were confirmed by DFT calculations (see below).

#### 4.8 NMR spectra of diphosphatetrylenes

The variable-temperature <sup>1</sup>H NMR spectra of **104Sn**, **145Ge**·C<sub>7</sub>H<sub>14</sub>, **145Sn**, **146Ge**·(C<sub>6</sub>H<sub>14</sub>)<sub>0.5</sub>, **146Sn** and **147Sn** are complex, exhibiting multiple broad and overlapping signals, which could not be unambiguously assigned. In contrast, the variable-temperature <sup>31</sup>P{<sup>1</sup>H} NMR spectra of **145Ge**, **145Sn**, **104Sn**, **146Ge**·(C<sub>6</sub>H<sub>14</sub>)<sub>0.5</sub>, **146Sn** and **147Sn** indicate dynamic processes occurring in solution and are shown in Figures 70, 72, 73, 76, 77 and 78, respectively.

#### 4.8.1 Dynamic behaviour of {(Tripp)<sub>2</sub>P}<sub>2</sub>Ge (145Ge)

The  $^{31}\text{P}\{^1\text{H}\}$  NMR spectrum of **145Ge** at room temperature consists of a singlet at 3.6 ppm (A, Fig. 70). As the temperature is reduced, this signal broadens and moves to slightly higher field. At -20 °C, the spectrum consists of a broad singlet at -0.6 ppm. As the temperature is further reduced, this signal broadens further and decoalesces, until, at -90 °C, the spectrum exhibits signals at 101.5 (B), 7.2 (C), -43.3 (D) and -84.7 ppm (E, doublet  $J_{\text{PP}} = 145.8$  Hz) in the approximate ratio of 1.0:1.5:1.3:1.0.

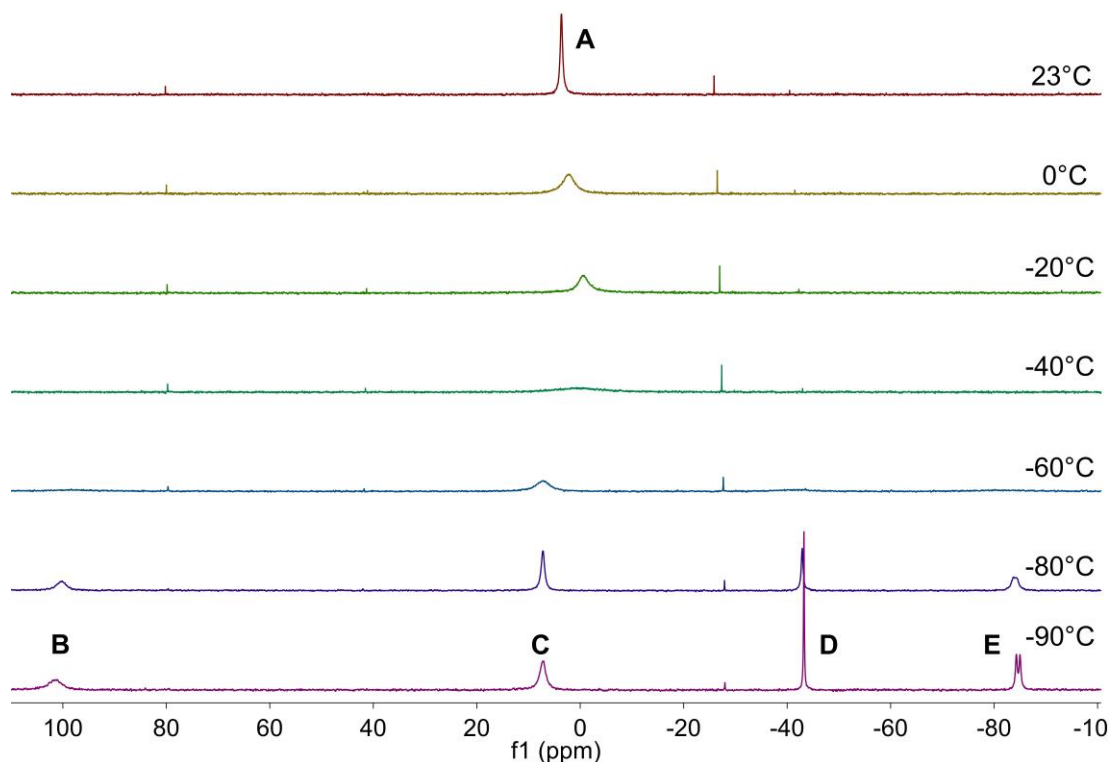
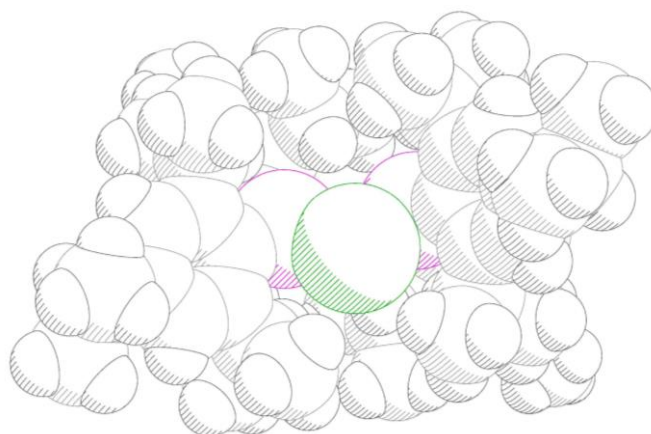


Figure 70: Variable-temperature  $^{31}\text{P}\{^1\text{H}\}$  NMR spectra of **145Ge** in  $d_8$ -toluene

The variable-temperature  $^{31}\text{P}\{^1\text{H}\}$  NMR spectra of **145Ge** follow a pattern similar to the corresponding spectra of **104Ge**.<sup>[1]</sup> In the low-temperature  $^{31}\text{P}\{^1\text{H}\}$  NMR spectrum of **104Ge**, the signals corresponding to peaks B and E were attributed to the planar and pyramidal phosphorus centres in the solid-state structure, respectively, on the basis of their correlation with the chemical shifts of the two centres observed in the  $^{31}\text{P}\{^1\text{H}\}$  magic-angle-spinning (MAS) NMR spectrum of **104Ge** and calculated chemical shifts from DFT studies.

DFT calculations of **145Ge** (see below) yield chemical shifts of 103 and -55 ppm for the planar and pyramidal phosphorus centres, respectively. However, the solid-state  $^{31}\text{P}\{^1\text{H}\}$  MAS NMR spectrum of the amorphous solid **145Ge**, resulting from the loss of solvent from **145Ge**·C<sub>7</sub>H<sub>14</sub> under vacuum, exhibits broad peaks at 3.3 and 5.5 ppm with multiple spinning side-bands, which is clearly inconsistent with the presence of a planar phosphorus centre. The

significantly paler colour of the amorphous solid of **145Ge** compared to the crystalline material of **145Ge**·C<sub>7</sub>H<sub>14</sub> is also consistent with the absence of a planar phosphorus centre, due to the absence of intense allowed  $\pi$ - $\pi^*$  absorptions. With these data in mind, we attribute the signals **B** and **E** to the planar and pyramidal phosphorus centres observed in the solid-state for **145Ge**·C<sub>7</sub>H<sub>14</sub>. The identities of the species responsible for the species **C** and **D** remain elusive. The inequivalent intensity of these signals and lack of <sup>31</sup>P-<sup>31</sup>P coupling indicate that these are separate species, rather than a dimer with bridging and terminal phosphide ligands. In addition, inspection of the space-filling model of **145Ge** reveals that the Ge centre is shrouded by the Tripp groups, making dimerization through the phosphorus or Ge centres to form a P<sub>2</sub>Ge<sub>2</sub> core or a Ge=Ge bond highly unlikely (Fig. 71).



**Figure 71:** Space-filling diagram of **145Ge**·C<sub>7</sub>H<sub>14</sub> with the molecule of solvation excluded for clarity

Given the foregoing and given that the four <sup>31</sup>P NMR signals observed at -90 °C coalesce at room temperature, we suggest that peaks **C** and **B** may be alternative configurations of **145Ge** with two pyramidal phosphorus centres. In support of this, two minimum-energy geometries with two pyramidal phosphorus centres were located by DFT calculations (see below); the calculated chemical shifts of these centres are -9 and -41 ppm in one (*syn,anti*) conformer and -15 ppm for both phosphorus centres in the second (*syn,syn*) conformer, i.e. in the same region as peaks **C** and **D**.

#### 4.8.2 Dynamic behaviour and SSNMR of {(Dipp)<sub>2</sub>P}<sub>2</sub>Sn (104Sn) and {(Tripp)<sub>2</sub>P}<sub>2</sub>Sn (145Sn)

The variable-temperature  $^{31}\text{P}\{^1\text{H}\}$  NMR spectra of **104Sn** and **145Sn** in  $d_8$ -toluene are very similar to each other (Fig. 73 and 72, respectively) but are somewhat different from those of **104Ge/145Ge**. The  $^{31}\text{P}\{^1\text{H}\}$  NMR spectrum of **145Sn** at room temperature exhibits a singlet (**F**) at -19.5 ppm [full-width at half maximum (FWHM) ca. 100 Hz] displaying tin satellites ( $J_{\text{PSn}} = 1420$  Hz). As the temperature is reduced, this signal broadens and moves to higher field. At -20 °C the spectrum consists of a very broad singlet at -35.6 ppm (FWHM ca. 1200 Hz) on which the tin satellites are not resolved. As the temperature is further reduced, this signal begins to sharpen and decoalesces, until, at -40 °C, the spectrum consists of a broad singlet (**G**) at -47.4 ppm (FWHM ca. 270 Hz) exhibiting poorly resolved tin satellites ( $J_{\text{PSn}} = \text{ca. } 960$  Hz), along with a very broad, low-intensity singlet (**H**) at 1.3 ppm (FWHM ca. 1500 Hz), on which tin satellites are not resolved in an approximate 14:1 ratio. Further reducing the temperature leads to the disappearance of peak **H** and the broadening of peak **G**, such that, at -80 °C, the spectrum consists of a broad singlet at -60.8 ppm (FWHM ca. 640 Hz). Below this temperature, this peak sharpens and moves to higher field until, at -100 °C, the spectrum consists of a broad singlet at -62.5 ppm (**J**; FWHM ca. 140 Hz) with well-resolved tin satellites ( $J_{\text{PSn}} = 820$  Hz).

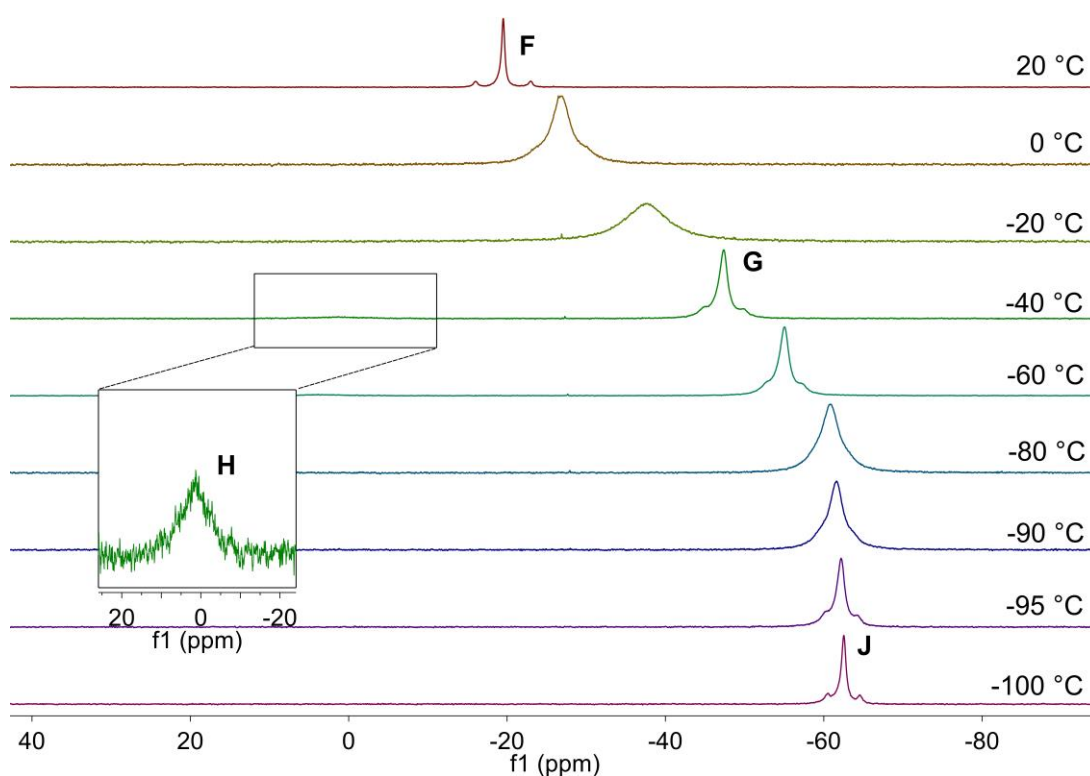
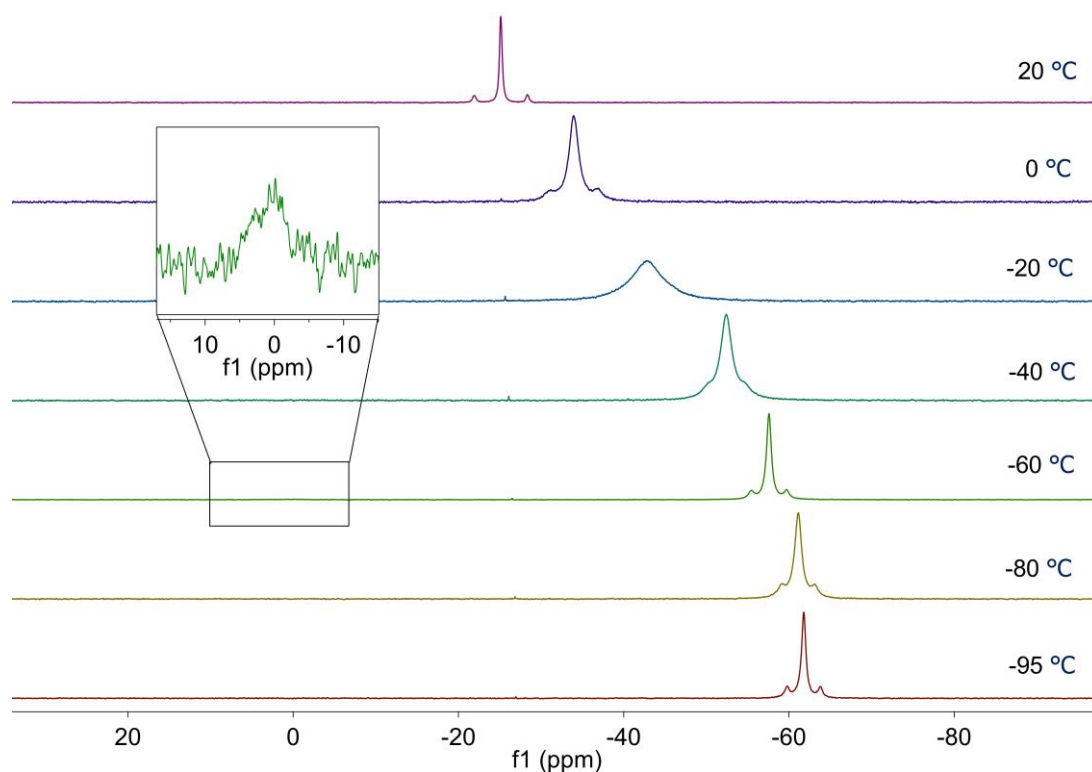


Figure 72: Variable-temperature  $^{31}\text{P}\{^1\text{H}\}$  NMR spectra of **145Sn** in  $d_8$ -toluene



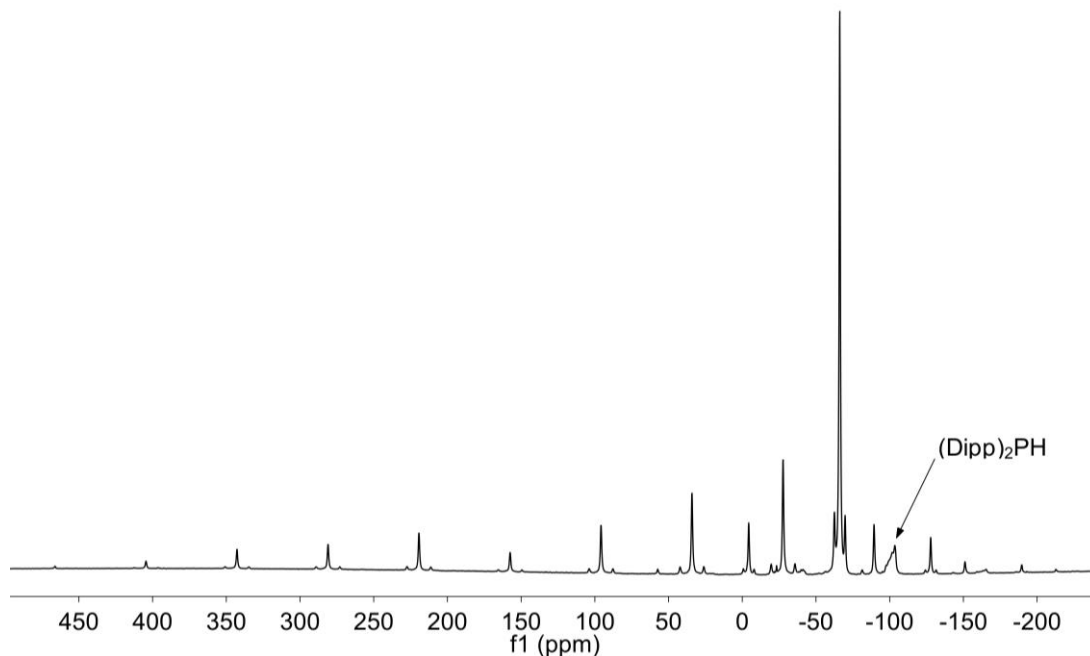
**Figure 73:** Variable-temperature  $^{31}\text{P}\{^1\text{H}\}$  NMR spectra of **104Sn** in  $d_8$ -toluene

The corresponding room temperature  $^{31}\text{P}\{^1\text{H}\}$  NMR spectrum of **104Sn** consists of a broad singlet at -25.1 ppm ( $J_{\text{PSn}} = 1300$  Hz), which decoalesces at -60 °C to give two signals at -57.6 ppm ( $J_{\text{PSn}} = 850$  Hz) and 0.8 ppm in an approximately 90:1 ratio. At low temperatures, the signal at 0.8 ppm disappears and, at -90 °C, the spectrum consists of a singlet at -61.8 ppm ( $J_{\text{PSn}} = 820$  Hz).

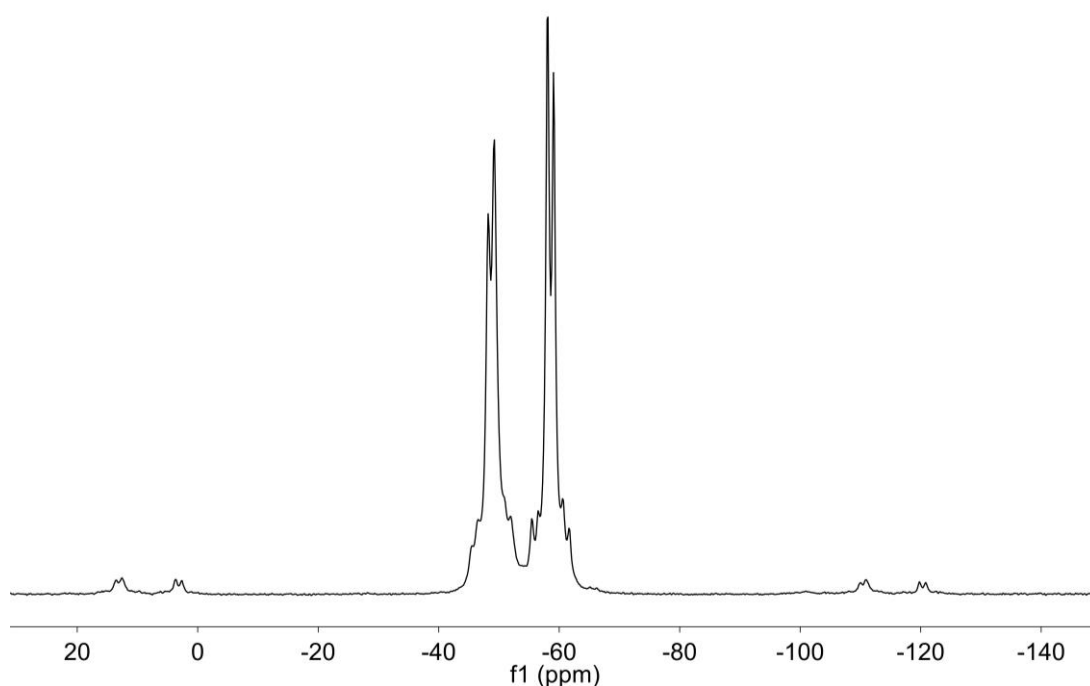
The solid-state  $^{31}\text{P}\{^1\text{H}\}$  MAS NMR spectrum of **104Sn** (Fig. 74) exhibits signals at 95.8 ppm ( $J_{\text{PSn}} = 2620$  Hz) and -66.2 ppm ( $J_{\text{PSn}} = 1180$ ), with the former exhibiting significant chemical shift anisotropy (with CSAs of ca. -350 and 50 for the two signals, respectively). We attribute these signals to the planar and pyramidal phosphorus centres, respectively, observed in the crystal structure. Consistent with this, the calculated  $^{31}\text{P}\{^1\text{H}\}$  chemical shifts for the planar and pyramidal centres in **104Sn** are 94 and -97 ppm, respectively.

The solid-state  $^{31}\text{P}\{^1\text{H}\}$  MAS NMR spectrum of **145Sn** (Fig. 75) consists of well-resolved doublets at -48.8 and -58.7 ppm ( $J_{\text{PP}} = 160.0$  Hz) exhibiting poorly resolved tin satellites ( $J_{\text{PSn}} = \text{ca. } 900$  and  $850$  Hz, respectively); both signals have few spinning side bands, typical of a low CSA. These signals are consistent with the two similar, but distinct, pyramidal phosphorus centres observed in the crystal structure and are in good correspondence with the calculated  $^{31}\text{P}\{^1\text{H}\}$  chemical shift of -41 ppm for the two pyramidal phosphorus centres of **145Sn**.

From the solid-state NMR data, we conclude that, in diphosphastannylenes, planar phosphorus centres are associated with low-field chemical shifts, large  $^{31}\text{P}$ - $^{117/119}\text{Sn}$  coupling constants ( $J_{\text{PSn}} > 1300$  Hz), and a substantial CSA, while pyramidal phosphorus centres are associated with high-field chemical shifts, reduced coupling constants ( $J_{\text{PSn}} < 1200$  Hz), and a small CSA. The phosphorus centres in the phosphastannenes **154** and **155** also exhibit low-field chemical shifts (204.7 and 170.7 ppm, respective) and large  $^{31}\text{P}$ - $^{119}\text{Sn}$  coupling constants (2295 and 2208 Hz, respectively).<sup>[6]</sup>

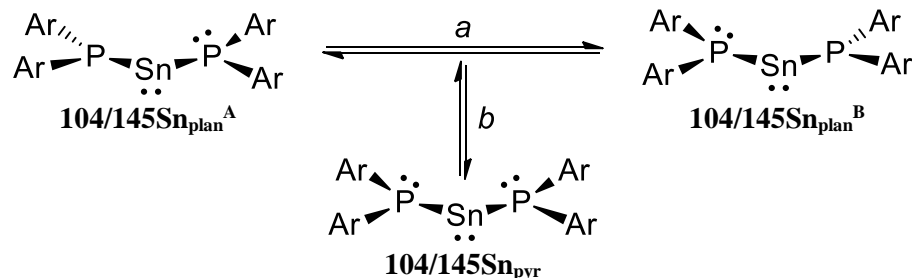


**Figure 74:** Solid-state  $^{31}\text{P}\{^1\text{H}\}$  MAS NMR spectrum of **104Sn** (spin rate 10 kHz)



**Figure 75:** Solid-state  $^{31}\text{P}\{^1\text{H}\}$  MAS NMR spectrum of **145Sn** (spin rate 10 kHz)

We interpret the solution behaviour of **104Sn** and **145Sn** according to Scheme 27. At room temperature, both compounds are subject to two dynamic processes: one (*a*) interconverts between the planar and pyramidal phosphorus centres (i.e., **104/145Sn<sub>plan</sub><sup>A</sup>** ↔ **104/145Sn<sub>plan</sub><sup>B</sup>**), while the second (*b*) interconverts between the configuration with one planar and one pyramidal phosphorus centre and a configuration with two pyramidal phosphorus centres (i.e., **104/145Sn<sub>plan</sub><sup>A</sup>** + **104/145Sn<sub>plan</sub><sup>B</sup>** ↔ **104/145Sn<sub>pyr</sub>**).



**Scheme 27:** Dynamic behaviour of **104Sn** and **145Sn** in solution

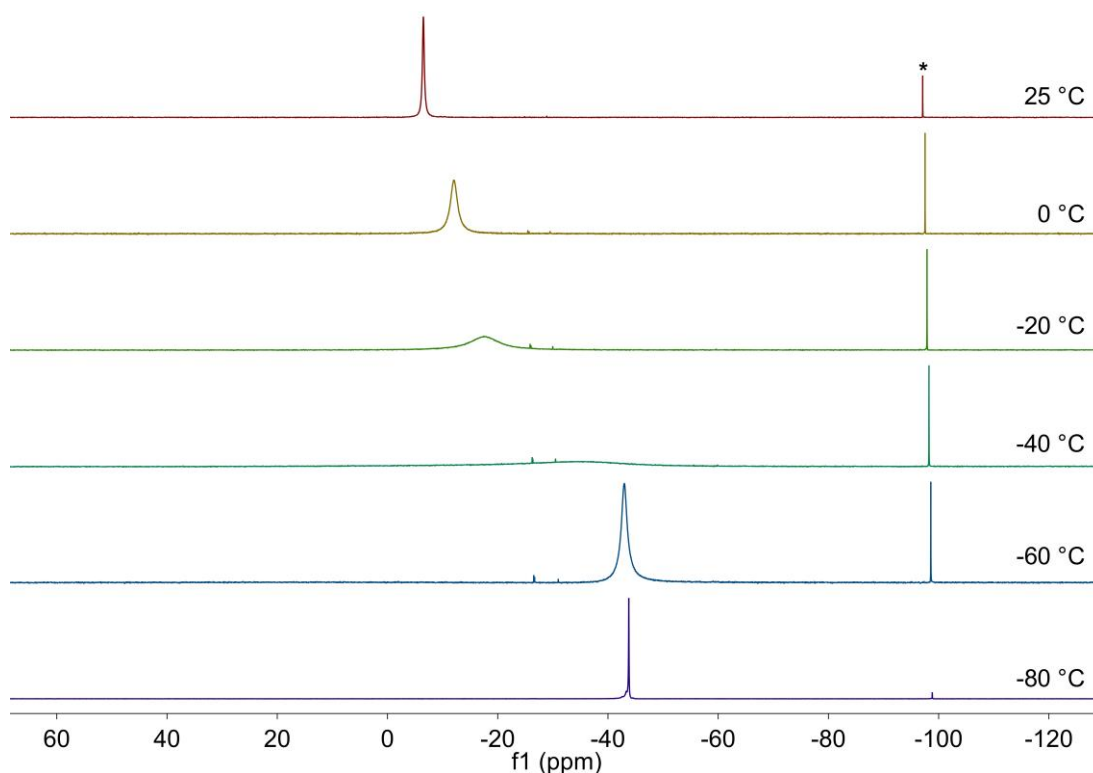
We expect the exchange between **104/145Sn<sub>plan</sub><sup>A</sup>** and **104/145Sn<sub>plan</sub><sup>B</sup>** to be rapid as it has been established that the barrier to inversion of phosphorus is reduced with electropositive and/or bulky substituents. Therefore, the single signal (**F**) observed in the  $^{31}\text{P}\{^1\text{H}\}$  NMR spectra of **104Sn** and **145Sn** at room temperature corresponds to a weighted average of the chemical shifts of the planar and pyramidal phosphorus centres in **104/145Sn<sub>plan</sub>** and the two pyramidal phosphorus centres in **104/145Sn<sub>pyr</sub>** and a weighted average of their  $^{31}\text{P}$ - $^{117/119}\text{Sn}$  coupling constants. This leads to a moderately low-field  $^{31}\text{P}$  chemical shift and a moderately large  $^{31}\text{P}$ - $^{117/119}\text{Sn}$  coupling constant. As the temperature is reduced, the rate of the exchange process *b* decreases and the signal decoalesces into the signals corresponding to the species **104/145Sn<sub>plan</sub>** (**H**) and **104/145Sn<sub>pyr</sub>** (**G**), with the former still being subject to the dynamic process *a*. At low temperatures the configuration **104/145Sn<sub>pyr</sub>** is favoured and increases in concentration at the expense of **104/145Sn<sub>plan</sub>**. Thus, as the temperature is reduced, **104/145Sn<sub>pyr</sub>** begins to predominate and the  $^{31}\text{P}$  NMR signal moves to higher field and exhibits a significantly smaller  $^{31}\text{P}$ - $^{117/119}\text{Sn}$  coupling constant, until, at  $-95\text{ }^{\circ}\text{C}$ , the signal (**J**) is essentially that of **104/145Sn<sub>pyr</sub>**.

A similar dynamic interconversion of the geometry at the phosphorus centre is observed for the transition-metal complexes  $\text{Cp}_2\text{M}(\text{PR}_2)_2$  [ $\text{M} = \text{Zr}, \text{Hf}$ ;  $\text{R} = \text{Et}, \text{Cy}, \text{Ph}$ ], which also contain one planar and one pyramidal phosphorus centre in the solid-state,<sup>[15]</sup> and for  $\text{Cp}_2\text{Nb}(\text{CO})(\text{P}i\text{PrPh})$ , for which the  $^1\text{H}$  and  $^{31}\text{P}$  NMR spectra suggest a rapid dynamic equilibrium between a pyramidal and planar geometry at the phosphorus centre at room temperature.<sup>[16]</sup>

Due to the significant broadening of the  $^{119}\text{Sn}$  signal for these species from the dynamic processes, no  $^{119}\text{Sn}$  NMR signal could be found at room temperature for either compound. However, at  $-95\text{ }^{\circ}\text{C}$ , compound **104Sn** exhibits an extremely broad signal at 440 ppm (FWHM ca. 2000 Hz), while no signal could be found for **145Sn** even at this low temperature.

#### 4.8.3 Dynamic behaviour of $\{(\text{Dipp})(\text{Mes})\text{P}\}_2\text{Ge}\cdot(n\text{-hexane})_{0.5}$ ( $^{146}\text{Ge}\cdot(\text{C}_6\text{H}_{14})_{0.5}$ )

The  $^{31}\text{P}\{^1\text{H}\}$  NMR spectrum of  $^{146}\text{Ge}\cdot(\text{C}_6\text{H}_{14})_{0.5}$  at  $25\text{ }^{\circ}\text{C}$  consists of a singlet at  $-6.5$  ppm that broadens and moves to higher field as the temperature is reduced, until, at  $-40\text{ }^{\circ}\text{C}$ , the spectrum consists of an extremely broad signal at approximately  $-35.0$  ppm (FWHM ca. 5000 Hz). As the temperature is further reduced the signal sharpens and continues to move upfield, until, at  $-80\text{ }^{\circ}\text{C}$ , the spectrum consists of a very sharp singlet at  $-44.1$  ppm.



**Figure 76:** Variable-temperature  $^{31}\text{P}\{^1\text{H}\}$  NMR spectra of  $^{146}\text{Ge}\cdot(\text{C}_6\text{H}_{14})_{0.5}$  in  $d_8$ -toluene (\* = free phosphine)

From the variable-temperature  $^{31}\text{P}\{^1\text{H}\}$  NMR spectra of  $^{146}\text{Ge}\cdot(\text{C}_6\text{H}_{14})_{0.5}$ , we interpret the solution behaviour of  $^{146}\text{Ge}\cdot(\text{C}_6\text{H}_{14})_{0.5}$  as a dynamic equilibrium between the configuration with one planar and one pyramidal phosphorus centre ( $^{146}\text{Ge}_{\text{plan}}$ ) and the configuration with two pyramidal phosphorus centres ( $^{146}\text{Ge}_{\text{pyr}}$ ), with the latter favoured at low temperatures. At room temperature, the signal exhibited by  $^{146}\text{Ge}\cdot(\text{C}_6\text{H}_{14})_{0.5}$  lies at a slighter higher field than the respective signals for **104Ge** and **145Ge**, which suggests a greater contribution of the configuration with two pyramidal phosphorus centres at this



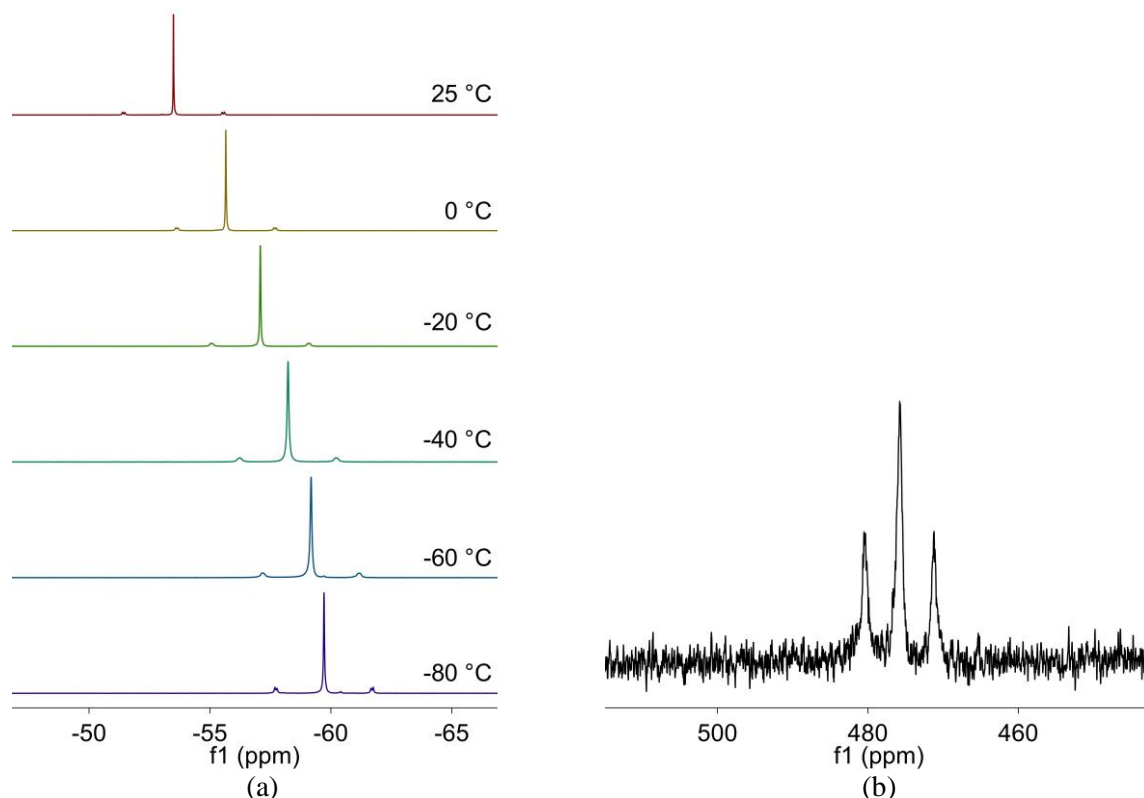
temperature. The low temperature  $^{31}\text{P}\{^1\text{H}\}$  NMR spectra of **104Ge** and **145Ge** exhibit signals corresponding to the individual phosphorus environments in a configuration with one planar and one pyramidal phosphorus centre, in addition to two unidentified peaks. In contrast, the sharp peak exhibited by **146Ge**·(C<sub>6</sub>H<sub>14</sub>)<sub>0.5</sub> in the  $^{31}\text{P}\{^1\text{H}\}$  NMR spectrum at -80 °C is consistent with the signal corresponding to **146Ge<sub>pyr</sub>**. These data suggest that **146Ge<sub>plan</sub>** is higher in relative energy than **146Ge<sub>pyr</sub>** and is inaccessible at low temperatures. This solution behaviour is similar to that observed in the variable temperature  $^{31}\text{P}\{^1\text{H}\}$  NMR spectra of **104Sn** and **145Sn**.

#### 4.8.4 Dynamic behaviour of {(Dipp)(Mes)P}<sub>2</sub>Sn (**146Sn**)

The  $^{31}\text{P}\{^1\text{H}\}$  NMR of **146Sn** at 25 °C consists of a singlet at -53.5 ppm (FWHM 4.8 Hz) with clearly defined tin satellites ( $J_{\text{P}^{117}\text{Sn}} = 815$  Hz,  $J_{\text{P}^{119}\text{Sn}} = 855$  Hz; Fig.77). As the temperature is reduced, this peak broadens slightly and moves to higher field, until, at -40 °C, the spectrum consists of a singlet at -58.2 ppm (FWHM 17.4 Hz) with poorly resolved tin satellites ( $J_{\text{PSn}} = 810$  Hz). As the temperature is further reduced, the signal continues to move to higher field and begins to sharpen. At -80 °C, the spectrum consists of a singlet at -59.7 ppm (FWHM 9.4 Hz) and the tin satellites are once again resolved ( $J_{\text{P}^{117}\text{Sn}} = 785$  Hz,  $J_{\text{P}^{119}\text{Sn}} = 820$  Hz). The  $^{119}\text{Sn}$  NMR spectrum of **146Sn** at 25 °C exhibits a triplet at -476 ppm ( $J_{\text{PSn}} = \text{ca. } 850$  Hz).

The sharp peaks exhibited by **146Sn** in the variable-temperature  $^{31}\text{P}\{^1\text{H}\}$  NMR spectra (FWHM ranging from 4.6 to 17.4 Hz) suggest there are no dynamic processes occurring between the different configurations of **146Sn**. The  $^{31}\text{P}\{^1\text{H}\}$  chemical shifts and  $^{31}\text{P}$ -Sn coupling constants exhibited by **146Sn** are remarkably similar to the signals observed in the  $^{31}\text{P}\{^1\text{H}\}$  MAS NMR spectra of **145Sn** (-48.8 and -58.7 ppm;  $J_{\text{PSn}} = \text{ca. } 900$  and 850 Hz, respectively), which correspond to two pyramidal phosphorus environments. In addition, the small  $^{31}\text{P}\{^1\text{H}\}$  chemical shift difference between the signals exhibited by **146Sn** at 25 °C and -80 °C suggests there is no change in the configuration of **146Sn** over this temperature range. The change in chemical shift is due to straightforward temperature dependence of the chemical shift caused by conformational changes and changes in intermolecular interactions with the solvent. These NMR data suggest that **146Sn** adopts exclusively a configuration with two pyramidal phosphorus centres (**146Sn<sub>pyr</sub>**) over the temperature range measured and there is minimal exchange with the configuration with one planar and one pyramidal phosphorus centre (**146Sn<sub>plan</sub>**). Furthermore, the relatively sharp triplet ( $J_{^{119}\text{SnP}} = 855$  Hz) exhibited by

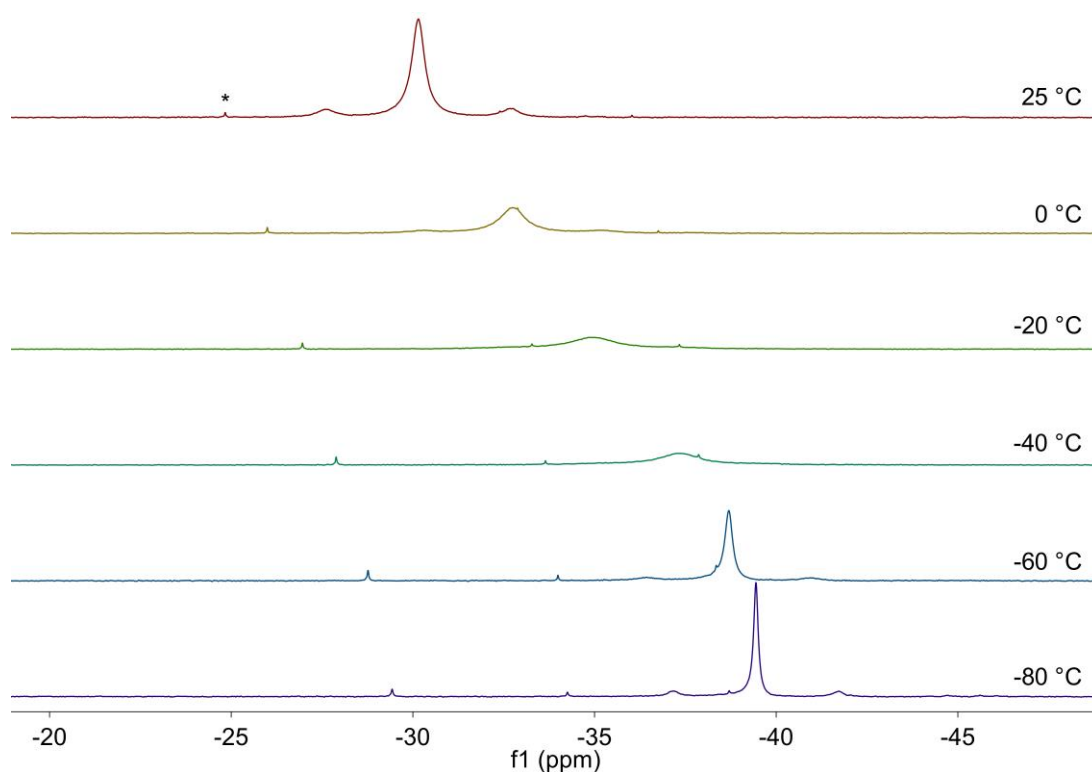
**146Sn** in the  $^{119}\text{Sn}$  spectrum is consistent with **146Sn<sub>pyr</sub>** and the absence of a dynamic equilibrium between **146Sn<sub>pyr</sub>** and **146Sn<sub>plan</sub>**. For **104Sn** and **145Sn**, no signal is observed in the  $^{119}\text{Sn}$  spectra at this temperature due to the significant line broadening due to the rapid exchange between the two configurations.



**Figure 77:** (a) Variable-temperature  $^{31}\text{P}\{^1\text{H}\}$  NMR spectra and (b) room temperature  $^{119}\text{Sn}$  NMR spectrum of **146Sn** in  $d_8$ -toluene

#### 4.8.4.1 Dynamic behaviour of $[(\text{Dipp})\{(\text{Me}_3\text{Si})_2\text{CH}\}\text{P}]_2\text{Sn}$ (**147Sn**)

The  $^{31}\text{P}\{^1\text{H}\}$  NMR spectrum of **147Sn** at 25 °C consists of a singlet at -30.2 ppm (FWHM ca. 90 Hz) with poorly resolved tin satellites ( $J_{\text{PSn}} = 1030$  Hz). As the temperature is reduced this signal begins to broaden and move to higher field, until, at -20 °C, the spectrum consists of a very broad singlet at -35.0 ppm (FWHM ca. 320 Hz) on which the tin satellites are not resolved. Below this temperature, this signal continues to move to higher field and begins to sharpen. At -80 °C the spectrum consists of a broad singlet at -39.4 ppm (FWHM ca. 28 Hz) with poorly resolved tin satellites ( $J_{\text{PSn}} = 920$  Hz).



**Figure 78:** Variable-temperature  $^{31}\text{P}\{^1\text{H}\}$  NMR spectra of **147Sn** in  $d_8$ -toluene (\* = free phosphine)

We interpret the solution behaviour of **147Sn** as a dynamic equilibrium between the configuration with one planar and pyramidal phosphorus centre (**147Sn<sub>plan</sub>**) and the configuration with two pyramidal phosphorus centres (**147Sn<sub>pyr</sub>**). As the temperature is reduced, the signal moves to a higher field and the  $^{31}\text{P}$ - $^{117/119}\text{Sn}$  coupling constant decreases, consistent with **147Sn<sub>pyr</sub>** predominating at low temperatures. This behaviour is similar to that of **146Ge**·( $\text{C}_6\text{H}_{14}$ )<sub>0.5</sub> and **146Sn**.

#### 4.8.4.2 NMR spectra of $\{[(\text{Me}_3\text{Si})_2\text{CH}]_2\text{P}\}_2\text{Sn}$ (**148Sn**)




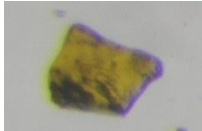




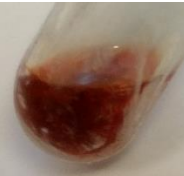



Unfortunately, we were unable to isolate bulk samples of **148Sn** because of the very low yield of crystalline material. Extraction of the products into toluene gives a dark red solution that exhibits a broad singlet in its  $^{31}\text{P}\{^1\text{H}\}$  NMR spectrum at 43.2 ppm with poorly resolved tin satellites ( $J_{\text{PSn}} = 1900$  Hz). The low-field nature of this signal and the relatively large  $^{31}\text{P}$ - $^{117/119}\text{Sn}$  coupling constant suggests a significant contribution of the planar configuration at this temperature.

#### 4.8.4.3 Conclusion from NMR spectra

The variable temperature  $^{31}\text{P}\{^1\text{H}\}$  NMR spectra of **104Sn**, **145Ge/Sn**, **146Ge** and **147Sn** suggest a dynamic equilibrium between the configuration with two pyramidal phosphorus centres and the configuration with one planar and one pyramidal phosphorus centre, where the pyramidal configuration is favoured at low temperatures. Only in the low temperature  $^{31}\text{P}\{^1\text{H}\}$  NMR spectra of **145Ge** and its previously reported analogue **104Ge** are separate signals observed for the planar and pyramidal phosphorus centres. From these spectra and the  $^{31}\text{P}\{^1\text{H}\}$  MAS SSNMR spectra of **104Sn** and **145Sn**, we associate planar phosphorus centres with high field chemical shifts and large  $^{31}\text{P}$ -Sn coupling constants for the stannylenes, compared to pyramidal phosphorus centres. Compound **146Sn** exhibits variable temperature  $^{31}\text{P}\{^1\text{H}\}$  spectra consistent with a pyramidal configuration over the temperature range measured, which is likely a consequence of the reduced steric bulk of the phosphide ligand (Dipp)(Mes)P.

#### 4.9 Crystal colouration, thermochromism and UV-visible spectra

The intense colour of the crystalline material of **104Ge**, **145Ge**·(C<sub>7</sub>H<sub>14</sub>) and **104Sn** is associated with the strong  $\pi \rightarrow \pi^*$  transition of the E=P bond. In contrast, the crystalline material of **145Sn** is significantly paler, consistent with the configuration with two pyramidal phosphorus centres having weaker absorptions, in the visible region, due to the absence of the P=Sn bond (Fig. 79). Similarly, the amorphous material **145Ge** is paler than the crystalline material **145Ge**·(C<sub>7</sub>H<sub>14</sub>) and exhibits a  $^{31}\text{P}$  MAS NMR spectrum suggesting two pyramidal phosphorus environments. However, dissolution of **145Ge** and **145Sn** in toluene give intensely coloured solutions that have colours and room temperature  $^{31}\text{P}\{^1\text{H}\}$  NMR spectra almost identical to **104Ge** and **104Sn**, respectively, consistent with a dynamic equilibrium between the weakly absorbing pyramidal configuration and strongly absorbing planar configuration for these four compounds (Fig. 79). In addition, frozen solutions of **104/145Ge** and **104/145Sn** in toluene at -196 °C are significantly paler than their respective room temperature solutions (Fig. 79). This is consistent with our observations from the variable-temperature  $^{31}\text{P}\{^1\text{H}\}$  NMR spectra that the pyramidal configuration, which is more weakly absorbing, is favoured at low temperatures, with the effect more visually pronounced for the diphosphagermylenes, **104Ge** and **145Ge**·(C<sub>7</sub>H<sub>14</sub>).

	<b>104Ge</b>	<b>145Ge·(C<sub>7</sub>H<sub>14</sub>)</b>	<b>104Sn</b>	<b>145Sn</b>
<b>Crystal</b>				
<b>Toluene (20 °C)</b>				
<b>Toluene (-196 °C)</b>				

**Figure 79:** Photographs of **104Ge**, **145Ge·(C<sub>7</sub>H<sub>14</sub>)**, **104Sn** and **145Sn** in the solid state and in solution at 20 °C and in frozen toluene solution

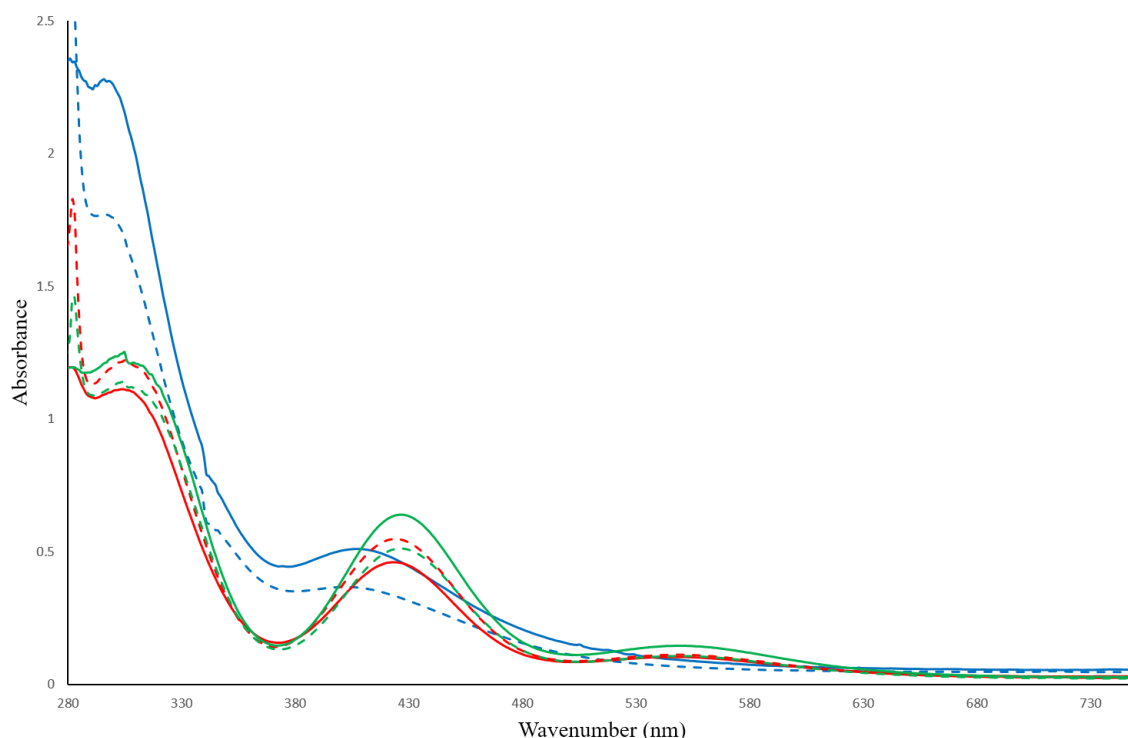
The pale red crystalline material of **146Ge·(C<sub>6</sub>H<sub>14</sub>)<sub>0.5</sub>** and **146Sn** is further consistent with pyramidal configurations being weakly absorbing. Dissolution of these crystalline materials into toluene either gave a dark red or purple solution, respectively, consistent with the dynamic equilibrium between the two configurations in solution. The dark green crystalline **147Sn** is somewhat unusual as it has a pyramidal configuration in the solid-state, however, solutions of **147Sn** in toluene have a dark purple colour. The strong absorptions of the crystals of **147Sn** may be a result of the electronic perturbation of the system from the alkyl substituents. While the dark red crystalline **148Sn** is further evidence of the strong absorptions resulting from the P=E bond, it is not suitable to comment on the colour of the crude solution of **148Sn** as it contains a large amount of unidentified impurities, some of which are strongly coloured.

	<b>146Ge·(C<sub>6</sub>H<sub>14</sub>)<sub>0.5</sub></b>	<b>146Sn</b>	<b>147Sn</b>	<b>148Sn</b>
<b>Crystal</b>				

**Figure 80:** Photographs of **146Ge·(C<sub>6</sub>H<sub>14</sub>)<sub>0.5</sub>**, **146Sn**, **147Sn** and **148Sn**

The absorptions of the diphosphagermylenes **104Ge**, **145Ge** and **146Ge·(C<sub>6</sub>H<sub>14</sub>)<sub>0.5</sub>** in solution were further probed by UV-visible spectroscopy. Unfortunately, it was not possible to obtain UV-visible spectra of the diphosphastannylenes **104Sn**, **145Sn**, **146Sn** and **147Sn** because of their rapid decomposition on exposure to ambient light. In toluene, the deep-red colour of **104Ge** and **145Ge** is associated with absorptions at 424 ( $\epsilon = 5480$  and  $5088 \text{ M}^{-1}\text{cm}^{-1}$

for **104Ge** and **145Ge**, respectively) and 548 nm ( $\epsilon = 1113$  and  $1053 \text{ M}^{-1}\text{cm}^{-1}$  for **104Ge** and **145Ge**, respectively). In addition, both compounds absorb strongly in the ultraviolet region at 304 nm ( $\epsilon = 12160$  and  $11390 \text{ M}^{-1}\text{cm}^{-1}$  for **104Ge** and **145Ge**, respectively). The UV-visible spectrum of **146Ge** in toluene exhibits strong absorptions at 408 nm ( $\epsilon = 3651 \text{ M}^{-1}\text{cm}^{-1}$ ) and at 296 nm ( $\epsilon = 17007 \text{ M}^{-1}\text{cm}^{-1}$ ), although this latter peak is obscured by the absorption from the toluene solvent and aromatic rings of the ligands. Surprisingly, the UV-visible spectra of **104/145/146Ge** in toluene and THF are essentially identical (Fig. 81); we attribute to the minor differences in absorptions of each compound in these two solvents to the inaccuracies of measuring such small amounts of these highly sensitive compounds. The similarity between the spectra suggest that the P=Ge  $\pi$  interaction is not perturbed in the strong donor solvent THF.



**Figure 81:** UV/Vis spectra of **104Ge** (blue), **145Ge** (red) **146Ge** (green) in THF (solid) and toluene (dashed)

Time-dependent DFT (TD-DFT) calculations indicate that the absorptions at 424 and 548 nm for **104Ge** and **145Ge** and the absorption at 408 nm for **146Ge** are largely due to the P=Ge  $\pi \rightarrow \pi^*$  transitions in the planar configuration. Furthermore, the TD-DFT calculations indicate that the absorptions at around 410 nm are an order of magnitude greater for the planar configuration than the pyramidal configuration. This is consistent with the reduced intensity of colour of **104/145Ge** and **104/145Sn** in solution at low temperatures, where the pyramidal configurations are favoured.

The similarity of the UV-visible spectra **104Ge** and **145Ge** suggests that both ligand systems have almost identical electronic properties. However, the UV-visible spectra of **146Ge** only exhibits a single peak in the visible region at 408 nm, which has a low intensity and is redshifted compared to the similar peaks at 424 nm for **104Ge** and **145Ge**. The differences in the UV-visible spectra of **104Ge** and **145Ge** with **146Ge** may be associated with **146Ge** having a greater contribution of the more pyramidal configuration in solution at room temperature, as indicated by the  $^{31}\text{P}\{^1\text{H}\}$  NMR spectra, which is more weakly absorbing than the planar configuration.

#### 4.10 Conclusions from UV-visible spectra

From crystalline material of **104Ge**, **145Ge**·( $\text{C}_7\text{H}_{14}$ ), **104Sn**, **145Sn**, **146Ge**·( $\text{C}_6\text{H}_{14}$ )<sub>0.5</sub>, **146Sn**, **147Sn** and **148Sn**, we conclude that the diphosphatetrylenes stabilised by  $\text{p}\pi\text{-p}\pi$  interactions in the solid-state have a significantly more intense colour than those that have pyramidal configurations, with the exception of **147Sn**. This was further supported by DFT calculations and the thermochromism of solutions of **104/145Ge** and **104/145Sn** in toluene. The UV-visible spectra of **104/145Ge** in toluene and THF are essentially identical, which suggests the (Dipp)<sub>2</sub>P and (Tripp)<sub>2</sub>P ligands have comparable electronic properties and the transitions have no solvent dependence. The difference in the UV-visible spectra of **146Ge**·( $\text{C}_6\text{H}_{14}$ )<sub>0.5</sub> compared to that of **104/145Ge** may be attributed to **146Ge**·( $\text{C}_6\text{H}_{14}$ )<sub>0.5</sub> having a greater contribution of the pyramidal configurations in solution.

## 4.11 DFT calculations

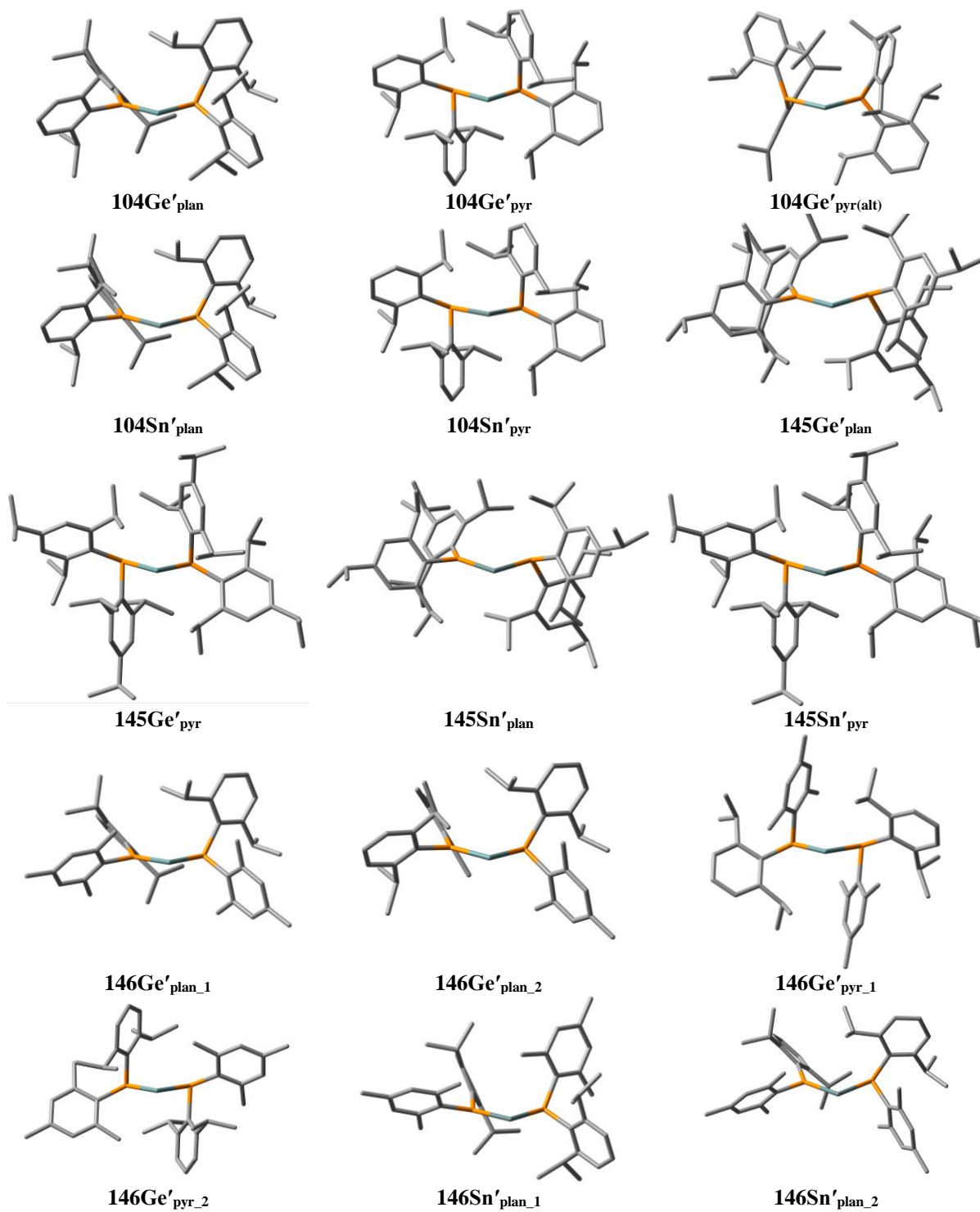
In order to gain insight into the relative stabilities of the two different configurations of the diphosphatetrylenes isolated and to better understand the bonding in these compounds, we carried out a DFT study (preliminary results for **104Ge** were published previously).<sup>[1]</sup> Minimum-energy geometries were located for both the planar and pyramidal configurations of **104/145Ge'**, **104/145Sn'** and **148Sn'** [primes are used to denote calculated geometries throughout]. The additional minimum-energy geometry **104Ge'**<sub>pyr(alt)</sub> was located, in which the phosphide-ligands adopt a *syn,anti* configuration, which lies 50.9 kJ mol<sup>-1</sup> higher in energy than the geometry **104Ge'**<sub>pyr</sub> with a *syn,syn* configuration. In addition, a minimum-energy geometry for **148Sn** was located with a near planar phosphorus centre (**148Sn'**<sub>plan\_2</sub>, sum of angles at P = 348.75°), which lies 23.6 kJ mol<sup>-1</sup> higher in energy than **148Sn'**<sub>plan\_1</sub>, which corresponds to the solid-state structure of **148Sn**.

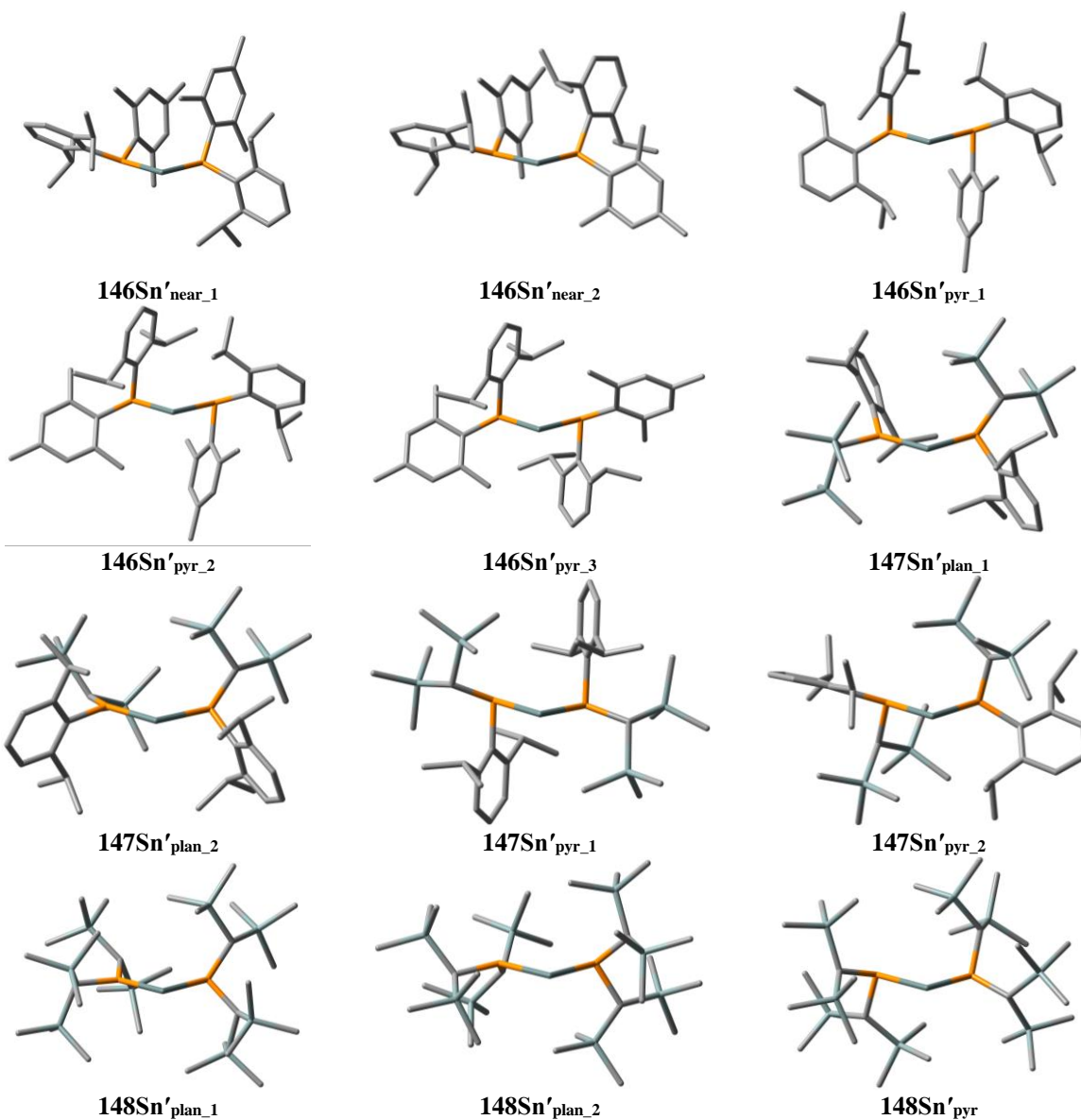
The heteroleptic phosphide ligands in **146Ge**·(C<sub>6</sub>H<sub>14</sub>)<sub>0.5</sub>, **146Sn** and **147Sn** lead to the possibility of multiple stereoisomers for both the planar and pyramidal configurations. For **146Ge** and **146/147Sn**, minimum-energy geometries were located for the pyramidal configurations with both mesityl or CH(SiMe<sub>3</sub>)<sub>3</sub> groups in the axial (**146Ge/Sn'**<sub>pyr\_1</sub> and **147Sn'**<sub>pyr\_2</sub>) or pseudo-equatorial positions (**146Ge/Sn'**<sub>pyr\_2</sub> and **147Sn'**<sub>pyr\_1</sub>), while an additional geometry with one mesityl and one Dipp group in the axial position was located for **146Sn** (**146Sn'**<sub>pyr\_3</sub>). Two minimum-energy geometries for the planar configuration were located for each of **146Ge** and **146/147Sn**. In addition, two minimum-energy geometries were located for **146Sn** which have moderately large sum of angles at both phosphorus centres in each, with one approaching planarity, these are denoted as **146Sn**<sub>near\_1</sub> and **146Sn**<sub>near\_2</sub>.

Attempts to locate minimum-energy geometries of these tetrylenes with two planar phosphorus centres were unsuccessful. The relative energies for all configurations are given in Table 3, and the corresponding minimum-energy geometries are shown in Chart 1. The calculated P-E distances are in good correspondence with the X-ray crystallographically obtained distances; however, DFT calculations underestimate the P-E-P angle in all cases, with the exception of **146Ge**. The discrepancy in this bond angle is small for the diphosphatetrylenes that have a pyramidal configuration in the solid-state, while it is significantly underestimated for **104Ge'**<sub>plan</sub>, **104Sn'**<sub>plan</sub>, **145Ge'**<sub>plan</sub> and **148Sn'**<sub>plan\_1</sub>. The E-P<sub>plan</sub> distances in these calculated structures with a planar configuration are approximately 4.1-8.1% longer than the E-P<sub>pyr</sub> distances, which is consistent with the crystallographic data



for **104/145Ge**, **104Sn** and **148Sn** and with the presence of multiple bond character in the former.



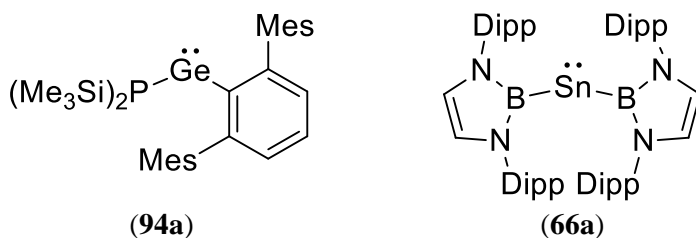


**Chart 1:** Minimum-energy configurations

**Table 3:** \*mean of the two molecules in the asymmetric unit. <sup>a</sup>Free energy of alternative form – free energy of the most stable planar or near planar form. (kJ mol<sup>-1</sup>). <sup>b</sup>Free energy of triplet – singlet (kJ mol<sup>-1</sup>). <sup>c</sup>HOMO-LUMO .gap (eV). <sup>d</sup>Experimental data from X-ray crystallography. <sup>e</sup>Experimental data from the <sup>31</sup>P{<sup>1</sup>H} NMR spectra at lowest recorded temperature (recorded temperature in parenthesis)

Compound	$\Delta G^a$	$\Delta_{S-T}^b$	$\Delta_{H-L}^c$	Sum of angles (°)		Bond distance (Å)		P-E-P angle (°)	<sup>31</sup> P NMR chemical shift (ppm)	
				P(1)	P(2)	E-P(1)	E-P(2)		P(1)	P(2)
<b>104Ge<sup>d</sup></b>				358.35	311.53	2.2337(11)	2.3823(12)	107.40(4)	98.5, 7.8, -43.1, -82.0 <sup>d</sup> (-95 °C)	
<b>104Ge'</b> <sub>plan</sub>		92.4	1.83	359.97	318.56	2.2232	2.3571	100.67	103.4	-56.0
<b>104Ge'</b> <sub>pyr</sub>	13.8	78.6	1.73	295.54	295.53	2.4118	2.4118	90.4	-15.1	-15.1
<b>104Ge'</b> <sub>pyr(alt)</sub>	57.1	35.3	1.30	335.89	299.92	2.4062	2.4569	107.41	-9.6	-41.9
<b>104Sn</b>				355.53	311.58	2.4458(8)	2.5757(7)	106.20(3)	-61.8 <sup>d</sup> (-90 °C)	
<b>104Sn'</b> <sub>plan</sub>		82.5	1.73	359.90	313.56	2.4560	2.5964	96.74	94.3	-66.8
<b>104Sn'</b> <sub>pyr</sub>	-2.5	80.0	1.77	295.13	295.13	2.6009	2.6009	88.24	-43.1	-43.1
<b>145Ge</b> ·(C <sub>7</sub> H <sub>14</sub> ) <sup>d</sup>				360.0	311.5	2.231(2)	2.367(2)	103.98(8)	101.5, 7.2, -43.3, 84.7 <sup>d</sup> (-90 °C)	
<b>145Ge'</b> <sub>plan</sub>		76.2	1.82	359.86	313.88	2.2519	2.3996	99.42	103.2	-55.2
<b>145Ge'</b> <sub>pyr</sub>	-3.0	79.3	1.88	291.66	291.66	2.4063	2.4063	91.04	-27.1	-27.1
<b>145Sn</b>				308.62	299.74	2.5836(6)	2.5673(7)	89.62(2)	-62.5 <sup>d</sup> (-100 °C)	
<b>145Sn'</b> <sub>plan</sub>		76.3	1.68	360.00	317.20	2.4535	2.5816	95.55	101.5	-66.6
<b>145Sn'</b> <sub>pyr</sub>	-4.2	80.4	1.80	295.28	295.28	2.5992	2.5992	86.22	-40.6	-40.6
<b>146Ge</b> ·(C <sub>6</sub> H <sub>14</sub> ) <sub>0.5</sub> <sup>d</sup>				294.95	290.80	2.3977(4)	2.3978(4)	91.873(13)	-44.1 <sup>d</sup> (-80 °C)	
<b>146Ge'</b> <sub>plan_1</sub>		72.8	1.82	359.19	317.42	2.2615	2.3971	99.46	117.4	-52.7
<b>146Ge'</b> <sub>plan_2</sub>	152.1	-79.3	1.85	359.05	311.91	2.2576	2.4218	98.29	122.6	-38.9
<b>146Ge'</b> <sub>pyr_1</sub>	-12.6	85.4	1.87	289.02	289.02	2.4305	2.4305	92.97	-18.3	-18.3
<b>146Ge'</b> <sub>pyr'_2</sub>	-8.0	80.8	1.75	294.75	294.85	2.4130	2.4134	91.90	-12.2	-12.6
<b>146Sn<sup>d</sup></b>				292.59	291.38	2.5882(4)	2.5847(4)	91.944(12)	-56.7 <sup>d</sup> (-80 °C)	
<b>146Sn'</b> <sub>plan_1</sub>	12.4	72.0	1.68	353.43	317.80	2.4824	2.5852	92.61	108.1	-34.8
<b>146Sn'</b> <sub>plan_2</sub>	26.9	57.5	1.77	359.84	304.81	2.4601	2.6280	96.98	116.5	-51.0
<b>146Sn'</b> <sub>near_1</sub>		84.4	1.52	344.06	335.14	2.5377	2.5547	90.47	111.6	1.2
<b>146Sn'</b> <sub>near_2</sub>	28.9	55.5	1.41	346.62	332.60	2.5188	2.5671	91.04	130.6	-9.6
<b>146Sn'</b> <sub>pyr_1</sub>	-10.2	94.6	1.94	290.98	290.15	2.6264	2.6313	91.08	-74.1	-75.6
<b>146Sn'</b> <sub>pyr_2</sub>	-2.2	86.6	1.93	288.03	295.22	2.6259	2.6018	90.80	-42.1	-35.7
<b>146Sn'</b> <sub>pyr'_3</sub>	70.9	13.5	1.81	296.19	296.19	2.6035	2.6035	88.87	-34.9	-34.9
<b>147Sn<sup>d</sup></b>				310.63	302.50	2.5726(5)	2.5810(5)	91.548(15)	-39.4 <sup>d</sup> (-80 °C)	
<b>147Sn'</b> <sub>plan_1</sub>		70.9	1.65	357.70	310.48	2.4483	2.6271	97.45	91.9	-98
<b>147Sn'</b> <sub>plan_2</sub>	14.1	56.8	1.63	357.57	308.97	2.4569	2.6329	102.96	112.0	-70.2
<b>147Sn'</b> <sub>pyr_1</sub>	1.0	69.9	1.48	312.47	302.40	2.5918	2.6051	86.31	-48.3	-41.3
<b>147Sn'</b> <sub>pyr'_2</sub>	83.4	-12.5	1.09	330.76	304.85	2.6019	2.9296	84.77	29.5	-2.1
<b>148Sn<sup>d</sup></b>				358.93*	311.98	2.4287(5)	2.6226(5)	101.614(18)	43.2 <sup>d</sup> (25 °C)	
<b>148Sn'</b> <sub>plan_1</sub>		87.8	1.61	359.01	309.94	2.4377	2.6381	92.18	120.4	-79.1
<b>148Sn'</b> <sub>plan_2</sub>	23.6	64.2	1.86	348.75	307.32	2.4786	2.6524	93.70	125.0	-24.9
<b>148Sn'</b> <sub>pyr</sub>	52.4	35.4	1.23	316.37	304.98	2.6155	2.6700	93.93	10.0	8.1

The reactivity of tetrylenes towards small molecules, such as  $\text{H}_2$  and  $\text{NH}_3$ , has been correlated to the calculated HOMO-LUMO energy gap ( $\Delta_{\text{H-L}}$ ) and singlet-triplet energy separation ( $\Delta_{\text{S-T}}$ ).<sup>[17]</sup> Triplet states were located for each compound by using the singlet minimum-energy geometries as the starting points for the optimization; in each case, the resulting minimum-energy geometries for the triplet states had two pyramidal phosphorus centres. In instances where multiple minimum-energy geometries were located for each compound, the lowest energy triplet state was used to calculate the singlet-triplet separation. Surprisingly, the calculated HOMO-LUMO gaps or singlet-triplet separations for the structures shown above do not correlate with the configurations of the phosphorus centres and range from 1.41 to 1.94 eV or 55.5 to 94.6  $\text{kJ mol}^{-1}$ , respectively (Table 3), with the values omitted for high energy geometries ( $>50 \text{ kJ mol}^{-1}$  higher in energy than the lowest energy structure for each compound). These  $\Delta_{\text{H-L}}$  values are significantly lower than the calculated  $\Delta_{\text{H-L}}$  of 2.10 eV for the  $\{(\text{Me}_3\text{Si})_2\text{P}\}(2,6\text{-Mes}_2\text{-C}_6\text{H}_3)\text{Ge}$  (**94a**), which has a pyramidal configuration at phosphorus in the solid-state.<sup>[18]</sup> The calculated  $\Delta_{\text{S-T}}$  values which lie at the lower end of the range are comparable to that calculated for  $\{(\text{CHNDipp})_2\text{B}\}_2\text{Sn}$  (**66a**,  $\Delta_{\text{H-L}} = 53.6 \text{ kJ mol}^{-1}$ ), in which the tin atom is substituted by two strongly  $\sigma$ -electron-withdrawing boryl groups.<sup>[19]</sup> The relatively low  $\Delta_{\text{H-L}}$  and  $\Delta_{\text{S-T}}$  values suggest the diphosphatetrylenes may exhibit interesting reactivity and may explain the thermal and light sensitivity of the diphosphastannylenes.



**Figure 82:** Tetrylenes with low  $\Delta_{\text{H-L}}$  and  $\Delta_{\text{S-T}}$  values

The Wiberg bond indices (WBIs) for the  $\text{E-P}_{\text{plan}}$  bonds in the calculated geometries with a planar configuration are significantly greater than 1, which implies a significant degree of multiple bond character, whereas the WBIs for the  $\text{E-P}_{\text{pyr}}$  bonds in these compounds lie in the range 0.7-0.9, which is typical for a  $\text{Ge-P}$  or  $\text{Sn-P}$   $\sigma$  bond (Table 4). As expected, the WBIs for the  $\text{Sn-P}_{\text{plan}}$  bonds are lower than that of the  $\text{Ge-P}_{\text{plan}}$  bonds due to the increased polarity in the latter. The WBIs of 0.979 and 1.026 for the  $\text{Sn-P}(1)$  bonds in **146Sn'**<sub>near\_1</sub> and **146Sn'**<sub>near\_2</sub>, respectively, suggest a substantially lower degree of multiple bond character than in the planar configurations. For the calculated geometries of **104-146Ge** and **104-148Sn** with a pyramidal configuration, the  $\text{E-P}$  WBIs lie in the range of 0.70-0.74.

Natural bond orbital (NBO) analysis of the calculated structures reveals that the lone pair on the tetrel centre has substantial s character. The s character of this lone pair is slightly higher in the pyramidal configurations.

Compound	WBI <sup>a</sup>			Compound	WBI <sup>a</sup>		
	E-P(1)	E-P(2)	% s E(lp)		E-P(1)	E-P(2)	% s E(lp) <sup>b</sup>
<b>104Ge'</b> <sub>plan</sub>	1.333	0.890	83.8	<b>104Ge'</b> <sub>pyr</sub>	0.732	0.732	90.3
<b>104Sn'</b> <sub>plan</sub>	1.131	0.774	86.4	<b>104Ge'</b> <sub>pyr(alt)</sub>	0.943	0.780	85.9
<b>145Ge'</b> <sub>plan</sub>	1.343	0.884	83.8	<b>104Sn'</b> <sub>pyr</sub>	0.700	0.700	88.9
<b>145Sn'</b> <sub>plan</sub>	1.138	0.787	86.1	<b>145Ge'</b> <sub>pyr</sub>	0.731	0.731	90.2
<b>146Ge'</b> <sub>plan_1</sub>	1.346	0.906	83.5	<b>145Sn'</b> <sub>pyr</sub>	0.704	0.704	88.6
<b>146Ge'</b> <sub>plan_2</sub>	1.343	0.877	84.1	<b>146Ge'</b> <sub>pyr_1</sub>	0.753	0.753	89.5
<b>146Sn'</b> <sub>plan_1</sub>	1.078	0.804	85.6	<b>146Ge'</b> <sub>pyr_2</sub>	0.757	0.757	88.9
<b>146Sn'</b> <sub>plan_2</sub>	1.144	0.757	87.3	<b>146Sn'</b> <sub>pyr_1</sub>	0.697	0.697	89.2
<b>146Sn'</b> <sub>near_1</sub>	0.979	0.885	85.6	<b>146Sn'</b> <sub>pyr_2</sub>	0.686	0.703	88.7
<b>146Sn'</b> <sub>near_2</sub>	1.026	0.837	85.7	<b>146Sn'</b> <sub>pyr_3</sub>	0.704	0.704	88.2
<b>147Sn'</b> <sub>plan_1</sub>	1.211	0.776	85.6	<b>147Sn'</b> <sub>pyr_1</sub>	0.777	0.725	86.6
<b>147Sn'</b> <sub>plan_2</sub>	1.232	0.769	86.6	<b>147Sn'</b> <sub>pyr_2</sub>	0.882	0.756	87.7
<b>148Sn'</b> <sub>plan_1</sub>	1.281	0.794	84.8	<b>148Sn'</b> <sub>pyr</sub>	0.838	0.819	86.4
<b>148Sn'</b> <sub>plan_2</sub>	1.168	0.780	85.3				

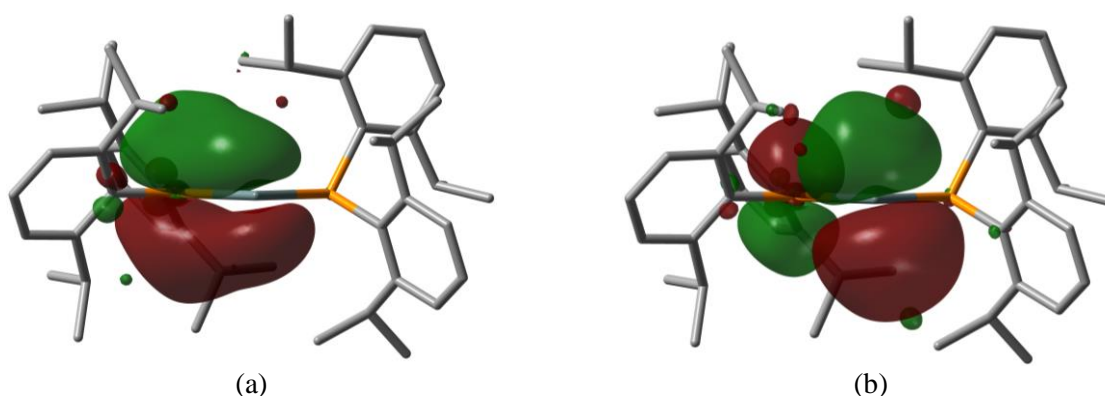
**Table 4:** NBO analyses and E-P WBIs for the calculated structures [<sup>a</sup>Wiberg bond indices of the E-P(1) and E-P(2) bonds, respectively. <sup>b</sup>Percentage of s character in the E lone pair.]

For **104Ge**, the planar form **104Ge'**<sub>plan</sub> is calculated to be 13.8 kJ mol<sup>-1</sup> more stable than **104Ge'**<sub>pyr</sub> and 64.7 kJ mol<sup>-1</sup> more stable than **104Ge'**<sub>pyr(alt)</sub>, consistent with the observed preference for the planar configuration of **104Ge**<sub>plan</sub> in the solid-state. In contrast, DFT calculations suggest **145Ge'**<sub>plan</sub> and **145Ge'**<sub>pyr</sub> are almost isoenergetic, with the pyramidal form **145Ge'**<sub>pyr</sub> more stable by 3.0 kJ mol<sup>-1</sup>. Similarly, for **104Sn'** and **145Sn'**, the pyramidal form **104/145Sn'**<sub>plan</sub> is more stable than the planar configurations by 2.5 and 4.2 kJ mol<sup>-1</sup>, respectively. For **104/145Sn'** this is consistent with the dynamic exchange between **104/145Sn'**<sub>pyr</sub> and **104/145Sn'**<sub>plan</sub> indicated in the variable-temperature <sup>31</sup>P{<sup>1</sup>H} NMR spectra. We attribute the isolation of **104Sn** and **145Sn** in the two different configurations in the solid-state to the small energy difference between the two forms and to the resulting influence of crystal packing effects on determining the solid-state structure. This is also consistent with the fact that **145Ge** crystallises as the methylcyclohexane solvate in the form **145Ge**<sub>plan</sub> but this reverts to an amorphous solid upon exposure to solvent and loss of methylcyclohexane, which, from its <sup>31</sup>P{<sup>1</sup>H} MAS NMR spectra, appears to contain two pyramidal phosphorus centres.

The lowest energy geometry of each configuration was used for the comparisons of the calculated structures of **146Ge'** and **146/147/148Sn'**. For **146Ge'** the pyramidal form **146Ge'**<sub>pyr\_1</sub> is calculated to be 12.6 kJ mol<sup>-1</sup> more stable than **146Ge'**<sub>plan</sub>, while the pyramidal form **146Sn'**<sub>pyr\_1</sub> is more stable than **146Sn'**<sub>near\_1</sub> by 10.2 kJ mol<sup>-1</sup> and **146Sn'**<sub>plan\_1</sub> by 33.6 kJ

mol<sup>-1</sup>. The instability of the planar (and near planar) forms of **146Ge'** and **146Sn'** is consistent with the observed preference for the pyramidal configurations of **146Ge<sub>pyr</sub>** and **146Sn<sub>pyr</sub>** in the crystal structures and in the variable-temperature <sup>31</sup>P{<sup>1</sup>H} NMR spectra, compared to **104/145Ge** and **104/145Sn**. For **147Sn'**, the planar form **147Sn'<sub>plan\_1</sub>** is essentially isoenergetic with the pyramidal form **147Sn'<sub>pyr</sub>**, with the former being more stable by 1.0 kJ mol<sup>-1</sup>. This is consistent with **147Sn** exhibiting similar variable-temperature <sup>31</sup>P{<sup>1</sup>H} NMR behaviour to **104/145Sn**. For **148Sn**, the planar configuration is significantly more stable than the pyramidal configuration **148Sn'<sub>pyr</sub>** by 52.4 kJ mol<sup>-1</sup>. Although we do not have complete NMR data for **148Sn**, the very large <sup>31</sup>P-<sup>117/119</sup>Sn coupling constant observed for the <sup>31</sup>P{<sup>1</sup>H} signal (*J*<sub>PSn</sub> = 1900 Hz) in the reaction mixture of **148Sn** supports the idea that the planar configuration **148Sn'<sub>plan\_1</sub>** has a large contribution in the equilibrium at room temperature.

Inspection of the molecular orbitals of the calculated structures with a planar configuration indicates that either the HOMO or HOMO -1 comprises the E-P π orbital while the LUMO or LUMO +1 comprises the corresponding π\* orbital (Table 5), with the exception of **148Sn'<sub>plan\_2</sub>**, for which the π or π\* molecular orbitals could not be located. For example, the HOMO and LUMO of **104Sn'<sub>plan</sub>** are shown in Figure 83. Although the sum of angles for P(1) in **146Sn'<sub>near\_1</sub>** and **146Sn'<sub>near\_2</sub>** are significantly lower than that in **148Sn'<sub>plan\_2</sub>**, the HOMO -1 and LUMO essentially comprise the π and π\* orbitals, respectively, in each case.



**Figure 83:** (a) HOMO and (b) LUMO of **104Sn'<sub>plan</sub>**

NBO analysis also reveals that, in addition to the stabilisation provided by the P-E π interaction, these structures are stabilised by the donation of the tetrel lone pair into the opposing P-C σ\* orbital of the planar phosphorus centre. Second-order perturbation theory analysis shows the approximate stabilisation afforded by these interactions range from 14.1 to 61.9 kJ mol<sup>-1</sup> (Table 5). For **146Sn'<sub>near\_1</sub>** and **146Sn'<sub>near\_2</sub>**, the sum of the approximate stabilisation provided by these interactions at both phosphorus centres is 18.2 and 21.5 kJ mol<sup>-1</sup>, respectively, in each case.

Compound	$E(2)$ for E-P(1)	$\pi$	$\pi^*$
<b>104Ge'</b> <sub>plan</sub>	55.0	HOMO -1	LUMO +1
<b>104Sn'</b> <sub>plan</sub>	45.1	HOMO	LUMO
<b>145Ge'</b> <sub>plan</sub>	54.8	HOMO	LUMO
<b>145Sn'</b> <sub>plan</sub>	46.5	HOMO	LUMO
<b>146Ge'</b> <sub>plan_1</sub>	51.5	HOMO -1	LUMO
<b>146Ge'</b> <sub>plan_2</sub>	44.0	HOMO -1	LUMO
<b>146Sn'</b> <sub>plan_1</sub>	23.6	HOMO -1	LUMO
<b>146Sn'</b> <sub>plan_2</sub>	43.5	HOMO -1	LUMO
<b>146Sn'</b> <sub>near_1</sub>	18.2*	HOMO -1	LUMO
<b>146Sn'</b> <sub>near_2</sub>	21.5*	HOMO -1	LUMO
<b>147Sn'</b> <sub>plan_1</sub>	40.0	HOMO -1	LUMO
<b>147Sn'</b> <sub>plan_2</sub>	61.9	HOMO -1	LUMO
<b>148Sn'</b> <sub>plan_1</sub>	28.2	HOMO -1	LUMO
<b>148Sn'</b> <sub>plan_2</sub>	14.1	-	-

**Table 5:**  $E(2)$  energy for the E(lone pair)  $\rightarrow$  [P(1)-C  $\sigma^*$ ] delocalization (kJ mol<sup>-1</sup>) and location of the molecular orbitals corresponding to the P-E  $\pi$  and  $\pi^*$  orbitals

The E $\cdots$ C<sub>ipso</sub> distances and C<sub>ipso</sub>-P-E angles for the calculated geometries with a pyramidal phosphorus configuration are shown in Table 6. The E $\cdots$ C<sub>ipso</sub> interactions in the calculated structures are rather symmetrical and closely match the longer interaction in the crystal structures of **146Ge**·(C<sub>6</sub>H<sub>14</sub>)<sub>0.5</sub> or **146Sn** with the exceptions of **104Ge'**<sub>pyr(alt)</sub> and **147Sn'**<sub>pyr\_1</sub>. As expected, the Sn $\cdots$ C<sub>ipso</sub> distances are longer than the corresponding Ge $\cdots$ C<sub>ipso</sub> interactions. The asymmetry of the Sn $\cdots$ C<sub>ipso</sub> interactions in the solid-state structure of **147Sn** is replicated in the corresponding minimum-energy geometry **147Sn'**<sub>pyr\_1</sub>, in which both interactions are slightly overestimated. Second order perturbation theory analysis showed significant stabilisation by delocalised of electron density from P-C<sub>ipso</sub>  $\sigma$  bonds and C<sub>ipso</sub>-C  $\pi$  bonds towards the vacant p-orbital at the tetrel centre. In support of the this, NBO deletions (in which the energy of the system is recalculated in the absence of the P-C<sub>ipso</sub>  $\sigma$  bond and C<sub>ipso</sub>-C  $\pi$  bond interactions) indicate that these interactions stabilise the calculated geometries of the diphosphagermylenes by 190 to 206 kJ mol<sup>-1</sup> and the diphosphastannynes by 131 to 146 kJ mol<sup>-1</sup>, with the exception of **147Sn'**<sub>pyr\_1</sub>, which is stabilised by 46.9 kJ mol<sup>-1</sup> from the single Sn $\cdots$ C<sub>ipso</sub> interaction.

Surprisingly, NBO analysis reveals that the “vacant” orbital on the tetrel centre for all the calculated geometries with a pyramidal geometry has an occupancy of 0.16 to 0.26 electrons, regardless of whether there are any E $\cdots$ C<sub>ipso</sub> interactions present (Table 6). This is unexpected as the Ge $\cdots$ C<sub>ipso</sub> distances in **104Ge'**<sub>pyr(alt)</sub> are relatively long and the faces of the corresponding arene rings are directed away from the vacant orbital. In addition, the arene groups in **147Sn'**<sub>pyr\_2</sub> are very remote to the tin centre and **148Sn'**<sub>pyr</sub> does not feature any arene groups. A potential source of this electron density is through agostic-type interactions. Inspection of **104Ge'**<sub>pyr(alt)</sub> revealed two very short Sn $\cdots$ H distances of 2.1509 and 2.2002 Å.

A NBO deletion of these two Sn $\cdots$ (H-C) interactions indicates that these interactions stabilise **104Ge'**<sub>pyr(alt)</sub> by 111.8 kJ mol<sup>-1</sup>. A preliminary DFT study was performed to investigate the magnitude of the stabilisation provided by agostic-type interactions in these systems. For **147Sn'**<sub>pyr\_1</sub> and **147Sn'**<sub>pyr\_2</sub>, NBO deletions of Sn $\cdots$ (H-C) interactions within 3 Å of the tin centre indicate that these interactions provided stabilisation of 52.9 and 52.5 kJ mol<sup>-1</sup>, respectively, which is remarkably similar to the stabilisation provided by the single long range Ge $\cdots$ C<sub>ipso</sub> interaction in **147Sn'**<sub>pyr\_1</sub>. In addition, a NBO deletion of the Sn $\cdots$ (H-C) interactions within 3.2 Å of the tin centre of **148Sn'**<sub>pyr</sub> indicate these interactions provide 80.8 kJ mol<sup>-1</sup> of stabilisation.

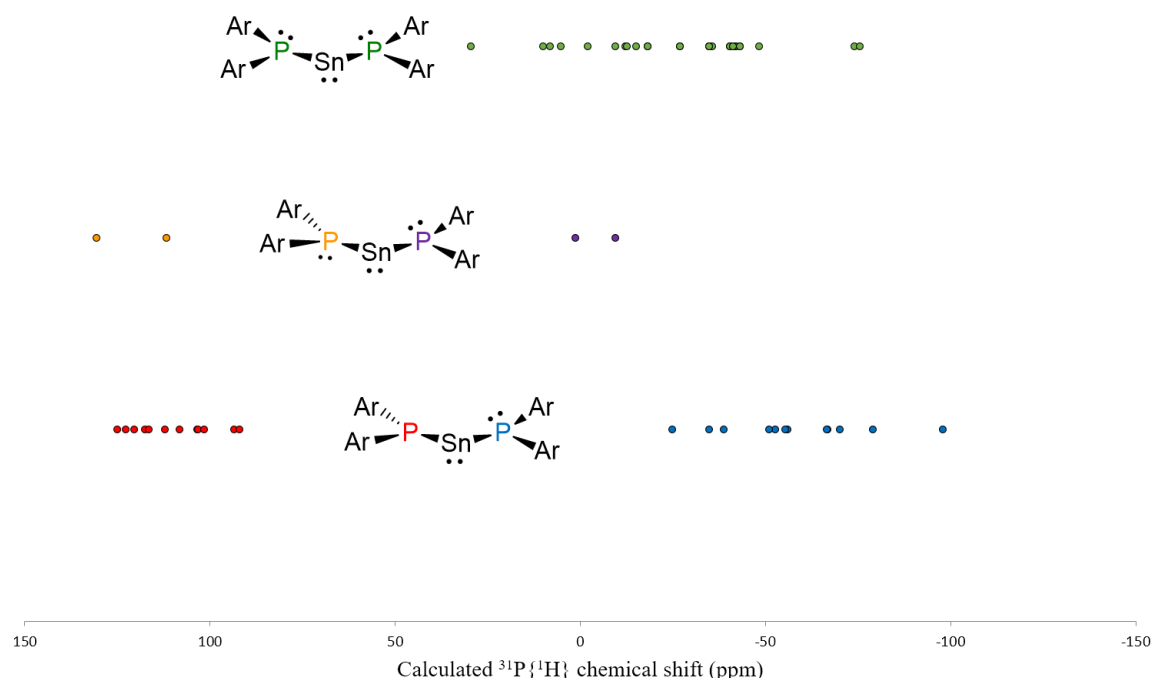
Compound	E $\cdots$ C <sub>ipso</sub> <sup>a</sup>		C <sub>ipso</sub> -P-E <sup>b</sup>		lp*occupancy <sup>c</sup>	E(NBOdel)	
	C <sub>ipso</sub> -P(1)	C <sub>ipso</sub> -P(2)	P(1)	P(2)		P-C <sub>ipso</sub> + C <sub>ipso</sub> -C <sup>d</sup>	C-H <sup>e</sup>
<b>104Ge'</b> <sub>pyr</sub>	2.6858	2.6862	76.04	76.05	0.19	206.2	-
<b>104Ge'</b> <sub>pyr(alt)</sub>	3.6110	3.1004	115.02	89.97	0.26	-	111.8
<b>104Sn'</b> <sub>pyr</sub>	2.8431	2.8431	76.63	76.63	0.17	146.4	-
<b>145Ge'</b> <sub>pyr</sub>	2.6549	2.6549	75.14	75.14	0.21	215.0	-
<b>145Sn</b>	2.9813(1)	2.882(2)	89.62(2)	79.20(8)			
<b>145Sn'</b> <sub>pyr</sub>	2.8336	2.8366	76.46	76.46	0.18	145.5	-
<b>146Ge'</b> (C <sub>6</sub> H <sub>14</sub> ) <sub>0.5</sub>	2.7008(14)	2.5736(14)	77.60(5)	73.13(5)			
<b>146Ge'</b> <sub>pyr_1</sub>	2.6720	2.6720	75.38	75.38	0.20	195.6	-
<b>146Ge'</b> <sub>pyr_2</sub>	2.7061	2.7049	76.82	76.77	0.20	190.0	-
<b>146Sn</b>	2.855(2)	2.7315(14)	78.02(6)	73.80(4)			
<b>146Sn'</b> <sub>pyr_1</sub>	2.8488	2.7911	76.41	74.34	0.16	138.3	-
<b>146Sn'</b> <sub>pyr_2</sub>	2.8540	2.7793	77.03	74.09	0.17	131.4	-
<b>146Sn'</b> <sub>pyr_3</sub>	2.8594	2.8594	77.15	77.15	0.17	139.2	-
<b>147Sn</b>	3.3245(16)	2.877(2)	98.56(5)	78.75(7)			
<b>147Sn'</b> <sub>pyr_1</sub>	3.378	3.0489	96.84	83.79	0.18	46.9	52.9
<b>147Sn'</b> <sub>pyr_2</sub>	-	-	-	-	0.22	-	52.5
<b>148Sn'</b> <sub>pyr</sub>	-	-	-	-	0.16	-	80.8

**Table 6:** <sup>a</sup>E $\cdots$ C<sub>ipso</sub> distances (Å) and <sup>b</sup>C<sub>ipso</sub>-P-E angles (°) of the E $\cdots$ C<sub>ipso</sub> interactions. <sup>c</sup>Electron occupancy of the vacant p-orbital at the tetrel centre. Energy change (kJ mol<sup>-1</sup>) from the NBO deletions of the interactions from the <sup>d</sup>P-C<sub>ipso</sub> σ bonds and C<sub>ipso</sub>-C π bonds and <sup>e</sup>agostic-type interactions from the C-H bonds.

The calculated <sup>31</sup>P NMR chemical shifts of **104-146Ge** and **104-148Sn** are listed in Table 3 and displayed in Figure 84, in which they are categorised by the configuration of the optimized geometry. The pyramidal phosphorus centres in the pyramidal, near planar and planar configurations have calculated <sup>31</sup>P NMR chemical shifts ranging from -98.0 to 29.5 ppm, while the calculated <sup>31</sup>P NMR chemical shifts of planar or near planar phosphorus environments have a smaller range from 91.9 to 130.6 ppm. The signals corresponding to the planar configurations in the low-temperature <sup>31</sup>P{<sup>1</sup>H} NMR spectra of **104Ge** and **145Ge** and the <sup>31</sup>P MAS SSNMR spectra of **104Ge** and **104Sn** have good correspondence with the respective calculated <sup>31</sup>P NMR chemical shifts. For example, the observed chemical shifts of 94.3 and -66.8 ppm in the <sup>31</sup>P{<sup>1</sup>H} MAS SSNMR spectrum of **104Sn** are closely replicated in **104Sn'**<sub>plan</sub> (95.8 and -66.2 ppm, respectively). The calculated <sup>31</sup>P{<sup>1</sup>H} NMR chemical shift of



-40.6 ppm for the two pyramidal phosphorus centres in **145Sn'**<sub>pyr</sub> less accurately matches the observed chemical shifts of -48.8 and -58.7 ppm in the  $^{31}\text{P}\{^1\text{H}\}$  MAS SSNMR spectra of **145Sn**. For compounds **146Ge**·(C<sub>6</sub>H<sub>14</sub>)<sub>0.5</sub>, **146Sn**, **147Sn** and **148Sn**, for which we only have solution-state  $^{31}\text{P}$  NMR data, comparison between the calculated and observed  $^{31}\text{P}$  NMR chemical shifts is complicated by the equilibrium between the planar and pyramidal configurations.



**Figure 84:** Calculated  $^{31}\text{P}\{^1\text{H}\}$  NMR shifts for the pyramidal (top), near planar (middle) and planar (bottom) configurations

## 4.12 Conclusion of DFT calculations

DFT calculations reveal that the relative energies of the planar, near planar and pyramidal configurations of the diphosphatetrylenes depend heavily on the sterics of the phosphide ligand system, with less bulky phosphides favouring the pyramidal configurations. Furthermore, the NBO calculations show that the planar configuration of the diphosphatetrylenes, as seen in the solid-state structures of **104Ge/Sn** and **145Ge**·(C<sub>7</sub>H<sub>14</sub>) and **148Sn**, is stabilised by a *push-pull* type interaction, in which the *push* arises from the  $\pi$  interaction from the planar phosphorus centre into the vacant p orbital at the tetrel centre and the *pull* from the delocalisation from the tetrel lone pair into a P-C  $\sigma^*$  orbital of the planar phosphorus centre. In contrast, the diphosphatetrylenes that adopt a pyramidal configuration in the solid-state (**145Sn**, **146Ge**·(C<sub>6</sub>H<sub>14</sub>)<sub>0.5</sub>, **146Sn** and **147Sn**) are stabilised by donation of

electron-density from the P- $C_{ipso}$   $\sigma$ -bonds and  $C_{ipso}$ -C  $\pi$ -bonds. The calculated  $^{31}\text{P}$  NMR chemical shifts further support the data from MAS SSNMR spectroscopy that planar phosphorus environments are associated with relatively low field signals, while high field signals are predicted for the pyramidal phosphorus environments.

#### 4.13 Overall conclusions

In conclusion, we have synthesised an array of diphosphatetrylenes featuring bulky phosphide substituents, including the first examples of diphosphastannylenes featuring  $p\pi$ - $p\pi$  interactions from a planar phosphorus centre. In the solid-state, compounds **104Sn**, **145Ge**·( $\text{C}_7\text{H}_{14}$ ) and **148Sn** are stabilised by  $\pi$ -interactions from a planar phosphorus centre while **145Sn**, **146Ge**·( $\text{C}_6\text{H}_{14}$ ) $_{0.5}$ , **146Sn** and **147Sn** are stabilised by short  $C_{ipso}$ -P-Ge/Sn contacts. However, in solution there is a dynamic equilibrium between the planar and pyramidal configurations, with the exception of **146Sn** in which only the pyramidal configuration is observed.

From the solid-state structures, variable-temperature  $^{31}\text{P}\{^1\text{H}\}$  NMR spectra and DFT calculations we have demonstrated that the stabilisation of these diphosphatetrylenes is dependent on the nature and sterics of the phosphide ligand. The stability of the planar configuration approximately correlates with the steric bulk of the substituents, decreasing in the order  $\{(\text{Me}_3\text{Si})_2\text{CH}\}_2\text{P} > (\text{Dipp})_2\text{P} \approx (\text{Tripp})_2\text{P} > \{(\text{Me}_3\text{Si})_2\text{CH}\}(\text{Dipp})_2 > (\text{Dipp})(\text{Mes})\text{P}$ . While, we were unable to isolate a clean sample of **148Sn** for characterisation by NMR spectroscopy, the large  $^{117/119}\text{Sn}$  coupling constant (1900 Hz) observed in the  $^{31}\text{P}\{^1\text{H}\}$  NMR spectrum of the crude reaction mixture suggests it has a larger contribution of the planar configuration at room temperature compared to **104Sn**, **145Sn**, **146Sn** and **147Sn**. The stability of the planar configuration of **148Sn** over the pyramidal configuration (52.4 kJ mol $^{-1}$  by DFT calculations) may be attributed the steric bulk of the  $\{(\text{Me}_3\text{Si})_2\text{CH}\}$  substituents and the inability for these substituents to stabilise the pyramidal configuration, as opposed to aryl substituted ligands that can provide arene $\cdots\text{E}$  interactions.

## 4.14 Experimental

### 4.14.1 Synthesis of {(Dipp)<sub>2</sub>P}<sub>2</sub>Ge (**104Ge**)

This is a modified synthesis of this compound, based on our previously published procedure.<sup>14</sup> A solution of *n*BuLi in hexanes (1.2 mL, 3.00 mmol) was added to a solution of (Dipp)<sub>2</sub>PH (1.01 g, 2.85 mmol) in THF (15 mL). The resulting red solution was stirred for 30 minutes and was then added, dropwise, to a solution of GeCl<sub>2</sub>(1,4-dioxane) (0.334 g, 1.44 mmol) in THF (10 mL) at room temperature and this mixture was stirred for 1 h. The solvent was removed *in vacuo* from the resulting dark red solution to give a sticky red solid. The product was extracted into *n*-hexane (30 mL) to give a dark red solution with pale solids. The solution was filtered and the dark red solution was reduced to 10 mL and stored at -25 °C. Dark red crystals of **104Ge** were isolated after 1 week. Yield 0.39 g, 34%.

<sup>31</sup>P and <sup>1</sup>H NMR data match those previously reported.

### 4.14.2 Synthesis of {(Dipp)<sub>2</sub>P}<sub>2</sub>Sn (**104Sn**)

A solution of *n*-BuLi in hexanes (1.0 mL, 2.50 mmol) was added to a solution of Dipp<sub>2</sub>PH (0.80 g, 2.27 mmol) in THF (15 mL). The resulting red solution was stirred for 1 h and was then added, dropwise, to a solution of SnCl<sub>2</sub> (0.216 g, 1.14 mmol) in THF (15 mL) at room temperature and this mixture was stirred for 1 h in the absence of light. The solvent was removed *in vacuo* from the resulting dark yellow solution to give a sticky orange solid. The product was extracted into toluene (15 mL) to give a purple solution containing pale solids. The solution was filtered and the dark purple filtrate was reduced to 5 mL and stored at -25°C. Dark purple crystals of **104Sn** suitable for X-ray crystallography were isolated after 1 week. Yield 0.37 g, 39%. Anal. Calcd. for C<sub>48</sub>H<sub>68</sub>P<sub>2</sub>Sn (825.73) C 69.80%, H 8.30%; found C 69.70%, H 8.33%.

<sup>1</sup>H NMR (d<sub>8</sub>-toluene, 298 K): δ 1.13 (d, *J*<sub>HH</sub> = 7.0 Hz, 48H, CHMe<sub>2</sub>), 3.88 (m, 8H, CHMe<sub>2</sub>), 7.05 (d, *J*<sub>HH</sub> = 7.5 Hz, 8H, ArH), 7.12 (m, 4H, ArH). <sup>13</sup>C{<sup>1</sup>H} NMR (d<sub>8</sub>-toluene, 298 K): δ 26.26 (CHMe<sub>2</sub>), 35.02 (m, CHMe<sub>2</sub>), 125.90 (Ar), 129.72 (Ar), 138.08 (m, Ar), 155.22 (m, Ar). <sup>31</sup>P{<sup>1</sup>H} NMR (d<sub>8</sub>-toluene, 298 K): δ -25.1 (br. s, *J*<sub>PSn</sub> = 1300 Hz).

No <sup>119</sup>Sn{<sup>1</sup>H} signal for **104Ge** could be located at room temperature or -80 °C.

#### 4.14.3 Synthesis of {(Tripp)<sub>2</sub>P}<sub>2</sub>Ge (145Ge)

A solution of *n*BuLi in hexanes (1.4 mL, 3.5 mmol) was added to a solution of (Tripp)<sub>2</sub>PH (1.55 g, 3.53 mmol) in THF (20 mL). The resulting dark red solution was stirred for 30 minutes and was then added, dropwise, to a solution of GeCl<sub>2</sub>(1,4-dioxane) (0.415 g, 1.79 mmol) in THF (20 mL) and this mixture was stirred for 1 h. The solvent was removed *in vacuo* from the resulting dark red solution to give a sticky red solid. The product was extracted into methylcyclohexane (20 mL) to give a dark red solution with pale solids. The solution was filtered and the dark red filtrate was reduced to 10 mL and stored at -25°C. Dark red crystals of **145Ge**·C<sub>7</sub>H<sub>14</sub> suitable for X-ray crystallography were isolated after 1 week and were washed with hexamethyldisiloxane (2 mL). The isolated compound, which lost crystallinity due to solvent loss, was brown. The following data relate to the solvent-free form **145Ge**. Yield: 0.52 g, 31%. Anal. Calcd. for C<sub>60</sub>H<sub>92</sub>P<sub>2</sub>Ge (947.97) C 76.02%, H 9.78%; found C 75.83%, H 9.89%.

<sup>1</sup>H NMR (d<sub>8</sub>-toluene, 298 K): δ ca. 1.2 (br. s, 48H, *o*-CHMe<sub>2</sub>), 1.21 (d, *J*<sub>HH</sub> = 7.0 Hz, 24H, *p*-CHMe<sub>2</sub>), 2.76 (sept, *J*<sub>HH</sub> = 7.0 Hz, 4H, *p*-CHMe<sub>2</sub>), 4.07 (br. s, 8H, *o*-CHMe<sub>2</sub>), 7.07 ppm (s, 8H, ArH). <sup>13</sup>C{<sup>1</sup>H} NMR (d<sub>8</sub>-toluene, 298 K): δ 25.05 (*p*-CHMe<sub>2</sub>), 26.10 (br. s, *o*-CHMe<sub>2</sub>), 35.54 (*o*-CHMe<sub>2</sub>), 36.69 (*p*-CHMe<sub>2</sub>), 123.69, 136.82, 150.51, 154.65 (Ar). <sup>31</sup>P{<sup>1</sup>H} NMR (d<sub>8</sub>-toluene, 298 K): δ 3.6 (br. s).

#### 4.14.4 Synthesis of {(Tripp)<sub>2</sub>P}<sub>2</sub>Sn (145Sn)

A solution of *n*BuLi in hexanes (1.1 mL, 2.75 mmol) was added to a solution of (Tripp)<sub>2</sub>PH (1.18 g, 2.69 mmol) in THF (20 mL). The resulting dark red solution was stirred for 1 h and was then added, dropwise, to a solution of SnCl<sub>2</sub> (0.256 g, 2.69 mmol) in THF (15 mL) at room temperature and this mixture was stirred for 1 h in the absence of light. The solvent was removed *in vacuo* from the resulting dark yellow solution to give a sticky orange solid. The product was extracted into *n*-hexane (15 mL) to give a purple solution containing pale solids. The solution was filtered and the dark purple filtrate was reduced to 5 mL and stored at -25 °C. Dark yellow crystals of **145Sn** suitable for X-ray crystallography were isolated after 2 days. Yield 0.39 g, 29%. Anal. Calcd. for C<sub>60</sub>H<sub>92</sub>P<sub>2</sub>Sn (994.05) C 72.50%, H 9.33%; found C 72.40%, H 9.14%.

<sup>1</sup>H NMR (d<sub>8</sub>-toluene, 298 K): δ 1.20 (br. s, 24H, *o*-CHMe<sub>2</sub>), 1.23 (d, *J*<sub>HH</sub> = 6.9 Hz, 12H, *p*-CHMe<sub>2</sub>), 2.74 (sept, *J*<sub>HH</sub> = 6.9 Hz, 4H, *p*-CHMe<sub>2</sub>), 4.02 (br. s, 8H, *o*-CHMe<sub>2</sub>), 7.08 (s,

8 H, ArH).  $^{13}\text{C}\{^1\text{H}\}$  NMR ( $d_8$ -toluene, 298 K):  $\delta$  25.06 (*p*-CHMe<sub>2</sub>), 26.29 (*o*-CHMe<sub>2</sub>), 35.21 (*o*-CHMe<sub>2</sub>), 35.52 (*p*-CHMe<sub>2</sub>), 123.87 (Ar), 135.97 (m, Ar), 149.85 (Ar), 155.30 (m, Ar).  $^{31}\text{P}\{^1\text{H}\}$  NMR ( $d_8$ -toluene, 298 K):  $\delta$  -19.5 (br. s,  $J_{\text{PSn}} = 1420$  Hz).

#### 4.14.5 Synthesis of (Dipp)<sub>2</sub>P-P(Dipp)<sub>2</sub> (150)

A solution of *n*-BuLi (1.0 mL, 2.3 mmol, 2.3 M) was added to a solution of Dipp<sub>2</sub>PH (0.84 g, 2.37 mmol) in THF (10 mL). The resulting red solution was stirred for 15 min and was then added rapidly to a suspension of PbI<sub>2</sub> (0.544 g, 1.20 mmol) in THF (10 mL). The mixture immediately formed a black precipitate and was stirred for 30 mins. The solvent was removed *in vacuo* and the product was extracted into Et<sub>2</sub>O (25 mL). The solution was filtered and solvent was removed *in vacuo* from the clear yellow filtrate to give a pale solid and a red oil. The coloured impurities were removed by heating the mixture in degassed ethanol (10 mL). The mixture was then cooled to 0 °C and the supernatant solution was decanted. This was repeated 3 more times until the supernatant was colourless. Removal of residual solvent *in vacuo* from the solid gave **150** as a pale yellow powder. Yield 0.39 g, 47%.

$^1\text{H}$  NMR (CDCl<sub>3</sub>):  $\delta$  = 0.04 (d,  $J_{\text{HH}} = 6.9$  Hz, 6H, CHMe<sub>2</sub>), 0.14 (d,  $J_{\text{HH}} = 6.4$  Hz, 6H, CHMe<sub>2</sub>), 0.42 (d,  $J_{\text{HH}} = 6.8$  Hz, 6H, CHMe<sub>2</sub>), 0.49 (d,  $J_{\text{HH}} = 6.4$  Hz, 6H, CHMe<sub>2</sub>), 1.13 (d,  $J_{\text{HH}} = 6.5$  Hz, 6H, CHMe<sub>2</sub>), 1.14 (d,  $J_{\text{HH}} = 6.5$  Hz, 6H, CHMe<sub>2</sub>), 1.22 (d,  $J_{\text{HH}} = 6.7$  Hz, 6H, CHMe<sub>2</sub>), 1.25 (d,  $J_{\text{HH}} = 6.5$  Hz, 6H, CHMe<sub>2</sub>), 3.61 (sept,  $J_{\text{HH}} = 6.6$  Hz, 2H, CHMe<sub>2</sub>), 3.74 (sept,  $J_{\text{HH}} = 6.1$  Hz, 2H, CHMe<sub>2</sub>), 3.96 (sept,  $J_{\text{HH}} = 5.8$  Hz, 2H, CHMe<sub>2</sub>), 4.90 (m, 2H, CHMe<sub>2</sub>), 6.96 (m, 4H, ArH), 7.02 (dd,  $J_{\text{HH}} = 7.8$  Hz,  $J_{\text{HH}} = 1.4$  Hz, 2H, ArH), 7.08 (dd,  $J_{\text{HH}} = 7.5$  Hz,  $J_{\text{HH}} = 1.4$  Hz, 2H, ArH), 7.16 (t,  $J_{\text{HH}} = 7.8$  Hz, 2H, ArH), 7.18 (t,  $J_{\text{HH}} = 7.8$  Hz, 2H, ArH).  $^{13}\text{C}\{^1\text{H}\}$  NMR (CDCl<sub>3</sub>): 22.58, 22.85, 23.94, 24.01, 24.03, 24.41, 25.48 (CHMe<sub>2</sub>), 31.57 (t,  $J_{\text{PC}} = 18.7$  Hz, CHMe<sub>2</sub>), 32.19 (t,  $J_{\text{PC}} = 20.5$  Hz, CHMe<sub>2</sub>), 32.63 (t,  $J_{\text{PC}} = 19.2$  Hz, CHMe<sub>2</sub>), 32.83 (CHMe<sub>2</sub>), 123.95 (t,  $J_{\text{PC}} = 3.1$  Hz, Ar), 124.24 (t,  $J_{\text{PC}} = 3.9$  Hz, Ar), 126.15, 126.51, 128.67, 129.72 (Ar), 134.07 (t,  $J_{\text{PC}} = 14.7$  Hz, Ar), 134.99 (t,  $J_{\text{PC}} = 18.9$  Hz), 154.27 (m, Ar), 154.77 (t,  $J_{\text{PC}} = 4.2$  Hz, Ar), 155.65 (t,  $J_{\text{PC}} = 19.3$  Hz, Ar).  $^{31}\text{P}$  NMR (CDCl<sub>3</sub>):  $\delta$  -38.1 (s).

#### 4.14.6 Synthesis of {(Dipp)(Mes)P}<sub>2</sub>Ge(*n*-hexane)<sub>0.5</sub> (146·(C<sub>6</sub>H<sub>14</sub>)<sub>0.5</sub>)

To a solution of (Dipp)(Mes)PH (0.81 g, 2.59 mmol) in THF (20 mL) was added a solution of *n*BuLi in hexanes (1.1 mL, 2.53 mmol). The resulting red solution was stirred for 1 h and added, dropwise, to a solution of GeCl<sub>2</sub>(1,4-dioxane) (0.300 g, 1.30 mmol) in THF (20

ml) and stirred for 1 h. The solvent was removed from the resulting dark red solution *in vacuo* to give a sticky red solid. The product was extracted into *n*-hexane (20 ml) to give a dark red solution with pale solids, which were removed by filtration. The filtrate was reduced to 5 ml *in vacuo* and deposited large pale red crystals of **146**·(**C<sub>6</sub>H<sub>14</sub>**)<sub>0.5</sub> suitable for X-ray crystallography on standing at room temperature overnight. The mixture was further stored at -25 °C for 1 day. The supernatant solution was removed by filtration and the crystals were washed with cold (-10 °C) *n*-hexane (5 ml) and the residual solvent was removed under vacuum. Yield: 0.34 g, 35%.

<sup>1</sup>H NMR: [*d*<sub>8</sub>-toluene]: δ 0.88 (t, *J*<sub>HH</sub> = 7.0 Hz, 3H, *n*-hexane), 1.02 (d, *J*<sub>HH</sub> = 6.8 Hz, 24H, CHMe<sub>2</sub>), 1.21-1.28 (m, 4H, *n*-hexane), 2.06 (s, 6H, *p*-Me), 2.40 (s, 12H, *o*-Me), 3.44 (m, 4H, CHMe<sub>2</sub>), 6.73 (s, 4H, ArH), 7.00 (d, *J*<sub>HH</sub> = 7.5 Hz, 4H, ArH), 7.10 (m, 2H, ArH). <sup>13</sup>C{<sup>1</sup>H} NMR: [*d*<sub>8</sub>-toluene]: δ 14.35 (*n*-hexane), 21.09 (*p*-Me), 23.11 (*n*-hexane), 24.88 (t, *J*<sub>PC</sub> = 9.2 Hz, *o*-Me), 25.03 (CHMe<sub>2</sub>), 32.05 (*n*-hexane), 33.80 (t, *J*<sub>PC</sub> = 5.8 Hz, CHMe<sub>2</sub>), 124.00, 128.51, 130.93 (ArH), 131.30 (t, *J*<sub>PC</sub> = 12.0 Hz, Ar), 136.16 (t, *J*<sub>PC</sub> = 6.4 Hz, Ar), 138.52 (Ar), 144.51 (t, *J*<sub>PC</sub> = 4.6 Hz, Ar), 153.11 (t, *J*<sub>PC</sub> = 4.2 Hz, Ar). <sup>31</sup>P{<sup>1</sup>H} NMR: [*d*<sub>8</sub>-toluene]: δ -6.5 (br. s).

#### 4.14.7 Synthesis of {(Dipp)(Mes)P}<sub>2</sub>Sn (**146Sn**)

To a solution of (Dipp)(Mes)PH (0.83 g, 2.66 mmol) in THF (15 ml) was added a solution of *n*BuLi in hexanes (2.3 M, 1.2 ml, 2.76 mmol). The resulting red solution was stirred for 1 h and added to a cold (-78 °C) solution of SnCl<sub>2</sub> (0.253 g, 1.33 mmol) in THF (15 ml) with the light excluded. The resulting red solution was allowed to warm to room temperature and the solvent was removed *in vacuo*. The product was extracted from the sticky red solid into methylcyclohexane to give a dark red/purple solution with pale solids. The pale solids were removed by filtration and the filtrate was reduced to 5 ml in volume. Storage at -25 °C for 1 week formed large purple crystals of **146Sn** suitable for characterisation by X-ray crystallography. The supernatant solution was removed by filtration and the purple crystals were washed with cold (0 °C) light petroleum (5 ml) and the residual solvent was removed under vacuum. Yield: 0.27 g, 27 %.

<sup>1</sup>H NMR [*d*<sub>8</sub>-toluene]: δ 0.97 (d, *J*<sub>HH</sub> = 6.7 Hz, 24H, CHMe<sub>2</sub>), 2.06 (s, 6H, *p*-Me), 2.43 (s, 12H, *o*-Me), 3.18 (sept, *J*<sub>HH</sub> = 6.7 Hz, 4H, CHMe<sub>2</sub>), 6.80 (s, 4H, ArH), 6.96 (d, *J*<sub>HH</sub> = 7.8 Hz, 4H, ArH), 7.05 (d, *J*<sub>HH</sub> = 7.8 Hz, 2H, ArH). <sup>13</sup>C{<sup>1</sup>H} NMR [*d*<sub>8</sub>-toluene]: δ 21.14 (*p*-Me), 24.77 (CHMe<sub>2</sub>), 25.49 (t, *J*<sub>PC</sub> = 11.0 Hz, *o*-Me), 33.56 (t, *J*<sub>PC</sub> = 5.5 Hz, CHMe<sub>2</sub>), 123.50,

127.50 (ArH), 129.33 (m, Ar, partially obscured by solvent peak), 132.26 (ArH), 136.98 (m, Ar), 137.82 (Ar), 144.92 (t,  $J_{PC} = 4.5$  Hz, Ar), 152.48 (t,  $J_{PC} = 4.4$  Hz, Ar).  $^{31}\text{P}\{^1\text{H}\}$  NMR [ $d_8$ -toluene]:  $\delta$  -53.5 ppm ( $J_{119\text{SnP}} = 855$  Hz,  $J_{117\text{SnP}} = 816$  Hz).  $^{119}\text{Sn}\{^1\text{H}\}$  NMR [ $d_8$ -toluene]:  $\delta$  476 (t,  $J_{\text{SnP}} = 855$  Hz).

#### 4.14.8 Synthesis of [(Dipp){(Me<sub>3</sub>Si)<sub>2</sub>CH}P]<sub>2</sub>Sn (147Sn)

To a cold (-78 °C) solution of (Dipp){(Me<sub>3</sub>Si)<sub>2</sub>CH}PH (0.63 g, 1.79 mmol) in THF (15 ml) was added a solution of *n*BuLi in hexanes (2.3 M, 0.8 ml, 1.84 mmol). The resulting mixture was allowed to warm to room temperature and was stirred for 30 min. The resulting red solution was added, dropwise, to a cold (-78 °C) solution of SnCl<sub>2</sub> (0.170 g, 1.79 mmol) in THF (15 ml). This mixture was allowed to warm to room temperature. The solvent was removed from the resulting orange solution *in vacuo* to give a sticky orange solid. The product was extracted into toluene (10 ml) and the dark purple mixture with pale solids was filtered. The solvent volume of the filtrate was reduced to 5 ml. Storage at -25 °C for 1 week resulted in the formation of crystals of **147Sn**. The supernatant was decanted and the residual solvent was removed from the remaining solid under vacuum to give the product as dark green crystals. Yield: 0.25 g, 34%.

$^1\text{H}$  NMR [ $d_8$ -toluene, 298 K]:  $\delta$  -0.01 (s, 36H, SiMe<sub>3</sub>), 1.43 (br. s, 24H, CHMe<sub>2</sub>), 1.96 (m, 2H, Si<sub>2</sub>CH), 4.31 (s, 4H, CHMe<sub>2</sub>), 7.05 (d,  $J_{\text{HH}} = 7.5$  Hz, 4H, ArH), 7.12 (t,  $J_{\text{HH}} = 7.5$  Hz, 2H, ArH).  $^{13}\text{C}\{^1\text{H}\}$  NMR [ $d_8$ -toluene, 298 K]:  $\delta$  2.56 (m, SiMe<sub>3</sub>), 10.72 (m, Si<sub>2</sub>CH), 25.97, 27.26 (br. s, CHMe<sub>2</sub>), 33.61 (t,  $J_{PC} = 9.5$  Hz, CHMe<sub>2</sub>), 125.58, 129.33 (ArH), 134.90 (m, Ar), 155.48 (Ar).  $^{31}\text{P}\{^1\text{H}\}$  NMR [ $d_8$ -toluene, 298 K]:  $\delta$  -30.1 (s,  $J_{\text{SnP}} = 1030$  Hz).

#### 4.15 References

- [1] K. Izod, D. G. Rayner, S. M. El-Hamruni, R. W. Harrington, U. Baisch, *Angew. Chem. Int. Ed. Engl.*, **2014**, 53, 3636-3640.
- [2] P. B. Hitchcock, M. F. Lappert, P. P. Power, S. J. Smith, *J. Chem. Soc., Chem. Commun.*, **1984**, 1669-1670.
- [3] M. Driess, R. Janoschek, H. Pritzkow, S. Rell, U. Winkler, *Angew. Chem. Int. Ed.*, **1995**, 34, 1614-1616.
- [4] F. J. Brady, C. J. Cardin, D. J. Cardin, D. J. Wilcock, *Inorg. Chim. Acta*, **2000**, 298, 1-8.
- [5] A. Dashti-Mommertz, B. Neumüller, *Z. Anorg. Allg. Chem.*, **1999**, 625, 954-960.
- [6] S. L. Hinchley, C. A. Morrison, D. W. H. Rankin, C. L. B. Macdonald, R. J. Wiacek, A. H. Cowley, M. F. Lappert, G. Gundersen, J. A. C. Clyburne, P. P. Power, *Chem. Commun.*, **2000**, 2045-2046.

- [7] (a) C. Couret, J. Escudie, J. Satge, A. Raharinirina, J. D. Andriamizaka, *J. Am. Chem. Soc.*, **1985**, *107*, 8280-8281; (b) H. Ranaivonjatovo, J. Escudie, C. Couret, J. Satge, *J. Chem. Soc., Chem. Commun.*, **1992**, 1047-1048.
- [8] S. Yao, M. Brym, K. Merz, M. Driess, *Organometallics*, **2008**, *27*, 3601-3607.
- [9] B. P. Johnson, S. Almstätter, F. Dielmann, M. Bodensteiner, M. Scheer, *Z. Anorg. Allg. Chem.*, **2010**, *636*, 1275-1285.
- [10] (a) J. Escudie, C. Couret, J. Satge, M. Andrianarison, J. D. Andriamizaka, *J. Am. Chem. Soc.*, **1985**, *107*, 3378-3379; (b) M. Draeger, J. Escudie, C. Couret, H. Ranaivonjatovo, J. Satge, *Organometallics*, **1988**, *7*, 1010-1013.
- [11] V. Y. Lee, M. Kawai, A. Sekiguchi, H. Ranaivonjatovo, J. Escudié, *Organometallics*, **2009**, *28*, 4262-4265.
- [12] K. Izod, J. Stewart, W. Clegg, R. W. Harrington, *Organometallics*, **2010**, *29*, 108-116.
- [13] (a) S. Duttwyler, Q. Q. Do, A. Linden, K. K. Baldrige, J. S. Siegel, *Angew. Chem. Int. Ed. Engl.*, **2008**, *47*, 1719-1722; (b) C. Gerdes, W. Saak, D. Haase, T. Muller, *J. Am. Chem. Soc.*, **2013**, *135*, 10353-10361.
- [14] (a) T. Probst, O. Steigelmann, J. Riede, H. Schmicklaur, *Angew. Chem. Int. Ed.*, **1990**, *29*, 1397-1398; (b) M. S. Weininger, P. F. Rodesiler, E. L. Amma, *Inorg. Chem.*, **1979**, *18*, 751-755; (c) A. G. Gash, P. F. Rodesiler, E. L. Amma, *Inorg. Chem.*, **1974**, *13*, 2429-2434; (d) P. F. Rodesiler, E. L. Amma, T. Auel, *J. Am. Chem. Soc.*, **1975**, *97*, 7405-7410; (e) A. Schafer, F. Winter, W. Saak, D. Haase, R. Pottgen, T. Muller, *Chem. Eur. J.*, **2011**, *17*, 10979-10984; (f) J. L. Lefferts, M. B. Hossain, K. C. Molloy, D. van der Helm, J. J. Zuckerman, *Angew. Chem. Int. Ed.*, **1980**, *19*, 309-310; (g) C. P. Sindlinger, F. S. Aicher, H. Schubert, L. Wesemann, *Angew. Chem. Int. Ed. Engl.*, **2017**, *56*, 2198-2202; (h) S. Hino, M. Olmstead, A. D. Phillips, R. J. Wright, P. P. Power, *Inorg. Chem.*, **2004**, *43*, 7346-7352; (i) J. Li, C. Schenk, F. Winter, H. Scherer, N. Trapp, A. Higelin, S. Keller, R. Pottgen, I. Krossing, C. Jones, *Angew. Chem. Int. Ed. Engl.*, **2012**, *51*, 9557-9561.
- [15] R. T. Baker, J. F. Whitney, S. S. Wreford, *Organometallics*, **1983**, *2*, 1049-1051.
- [16] G. Bonnet, M. M. Kubicki, C. Moise, R. Lazzaroni, P. Salvadori, G. Vitulli, *Organometallics*, **1992**, *11*, 964-967.
- [17] P. P. Power, *Nature*, **2010**, *463*, 171-177.
- [18] M. Usher, A. V. Protchenko, A. Rit, J. Campos, E. L. Kolychev, R. Tirfoin, S. Aldridge, *Chem. Eur. J.*, **2016**, *22*, 11685-11698.
- [19] A. V. Protchenko, D. Dange, A. D. Schwarz, C. Y. Tang, N. Phillips, P. Mountford, C. Jones, S. Aldridge, *Chem. Commun.*, **2014**, *50*, 3841-3844.



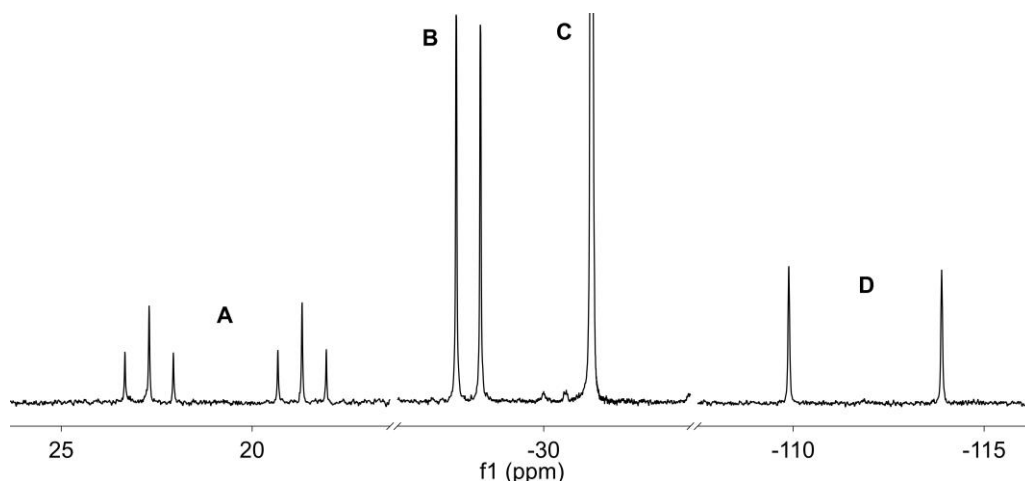
## Chapter 5. Isolation of an unusual Ge(I) cluster

### 5.1 Introduction

In the previous chapter, the synthesis and structures of an array of diphosphatetrylenes featuring bulky phosphide ligands were described. This chapter details the attempted synthesis of the diphosphatetrylenes  $\{(\text{Mes})_2\text{P}\}_2\text{E}$  [ $\text{E} = \text{Ge}$  (**160Ge**) and  $\text{Sn}$  (**160Sn**)], featuring the less bulky  $(\text{Mes})_2\text{P}$  phosphide ligand and the isolation of unexpected decomposition products.

### 5.2 Attempted synthesis of $\{(\text{Mes})_2\text{P}\}_2\text{Ge}$ (**160Ge**)

The reaction between two equivalents of *in-situ* generated  $[(\text{Mes})_2\text{P}]\text{K}$  and  $\text{GeCl}_2(1,4\text{-dioxane})$  in cold THF initially gave a dark blue solution, from which no material suitable for characterisation could be obtained. The  $^{31}\text{P}\{^1\text{H}\}$  NMR spectrum of this mixture exhibits a broad signal at  $-18.0$  ppm (FWHM ca. 130 Hz), which we attribute to the putative diphosphagermylene  $\{(\text{Mes})_2\text{P}\}_2\text{Ge}$  (**160Ge**). This solution degrades on standing at room temperature to give, after three days, a dark red solution that appears to contain new two phosphorus-containing species. The  $^{31}\text{P}\{^1\text{H}\}$  NMR spectrum of the resulting dark red solution consists of a doublet of triplets at  $20.7$  ppm (**A**,  $J_{\text{PP}} = 485$  Hz,  $J_{\text{PP}} = 80$  Hz), a doublet at  $-28.0$  ppm (**B**,  $J_{\text{PP}} = 80$  Hz), a singlet at  $-31.3$  ppm (**C**) and a doublet at  $-111.9$  ppm (**D**,  $J_{\text{PP}} = 485$  Hz) in a 1:2:7:1 ratio (Fig. 85). We assigned the identity of the species responsible for peak **C** to the diphosphine  $(\text{Mes})_2\text{P-P}(\text{Mes})_2$  (**161**), based on its chemical shift,<sup>[1]</sup> while peaks **A**, **B** and **D** are consistent with the structure of  $[\{(\text{Mes})_2\text{P}\}\text{Ge}]_4$  (**162**) (see below).

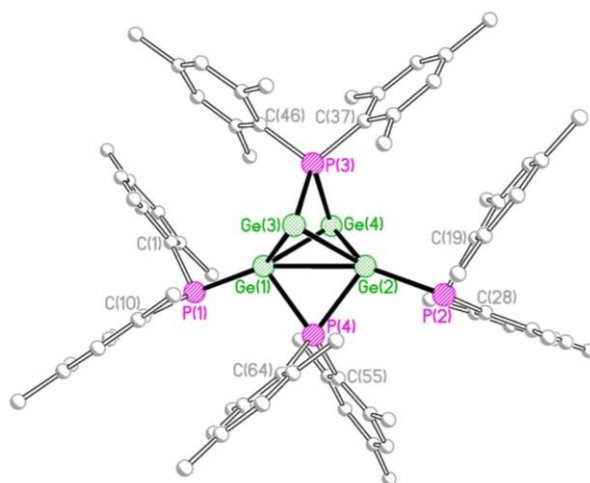


**Figure 85:**  $^{31}\text{P}\{^1\text{H}\}$  NMR spectrum of reaction mixture between two equivalents of  $[(\text{Mes})_2\text{P}]\text{K}$  and  $\text{GeCl}_2(1,4\text{-dioxane})$  after 3 days

Storage of the dark red reaction mixture in cold methylcyclohexane deposited a large amount of colourless crystalline material and a very small amount of single red crystals, which X-ray crystallography revealed to be the diphosphine (Mes)<sub>2</sub>P-P(Mes)<sub>2</sub> (**161**)<sup>[2]</sup> and [{(Mes)<sub>2</sub>P}Ge]<sub>4</sub>·(C<sub>7</sub>H<sub>14</sub>)<sub>5</sub> (**162**·(C<sub>7</sub>H<sub>14</sub>)), respectively. Unfortunately, we have not been able to isolate clean bulk material of **162**·(C<sub>7</sub>H<sub>14</sub>) for further analysis.

### 5.3 Solid-state structure of [{(Mes)<sub>2</sub>P}Ge]<sub>4</sub>(C<sub>7</sub>H<sub>14</sub>)<sub>5</sub> (**162**·(C<sub>7</sub>H<sub>14</sub>))

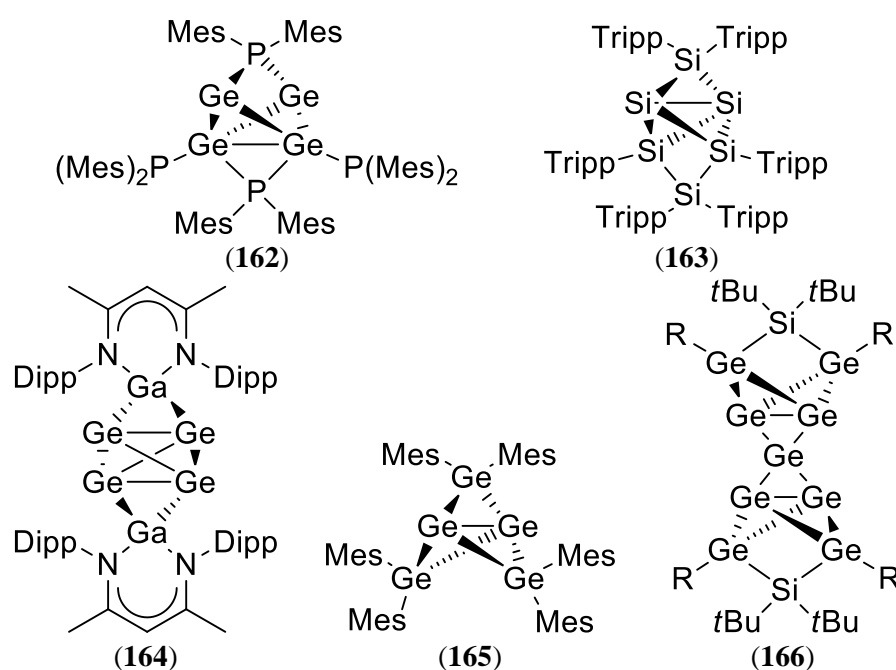
Compound **162**·(C<sub>7</sub>H<sub>14</sub>) crystallises as a tetranuclear cluster **162**, along with five molecules of methylcyclohexane, which were highly disordered but which were successfully modelled crystallographically (Fig. 86). The four germanium centres are formally in the +1 oxidation state and adopt a butterfly configuration that has a short Ge(1)-Ge(2) distance [2.9215(15) Å] that is significantly shorter than the sum of van der Waals radii of two Ge atoms (4.22 Å), suggesting a significant Ge-Ge interaction.<sup>[3]</sup> In contrast, the Ge(3)-Ge(4) distance of 3.510(5) Å is significantly longer and suggests at best a very weak interaction between these atoms. Two phosphide ligands separately bridge the pairs Ge(1)-Ge(2) and Ge(3)-Ge(4), while Ge(1) and Ge(2) are each further coordinated by a terminal phosphide ligand.



**Figure 86:** Molecular structure of **162**·(C<sub>7</sub>H<sub>14</sub>) with the molecules of solvation and hydrogen atoms omitted for clarity. Selected bond lengths (Å) and angles (°): Ge(1)-P(1) 2.3518(7), Ge(1)-P(4) 2.4057(7), Ge(2)-P(2) 2.3595(8), Ge(2)-P(4) 2.3957(7), Ge(3)-P(3) 2.4661(8), Ge(4)-P(3) 2.4837(8), Ge(1)-Ge(2) 2.9215(15), Ge(1)-Ge(3) 2.5745(4), Ge(1)-Ge(4) 2.5635(4), Ge(2)-Ge(3) 2.5784(4), Ge(2)-Ge(4) 2.5617(4), Ge(3)-P(3)-Ge(4) 92.68(3), Ge(1)-P(4)-Ge(2) 74.96(2), Ge(3)-Ge(1)-Ge(4) 88.367(13), Ge(3)-Ge(2)-Ge(4) 88.322(14).

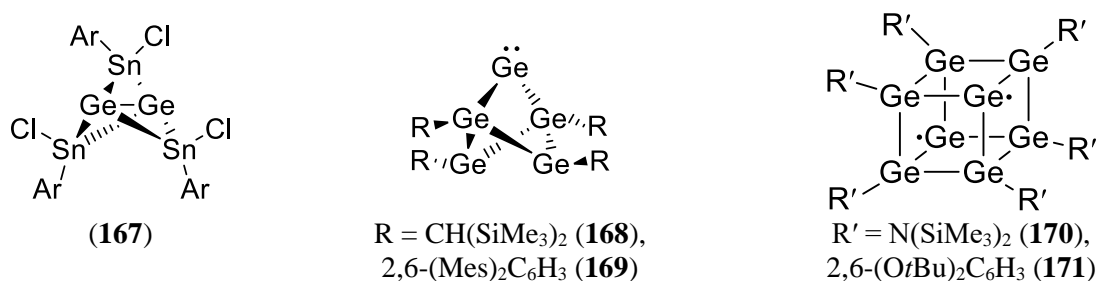
The overall structure of **162** is remarkably similar to that of the silicon cluster Si<sub>6</sub>Tripp<sub>6</sub> (**163**) reported by Scheschkewitz,<sup>[4]</sup> while the gallylene stabilised cluster **164** reported by Fischer and Frenking has a similar arrangement of its Ge<sub>4</sub> core to **162**, although all four bridgehead germanium centres are unsubstituted (Fig. 87).<sup>[5]</sup> It is notable that the

germanium and silicon centres in **162**, **163** and **164** are all in unusual low oxidation states. However, the location of the Ge-Ge bridge in **162** contrasts with those in compounds **163**, **164** and with metalla[1.1.1]propellanes ( $M_3R_6$ ,  $M = \text{Si, Ge, Sn}$ ), in which the M-M bridges occur between two unsubstituted bridgehead atoms (Fig. 87). Despite the increased substitution at the bridging germanium centres in **162**, the Ge-Ge bridging distance [2.9215(15) Å] is comparable to the Ge-Ge bridging distances in **164** [2.9517(7) Å] and the pentagerma[1.1.1]propellanes **165**<sup>[6]</sup> and **166**<sup>[7]</sup> [2.869(2) and 2.8292(5) Å, respectively] (Fig. 87).



**Figure 87:** Structurally similar compounds to **162**·( $C_7H_{14}$ )

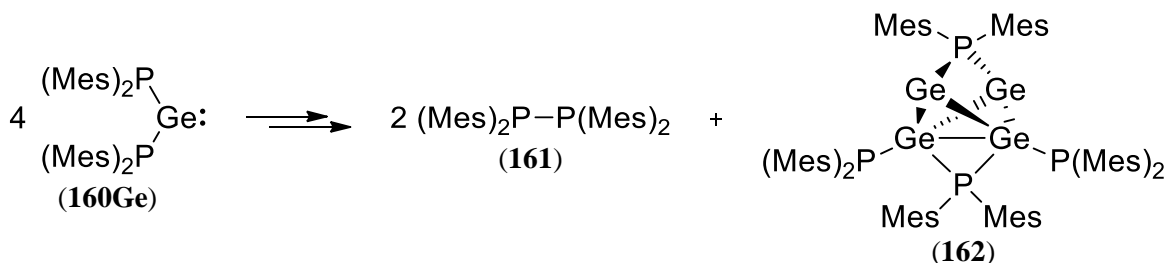
The distance between the two unsubstituted bridgehead germanium centres in **162** [Ge(3)-Ge(4) 3.510(5) Å] is significantly greater than the Ge-Ge bridging distances discussed above. It has been proposed that the diradical character of metalla[1.1.1]propellanes and related species correlates with the distance between the unsubstituted bridgehead atoms, with greater distances being associated with greater biradicaloid behaviour.<sup>[8]</sup> For comparison, compounds **167**<sup>[8a]</sup>, **168** and **169**<sup>[9]</sup> are suspected of having singlet diradical character, with Ge-Ge distances that are greater than typical germa[1.1.1]propellanes [3.363(1), 3.3292(10) and 3.541(3) Å, respectively] (Fig. 88). The singlet diradical germanium clusters **170** and **171** have a separation of the unsubstituted bridgehead germanium atoms that is significantly greater than the sum of their van der Waals radii [5.175(1) and 4.4830(11) Å, respectively] (Fig. 88). Given the foregoing, we suggest that **162** has significant diradical character located on Ge(3) and Ge(4). While there is the possibility for the triplet diradical state of **162**, this is unlikely given that we observe sharp signals in its  $^{31}\text{P}\{^1\text{H}\}$  NMR spectrum.



**Figure 88:** Compounds with biradical character

#### 5.4 Proposed formation of $[(\text{Mes})_2\text{P}\text{Ge}]_4$ (**162**)

A preliminary NMR study to monitor the reaction between two equivalents of  $[(\text{Mes})_2\text{P}]\text{K}$  and  $\text{GeCl}_2(1,4\text{-dioxane})$  in THF reveals that the initial signal at  $-18.0$  ppm in the  $^{31}\text{P}\{^1\text{H}\}$  NMR spectrum cleanly converts to the signals corresponding to **161** and **162** in an approximate 2:1 ratio over approximately 48 hours. Given the foregoing, we propose that **160Ge** decomposes through an unknown mechanism to the fragments  $(\text{Mes})_2\text{P}\cdot$  and  $\{(\text{Mes})_2\text{P}\}\text{Ge}\cdot$ , which combine to give **161** and **162**, respectively, with the stoichiometry shown in Scheme 28. The decomposition of **160Ge** contrasts with that of the diphosphastannylenes  $\{(\text{Ar})_2\text{P}\}_2\text{Sn}$  [ $\text{Ar} = \text{Dipp}$  (**104Sn**),  $\text{Tripp}$  (**145Sn**)] and  $[(\text{Me}_3\text{Si})_2\text{CH}\text{P}]_2\text{Sn}$  (**148Sn**), which decompose to give metallic tin and either the corresponding diphosphine or phosphanyl radical, respectively, and that of  $\{(\text{Dipp})_2\text{P}\}_2\text{Ge}$  (**104Ge**), which is stable for long periods, both in solution and the solid state. The reactivity of **160Ge** also contrasts that of tetrylene featuring relatively small phosphide substituents, which typically dimerize to give phosphorus-bridged dimers (see Section 1.8.8). However, it is worth noting that the *P*-heterocyclic tetrylenes  $\{\text{CH}_2\text{P}(\text{Ph})\}_2\text{E}$  [ $\text{E} = \text{Ge}$  (**172Ge**),  $\text{Sn}$  (**172Sn**)] are not stable at room temperature, although the decomposition products are not reported.<sup>[10]</sup>



**Scheme 28:** Proposed stoichiometry for the formation of **162**·( $\text{C}_7\text{H}_{14}$ )

The broadness of the initial signal at  $-18.0$  ppm in the  $^{31}\text{P}\{^1\text{H}\}$  NMR spectrum, which we tentatively assign to **160Ge**, suggests the operation of a dynamic process. A dynamic equilibrium between the pyramidal and planar configurations of **160Ge**, similar to that we observe for the diphosphagermylenes **104Ge** and **145Ge**, is unlikely given the low steric bulk

of the phosphide ligands, which we expect to result in a higher energy barrier to inversion of the phosphorus centres. Since the direct silylene analogue  $\{(\text{Mes})_2\text{P}\}_2\text{Si}$  (**173**) readily dimerizes to the disilene  $\{(\text{Mes})_2\text{P}\}_2\text{Si}=\text{Si}\{\text{P}(\text{Mes})_2\}_2$  (**181**) (see Chapter 6), we anticipate that **160Ge** is in a dynamic equilibrium with a dimeric species, either of the form  $\{(\text{Mes})_2\text{P}\}_2\text{Ge}=\text{Ge}\{\text{P}(\text{Mes})_2\}_2$  or the phosphorus-bridged dimer  $[\{(\text{Mes})_2\text{P}\}\text{Ge}\{\mu\text{-P}(\text{Mes})_2\}]_2$ .

### 5.5 Attempted synthesis of $\{(\text{Mes})_2\text{P}\}_2\text{Sn}$ (**160Sn**)

A similar reaction between two equivalents of *in-situ* prepared  $[(\text{Mes})_2\text{P}]\text{Li}$  and  $\text{SnCl}_2$  in cold THF gives a yellow solution. Removal of the solvent under vacuum and extraction of the resulting sticky yellow solid into toluene gives a dark red solution with pale solids, which were removed by filtration. The  $^{31}\text{P}\{^1\text{H}\}$  NMR spectrum of the dark red filtrate exhibits a singlet at -53.4 ppm with well resolved tin satellites ( $J_{\text{Sn}} = 820$  Hz). The chemical shift and  $^{31}\text{P}$ - $^{117/119}\text{Sn}$  coupling constant of this species is very similar to that we observe in the  $^{31}\text{P}\{^1\text{H}\}$  MAS NMR spectrum of  $\{(\text{Tripp})_2\text{P}\}_2\text{Sn}$  (**145Sn**) (-48.8 and -58.7 ppm,  $J_{\text{PSn}} = 900$  and 850 Hz, respectively), suggesting **160Sn** has a pyramidal configuration in solution. Unfortunately, we have been unable to isolate **160Sn** in a form suitable for characterisation nor monitored its stability in solution.

### 5.6 Conclusions and future work

From the reaction between  $\text{GeCl}_2(1,4\text{-dioxane})$  and two equivalents  $[(\text{Mes})_2\text{P}]\text{K}$  we isolated crystalline material of the diphosphine **161** and the Ge(I) cluster **162**. The NMR data suggests these species are formed by the decomposition of the putative diphosphagermylene **160Ge**, although there is insufficient data to determine the configuration and aggregation state of **160Ge** in solution. The apparent instability of **160Ge** contrasts that of the diphosphagermylenes **104Ge** and **145Ge** and the tetraphosphadisilene **181** that are stable in solution and in the solid state. Compound **162** has a unique configuration of its Ge(I) centres that suggests it may have biradicaloid character and so may exhibit reactivity with small molecules.

Similarly, the reaction between  $\text{SnCl}_2$  and two equivalents of  $[(\text{Mes})_2\text{P}]\text{Li}$  cleanly gives the putative diphosphastannylene **160Sn**. The  $^{31}\text{P}\{^1\text{H}\}$  NMR data of which suggest it has a pyramidal configuration at both phosphorus centres in solution.

Further work is required to characterise **160Ge** and **160Sn** by X-ray crystallography, which may be achieved by recrystallization from a wider range of solvents. In addition, the

decomposition of **160Ge** and stability of **160Sn** requires a detailed investigation by NMR spectroscopy and DFT studies. The nature of the bonding in **162** may be explored by DFT calculations.

## 5.7 Experimental

### 5.7.1 Attempted synthesis of $\{(\text{Mes})_2\text{P}\}_2\text{Ge}$ (**160Ge**)

To a cold (-78 °C) solution of  $\text{GeCl}_2$ (dioxane) (0.36 g, 1.55 mmol) in THF (30 ml) was added, dropwise, a solution of  $[(\text{Mes})_2\text{P}]\text{K}$  (0.97 g, 3.15 mmol) in THF (30 ml). The resulting dark blue solution was allowed to warm to room temperature. The  $^{31}\text{P}\{^1\text{H}\}$  NMR spectrum of the resulting dark blue reaction mixture exhibits a broad signal at -18.0 ppm. The solvent was removed *in vacuo* and the product was extracted into  $\text{Et}_2\text{O}$  (30 ml). The resulting pale solids were removed by filtration and the solvent was removed *in vacuo*. The resulting blue foam was dissolved into THF (30ml) and stood for 3 days at room temperature in the absence of light. The  $^{31}\text{P}\{^1\text{H}\}$  NMR spectrum of the resulting dark red solution exhibits a doublet of triplets at 20.7 ppm ( $J_{\text{PP}} = 485$  Hz,  $J_{\text{PP}} = 80$  Hz), a doublet at -28.0 ppm ( $J_{\text{PP}} = 80$  Hz), a singlet at -31.3 ppm and a doublet at -111.9 ppm ( $J_{\text{PP}} = 485$  Hz) in a 1:2:7:1 ratio. The solvent was removed *in vacuo* and the sticky red solvent was dissolved in methylcyclohexane (10 ml). Storage of this mixture at -25 °C overnight deposited a large quantity of colour crystal and a small amount of red crystals, which X-ray crystallography revealed to be **161** and **162**.

### 5.7.2 Attempted synthesis of $\{(\text{Mes})_2\text{P}\}_2\text{Sn}$ (**160Sn**)

A solution of *n*BuLi in hexanes (2.45 M, 1.2 ml, 1.74 mmol) was added to a solution of  $(\text{Mes})_2\text{PH}$  (**108**) in THF (15 ml). The resulting red solution was stirred for 30 min and added, dropwise, to a cold (-78 °C) solution of  $\text{SnCl}_2$  (0.278 g, 1.46 mmol) in THF (15 ml). The resulting pale red solution was allowed to warm to room temperature and the solvent was removed *in vacuo*. The addition of toluene (15 ml) to the resulting sticky red solution gave a dark red solution with pale solids, which were removed by filtration. No material suitable for characterisation could be obtained from the dark red filtrate by recrystallization from a range of solvents. The  $^{31}\text{P}\{^1\text{H}\}$  NMR spectrum of the crude reaction mixture in toluene consists of a singlet at -53.4 ppm ( $J_{\text{PSn}} = 820$  Hz).

## 5.8 References

- [1] S. Sasaki, F. Murakami, M. Yoshifuji, *Tetrahedron Lett.*, **1997**, 38, 7095-7098.
- [2] S. G. Baxter, A. H. Cowley, R. E. Davis, P. E. Riley, *J. Am. Chem. Soc.*, **1981**, 103, 1699-1702.
- [3] M. Mantina, A. C. Chamberlin, R. Valero, C. J. Cramer, D. G. Truhlar, *J. Phys. Chem. A*, **2009**, 113, 5806-5812.
- [4] K. Abersfelder, A. J. White, R. J. Berger, H. S. Rzepa, D. Scheschkewitz, *Angew. Chem. Int. Ed. Engl.*, **2011**, 50, 7936-7939.
- [5] A. Doddi, C. Gemel, M. Winter, R. A. Fischer, C. Goedecke, H. S. Rzepa, G. Frenking, *Angew. Chem. Int. Ed. Engl.*, **2013**, 52, 450-454.
- [6] D. Nied, W. Klopper, F. Breher, *Angew. Chem. Int. Ed. Engl.*, **2009**, 48, 1411-1416.
- [7] Y. Ito, V. Y. Lee, H. Gornitzka, C. Goedecke, G. Frenking, A. Sekiguchi, *J. Am. Chem. Soc.*, **2013**, 135, 6770-6773.
- [8] (a) A. F. Richards, M. Brynda, P. P. Power, *Organometallics*, **2004**, 23, 4009-4011;  
(b) F. Breher, *Coord. Chem. Rev.*, **2007**, 251, 1007-1043.
- [9] A. F. Richards, M. Brynda, M. M. Olmstead, P. P. Power, *Organometallics*, **2004**, 23, 2841-2844.
- [10] D. M. Anderson, P. B. Hitchcock, M. F. Lappert, I. Moss, *Inorg. Chim. Acta*, **1988**, 141, 157-159.

## Chapter 6. A fully phosphide-substituted disilene

### 6.1 Introduction

In Chapter 3, we described the synthesis and structures of a range of diphosphagermylenes and –stannylenes, in which the stabilisation mode is determined by the sterics of the substituents and the tetrel centre. We therefore sought to prepare a diphosphasilylene, as the increased orbital overlap between the Si(II) centre and a planar phosphorus should lead to stronger  $p\pi$ - $p\pi$  interactions than its heavier analogues. To the best of our knowledge, the only examples of monomeric, phosphide-substituted Si(II) centres are the donor-stabilised phosphasilylenes **99**<sup>[1]</sup> and **100**.<sup>[2]</sup> The scarcity of phosphide-substituted Si(II) centres and absence of two-coordinate phosphasilylenes may be attributed to the increased difficulty of synthesising silylenes. In contrast to the typical synthesis of silylenes by the reduction or dehydrochlorination of Si(IV) precursors (see Section 1.6.2), compounds **99** and **100** were prepared by a metathesis reaction between the respective donor-stabilised Si(II) chloride and lithium phosphide.

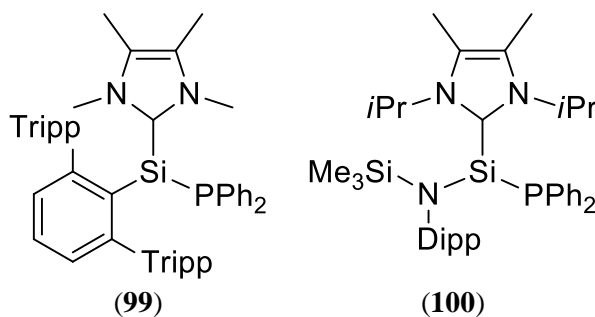


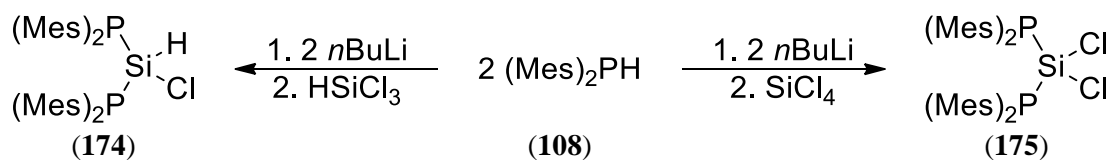
Figure 89: Phosphasilylenes

In addition, the synthesis of silylenes is further complicated by the expansion of the silicon radius going from Si(IV) to Si(II). This limits the steric encumbrance that can be installed from the substituents in a Si(IV) precursor and so limits kinetic stabilisation of the corresponding silylene. Therefore, we chose the moderately bulky (Mes)<sub>2</sub>P phosphide as a ligand to initially explore strategies for synthesising of the corresponding diphosphasilylene {(Mes)<sub>2</sub>P}<sub>2</sub>Si (**173**).

### 6.2 Synthesis of Si(IV) precursors {(Mes)<sub>2</sub>P}<sub>2</sub>SiHCl (**174**) and {(Mes)<sub>2</sub>P}<sub>2</sub>SiCl<sub>2</sub> (**175**)

The reaction between two equivalents of [(Mes)<sub>2</sub>P]Li and either HSiCl<sub>3</sub> or SiCl<sub>4</sub> gave the Si(IV) precursors {(Mes)<sub>2</sub>P}<sub>2</sub>SiHCl (**174**) and {(Mes)<sub>2</sub>P}<sub>2</sub>SiCl<sub>2</sub> (**175**), respectively, in good purity and yield as colourless solids (Scheme 29).

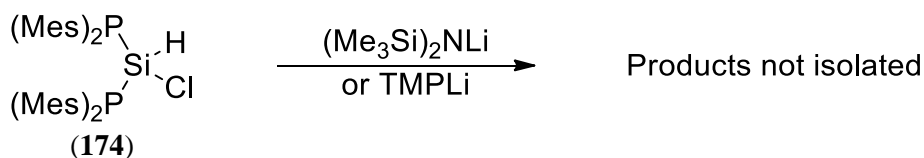




Scheme 29: Synthesis of compounds **174** and **175**

### 6.3 Attempted dehydrochlorination of $\{(\text{Mes})_2\text{P}\}_2\text{SiHCl}$ (**174**)

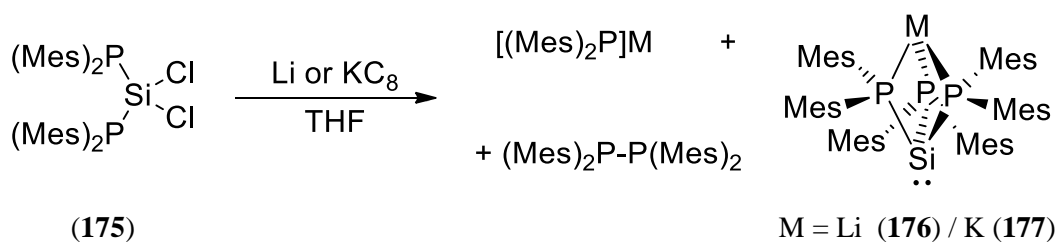
The attempted dehydrochlorination of **174** with  $(\text{Me}_3\text{Si})_2\text{NLi}$  or  $\text{TMPLi}$  gave highly coloured solutions that contained a complex mixture of species according to  $^{31}\text{P}\{^1\text{H}\}$  NMR spectra of the crude solutions (Scheme 30), which we were unable to identify (TMP = 2,2,6,6-tetramethylpiperidiny). On the basis of the complex mixture of products obtained from this reaction we propose that the resulting amine side-products are reacting with the initially generated Si(II) species.



Scheme 30: Reactivity of **174** with lithium amides (TMP = 2,2,6,6-tetramethylpiperidiny)

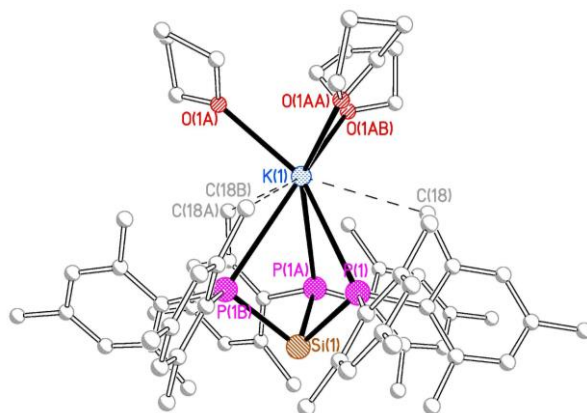
### 6.4 Attempted reduction of $\{(\text{Mes})_2\text{P}\}_2\text{SiCl}_2$ (**175**)

The reduction of **175** with lithium shot or potassium graphite in THF gave a mixture of the corresponding alkali metal phosphides as the major product, a small amount of the diphosphine **150** and the triphosphasilanate complexes  $[\{(\text{Mes})_2\text{P}\}_3\text{Si}]\text{M}$  [ $\text{M} = \text{Li}$  (**176**),  $\text{K}$  (**177**)] (Scheme 31). Compound **176** was identified in solution by its distinctive equal intensity quartet in the  $^{31}\text{P}\{^1\text{H}\}$  NMR spectrum in non-donor solvents and was later prepared cleanly by an alternative route (see below). In a single instance, we were able to obtain a small number of orange crystals that were shown to be  $[\{(\text{Mes})_2\text{P}\}_3\text{Si}]\text{K}(\text{THF})_3$  (**177**·THF) by X-ray crystallography.



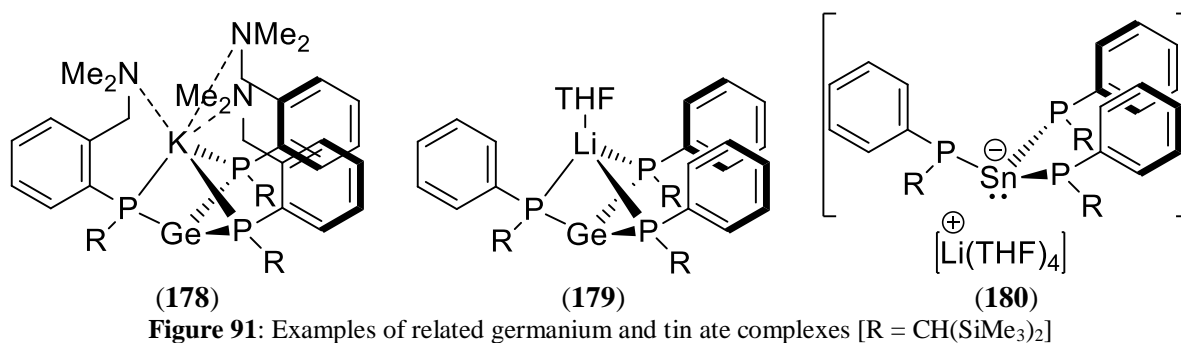
Scheme 31: Reactivity of **175** with Li or  $\text{KC}_8$

The structure of **177**·THF is shown in Figure 90, along with selected bond lengths and angles. Compound **177**·THF crystallises with three-fold rotational symmetry about the three-coordinate, trigonal pyramidal Si(II) centre that is bonded to three phosphide ligands. The potassium ion is coordinated to these phosphide ligands and three THF molecules. In addition, there are three short K···Me contacts [K(1)···C(18) 3.363(3) Å].



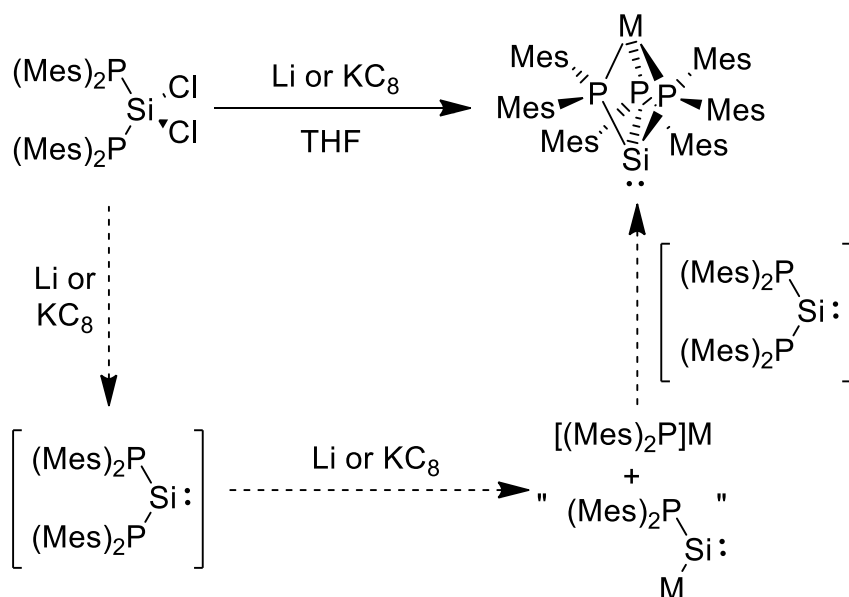
**Figure 90:** Molecular structure of **177**·THF with H atoms and minor disorder components omitted for clarity. Selected bond lengths (Å) and angles (°): K(1)-P(1) 3.4494(8), K(1)-O(1A) 2.780(14), K(1)···C(18) 3.362(3), Si(1)-P(1) 2.3972(8), C(1)-P(1) 1.870(2), C(10)-P(1) 1.866(2), P(1)-K(1)-P(1A) 58.01(2), P(1)-Si(1)-P(1A) 88.49(3), Si(1)-P(1)-K(1) 92.28(3).

The P-K distances in **177**·THF [3.4494(8) Å] are significantly shorter than the corresponding P-K distances in the similar germanium complex  $[\{(\text{Me}_3\text{Si})_2\text{CH}\}\text{P}(\text{C}_6\text{H}_4\text{-2-CH}_2\text{-NMe}_2)\}_3\text{GeK}$  (**178**), in which the potassium ion is intra-molecularly solvated by three benzylamine groups.<sup>[3]</sup> In the solid-state, the related germanium complex  $[\{(\text{Me}_3\text{Si})_2\text{CH}\}(\text{Ph})\text{P}\}_3\text{GeLi}(\text{THF})$  (**179**) has an analogous structure to **177**·THF, while the tin complex  $[\{(\text{Me}_3\text{Si})_2\text{CH}\}(\text{Ph})\text{P}\}_3\text{Sn}\cdot\text{Li}(\text{THF})_4$  (**180**) is a separated ion pair. Compounds **179** and **180** both exhibit NMR spectra in  $d_8$ -toluene consistent with the cage-like structure observed in the crystal structure of **179**.<sup>[4]</sup>



The formation of **176** and **177**·THF demonstrates that the Si(IV) centre in **175** is being reduced to Si(II) by either lithium or potassium graphite. However, the corresponding alkali metal phosphides are the major product in these reactions and compounds **176** and **177**(THF)<sub>3</sub>

are complexes between **173** and these phosphides. This suggests the reduction of **175** initially forms the silylene **173** but this species is further reduced to give  $[(\text{Mes})_2\text{P}]\text{M}$  and an unidentified silicon-containing species (Scheme 32). Magnesium was trialled as a milder reducing agent, in an attempt to prevent this over-reduction, but was found not to react with **175**.



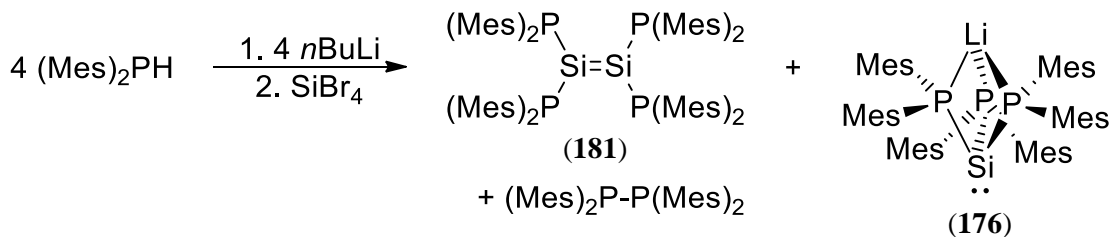
**Scheme 32:** Reactivity of **175** with  $\text{Li}$  or  $\text{KC}_8$  to form complexes **176** and **177**

## 6.5 Synthesis of $\{(\text{Mes})_2\text{P}\}_2\text{Si}=\text{Si}\{\text{P}(\text{Mes})_2\}_2$ (**181**)

As the use of lithium and potassium graphite as reducing agents resulted in the over-reduction of **175**, we sought to prepare  $\{(\text{Mes})_2\text{P}\}_2\text{SiBr}_2$  since this should require less aggressive reducing agents, such as magnesium, to cleave the  $\text{P-Br}$  bonds. Unexpectedly, the reaction between  $\text{SiBr}_4$  and two equivalents of  $[(\text{Mes})_2\text{P}]\text{Li}$  in  $\text{Et}_2\text{O}$  gave a deep blue solution, which slowly decolourised and deposited a small number of dark purple crystals that were shown to be  $\{(\text{Mes})_2\text{P}\}_2\text{Si}=\text{Si}\{\text{P}(\text{Mes})_2\}_2$  (**181**) by X-ray crystallography.

The isolation of **181** demonstrates that  $[(\text{Mes})_2\text{P}]\text{Li}$  is acting as a reducing agent in this system.<sup>[5]</sup> Therefore, the stoichiometry of the reaction was adjusted to account for  $[(\text{Mes})_2\text{P}]\text{Li}$  acting as both a ligand transfer reagent and a sacrificial reducing agent. The reaction between  $\text{SiBr}_4$  and four equivalents of  $[(\text{Mes})_2\text{P}]\text{Li}$  in  $\text{Et}_2\text{O}$  once again gave a blue solution (Scheme 33). Removal of the solvent from this solution and extraction of the resulting residue into *n*-hexane caused the precipitation of the  $\text{LiBr}$  by-product, which was separated by filtration. The resulting brown filtrate exhibited four major signals in its  $^{31}\text{P}\{^1\text{H}\}$  NMR spectrum: a singlet at -31.4 ppm that is due to  $(\text{Mes})_2\text{P-P}(\text{Mes})_2$ , a broad singlet at -41.3 ppm that we tentatively assign to the silylene **173**, a 1:1:1:1 quartet at -62.5

corresponding to **176** and a singlet at -90.8 ppm from an unknown species (approximate ratio of peaks 1.0:2.2:1.3:1.0). Upon standing at room temperature for several days the brown solution deposited large deep purple crystals of **181** in moderate yield. This deposition is accelerated by heating the solution under reflux where it is complete after 4 hours.



**Scheme 33:** Synthesis of complexes **176** and **181** from  $\text{SiBr}_4$

The structure of **181** is somewhat unexpected as previous diphosphatetrylenes dimers are formed through the phosphorus centres to give  $\text{E}_2\text{P}_2$  cores (Section 1.8.8). In addition, there are few examples of ditetrelenes ( $\text{R}_2\text{E}=\text{ER}_2$ ) substituted by heteroatoms from groups 15–17, since such heteroatoms usually favour the formation of the corresponding monomeric tetrylenes ( $\text{ER}_2$ ). These ditetrelenes feature a maximum of two such heteroatom substituents, which are installed in the ditetrelene by a variety of methods. For example, the phosphide- or iodide-substituted disilenes **182** and **183** were prepared by the treatment of  $(\text{Tripp})_2\text{Si}=\text{Si}(\text{Tripp})(\text{Li})$  with  $\text{R}_2\text{PCl}$  or iodine, respectively [ $\text{R} = \text{Ph}, i\text{Pr}, \text{Cy}, t\text{Bu}, \text{NR}'_2$  ( $\text{R}' = \text{Me}, \text{Et}, i\text{Pr}$ )],<sup>[6]</sup> while the 1,2-addition of amines to disilynes gave the disilenes **184** (Fig. 92).<sup>[7]</sup> Compound **185** was first prepared by the reaction between  $[\text{Cp}^*\text{Si}][\text{B}(\text{C}_6\text{F}_5)_4]$  and  $[(\text{Me}_3\text{Si})_2\text{N}]\text{Li}$ <sup>[8]</sup> and later from the reaction of  $\text{Cp}^*\text{SiCl}_2\text{H}$  and  $[(\text{Me}_3\text{Si})_2\text{N}]\text{K}$ ,<sup>[9]</sup> presumably through the transient silylene  $\text{Cp}^*\{(\text{Me}_3\text{Si})_2\text{N}\}\text{Si}$  (Fig. 92). The cyclic diaminosilylene  $(\text{CH}_2\text{N}t\text{Bu})_2\text{Si}$  aggregates to the unusual amino-substituted **186** on standing at room temperature (Fig. 92), rather than the corresponding tetraaminodisilene;<sup>[10]</sup> in solution there is a dynamic equilibrium between the silylene and **186** (closely related digermenes has also been reported).<sup>[11]</sup> A dynamic equilibrium was also proposed for the dibromodisilene **187** and its bromosilylene analogue (Fig. 92).<sup>[12]</sup> A similar dynamic equilibrium has been proposed between  $(i\text{Pr}_2\text{N})_2\text{Si}$  and its disilene dimer, based on variable temperature UV/VIS spectroscopy; although this dimer has not been isolated and is a minor component.<sup>[13]</sup>

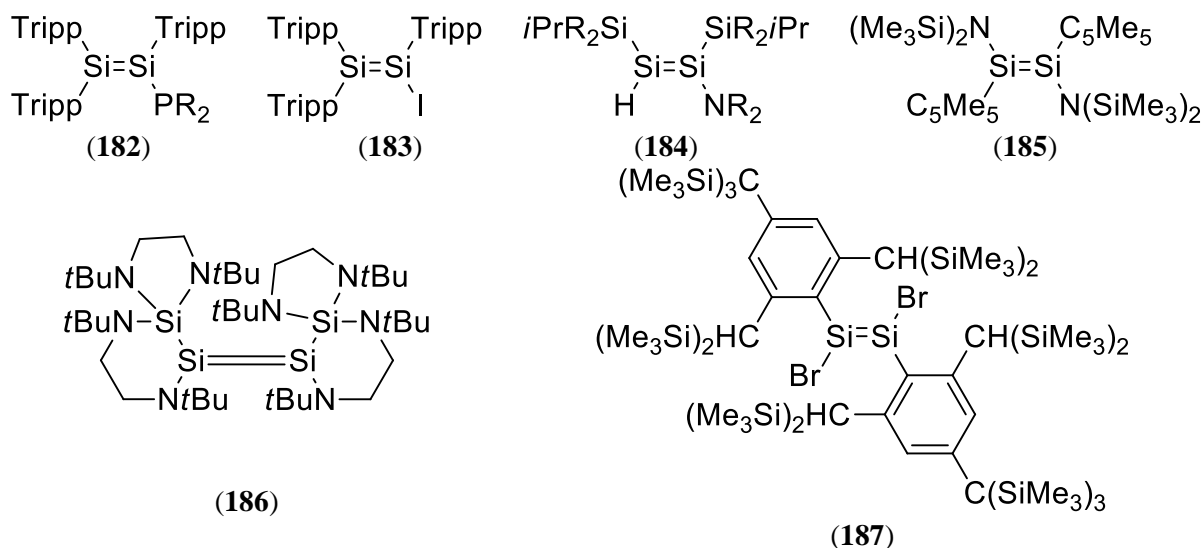
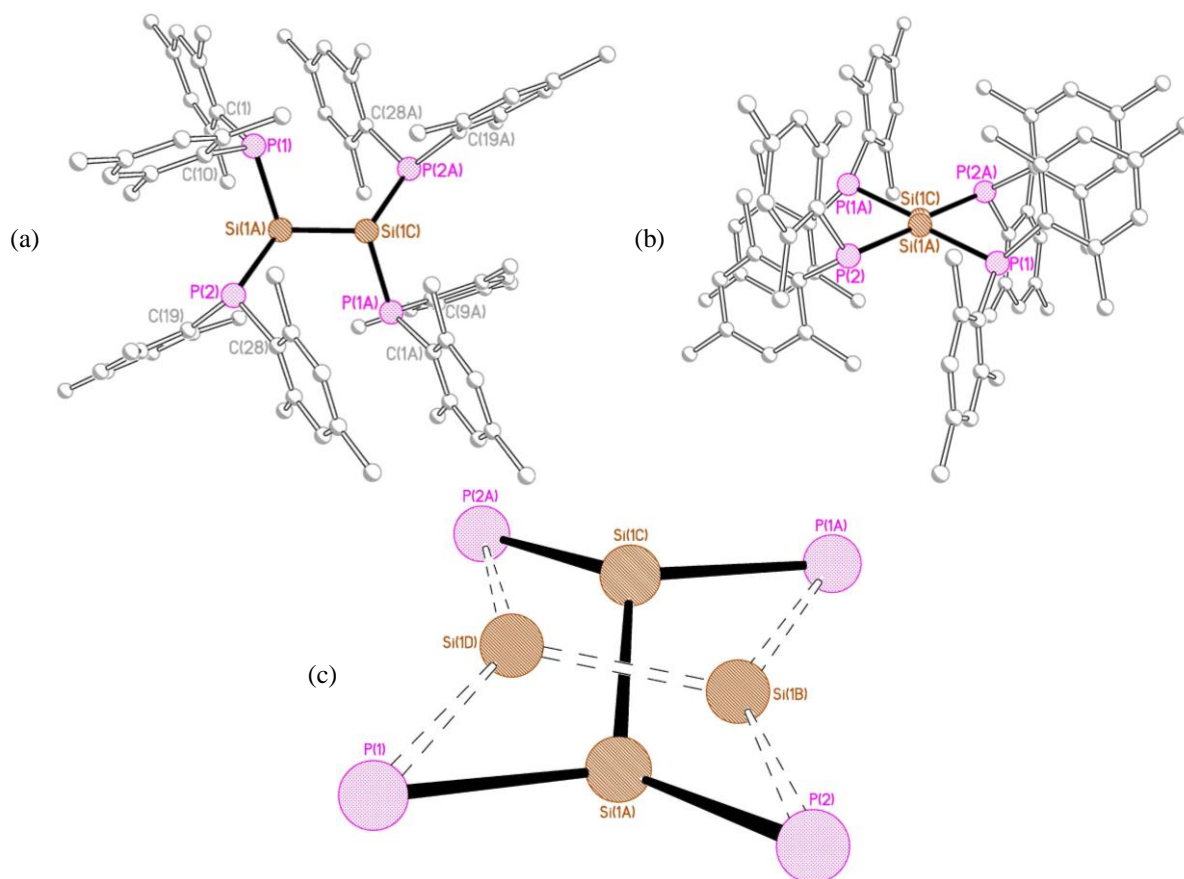


Figure 92: Disilenes substituted by group 14-17 atoms

## 6.6 Solid-state structure of $\{(\text{Mes})_2\text{P}\}_2\text{Si}=\text{Si}\{\text{P}(\text{Mes})_2\}_2$ (**181**)

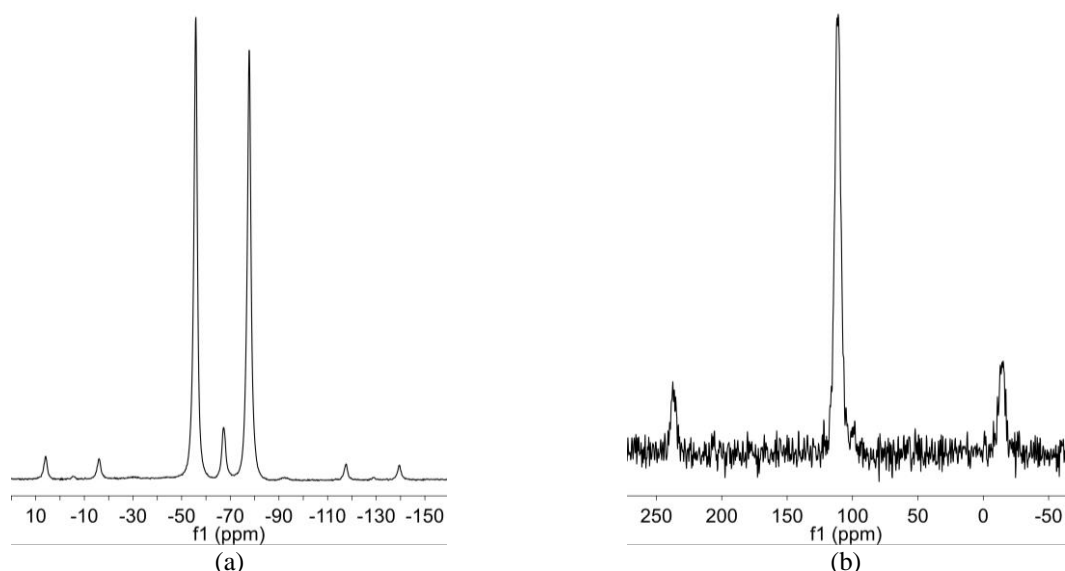
The structure of **181** is shown in Figure 93, along with selected bond lengths and angles. Compound **181** crystallises as a discrete molecular species in which the silicon atoms are disordered over two positions with 92:8 occupancy, with crystallographic inversion symmetry at the centre of the Si-Si bonds (Fig. 93c). The Si-Si distances in the two components are essentially identical [Si(1A)-Si(1C) 2.1901(12) and Si(1B)-Si(1D) 2.190(11) Å]. The major disorder component has a strongly *trans*-bent geometry (40.6° deviation of the SiP<sub>2</sub> mean plane from the Si-Si vector), which contrasts with the near-planar geometries adopted by most silicon-substituted disilenes,<sup>[14]</sup> while the minor disorder component has a smaller *trans*-bending angle of 23.8°. Similar large *trans*-bending angles to that of the major component have been observed in heteroatom-substituted disilenes.<sup>[15]</sup> For example, the *trans*-bending angle at the phosphorus-substituted silicon in (Tripp)<sub>2</sub>Si=Si(Tripp){P(NiPr<sub>2</sub>)} is 30.8°,<sup>[6b]</sup> while the *trans*-bending angles in (Bbt)BrSi=SiBr(Bbt) (**187**) are 32.4 and 39.8° (Bbt = 2,6-{(Me<sub>3</sub>Si)CH}<sub>2</sub>-4-{(Me<sub>3</sub>Si)<sub>3</sub>C}C<sub>6</sub>H<sub>2</sub>).<sup>[12]</sup> The phosphorus atoms in **181** have pyramidal geometries [sum of angles at P(1) 325.62°, P(2) 337.94°], and the Si-P distances are 2.2668(8) and 2.2392(8) Å, which are similar to Si-P distances in the small number of known Si(II) phosphides. For example, the Si-P distances in (Tripp)<sub>2</sub>Si=Si(Tripp)(PCy<sub>2</sub>) and {PhC(NtBu)<sub>2</sub>}Si(PiPr<sub>2</sub>) are 2.2367(12)<sup>[16]</sup> and 2.307(8) Å,<sup>[6c]</sup> respectively. In addition, an aromatic ring on each phosphorus centre lies parallel to the corresponding ring in the opposite Si(PR<sub>2</sub>)<sub>2</sub> moiety with an interplane separation of 3.6 Å, consistent with an offset  $\pi$ - $\pi$  interaction.



**Figure 93:** Molecular structure of the major disorder component of **181** viewed a) above and b) along the Si-Si vector (H atoms omitted for clarity). c) The core of **181**, showing the relationship of the two disorder components (minor component shown with dashed lines). Selected bond lengths [Å] and angles [°] for the major disorder component: Si(1A)-Si(1C) 2.1901(12), Si(1A)-P(1) 2.2666(8), Si(1A)-P(2) 2.2392(8), P(1)-C(1) 1.847(2), P(1)-C(10) 1.835(2), P(2)-C(19) 1.835(2), P(2)-C(28) 1.843(2); C(1)-P(1)-Si(1A) 116.34(8), C(10)-P(1)-Si(1A) 103.55(7), C(1)-P(1)-C(10) 105.73(10), C(19)-P(2)-Si(1A) 115.03(5), C(28)-P(2)-Si(1A) 112.76(7), C(28)-P(2)-C(19) 110.15(10), P(1)-Si(1A)-Si(1C) 108.19(4), P(2)-Si(1A)-Si(1C) 121.45(4), P(1)-Si(1A)-P(2) 113.52(3).

## 6.7 CP-MAS NMR spectra of $\{(\text{Mes})_2\text{P}\}_2\text{Si}=\text{Si}\{\text{P}(\text{Mes})_2\}_2$ (**181**)

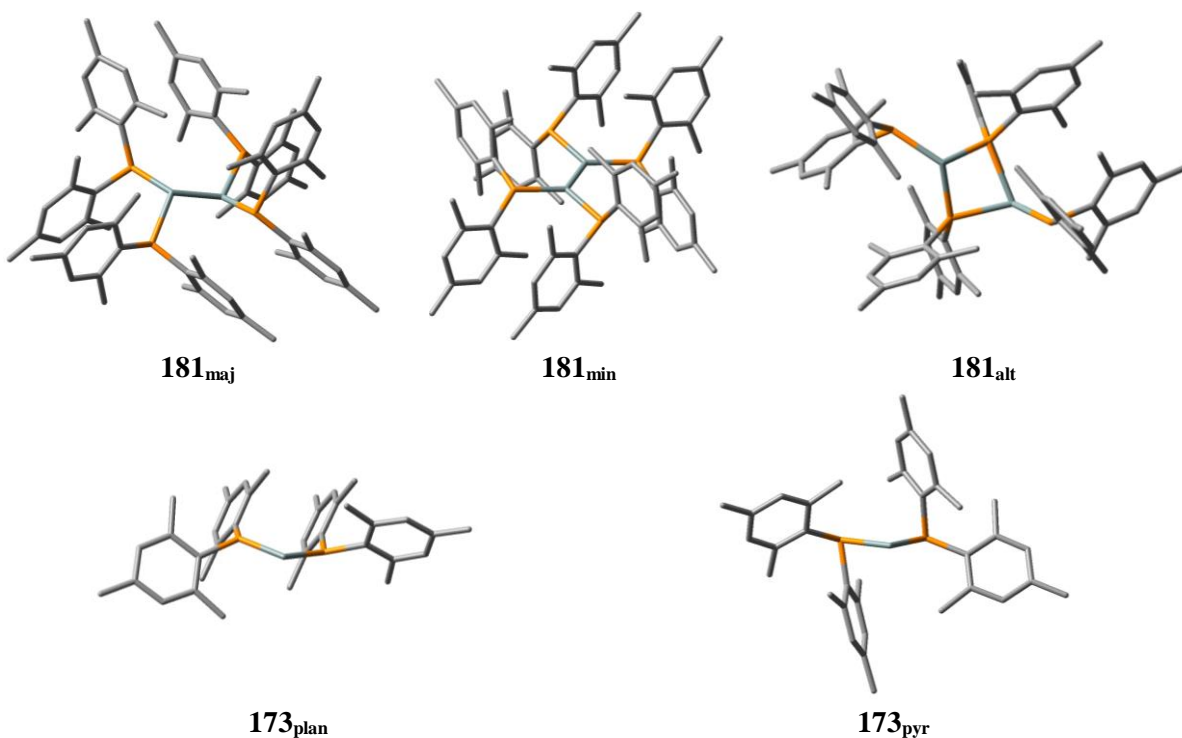
Compound **181** has low solubility in common organic solvents, which prevents characterisation by solution-state NMR spectroscopy. The solid-state cross-polarisation magic angle spinning (CP-MAS)  $^{31}\text{P}\{^1\text{H}\}$  NMR spectrum of **181** consists of a pair of singlets at -55.9 and -77.9 ppm, consistent with the two distinct phosphorus environments observed by X-ray crystallography, and a minor peak at -67.4 ppm, which we tentatively assign to the minor disorder component (Fig. 94a). However, the CP-MAS  $^{29}\text{Si}\{^1\text{H}\}$  NMR spectrum of **181** consists of a broad singlet at 111.7 ppm (Fig. 94b); no  $^{31}\text{P}$ - $^{29}\text{Si}$  coupling is resolved. The  $^{29}\text{Si}$  chemical shift of **181** is in the typical range for disilenes.<sup>[14]</sup>



**Figure 94:** (a)  $^{31}\text{P}\{^1\text{H}\}$  and (b)  $^{29}\text{Si}\{^1\text{H}\}$ -INEPT solid-state CP-MAS NMR spectra of **181**

## 6.8 DFT calculations

We undertook a DFT study to better understand the bonding in and stability of **181**. The minimum energy geometries **181<sub>maj</sub>** and **181<sub>min</sub>** were located using the crystallographic coordinates of the major and minor disorder components, respectively, in the X-ray crystal structure as the starting points for the optimizations (Table 7). In addition, we located the minimum energy geometry for the alternative phosphide-bridge dimer  $[(\text{Mes})_2\text{PSi}\{\mu\text{-P}(\text{Mes})_2\}]_2$  (**181<sub>alt</sub>**).



**Table 7:** Calculated geometries for **181<sub>maj</sub>**, **181<sub>min</sub>**, **181<sub>alt</sub>**, **173<sub>plan</sub>** and **173<sub>pyr</sub>**

Although the calculated minimum energy geometry **181<sub>maj</sub>** is similar to the crystallographically determined structure, with *trans*-bending angles of 38.42° and 40.04°, which are close to those observed in the solid-state structure, the calculated structure exhibits a twist between the two SiP<sub>2</sub> units (14.75° dihedral angle between the two normals of the SiP<sub>2</sub> planes). The calculated Si-Si bond distance of 2.2386 Å is somewhat longer than that observed in the solid-state, which is likely a result of the twisted geometry reducing the Si-Si  $\pi$ -overlap. The *trans*-bending angle in **181<sub>min</sub>** (6.22°) is significantly smaller than that in the solid-state structure (23.8°), although the calculated Si-Si distance (2.182 Å) is close to that determined crystallographically (2.190(11) Å). The observed <sup>31</sup>P and <sup>29</sup>Si chemical shifts of **181** correlate reasonably well to the calculated <sup>31</sup>P and <sup>29</sup>Si chemical shifts of **181<sub>maj</sub>** and **181<sub>min</sub>** (Table 8).

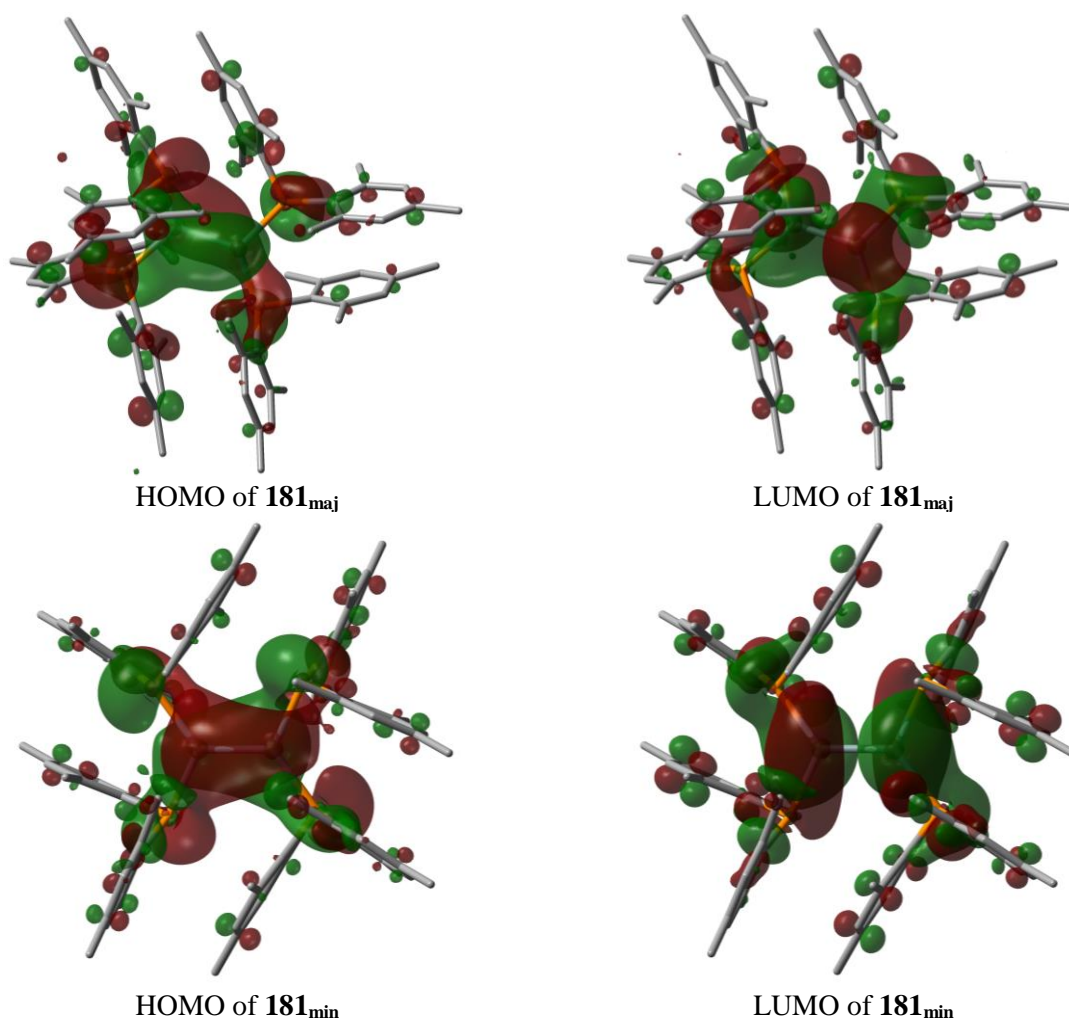
	<b>181<sub>maj</sub></b>	<b>181<sub>min</sub></b>	<b>181</b>
<sup>31</sup> P (ppm)	-28.7, -41.5, -57.2, -61.8	-53.6, -59.1	-55.9, -77.9, -67.4 (minor)
<sup>29</sup> Si (ppm)	168.7, 112.8	103.1	111.7

**Table 8:** Calculated <sup>31</sup>P and <sup>29</sup>Si NMR shifts for **181<sub>maj</sub>** and **181<sub>min</sub>** and observed shifts for **181**

The DFT calculations reveal that **181<sub>maj</sub>** is more stable than **181<sub>min</sub>** by 9.0 kJ mol<sup>-1</sup>, while the alternative geometry **181<sub>alt</sub>**, containing a P<sub>2</sub>Si<sub>2</sub> core, lies 82.7 kJ mol<sup>-1</sup> higher in free energy than the former.

The HOMO and LUMO of **181<sub>maj</sub>** and **181<sub>min</sub>** are essentially the Si=Si  $\pi$  and  $\pi^*$  orbitals, although there is a significant component of these orbitals on the phosphorus atoms (Fig. 95). Natural Bond Orbital (NBO) analysis yields Wiberg Bond Indices (WBIs) for the Si=Si bonds in **181<sub>maj</sub>** and **181<sub>min</sub>** of 1.411 and 1.551, respectively, which is consistent with substantial double bond character. The WBIs for the Si-P bonds in **181<sub>maj</sub>** and **181<sub>min</sub>** range from 0.934 and 1.016, which is significantly greater than we calculate for a straightforward P-Si(II)  $\sigma$ -bond (see below) and suggests there is an interaction between the phosphorus lone pairs and the Si=Si bond.





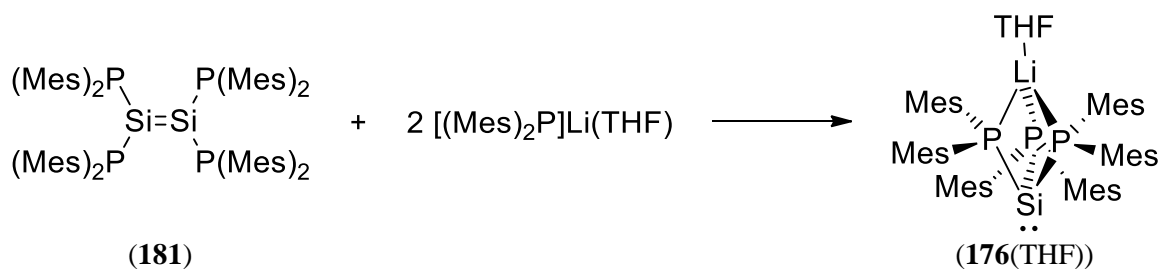
**Figure 95:** HOMO and LUMOs of **181**<sub>maj</sub> and **181**<sub>min</sub>

In order to explore the dimerization energy of the proposed intermediate **173** to the tetraphosphadisilene **181**, we calculated the minimum energy geometries of the two extreme forms of the diphosphasilylene. The minimum energy geometry **173**<sub>plan</sub> has two phosphorus centres that approach planarity while **173**<sub>pyr</sub> has two pyramidal phosphorus centres (Table 7). All attempts to obtain a minimum energy geometry with one planar and pyramidal phosphorus centre, as observed for the diphosphagermylenes and –stannylenes in Chapter 4, converged to **173**<sub>plan</sub>. For **173**<sub>plan</sub> both phosphorus centres are close to planar (sum of angles at P = 352.71 and 352.76°) and the Si-P distances (2.208 and 2.207 Å) are shorter than typical Si-P single bonds. However, these Si-P distances are shorter than previously reported Si=P bonds in phosphasilenes such as (*t*Bu)(Tripp)Si=P-Si(*i*Pr)<sub>3</sub> (Si=P 2.062(1) and Si-P 2.255(1) Å).<sup>[17]</sup> In addition, the Si-P WBIs of 1.221 and 1.222 suggest significant pπ-pπ interactions in **173**<sub>plan</sub>, even though the phosphorus centres deviate slightly from planarity. In contrast, the Si-P distances in **173**<sub>pyr</sub> are both 2.337 Å and the Si-P bonds have WBIs of 0.804, which is consistent with Si-P single bonds.

These calculations show that **173<sub>plan</sub>** is more stable than **173<sub>pyr</sub>** by 16.4 kJ mol<sup>-1</sup> and that the dimerization to **181<sub>maj</sub>** is strongly favoured; the difference in Gibbs free energy between the disilene **181<sub>maj</sub>** and two equivalents of **173<sub>plan</sub>** is +71.0 kJ mol<sup>-1</sup>. These results contrast with recent calculations on the putative tetraamino-substituted ditetrelenes {(Me<sub>3</sub>Si)<sub>2</sub>N}<sub>2</sub>E=E{N(SiMe<sub>3</sub>)<sub>2</sub>}<sub>2</sub> that suggest that dissociation to the corresponding tetrylene monomers {(Me<sub>3</sub>Si)<sub>2</sub>N}<sub>2</sub>E is strongly favoured (E = Ge, ΔG = -69 kJ mol<sup>-1</sup>; E = Sn, ΔG = -75 kJ mol<sup>-1</sup>; E = Pb, ΔG = -45 kJ mol<sup>-1</sup>).<sup>[18]</sup>

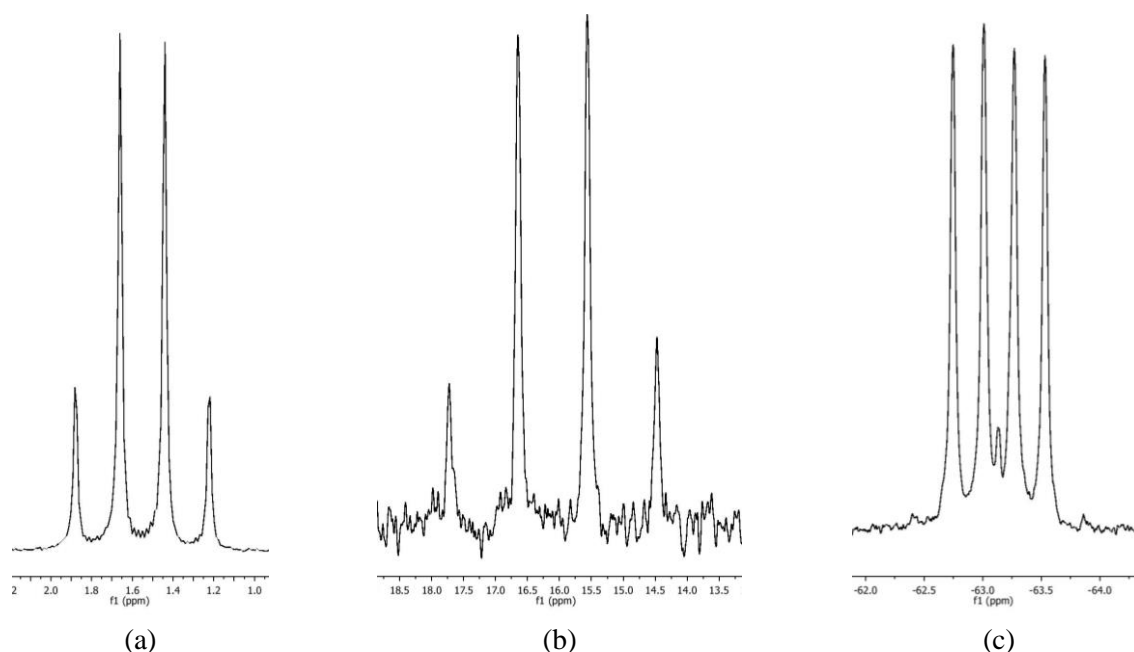
## 6.9 Synthesis of [(Mes)<sub>2</sub>P]<sub>3</sub>SiLi(THF) (**176(THF)**)

Treatment of **181** with either lithium or KC<sub>8</sub> gave the corresponding phosphides [(Mes)<sub>2</sub>P]M (M = Li, K) as the sole products as observed by <sup>31</sup>P NMR spectroscopy. This is consistent with our premise that the formation of the triphosphasilanates **176** and **177** result from the cleavage of a P-C bond in **173** (or **181**), followed by the complexation of the resulting [(Mes)<sub>2</sub>P]M (M = Li, K) with **173**. Consistent with this, the reaction between **181** and two equivalents of [(Mes)<sub>2</sub>P]Li in THF gave **176(THF)** after precipitation from Et<sub>2</sub>O (Scheme 34). Unfortunately, we were unable to isolate crystalline material suitable for characterisation by X-ray crystallography.



Scheme 34: Synthesis of **176(THF)**

Compound **176(THF)** exhibits well-resolved 1:3:3:1 quartets in its <sup>7</sup>Li and <sup>29</sup>Si{<sup>1</sup>H}-INEPT NMR spectra at 1.6 ppm (*J*<sub>PLi</sub> = 42 Hz) and 16.1 ppm (*J*<sub>PSi</sub> = 110 Hz), respectively, and a 1:1:1:1 quartet in its <sup>31</sup>P{<sup>1</sup>H} NMR spectrum at -63.1 ppm (*J*<sub>PLi</sub> = 42 Hz) in C<sub>6</sub>D<sub>6</sub> (Fig. 96). These spectra are consistent with **176(THF)** maintaining a similar core structure to **177(THF)**<sub>3</sub> in solution. Similar <sup>7</sup>Li and <sup>31</sup>P{<sup>1</sup>H} spectra are observed for compounds **179** and **180** in solution.



**Figure 96:** (a)  $^7\text{Li}$ , (b)  $^{29}\text{Si}\{^1\text{H}\}$ -INEPT and (c)  $^{31}\text{P}\{^1\text{H}\}$  NMR spectra of **176**·(THF) in  $\text{C}_6\text{D}_6$

## 6.10 Conclusions

Compounds **174** and **175** were prepared by the reaction between two equivalents of  $[(\text{Mes})_2\text{P}]\text{Li}$  and  $\text{HSiCl}_3$  or  $\text{SiCl}_3$  in good yields but these compounds were not suitable precursors for the synthesis of Si(II) compounds. In contrast, the reaction between four equivalents  $[(\text{Mes})_2\text{P}]\text{Li}$  and  $\text{SiBr}_4$  gave the unique tetraphosphadisilene **181**, in which the lithium phosphide acts as a sacrificial reducing agent, in moderate yield. This is the first example of a ditetrelene substituted by more than two heteroatoms from groups 15-17. The triphoshasilanate complex **176**·(THF) was prepared by the reaction between **181** and two equivalents of  $[(\text{Mes})_2\text{P}]\text{Li}$ .

The isolation of **181** demonstrates that the phosphide  $(\text{Mes})_2\text{P}$  does not have the steric bulk to prevent dimerization of the respective diphosphasilylene **173**. This is further highlighted by the isolation of the triphoshasilanate complexes **176**·(THF) and **177**(THF)<sub>3</sub> that contain three of these phosphides at each of the Si(II) centres. The dimerization of a diphosphasilylene and the formation of triphoshasilanate complexes may possibly be suppressed by the use of a more sterically demanding phosphide.

## 6.11 Experimental

### 6.11.1 Synthesis of $\{(\text{Mes})_2\text{P}\}_2\text{SiHCl}$ (**174**)

To a solution of  $(\text{Mes})_2\text{PH}$  (1.70 g, 6.29 mmol) in  $\text{Et}_2\text{O}$  (30 mL) was added a solution of  $n\text{BuLi}$  in hexanes (2.7 mL, 6.21 mmol). The resulting orange solution was stirred for 1 h

then added, dropwise, to a cold (-78 °C) solution of  $\text{SiHCl}_3$  (0.3 mL, 2.97 mmol) in  $\text{Et}_2\text{O}$  (25 mL) to give a yellow solution with a pale precipitate that was allowed to warm to room temperature. The solvent was removed *in vacuo* to give a sticky pale yellow solid. The product was extracted into light petroleum (50 mL) and the resulting pale solids were removed by filtration. The solvent was removed *in vacuo* from the pale yellow filtrate to give a pale yellow foam. The foam was dissolved in *n*-hexane (5 mL) and the product was precipitated as a white solid by the addition of hexamethyldisiloxane (10 mL). Further material was obtained by storage of this mixture at -25 °C overnight. The supernatant was removed by filtration and the residual solvent was removed under vacuum to give a white solid. Yield: 1.14 g, 71%.

$^1\text{H}$  NMR [ $\text{C}_6\text{D}_6$ ]:  $\delta$  2.04 (s, 12H, *p*-Me), 2.48 (s, 24H, *o*-Me), 6.70 (s, 8H, ArH), 6.85 (t,  $J_{\text{PH}} = 20.0$ , 1H, SiH).  $^{13}\text{C}\{^1\text{H}\}$  NMR [ $\text{C}_6\text{D}_6$ ]: 20.90 (*p*-Me), 24.63 (t,  $J_{\text{PC}} = 8.2$  Hz, *o*-Me), 129.78 (t,  $J_{\text{PC}} = 5.7$  Hz, Ar), 130.03 (m, ArH), 138.10 (Ar), 143.64 (t,  $J_{\text{PC}} = 7.5$  Hz, Ar).  $^{29}\text{Si}$ -INEPT NMR [ $\text{C}_6\text{D}_6$ ]: 2.4 (dt,  $J_{\text{SiH}} = 240$  Hz,  $J_{\text{SiP}} = 80$  Hz).  $^{31}\text{P}\{^1\text{H}\}$  NMR [ $\text{C}_6\text{D}_6$ ]:  $\delta$  -75.8 (d,  $J_{\text{PH}} = 20.0$  Hz).

### 6.11.2 Synthesis of $\{(\text{Mes})_2\text{P}\}_2\text{SiCl}_2$ (175)

To a solution of  $(\text{Mes})_2\text{PH}$  (1.49 g, 5.51 mmol) in  $\text{Et}_2\text{O}$  (20 mL) was added a solution of *n*BuLi in hexanes (2.4 mL, 5.5 mmol). The resulting orange solution was stirred for 1 h then added, dropwise, to a solution of  $\text{SiCl}_4$  (0.3 mL, 2.6 mmol) in  $\text{Et}_2\text{O}$  (20 mL) at -78 °C to give a yellow solution with a pale precipitate that was allowed to warm to room temperature. The solvent was removed *in vacuo* to give a sticky pale yellow solid. The product was extracted into light petroleum (40 mL) and the resulting pale solids were removed by filtration. The solvent was removed *in vacuo* from the pale yellow filtrate to give a pale yellow foam. The foam was dissolved in *n*-hexane (5 mL) and the product was precipitated as a white solid by the addition of hexamethyldisiloxane (10 mL). Further material was obtained by storage of this mixture at -25 °C overnight. The supernatant was removed by filtration and the residual solvent was removed from the remaining white powder under vacuum. Yield: 1.33 g, 76%.

$^1\text{H}$  NMR [ $\text{C}_6\text{D}_6$ ]:  $\delta$  2.01 (s, 12H, *o*-Me), 2.59 (s, 24H, *p*-Me), 6.68 (s, 8H, ArH).  $^{13}\text{C}\{^1\text{H}\}$  NMR [ $\text{C}_6\text{D}_6$ ]: 20.85 (*p*-Me), 24.79 (t,  $J_{\text{PC}} = 8.1$  Hz, *o*-Me), 128.90 (t,  $J_{\text{PC}} = 5.5$  Hz, Ar), 130.11 (t,  $J_{\text{PC}} = 2.6$  Hz, ArH), 138.65 (Ar), 144.16 (t,  $J_{\text{PC}} = 7.9$  Hz, Ar).  $^{29}\text{Si}\{^1\text{H}\}$ -INEPT NMR [ $\text{C}_6\text{D}_6$ ]: 18.5 (t,  $J_{\text{SiP}} = 120$  Hz).  $^{31}\text{P}\{^1\text{H}\}$  NMR [ $\text{C}_6\text{D}_6$ ]:  $\delta$  -57.3.

### 6.11.3 Synthesis of $\{(\text{Mes})_2\text{P}\}_2\text{Si}=\text{Si}\{\text{P}(\text{Mes})_2\}_2$ (**181**)

To a solution of  $\text{Mes}_2\text{PH}$  (1.09 g, 4.03 mmol) in  $\text{Et}_2\text{O}$  (20 mL) was added a solution of  $n\text{BuLi}$  in hexanes (2.3 M, 1.8 mL, 4.14 mmol). The resulting orange solution was stirred for 1 h and added, dropwise, over 30 min to a solution of  $\text{SiBr}_4$  (2.0 mL of a 0.5 M solution in light petroleum, 1.0 mmol) in  $\text{Et}_2\text{O}$  (20 mL). The resulting dark blue solution gradually became brown while stirring at room temperature for 15 h. This crude reaction mixture contains 4 major species, as observed in the  $^{31}\text{P}\{^1\text{H}\}$  NMR spectrum [-31.4 (s,  $\text{Mes}_2\text{P}-\text{PMes}_2$ ), -41.3 (br. s), -62.5 (q,  $J_{\text{PLi}} = 44$  Hz,  $[(\text{Mes}_2\text{P})_3\text{Si}]\text{Li}$ ) and -90.8 (br. s) in a 1.0:2.2:1.3:1.0 ratio, respectively]. The solvent was removed *in vacuo* from this solution and the product was extracted from the resulting sticky brown solid into *n*-hexane (25 mL). The resulting pale solids were removed by filtration and the filtrate was heated at reflux for 4 h, during which time **181** deposited as a dark purple microcrystalline solid. The supernatant solution was removed by filtration and the purple solid was washed with  $\text{Et}_2\text{O}$  (10 mL) and residual solvent was removed under vacuum. Single crystals suitable for characterization by X-ray crystallography were obtained by standing the crude reaction mixture in *n*-hexane at room temperature for 3 days. Yield: 0.23 g, 41%.

Solid-state  $^{31}\text{P}\{^1\text{H}\}$  CP-MAS NMR:  $\delta$  -55.9, -77.9. Solid-state  $^{29}\text{Si}\{^1\text{H}\}$ -INEPT CP-MAS NMR:  $\delta$  111.7.

### 6.11.4 Synthesis of $[(\text{Mes}_2\text{P})_3\text{Si}]\text{Li}(\text{THF})$ (**176**·(THF))

A mixture of  $[(\text{Mes}_2\text{P})_2\text{Si}]_2$  (**181**) (0.178 g, 0.16 mmol) and  $[(\text{Mes}_2\text{P})\text{Li}(\text{THF})_2]$  (0.132 g, 0.31 mmol) was dissolved in THF (5 mL) and stirred for 3 days. The resulting red solution was filtered to remove a small amount of dark solid and the solvent was removed from the filtrate *in vacuo*. Diethyl ether (5 mL) was added to the resulting sticky orange solid to give a yellow solution that rapidly precipitated a yellow solid. The supernatant solution was removed by filtration and the yellow solid was washed with cold (-10 °C)  $\text{Et}_2\text{O}$  (2 mL) and residual solvent was removed *in vacuo*. Yield: 0.20 g, 70%.

$^1\text{H}$  NMR [ $\text{C}_6\text{D}_6$ ]:  $\delta$  1.37 (m, THF, 4H) 2.07 (s, 9H, Me), 2.10 (s, 9H, Me), 2.36 (s, 9H, Me), 2.63 (s, 9H, Me), 2.65 (s, 9H, Me), 2.83 (s, 9H, Me), 3.85 (m, 4H, THF), 6.28 (s, 3H, ArH), 6.35 (s, 3H, ArH), 6.67 (s, 6H, ArH).  $^{13}\text{C}\{^1\text{H}\}$  NMR [ $\text{C}_6\text{D}_6$ ]:  $\delta$  20.84, 20.94 (Me), 24.15 (m, Me), 25.33 (Me), 25.50 (THF) 25.89 (m, Me), 28.05 (Me), 69.59 (THF), 129.01 (ArH), 129.56 (d,  $J_{\text{PC}} = 2.9$  Hz, ArH), 130.09, 130.36 (ArH), 133.24 (m, ArH), 133.59 (m,

ArH), 135.41, 136.80 (Ar), 143.30 (m, 2Ar), 145.67, 146.34 (Ar).  $^7\text{Li}$  NMR [ $\text{C}_6\text{D}_6$ ]:  $\delta$  1.6 (q,  $J_{\text{LiP}} = 42$  Hz).  $^{29}\text{Si}\{^1\text{H}\}$ -INEPT NMR [ $\text{C}_6\text{D}_6$ ]:  $\delta$  16.1 (q,  $J_{\text{SiP}} = 110$  Hz).  $^{31}\text{P}\{^1\text{H}\}$  NMR [ $\text{C}_6\text{D}_6$ ]:  $\delta$  -63.1 (q,  $J_{\text{LiP}} = 42$  Hz).

## 6.12 References

- [1] K. Hansen, T. Szilvasi, B. Blom, E. Irran, M. Driess, *Chem. Eur. J.*, **2015**, *21*, 18930-18933.
- [2] H. Cui, J. Zhang, Y. Tao, C. Cui, *Inorg. Chem.*, **2016**, *55*, 46-50.
- [3] K. Izod, W. McFarlane, B. Allen, W. Clegg, R. W. Harrington, *Organometallics*, **2005**, *24*, 2157-2167.
- [4] K. Izod, J. Stewart, E. R. Clark, W. Clegg, R. W. Harrington, *Inorg. Chem.*, **2010**, *49*, 4698-4707.
- [5] (a) M. Usher, A. V. Protchenko, A. Rit, J. Campos, E. L. Kolychev, R. Tirfoin, S. Aldridge, *Chem. Eur. J.*, **2016**, *22*, 11685-11698; (b) B. P. Johnson, S. Almstätter, F. Dielmann, M. Bodensteiner, M. Scheer, *Z. Anorg. Allg. Chem.*, **2010**, *636*, 1275-1285.
- [6] (a) D. Scheschkewitz, *Angew. Chem. Int. Ed. Engl.*, **2004**, *43*, 2965-2967; (b) P. Willmes, M. J. Cowley, M. Hartmann, M. Zimmer, V. Huch, D. Scheschkewitz, *Angew. Chem. Int. Ed. Engl.*, **2014**, *53*, 2216-2220; (c) M. Hartmann, A. Haji-Abdi, K. Abersfelder, P. R. Haycock, A. J. White, D. Scheschkewitz, *Dalton Trans.*, **2010**, *39*, 9288-9295.
- [7] (a) K. Takeuchi, M. Ikoshi, M. Ichinohe, A. Sekiguchi, *J. Am. Chem. Soc.*, **2010**, *132*, 930-931; (b) K. Takeuchi, M. Ikoshi, M. Ichinohe, A. Sekiguchi, *J. Organomet. Chem.*, **2011**, *696*, 1156-1162.
- [8] P. Jutzi, A. Mix, B. Neumann, B. Rummel, W. W. Schoeller, H. G. Stammli, A. B. Rozhenko, *J. Am. Chem. Soc.*, **2009**, *131*, 12137-12143.
- [9] S. Khan, S. S. Sen, H. W. Roesky, D. Kratzert, R. Michel, D. Stalke, *Inorg. Chem.*, **2010**, *49*, 9689-9693.
- [10] T. A. Schmedake, M. Haaf, Y. Apeloig, T. Müller, S. Bukalov, R. West, *J. Am. Chem. Soc.*, **1999**, *121*, 9479-9480.
- [11] (a) A. Schäfer, W. Saak, M. Weidenbruch, H. Marsmann, G. Henkel, *Chem. Ber.*, **1997**, *130*, 1733-1737; (b) A. Schäfer, W. Saak, M. Weidenbruch, *Z. Anorg. Allg. Chem.*, **1998**, *624*, 1405-1408.
- [12] K. Suzuki, T. Matsuo, D. Hashizume, K. Tamao, *J. Am. Chem. Soc.*, **2011**, *133*, 19710-19713.
- [13] M. Takahashi, S. Tsutsui, K. Sakamoto, M. Kira, T. Müller, Y. Apeloig, *J. Am. Chem. Soc.*, **2001**, *123*, 347-348.
- [14] (a) P. P. Power, *Chem. Rev.*, **1999**, *99*, 3463-3504; (b) R. C. Fischer, P. P. Power, *Chem. Rev.*, **2010**, *110*, 3877-3923; (c) C. Prasang, D. Scheschkewitz, *Chem. Soc. Rev.*, **2016**, *45*, 900-921.
- [15] (a) I. Bejan, D. Scheschkewitz, *Angew. Chem. Int. Ed. Engl.*, **2007**, *46*, 5783-5786; (b) R. Tanaka, T. Iwamoto, M. Kira, *Angew. Chem. Int. Ed. Engl.*, **2006**, *45*, 6371-6373; (c) J. Jeck, I. Bejan, A. J. White, D. Nied, F. Breher, D. Scheschkewitz, *J. Am. Chem. Soc.*, **2010**, *132*, 17306-17315.
- [16] C. W. So, H. W. Roesky, P. M. Gurubasavaraj, R. B. Oswald, M. T. Gamer, P. G. Jones, S. Blaurock, *J. Am. Chem. Soc.*, **2007**, *129*, 12049-12054.
- [17] M. Driess, S. Rell, H. Pritzkow, *J. Chem. Soc., Chem. Commun.*, **1995**, 253-254.
- [18] J.-D. Guo, D. J. Liptrot, S. Nagase, P. P. Power, *Chem. Sci.*, **2015**, *6*, 6235-6244.

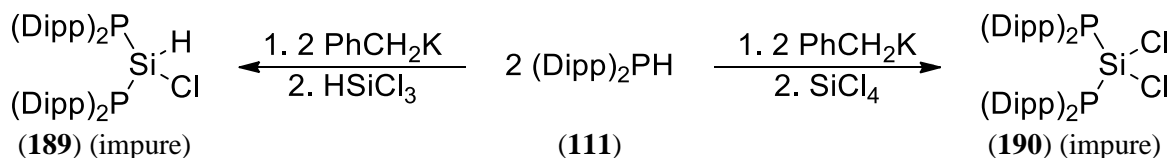
## Chapter 7. Rearrangement of a transient diphosphasilylene

### 7.1 Introduction

In the previous chapter we developed the synthesis of phosphide-substituted Si(II) species, which led to the isolation of the disilene  $\{(\text{Mes})_2\text{P}\}_2\text{Si}=\text{Si}\{\text{P}(\text{Mes})_2\}_2$  (**181**). We proposed that the use of a more sterically demanding phosphide ligand would inhibit dimerization and allow the isolation of a monomeric diphosphasilylene. We sought to utilise the bulky  $(\text{Dipp})_2\text{P}$  phosphide that has been successfully employed in the synthesis of  $\{(\text{Dipp})_2\text{P}\}_2\text{Ge}$  (**104Ge**) and  $\{(\text{Dipp})_2\text{P}\}_2\text{Sn}$  (**104Sn**), which are stabilised by a planar phosphorus centre in the solid state. Due to the similarity in the radii of silicon and germanium, we were confident that this ligand system would prevent dimerization of the silylene  $\{(\text{Dipp})_2\text{P}\}_2\text{Si}$  (**188**). Although the less sterically demanding Si(IV) precursors **174** and **175** were unsuccessful in the synthesis of **181**, we initially pursued the synthesis of the Dipp-substituted analogues to investigate whether the bulky groups stabilise the resulting silylene **188** from side-reactions.

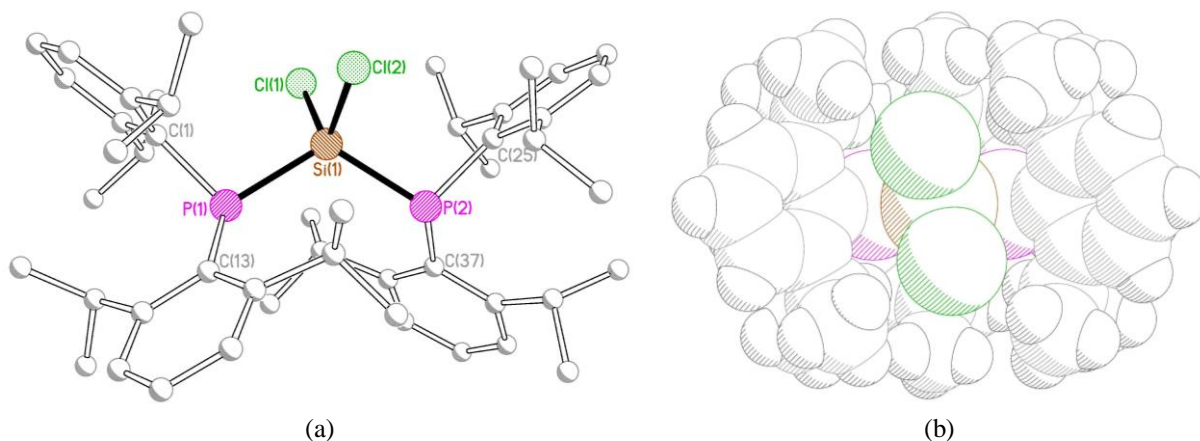
### 7.2 Synthesis of Si(IV) precursors $\{(\text{Dipp})_2\text{P}\}_2\text{SiHCl}_3$ (**189**) and $\{(\text{Dipp})_2\text{P}\}_2\text{SiCl}_2$ (**190**)

The reactions between two equivalents  $[(\text{Dipp})_2\text{P}]\text{Li}$  and either  $\text{HSiCl}_3$  or  $\text{SiCl}_4$  at low temperatures gave mixtures of products containing the mono-substituted species, free phosphine and the diphosphine  $(\text{Dipp})_2\text{P}-\text{P}(\text{Dipp})_2$ , as observed by  $^{31}\text{P}$  NMR spectroscopy. We propose that the lithium phosphide transfer reagent  $[(\text{Dipp})_2\text{P}]\text{Li}$  was insufficiently nucleophilic for the second metathesis reaction at low temperatures and that this underwent side reactions as the solution was warmed to room temperature. The reaction between two equivalents  $[(\text{Dipp})_2\text{P}]\text{K}$  and  $\text{HSiCl}_3$  gave  $\{(\text{Dipp})_2\text{P}\}_2\text{SiHCl}$  (**189**), which was contaminated with the free phosphine **111** (approx. 20%), while the respective reaction with  $\text{SiCl}_4$  gave a mixture of  $\{(\text{Dipp})_2\text{P}\}_2\text{SiCl}_2$  (**190**) and  $\{(\text{Dipp})_2\text{P}\}\text{SiCl}_3$  in a 3.4:1 ratio. Attempts to obtain **189** and **190** as clean solids by recrystallization were unsuccessful, but a small number of single crystals of  $\textbf{190}\cdot(\text{C}_7\text{H}_{14})_2$  suitable for characterisation by X-ray crystallography were obtained from methylcyclohexane.



Scheme 35: Synthesis of compounds **189** and **190**

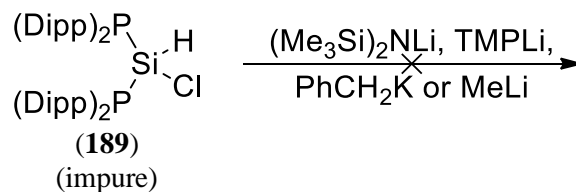
The structure of **190**·(C<sub>7</sub>H<sub>14</sub>)<sub>2</sub> is shown in Figure 97a, along with selected bond lengths and angles. Compound **190**·(C<sub>7</sub>H<sub>14</sub>)<sub>2</sub> crystallises as a methylcyclohexane disolvate, in which the bond angle between the two phosphide ligands [P(1)-Si(1)-P(2) 116.67(3)°] is significantly larger than the respective angle between the two chlorides [Cl(1)-P(1)-Cl(2) 101.95(3)°]. The space-filling diagram (Fig. 97b) illustrates the steric demands of the two phosphide ligands at the Si(IV) centre.



**Figure 97:** (a) Molecular structure of **190**·(C<sub>7</sub>H<sub>14</sub>)<sub>2</sub> with the solvent of crystallisation and hydrogen atoms omitted for clarity and (b) space-filling diagram. Selected bond lengths (Å) and angles (°): Si(1)-P(1) 2.2448(7), Si(1)-P(2) 2.2483(7), Si(1)-Cl(1) 2.0654(8), Si(1)-Cl(2) 2.0592(7), P(1)-C(13) 1.861(2), P(1)-C(1) 1.864(2), P(2)-C(25) 1.8638(19), P(2)-C(37) 1.857(2), P(1)-Si(1)-P(2) 116.67(3), Cl(1)-Si(1)-Cl(2) 101.95(3).

### 7.3 Attempted dehydrochlorination of **189** and reduction of **190**

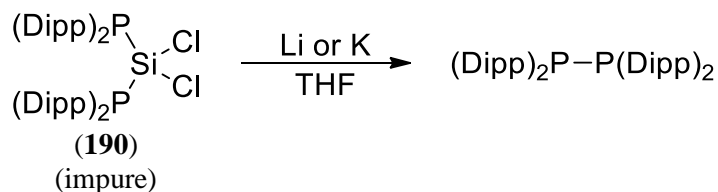
Since it was not possible to isolate clean compounds, the precursors **189** and **190** were used as the impure mixtures prepared *in-situ*. Compound **189** was found not to react with the strong, non-nucleophilic bases [(Me<sub>3</sub>Si)<sub>2</sub>N]Li or TMPLi or the strong, nucleophilic bases benzylpotassium or methyllithium under reflux in THF (Scheme 36) [TMP = 2,2,6,6-tetramethylpiperidide]. This suggests that the silicon-bound hydrogen is too sterically encumbered by the bulky phosphide ligands, which renders **189** inert towards dehydrochlorination by these bases.



**Scheme 36:** Reactivity of **189** towards strong bases



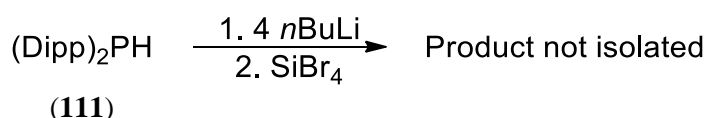
The reaction between **190** and either lithium or potassium in THF gave  $(\text{Dipp})_2\text{P}-\text{P}(\text{Dipp})_2$  (**150**) as the sole product according to  $^{31}\text{P}\{^1\text{H}\}$  NMR spectroscopy. It is surprising that the reduction of **190** gives a different product to the less sterically encumbered analogue **175**, which gives  $[(\text{Mes})_2\text{P}]\text{M}$  as the over-reduction products.



**Scheme 37:** Reactivity of **190** with either Li or K

#### 7.4 Attempted reaction between $\text{SiBr}_4$ and $[(\text{Dipp})_2\text{P}]\text{Li}$

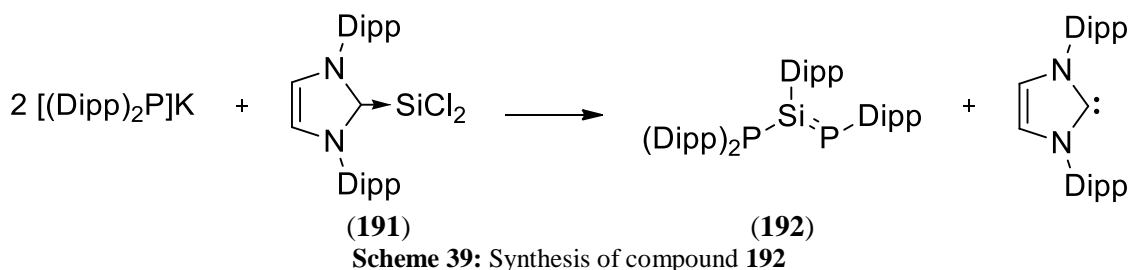
As the Si(IV) precursors **189** and **190** were not suitable for the preparation of **188**, we opted to use a modification of the synthetic approach developed in the previous chapter for synthesis of the disilene **181**, in which the lithium phosphide acts as a metathesis and sacrificial reducing agent with  $\text{SiBr}_4$ . The reaction between  $\text{SiBr}_4$  and four equivalents of  $[(\text{Dipp})_2\text{P}]\text{Li}$  gave a deep purple solution that exhibited a broad signal at -15.2 ppm in the  $^{31}\text{P}\{^1\text{H}\}$  NMR spectrum of the reaction mixture. Unfortunately, we have been unable to isolate any species from this mixture. We do not believe that the species responsible for the signal in the  $^{31}\text{P}\{^1\text{H}\}$  NMR spectrum is **188** as we suspect the diphosphasilylene is inherently unstable at room temperature (see below). In addition, the data do not support the formation of an ate complex of the form  $\{(\text{Dipp})_2\text{P}\}_2\text{SiBrLi}(\text{OEt}_2)_n$  because this species is expected to be lightly coloured and unstable towards  $\text{LiBr}$  elimination in non-donor solvents in a similar manner to its heavier analogue  $\{(\text{Dipp})_2\text{P}\}_2\text{SnClLi}(\text{THF})$ . However, this unidentified species remains unchanged in colour and by  $^{31}\text{P}$  NMR spectroscopy in non-donor solvents such as *n*-hexane. One possibility is that it is a singly phosphide-substituted low oxidation state silicon species of the form  $\{(\text{Dipp})_2\text{P}\}\text{SiBr}_n$  ( $n = 0-2$ ), which may result from the reduction of the silicon centre being favoured over substitution of the bromide. The reaction between four equivalents  $[(\text{Dipp})_2\text{P}]\text{K}$  and  $\text{SiBr}_4$  in THF gave **150** as the sole product according to  $^{31}\text{P}\{^1\text{H}\}$  NMR spectroscopy, which suggests the potassium phosphide is too reducing.



**Scheme 38:** Reactivity of  $[(\text{Dipp})_2\text{P}]\text{Li}$  with  $\text{SiBr}_4$

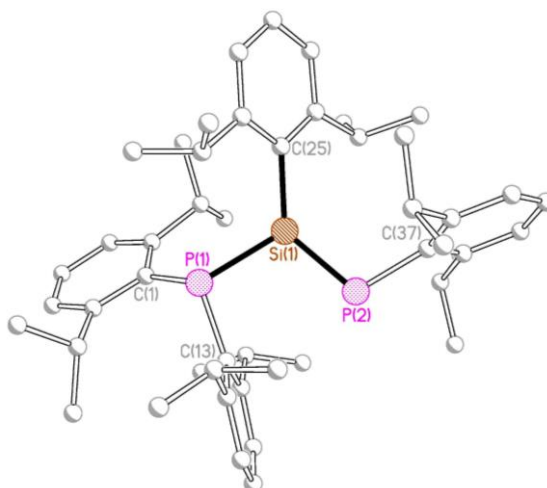
## 7.5 Synthesis of the phosphasilene {(Dipp)<sub>2</sub>P}Si(Dipp){P(Dipp)} (192)

Due to the lack of success in using Si(IV) precursors in the synthesis of **188**, we opted to use the NHC-stabilised dichlorosilylene (IPr-SiCl<sub>2</sub>) **191**<sup>[1]</sup> as the silicon source. The reaction between **191** and two equivalents of [(Dipp)<sub>2</sub>P]K gave a small number of orange crystals, which were shown by X-ray crystallography to be the unexpected phosphasilene {(Dipp)<sub>2</sub>P}Si(Dipp){P(Dipp)} (**192**), along with a colourless powder, after crystallisation from *n*-hexane (Scheme 39). Although we have not yet been able to isolate clean bulk material of **192**, a sample for NMR spectroscopy was prepared by manually separating the orange crystals from the colourless powder. Compound **192** exhibits a pair of doublets at -68.0 and 112.8 ppm ( $J_{\text{PP}} = 45.0$  Hz) in the <sup>31</sup>P{<sup>1</sup>H} NMR spectrum, in which we attribute the low-field signal to the two-coordinate phosphorus centre, and a doublet of doublets in the <sup>29</sup>Si{<sup>1</sup>H}-INEPT spectrum at 167.4 ppm ( $J_{\text{SiP}} = 206$  Hz,  $J_{\text{SiP}'} = 107$  Hz). We have trialled the removal of the NHC side-product by the addition of SiBr<sub>4</sub> to the crude reaction mixture or stirring under an atmosphere of CO<sub>2</sub>, with the former giving the most promising results.<sup>[2]</sup>



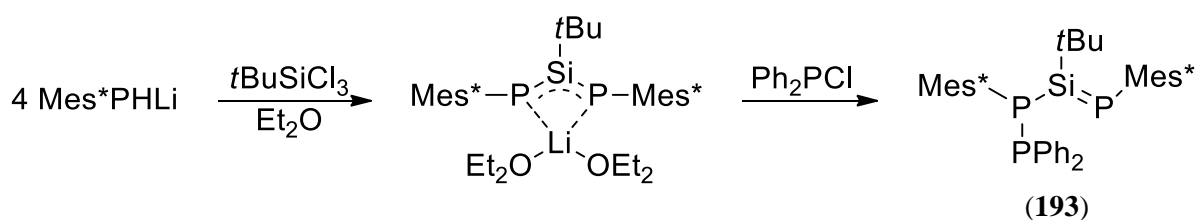
## 7.6 Solid-state structure of {(Dipp)<sub>2</sub>P}Si(Dipp){P(Dipp)} (192)

The structure of **192** is shown in Figure 98, along with selected bond lengths and angles. Compound **192** crystallises with two independent molecules in the asymmetric unit, which has nearly identical conformations. The silicon atoms adopt a trigonal planar geometry [sum of angles at Si(1) = 357.13° and Si(2) = 356.65°] while the three-coordinate phosphorus atoms adopt a pyramidal geometry. The Si-P distances to the three-coordinate phosphorus centres [2.2336(7) and 2.2279(6) Å] are significantly longer than the Si-P distances to the two-coordinate phosphorus centres [2.0893(7) and 2.0959(6) Å], which is consistent with the presence of an Si=P double bond at P(2) and P(4). This compound has an almost identical core structure to the first X-ray crystallographically characterised phosphasilene {(Ph<sub>2</sub>P)(Mes\*)P}Si(*t*Bu)(Mes\*) (**193**) [Si-P 2.254(3) Å, Si=P 2.094(3) Å and sum of angles at Si = 356.7°].<sup>[3]</sup>



**Figure 98:** Molecular structure of one of the two independent molecules of **192** with hydrogen atoms omitted for clarity. Selected bond lengths (Å) and angles (°): (molecule 1) Si(1)-P(1) 2.2336(7), Si(1)-P(2) 2.0893(7), Si(1)-C(25) 1.8926(16), P(1)-C(1) 1.8529(19), P(1)-C(13) 1.8563(17), P(2)-C(37) 1.8563(17), P(1)-Si(1)-P(2) 107.70(3), P(1)-Si(1)-C(25) 117.89(6), P(2)-Si(1)-C(25) 131.54(6), C(1)-P(1)-Si(1) 120.18(6), C(1)-P(1)-C(13) 106.28(8), C(13)-P(1)-Si(1) 102.29(6), C(37)-P(2)-Si(1) 108.81(6), (molecule 2) Si(2)-P(3) 2.2279(6), Si(2)-P(4) 2.0959(6), Si(2)-C(73) 1.8922(18), P(3)-C(49) 1.8506(17), P(3)-C(61) 1.8471(19), P(4)-C(85) 1.8540(17), P(3)-Si(2)-P(4) 107.17(3), P(3)-Si(2)-C(73) 116.46(6), P(4)-C(2)-C(73) 133.02(5), C(49)-P(3)-Si(2) 121.44(6), C(61)-P(3)-Si(2) 101.44(6), C(49)-P(3)-C(61) 107.34(8), C(85)-P(4)-Si(2) 107.70(3).

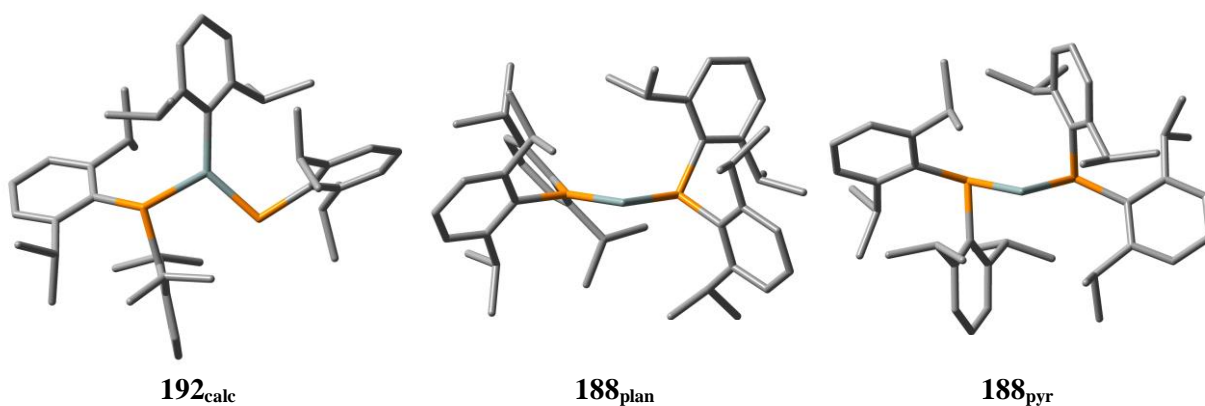
Phosphasilylenes are typically synthesised from Si(IV) chloride precursors and primary lithium phosphides.<sup>[4]</sup> For example, the synthesis of **193** from *t*BuSiCl<sub>3</sub> is shown in Scheme 40.<sup>[3]</sup> In contrast, compound **192** must form by a 1,2-aryl migration from the corresponding diphosphasilylene **188**. Similar migrations have been observed in the first example of a (phospha)(boryl)carbene **62** and of a dialkylsilylene **52**.



**Scheme 40:** Synthetic route to **193**

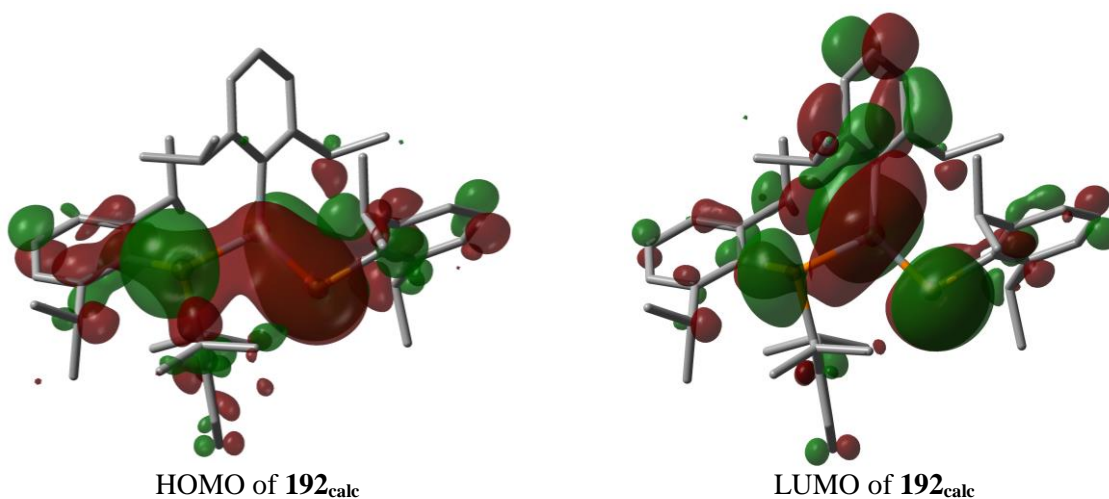
## 7.7 DFT calculations

In order to gain an insight into the relative stability of **192** and the two different configurations of **188** we carried out a DFT study. The minimum energy geometry **192<sub>calc</sub>** was located by using the crystallographic coordinates of a single molecule of **192** as the starting geometry for the optimisation while **188<sub>plan</sub>** and **188<sub>pyr</sub>** were located by starting from the previously optimised geometries of the germylene {(Dipp)<sub>2</sub>P}<sub>2</sub>Ge (**104Ge**) (Fig. 99).



**Figure 99:** Calculated geometries of **192<sub>calc</sub>**, **188<sub>plan</sub>** and **188<sub>pyr</sub>**

The minimum energy geometry **192<sub>calc</sub>** accurately reproduces the geometry of the X-ray crystallographically determined structure of **192**. Inspection of the molecular orbitals of **192<sub>calc</sub>** reveals that the HOMO is mainly comprised of the lone pair at the three-coordinate phosphorus centre (P(1)) and the Si-P  $\pi$  orbital while the LUMO is comprised from the lone pair at P(1) and the Si-P  $\pi^*$  orbital, with both of these orbitals having a significant component on the aromatic rings (Fig. 100). Natural Bond Orbital (NBO) analysis yields a Wiberg Bond Index (WBI) for the P(1)-Si(1) bond of 0.9919, which is significantly higher than that calculated for the straightforward P-Si(II)  $\sigma$ -bond in **173<sub>pyr</sub>** (0.804, see the previous chapter). This may be attributed to the tetravalent Si centre providing better orbital overlap compared to the Si(II) centres. The WBI of the P(2)-Si(1) bond at the two-coordinate phosphorus centre of 1.6714 is consistent with the P=Si double bond. The calculated  $^{31}\text{P}\{^1\text{H}\}$  chemical shifts at P(1) and P(2) of -65.4 and 116.4 ppm, respectively, and the calculated  $^{29}\text{Si}\{^1\text{H}\}$  chemical shift of 188.0 ppm are in very good agreement with the observed chemical shifts of -68.0 and 112.8 ppm in the  $^{31}\text{P}\{^1\text{H}\}$  NMR spectrum and 167.4 ppm in the  $^{29}\text{Si}\{^1\text{H}\}$ -INEPT spectrum.



**Figure 100:** HOMO and LUMO of **192<sub>calc</sub>**

While the overall structures of **188<sub>plan</sub>** and **188<sub>pyr</sub>** are similar to that of the corresponding minimum energy geometries of **104Ge** the P-Si distances are approximately 4% shorter than the respective P-Ge distances. The minimum energy geometry **188<sub>plan</sub>** has one planar and one pyramidal phosphorus centre (sum of angles at P1 = 359.88 and P(2) = 320.29°) and P-Si distances of 2.1752 and 2.2972 Å, respectively. In addition, the WBIs of the P(1)-Si(1) and P(2)-Si(1) bonds of 1.3833 and 0.9364 are consistent with **188<sub>plan</sub>** featuring  $\pi$ - $\pi$  interactions from the planar phosphorus centre, which are analogues to the interactions we observe in the diphosphagermylenes and -stannylenes in Chapter 4. The minimum energy geometry **188<sub>pyr</sub>** has two symmetrical pyramidal phosphorus centres (sum of angles at P = 293.92°) and P-Si distances of 2.3182 Å. The WBIs of the P-Si bonds of 0.7916 are consistent with straightforward P-Si  $\sigma$ -bonds.

The calculations reveal that **188<sub>plan</sub>** is more stable than **188<sub>pyr</sub>** by 14.1 kJ mol<sup>-1</sup>, which is remarkably similar to the difference in energy between **104Ge<sub>plan</sub>** and **104Ge<sub>pyr</sub>** (13.8 kJ mol<sup>-1</sup>). Although we were unable to locate a transition state for the formation **192<sub>calc</sub>** from either **188<sub>plan</sub>** or **188<sub>pyr</sub>**, the 1,2-aryl migration is strongly favoured; the difference in Gibbs free energy between **192<sub>calc</sub>** and **188<sub>pyr</sub>** is -62.9 kJ mol<sup>-1</sup>.

## 7.8 Conclusions

The reactions between two equivalents of [(Dipp)<sub>2</sub>P]K and either HSiCl<sub>3</sub> or SiCl<sub>4</sub> gave **189** and **190** as impure mixtures. Compound **189** proved inert towards dehydrochlorination by a range of strong bases while the reaction of **190** with alkali metals gave the diphosphine **150**.

Treatment of the NHC-stabilised dichlorosilylene **191** with two equivalents of [(Dipp)<sub>2</sub>P]K gave the phosphasilene **192**. This compound must form from a 1,2-aryl migration of the diphosphasilylene **188**. While we have insufficient data to indicate if the migration is occurring in the silylene with one planar and one pyramidal phosphorus centre (**188<sub>plan</sub>**) or with two pyramidal phosphorus centres (**188<sub>pyr</sub>**), we have shown that these geometries are thermodynamically unstable with respect to the formation of the phosphasilene **192<sub>calc</sub>**.

We propose a stable diphosphasilylene may be accessible through the use of phosphide ligands with substituents less prone to migration. The bulky dialkylphosphide {(Me<sub>3</sub>Si)<sub>2</sub>CH}<sub>2</sub>P, which was previously prepared in Chapter 3, may be a suitable ligand. The alkyl substituents should destabilise the migration transition state.

## 7.9 Experimental

The NHC-stabilised dichlorosilylene **191** was prepared by the previously reported procedure.<sup>[1]</sup>

### 7.9.1 Attempted synthesis of $\{(\text{Dipp})_2\text{P}\}_2\text{SiHCl}$ (**189**)

To a solution of  $(\text{Dipp})_2\text{PH}$  (1.52 g, 4.29 mmol) in THF (30 ml) was added a solution of  $\text{PhCH}_2\text{K}$  (0.558 g, 4.29 mmol) in THF (15 ml). The resulting red solution was stirred for 30 min and added, dropwise, to a cold ( $-78\text{ }^\circ\text{C}$ ) solution of  $\text{SiHCl}_3$  (0.20 ml, 1.98 mmol) in THF (15 ml). The resulting mixture was allowed to warm to room temperature to give a yellow solution with pale solids. A  $^{31}\text{P}\{^1\text{H}\}$  NMR spectrum of this crude reaction mixture contained a very broad multiplet at  $-89$  ppm and  $(\text{Dipp})_2\text{PH}$  as a contaminant (20%) at  $-102$  ppm. Attempts to purify this compound by recrystallization proved unsuccessful.

### 7.9.2 Attempted synthesis of $\{(\text{Dipp})_2\text{P}\}_2\text{SiCl}_2$ (**190**)

To a solution of  $(\text{Dipp})_2\text{PH}$  (2.19 g, 6.17 mmol) in THF (25 mL) was added a solution of  $\text{PhCH}_2\text{K}$  (0.808 g, 6.17 mmol) in THF (20 mL). The resulting red solution was stirred for 30 min and added, dropwise, to a cold ( $-78\text{ }^\circ\text{C}$ ) solution of  $\text{SiCl}_4$  (0.35 mL, 3.05 mmol) in THF (15 mL). The resulting mixture was allowed to warm to room temperature to give a yellow solution with pale solids. A  $^{31}\text{P}\{^1\text{H}\}$  NMR spectrum of this crude reaction mixture contained major peaks at  $-57$  and  $-70$  ppm in a 1:3.4 ratio, which were tentatively assigned as  $\{(\text{Dipp})_2\text{P}\}\text{SiCl}_3$  and  $\{(\text{Dipp})_2\text{P}\}_2\text{SiCl}_2$  (**190**), respectively. Attempts to obtain **190** as a clean solid were unsuccessful, but a small number of single crystals suitable for X-ray crystallography were isolated from cold ( $-30\text{ }^\circ\text{C}$ ) methylcyclohexane.

### 7.10 Synthesis of $\{(\text{Dipp})_2\text{P}\}\text{Si}(\text{Dipp})\{\text{P}(\text{Dipp})\}$ (**192**)

To a solution of  $\text{IPr-SiCl}_2$  (**191**) (0.293 g, 0.60 mmol) in THF (15 ml) was added, slowly, a solution of  $[(\text{Dipp})_2\text{P}]\text{K}$  (0.472 g, 1.20 mmol). The resulting light red solution was stirred for 30 min and the solvent was removed *in vacuo* to give a sticky red residue. The product was extracted into *n*-hexane (10 ml) to give an orange solution with pale solids, which were removed by filtration. Storage of the orange filtrate at  $-25\text{ }^\circ\text{C}$  overnight gave a small number of large orange crystals of **192**, which were characterised by X-ray crystallography, and a fine colourless powder. The supernatant solution was removed by filtration and the residual solvent was removed under vacuum. A sample of **192** for NMR

spectroscopy was obtained by manually separating the orange crystals from the colourless powder, although the  $^1\text{H}$  NMR spectrum of **192** shows peaks due to a small amount of contamination from the free NHC side-product.

$^1\text{H}$  NMR [ $\text{d}_8$ -toluene]:  $\delta$  1.05 (br. m, 48H,  $\text{CHMe}_2$ ), 3.96 (br. m, 8H,  $\text{CHMe}_2$ ), 6.95 (m, 4H, ArH), 7.02-7.10 (m, 6H, ArH), 7.15 (d,  $J_{\text{HH}} = 7.8$  Hz, ArH).  $^{29}\text{Si}\{^1\text{H}\}$ -INEPT [ $\text{d}_8$ -toluene]:  $\delta$  167.4 (dd,  $J_{\text{SiP}} = 206$  Hz,  $J_{\text{SiP}'} = 107$  Hz).  $^{31}\text{P}\{^1\text{H}\}$  NMR [ $\text{d}_8$ -toluene]:  $\delta$  -68.0 (d,  $J_{\text{PP}} = 45.0$  Hz,  $J_{\text{SiP}} = 206$  Hz,  $\text{SiPAr}_2$ ), 112.8 (d,  $J_{\text{PP}} = 45.0$  Hz,  $J_{\text{SiP}} = 107$  Hz,  $\text{Si=PAr}$ ).

## 7.11 References

- [1] R. S. Ghadwal, H. W. Roesky, S. Merkel, J. Henn, D. Stalke, *Angew. Chem. Int. Ed. Engl.*, **2009**, *48*, 5683-5686.
- [2] T. J. Hadlington, J. A. Abdalla, R. Tirfoin, S. Aldridge, C. Jones, *Chem. Commun.*, **2016**, *52*, 1717-1720.
- [3] H. R. G. Bender, E. Niecke, M. Nieger, *J. Am. Chem. Soc.*, **1993**, *115*, 3314-3315.
- [4] V. Nesterov, N. C. Breit, S. Inoue, *Chem. Eur. J.*, **2017**, *23*, 12014-12039.

## Chapter 8. A diphospharsenium cation stabilised a planar phosphorus

### 8.1 Introduction to pnictenium cations

Two-coordinate pnictenium cations ( $R_2E^+$ ;  $E = P, As, Sb, Bi$ ) are isoelectronic analogues of singlet tetrylenes, with the cationic pnictogen centre possessing a lone pair and a vacant p-orbital (Fig. 101). The positive charge at the pnictogen centre makes these compounds substantially less nucleophilic but more electrophilic than their tetrylene counterparts. Curiously, the first two-coordinate pnictenium cations **194** and **195**<sup>[1]</sup> predate the stable carbenes reported by Bertrand and Arduengo by three decades (Fig. 102).<sup>[2]</sup> However, such phosphacyanines are typically not viewed as “true” phosphonium cations ( $R_2P^+$ ) as the positive charge is not located primarily at the phosphorus centre, and so will not be discussed in this chapter. Similarly, we exclude diphosphapnictenium cations of the form  $(R_3P)_2E^+$  [ $E = P, As$ ] that contain pnictogen centres in the +1 oxidation state that are not isoelectronic with tetrylenes.

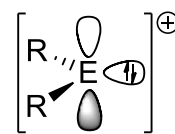


Figure 101

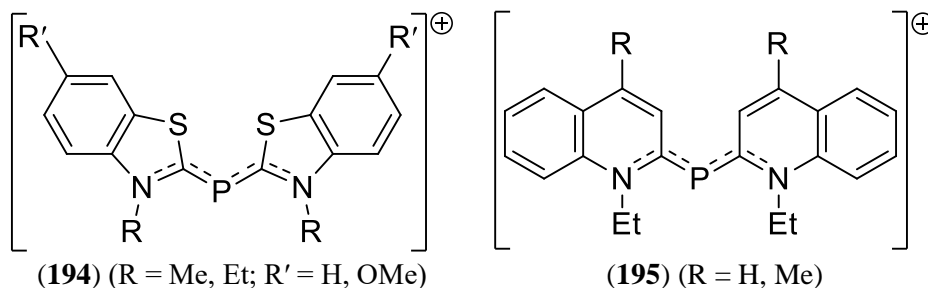


Figure 102: Phosphacyanines

Since the electron deficiency of the two-coordinate pnictogen centre may be partially alleviated by  $\pi$  interactions from heteroatom substituents, in a manner analogous to tetrylenes (see Section 1.3), the vast majority of isolated pnictenium cations are *N*-heterocyclic species of the form **196** (Fig. 103). The first crystallographically characterised phosphonium cation  $[{(iPr)_2N}_2P][OTf]$  (**197**)<sup>[3]</sup> is essentially isostructural with the carbene analogue  $\{(iPr)_2N\}_2C:$  (**37**)<sup>[4]</sup>, in which the two-coordinate phosphorus centre and carbenic carbon are stabilised by  $\pi$  interactions from the two nitrogen centres.

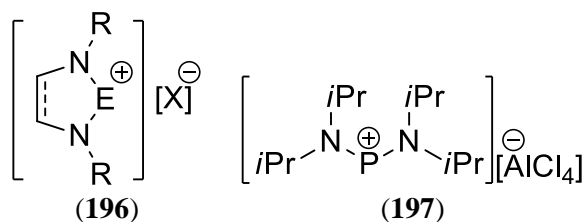


Figure 103: Diaminopnictenium cations



### 8.1.1 Phosphorus-substituted pnictenium cations

Similarly to tetrylenes, there are significantly fewer examples of phosphorus-substituted pnictenium cations compared to their nitrogen analogues, with compounds **198**,<sup>[5]</sup> **199**<sup>[6]</sup> and **200**<sup>[7]</sup> being the only structurally characterised examples. The two-coordinate phosphorus centre in the diposphene salt  $[\text{Mes}^*\text{MeP}=\text{PMes}^*][\text{OTf}]$  (**198**) reported by Grützmacher is stabilised by  $p\pi$ - $p\pi$  interactions from the perfectly planar phosphide ligand, while the two-coordinate phosphorus centres in the phosphaphosponium salts **199** and **200** by Romanenko and Goicoechea, respectively, have a formal  $\text{P}=\text{P}$  double bond to the phosphinidine substituent and are further coordinated to a tertiary phosphine or NHC, respectively (Fig. 104).

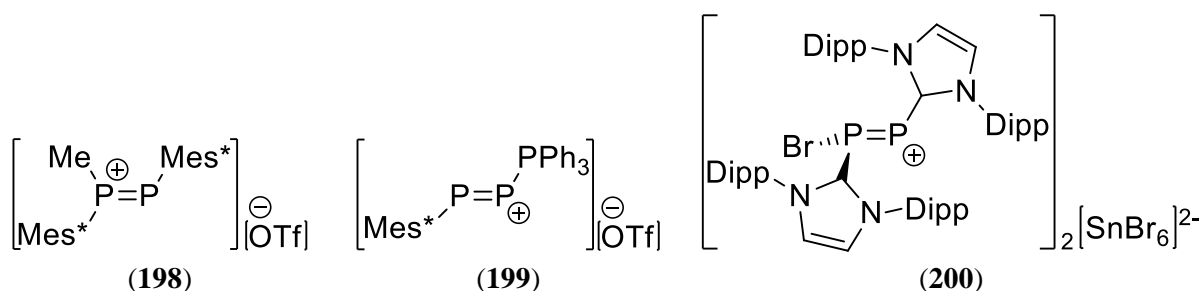


Figure 104: Phosphorus-substituted pnictenium cations

### 8.1.2 Heavier acyclic pnictenium cations

It is notable that there are significantly fewer acyclic examples of heavier pnictenium cations; structurally characterised examples of acyclic arsenium cations are limited to **201**-**204**. The sandwich compound **201** was reported in 1983 Jutzi and co-workers,<sup>[8]</sup> which has an analogous structure to the metallocenes **1-4**, while Krossing and co-workers subsequently reported the half-sandwich **202**.<sup>[9]</sup> Although the diaminoarsenium cations **203** and **204** are stabilised by  $\pi$  interactions from the two amido ligands and a close  $\text{As}\cdots\text{Cl}$  contact from the counterion in the solid-state, they exhibit poor thermal stability in solution, which is in marked contrast to typical acyclic diaminotetrylenes.<sup>[10]</sup> In addition, only a very small number of related acyclic stibenium ( $\text{R}_2\text{Sb}^+$ ) and bismuthenium ( $\text{R}_2\text{Bi}^+$ ) cations have been reported.<sup>[11]</sup>

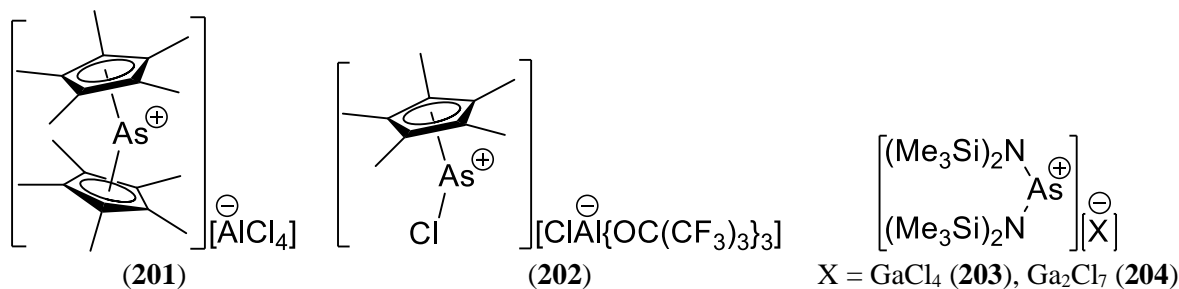


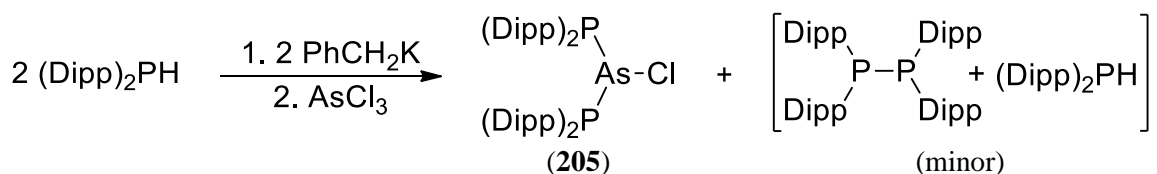
Figure 105: Acyclic heavier pnictenium cations

### 8.1.3 Proposed diphosphapnictenium cation

In Chapter 3, we have demonstrated that the stabilisation of diphosphatetrylenes by  $p\pi-p\pi$  interactions from a planar phosphorus centre through the appropriate choice of bulky phosphide ligands. Since the diphosphatetrylenes **104Ge** and **104Sn** are isoelectronic with the corresponding diphosphaarsenium cation, we speculated that the P-As  $\pi$  stabilised diphosphaarsenium cation  $\{(\text{Dipp})_2\text{P}\}_2\text{As}^+$  may be accessible.

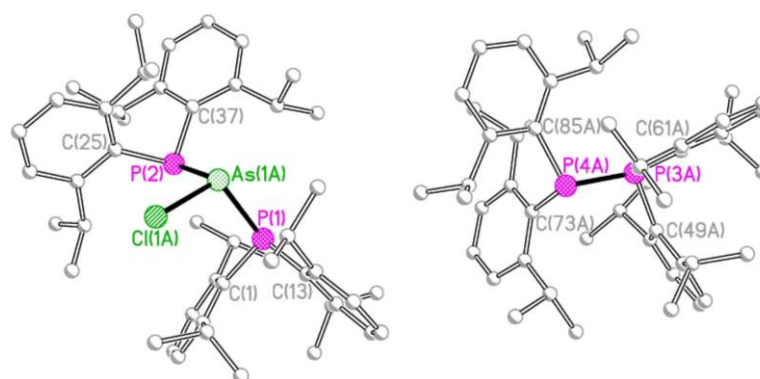
## 8.2 Synthesis of $\{(\text{Dipp})_2\text{P}\}_2\text{AsCl}$

The reaction between two equivalents of  $[(\text{Dipp})_2\text{P}]\text{K}$  (**A**) and  $\text{AsCl}_3$  in cold THF gives  $\{(\text{Dipp})_2\text{P}\}_2\text{AsCl}$  (**205**) as a yellow powder, along with a small amount of the diphosphine  $(\text{Dipp})_2\text{P}-\text{P}(\text{Dipp})_2$  and the free phosphine  $(\text{Dipp})_2\text{PH}$  (approximately 20%) (Scheme 41). While it was not possible to remove these impurities by selective recrystallization, storage of a solution of this material in a mixture of MeCN and  $\text{Et}_2\text{O}$  at  $-25^\circ\text{C}$  lead to the deposition of yellow co-crystals of  $\{(\text{Dipp})_2\text{P}\}_2\text{AsCl}\cdot(\text{Dipp})_2\text{P}-\text{P}(\text{Dipp})_2$  (**205·150**).



Scheme 41: Synthesis of **205**

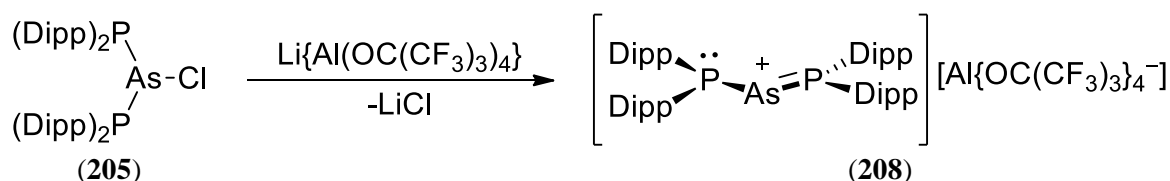
The structure of **205·150** is shown in Figure 207, along with selected bond lengths and angles. The P-As distances in **205·150** [2.3401(7) and 2.3879(7) Å] are rather unsymmetrical, with the shorter P-As distance being similar to the respective distances in  $\{(\mu-(2,6\text{-Mes}_2\text{C}_6\text{H}_3)\text{PAsCl})_2$  (**206**) [2.3346(7) and 2.3498(7) Å]. The As-Cl distance [2.250(7) Å] in **205·150** is similar to the larger respective distance in **206** [2.2681(8) and 2.2208(7) Å].<sup>[12]</sup>



**Figure 207.** Structure of **205·150** with minor disorder components and H atoms omitted for clarity. Selected bond lengths (Å) and angles (°): As(1A)-P(1) 2.3401(7), As(1A)-P(2) 2.3879(7), As(1A)-Cl(1A) 2.2250(7), P(1)-C(1) 1.859(3), P(1)-C(13) 1.870(3), P(2)-C(25) 1.857(3), P(2)-C(37) 1.875(2), P(3A)-P(4A) 2.2275(12), P(3A)-C(49A) 1.865(5), P(3A)-C(61A) 1.848(4), P(4A)-C(73A) 1.875(4), P(4A)-C(85A) 1.860(5), P(1)-As(1A)-P(2) 92.29(2), P(1)-As(1A)-Cl(1A) 108.15(3), P(2)-As(1A)-Cl(1A) 95.75(3), As(1A)-P(1)-C(1) 110.15(7), As(1A)-P(1)-C(13) 114.81(8), C(1)-P(1)-C(13) 105.07(11), As(1A)-P(2)-C(25) 97.40(8), As(1A)-P(2)-C(37) 109.52(8), C(25)-P(2)-C(37) 102.51(11).

### 8.3 Synthesis of $[(\text{Dipp})_2\text{P}]_2\text{As}[\text{Al}\{\text{OC}(\text{CF}_3)_3\}_4]\cdot(\text{PhMe})_{0.5}$

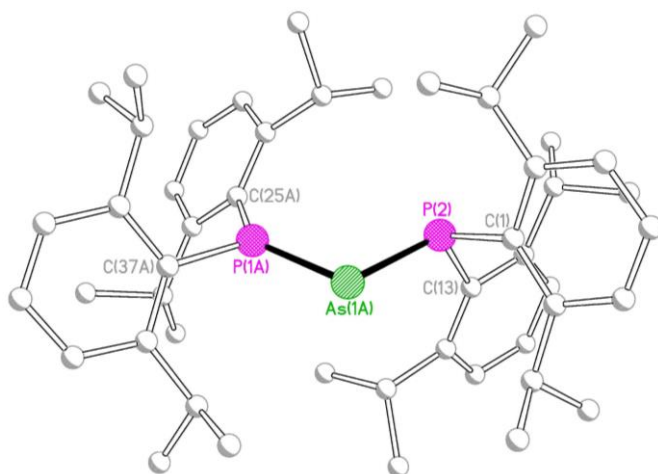
Treatment of **205** with either one equivalent of  $\text{GaCl}_3$  or  $\text{Na}[\text{B}\{3,5\text{-(CF}_3)_2\text{-C}_6\text{H}_3\}_4]$  in fluorobenzene give dark green solutions, which, unexpectedly, exhibit no discernible signals in the  $^{31}\text{P}\{^1\text{H}\}$  NMR spectra at room temperature. Although we were able to obtain green crystalline material of the supposed arsenium salts  $[(\text{Dipp})_2\text{P}]_2\text{As}^+[\text{M}]^-$  ( $[\text{M}]^- = \text{GaCl}_4^-$ ,  $[\text{B}\{3,5\text{-(CF}_3)_2\text{-C}_6\text{H}_3\}_4]^-$ ) from these mixtures, the crystals were not suitable for characterisation by X-ray crystallography so their identities could not be verified. However, the reaction between **205** and  $\text{Li}[\text{Al}\{\text{OC}(\text{CF}_3)_3\}_4]$  in fluorobenzene initially gave a dark green oil from an attempted crystallisation in a mixture toluene and fluorobenzene. Storage of this oil at  $-25^\circ\text{C}$  for approximately one week gives  $[(\text{Dipp})_2\text{P}]_2\text{As}[\text{Al}\{\text{OC}(\text{CF}_3)_3\}_4]\cdot(\text{PhMe})_{1.5}$  (**208**) after gradual crystallisation of the material, which was characterised by X-ray crystallography. The solvent of crystallisation in **208** is only weakly held; the alternative solvate  $[(\text{Dipp})_2\text{P}]_2\text{As}[\text{Al}\{\text{OC}(\text{CF}_3)_3\}_4]\cdot(\text{PhMe})_{0.5}$  (**208a**) was isolated after exposing the crystalline material of **208** to vacuum for 10 minutes, as judged by  $^1\text{H}$  NMR spectroscopy. Compound **208a** is stable in the solid-state for long periods and decomposes very slow in solution at room temperature, which contrasts the thermal instability of previously isolated acyclic diaminoarsenium salts; for example, the recently isolated diaminoarsenium salts **203** and **204** decompose above  $-10^\circ\text{C}$  in solution.



**Scheme 42:** Synthesis of **208**

## 8.4 Solid-state structure of $[(\text{Dipp})_2\text{P}]_2\text{As}[\text{Al}\{\text{OC}(\text{CF}_3)_3\}(\text{PhMe})_{1.5}]$ (**208**)

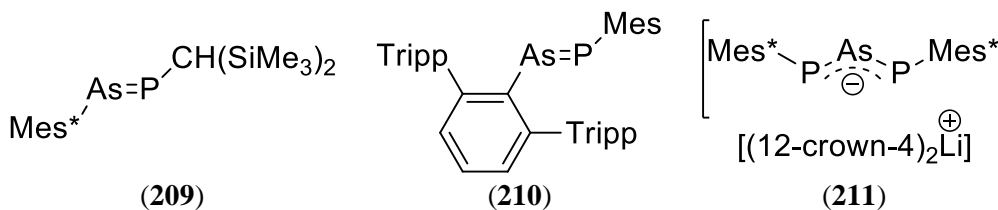
Compound **208** crystallises with two crystallographically independent cation/anion pairs in the asymmetrical unit, along with three molecules of toluene (Fig. 106); the cations and anions are well separated (closest As $\cdots$ F contact  $>5\text{\AA}$ ). The two independent cations in **208** both have a major (**208**<sup>1</sup><sub>maj</sub> and **208**<sup>2</sup><sub>maj</sub>, with 94 and 92% occupancy, respectively) and minor (**208**<sup>1</sup><sub>min</sub> and **208**<sup>2</sup><sub>min</sub>) disorder component.



**Figure 106:** Solid-state structure of the **208**<sup>1</sup><sub>maj</sub> disorder component of 1 of 2 independent cations of **208** with H atoms omitted for clarity. Selected bond lengths ( $\text{\AA}$ ) and angles ( $^\circ$ ) for **208**<sup>1</sup><sub>maj</sub>: P(1A)-As(1A) 2.1501(9), P(2)-As(1A) 2.2925(7), P(1A)-C(25A) 1.834(3), P(1A)-C(37A) 1.809(3), P(2)-C(1) 1.849(3), P(2)-C(13) 1.845(3), P(1A)-As(1A)-P(2) 105.45(3), As(1A)-P(1A)-C(25A) 135.75(11), As(1A)-P(1A)-C(37A) 111.28(10), C(25A)-P(1A)-C(37A) 112.72(14), As(1A)-P(2)-C(1) 95.72(8), As(1A)-P(2)-C(13) 118.30(10), C(1)-P(2)-C(13) 106.15(13).

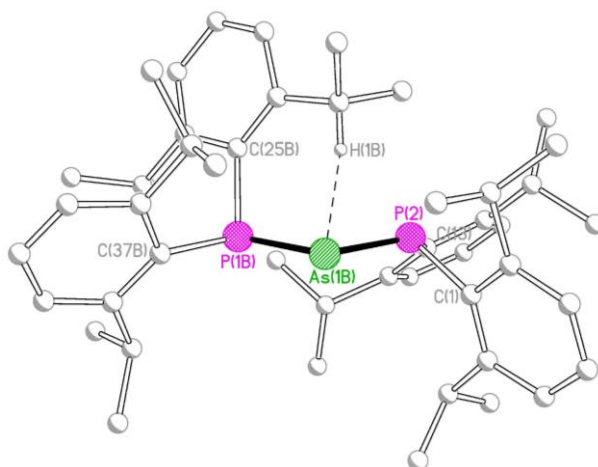
The major disorder components (**208**<sup>1</sup><sub>maj</sub> and **208**<sup>2</sup><sub>maj</sub>) each possess one planar and one pyramidal phosphorus centre [sum of angles at P(1A) = 359.74, P(2) = 320.16, P(3A) = 359.87, P(4A) = 319.49 $^\circ$ ]. The  $P_{\text{plan}}$ -As distances [2.1501(9) and 2.1482(9)  $\text{\AA}$  for **208**<sup>1</sup><sub>maj</sub> and **208**<sup>2</sup><sub>maj</sub>, respectively] are approximately 6% shorter than the  $P_{\text{pyr}}$ -As distances [2.2925(7) and 2.3028(11)  $\text{\AA}$  for **208**<sup>1</sup><sub>min</sub> and **208**<sup>2</sup><sub>min</sub>, respectively], suggesting a significant degree of multiple bond character of the former bonds. The short P-As distances in **208**<sup>1</sup><sub>maj</sub> and **208**<sup>2</sup><sub>maj</sub> are at the longer end of the range of P=As distances in phospharsenes (RP=AsP), in which there are true P=As double bonds; for example, the P-As distances in (Mes\*)P=As{CH(SiMe<sub>3</sub>)<sub>2</sub>} (**209**)<sup>[13]</sup> and (2,6-Tripp<sub>2</sub>C<sub>6</sub>H<sub>3</sub>)As=P(Mes) (**210**)<sup>[14]</sup> are 2.125(1) and 2.134(2)  $\text{\AA}$ , respectively (Fig. 107). However, the  $P_{\text{plan}}$ -As distances in **208**<sup>1</sup><sub>maj</sub> and **208**<sup>2</sup><sub>maj</sub> are similar to the P-As distances in the 1,3-diphospha-2-arsaallyl anion in (Mes\*P)<sub>2</sub>AsLi(TMEDA)(Me<sub>2</sub>NH) (**211**) [As-P 2.176(1) and 2.170(1)  $\text{\AA}$ ], while the  $P_{\text{pyr}}$ -As distances in **208**<sup>1</sup><sub>maj</sub> and **208**<sup>2</sup><sub>maj</sub> are significantly shorter than the respective distances in **205** (Fig. 107).<sup>[15]</sup> The P-As-P distances in **208**<sup>1</sup><sub>maj</sub> and **208**<sup>2</sup><sub>maj</sub> are 105.45(3) and 109.95(4) $^\circ$ . Overall, the structures of **208**<sup>1</sup><sub>maj</sub> and **208**<sup>2</sup><sub>maj</sub> are remarkably similar to that of the

isoelectronic  $\{(\text{Dipp})_2\text{P}\}_2\text{Ge}$  (**104Ge**) [sum of angles at P = 358.35 and 311.53°, P-Ge-P angle 107.4(4)°].<sup>[16]</sup>



**Figure 107:** Phosphaarsenes and an arsallyl anion

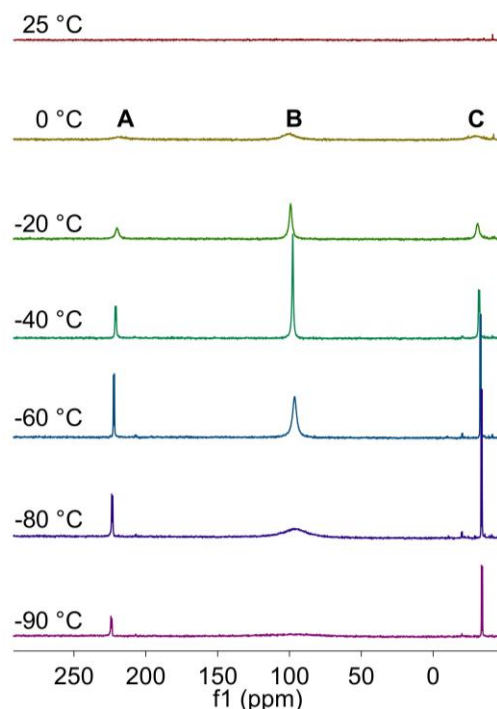
As the minor disorder components of the two independent cations have low occupancies (6% and 8% for **208**<sup>1</sup><sub>min</sub> and **208**<sup>2</sup><sub>min</sub>, respectively), it is not appropriate to discuss their structures in detail; however, their gross structures are clear. The disorder component **208**<sup>2</sup><sub>min</sub> adopts the same planar configuration of **208**<sup>1</sup><sub>maj</sub> and **208**<sup>2</sup><sub>maj</sub>. In contrast, **208**<sup>1</sup><sub>min</sub> adopts a configuration with two pyramidal phosphorus centres [sum of angles at P(1B) 324.5, P(2) 339.97°], in which there is a close contact between a methine hydrogen of one isopropyl group and the arsenic centre [H(1B)⋯As(1B) 2.02(1) Å] (Fig. 108). While related B-H⋯E (E = Sn, Pb) in phosphine-borane stabilised dialkylstannylenes and –plumbylenes have been reported by the Izod group,<sup>[17]</sup> this C-H⋯As agostic-type interaction is the first of its type observed crystallographically in a heavier group 14 analogue (the nature of this interaction is supported by DFT calculations, see below).



**Figure 108:** Solid-state structure of the **208**<sup>1</sup><sub>min</sub> disorder component of 1 of 2 independent cations of **208** with H atoms omitted for clarity, with the exception of H(1B). Selected bond lengths (Å) and angles (°) for **208**<sup>1</sup><sub>min</sub>: P(1B)-As(1B) 2.077(14), P(2)-As(1B) 2.192(5), P(1B)-C(25B) 1.874(15), P(1B)-C(37B) 1.834(17), P(2)-C(1) 1.849(3), P(2)-C(13) 1.845(3), H(1B)-As(1B) 2.02(1), P(2)-As(1B)-P(1B) 108.4(4), C(25B)-P(1B)-As(1B) 108.7(11), C(37B)-P(1B)-As(1B) 106.9(16), C(37B)-P(1B)-C(25B) 108.9(12), C(1)-P(2)-As(1B) 95.04(16), C(13)-As(1B)-As(1B) 138.78(19), C(14)-P(2)-C(1) 106.15(13).

## 8.5 Variable-temperature $^{31}\text{P}\{^1\text{H}\}$ and solid-state CP-MAS $^{31}\text{P}\{^1\text{H}\}$ NMR spectra of $[(\text{Dipp})_2\text{P}]_2\text{As}[\text{Al}\{\text{OC}(\text{CF}_3)_3\}\cdot(\text{PhMe})_{0.5}]$ (**208a**)

At room temperature, the  $^1\text{H}$  and  $^{13}\text{C}\{^1\text{H}\}$  NMR spectra of **208a** exhibit broad signals that are consistent with a single ligand environment. At lower temperatures the  $^1\text{H}$  NMR spectra consists of multiple broad, overlapping signals that are difficult to interpret. However, the  $^{31}\text{P}\{^1\text{H}\}$  NMR spectra of **208a** are more informative. While at room temperature no signals are observed, as the temperature is reduced, the spectrum resolved into three broad signals, **A**, **B** and **C**, which, at  $-20\text{ }^\circ\text{C}$  are in a 1:3:1 ratio (Fig. 109). As the temperature is reduced further, peaks **A** and **B** sharpen and resolve into a pair of doublets, while peak **B** sharpens then broadens, although the ratio of **A**:**B**:**C** remains approximately 1:3:1. At  $-90\text{ }^\circ\text{C}$  the spectrum consists of a pair of doublets at 223.9 (A) and  $-34.0\text{ ppm}$  ( $J_{\text{PP}} = 151.8\text{ Hz}$ ), while the signal at 95.2 ppm has significantly broadened to the extent that it is barely resolved, which clearly suggests further decoalesces of this peak. Unfortunately, we were unable to obtain a temperature low enough to observe this behaviour nor observed complete coalescence of the peaks at higher temperatures due to the instability of **208a** above  $40\text{ }^\circ\text{C}$ .

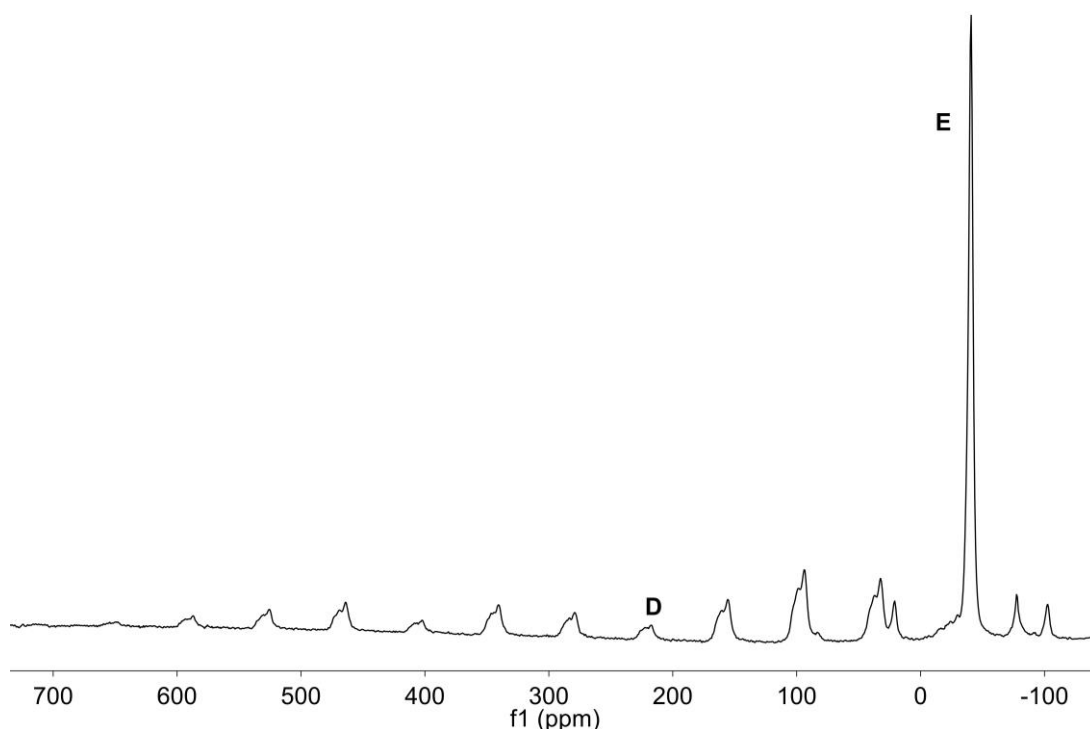


**Figure 109:** Variable-temperature  $^{31}\text{P}\{^1\text{H}\}$  NMR spectra of **208a** in  $\text{CD}_2\text{Cl}_2$

The solid-state  $^{31}\text{P}\{^1\text{H}\}$  CP-MAS NMR spectrum of **208a** exhibits a sharp singlet at  $-40.7\text{ ppm}$  (**D**) with few spinning side bands and a broad signal at  $217.4\text{ ppm}$  (**E**) exhibiting a large degree of chemical shift anisotropy (Fig. 110). The low field signal **D** exhibits some fine structure, which may be associated with the two independent molecules in the asymmetric

unit cell, with the signals due the pyramidal phosphorus centres being coincident but the signals due to the planar phosphorus centres appearing to be slightly different. These signals are clearly consistent with the signals **A** and **C** in the low temperature  $^{31}\text{P}\{^1\text{H}\}$  NMR spectrum. On the basis of their chemical shifts and the large chemical shift anisotropy of the low field signal in the solid-state spectrum, attributed peaks **A** and **B** to the planar and pyramidal phosphorus centres in **208a**, respectively. For comparison, the chemical shifts of the two-coordinate phosphorus centres in phospharsenes typically lie in the range 530-670 ppm; the chemical shift of the planar phosphorus centre in **208a** is closer to that observed for the arsaallyl anion **211** (235.3 ppm for the *E,E*-isomer).<sup>[15]</sup>

However, the identity of the species responsible for peak **B** is less clear. We have previously observed similar NMR behaviour for the isoelectronic diphosphagermylenes **104Ge** and **145Ge**; at -90 °C, the NMR spectrum of **145Ge** consists of a broad signal at 101.5 ppm and a doublet at -84.7 ppm ( $J_{\text{PP}} = 146$  Hz), corresponding the planar and pyramidal phosphorus centres, respectively, along with two signals at 7.2 and -43.3 ppm, which we assigned to two pyramidal phosphorus centres. Therefore, it is likely that the broadening of peak **B** at low temperatures is due to decoalescence into two peaks arising from configurations of **208** with two pyramidal phosphorus centres. DFT calculations support this, as an alternative configuration of **208** with two pyramidal phosphorus centres would give rise to a signal at 34 ppm.



**Figure 110:** Solid-state  $^{31}\text{P}\{^1\text{H}\}$  CP-MAS NMR spectrum of **208a**

## 8.6 DFT calculations

In order to investigate the bonding in **208** and the relative stabilities of the different configurations we carried out a DFT study. We located the minimum energy geometry with one planar and one planar phosphorus centre (**208<sub>plan</sub>**), corresponding to the solid-state structure of **208<sup>1</sup><sub>maj</sub>**, along with the configuration with two pyramidal phosphorus centres (**208<sub>pyr</sub>**) (Fig. 111). We were unable to locate a minimum energy geometry corresponding to **208<sup>1</sup><sub>min</sub>** as each attempt converged to a geometry corresponding to **208<sup>1</sup><sub>maj</sub>**. Geometry **208<sub>plan</sub>** is 25.7 kJ mol<sup>-1</sup> lower in free energy than **208<sub>pyr</sub>**.

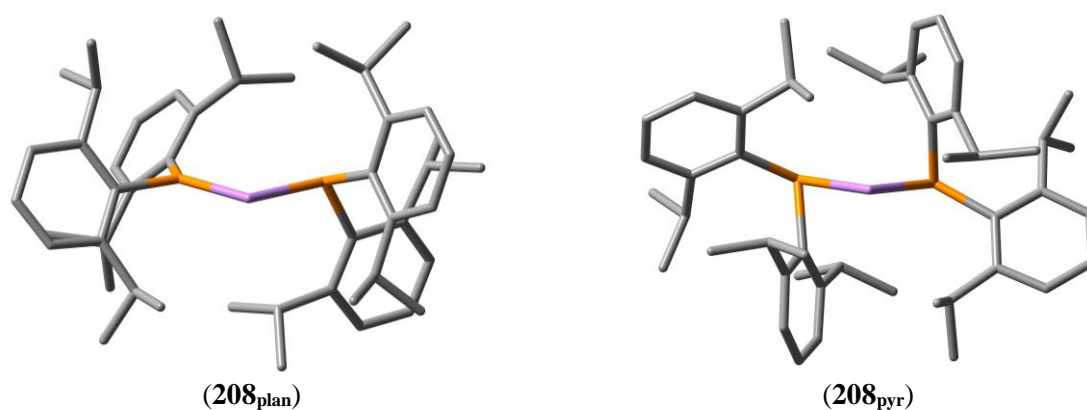


Figure 111: Calculated minimum energy geometries of **208<sup>1</sup><sub>maj</sub>** and **208<sup>2</sup><sub>maj</sub>**

The calculated geometry of **208<sub>plan</sub>** rather accurately reproduces the disorder components **208<sup>1</sup><sub>maj</sub>** and **208<sup>2</sup><sub>maj</sub>** in the solid state structure [P(1A)-As(1A) 2.1501(9), P(2)-As(1A) 2.2925(7) Å, P(1A)-As(1A)-P(2) 105.45(3)°; calculated P-As distances 2.1765 and 2.3003 Å, respectively, and P-As-P angle of 105.748°]. Inspection of the molecular orbitals reveals that the HOMO is a widely distributed orbital with components on the arsenic centre, the two phosphorus atoms and one of the aromatic rings. The P-As  $\pi$ -bond was located in the HOMO-5, although this orbital also has components on the aromatic rings, while the P-As  $\pi^*$ -orbital is the LUMO (Fig. 112). Natural Bond Orbital (NBO) analysis of **208<sub>plan</sub>** reveals that the P-As  $\pi$ -orbital is 57% based on the phosphorus atom and that the lone pair on the arsenic has predominantly s-character, while the lone pair at the pyramidal phosphorus centre has essentially sp-character. NBO analysis also yields Wiberg bond indices of 1.558 and 1.055 for the As-P<sub>plan</sub> and As-P<sub>pyr</sub> bond respectively, which indicates significant multiple bond character of the former bond. For **208<sub>pyr</sub>**, the Wiberg bond indices are both 0.936, suggesting no As-P multiple bond character.



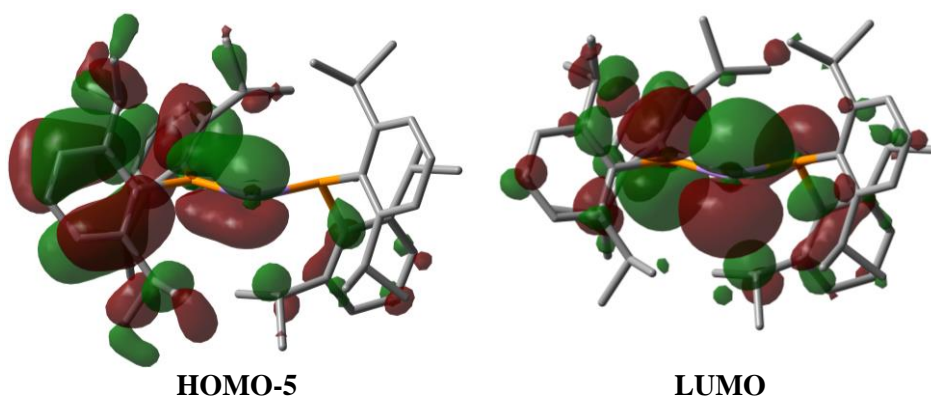


Figure 112: Calculated molecular orbital of **208<sub>plan</sub>**

NBO analysis reveals that, in addition to the P=As  $\pi$  interaction, **208<sub>plan</sub>** is further stabilised by delocalisation of the arsenic lone pair into a P-C  $\sigma^*$ -orbital associated with the planar phosphorus centre. Second order perturbation theory analysis indicates that approximate stabilisation afforded by this interaction [the E(2) energy] is 45 kJ mol<sup>-1</sup>, which is similar in energy to the respective interactions from the Ge/Sn lone pairs in the diphosphatetrylenes **104Ge/Sn** and **145Ge/Sn** [45.1-55.0 kJ mol<sup>-1</sup>] (see Section 4.11). The stabilisation of **208<sub>plan</sub>** may be interpreted as a “push-pull” type, with the *push* arising from the  $\pi$ -donation of the lone pair of the planar phosphorus centre into vacant p-orbital and *pull* arising from the delocalisation of the arsenic lone pair into the P-C  $\sigma^*$ -orbital of the same planar phosphorus centre.

In **208<sub>pyr</sub>** two of the aromatic rings are significantly canted towards the arsenic atom, with  $C_{ipso}\cdots As$  distances of 2.4801 Å, which lie well within the sum of the van der Waals radii of C and As (3.55 Å) and suggests a significantly bonding interaction between these two atoms.<sup>[18]</sup> Consistent with this, NBO analysis of **208<sub>pyr</sub>** reveals significant delocalisation of electron density from the aromatic rings into the “vacant” p-orbital into the arsenic centres, such that the latter orbital has an occupancy of 0.53 electrons and these interactions stabilise **208<sub>pyr</sub>** by 208 kJ mol<sup>-1</sup>. While we observe similar interactions in the calculated pyramidal configurations of the diphosphatetrylenes **104Ge/Sn**, **145Ge/Sn**, **146Ge/Sn**, **147Sn** and **148Sn** the occupancy of the “vacant” p-orbital on the tellurium centres is significantly lower [0.16-0.26 electrons], although the strength of the interaction in **104Ge** and **145Ge** are very similar [206.2 and 215.0 kJ mol<sup>-1</sup>, respectively]. In addition, the arene $\cdots As$  interactions in **208<sub>pyr</sub>** are related to the arene $\cdots As$  interactions in Menshutkin complexes such as SbCl<sub>3</sub>.C<sub>6</sub>H<sub>6</sub>.<sup>[19]</sup> However, the interactions in these systems are significantly lower than that observed in **208<sub>pyr</sub>** (e.g. for AsCl<sub>3</sub> $\cdots$ C<sub>6</sub>H<sub>6</sub> the interaction strength is calculated to be just 27.1 kJ mol<sup>-1</sup>),<sup>[20]</sup> which may be a result of the electron-precise pnictogen centres.

## 8.7 Conclusions

The diphosphachloroarsine **205** was prepared by the reaction between two equivalents of [(Dipp)<sub>2</sub>P]K and AsCl<sub>3</sub>, although it could not be isolated cleanly. Treatment of **205** with Li[Al{OC(CF<sub>3</sub>)<sub>3</sub>}<sub>4</sub>] gave the unusually stable diphosphaarsenium cation **208**, which is the first example of an arsenium cation to have two phosphorus substituents. This compound possesses one planar and one pyramidal phosphorus centre in the solid state, which leads to substantial stabilisation through a P-As interactions. In solution there is a dynamic equilibrium between the configuration with one planar and one pyramidal phosphorus centre and the configuration with two pyramidal phosphorus centres.

## 8.8 Experimental

### 8.8.1 Synthesis of {(Dipp)<sub>2</sub>P}<sub>2</sub>AsCl (**205**)

To a cold (-78 °C) solution of freshly distilled AsCl<sub>3</sub> (0.19 ml, 2.26 mmol) in THF (15 ml) was added a solution of [(Dipp)<sub>2</sub>P]K (1.77 g, 4.51 mmol) in THF (20 ml). The resulting dark brown mixture was allowed to warm to room temperature to give a yellow solution with pale solids. The solvent was removed *in vacuo* to give a sticky yellow solid and the product was extracted into Et<sub>2</sub>O (15 ml). The pale solids were removed by filtration and the solvent from the yellow filtrate was removed *in vacuo* to give **205** as a yellow foam, which contains approximately 20% (Dipp)<sub>2</sub>PH as shown by <sup>31</sup>P NMR spectroscopy. Yield: 1.45 g, 79%.

<sup>31</sup>P{<sup>1</sup>H} NMR [d<sub>8</sub>-toluene, 253 K]: δ -25.77 (d, *J*<sub>PP</sub> = 135 Hz), -21.92 (d, *J*<sub>PP</sub> = 135 Hz).

### 8.8.2 Synthesis of [{(Dipp)<sub>2</sub>P}<sub>2</sub>As][Al{OC(CF<sub>3</sub>)<sub>3</sub>}<sub>4</sub>].(PhMe)<sub>0.5</sub> (**208a**)

To a mixture of {(Dipp)<sub>2</sub>P}AsCl (0.358 g, 0.44 mmol) and Li[Al{OC(CF<sub>3</sub>)<sub>3</sub>}<sub>4</sub>] (0.427 g, 0.44 mmol) was added PhF (15 ml). The resulting dark green solution with pale solids was stirred for 1 h and filtered. The solvent was removed from the filtrate *in vacuo* to give a sticky dark green solid. This solid was dissolved in a mixture of toluene (15 ml) and PhF (2 ml). Storage at -25 °C caused the precipitation of a dark green oil that slowly turned into dark green crystals of ([{(Dipp)<sub>2</sub>P}<sub>2</sub>As][Al{OC(CF<sub>3</sub>)<sub>3</sub>}<sub>4</sub>])<sub>2</sub>.(PhMe)<sub>3</sub> (**208**). The supernatant solution was removed by decantation and the remaining solid was washed with cold (0 °C) light petroleum (2 x 5 ml). The residual solvent was removed under vacuum to give the alternate

solvate  $[(\text{Dipp})_2\text{P}]_2\text{As}[\text{Al}\{\text{OC}(\text{CF}_3)_3\}_4](\text{PhMe})_{0.5}$  (**208a**) as a green solid. Yield: 0.51 g, 65%.

$^1\text{H}$  NMR [ $\text{CD}_2\text{Cl}_2$ , 298 K]:  $\delta$  1.11 (br. s, 48H,  $\text{CHMe}_2$ ), 3.40 (s, 1.5H,  $\text{PhMe}$ ), 3.40 (br. s, 8H,  $\text{CHMe}_2$ ), 7.14-7.14 (m, 1H,  $\text{PhMe}$ ), 7.23-7.26 (m, 1H,  $\text{PhMe}$ ), 7.35 (br. m, 8H, ArH), 7.60 (t,  $J_{\text{HH}} = 7.7$  Hz, 4H, ArH).  $^{13}\text{C}\{^1\text{H}\}$  NMR [ $\text{CD}_2\text{Cl}_2$ , 298 K]:  $\delta$  21.72 ( $\text{PhMe}$ ), 24.98 (br. s,  $\text{CHMe}_2$ ), 36.69 (br. s,  $\text{CHMe}_2$ ), 121.87 (q,  $J_{\text{CF}} = 290$  Hz,  $\text{OC}(\text{CF}_3)_3$ ), 125.83 ( $\text{PhMe}$ ), 127.15 (br. s, ArH), 128.76, 129.57 ( $\text{PhMe}$ ), 131.83 (br. s, Ar), 134.55 (br. s, ArH), 138.57 ( $\text{PhMe}$ ), 153.89 (br. s, Ar).

## 8.9 References

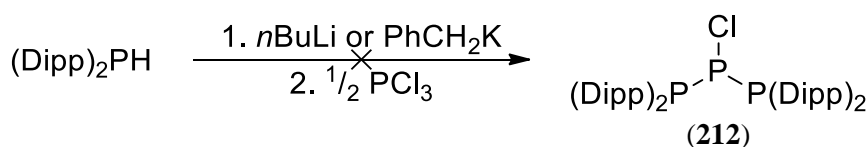
- [1] K. Dimroth, P. Hoffmann, *Angew. Chem. Int. Ed.*, **1964**, 3, 384-384.
- [2] (a) A. Igau, H. Grutzmacher, A. Baceiredo, G. Bertrand, *J. Am. Chem. Soc.*, **1988**, 110, 6463-6466; (b) A. J. Arduengo, R. L. Harlow, M. Kline, *J. Am. Chem. Soc.*, **1991**, 113, 361-363.
- [3] A. H. Cowley, M. C. Cushner, J. S. Szobota, *J. Am. Chem. Soc.*, **1978**, 100, 7784-7786.
- [4] R. W. Alder, P. R. Allen, M. Murray, A. G. Orpen, *Angew. Chem. Int. Ed.*, **1996**, 35, 1121-1123.
- [5] S. Loss, C. Widauer, H. Grützacher, *Angew. Chem. Int. Ed.*, **1999**, 38, 3329-3331.
- [6] V. D. Romanenko, V. L. Rudzevich, E. B. Rusanov, A. N. Chernega, A. Senio, J.-M. Sotiropoulos, G. Pfister-Guillouzo, M. Sanchez, *J. Chem. Soc., Chem. Commun.*, **1995**, 1383.
- [7] J. B. Waters, T. A. Everitt, W. K. Myers, J. M. Goicoechea, *Chem Sci*, **2016**, 7, 6981-6987.
- [8] (a) P. Jutzi, T. Wippermann, C. Krüger, H.-J. Kraus, *Angew. Chem. Int. Ed.*, **1983**, 22, 250-250; (b) R. J. Wiacek, J. N. Jones, C. L. B. Macdonald, A. H. Cowley, *Can. J. Chem.*, **2002**, 80, 1518-1523.
- [9] A. Kraft, J. Beck, I. Krossing, *Chem. Eur. J.*, **2011**, 17, 12975-12980.
- [10] C. Hering, J. Rothe, A. Schulz, A. Villinger, *Inorg. Chem.*, **2013**, 52, 7781-7790.
- [11] (a) C. Hering, M. Lehmann, A. Schulz, A. Villinger, *Inorg. Chem.*, **2012**, 51, 8212-8224; (b) W. Baumann, A. Schulz, A. Villinger, *Angew. Chem. Int. Ed. Engl.*, **2008**, 47, 9530-9532.
- [12] A. Hinz, A. Schulz, A. Villinger, *Inorg. Chem.*, **2016**, 55, 3692-3699.
- [13] A. H. Cowley, J. E. Kilduff, J. G. Lasch, S. K. Mehrotra, N. C. Norman, M. Pakulski, B. R. Whittlesey, J. L. Atwood, W. E. Hunter, *Inorg. Chem.*, **1984**, 23, 2582-2593.
- [14] B. Twamley, P. P. Power, *Chem. Commun.*, **1998**, 1979-1980.
- [15] L. S. Dixon, L. K. Allen, R. J. Less, D. S. Wright, *Chem. Commun.*, **2014**, 50, 3007-3009.
- [16] K. Izod, D. G. Rayner, S. M. El-Hamruni, R. W. Harrington, U. Baisch, *Angew. Chem. Int. Ed. Engl.*, **2014**, 53, 3636-3640.
- [17] (a) K. Izod, C. M. Dixon, R. W. Harrington, M. R. Probert, *Chem. Commun.*, **2015**, 51, 679-681; (b) K. Izod, C. Wills, M. R. Probert, R. W. Harrington, *Main Group Met. Chem.*, **2014**, 37; (c) K. Izod, C. Wills, W. Clegg, R. W. Harrington, *Organometallics*, **2009**, 28, 2211-2217; (d) K. Izod, C. Wills, W. Clegg, R. W. Harrington, *Organometallics*, **2009**, 28, 5661-5668; (e) K. Izod, W. McFarlane, C. Wills, W.

- Clegg, R. W. Harrington, *Organometallics*, **2008**, 27, 4386-4394; (f) K. Izod, W. McFarlane, B. V. Tyson, I. Carr, W. Clegg, R. W. Harrington, *Organometallics*, **2006**, 25, 1135-1143.
- [18] M. Mantina, A. C. Chamberlin, R. Valero, C. J. Cramer, D. G. Truhlar, *J. Phys. Chem. A*, **2009**, 113, 5806-5812.
- [19] (a) I. Caracelli, I. Haiduc, J. Zukerman-Schpector, E. R. T. Tiekink, *Coord. Chem. Rev.*, **2013**, 257, 2863-2879; (b) H. Schmidbaur, A. Schier, *Organometallics*, **2008**, 27, 2361-2395; (c) H. Schmidbaur, R. Nowak, O. Steigelmann, G. Müller, *Chem. Ber.*, **1990**, 123, 1221-1226; (d) H. Schmidbaur, R. Nowak, B. Huber, G. Mueller, *Organometallics*, **1987**, 6, 2266-2267; (e) D. Mootz, V. Handler, *Z. Anorg. Allg. Chem.*, **1986**, 533, 23-29; (f) B. Twamley, C. D. Sofield, M. M. Olmstead, P. P. Power, *J. Am. Chem. Soc.*, **1999**, 121, 3357-3367; (g) G. Bombieri, G. Peyronel, I. M. Vezzosi, *Inorg. Chim. Acta*, **1972**, 6, 349-354.
- [20] J. Zukerman-Schpector, A. Otero-de-la-Roza, V. Luana, E. R. Tiekink, *Chem. Commun.*, **2011**, 47, 7608-7610.

## Chapter 9. Attempted synthesis of a phosphonium cation

### 9.1 Attempted synthesis of $\{(\text{Dipp})_2\text{P}\}_2\text{PCl}$ (**212**)

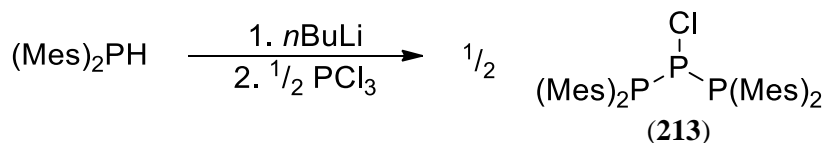
Given the successful use  $\{(\text{Dipp})_2\text{P}\}_2\text{AsCl}$  (**205**) in the synthesis of the arsenium cation **208**, which is stabilised by a planar phosphorus centre, we attempted to prepare the chlorophosphine analogue  $\{(\text{Dipp})_2\text{P}\}_2\text{PCl}$  (**212**) as a precursor to a diphosphaphosphenium cation (Scheme 43). However, the reaction between two equivalents of either *in-situ* generated  $[(\text{Dipp})_2\text{P}]\text{Li}$  or  $[(\text{Dipp})_2\text{P}]\text{K}$  with  $\text{PCl}_3$  in cold THF or  $\text{Et}_2\text{O}$  gave a multitude of unidentifiable phosphorus-containing species, as judged by  $^{31}\text{P}\{^1\text{H}\}$  NMR spectroscopy. We propose that the transfer reagents  $[(\text{Dipp})_2\text{P}]\text{M}$  ( $\text{M} = \text{Li}, \text{K}$ ) are insufficiently nucleophilic and that the intermediate  $\{(\text{Dipp})_2\text{P}\}\text{PCl}_2$  is too hindered for the second metathesis reaction to proceed, such that side reactions occur as the solution is warmed to room temperature; this is similar to the behaviour we observed in the attempted synthesis of  $\{(\text{Dipp})_2\text{P}\}_2\text{SiCl}_2$  (**190**) using  $[(\text{Dipp})_2\text{P}]\text{Li}$  as the transfer reagent. Therefore, we anticipated that a less bulky phosphide ligand would be more suitable and so targeted the diphosphachlorophosphine  $\{(\text{Mes})_2\text{P}\}_2\text{PCl}$  (**213**).



Scheme 43: Attempted synthesis of **212**

### 9.2 Synthesis of $\{(\text{Mes})_2\text{P}\}_2\text{PCl}$ (**213**)

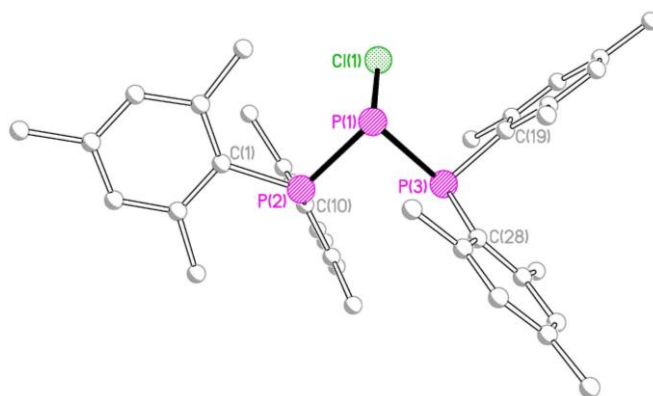
Treatment of  $\text{PCl}_3$  with two equivalents of *in-situ* generated  $[(\text{Mes})_2\text{P}]\text{Li}$  in cold  $\text{Et}_2\text{O}$  gives  $\{(\text{Mes})_2\text{P}\}_2\text{PCl}$  (**213**) as a yellow solid (Scheme 44). As expected, compound **213** exhibits an  $\text{AX}_2$  pattern in its  $^{31}\text{P}\{^1\text{H}\}$  NMR spectrum in  $\text{CDCl}_3$ , with a triplet at 117.2 ppm ( $J_{\text{PP}} = 255$  Hz) corresponding to the  $\text{PCl}$  environment and the doublet at -22.7 ppm ( $J_{\text{PP}} = 255$  Hz) corresponding to the  $(\text{Mes})_2\text{P}$  environments.



Scheme 44: Synthesis of **213**

### 9.3 Solid-state structure of {(Mes)<sub>2</sub>P}<sub>2</sub>PCl (**213**)

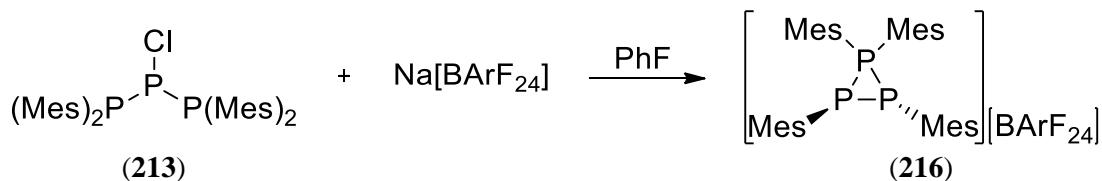
The structure of **213** is shown in Figure 113, along with selected bond lengths and angles. Compound **213** is the first example of an acyclic diphosphachlorophosphine to be characterised by X-ray crystallography.<sup>[1]</sup> The P-P distances [2.1849(6) and 2.2437(6) Å] are rather unsymmetrical, but are typical of P-P distances in chlorophosphines; for example, the P-P distance in the cyclic triphosphine {(μ-Mes\*P)PCl}<sub>2</sub> (**214**) range from 2.1905(5) to 2.2731(5) Å.<sup>[1a]</sup> The P-Cl distance [2.1017(6) Å] is similar to the respective distances in **214** [2.0967(5) and 2.1061(6) Å] and (tBuP)<sub>3</sub>PCl (**215**) [2.0971(8) Å].<sup>[1]</sup>



**Figure 113:** Molecular structure of **213** with H atoms omitted for clarity. Selected bond lengths (Å) and angles (°): P(1)-Cl(1) 2.1017(6), P(1)-P(2) 2.1849(6), P(1)-P(3) 2.2437(6), P(2)-C(1) 1.8442(16), P(2)-C(10) 1.8393(17), P(3)-C(19) 1.8508(17), P(3)-C(28) 1.8524

### 9.4 Chloride abstraction from {(Mes)<sub>2</sub>P}<sub>2</sub>PCl (**213**)

The reaction between **213** and Na[BArF<sub>24</sub>] in fluorobenzene initially gives a dark purple solution that gradually fades to pale yellow over 5 minutes to give the diphosphaphosphonium cation [{μ-(Mes)P}<sub>2</sub>P(Mes)<sub>2</sub>][BArF<sub>24</sub>] (**216**) in near quantitative yield, as judged by <sup>31</sup>P{<sup>1</sup>H} NMR spectroscopy (Scheme 45). A small amount of single colourless crystals of **216**·(C<sub>7</sub>H<sub>14</sub>) were obtained by layering a concentrated solution of **216** in fluorobenzene with methylcyclohexane and were characterised by X-ray crystallography.



**Scheme 45:** Synthesis of **216**

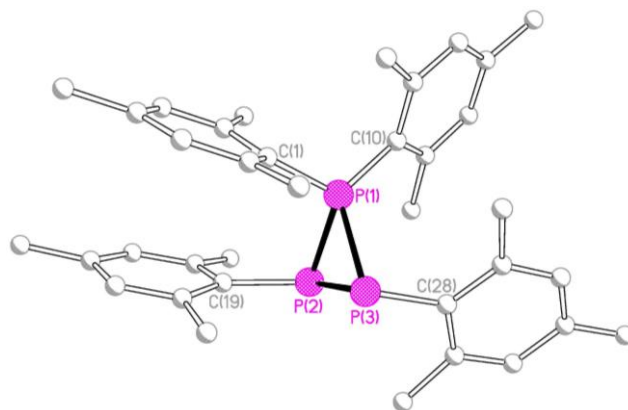
Similarly, the reactions between **213** and either Li[Al{OC(CF<sub>3</sub>)<sub>3</sub>}<sub>4</sub>] or GaCl<sub>3</sub> undergo the same colour changes, with the resulting pale yellow reaction mixtures exhibiting identical <sup>31</sup>P{<sup>1</sup>H} NMR spectra to **216**·(C<sub>7</sub>H<sub>14</sub>)<sub>0.5</sub> (see below). However, the putative salts

$[\{\mu\text{-(Mes)P}\}_2\text{P(Mes)}_2][\text{M}]$  ( $[\text{M}] = \text{GaCl}_4^-, [\text{Al}\{\text{OC}(\text{CF}_3)_3\}_4]^-$ ) were only obtained as pale yellow oils, which were not suitable for further characterisation.

Although the reaction between **213** and  $\text{Na}[\text{BArF}_{24}]$  to give **216** proceeds almost quantitatively, as judged by  $^{31}\text{P}\{^1\text{H}\}$  NMR spectroscopy, the isolated yield of the alternative solvate **216**· $(\text{C}_7\text{H}_{14})_{0.5}$  was very low (<5%), which likely a result of the quantity of fluorobenzene required for the growth of high quality crystals also solvating the majority of the product. The solvent of crystallisation is only very weakly held and partially lost under vacuum. Compound **216**· $(\text{C}_7\text{H}_{14})_{0.5}$  exhibits a triplet at -46.2 ppm ( $J_{\text{PP}} = 312$  Hz) and a doublet at -97.9 ppm ( $J_{\text{PP}} = 312$  Hz) in its  $^{31}\text{P}\{^1\text{H}\}$  NMR spectrum in  $\text{CDCl}_3$ , which correspond to the  $(\text{Mes})_2\text{P}$  and  $(\text{Mes})\text{P}$  environments, respectively. In an attempt to improve the yield of isolated material, addition of neat methylcyclohexane to the reaction mixture after the removal of the  $\text{LiCl}$  side-product and solvent immediately precipitated **216**· $(\text{C}_7\text{H}_{14})_{0.5}$ , as a pale yellow microcrystalline material. However, this crop of **216**· $(\text{C}_7\text{H}_{14})_{0.5}$  was contaminated with a small quantity (approximately 10%) of  $[(\text{Mes})_2\text{P(H)P(Mes)}_2][\text{BArF}_{24}]$ , which was identified by  $^{31}\text{P}$  NMR spectroscopy.

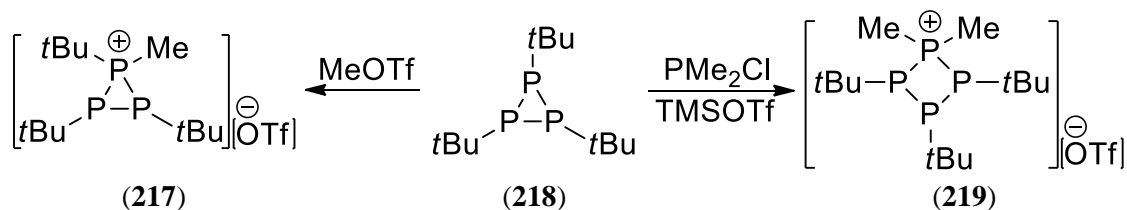
### 9.5 Solid-state structure of $[\{\mu\text{-(Mes)P}\}_2\text{P(Mes)}_2][\text{BArF}_{24}]\cdot(\text{C}_7\text{H}_{14})$ (**216**)· $(\text{C}_7\text{H}_{14})$

Compound **216**· $(\text{C}_7\text{H}_{14})$  crystallizes with two crystallographically independent cation/anion pairs in the asymmetric unit, the conformations of which differ only slightly, along with two highly disordered methylcyclohexane molecules that could not be sensibly modelled (Fig. 114); the cations and anions are reasonably well separated (closest P...F distance >3.5 Å). Compound **216** has a cyclic  $\text{P}_3$  core, in which the P-P-P angles at the four-coordinate phosphorus centres [P-P-P angles at P(1) and P(4) both  $61.90(4)^\circ$ ] are slightly larger than the respective angles at the three-coordinate phosphorus centres [P-P-P angles at P(2)  $58.91(3)$ ; P(3)  $59.19(3)$ ; P(5)  $58.91(4)$ ; P(6)  $59.19(4)^\circ$ ]. In addition, the P-P distances at the four-coordinate centres [ranging from  $2.1984(10)$  to  $2.2075(11)$  Å] are greater than the distances between the two pairs of three-coordinate phosphorus centres [P(2)-P(3)  $1.798(3)$ , P(5)-P(6)  $1.858(3)$  Å]. Almost identical bond lengths and angles are observed in  $[(t\text{BuP})_3\text{Me}][\text{OTf}]$  (**217**), which has an analogous framework (see below).<sup>[2]</sup> The mesityl groups on the three coordinate phosphorus centres adopt a *trans*-arrangement with the planes of the aromatic rings on the P(2) and P(5) centres lying parallel to the corresponding ring of the respective  $\text{P(Mes)}_2$  group. These rings have an interplane separation of 3.6 Å and this stacking interaction may contribute to the overall stability of the cationic species.



**Figure 114:** Molecular structure of one of the two independent cation of **216** ( $C_7H_{14}$ ) with hydrogen atoms omitted for clarity. Selected bond lengths (Å) and bond angles ( $^\circ$ ): (molecule 1) P(1)-P(2) 2.2048(11), P(1)-P(3) 2.1984(10), P(2)-P(3) 2.2645(11), P(1)-C(1) 1.798(3), P(1)-C(10) 1.807(3), P(2)-C(19) 1.834(3), P(3)-C(28) 1.845(3), P(2)-P(1)-P(3) 61.90(4), P(1)-P(2)-P(3) 58.91(3), P(1)-P(3)-P(2) 59.19(3), (molecule 2) P(4)-P(5) 2.2075(11), P(4)-P(6) 2.2010(10), P(5)-P(6) 2.2673(12), P(4)-C(37) 1.795(3), P(4)-C(46) 1.813(3), P(5)-C(55) 1.830(4), P(6)-C(64) 1.858(3), P(5)-P(4)-P(6) 61.90(4), P(4)-P(5)-P(6) 58.91(4), P(4)-P(6)-P(5) 59.19(4).

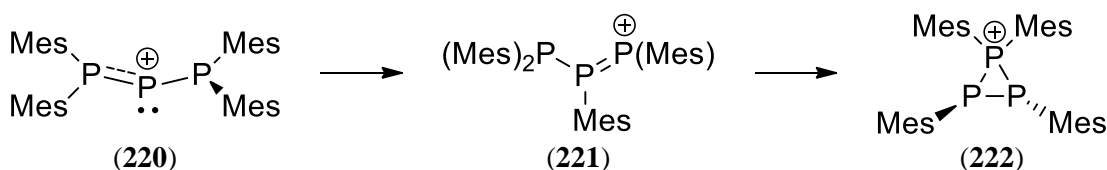
In addition to **217**, a series of *catena*-polyphosphorus cations  $(PR)_nR'P_2^+$  ( $n = 2, 3, 4$ ;  $R = \text{Me}, t\text{Bu}, \text{Cy}, \text{Ph}$ ;  $R' = \text{H}, \text{Me}, t\text{Bu}$ ) have been reported by Burford and co-workers.<sup>[2-3]</sup> These compounds were prepared by either the alkylation or the insertion of a dialkylphosphenium cation into the P-P bond of the corresponding cyclic phosphine, as shown in Scheme 46 for the synthesis of **217** or **219** from the triphosphine **218**.<sup>[2]</sup>



**Figure 46:** Synthesis of *catena*-polyphosphorus cations

## 9.6 Proposed mechanisms for the formation of $[\{\mu-(\text{Mes})\text{P}\}_2\text{P}(\text{Mes})_2][\text{BArF}_4]$ (**216**)

We propose that the initial halide abstraction from **213** gives the putative diphosphaphosphenium cation  $\{(\text{Mes})_2\text{P}\}_2\text{P}^+$  (**220**) and that this first undergoes a 1,2-aryl migration to form the diphosphene cation **221**, which subsequently undergoes cyclization to give the diphosphaphosphenium **222** (Scheme 47).

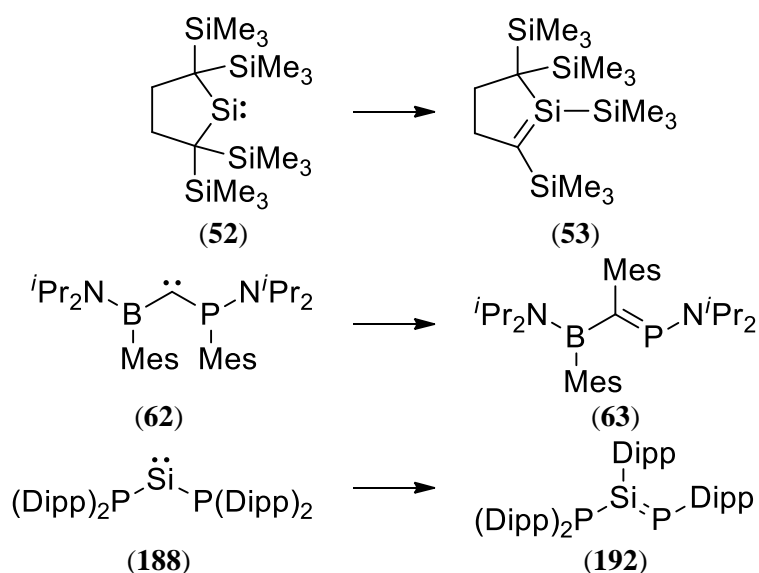


**Scheme 47:** Proposed rearrangement of **220**



In support of this, the diphosphene salt  $[\text{Mes}^*\text{MeP}=\text{PMes}^*][\text{OTf}]$  (**198**) reported has been isolated previously by Grützmacher and has a similar structure to that of the proposed intermediate **221**, in which the cationic two-coordinate phosphorus centre is stabilised by the adjacent phosphide ligand.<sup>[4]</sup>

Similar aryl and alkyl migrations have been observed for the dialkylsilylene **52**,<sup>[5]</sup> (boryl)(phospha)carbene **62**<sup>[6]</sup> and putative diphosphasilylene **188** to give the rearranged species **53**, **63** and **192**, respectively (Scheme 48). However, **63** and **192** do not undergo cyclization, which may be a result of the electronic and steric stabilisation of the boron and phosphorus centres, respectively, or the difference in the charges of these systems compared to **221**.



**Scheme 48:** Previously observed migrations of tetrylenes

The reactivity of the putative intermediate **220** contrasts with that of its isoelectronic and isosteric silicon analogue  $\{(\text{Mes})_2\text{P}\}_2\text{Si}$  (**173**), which dimerizes to give the disilene **181**, and is more similar to the bulkier derivative  $\{(\text{Dipp})_2\text{P}\}_2\text{Si}$  (**188**). It is possible that the aryl-migrations of **188** and **220** occur through a configuration with a planar geometry of one of the phosphide ligands; we anticipate such configurations would be stabilised by the  $\pi$ -accepting ability of the two-coordinate phosphorus centre in **220** and the steric bulk of the phosphide ligands in **188**. If the aryl-migrations occur through a planar configuration this may offer an explanation as to why **173** is stable towards such migrations, since DFT calculations predict the planar configuration of this compound is highly disfavoured, although a detailed DFT and NMR study is required to confirm this hypothesis.

We tentatively suggest that the intense purple colour of the initial reaction mixtures of **213** with a range of chloride abstraction reagents is due to the  $n \rightarrow \pi^*/\pi \rightarrow \pi^*$  transitions of the P=P bonds in either the diphosphaphosphenium cation **220**, with a planar configuration at one of the substituent phosphorus atoms, or the cationic diphosphene **221**. Similar strong absorptions have been observed in species with P=E bonds [E = Ge, Sn, As]. Unfortunately, we have not yet been able to obtain  $^{31}\text{P}\{^1\text{H}\}$  NMR spectra of the initial purple solutions to determine the species present.

## 9.7 Conclusions

The diphosphachlorophosphine **213** was prepared in excellent yield and purity from the reaction between two equivalents of  $[(\text{Mes})_2\text{P}]\text{Li}$  and  $\text{PCl}_3$  in  $\text{Et}_2\text{O}$ . The reaction between **213** and a range of chloride abstraction reagents gives the corresponding diphosphaphosphonioum salts  $[\{\mu-(\text{Mes})\text{P}\}_2\text{P}(\text{Mes})_2][\text{M}]$  ( $[\text{M}] = \text{BArF}_{24}, \text{GaCl}_4, [\text{Al}\{\text{OC}(\text{CF}_3)_3\}_4]$ ) in near quantitative yields, as judged by  $^{31}\text{P}\{^1\text{H}\}$  NMR spectroscopy of the crude reaction mixtures, although only the  $\text{BArF}_{24}$  salt **216**· $(\text{C}_7\text{H}_{14})_{0.5}$  was isolated as a solid material. The rearrangement of the **220** is similar to that we observe for the putative diphosphasilylene **188**, although the proposed intermediate **221** undergoes a further cyclization.

The apparent instability of **220** contrasts that of the diphosphaarsenium cation  $[\{(\text{Dipp})_2\text{P}\}_2\text{As}][\text{Al}\{\text{OC}(\text{CF}_3)_3\}_4]$  (**208**), which is stable in the solid state for long periods and decomposes slowly in solution.

## 9.8 Experimental

### 9.8.1 Synthesis of $\{(\text{Mes})_2\text{P}\}_2\text{PCl}$ (**213**)

To a solution of  $(\text{Mes})_2\text{PH}$  (1.59 g, 5.88 mmol) in  $\text{Et}_2\text{O}$  (20 ml) a solution of  $n\text{BuLi}$  in hexanes (2.3 M, 2.6 ml, 5.98 mmol) was added. The resulting orange solution was stirred for 1 h and added, dropwise, to a cold ( $-78^\circ\text{C}$ ) solution of  $\text{PCl}_3$  (0.25 ml, 2.86 mmol) in  $\text{Et}_2\text{O}$  (20 ml). The yellow solution with pale solids was allowed to warm to room temperature and the solvent removed *in vacuo*. The product was extracted into toluene (20 ml) and the pale solids were removed by filtration. The solvent was removed from the yellow filtrate *in vacuo* to give **213** as a yellow foam. Yield: 1.69 g, 95%. Alternatively, crystalline material was obtained, albeit in a lower yield, by allowing a hot ( $60^\circ\text{C}$ ) solution of the previously isolated material in a mixture of toluene (10 ml) and light petroleum (5 ml) to cool to room temperature and stand overnight, giving the product as large yellow crystals. Further crystalline material was deposited by storing this mixture at  $-25^\circ\text{C}$  overnight. The supernatant solution was removed by filtration and the yellow crystalline material was washed with light petroleum (5 ml) before the residual solvent was removed under vacuum. Yield: 0.61 g, 34%. The two batches of **213** have identical composition, as judged by  $^1\text{H}$  and  $^{31}\text{P}\{^1\text{H}\}$  NMR spectroscopy.

$^1\text{H}$  NMR [ $\text{CDCl}_3$ ]:  $\delta$  2.24 (s, 12 H, *p*-Me), 2.37 (br. s, 24 H, *o*-Me), 6.80 (s, 8 H, ArH).  $^{13}\text{C}\{^1\text{H}\}$  NMR [ $\text{CDCl}_3$ ]:  $\delta$  21.01 (*p*-Me), 24.45 (*o*-Me), 129.75 (ArH), 130.48, 138.31, 143.63 (br., Ar).  $^{31}\text{P}$  NMR [ $\text{CDCl}_3$ ]:  $\delta$  -22.7 (d,  $J_{\text{PP}} = 255$  Hz,  $\text{P}(\text{Mes})_2$ ), 117.2 (t,  $J_{\text{PP}} = 255$  ppm, PCl).

### 9.9 Synthesis of $\{[\mu-(\text{Mes})\text{P}]_2\text{P}(\text{Mes})_2\}[\text{BArF}_{24}] \cdot (\text{C}_7\text{H}_{14})$ (**216**) $\cdot (\text{C}_7\text{H}_{14})$

To a mixture of  $\{(\text{Mes})_2\text{P}\}_2\text{PCl}$  (0.388 g, 0.64 mmol) and  $\text{NaBArF}_{24}$  (0.568 g, 0.64 mmol) was added PhF (15 ml). The resulting dark purple solution gradually faded to a pale yellow solution with pale solids over a period of 5 minutes and was further stirred for 30 min. The resulting mixture was filtered and the filtrate was reduced in volume to  $\sim 3$  ml. Methylcyclohexane (20 ml) was carefully layered onto this concentrated yellow solution. Standing of this mixture at room temperature over one week formed a small amount of white crystalline material that was shown by X-ray crystallography to be (**216**) $\cdot (\text{C}_7\text{H}_{14})$ .

The NMR data reported below are for the alternative solvate (**216**) $\cdot (\text{C}_7\text{H}_{14})_{0.5}$ .

$^1\text{H}$  NMR [ $\text{CDCl}_3$ ]:  $\delta$  0.86 (d,  $J_{\text{HH}} = 6.5$  Hz, 2.1H,  $\text{C}_7\text{H}_{14}\text{-CH}_3$ ), 1.08-1.26 (m, 1.8H,  $\text{C}_7\text{H}_{14}\text{-CH}_2$ ), 1.33 (m, 0.5H,  $\text{C}_7\text{H}_{14}\text{-CH}$ ), 1.62-1.68 (m, 2.7H,  $\text{C}_7\text{H}_{14}\text{-CH}_2$ ), 2.15 (s, 18H, *o*-Me), 2.16 (s, 6H, *o*-Me), 2.50 (s, 12H, *p*-Me), 6.64 (s, 2H, Mes-ArH), 6.73 (s, 2H, Mes-ArH), 6.74 (s, 4H, Mes-ArH), 7.51 (s, 4H, BArF<sub>24</sub>-ArH), 7.71 (s, 8H, BArF<sub>24</sub>-ArH).  $^{13}\text{C}\{^1\text{H}\}$  NMR [ $\text{CDCl}_3$ ]:  $\delta$  20.94 (*o*-Me), 21.07 (d,  $J_{\text{PC}} = 1.7$  Hz, *o*-Me), 23.07 ( $\text{C}_7\text{H}_{14}\text{-CH}_3$ ), 24.27 (t,  $J_{\text{PC}} = 10.3$  Hz, *p*-Me), 24.82 (br. m, *o*-Me), 26.49, 26.61 ( $\text{C}_7\text{H}_{14}\text{-CH}_2$ ), 32.89 ( $\text{C}_7\text{H}_{14}\text{-CH}$ ), 35.60 ( $\text{C}_7\text{H}_{14}\text{-CH}_2$ ), 113.98 (d,  $J_{\text{PC}} = 56.1$  Hz, Mes-Ar), 117.57 (m, BArF<sub>24</sub>-Ar), 118.53 (td,  $J_{\text{PC}} = 22.2$  Hz,  $J_{\text{PC}} = 8.6$  Hz, Mes-Ar), 124.70 (q,  $J_{\text{CF}} = 272$  Hz, BArF<sub>24</sub>-Ar), 129.03 (qm,  $J_{\text{CF}} = 31.3$  Hz, BArF<sub>24</sub>-Ar), 130.53 (d,  $J_{\text{PC}} = 2.6$  Hz, Mes-ArH), 132.06 (d,  $J_{\text{PC}} = 13.0$  Hz, Mes-ArH), 134.96 (Mes-ArH), 142.18 (d,  $J_{\text{PC}} = 3.3$  Hz, Mes-Ar), 143.93 (m, Mes-Ar), 145.30 (d,  $J_{\text{PC}} = 4.0$  Hz, Mes-Ar), 161.84 (q,  $J_{\text{CB}} = 49.7$  Hz, BArF<sub>24</sub>).  $^{19}\text{F}\{^1\text{H}\}$  NMR [ $\text{CDCl}_3$ ]:  $\delta$  -62.5 (s).  $^{31}\text{P}\{^1\text{H}\}$  NMR [ $\text{CDCl}_3$ ]:  $\delta$  97.7 (d,  $J_{\text{PP}} = 312$  Hz, 2P, (Mes)P), -46.2 (t,  $J_{\text{PP}} = 312$  Hz, 1P, (Mes)<sub>2</sub>P).

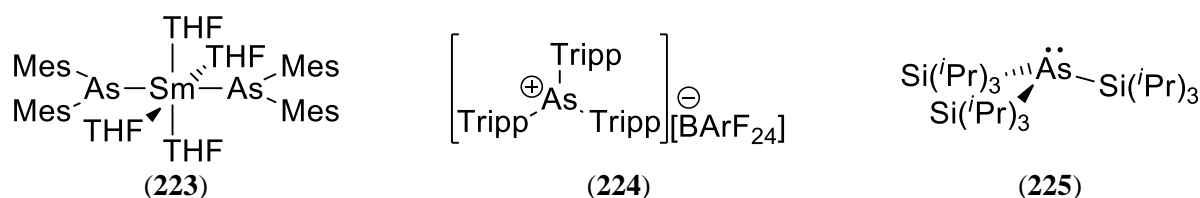
## 9.10 References

- [1] (a) J. Bresien, C. Hering, A. Schulz, A. Villinger, *Chem. Eur. J.*, **2014**, *20*, 12607-12615; (b) B. Riegel, A. Pfitzner, G. Heckmann, H. Binder, E. Fluck, *Z. Anorg. Allg. Chem.*, **1995**, *621*, 1365-1372.
- [2] N. Burford, C. A. Dyker, M. Lumsden, A. Decken, *Angew. Chem. Int. Ed. Engl.*, **2005**, *44*, 6196-6199.
- [3] C. A. Dyker, N. Burford, G. Menard, M. D. Lumsden, A. Decken, *Inorg. Chem.*, **2007**, *46*, 4277-4285.
- [4] S. Loss, C. Widauer, H. Grützmacher, *Angew. Chem. Int. Ed.*, **1999**, *38*, 3329-3331.
- [5] M. Kira, S. Ishida, T. Iwamoto, C. Kabuto, *J. Am. Chem. Soc.*, **1999**, *121*, 9722-9723.
- [6] F. Lavigne, E. Maerten, G. Alcaraz, N. Saffon-Merceron, C. Acosta-Silva, V. Branchadell, A. Baceiredo, *J. Am. Chem. Soc.*, **2010**, *132*, 8864-8865.

## Chapter 10. Diarsatetrylenes

### 10.1 Background

In Chapter 4, we discussed the synthesis of an array of diphosphatetrylenes, of which compounds **104Sn**, **145Ge** and **148Sn** are stabilised by P-Ge/Sn  $p\pi$ - $p\pi$  interactions from a planar phosphorus centre in the solid-state.<sup>[1]</sup> We now sought to prepare heavier tetrylenes featuring bulky arsenide ligands as it has been predicted that phosphorus and arsenic have similar  $\pi$ -donor capacity to that of nitrogen, if the energy of planarization is ignored.<sup>[2]</sup> We were intrigued to see whether a tetrylene featuring two bulky arsenide substituents would promote planarization of an arsenic centre. The resulting  $p\pi$ - $p\pi$  interactions from the planar arsenic should be weaker than in their phosphorus analogues, which may result in increased reactivity towards small molecules (see Section 1.7.2). However, examples of planar, three-coordinate arsenic centres are very rare, as the energy barrier of planarization for arsenic is higher than that of phosphorus. For example, the energy barrier to inversion, which correlates directly to the energy of planarization, of  $\text{PH}_3$  and  $\text{AsH}_3$  has been calculated to be 146.8 and 164.0 kJ mol<sup>-1</sup>, respectively, at the MP2 level of theory.<sup>[3]</sup> Compounds featuring planar arsenic centres include a small number of transition metal arsenide complexes,<sup>[4]</sup> the samarium(II) arsenide complex **223**<sup>[5]</sup>, in which the planar configuration is a consequence of the ionic bonding in Ln(II) compounds, and the arsinyl radical **224**<sup>[6]</sup> (Fig. 115). To the best of our knowledge, no examples of main group compounds containing a neutral, three-coordinate arsenic have been reported. For comparison, the bulky silyl arsine (*i*Pr<sub>3</sub>Si)<sub>3</sub>As (**225**) has a near-planar arsenic centre with a sum of angles at arsenic of 348.0°.<sup>[7]</sup>



**Figure 115:** Compounds with planar or near-planar arsenic centres  $\text{BArF}_{24} = [\text{B}\{3,5-(\text{CF}_3)_2\text{C}_6\text{H}_3\}_4]^-$

The chemistry of arsatetrylenes is less established than that of diphosphatetrylenes, with only three arsatetrylenes having been crystallographically authenticated (**227-229**); of these, compound **229** is the only example that is monomeric (Fig. 116).<sup>[8]</sup> Due to the success of the bulky phosphide ligand  $(\text{Dipp})_2\text{P}$  in the synthesis of the diphosphatetrylenes  $\{(\text{Dipp})_2\text{P}\}_2\text{E}$  [E = Ge (**104Ge**), Sn (**104Sn**)] that are stabilised by a planar phosphorus in the solid-state, we chose to prepare the analogous arsine pro-ligand  $(\text{Dipp})_2\text{AsH}$  (**226**).

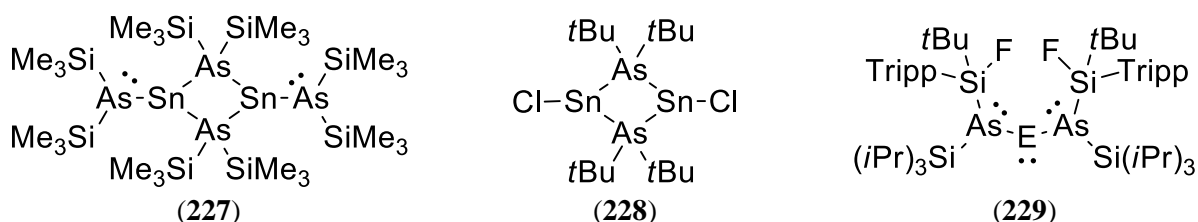
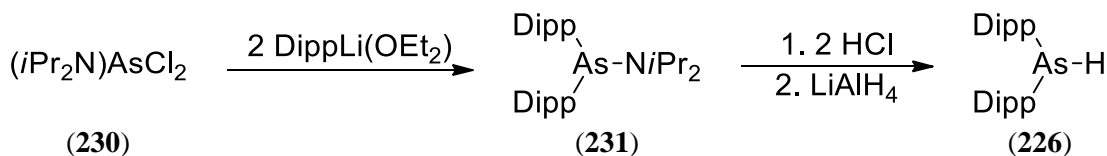


Figure 116: Previous arsatetrylenes

## 10.2 Synthesis of (Dipp)<sub>2</sub>AsH

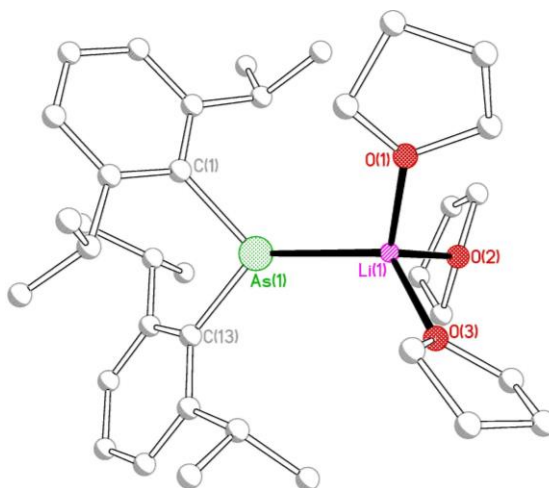
Since the large covalent radii of arsenic, compared to phosphorus, potentially allows for the over-substitution of the arsenic centre in AsCl<sub>3</sub> during a metathesis reaction with DippLi(OEt<sub>2</sub>) (**119**), the amide-protected (iPr<sub>2</sub>N)AsCl<sub>2</sub> (**230**) was first prepared by the reaction of AsCl<sub>3</sub> with two equivalents of iPr<sub>2</sub>NH. Treatment of **230** with two equivalents of DippLi(OEt<sub>2</sub>) (**119**) cleanly gave (Dipp)<sub>2</sub>As(NiPr<sub>2</sub>) (**231**), which was deprotected by the addition of two equivalents of ethereal HCl to give the chloroarsine (Dipp)<sub>2</sub>AsCl (**232**). The reaction between **232** and LiAlH<sub>4</sub> gave the secondary arsine (Dipp)<sub>2</sub>AsH (**226**) in excellent yield and purity (81% yield over the four steps from AsCl<sub>3</sub>, Scheme 49).



Scheme 49: Synthesis of **226**

## 10.3 Synthesis and solid-state structure of [(Dipp)<sub>2</sub>As]Li(THF)<sub>2.5</sub>(OEt<sub>2</sub>)<sub>0.25</sub>

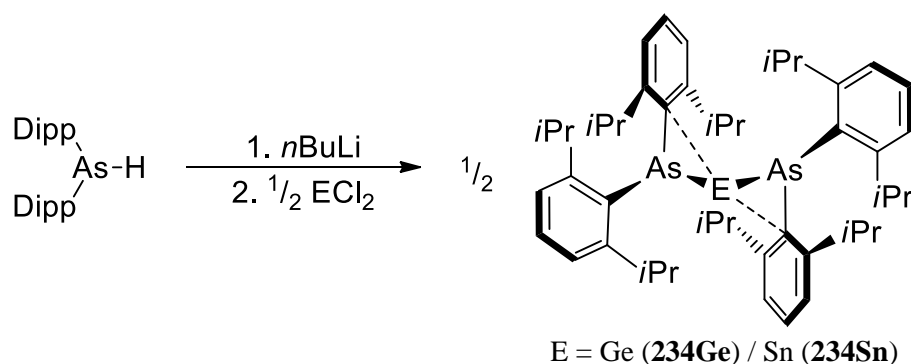
Treatment of **226** with *n*BuLi in THF gave [(Dipp)<sub>2</sub>As]Li(THF)<sub>2.75</sub>(OEt<sub>2</sub>)<sub>0.25</sub> (**233**) after crystallisation from Et<sub>2</sub>O. Compound **233** crystallises with two independent molecules of lithium arsenide in the asymmetric unit (Fig. 117). The two molecules are essentially isostructural with each lithium ion coordinated by a single arsenide ligand and three molecules of THF; however, one of the independent lithium arsenide molecules has partial occupancy disorder of a THF molecule with a molecule of Et<sub>2</sub>O. The structure of **233** is very similar to that of its phosphide analogue, [(Dipp)<sub>2</sub>P]Li(THF)<sub>3</sub> (**128a**), albeit with a slightly more pyramidal pnictide centre [sum of angles at As = 355.23/352.02° (**233**) and P = 358.13/356.73° (**128a**)]. The Li-As distances [2.568(3) and 2.584(4) Å] lie at the shorter end of the scale for such contacts.<sup>[9]</sup> Compound **233** is stable towards solvent loss on exposure to vacuum for extended periods.



**Figure 117:** Molecular structure of one of the two independent molecules of **233** with H atoms and minor disorder components omitted for clarity. Selected bond lengths (Å) and angles (°): molecule 1, Li(1)-As(1) 2.568(3), Li(1)-O(1) 1.921(4), Li(1)-O(2) 1.974(4), Li(1)-O(3) 1.940(4), As(1)-C(1) 1.9752(18), As(1)-C(13) 1.9712(19), Li(1)-As(1)-C(1) 123.65(9), Li(1)-As(1)-C(13) 131.74(10), C(1)-As(1)-C(13) 99.84(8); molecule 2, Li(2)-As(2) 2.584(4), Li(2)-O(4A) 1.953(10), Li(2)-O(5) 1.919(4), Li(2)-O(6A) 1.947(11), As(2)-C(37) 1.9779(18), As(2)-C(49) 1.9795(18), Li(2)-As(2)-C(37) 129.18(10), Li(2)-As(2)-C(49) 123.16(9), C(37)-As(2)-C(49) 99.68(7).

#### 10.4 Synthesis of {(Dipp)<sub>2</sub>As}<sub>2</sub>Ge.PhMe (**234Ge**) and {(Dipp)<sub>2</sub>As}<sub>2</sub>Sn.PhMe (**234Sn**)

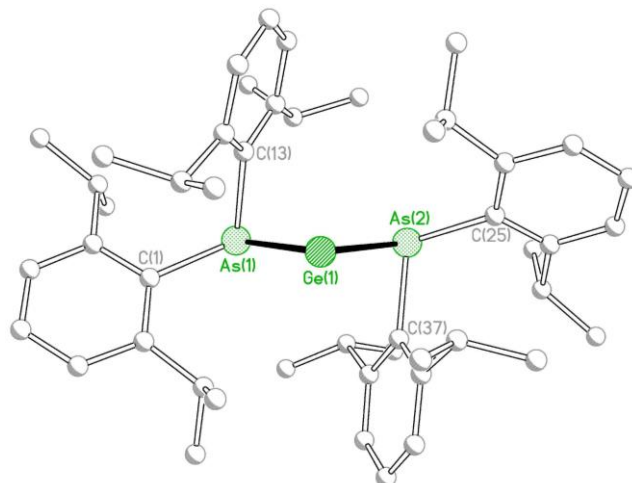
The reaction between two equivalents of *in-situ* generated [(Dipp)<sub>2</sub>As]Li with either GeCl<sub>2</sub>(1,4-dioxane) or SnCl<sub>2</sub> in cold THF gives the diarsagermylene{(Dipp)<sub>2</sub>As}<sub>2</sub>Ge.PhMe (**234Ge**) or diarsastannylene {(Dipp)<sub>2</sub>As}<sub>2</sub>Sn.PhMe (**234Sn**), respectively, after crystallisation from toluene (Scheme 50). We attribute the low isolated yield of **234Ge** and **234Sn** to their high solubility in non-polar solvents and their thermal and light sensitivity. While compounds **234Ge** and **234Sn** are moderately stable in the solid-state, they decompose rapidly in solution at room temperature, or very rapidly on exposure to ambient light.



**Scheme 50:** Synthesis of **234Ge/Sn**

## 10.5 Solid-state structures of {(Dipp)<sub>2</sub>As}<sub>2</sub>E·PhMe [E = Ge (**234Ge**), Sn (**234Sn**)]

In the solid-state, compounds **234Ge** and **234Sn** are isostructural and isomorphous; each compound crystallises as a discrete monomeric species with two pyramidal arsenic centres [sum of angles at As for **234Ge** = 285.86 and 287.76°; **234Sn** = 285.96 and 289.58°] along with a molecule of toluene (Fig. 118). Compound **234Ge** is the first X-ray crystallographically characterised diarsagermylene, while **234Sn** is only the second diarsastannylene to be structurally authenticated.



**Figure 118:** Molecular structure of **234Ge** with H atoms and solvent of crystallisation omitted for clarity [compound **234Sn** is isostructural]. Selected bond lengths (Å) and angles (1): **234Ge** As(1)–Ge(1) 2.4851(4), As(2)–Ge(1) 2.4771(4), As(1)–C(1) 2.020(3), As(1)–C(13) 2.000(3), As(2)–C(37) 2.023(3), As(2)–C(37) 2.001(3), Ge(1)···C(1) 2.666(3), Ge(1)···C(25) 2.710(2), As(1)–Ge–As(2) 90.808(13), Ge(1)–As(1)–C(1) 71.75(7), Ge(1)–As(1)–C(13) 108.70(8), Ge(1)–As(2)–C(25) 73.28(7), Ge(1)–As(2)–C(37) 109.94(8); **234Sn** As(1)–Sn(1) 2.6579(4), As(2)–Sn(1) 2.6644(4), As(1)–C(1) 1.994(3), As(1)–C(13) 2.020(3), As(2)–C(37) 1.995(3), As(2)–C(37) 2.014(3), Sn(1)···C(1) 2.858(2), Sn(1)···C(37) 2.762(3), As(1)–Sn(1)–As(2) 91.004(11), Sn(1)–As(1)–C(1) 110.57(8), Sn(1)–As(1)–C(13) 73.91(7), Sn(1)–As(2)–C(25) 108.49(8), Sn(1)–As(2)–C(37) 70.79(8).

As expected, the As-Ge distances in **234Ge** [2.4851(4) and 2.4771(4) Å] are significantly shorter than the corresponding distances in the tertiary arsine complexes **235** and **236**, which are the only other reported examples of As-Ge(II) distances (Fig. 119).<sup>[10]</sup> The As-Sn distances in **234Sn** [2.6210(11) and 2.6313(11) Å] are similar to the As-Sn distances in **229** [average 2.652(1) Å for the two crystallographically independent molecules in the asymmetric unit]. The As-E-As angles of 90.808(13) and 91.004(11)° for **234Ge** and **234Sn**, respectively, suggest negligible hybridisation of the tetrel centres in these compounds; this is supported by DFT calculations (see below). The As-Sn-As angle in **234Sn** is slightly smaller than the corresponding angle in **229** [94.64(4)°].<sup>[11]</sup>





**Figure 119:** Compounds with crystallographically authenticated As-Ge(II) distances

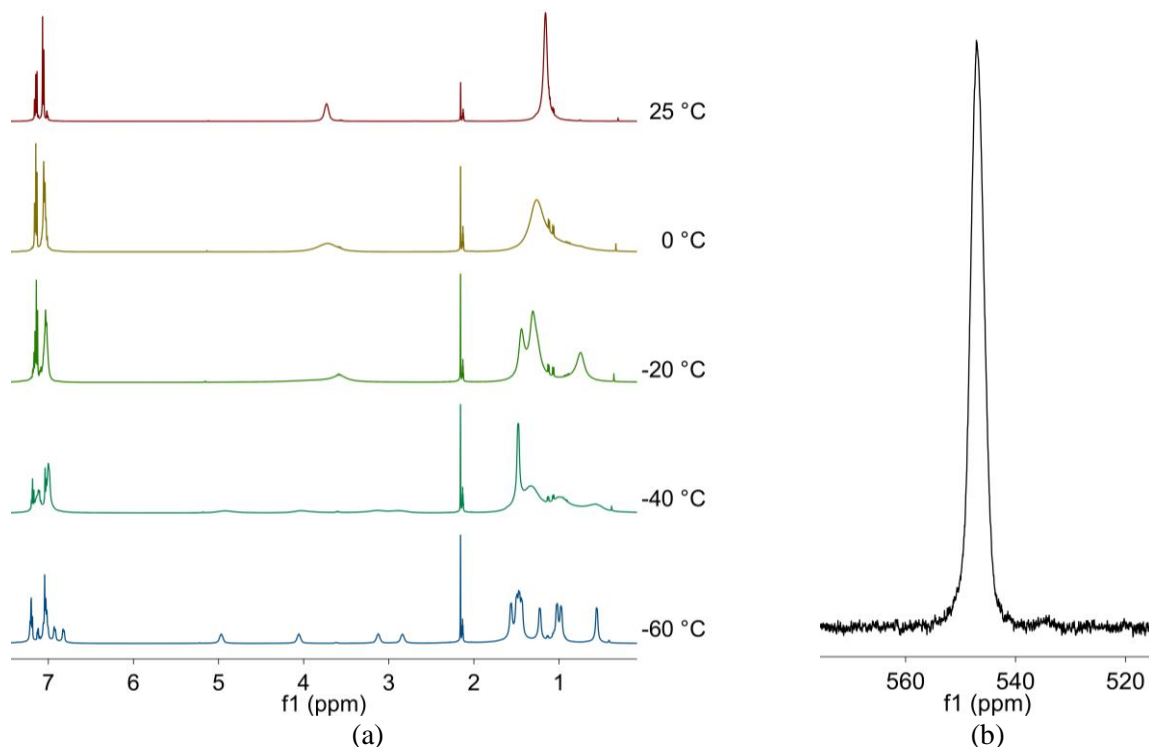
The structures of **234Ge** and **234Sn** are similar to those of the diphosphatetrylenes **145Sn**, **146Ge**, **146Sn** and **147Sn**, which are stabilised by Ge/Sn $\cdots$ C<sub>ipso</sub> interactions. Although the pyramidal arsenic centres in **234Ge** and **234Sn** inhibit stabilization of the tetrel centres by  $\pi$ -interactions, the *ipso*-carbon of one of the phenyl rings from each arsenide ligand lies in close proximity to the tetrel centre [Ge $\cdots$ C<sub>ipso</sub> 2.710(2) and 2.666(3) Å; Sn $\cdots$ C<sub>ipso</sub> 2.762(3) and 2.858(2) Å]. These distances are well within the sums of the van der Waals radii of Ge and C (3.81 Å) and of Sn and C (3.87 Å) and suggest significant interactions.<sup>[11]</sup>

We have previously discussed other examples of compounds exhibiting Group 14 element $\cdots$ arene interactions in Chapter 4. In summary, these mostly consist of molecules with cationic group 14 centres in the +2 and +4 oxidation states and the diphosphatetrylenes discussed above. The arene groups in **234Ge** and **234Sn** featuring short Ge/Sn $\cdots$ C<sub>ipso</sub> contacts lie rather symmetrically above the tetrel centres, with respect to the two ortho carbons, while the arene groups in **145Sn**, **146Ge** and **146Sn** lie offset above the tetrel centre. Given the larger covalent radii of arsenic compared to phosphorus, one might expect the aryl substituents to be located more remotely to the tetrel centre because of the increased As-Ge/Sn and As-C distances. However, the short Ge/Sn $\cdots$ C<sub>ipso</sub> contacts in **234Ge** and **234Sn** are almost identical to the corresponding distances in **146Ge** and **146Sn**, respectively. This suggests that the Ge/Sn $\cdots$ C<sub>ipso</sub> interactions in **234Ge** and **234Sn** are substantially stronger than for those observed in the diphosphatetrylenes **145Sn**, **146Ge** and **146Sn**; this was confirmed by DFT calculations (see below).

### 10.6 NMR spectra of {(Dipp)<sub>2</sub>As}<sub>2</sub>E·PhMe [E = Ge (**234Ge**), Sn (**234Sn**)]

The <sup>1</sup>H NMR spectra of **234Ge** and **234Sn** in d<sub>8</sub>-toluene at 25 °C consist of a single set of extremely broad signals due to the isopropyl and aromatic protons of the ligands, which indicates dynamic exchange between the aromatic rings engaged in the Ge/Sn $\cdots$ C<sub>ipso</sub> interactions and those that are not (Figure 120a for **234Sn**). As the temperature is reduced, these signals begin to decoalesce, until, at -60 °C, the broad signals separate into eight methyl signals (spanning the range of 0.48-1.42 for **234Ge** and 0.51-1.52 for **234Sn**) and four

methine signals (spanning the range of 2.51–4.86 ppm for **234Ge** and 2.80–2.93 for **234Sn**), which is consistent with the  $C_2$  symmetry of the solid-state structures. The large range of methyl and methine environments in the low temperature  $^1\text{H}$  NMR spectra is due to the protons' proximity (or not) to the aromatic rings or the arsenic and tellurium centre lone pairs.



**Figure 120:** (a) Variable-temperature  $^1\text{H}$  NMR spectra and (b)  $^{119}\text{Sn}\{^1\text{H}\}$  NMR spectra at -60 °C of **234Sn** in  $d_8$ -toluene

Due to the rapid exchange between the planar and pyramidal configurations of **104Sn**, **145Sn** and **147Sn** in solution, we were unable to locate  $^{119}\text{Sn}$  signals for these diphosphastannylenes at room temperature and only a very broad signal [FWHM ca. 2000 Hz] at 440 ppm for **145Sn** could be observed at -95 °C. In contrast, compound **146Sn** exhibits a triplet in its  $^{119}\text{Sn}\{^1\text{H}\}$  NMR spectrum at 476 ppm; we attribute the relative sharpness of this signal [FWHM 855 Hz] to the absence of the exchange process between the planar and pyramidal configurations, with both phosphorus centres adopting pyramidal geometries. While we were not able to locate a  $^{119}\text{Sn}$  signal for **234Sn** at room temperature, which is in part due to the thermal instability of this compound and quadrupolar nature of  $^{75}\text{As}$ , at -60 °C the  $^{119}\text{Sn}\{^1\text{H}\}$  NMR spectrum exhibits a broad signal [FWHM 500 Hz] at 547 ppm (Fig. 120b). Although no  $^{119}\text{Sn}$  NMR data are available for the arsastannylenes **228**<sup>[8a]</sup> and **229**<sup>[8c]</sup>, the  $^{119}\text{Sn}$  chemical shift of **234Sn** is similar to that observed for **227**<sup>[8b]</sup> (475 and 671 ppm for the *cis* and *trans* isomers, respectively) and the diphosphastannylenes **145Sn** (440 ppm) and **146Sn** (476 ppm).

## 10.7 DFT calculations

The optimised geometries **234Ge<sub>pyr</sub>** and **234Sn<sub>pyr</sub>** correlate well with the X-ray crystallographically derived structures (Fig. 121). In particular, the calculated structures replicate the short E...C<sub>ipso</sub> interactions rather accurately (Table 9).

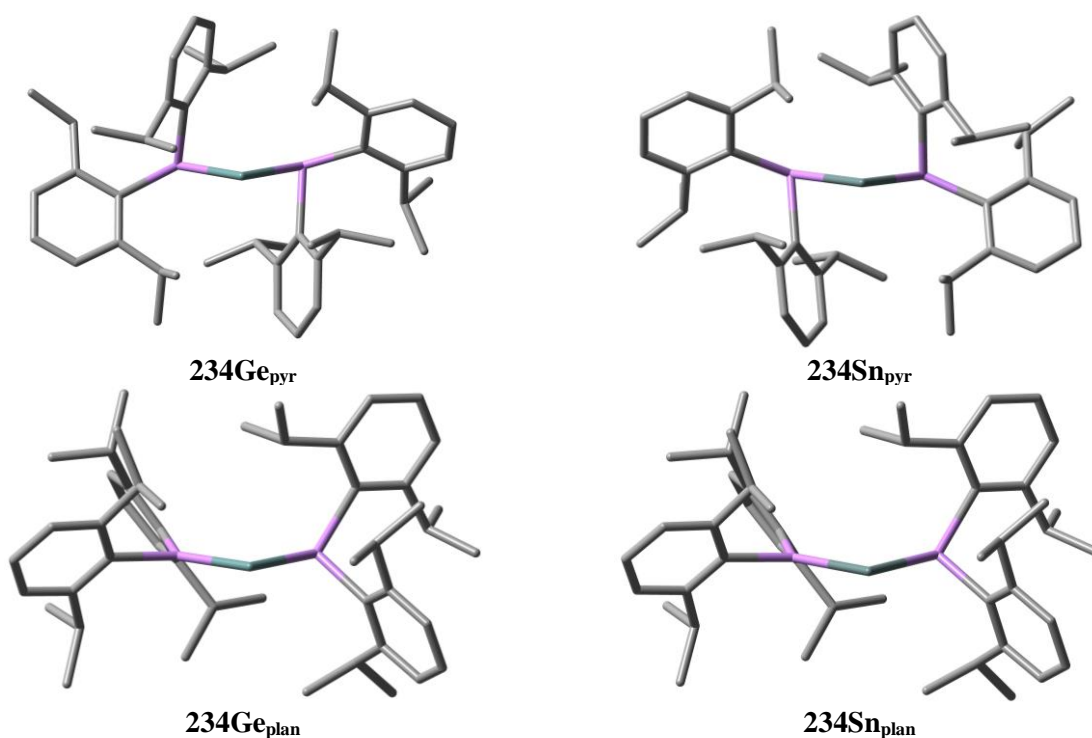
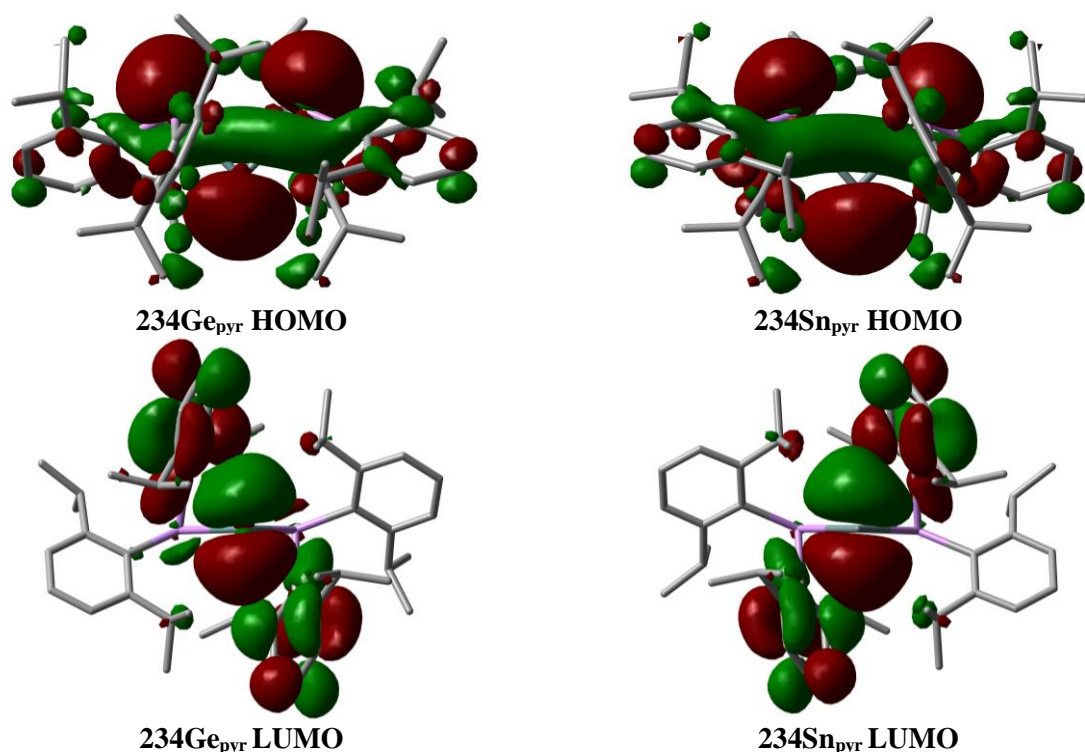


Figure 121: Calculation structures of **234Ge** and **234Sn**

Inspection of the molecular orbitals reveals that the HOMO for both **234Ge** and **234Sn** is largely based on the tetrel and arsenic lone pairs, while the LUMOs consist of the vacant p-orbital at the tetrel centre, although there is a significant component of the LUMO on the two nearby aromatic rings in each case (Fig. 122). Natural Bond Orbital (NBO) analysis reveals that the lone pair on the tetrel centre has >90% s-character, while the “vacant” orbital has essentially pure p-character. NBO analysis also reveals that this “vacant” orbital has an occupancy of 0.21 electrons for **234Ge<sub>pyr</sub>** and 0.18 electrons for **234Sn<sub>pyr</sub>**. This is associated with delocalisation of electron density from the As-C<sub>ipso</sub> σ-bonds and C<sub>ipso</sub>-C π-bonds. Similar p-orbital occupancies were calculated for the optimised geometries of the diphosphatetrylenes **104Ge/Sn**, **145Ge/Sn**, **146Ge/Sn**, **147Sn** and **148Sn** with pyramidal configurations (with occupancies ranging from 0.16 to 0.26 electrons).



**Figure 122:** Calculation molecular orbitals for **234Ge** and **234Sn**

Second order perturbation theory showed significant delocalisation from the As-  $C_{ipso}$   $\sigma$ -bonds and  $C_{ipso}$ -C  $\pi$ -bonds towards the “vacant” p-orbital on the tetrel centres. In support of this, NBO deletions (in which the energy of the system is recalculated in the absence of the As- $C_{ipso}$   $\sigma$ -bond and  $C_{ipso}$ -C  $\pi$ -bond interactions) indicate that these interactions stabilise **234Ge<sub>pyr</sub>** and **234Sn<sub>pyr</sub>** by a total of 283.5 and 180.8 kJ mol<sup>-1</sup>, respectively. These values are approximately 35% larger than those calculated for the phosphorus analogues **104Ge<sub>pyr</sub>** and **104Sn<sub>pyr</sub>** (206.2 and 146.4 kJ mol<sup>-1</sup>, respectively).

Compound	$E \cdots C_{ipso}^a$		$C_{ipso}$ -As-E <sup>b</sup>		lp*occupancy <sup>c</sup>	$E(NBO_{del})$ As- $C_{ipso}$ + $C_{ipso}$ -C <sup>d</sup>
	$C_{ipso}$ -As(1)	$C_{ipso}$ -As(2)	As(1)	As(2)		
<b>12Ge</b>	2.710(2)	2.666(3)	71.75(7)	73.28(7)	0.21	283.5
	2.757	2.644	73.39	69.77		
<b>12Sn</b>	2.762(3)	2.858(2)	70.79(8)	73.91(7)	0.18	180.8
	2.849	2.849	71.92	71.91		

Table 9: <sup>a</sup> $E \cdots C_{ipso}$  distances (Å) and <sup>b</sup> $C_{ipso}$ -P-E angles (°) of the  $E \cdots C_{ipso}$  interactions. <sup>c</sup>Electron occupancy of the vacant p-orbital at the tetrel centre. Energy change (kJ mol<sup>-1</sup>) from the NBO deletions of the interactions from the <sup>d</sup>P- $C_{ipso}$   $\sigma$  bonds and  $C_{ipso}$ -C  $\pi$  bonds.

In addition, we have located minimum energy geometries of **234Ge** and **234Sn** in which one of the arsenic centres is planar, **234Ge<sub>plan</sub>** and **234Sn<sub>plan</sub>** (Fig. 121). These structures possess As-Ge/Sn  $p\pi$ - $p\pi$  interactions and are the direct analogues of **104Ge** and **104Sn**, respectively. The geometries **234Ge<sub>plan</sub>** and **234Sn<sub>plan</sub>** lie 18.0 and 32.1 kJ mol<sup>-1</sup>, respectively, higher in energy than the ground state forms **234Ge<sub>pyr</sub>** and **234Sn<sub>pyr</sub>**. For

comparison, the calculated energy barrier to inversion, and so planarization, for AsH<sub>3</sub> at MP2 level is 164 kJ mol<sup>-1</sup>.<sup>[3]</sup>

As previously discussed in Chapter 4, it has been suggested that the singlet-triplet energy separation ( $\Delta_{S-T}$ ) and HOMO-LUMO energy gap ( $\Delta_{H-L}$ ) of tetrylenes correlate with their reactivities, with smaller gaps indicating higher reactivities. For **234Ge<sub>pyr</sub>** and **234Sn<sub>pyr</sub>** the  $\Delta_{S-T}$  are calculated to be 79.8 and 90.0 kJ mol<sup>-1</sup>, respectively, while the  $\Delta_{H-L}$  are 1.91 and 1.98 eV. These are comparable to the values at the high end of the scale for the  $\Delta_{S-T}$  and  $\Delta_{H-L}$  calculated values for the diphosphatetetrylenes **104Ge/Sn**, **145Ge/Sn**, **146Ge/Sn**, **147Sn** and **148Sn**, which range from 55.5 to 94.6 kJ mol<sup>-1</sup> and 1.41 to 1.94 eV, respectively.

## 10.8 Conclusions

The bulky secondary arsine **226** was prepared in excellent yield and readily undergoes deprotonation by *n*BuLi in THF to give the corresponding lithium arsenide **233** after crystallisation. Compounds **234Ge** and **234Sn** were prepared from *in-situ* generated [(Dipp)<sub>2</sub>As]Li and isolated in low yield, which we attribute to their low thermal stability in solution. In the solid-state, compounds **234Ge** and **234Sn** adopt a configuration with two pyramidal phosphorus centres as a result of the high barrier to planarization of phosphorus. In the absence of stabilising by  $p\pi$ - $p\pi$  interactions, these compounds are stabilised through interactions between the As-*C<sub>ipso</sub>*  $\sigma$ -bonds and *C<sub>ipso</sub>*-C  $\pi$ -bonds and the vacant orbital at the tetrel centre, stabilising **234Ge** and **234Sn** by up to 283.5 kJ mol<sup>-1</sup>.

## 10.9 Experimental

### 10.9.1 Synthesis of (*i*Pr<sub>2</sub>N)AsCl<sub>2</sub> (**230**)

To a solution of AsCl<sub>3</sub> (1.0 ml, 11.9 mmol) in Et<sub>2</sub>O (60 ml) was added *i*Pr<sub>2</sub>NH (3.3 ml, 23.5 mmol) and the mixture was stirred for 2 h. The resulting solid was removed by filtration and washed with Et<sub>2</sub>O (20 ml). The solvent was removed under reduced pressure (10 Torr) from the combined Et<sub>2</sub>O solutions to give the product as an orange oil. Yield: 2.77 g, 95%.

<sup>1</sup>H NMR [CDCl<sub>3</sub>]:  $\delta$  1.31 (d,  $J_{HH}$  = 6.8 Hz, 1H, CHMe<sub>2</sub>), 4.03 (sept,  $J_{HH}$  = 6.8 Hz, 6H, CHMe<sub>2</sub>). <sup>13</sup>C{<sup>1</sup>H} NMR [CDCl<sub>3</sub>]:  $\delta$  25.10 (CHMe<sub>2</sub>), 49.37 (CHMe<sub>2</sub>).

### 10.9.2 Synthesis of (Dipp)<sub>2</sub>As(NiPr<sub>2</sub>) (231)

To a solution of (iPr<sub>2</sub>N)AsCl<sub>2</sub> (**230**) (2.77 g, 11.3 mmol) in Et<sub>2</sub>O (40 ml) was added, dropwise, a solution of DippLi.OEt<sub>2</sub> (5.46 g, 22.5 mmol) in Et<sub>2</sub>O (40 ml). The resulting brown solution with pale solids was stirred for 30 min. The solvent was removed *in vacuo* and the product was extracted into *n*-hexane (50 ml) and filtered. The solvent was removed from the filtrate *in vacuo* to give a pale brown powder. Yield: 5.45 g, 97%.

<sup>1</sup>H NMR [d<sub>8</sub>-toluene, 213 K]: δ 0.35 (d, *J*<sub>HH</sub> = 6.3 Hz, 3H, ArCHMe), 0.45 (d, *J*<sub>HH</sub> = 6.4 Hz, 3H, ArCHMe), 0.71 (d, *J*<sub>HH</sub> = 6.2 Hz, 3H, NCHMe), 1.13 (d, *J*<sub>HH</sub> = 6.6 Hz, 3H, ArCHMe), 1.17 (d, *J*<sub>HH</sub> = 6.6 Hz, 3H, ArCHMe), 1.21 (d, *J*<sub>HH</sub> = 6.4 Hz, 3H, ArCHMe), 1.30 (d, *J*<sub>HH</sub> = 6.4 Hz, 3H, NCHMe), 1.36 (d, *J*<sub>HH</sub> = 6.5 Hz, 3H, ArCHMe), 1.41 (m, 6H, ArCHMe), 1.55 (d, *J*<sub>HH</sub> = 6.5 Hz, 3H, NCHMe), 3.25 (sept, *J*<sub>HH</sub> = 6.7 Hz, 1H, NCHMe), 3.38 (sept, *J*<sub>HH</sub> = 6.5 Hz, 1H, ArCHMe), 3.65 (sept, *J*<sub>HH</sub> = 6.5 Hz, 1H, ArCHMe), 3.81 (sept, *J*<sub>HH</sub> = 6.7 Hz, 1H, NCHMe), 4.57 (sept, *J*<sub>HH</sub> = 6.7 Hz, 1H, ArCHMe), 5.32 (sept, *J*<sub>HH</sub> = 6.6 Hz, 1H, ArCHMe), 6.83 (dd, *J*<sub>HH</sub> = 6.9 Hz, *J*<sub>HH</sub> = 2.0 Hz, 1H, ArH), 6.91 (dd, *J*<sub>HH</sub> = 7.7 Hz, *J*<sub>HH</sub> = 1.1 Hz, 1H, ArH), 7.06 (dd, *J*<sub>HH</sub> = 7.6 Hz, *J*<sub>HH</sub> = 1.1 Hz, 1H, ArH), 7.16 (m, 3H, ArH). <sup>13</sup>C{<sup>1</sup>H} NMR [d<sub>8</sub>-toluene, 213 K]: δ 20.81 (NCHMe), 22.34, 22.64 (ArCHMe), 23.60 (NCHMe), 23.70, 24.75, 24.98, 25.01 (ArCHMe), 25.13 (ArCHMe), 25.41 (ArCHMe), 25.88 (NCHMe), 26.88 (ArCHMe), 27.32 (NCHMe), 29.90, 32.42, 35.42 (ArCHMe), 46.10, 53.40 (NCHMe), 123.92, 124.52, 125.43, 125.83, 130.15 (ArH), 140.70, 141.64, 150.21, 152.58, 152.75, 152.78 (Ar).

### 10.9.3 Synthesis of (Dipp)<sub>2</sub>AsCl (232)

To a solution of Dipp<sub>2</sub>As(NiPr<sub>2</sub>) (**232**) (5.45 g, 11.0 mmol) in Et<sub>2</sub>O (60 ml) was added a solution of HCl in diethyl ether (2.0 M, 10 ml, 20.0 mmol) and the mixture was stirred for 3 h. The solid was removed by filtration and washed with Et<sub>2</sub>O (20 ml). The solvent from the combined filtrate and washings was removed *in vacuo* to give a white microcrystalline solid. Yield: 4.19 g, 96%.

<sup>1</sup>H NMR [CDCl<sub>3</sub>]: δ 1.04 (d, *J*<sub>HH</sub> = 6.7 Hz, 12H, CHMeMe), 1.04 (d, *J*<sub>HH</sub> = 6.7 Hz, 12H, CHMeMe), 3.57 (sept, *J*<sub>HH</sub> = 6.7 Hz, 4H, CHMeMe), 7.12 (d, *J*<sub>HH</sub> = 7.8 Hz, 4H, ArH), 7.28 (m, 2H, ArH). <sup>13</sup>C{<sup>1</sup>H} NMR [CDCl<sub>3</sub>]: δ 24.12 (CHMeMe), 24.87 (CHMeMe), 32.60 (CHMeMe), 124.73, 129.96 (ArH), 141.77, 151.91 (Ar).

#### 10.9.4 Synthesis of (Dipp)<sub>2</sub>AsH (**226**)

To a cold (0 °C) solution of Dipp<sub>2</sub>AsCl (**232**) (4.19 g, 9.68 mmol) in Et<sub>2</sub>O (50 ml) was added solid LiAlH<sub>4</sub> (0.370 g, 9.74 mmol) in portions. The mixture was stirred for 3 h at room temperature then quenched by the careful addition of degassed water (40 ml). The organic phase was separated and the aqueous phase was extracted into light petroleum (3 x 15 ml). The combined organic phases were dried over 4 Å molecular sieves. The solution was filtered and the solvent was removed from the filtrate *in vacuo* to give a white microcrystalline solid. Residual solvent was removed by heating (~80 °C) under vacuum. Yield: 3.53 g, 92%.

<sup>1</sup>H NMR [CDCl<sub>3</sub>]: δ 1.03 (d, *J*<sub>HH</sub> = 6.8 Hz, 12H, CHMeMe), 1.06 (d, *J*<sub>HH</sub> = 6.8 Hz, 12H, CHMeMe), 3.40 (sept, *J*<sub>HH</sub> = 6.8 Hz, 4H, CHMeMe), 4.67 (s, 1H, AsH), 7.09 (d, *J*<sub>HH</sub> = 7.6 Hz, 4H, ArH), 7.24 (m, 2H, ArH). <sup>13</sup>C{<sup>1</sup>H} NMR [CDCl<sub>3</sub>]: δ 23.92 (CHMeMe), 24.30 (CHMeMe), 34.31 (CHMeMe), 123.46, 128.54 (ArH), 136.69, 152.50 (Ar).

#### 10.9.5 Synthesis of (Dipp<sub>2</sub>As)Li(THF)<sub>2.5</sub>(OEt<sub>2</sub>)<sub>0.5</sub> (**233**)

To a solution of Dipp<sub>2</sub>AsH (**226**) (0.78 g, 1.96 mmol) in THF (10 mL) was added a solution of *n*BuLi in hexanes (0.85 mL, 2.0 mmol). The resulting red solution was stirred for 1 h. The solvent was removed *in vacuo* and the resulting yellow solid was dissolved in Et<sub>2</sub>O (5 mL). On standing at -25 °C overnight yellow crystals of (Dipp<sub>2</sub>As)Li(THF)<sub>2.75</sub>(OEt<sub>2</sub>)<sub>0.25</sub> (**233**) suitable for X-ray crystallography formed. These were washed with cold (-10 °C) light petroleum (2 x 5 mL) and residual solvent was removed *in vacuo* to give **233** as a yellow crystalline solid. Yield: 0.69 g, 60%.

<sup>1</sup>H NMR [d<sub>8</sub>-toluene]: δ 1.08 (t, 1.5H, Et<sub>2</sub>O), 1.11 (d, *J*<sub>HH</sub> = 6.9 Hz, 24H, CHMe<sub>2</sub>), 1.39 (m, 11H, THF), 3.25 (q, 1H, Et<sub>2</sub>O), 3.47 (m, 11H, THF), 4.40 (sept, *J*<sub>HH</sub> = 6.9 Hz, 4H, CHMe<sub>2</sub>), 7.08 (m, 4H, ArH), 7.16 (m, 2H, ArH). <sup>13</sup>C{<sup>1</sup>H} NMR [d<sub>8</sub>-toluene]: δ 15.49 (Et<sub>2</sub>O), 25.03 (CHMe<sub>2</sub>), 25.57 (THF), 35.82 (CHMe<sub>2</sub>), 65.92 (Et<sub>2</sub>O), 68.47 (THF), 122.54, 125.17 (ArH), 150.66 (br. s, Ar), 152.93 (Ar). <sup>7</sup>Li NMR [d<sub>8</sub>-toluene]: δ 1.7 (s).

#### 10.9.6 Synthesis of {(Dipp)<sub>2</sub>As}<sub>2</sub>Ge.C<sub>7</sub>H<sub>8</sub> (**234Ge**)

To a solution of (Dipp)<sub>2</sub>AsH (0.66 g, 1.66 mmol) in THF (10 ml) was added a solution of *n*BuLi in hexanes (2.3 M, 0.7 ml, 1.61 mmol). The resulting red solution was stirred for 30 min and added, dropwise, to a cold (-78 °C) solution of GeCl<sub>2</sub>(1,4-dioxane) (0.192 g, 0.83 mmol) in THF (10 ml). The resulting red solution was allowed to warm to room temperature

and the solvent was removed *in vacuo* to give a sticky red solid. The product was extracted into toluene (15 ml) to give a dark red solution with pale solids. The mixture was filtered and the dark red filtrate was reduced under vacuum to 5 ml in volume. Storage at -25 °C overnight gave red crystals of  $\{(\text{Dipp})_2\text{As}\}_2\text{Ge.C}_7\text{H}_8$  (**234Ge**). The supernatant was removed by filtration and the remaining solid was washed with cold (0 °C) light petroleum (10 ml). Residual solvent was removed under vacuum to give a red crystalline powder. Yield: 0.20 g, 25%.

$^1\text{H}$  NMR [213 K,  $d_8$ -toluene]:  $\delta$  0.49 (d,  $J_{\text{HH}} = 5.8$  Hz, 6H,  $^{\text{B}}\text{CHMeMe}$ ), 0.84 (d,  $J_{\text{HH}} = 5.2$  Hz, 6H,  $^{\text{A}}\text{CHMeMe}$ ), 0.87 (d,  $J_{\text{HH}} = 5.6$  Hz, 6H,  $^{\text{C}}\text{CHMeMe}$ ), 1.20 (d,  $J_{\text{HH}} = 5.8$  Hz, 6H,  $^{\text{A}}\text{CHMeMe}$ ), 1.37 (d,  $J_{\text{HH}} = 5.8$  Hz, 6H,  $^{\text{D}}\text{CHMeMe}$ ), 1.43 (m, 12H,  $^{\text{C}}\text{CHMeMe} + ^{\text{D}}\text{CHMeMe}$ ), 1.53 (d,  $J_{\text{HH}} = 5.9$  Hz, 6H,  $^{\text{B}}\text{CHMeMe}$ ), 2.11 (s, 3H, *PhMe*), 2.53 (br. m, 2H,  $^{\text{A}}\text{CHMeMe}$ ), 3.27 (br. m, 2H,  $^{\text{B}}\text{CHMeMe}$ ), 3.99 (br. m, 2H,  $^{\text{C}}\text{CHMeMe}$ ), 4.87 (br. m, 2H,  $^{\text{D}}\text{CHMeMe}$ ), 6.70-7.25 (br. m, 17H, ArH + *PhMe*).  $^{13}\text{C}\{^1\text{H}\}$  NMR [213 K,  $d_8$ -toluene]:  $\delta$  21.34 (*PhMe*), 21.53 ( $^{\text{C}}\text{CHMeMe}$ ), 23.85 ( $^{\text{D}}\text{CHMeMe}$ ), 24.20 ( $^{\text{B}}\text{CHMeMe}$ ), 25.46 ( $^{\text{A}}\text{CHMeMe}$ ), 26.01 ( $^{\text{D}}\text{CHMeMe}$ ), 26.29 ( $^{\text{C}}\text{CHMeMe}$ ), 26.76 ( $^{\text{A}}\text{CHMeMe}$ ), 28.21 ( $^{\text{B}}\text{CHMeMe}$ ), 34.06 ( $^{\text{B}}\text{CHMeMe}$ ), 34.34 ( $^{\text{C}}\text{CHMeMe}$ ), 35.01 ( $^{\text{A}}\text{CHMeMe}$ ,  $^{\text{D}}\text{CHMeMe}$ ), 123.12, 124.52, 124.59 (ArH), 125.57 (*PhMe*), 126.11, 126.78 (ArH), 128.43, 129.21 (*PhMe*), 130.78 (Ar), 131.12 (ArH), 140.72, 152.17, 152.58, 157.20, 158.67 (Ar).

#### 10.10 Synthesis of $\{(\text{Dipp})_2\text{As}\}_2\text{Sn.C}_7\text{H}_8$ (**234Sn**)

To a solution of  $(\text{Dipp})_2\text{AsH}$  (0.67 g, 1.68 mmol) in THF (10 ml) was added a solution of *n*BuLi in hexanes (2.3 M, 0.7 ml, 1.61 mmol). The resulting red solution was stirred for 30 min and added, dropwise, to a cold (-78 °C) solution of  $\text{SnCl}_2$  (0.159 g, 0.84 mmol) in THF (10 ml). The resulting orange solution was allowed to warm to room temperature and the solvent was removed *in vacuo* to give a sticky orange solid. The product was extracted into toluene (10 ml) to give a very dark purple solution with pale solids. The mixture was filtered and the dark purple filtrate was reduced to 5 ml in volume. Storage at -25 °C overnight gave purple crystals of  $\{(\text{Dipp})_2\text{As}\}_2\text{Sn.C}_7\text{H}_8$  (**234Sn**). The supernatant was removed by filtration and the remaining solid was washed with cold (-10 °C) light petroleum (10 ml). Residual solvent was removed under vacuum to give purple crystalline material. Yield: 0.25 g, 30%.

$^1\text{H}$  NMR [213 K,  $d_8$ -toluene]:  $\delta$  0.51 (d,  $J_{\text{HH}} = 4.5$  Hz, 6H,  $^{\text{B}}\text{CHMeMe}$ ), 0.93 (d,  $J_{\text{HH}} = 3.0$  Hz, 6H,  $^{\text{A}}\text{CHMeMe}$ ), 0.98 (d,  $J_{\text{HH}} = 4.1$  Hz, 6H,  $^{\text{C}}\text{CHMeMe}$ ), 1.18 (d,  $J_{\text{HH}} = 3.9$  Hz, 6H,



<sup>A</sup>CHMeMe), 1.40 (br. m, 6H, <sup>D</sup>CHMeMe), 1.42 (d,  $J_{\text{HH}} = 5.8$  Hz, 6H, <sup>B</sup>CHMeMe), 1.45 (br. m, 6H, <sup>D</sup>CHMeMe), 1.52 (br. m, 6H, <sup>C</sup>CHMeMe), 2.11 (s, 3H, PhMe), 2.80 (br. m, 2H, <sup>A</sup>CHMeMe), 3.08 (br. m, 2H, <sup>B</sup>CHMeMe), 4.01 (br. m, 2H, <sup>C</sup>CHMeMe), 4.93 (br. m, 2H, <sup>D</sup>CHMeMe), 6.78 (d,  $J_{\text{HH}} = 7.1$  Hz, 2H, ArH), 6.88 (d,  $J_{\text{HH}} = 7.3$  Hz, 2H, ArH), 6.74-7.04 (m, 8H, ArH and PhMe), 7.08 (m, 1H, PhMe), 7.16 (m, 4H, ArH). <sup>13</sup>C{<sup>1</sup>H} NMR [213 K, *d*<sub>8</sub>-toluene]:  $\delta$  21.34 (PhMe), 21.43 (<sup>C</sup>CHMeMe), 23.61 (<sup>D</sup>CHMeMe), 24.89 (<sup>B</sup>CHMeMe), 25.30 (<sup>A</sup>CHMeMe), 26.30 (<sup>D</sup>CHMeMe), 26.33 (<sup>A</sup>CHMeMe), 26.62 (<sup>C</sup>CHMeMe), 28.33 (<sup>B</sup>CHMeMe), 33.73 (<sup>B</sup>CMeMe), 34.96 (<sup>C</sup>CMeMe and <sup>D</sup>CMeMe), 35.04 (<sup>A</sup>CMeMe), 122.79, 124.45 (ArH), 125.58 (PhMe), 126.29, 126.76 (ArH), 128.43, 129.21 (PhMe), 129.69 (ArH), 133.33 (Ar), 137.66 (PhMe), 139.92, 151.90, 153.18, 155.11, 157.22 (Ar). <sup>119</sup>Sn{<sup>1</sup>H} NMR [213 K, *d*<sub>8</sub>-toluene]:  $\delta$  547 (HHFW 500 Hz).

## 10.11 References

- [1] K. Izod, D. G. Rayner, S. M. El-Hamruni, R. W. Harrington, U. Baisch, *Angew. Chem. Int. Ed. Engl.*, **2014**, 53, 3636-3640.
- [2] (a) J. Kapp, C. Schade, A. M. El-Nahas, P. v. R. Schleyer, *Angew. Chem.*, **1996**, 108, 2373-2376; (b) J. Kapp, C. Schade, A. M. El-Nahas, P. von Ragué Schleyer, *Angew. Chem. Int. Ed.*, **1996**, 35, 2236-2238.
- [3] P. Schwerdtfeger, L. J. Laakkonen, P. Pyykkö, *J. Chem. Phys.*, **1992**, 96, 6807-6819.
- [4] (a) M. Stubenhofer, C. Kuntz, M. Bodensteiner, U. Zenneck, M. Sierka, M. Scheer, *Chem. Eur. J.*, **2010**, 16, 7488-7495; (b) C. Elschenbroich, J. Six, K. Harms, *Dalton Trans.*, **2008**, 92-95; (c) M. Westerhausen, W. Schwarz, *Z. Naturforsch., B: Chem. Sci.*, **1995**, 50b, 106-114.
- [5] F. Nief, L. Ricard, *J. Organomet. Chem.*, **1997**, 529, 357-360.
- [6] T. Li, G. Tan, C. Cheng, Y. Zhao, L. Zhang, X. Wang, *Chem. Commun.*, **2018**, 54, 1493-1496.
- [7] C. v. Hänisch, *Z. Anorg. Allg. Chem.*, **2001**, 627, 1414-1416.
- [8] (a) A. H. Cowley, D. M. Giolando, R. A. Jones, C. M. Nunn, J. M. Power, W.-W. du Mont, *Polyhedron*, **1988**, 7, 1317-1319; (b) M. Westerhausen, M. M. Enzelberger, W. Schwarz, *J. Organomet. Chem.*, **1995**, 491, 83-90; (c) M. Driess, R. Janoschek, H. Pritzkow, S. Rell, U. Winkler, *Angew. Chem. Int. Ed.*, **1995**, 34, 1614-1616.
- [9] K. Izod, *Adv. Inorg. Chem.*, **2000**, 50, 33-107.
- [10] F. Cheng, A. L. Hector, W. Levason, G. Reid, M. Webster, W. Zhang, *Inorg. Chem.*, **2010**, 49, 752-760.
- [11] M. Mantina, A. C. Chamberlin, R. Valero, C. J. Cramer, D. G. Truhlar, *J. Phys. Chem. A*, **2009**, 113, 5806-5812.

## Chapter 11. Synthesis of diphosphines and dilithium diphosphides

### 11.1 Introduction

Bidentate diphosphine ligands such as bis(diphenylphosphino)methane and -ethane are routinely used in transition metal coordination chemistry and catalysis. In contrast, the corresponding alkyl-bridged diphosphides  $[\text{RP}(\text{CH}_2)_n\text{PR}]^{2-}$  have been less extensively utilized as ligands, although they offer the formation of phosphorus-element or phosphorus-metal  $\sigma$ -bonds and for the synthesis of novel phosphorus-containing heterocycles.

Isslieb and co-workers first reported compounds of the form  $[\text{RP}(\text{CH}_2)_n\text{PR}]\text{M}$  [ $\text{R} = \text{Cy}, \text{Ph}$ ;  $\text{M} = \text{Li}_2, \text{Na}_2, \text{K}_2, \text{Mg}, \text{Sn}, \text{AlX}$ ;  $n = 2-6$ ] in the 1960s, but these species were not investigated in detail; no structural data and only very limited spectroscopic data were presented.<sup>[1]</sup> Subsequently, only a few dialkali metal alkyl-bridged diphosphides have been characterised by X-ray crystallography. In the 1980s Lappert and co-workers and Craig and co-workers independently reported the structure of  $[\{\text{PhPCH}_2\text{CH}_2\text{PPh}\}\text{Li}_2(\text{THF})_4]_2$  (**237**), which was prepared by Ph-P cleavage of  $\text{Ph}_2\text{PCH}_2\text{CH}_2\text{PPh}_2$  with elemental lithium.<sup>[2]</sup> Compound **237** and the *meta*-xylene-bridged dipotassium diphosphide **238** reported by Hayes have dimeric structures in the solid-state (Fig. 123).<sup>[3]</sup>

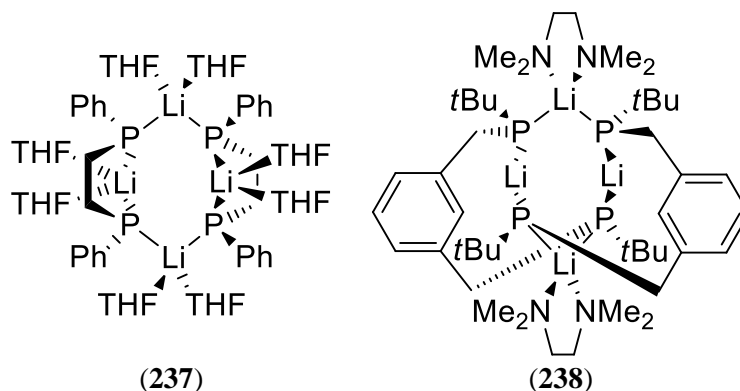
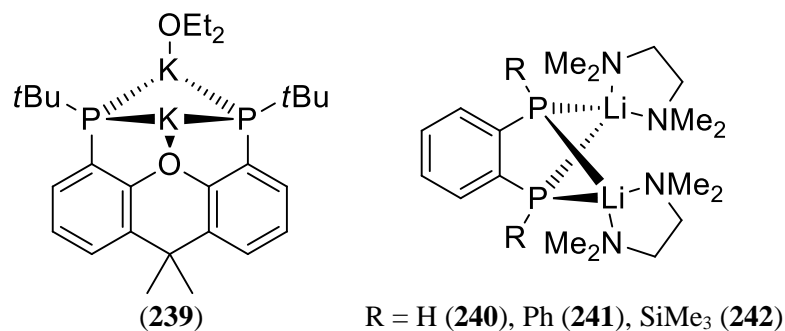


Figure 123: Dimeric dialkali metal diphosphides

Stelzer and co-workers have reported that the methylene-bridged diphosphines  $\text{RP}(\text{H})\text{CH}_2\text{PR}(\text{H})$  [ $\text{R} = \text{Me}, i\text{Pr}, t\text{Bu}, \text{Ph}, \text{Mes}$ ] undergo double deprotonation on treatment with  $\text{MeLi}$  to give the dilithium diphosphides  $[\text{RPCH}_2\text{PR}]\text{Li}_2$ , which were characterised by multinuclear NMR spectroscopy.<sup>[4]</sup> Variable-temperature  $^{31}\text{P}\{^1\text{H}\}$  and  $^7\text{Li}$  NMR spectroscopy of these compounds suggested the operation of a monomer-oligomer equilibrium in solution. In addition, a related dipotassium diphosphide-borane complex has been reported by Wagner.<sup>[5]</sup> A small number of transition metal complexes of alkyl-bridged diphosphides have also been reported,<sup>[6]</sup> along with a selection of variously-substituted aryl- or alkenyl-bridged

diphosphide compounds.<sup>[3, 7]</sup> The “pincer” dipotassium diphosphide complex **239** reported by Emslie<sup>[7h]</sup> and the phenyl-bridged dilithium diphosphides **240-242** are monomeric in the solid-state (Fig. 124).<sup>[7a, 7c]</sup>

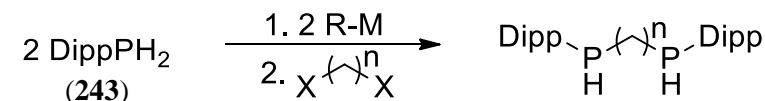


**Figure 124:** Monomeric dialkali metal diphosphides

Our interest in alkyl-bridged diphosphides lies in their use as ligands for tetrylenes. In the previous chapter, we have shown that the planar geometry of a single phosphorus centre in diphosphatetrylenes can be achieved with bulky phosphide ligands of the form (R)<sub>2</sub>P. Since the energy of planarization for phosphorus is also lowered by incorporation of the phosphorus centre into a ring, we have investigated whether similar  $\pi$ -interactions could be invoked in *P*-heterocyclic tetrylenes featuring alkyl-bridged diphosphide ligands.

### 11.1.1 Proposed synthetic strategy to alkyl-bridged diphosphines

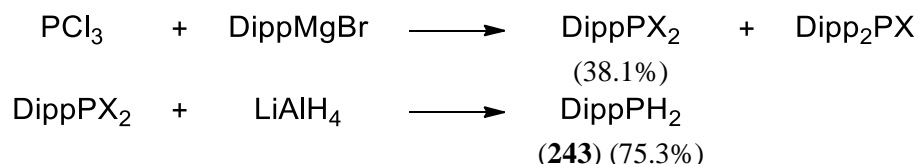
We propose that the alkyl-bridged diphosphine pro-ligands DippPH(CH<sub>2</sub>)<sub>n</sub>PHDipp [*n* = 1-5] may be prepared the addition of the primary phosphide [DippPH]M [M = Li, K] to half an equivalent of the corresponding alkyl dihalide (Scheme 51). Similar strategies were employed by Issleib in the synthesis of the alkyl-bridged diphosphines RPHCH<sub>2</sub>CH<sub>2</sub>PHR [R = H, Et, Cy, NR'<sub>2</sub>; R' = H, Et].<sup>[8]</sup>



**Scheme 51:** Proposed synthesis of alkyl-bridged diphosphines (*n* = 1-5)

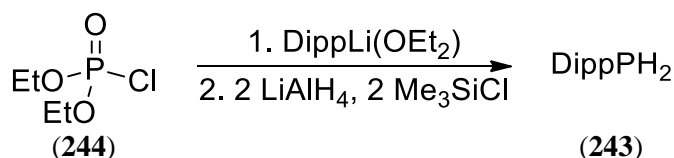
## 11.2 Synthesis of DippPH<sub>2</sub> (**243**)

The primary phosphine DippPH<sub>2</sub> (**243**) has previously been synthesised through the two-step reaction shown in Scheme 52.<sup>[9]</sup> However, the overall yield of **243** is rather low (29%) as a result of the initial metathesis reaction between DippMgBr and PCl<sub>3</sub> giving a mixture of products, from which DippPX<sub>2</sub> is isolated by distillation in low yield (X = Cl/Br).



Scheme 52: Previously reported synthesis of **243**

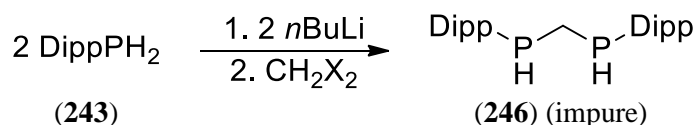
We sought to develop a higher yielding route to preparing **243** to increase the viability of further reactions. This was achieved by using (Et<sub>2</sub>O)<sub>2</sub>P(O)Cl (**244**) as the phosphorus source to protect the phosphorus centre from multiple additions of the nucleophile. The metathesis reaction of **244** with DippLi(OEt<sub>2</sub>) (**119**), followed by the *in-situ* reduction of (Dipp)(EtO)<sub>2</sub>P(O) with a mixture of LiAlH<sub>4</sub> and Me<sub>3</sub>SiCl and an aqueous workup gave **243** with a higher overall yield of 81% in a “one-pot” reaction (Scheme 53).



Scheme 53: Improved synthesis of **243**

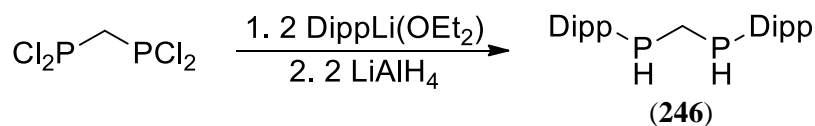
## 11.3 Synthesis of CH<sub>2</sub>(PHDipp)<sub>2</sub> (**246**)

Treatment of **243** with *n*BuLi gave the primary lithium phosphide DippPHLi (**245**), which was added to half an equivalent of either dichloromethane or dibromomethane at low temperature (-78 °C) to give the methylene-bridged diphosphine CH<sub>2</sub>(PHDipp)<sub>2</sub> (**246**) as an impure mixture (Scheme 54). The <sup>31</sup>P NMR spectrum of **246** showed a small amount (5-10%) of unknown PH-containing species, while the <sup>1</sup>H NMR spectrum showed a significant amount of contamination. The impurities could not be removed by distillation under reduced pressure and further reactions were not attempted with this mixture.



Scheme 54: Attempted synthesis of **246** (X = Cl or Br)

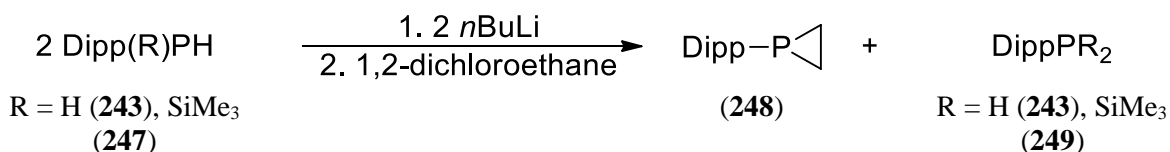
In contrast to the above, the metathesis reaction between  $\text{Cl}_2\text{PCH}_2\text{Cl}_2$  and two equivalents of  $\text{DippLi}(\text{OEt}_2)$  (**119**) gave the chlorophosphine  $(\text{Dipp})(\text{Cl})\text{PCH}_2\text{P}(\text{Dipp})(\text{Cl})$ , which was reacted *in-situ* with  $\text{LiAlH}_4$  to give **246** cleanly and in a high yield, following an aqueous work-up (Scheme 55). Due to the presence of two chiral phosphorus centres, compound **246** was isolated as a mixture of two diastereomers in a 1.1:1 ratio.



Scheme 55: Synthesis of **246**

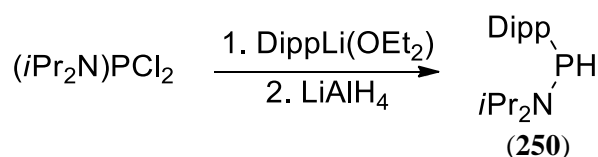
#### 11.4 Synthesis of $\{\text{CH}_2(\text{PHDipp})\}_2$ (**253**)

Initial attempts to synthesise the ethylene-bridged diphosphine  $\{\text{CH}_2(\text{PHDipp})\}_2$  (**253**) from **243** were unsuccessful. Treatment of **243** with  $n\text{BuLi}$ , followed by the addition of the resulting **245** to half an equivalent of 1,2-dichloroethane gave the phosphirane **248** and **243** in equal ratios, as judged by  $^{31}\text{P}$  NMR spectroscopy (Scheme 56). We propose that the intermediate  $\text{DippPHCH}_2\text{CH}_2\text{Cl}$  is deprotonated by a molecule of **245**, which reforms **243**, and the resulting  $\text{DippPLiCH}_2\text{CH}_2\text{Cl}$  undergoes a rapid intramolecular cyclization to form **248**. In an attempt to prevent the second deprotonation, the silyl-protected phosphine  $(\text{Dipp})(\text{Me}_3\text{Si})\text{PH}$  (**247**) was prepared by the addition of **245** to a solution  $\text{Me}_3\text{SiCl}$  in cold THF. Surprisingly, the reaction between **247**,  $n\text{BuLi}$  and 1,2-dichloroethane under the same reaction conditions resulted in the formation of the **248** and the tertiary phosphine  $(\text{Dipp})(\text{Me}_3\text{Si})_2\text{P}$  (**249**) (Scheme 56). We propose that the initially formed  $\text{DippP}(\text{SiMe}_3)\text{CH}_2\text{CH}_2\text{Cl}$  undergoes an intramolecular cyclization by elimination of  $\text{Me}_3\text{SiCl}$ , which readily reacts with **245** to form **249**. Similar methods have previously been used in the synthesis of aryl and silyl phosphiranes.<sup>[10]</sup>



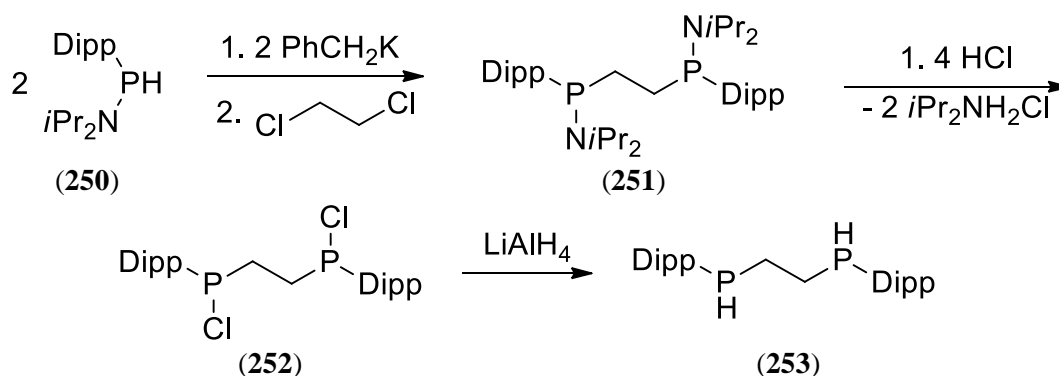
Scheme 56: Attempted synthesis of  $\{\text{CH}_2(\text{PHDipp})\}_2$

Compound **253** was successfully prepared by the following procedure. The amido-protected phosphine  $(\text{Dipp})(i\text{Pr}_2\text{N})\text{PH}$  (**250**) was prepared in a good yield by a metathesis reaction between  $(i\text{Pr}_2\text{N})\text{PCl}_2$  and  $\text{DippLi}(\text{OEt}_2)$ , followed by the addition of  $\text{LiAlH}_4$  and an aqueous work-up (Scheme 58).



Scheme 57: Synthesis of **250**

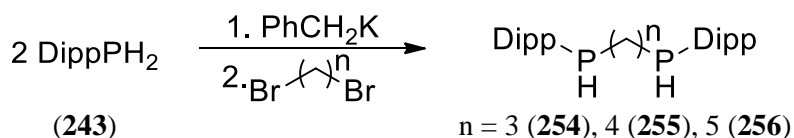
Treatment of **250** with benzylpotassium, followed by the addition of the resulting potassium phosphide (Dipp)(*i*Pr<sub>2</sub>N)PK to half an equivalent of 1,2-dichloroethane gave [CH<sub>2</sub>{P(*Ni*Pr<sub>2</sub>)(Dipp)}]<sub>2</sub> (**251**), which was subsequently deprotected with ethereal HCl to give [CH<sub>2</sub>{P(Cl)(Dipp)}]<sub>2</sub> (**252**). Compounds **251** and **252** were not isolated in high purity and were used without further purification. However, addition of LiAlH<sub>4</sub> to **252**, followed by an aqueous work-up gave {CH<sub>2</sub>(PHDipp)}<sub>2</sub> (**253**) in good yield (61%) over the four steps (Scheme 58) as a mixture of two diastereoisomers in a 1.1:1 ratio.



Scheme 58: Synthesis of **253**

### 11.5 Synthesis of CH<sub>2</sub>{CH<sub>2</sub>(PHDipp)}<sub>2</sub>, (**254**) {CH<sub>2</sub>CH<sub>2</sub>(PHDipp)}<sub>2</sub> (**255**) and CH<sub>2</sub>{CH<sub>2</sub>CH<sub>2</sub>(PHDipp)}<sub>2</sub> (**256**)

Treatment of **243** with benzylpotassium, followed by the addition of the resulting DippPHK to half an equivalent of either 1,3-dibromopropane, 1,4-dibromopropane or 1,5-dibromopentane gave the diphosphines CH<sub>2</sub>{CH<sub>2</sub>(PHDipp)}<sub>2</sub>, (**254**) {CH<sub>2</sub>CH<sub>2</sub>(PHDipp)}<sub>2</sub> (**255**) and CH<sub>2</sub>{CH<sub>2</sub>CH<sub>2</sub>(PHDipp)}<sub>2</sub> (**256**), respectively, in high yields (Scheme 59).



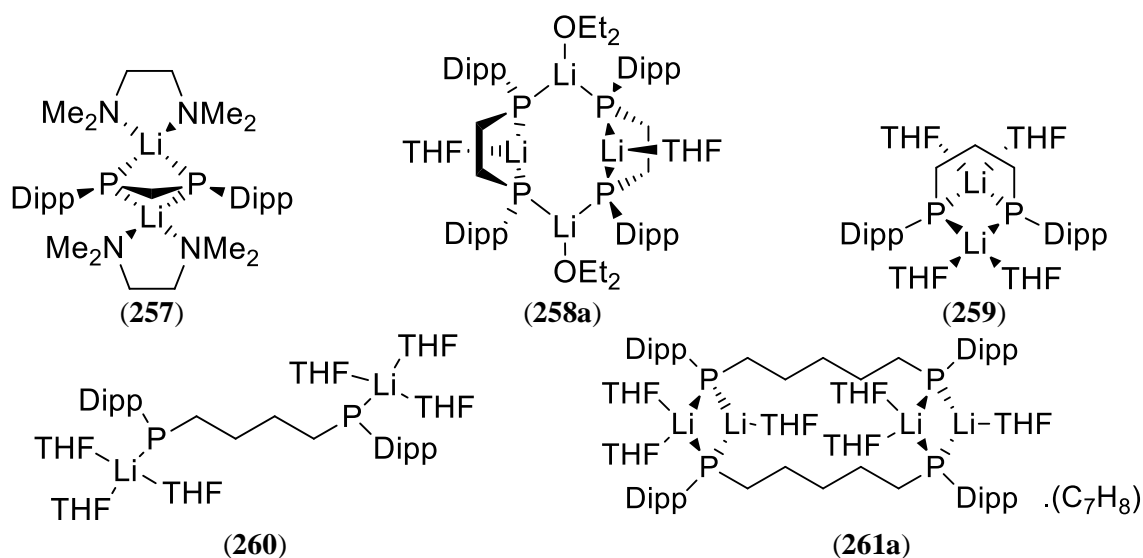
Scheme 59: Synthesis of **254**, **255** and **256**

While it is evident that compound **254** consists of a mixture of two diastereomers from its <sup>31</sup>P{<sup>1</sup>H} NMR spectrum, in which it exhibits two signals in a 1:1.2 ratio, this is not the case for **255** and **256** as these compounds each only exhibit a single signal in their <sup>31</sup>P{<sup>1</sup>H} NMR spectra. However, the asymmetry of the peaks corresponding to the phosphorus-bound

hydrogen in the  $^1\text{H}$  NMR spectra of **255** and **256** indicate these compounds consist of a mixture of diastereomers. We suggest that the difference in chemical shift between the two diastereomers decreases with increasing alkyl chain length, and, as a result, the  $^{31}\text{P}\{^1\text{H}\}$  NMR signals for the diastereomers of **255** and **256** are coincident in both cases. We also suspect the phosphines **254-256** are contaminated with a small amount of KBr as we later isolate a product containing a bromide ion, which could only originate from the initial phosphine **254**. The use of the lithium transfer reagent DippPHLi (**245**), in the analogous reaction shown in Scheme 59, gave the corresponding phosphines that were pure by  $^{31}\text{P}\{^1\text{H}\}$  and  $^1\text{H}$  NMR spectroscopy but had greater than 100% yield by weight, which we attribute to significant LiBr contamination.

**11.6 Synthesis and solid-state structures of  $[\text{CH}_2(\text{PLiDipp})_2](\text{TMEDA})_2$  (**257**),  $\{\text{CH}_2(\text{PLiDipp})\}_2(\text{THF})(\text{OEt}_2)_{1.5}$  (**258a**),  $[\text{CH}_2\{\text{CH}_2(\text{PLiDipp})\}_2(\text{THF})_4$  (**259**),  $\{\text{CH}_2\text{CH}_2(\text{PLiDipp})\}_2(\text{THF})_6$  (**260**) and  $[\text{CH}_2\{\text{CH}_2\text{CH}_2\text{P}(\text{Dipp})\}_2]\text{Li}_2(\text{THF})_6(\text{C}_7\text{H}_8)$  (**261a**)**

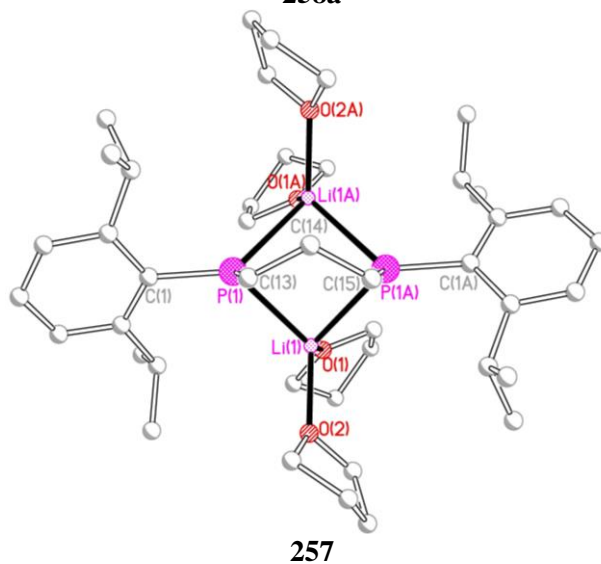
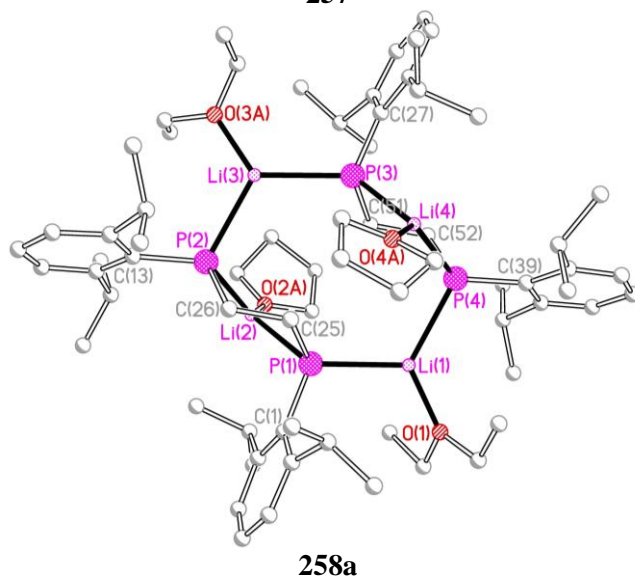
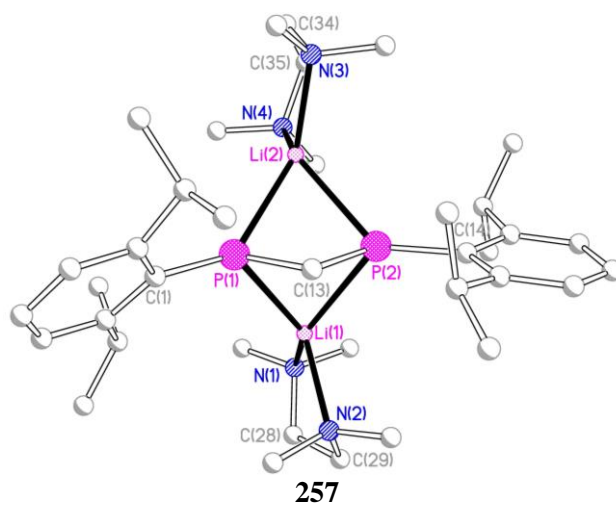
Treatment of **246** with two equivalents of  $n\text{BuLi}$  in THF generated the corresponding lithium diphosphide cleanly, as observed by  $^{31}\text{P}$  NMR spectroscopy, but no material suitable for characterisation by X-ray crystallography could be obtained. The addition of two equivalents of  $N,N,N',N'$ -tetramethylethylene-diamine (TMEDA) allowed for the isolation of  $[\text{CH}_2(\text{PLiDipp})_2](\text{TMEDA})_2$  (**257**) by crystallization from methylcyclohexane (Chart 2). The reaction between **253** and two equivalents of  $n\text{BuLi}$  in THF gave  $\{\text{CH}_2(\text{PLiDipp})\}_2(\text{THF})(\text{OEt}_2)_{1.5}$  (**258b**) after crystallisation from a mixture of  $\text{Et}_2\text{O}$  and light petroleum. A crystal of the alternative solvate  $\{\text{CH}_2(\text{PLiDipp})\}_2(\text{THF})(\text{OEt}_2)$  (**258a**) was obtained by crystallisation from  $\text{Et}_2\text{O}$  and characterised by X-ray crystallography. The difference in solvation between **258a** and **258b** suggests that the bulk material contained more highly solvated lithium ions than in the crystal of **258a**. Treatment of **254**, **255** or **256** with two equivalents of  $n\text{BuLi}$  in THF gave the corresponding lithium diphosphides  $[\text{CH}_2\{\text{CH}_2(\text{PLiDipp})\}_2(\text{THF})_4$  (**259**),  $\{\text{CH}_2\text{CH}_2(\text{PLiDipp})\}_2(\text{THF})_6$  (**260**) and  $[\text{CH}_2\{\text{CH}_2\text{CH}_2\text{P}(\text{Dipp})\}_2]\text{Li}_2(\text{THF})_6(\text{C}_7\text{H}_8)$  (**261a**) after crystallisation from light petroleum, THF or toluene, respectively (Chart 2). Compounds **259** and **260** were stable for extended periods under vacuum (~30 min) while **261a** rapidly loses coordinated solvent to give the alternative solvate  $[\text{CH}_2\{\text{CH}_2\text{CH}_2(\text{PLiDipp})\}_2](\text{THF})_{2.5}$  (**261b**). Although the yield of isolated crystalline material of the dilithium diphosphides ranged from moderate to high, the deprotonations proceeded almost quantitatively according to  $^{31}\text{P}$  NMR spectroscopy.

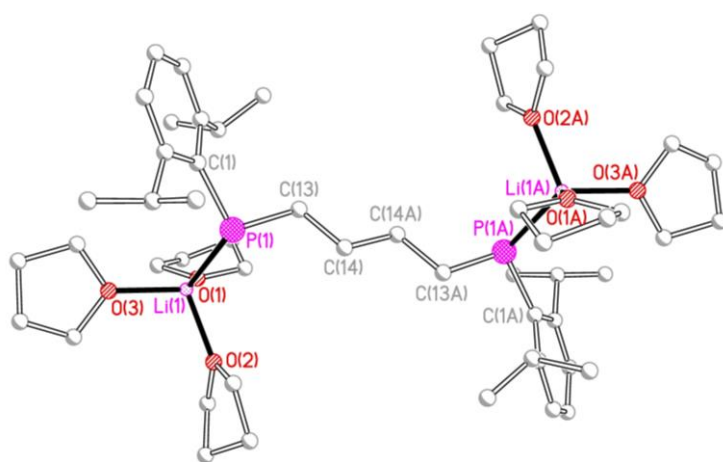


**Chart 2:** Structures of **257**, **258**, **259**, **260** and **261a**

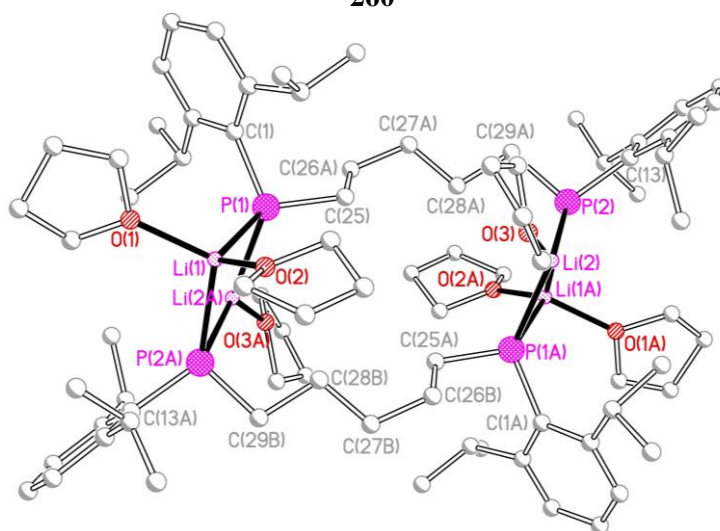
The molecular structures of **257**, **258a**, **259**, **260** and **261a** are shown in Figure 125, along with selected bond lengths and angles. The two lithium ions in compound **257** bridge the two phosphorus atoms and are each further coordinated by the two nitrogen atoms of molecule of TMEDA in a distorted tetrahedral geometry. In contrast, compound **258a** crystallises as a dimer with minor disorder of the isopropyl groups and coordinated solvent molecules. Each of the diphosphide ligands in **258a** chelates a lithium ion that is further coordinated by the oxygen atom of a molecule of THF. The diphosphide ligands are bridged by two lithium ions, which are further coordinated to an oxygen atom of a molecule of Et<sub>2</sub>O, to form an eight-membered ring of alternating lithium ions and phosphorus atoms. The structure of **258a** is analogous to its less bulky derivative {CH<sub>2</sub>(PLiPh)}<sub>2</sub>(THF)<sub>8</sub> (**237**). Compound **259** has a similar framework to **257**; the two lithium ions bridge the two phosphorus centres and are each further coordinated by two oxygen atoms from two THF molecules. Compound **260** crystallises as discrete monomers with crystallographic inversion symmetry, in which the lithium ions are coordinated in a distorted tetrahedral geometry by one phosphorus atom and three molecules of THF. Compound **261a** has an alternative dimeric structure to **258a**. Each P<sub>2</sub>Li<sub>2</sub> square is comprised of a phosphorus atom from each diphosphide ligand and two different lithium ions. The lithium ions are further coordinated by either one or two oxygen atoms from THF molecules. The P-Li distances [2.500(4), 2.537(4) (**257**), 2.470(6)-2.503(5) (**258a**), 2.547(3), 2.555(3) (**259**), 2.530(3) (**260**) and 2.485(3), 2.578(4) Å (**261a**)] all lie within the typical range for such contacts.<sup>[11]</sup> For example, the P-Li distances in {CH<sub>2</sub>(PLiPh)}<sub>2</sub>(THF)<sub>8</sub> (**237**) range from 2.53(2) to 2.57(2) Å.<sup>[12]</sup>







**260**



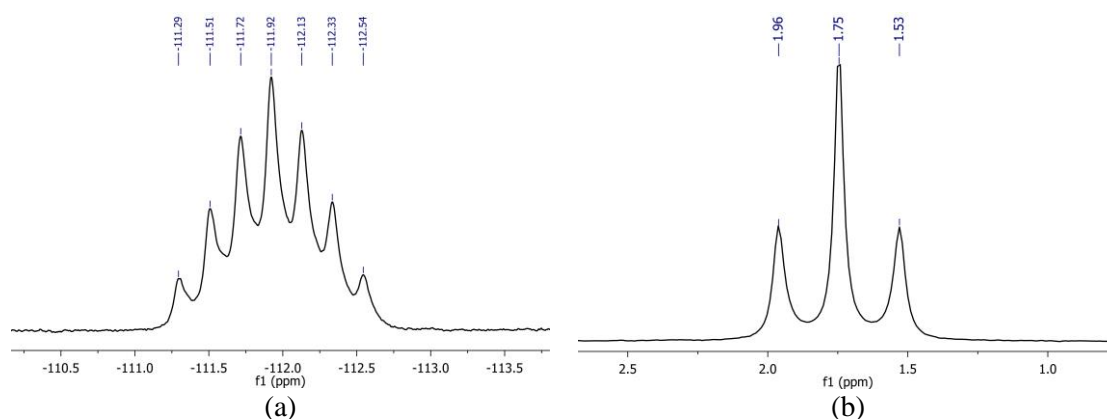
**261a**

**Figure 125:** Molecular structures of **257**, **258a**, **259**, **260** and **261a** with minor disorder components and H atoms omitted for clarity. Selected bond lengths (Å) and angles (°): **257** P(1)-C(1) 1.8546(19), P(1)-C(1) 1.889(2), P(1)-Li(1) 2.537(4), P(1)-Li(2) 2.500(4), P(2)-C(13) 1.874(2), P(2)-C(14) 1.841(2), P(2)-Li(1) 2.559(4), P(2)-Li(2) 2.533(4), N(1)-Li(1) 2.118(4), N(2)-Li(1) 2.099(5), N(3)-Li(2) 2.071(5), N(4)-Li(2) 2.082(4), C(1)-P(1)-C(13) 106.51(9), Li(2)-P(1)-Li(1) 94.45(14), C(14)-P(1)-C(13) 115.24(9), Li(2)-P(2)-Li(1) 93.11(13), P(1)-Li(1)-P(2) 67.27(10), N(2)-Li(1)-N(1) 87.25(17), P(1)-Li(2)-P(2) 68.23(10), N(3)-Li(2)-N(4) 88.63(16); **258a** P(1)-C(1) 1.862(3), P(1)-C(25) 1.872(3), P(1)-Li(2) 2.496(6), P(1)-Li(1) 2.503(5), P(2)-C(13) 1.861(3), P(2)-C(26) 1.883(3), P(2)-Li(2) 2.470(6), P(2)-Li(3) 2.498(5), P(3)-C(27) 1.859(3), P(3)-C(51) 1.870(3), P(3)-Li(4) 2.489(6), P(3)-Li(3) 2.486(5), P(4)-C(39) 1.860(3), P(4)-C(52) 1.872(3), P(4)-Li(4) 2.469(6), P(4)-Li(1) 2.496(5), Li(1)-O(1) 1.963(7), Li(2)-O(2A) 1.912(8), Li(2)-O(2B) 1.801(10), Li(3)-O(3A) 1.907(10), Li(3)-O(3B) 1.918(17), Li(3)-O(3C) 2.088(15), Li(4)-O(4A) 1.882(11), Li(4)-O(4B) 1.884(9), C(1)-P(1)-C(25) 106.49(14), Li(2)-P(1)-Li(1) 126.1(2), C(13)-P(2)-C(26) 102.16(13), Li(2)-P(2)-Li(3) 106.0(2), C(27)-P(3)-C(51), Li(3)-P(3)-Li(4) 124.0(2), C(39)-P(4)-C(52) 104.49(14), Li(4)-P(4)-Li(1) 107.0(2); **259** P(1)-C(1) 1.8583(16), P(1)-Li(1) 2.555(3), P(1)-Li(1A) 2.547(3), P(1)-C(13) 1.893(4), P(1A)-Li(1) 2.574(3), P(1A)-C(15) 1.879(4), Li(1)-O(1) 1.946(3), Li(1)-O(2) 1.967(3), C(1)-P(1)-Li(1A) 133.89(8), C(1)-P(1)-Li(1) 129.33(8), C(1)-P(1)-C(13) 100.8(2), Li(1A)-P(1)-Li(1) 81.05(11), C(13)-P(1)-Li(1A) 107.5(2), P(1A)-Li(1)-P(1) 82.11(8), O(1)-Li(1)-O(2) 98.88(13); **260** P(1)-C(1) 1.8399(15), P(1)-C(13) 1.8835(16), P(1)-Li(1) 2.530(3), Li(1)-O(1) 1.968(3), Li(1)-O(2) 1.960(3), Li(1)-O(3) 1.941(3), C(1)-P(1)-C(13) 102.72(7), C(1)-P(1)-Li(1) 114.08(8), C(13)-P(1)-Li(1) 107.17(8); **261a** P(1)-C(1) 1.858(2), P(1)-C(25) 1.873(2), P(1)-Li(1) 2.578(4), P(1)-Li(2A) 2.485(3), P(2)-C(13) 1.8520(18), P(2)-Li(1A) 2.600(4), P(2)-Li(2) 2.492(4), P(2)-C(29A) 1.807(8), P(2)-C(29B) 1.940(11), P(1A)-Li(2) 2.485(3), P(2A)-Li(1) 2.600(4), Li(1)-O(1) 1.997(7), Li(1)-O(2) 2.004(9), Li(2)-O(3) 1.915(9), Li(2)-O(3A) 1.915(7), C(1)-P(1)-C(25) 103.55(9), Li(2A)-P(1)-Li(1) 80.32(12), C(13)-P(2)-C(29B) 100.2(4), C(29A)-P(2)-C(13) 100.6(3), Li(2A)-P(2)-Li(1) 803.32(12), Li(2)-P(2)-Li(1) 79.77(12), P(1)-Li(1)-P(2A) 96.40(12), O(1)-Li(1)-O(2) 112.7(5), O(1A)-P(1)-O(2A) 95.9(5), P(1A)-Li(2)-P(2) 101.74(13).

## 11.7 Solution behaviour of dilithium diphosphides **257**, **258b**, **259**, **260** and **261b**

### 11.7.1 NMR spectra of $[\text{CH}_2(\text{PLiDipp})_2](\text{TMEDA})_2$ (**257**),

At room temperature, compound **257** exhibits a well-resolved 1:2:3:4:3:2:1 septet ( $J_{\text{PLi}}$  41 Hz) and 1:2:1 triplet ( $J_{\text{PLi}} = 41$  Hz), respectively, in its  $^{31}\text{P}\{^1\text{H}\}$  and  $^7\text{Li}$  NMR spectra, as shown in Figure 126. The  $^{31}\text{P}\{^1\text{H}\}$  and  $^7\text{Li}$  NMR spectra of this compound do not display any variable-temperature behaviour. These signals are consistent with a  $\text{P}_2\text{Li}_2$  unit and with **257** maintaining its monomeric structure in solution.

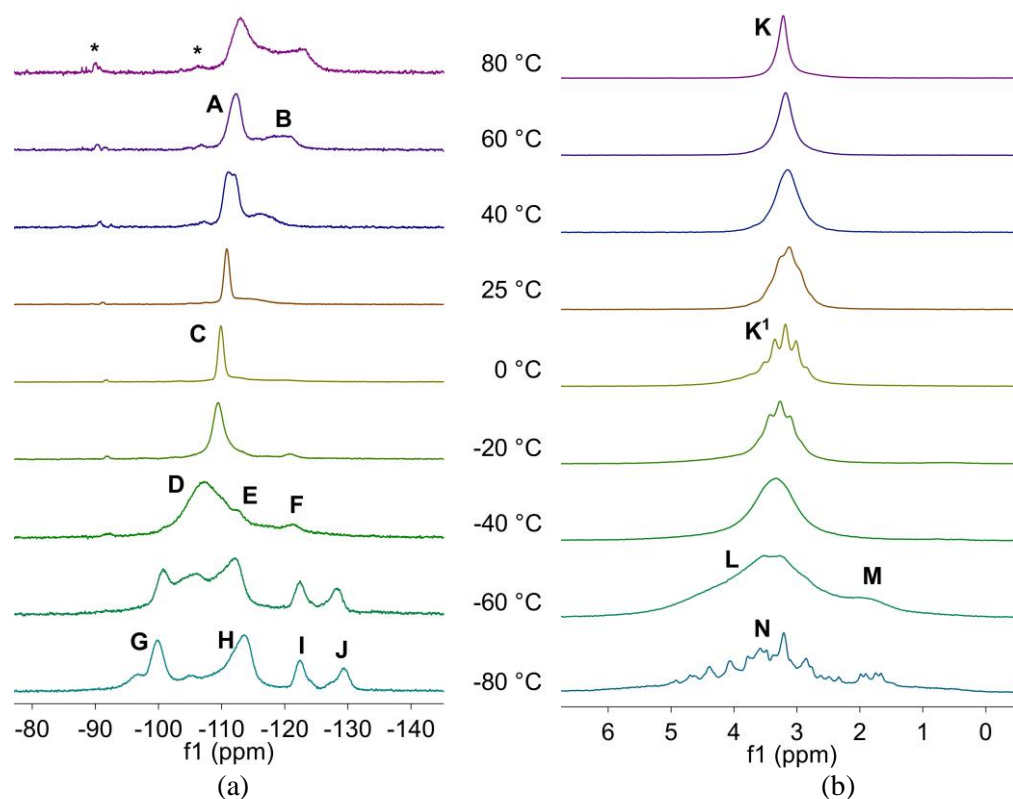


**Figure 126:** Variable-temperature (a)  $^{31}\text{P}\{^1\text{H}\}$  and (b)  $^7\text{Li}$  NMR spectra of **257** in  $\text{d}_8$ -toluene

### 11.7.2 Dynamic behaviour of $\{\text{CH}_2(\text{PLiDipp})\}_2(\text{THF})(\text{OEt}_2)_{1.5}$ (**258b**)

The variable-temperature  $^{31}\text{P}\{^1\text{H}\}$  and  $^7\text{Li}$  NMR spectra of **258b** are shown in Figure 127. At 80 °C the  $^{31}\text{P}\{^1\text{H}\}$  NMR spectrum of **258b** consists of two broad, overlapping signals at approximately -113.0 and -122.8 ppm. As the temperature is reduced, the two signals begin to sharpen, initially into the broad signals -112.3 (**A**) and -119.3 ppm (**B**) at 60 °C, and begin to merge as **B** moves downfield while decreasing in intensity, until, at 0 °C, the spectrum consists of a singlet at -109.9 ppm (**C**). As the temperature is reduced further, peak **C** broadens and decoalesces. At -40 °C, the spectrum consists of a very broad signal at approximately -107.1 (**D**) and two low intensity broad signals at -112.6 (**E**) and -121.6 ppm (**F**). Below this temperature, peak **D** decoalesces into multiple broad signals, until, at -80 °C, the spectrum consists of four major signals at -99.9 (**G**), -113.6 (**H**), -122.4 (**I**) and -129.3 ppm (**J**). At 80 °C the  $^7\text{Li}$  NMR spectrum of **258b** consists of a singlet at 3.2 ppm (**K**). As the temperature is reduced, peak **K** broadens and gradually resolves, until, at 0 °C, the spectrum consists of a broad quintet ( $J_{\text{PLi}} = 33$  Hz) at 3.2 ppm. As the temperature is further reduced, peak **K** broadens and decoalesces, until, at -60 °C, the spectrum consists of a very broad multiplet at approximately 3.4 ppm (**L**) and a low intensity signal at 1.9 ppm (**M**). At -80 °C,

peaks **L** and **M** decoalesce and resolve into multiple overlapping signals between 1.6 and 4.9 ppm (**N**).

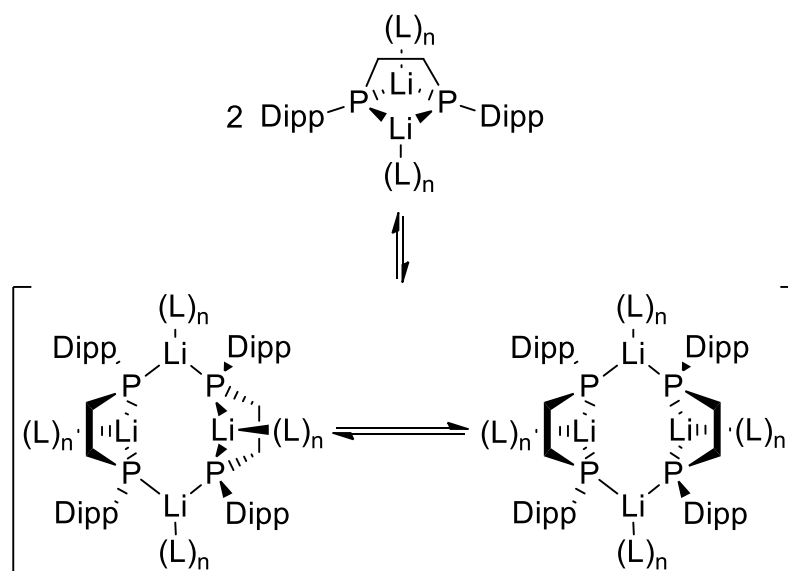


**Figure 127:** Variable-temperature (a)  $^{31}\text{P}\{^1\text{H}\}$  and (b)  $^7\text{Li}$  NMR spectra of **258b** in  $d_8$ -toluene (\*DippPLiCH<sub>2</sub>CH<sub>2</sub>PHDipp impurity)

The variable-temperature  $^{31}\text{P}\{^1\text{H}\}$  NMR spectra of **258b** indicate there are at least two dynamic processes in solution. At -80 °C, we suggest that the species responsible for the two pairs of peaks (**G/H**, **I/J**) are two stereoisomers of dimeric species of the form  $[\{\text{CH}_2(\text{PLiDipp})\}_2(\text{L})_n]$  that differ by the *cis/trans* arrangement of the ethyl bridge. Above -40 °C these stereoisomers are in dynamic equilibrium. At higher temperatures (> 0 °C) the spectra are consistent with a complex equilibrium between the two stereoisomers of the dimeric species, which are responsible for peak **A**, and a monomeric species of the form  $\{\text{CH}_2(\text{PLiDipp})\}_2(\text{L})_n$  (peak **B**). These processes are illustrated in Scheme 60.

The variable-temperature  $^7\text{Li}$  NMR spectra indicate that **258b** undergoes an unusual dynamic process in solution. At 0 °C, the spectrum consists of a quintet (peak **K**<sup>1</sup>) consistent with a single lithium environment that exhibits coupling to four equivalent phosphorus atoms. A static arrangement of four equivalent lithium ions each coordinating to four equivalent phosphorus atoms in this system is not possible. Therefore, we propose that the signal arises from the rapid exchange of the two lithium environments between four equal phosphorus atoms in each of the dimer stereoisomers, which are also in rapid exchange. Since the lithium

ions are only coordinated to two phosphorus atoms at any instance in these structures, this results in a time-averaged  $^{31}\text{P}$ - $^7\text{Li}$  coupling constant (33 Hz) that is approximately half of that observed in the spectra of the longer chain dilithium diphosphides **259**, **260** and **261b** (52 to 63 Hz). Similar dynamic NMR processes have been observed in  $[\text{MeP}(\text{C}_6\text{H}_4\text{-2-CH}_2\text{NMe}_2)\{\text{C}_6\text{H}_4\text{-2-CH}(\text{Li})\text{-NMe}_2\}]_2$ <sup>[13]</sup>,  $[(\text{dimethylamino})\text{methyl}]\text{phenyllithium}$ <sup>[14]</sup> and  $[\text{Sb}(\text{PCy})_3]_2\text{Li}_6\cdot_6\text{HNMe}_2\cdot_2\text{C}_7\text{H}_8$ .<sup>[15]</sup>

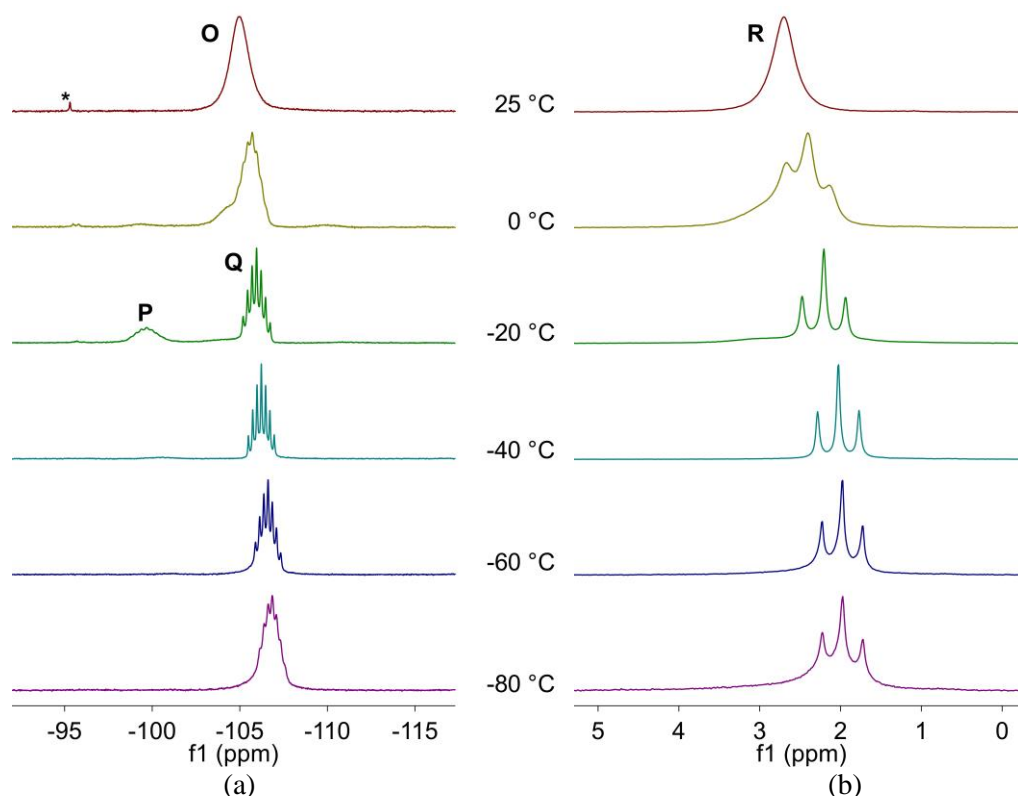


**Scheme 60:** Proposed equilibria of **258b** in solution (L = THF / Et<sub>2</sub>O)

### 11.7.3 Dynamic behaviour of $[\text{CH}_2\{\text{CH}_2(\text{PLiDipp})\}_2](\text{THF})_4$ (**259**),

The variable-temperature  $^{31}\text{P}\{^1\text{H}\}$  and  $^7\text{Li}$  NMR spectra of **259** are shown in Figure 128. At 25 °C the  $^{31}\text{P}\{^1\text{H}\}$  NMR spectrum of **259** consists of a broad singlet at -104.9 ppm (**O**). As the temperature is reduced, peak **O** sharpens and decoalesces below 0 °C into two overlapping signals, until, at -20 °C, the  $^{31}\text{P}\{^1\text{H}\}$  NMR spectrum consists of a broad multiplet at -99.7 ppm (**P**) and a well-resolved septet ( $J_{\text{PLi}} = 52$  Hz) at -106.0 ppm (**Q**) in an approximate 0.35:1 ratio. As the temperature is further reduced, peak **P** rapidly loses intensity while peak **Q** begins to broaden and move upfield slightly, until, at -80 °C, the spectrum consists of a broad multiplet **Q** at -106.9 ppm. The  $^7\text{Li}$  NMR spectrum of **259** at 80 °C consists of a broad singlet at 2.7 ppm (**R**), which moves to higher field and gradually resolves at -20 °C into a well-resolved triplet ( $J_{\text{PLi}} = 52$  Hz) at 2.2 ppm (**R**). At lower temperatures, peak **R** moves to slightly higher field.

The variable-temperature  $^{31}\text{P}\{^1\text{H}\}$  and  $^7\text{Li}$  NMR spectra of **259** indicate that at 100 °C there is a dynamic equilibrium between the species responsible for peaks **P** and **Q**. The low temperature  $^{31}\text{P}\{^1\text{H}\}$  and  $^7\text{Li}$  NMR spectra of **259** are consistent with a  $\text{P}_2\text{Li}_2$  unit in the predominant species. The chemical shift difference between peaks **P** and **Q** in the spectrum of **259** (6 ppm) is similar to that chemical shift difference between peaks **A** and **B** in the spectrum of spectrum of **258b** at 80 °C (7 ppm), in which we assigned the higher-field signal to the monomeric species. On this basis, we tentatively assign the lower field signal **P** to a dimeric species of the form  $[\text{CH}_2\{\text{CH}_2(\text{PLiDipp})\}_2]_2(\text{THF})_n$  and the higher field signal **Q** to monomeric species of the form  $[[\text{CH}_2\{\text{CH}_2(\text{PLiDipp})\}_2]_2]_2(\text{THF})_n$ .

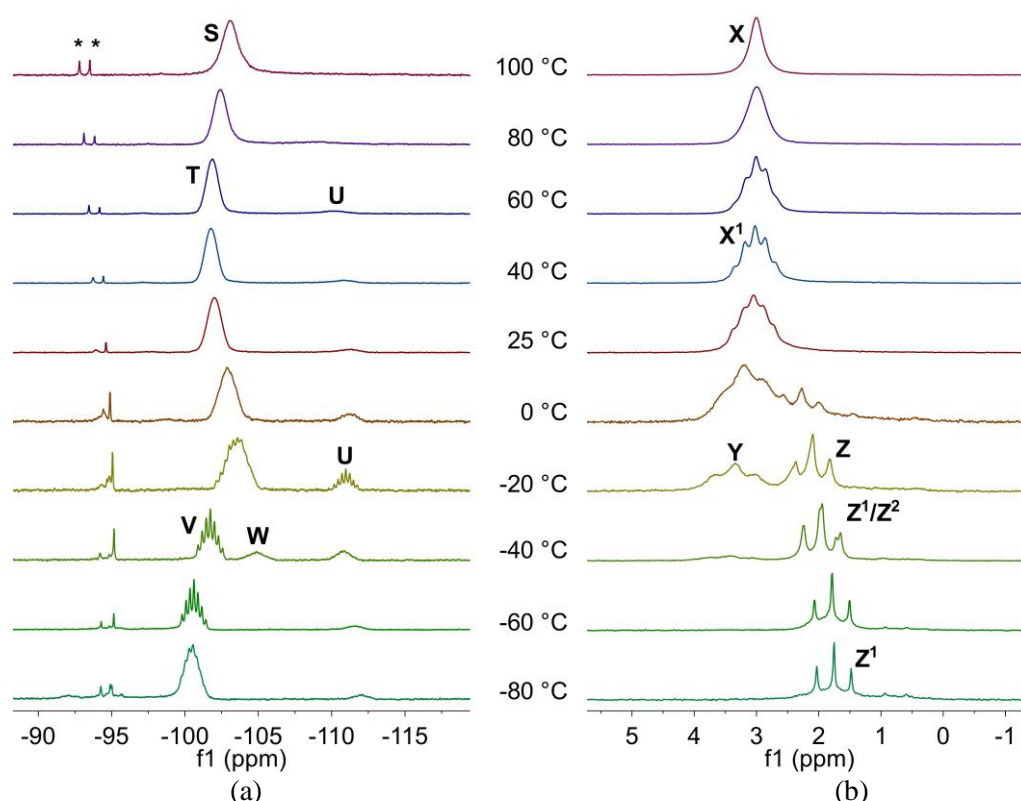


**Figure 128:** Variable-temperature (a)  $^{31}\text{P}\{^1\text{H}\}$  and (b)  $^7\text{Li}$  NMR spectra of **259** in  $d_8$ -toluene (\* free phosphine **254**)

#### 11.7.4 Dynamic behaviour of $\{\text{CH}_2\text{CH}_2(\text{PLiDipp})\}_2(\text{THF})_6$ (**260**)

The variable-temperature  $^{31}\text{P}\{^1\text{H}\}$  and  $^7\text{Li}$  NMR spectra of **260** are shown in Figure 129. At 100 °C the  $^{31}\text{P}\{^1\text{H}\}$  NMR spectrum of **260b** consists of a singlet at -103.1 ppm (**S**). As the temperature is reduced, peak **S** moves to slightly lower field and gradually decoalesces. At 60 °C the spectrum consists of a broad singlet at -101.0 ppm (**T**) and a low intensity signal at approximately -110.0 ppm (**U**). As the temperature is further reduced, peak **T** moves to slightly higher field and broadens, while peak **U** gains intensity, until, at -20 °C, peak **T** consists of two-overlapped signals at approximately -103.6 ppm and peak **U** resolves

into a septet ( $J_{\text{PLi}} = 54$  Hz) at -111.0 ppm in an approximate 1:0.2 ratio. At -40 °C the spectrum consists of three signals in an approximate 1:0.3:0.3 ratio: peak **T** decoalesces into a well-resolved septet ( $J_{\text{PLi}} = 56$  Hz) at -107.7 ppm (**V**) and a broad multiplet at -104.9 ppm, while peak **U** broadens again. Below this temperature, peak **V** broadens and moves to lower field and the intensities of peaks **U** and **W** decrease, until, at -80 °C, the spectrum consists of a broad multiplet at -100.6 ppm (**V**) and a low intensity broad signal at -112.1 ppm (**U**) in an approximate 1:0.07 ratio. The  $^7\text{Li}$  NMR spectrum of **260** at 100 °C consists of a singlet at 3.00 ppm (**X**). As the temperature is reduced, the signal resolves at 40 °C into an approximate quintet ( $J_{\text{PLi}} = 31$  Hz) at 3.0 ppm (**X**<sup>1</sup>). As the temperature is further reduced, peak **X**<sup>1</sup> broadens and gradually decoalesces, until, at -20 °C, the spectrum consists of a broad triplet ( $J_{\text{PLi}} = 63$  Hz) at 3.3 ppm (**Y**) and a sharp triplet ( $J_{\text{PLi}} = 53$  Hz) at 2.1 ppm (**Z**) in an approximate 1:1.1 ratio. At -40 °C, the spectrum consists of two overlying triplets at -2.0 ppm (**Z**<sup>1</sup>/**Z**<sup>2</sup>) as the predominant species. At low temperatures, peaks **Z**<sup>1</sup>/**Z**<sup>2</sup> move to slightly higher field and **Z**<sup>2</sup> reduces in intensity, until, at -80 °C, the spectrum consists of a triplet ( $J_{\text{PLi}} = 54$  Hz) at 1.8 ppm (**Z**<sup>1</sup>).



**Figure 129:** Variable-temperature (a)  $^{31}\text{P}\{^1\text{H}\}$  and (b)  $^7\text{Li}$  NMR spectra of **260** in  $d_8$ -toluene (\* mono deprotonated phosphine  $\{(\text{DippHP})\text{CH}_2\text{CH}_2\text{CH}_2\text{CH}_2(\text{PLiDipp})\}(\text{THF})_n$ )

The variable-temperature  $^{31}\text{P}\{^1\text{H}\}$  and  $^7\text{Li}$  NMR spectra of **260** indicate three dynamic exchange processes occurring in solution. At -80 °C, a  $\text{P}_2\text{Li}_2$  containing species (**Z**<sup>1</sup>/**V**) is the



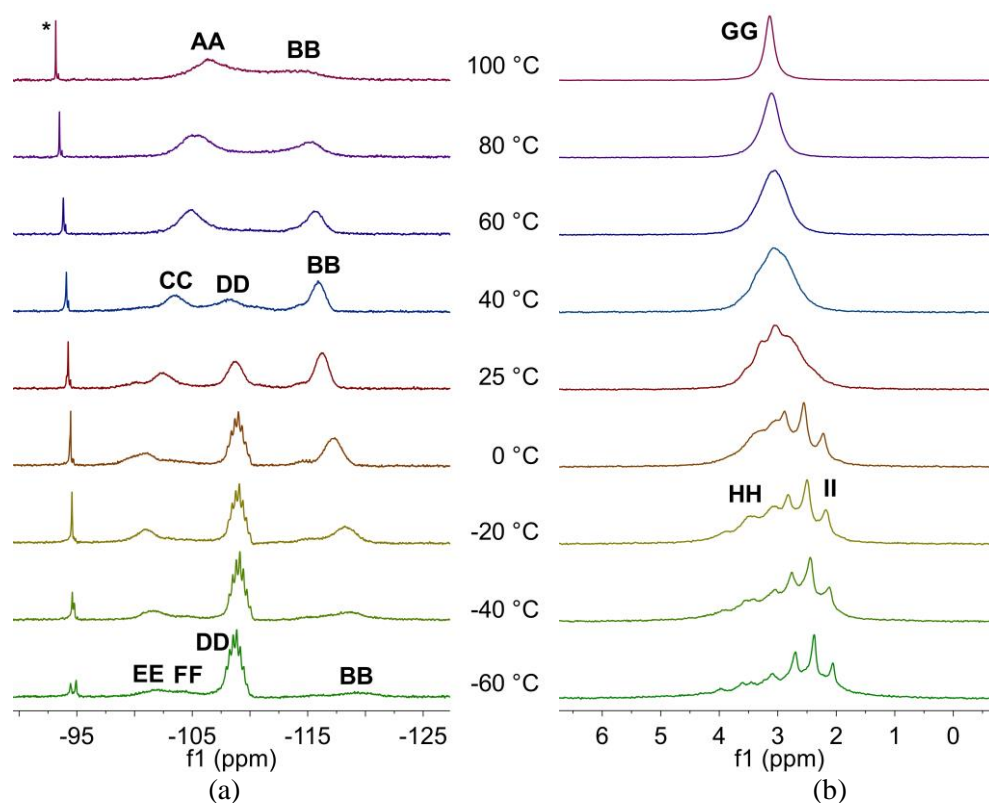
dominant species and at higher temperatures, other  $P_2Li_2$  containing species (**Z2/W** and **U/Y**) increase in concentration. Above 0 °C, the species responsible for the peaks **U/Y**, **V/Z<sup>1</sup>** and **W/Z<sup>2</sup>** are in dynamic equilibrium. The resulting signal in the  $^7Li$  NMR spectrum resolves into a quintet (**X<sup>1</sup>**) at 40 °C and at higher temperatures, the coupling is unresolved. Due to the similarity of peak **X<sup>1</sup>** and peak **K<sup>1</sup>** in the spectra of **258b** we suggest this quintet ( $J_{PLi} = 31$  Hz) results from a similar process (see Section 4.8.2), in which the lithium environments are rapid exchange with four equal phosphorus atoms in a dimeric species of the form  $[CH_2CH_2(PLiDipp)]_2(THF)_n$ .

### 11.7.5 Dynamic behaviour of $[CH_2\{CH_2CH_2(PLiDipp)\}_2](THF)_{2.5}$ (**261b**)

The variable-temperature  $^{31}P\{^1H\}$  and  $^7Li$  NMR spectra of **261b** are shown in Figure 130. The  $^{31}P\{^1H\}$  NMR spectrum of **261b** at 100 °C consists of two broad signals at approximately -106.4 (**AA**) and -114.6 ppm (**BB**). As the temperature is reduced, peak **AA** moves to slightly lower field and gradually decoalesces while peak **BB** moves to slightly higher field, until, at 40 °C, the spectrum consists of broad signals at -103.4 (**CC**) and -108.4 ppm (**DD**) of approximate equal intensity and a broad singlet at -115.9 ppm (**BB**). As the temperature is further reduced, peak **BB** moves to slightly higher field and decreases in intensity, while **CC** broadens and decoalesces and peak **DD** resolves at 0 °C into a septet ( $J_{PLi} = 63$  Hz) at -109.00 ppm. At -60 °C the spectrum consists of two low intensity, broad signals at -101.8 (**EE**) and -104.8 (**FF**), a septet ( $J_{PLi} = 61$  Hz) at -108.9 ppm (**DD**) and a very broad signal at -119.4 ppm (**BB**). The  $^7Li$  NMR spectrum of **261b** at 100 °C consists of a singlet at 3.3 ppm (**GG**), which gradually broadens and resolves as the temperature is reduced, until, at 25 °C, the spectrum consists of a broad multiplet at 3.0 ppm (**GG**). As the temperature is further reduced, peak **GG** decoalesces. At -20 °C the spectrum consists of two broad overlapping signals, a multiplet at 3.5 ppm (**HH**) and a triplet ( $J_{PLi} = 63$  Hz) at 2.5 ppm (**II**). At lower temperatures, peak **II** moves to slightly higher field and increases in intensity with respect to the remaining signals.

The variable-temperature  $^{31}P\{^1H\}$  and  $^7Li$  NMR spectra of **261b** suggest there are at least three dynamic processes occurring in solution. At -80 °C, the  $^{31}P\{^1H\}$  NMR spectrum consists of a major  $P_2Li_2$  containing species (**DD/II**) and three other low intensity signals (**EE**, **FF** and **BB**), which gain in relative intensity at higher temperatures. Above -40 °C the species responsible for the signals **EE** and **FF** are in dynamic exchange to give a new signal (**CC**), which is in dynamic equilibrium with **DD** above 40 °C.





**Figure 130:** Variable-temperature (a)  $^{31}\text{P}\{^1\text{H}\}$  and (b)  $^7\text{Li}$  NMR spectra of **261b** in  $d_8$ -toluene (\* free phosphine **256**)

## 11.8 Conclusions

The alkyl-bridged diphosphines **246**, **253**, **254**, **255** and **256** were successfully synthesised; the synthetic route is dependent on the chain length. The corresponding dilithium diphosphides **257**, **258a**, **259**, **260a** and **261a** were characterised by X-ray crystallography and display a diverse range of monomeric and dimeric structures. Compounds **258b**, **259**, **260** and **261b** exhibit complex variable-temperature  $^{31}\text{P}\{^1\text{H}\}$  and  $^7\text{Li}$  NMR behaviour due to dynamic equilibria between monomeric and oligomeric species in solution. Unfortunately, no correlation between the dilithium diphosphides can be drawn between their solid-state structures and NMR data with either the alkyl chain length or solvation.

## 11.9 Experimental

The compounds  $\text{Cl}_2\text{PCH}_2\text{PCl}_2$ <sup>[16]</sup> and  $(i\text{Pr}_2\text{N})\text{PCl}_2$ <sup>[17]</sup> were prepared by previously report procedures.

### 11.9.1 Synthesis of DippPH<sub>2</sub> (**243**)

To a cold ( $-78\text{ }^\circ\text{C}$ ) solution of  $(\text{EtO})_2\text{P}(\text{O})\text{Cl}$  (5.0 ml, 34.6 mmol) in  $\text{Et}_2\text{O}$  (80 ml) was added, slowly, a solution of  $\text{DippLi}(\text{OEt}_2)$  (8.46 g, 34.9 mmol) in  $\text{Et}_2\text{O}$  (80 ml). The resulting

solution was allowed to warm to room temperature and was stirred for 2 h. The resulting pale orange solution with pale solids was cooled to -78 °C and solid LiAlH<sub>4</sub> (2.64 g, 64.8 mmol) and chlorotrimethylsilane (9.0 ml, 70.9 mmol) were added. The resulting grey mixture was allowed to warm to room temperature and was stirred for 1 h. The resulting mixture was cooled to 0 °C and degassed water (40 ml) was slowly added. The product was extracted into light petroleum (3 x 20 ml) and the combined organic phases were dried over 4 Å molecular sieves overnight. The solution was filtered and the solvent was removed *in vacuo* from the filtrate to give a cloudy, colourless oil. The product was purified by distillation under reduced pressure (oil bath temperature 100 °C, 0.01 Torr) to give **243** as a colourless clear oil. Yield: 5.52 g, 81%.

<sup>1</sup>H NMR [CDCl<sub>3</sub>]: δ 1.27 (d, *J*<sub>HH</sub> = 6.8 Hz, 12H, CHMe<sub>2</sub>), 3.37 (m, 2H, CHMe<sub>2</sub>), 3.89 (d, *J*<sub>PH</sub> = 208 Hz, 2H, PH<sub>2</sub>), 7.15 (dd, *J*<sub>HH</sub> = 7.7 Hz, *J*<sub>HH</sub> = 2.5 Hz, 2H, ArH), 7.28 (m, 1H, ArH). <sup>13</sup>C{<sup>1</sup>H} NMR [CDCl<sub>3</sub>]: δ 23.77 (CHMe<sub>2</sub>), 33.07 (d, *J*<sub>PC</sub> = 11.4 Hz, CHMe<sub>2</sub>), 122.83 (d, *J*<sub>PC</sub> = 2.5 Hz, ArH), 126.06 (d, *J*<sub>PC</sub> = 13.1 Hz, ArH), 128.38 (Ar), 151.87 (d, *J*<sub>PC</sub> = 9.3 Hz, Ar). <sup>31</sup>P NMR [CDCl<sub>3</sub>]: δ -157.1 (t, *J*<sub>PH</sub> = 208 Hz).

### 11.9.2 Synthesis of CH<sub>2</sub>(PHDipp)<sub>2</sub> (246)

To a cold (-78 °C) solution of Cl<sub>2</sub>PCH<sub>2</sub>PCl<sub>2</sub> (1.87 g, 8.59 mmol) in Et<sub>2</sub>O (40 ml) was added, dropwise, a solution of DippLi(OEt<sub>2</sub>) (4.162 g, 17.17 mmol) in Et<sub>2</sub>O (40 ml). The resulting solution was allowed to warm to room temperature and was stirred for 2 h. The resulting colourless solution with pale solids was cooled to -78 °C and solid LiAlH<sub>4</sub> (0.651 g, 17.15 mmol) was added in portions. The resulting mixture was allowed to warm to room temperature and was stirred for 2 h. The mixture was cooled to 0 °C and degassed water (30 ml) was added slowly. The product was extracted into light petroleum (3 x 15 ml) and the combined organic phases were dried over 4 Å molecular sieves overnight. The solution was filtered and the solvent was removed from the filtrate under vacuum to give **246** as a turbid colourless oil that slowly formed a colourless crystalline solid. Yield: 3.13 g, 91%.

The NMR spectra of **246** indicate a mixture of two diastereoisomers with approximately equal intensity that gave rise to multiple, overlapping peaks in the <sup>1</sup>H{<sup>31</sup>P} NMR spectrum, corresponding to the methine and methylene environments. Due to strong <sup>1</sup>H-<sup>31</sup>P coupling from the methylene group and P-bound hydrogen atoms, <sup>1</sup>H{<sup>31</sup>P} and <sup>31</sup>P{<sup>1</sup>H} decoupled spectra were required to simplify the spectra.

$^1\text{H}\{^{31}\text{P}\}$  NMR [ $\text{CDCl}_3$ ]:  $\delta$  1.14-1.28 (m, 24H,  $\text{CHMe}_2$ ), 1.77-2.07 (m, 2H,  $\text{PCH}_2$ ), 3.45-3.68 (m,  $\text{CHMe}_2$ ), 4.39 (m, 2H, PH), 7.13-7.16 (m, 4H, ArH), 7.26-7.33 (m, 2H, ArH).  $^{13}\text{C}\{^1\text{H}\}$  NMR [ $\text{CDCl}_3$ ]:  $\delta$  16.83 (t,  $J_{\text{PC}} = 23.8$  Hz,  $\text{PCH}_2$ ), 24.65 ( $\text{CHMe}_2$ ), 32.82 (t,  $J_{\text{PC}} = 7.1$  Hz,  $\text{CHMe}_2$ ), 123.28 (t,  $J_{\text{PC}} = 1.6$  Hz, ArH), 129.48 (ArH), 132.02 (t,  $J_{\text{PC}} = 6.3$  Hz, Ar), 152.76 (t,  $J_{\text{PC}} = 5.6$  Hz, Ar).  $^{31}\text{P}\{^1\text{H}\}$  NMR [ $\text{CDCl}_3$ ]:  $\delta$  -98.2 (s), 98.8 (s) in a 1.1:1 ratio

### 11.9.3 Synthesis of $[\text{CH}_2(\text{PLiDipp})_2](\text{TMEDA})_2$ (**257**)

To a solution of  $\text{CH}_2(\text{PHDipp})_2$  (0.72 g, 1.80 mmol) in  $\text{Et}_2\text{O}$  (10 ml) was added a solution of  $n\text{BuLi}$  (2.3 M, 1.6 ml, 3.7 mmol) in hexanes and the resulting orange solution was stirred for 1 h. To this mixture, TMEDA (0.55 ml, 3.7 mmol) was added and the mixture was stirred for 1 h. The solvent was removed *in vacuo* and the resulting sticky orange solid was dissolved in hot (80 °C) methylcyclohexane (15 ml) and allowed to cool. Storage of this solution at -25 °C overnight yielded large yellow crystals of **257**. These were washed with cold (-10 °C) light petroleum (2 x 5 ml) and the residual solvent was removed under vacuum. Yield: 0.51 g, 44%.

$^1\text{H}$  NMR [ $d_8$ -toluene]:  $\delta$  1.40 (d,  $J_{\text{HH}} = 6.9$  Hz, 24H,  $\text{CHMe}_2$ ), 1.88 (s, 8H,  $\text{CH}_2\text{N}$ ), 2.08 (s, 24H,  $\text{Me}_2\text{N}$ ), 3.46 (t,  $J_{\text{PH}} = 4.2$ , 2H,  $\text{PCH}_2\text{P}$ ), 4.54 (m, 4H,  $\text{CHMe}_2$ ), 7.09-7.13 (m, 6H, ArH).  $^{13}\text{C}\{^1\text{H}\}$  NMR [ $d_8$ -toluene]: 21.83 (t,  $J_{\text{PC}} = 34$  Hz,  $\text{PCH}_2\text{P}$ ), 25.37 ( $\text{CHMe}_2$ ), 32.04 (t,  $J_{\text{PC}} = 8$  Hz,  $\text{CHMe}_2$ ), 46.01 ( $\text{Me}_2\text{N}$ ), 56.73 ( $\text{CH}_2\text{N}$ ), 121.61, 121.95 (ArH), 149.93 (t,  $J_{\text{PC}} = 3$  Hz, Ar), 151.16 (m, Ar).  $^7\text{Li}$  NMR [ $d_8$ -toluene]:  $\delta$  1.75 (t,  $J_{\text{PLi}} = 42$  Hz).  $^{31}\text{P}\{^1\text{H}\}$  NMR [ $d_8$ -toluene]:  $\delta$  -111.9 (sept,  $J_{\text{PLi}} = 42$  Hz).

### 11.9.4 Synthesis of $(\text{Dipp})(i\text{Pr}_2\text{N})\text{PH}$ (**250**)

To a cold (-78 °C) solution of  $(i\text{Pr}_2\text{N})\text{PCl}_2$  (3.73 g, 18.5 mmol) in  $\text{Et}_2\text{O}$  (40 ml) was added, dropwise, a solution of  $\text{DippLi}(\text{OEt}_2)$  (4.47 g, 18.5 mmol) in  $\text{Et}_2\text{O}$  (20 ml). The mixture was allowed to warm to room temperature and was stirred for 1 h to give a pale yellow solution containing pale solids. The mixture was cooled to 0 °C and solid  $\text{LiAlH}_4$  (0.703 g, 18.5 mmol) was added in portions. The resulting mixture was allowed to warm to room temperature and was stirred for 1 h. The mixture was cooled to 0 °C and degassed water (50 ml) was added slowly. The product was extracted into light petroleum (3 x 15 ml) and the combined organic phases were dried over 4 Å molecular sieves overnight. The solution was filtered and the solvent was removed from the filtrate *in vacuo* to give **250** as a pale yellow oil. Yield: 4.50 g, 83%.

$^1\text{H}$  NMR [ $\text{CDCl}_3$ ]:  $\delta$  1.10 (d,  $J_{\text{HH}} = 6.7$  Hz, 6H,  $\text{NCHMeMe}$ ), 1.15 (d,  $J_{\text{HH}} = 6.7$  Hz, 6H,  $\text{NCHMeMe}$ ), 1.19 (d,  $J_{\text{HH}} = 6.8$  Hz, 6H,  $\text{ArCHMeMe}$ ), 1.29 (d,  $J_{\text{HH}} = 6.8$  Hz, 6H,  $\text{ArCHMeMe}$ ), 3.18 (m, 2H,  $\text{NCHMeMe}$ ), 3.83 (m, 2H,  $\text{ArCHMeMe}$ ), 6.00 (d,  $J_{\text{PH}} = 208$  Hz, 1H, PH), 7.17 (d,  $J_{\text{HH}} = 7.8$  Hz, 1H, ArH), 7.18 (d,  $J_{\text{HH}} = 7.8$  Hz, 1H, ArH), 7.31 (t,  $J_{\text{HH}} = 7.8$  Hz, 1H, ArH).  $^{13}\text{C}\{^1\text{H}\}$  NMR [ $\text{CDCl}_3$ ]:  $\delta$  21.63 (d,  $J_{\text{PC}} = 11.6$  Hz,  $\text{NCHMeMe}$ ), 22.96 (d,  $J_{\text{PC}} = 2.8$  Hz,  $\text{NCHMeMe}$ ), 24.09 ( $\text{ArCHMeMe}$ ), 25.44 ( $\text{ArCHMeMe}$ ), 31.72 (d,  $J_{\text{PC}} = 10.3$  Hz,  $\text{ArCHMeMe}$ ), 48.39 (d,  $J_{\text{PC}} = 6.9$  Hz,  $\text{NCHMeMe}$ ), 123.23 (d,  $J_{\text{PC}} = 2.3$  Hz, ArH), 129.24 (ArH), 132.14 (d,  $J_{\text{PC}} = 6.6$  Hz, Ar), 153.33 (d,  $J_{\text{PC}} = 13.0$  Hz, Ar).  $^{31}\text{P}$  NMR [ $\text{CDCl}_3$ ]:  $\delta$  36.8 (d,  $J_{\text{PH}} = 208$  Hz).

#### 11.9.5 Synthesis of $\{\text{CH}_2(\text{PHDipp})\}_2$ (**253**)

To a solution of  $(\text{Dipp})(i\text{Pr}_2\text{N})\text{PH}$  (**250**) (2.09 g, 7.12 mmol) in THF (25 ml) was added a solution of  $\text{PhCH}_2\text{K}$  (0.930 g, 7.14 mmol) in THF (10 ml). The resulting very dark red solution was stirred for 30 min and added, dropwise, to a cold ( $-78^\circ\text{C}$ ) solution of 1,2-dichloroethane (0.28 g, 3.55 mmol) in THF (20 ml). The resulting red solution was allowed to warm to room temperature and was stirred for 1 h. The solvent was removed *in vacuo* and the product was extracted into warm ( $40^\circ\text{C}$ ) light petroleum (50 ml). The petroleum extract was filtered and the solvent was removed from the filtrate *in vacuo* to give  $[\text{CH}_2\{\text{P}(\text{Dipp})(\text{NiPr}_2)\}]_2$  (**251**) as a pale yellow solid (1.98 g, 3.23 mmol). This solid was dissolved in light petroleum (60 ml) and cooled to  $0^\circ\text{C}$  before a solution of anhydrous  $\text{HCl}$  in  $\text{Et}_2\text{O}$  (2.0 M, 6.5 ml, 13.0 mmol) was slowly added. A white solid immediately formed and the resulting mixture was stirred for 1 h. The mixture was filtered through celite and the solvent was removed from the filtrate *in vacuo* to give  $\{\text{CH}_2(\text{PClDipp})\}_2$  (**252**) as a white solid (1.25 g, 2.59 mmol). This solid was dissolved in  $\text{Et}_2\text{O}$  (40 ml) and cooled to  $0^\circ\text{C}$  before solid  $\text{LiAlH}_4$  (0.101 g, 2.66 mmol) was added in portions. The mixture was allowed to warm to room temperature and was stirred for 1 h. The mixture was cooled to  $0^\circ\text{C}$  and degassed water (30 ml) was slowly added. The product was extracted into light petroleum (2 x 15 ml) and the combined organic phases were dried over  $4\text{ \AA}$  molecular sieves overnight. The solution was filtered and the solvent was removed *in vacuo*. Volatile impurities were removed by vacuum distillation ( $100^\circ\text{C}$ ,  $10^{-3}$  Torr) to leave **253** as a white crystalline solid on cooling. Yield: 0.90 g, 61% based on **250**.

The two diastereoisomers of **253** (A and B) exhibit coincident peaks in the  $^1\text{H}$  and  $^{13}\text{C}\{^1\text{H}\}$  NMR spectra with the exception of the methyl environments.

$^1\text{H}$  NMR [ $\text{CDCl}_3$ ]:  $\delta$  1.15 (m, 12H,  $^A\text{CHMe}_2$ ), 1.22 (d,  $J_{\text{HH}} = 6.7$  Hz, 12H,  $^B\text{CHMe}_2$ ), 1.75 (m, 2H, PCHH), 1.87 (m, 2H, PCHH), 3.55 (m, 4H, CHMeMe), 4.36 (d,  $J_{\text{HH}} = 216$  Hz, 2H, PH), 7.13 (d,  $J_{\text{HH}} = 7.6$  Hz, 4H, ArH), 7.27 (t,  $J_{\text{HH}} = 7.6$  Hz, 2H ArH).  $^{13}\text{C}\{^1\text{H}\}$  NMR [ $\text{CDCl}_3$ ]:  $\delta$  22.73 (m, PCHH), 24.31 ( $^B\text{CHMeMe}$ ), 24.35 ( $^B\text{CHMeMe}$ ), 24.86 ( $^A\text{CHMe}_2$ ), 32.81 (CHMeMe), 123.27, 129.22 (ArH), 132.68 (m, Ar), 152.85 (m, Ar).  $^{31}\text{P}$  NMR [ $\text{CDCl}_3$ ]:  $\delta$  -88.8 (d,  $J_{\text{PH}} = 216$  Hz), -88.2 (d,  $J_{\text{PH}} = 216$  Hz) in a 1.1:1 ratio.

#### 11.9.6 Synthesis of $\{\text{CH}_2(\text{PLiDipp})\}_2(\text{THF})(\text{OEt}_2)_{1.5}$ (**258b**)

To a solution of  $\{\text{CH}_2(\text{PHDipp})\}_2$  (0.48 g, 1.16 mmol) in THF (10 ml) was added a solution of  $n\text{BuLi}$  in hexanes (2.47 M, 0.95 ml, 2.34 mmol). The resulting red solution was stirred for 30 min and the solvent was removed *in vacuo*. The resulting sticky yellow solid was dissolved in  $\text{Et}_2\text{O}$  (5 ml). The resulting yellow solution was left to stand overnight to give yellow crystals of  $[\{\text{CH}_2(\text{PLiDipp})\}_2(\text{THF})_2(\text{OEt}_2)_2]$  (**258a**). Further crystalline material was obtained by storage at  $-25$  °C overnight. The supernatant solution was removed by filtration and the remaining crystalline solid was washed with cold ( $-10$  °C) light petroleum (5 ml). The residual solvent was removed under vacuum to give the alternative solvate  $\{\text{CH}_2(\text{PLiDipp})\}_2(\text{THF})(\text{OEt}_2)_{1.5}$  (**258b**) as a yellow powder. Combined yield: 0.28 g, 40%.

$^1\text{H}$  NMR [ $d_8$ -toluene, 253 K]:  $\delta$  0.96 (t, 9H,  $\text{Et}_2\text{O}$ ), 1.16 (br. s, 4H, THF), 1.41 (d,  $J_{\text{HH}} = 6.8$  Hz, 24H, CHMe<sub>2</sub>), 2.68 (br. s, 4H, PCH<sub>2</sub>), 3.16 (q, 6H,  $\text{Et}_2\text{O}$ ), 3.34 (br. s, 4H, THF), 4.47 (br. m, 4H, CHMe<sub>2</sub>), 7.16 (d,  $J_{\text{HH}} = 7.3$  Hz, 4H, ArH), 7.21 (m, 2H, ArH).  $^{13}\text{C}\{^1\text{H}\}$  NMR [ $d_8$ -toluene, 253 K]:  $\delta$  15.23 ( $\text{Et}_2\text{O}$ ), 25.27 (THF), 28.92 (PCH<sub>2</sub>), 33.93 (CHMe<sub>2</sub>), 65.82 ( $\text{Et}_2\text{O}$ ), 69.08 (THF), 122.47, 125.33 (ArH), 146.40, 152.34 (Ar).  $^7\text{Li}$  NMR [ $d_8$ -toluene, 253 K]:  $\delta$  3.3 (br. m).  $^{31}\text{P}\{^1\text{H}\}$  NMR [ $d_8$ -toluene, 253 K]:  $\delta$  -109 (br. s), -121 (br. s) in a 15:1 ratio.

#### 11.9.7 Synthesis of $\text{CH}_2\{\text{CH}_2(\text{PHDipp})\}_2$ (**254**)

A solution of  $\text{PhCH}_2\text{K}$  (1.116 g, 8.57 mmol) in THF (20 ml) was added to a solution of  $\text{DippPH}_2$  (**243**) (1.66 g, 8.55 mmol) in THF (20 ml). The resulting red solution was stirred for 15 min and added, dropwise, to a cold ( $-78$  °C) solution of 1,3-dibromopropane (0.43 ml, 4.24 mmol) in THF (30 ml). The resulting mixture was allowed to warm to room temperature and the solvent was removed *in vacuo* to give a sticky grey solid. The product was extracted into light petroleum (40 ml), filtered and the solvent was removed from the filtrate *in vacuo* to give **254** as a turbid colourless oil. Yield: 1.68 g, 92%.

$^1\text{H}$  NMR [ $\text{CDCl}_3$ ]:  $\delta$  1.21 (d,  $J_{\text{HH}} = 6.8$  Hz, 12H,  $\text{CHMeMe}$ ), 1.28 (d,  $J_{\text{HH}} = 6.8$  Hz, 12H,  $\text{CHMeMe}$ ), 1.67 (br. m, 4H,  $\text{PCH}_2\text{CH}_2$ ), 1.90 (br. m, 2H,  $\text{PCH}_2\text{CH}_2$ ), 3.61 (m, 4H,  $\text{CHMeMe}$ ), 4.28 (dm,  $J_{\text{PH}} = 215$  Hz, 2H, PH), 7.16 (dd,  $J_{\text{HH}} = 7.9$  Hz,  $J_{\text{HH}} = 2.2$  Hz, 4H, ArH), 7.30 (m, 2H, ArH).  $^{13}\text{C}\{^1\text{H}\}$  [ $\text{CDCl}_3$ ]:  $\delta$  24.43 ( $\text{CHMeMe}$ ), 24.95 ( $\text{CHMeMe}$ ), 25.38 (m,  $\text{PCH}_2\text{CH}_2$ ), 27.52 (t,  $J_{\text{PC}} = 11.5$  Hz,  $\text{PCH}_2\text{CH}_2$ ), 32.80 (d,  $J_{\text{PC}} = 13.8$  Hz,  $\text{CHMeMe}$ ), 123.27 (d,  $J_{\text{PC}} = 3.3$  Hz, ArH), 129.19 (ArH), 131.25 (d,  $J_{\text{PC}} = 16.2$  Hz, Ar), 152.89 (d,  $J_{\text{PC}} = 10.8$  Hz).  $^{31}\text{P}$  NMR [ $\text{CDCl}_3$ ]:  $\delta$  -95.6 (d,  $J_{\text{PH}} = 215$  Hz), -95.4 (d,  $J_{\text{PH}} = 215$  Hz) in a 1:1.2 ratio.

### 11.9.8 Synthesis of $[\text{CH}_2\{\text{CH}_2(\text{PLiDipp})\}_2(\text{THF})_4]$ (**259**)

To a solution of  $\text{CH}_2\{\text{CH}_2(\text{PHDipp})\}_2$  (**254**) (1.84 g, 4.29 mmol) in THF (20 ml) was added a solution of  $n\text{BuLi}$  in hexanes (2.3 M, 3.7 ml, 8.51 mmol). The resulting red solution was stirred for 1 h and the solvent was removed *in vacuo* to give a sticky yellow solid. The solid was dissolved in  $\text{Et}_2\text{O}$  (15 ml) and the resulting orange solution was stored at  $-25^\circ\text{C}$  overnight to give large yellow crystals of  $[\text{CH}_2\{\text{CH}_2(\text{PLiDipp})\}_2(\text{THF})_4]$  (**259**). The supernatant solution was removed by filtration and the crystals were washed with cold ( $-10^\circ\text{C}$ ) light petroleum (2 x 5ml) and the residual solvent was removed from the remaining solid under vacuum to give a yellow crystalline powder (1.03 g, 33%). A second crop of material was obtained by reducing the volume of the combined filtrate and washings to 10 ml followed by storage at  $-25^\circ\text{C}$  for 1 week. The supernatant solution was removed by filtration and the residual solvent was removed under vacuum from the remaining solid to give a yellow microcrystalline powder (0.67 g, 22%). Combined yield: 1.70 g, 55%.

$^1\text{H}$  NMR [ $d_8$ -toluene]:  $\delta$  1.38-1.40 (m, THF +  $\text{CHMe}_2$ , 40H), 2.41 (br. s,  $\text{PCH}_2\text{CH}_2$ , 2H), 2.53 (br. s,  $\text{PCH}_2\text{CH}_2$ , 4H), 3.59 (m, THF, 16H), 4.68 (br. s,  $\text{CHMe}_2$ , 4H), 7.17 (s, ArH, 6H).  $^{13}\text{C}\{^1\text{H}\}$  NMR [ $d_8$ -toluene]:  $\delta$  25.52 ( $\text{CHMe}_2$ ), 25.66 (THF), 30.20 (br. s,  $\text{PCH}_2\text{CH}_2$ ), 33.54 (br. s,  $\text{PCH}_2\text{CH}_2$ ), 68.59 (THF), 122.33, 124.68 (ArH), 148.82, 152.51 (br. s, Ar).  $^7\text{Li}$  NMR [ $d_8$ -toluene]:  $\delta$  -2.7 (s).  $^{31}\text{P}\{^1\text{H}\}$  NMR [ $d_8$ -toluene]:  $\delta$  -105.0 (br. s).

### 11.9.9 Synthesis of $\{\text{CH}_2\text{CH}_2(\text{PHDipp})\}_2$ (**255**)

A solution of  $\text{PhCH}_2\text{K}$  (1.126 g, 8.95 mmol) in THF (15 ml) was added to a solution of  $\text{DippPH}_2$  (**243**) (1.68 g, 8.65 mmol) in THF (15 ml). The resulting solution was stirred for 30 min and added, dropwise, to a solution of 1,4-dibromobutane (0.52 ml, 4.35 mmol) in THF (20 ml) and this mixture was stirred for 30 min. The solvent was removed *in vacuo* and the

product was extracted into light petroleum (30 ml). The resulting mixture with pale solids was filtered and the solvent was removed from the filtrate *in vacuo* to give **255** as a white powder. Yield: 1.64 g, 86%.

$^1\text{H}$  NMR [ $\text{CDCl}_3$ ]:  $\delta$  1.22 (d,  $J_{\text{HH}} = 6.8$  Hz, 12H,  $\text{CHMeMe}$ ), 1.28 (d,  $J_{\text{HH}} = 6.8$  Hz, 12H,  $\text{CHMeMe}$ ), 1.48-1.87 (m, 8H,  $\text{PCH}_2\text{CH}_2$ ), 4.28 (dm,  $J_{\text{PH}} = 215$  Hz, PH), 7.14-7.18 (m, 4H, ArH), 7.30 (m, 2H, ArH).  $^{13}\text{C}\{^1\text{H}\}$  [ $\text{CDCl}_3$ ]:  $\delta$  23.70 (dd,  $J_{\text{PC}} = 11.4$  Hz,  $J_{\text{PC}} = 1.4$  Hz,  $\text{PCH}_2\text{CH}_2$ ), 24.42 ( $\text{CHMeMe}$ ), 24.96 ( $\text{CHMeMe}$ ), 30.03 (m,  $\text{PCH}_2\text{CH}_2$ ), 32.76 (d,  $J_{\text{PC}} = 13.8$  Hz,  $\text{CHMeMe}$ ), 123.24 (d,  $J_{\text{PC}} = 3.2$  Hz, ArH), 129.16 (ArH), 131.41 (d,  $J_{\text{PC}} = 16.3$  Hz, Ar), 152.90 (d,  $J_{\text{PC}} = 10.8$  Hz, Ar).  $^{31}\text{P}$  NMR [ $\text{CDCl}_3$ ]:  $\delta$  -94.6 (d,  $J_{\text{PH}} = 215$  Hz).

#### 11.9.10 Synthesis of $\{\text{CH}_2\text{CH}_2(\text{PLiDipp})\}_2(\text{THF})_6$ (**260**)

To a solution of  $\{\text{CH}_2\text{CH}_2(\text{PHDipp})\}_2$  (**255**) (0.86 g, 1.94 mmol) in THF (15 ml) was added a solution of *n*BuLi in hexanes (2.3 M, 1.7 ml, 3.9 mmol) and the resulting red solution was stirred for 1 h. The resulting solution was reduced to 5 ml and heated to dissolve a small amount of yellow solid that had formed. Storage at 4 °C overnight yielded large yellow crystals of  $\{\text{CH}_2\text{CH}_2(\text{PLiDipp})\}_2(\text{THF})_6$  (**260**). The supernatant solution was removed by filtration and the remaining solid material was washed with light petroleum (3 x 5 ml). The residual solvent was removed under vacuum to give the product as a yellow powder. Yield: 1.11 g, 64%.

$^1\text{H}$  NMR [ $\text{d}_8$ -toluene]:  $\delta$  1.35 (m, 24H, THF), 1.43 (s,  $\text{CHMeMe}$ , 12H), 1.45 (s, 12H,  $\text{CHMeMe}$ ), 2.10 (br. s, 4H,  $\text{PCH}_2\text{CH}_2$ ), 2.59 (br. s, 4H,  $\text{PCH}_2\text{CH}_2$ ), 3.46 (m, 24H, THF), 4.13 (br. s, 4H,  $\text{CHMeMe}$ ), 7.07-7.11 (m, 6H, ArH).  $^{13}\text{C}\{^1\text{H}\}$  NMR [ $\text{d}_8$ -toluene]: 25.59 ( $\text{CHMe}_2$ ), 25.67 (THF), 27.55 (m,  $\text{PCH}_2\text{CH}_2$ ), 33.50 ( $\text{CHMe}_2$ ), 36.34 ( $\text{PCH}_2\text{CH}_2$ ), 68.15 (THF), 122.45, 123.60 (ArH), 149.78 (d,  $J_{\text{PC}} = 38$  Hz, Ar), 150.88 (Ar).  $^7\text{Li}$  NMR [ $\text{d}_8$ -toluene]: 3.1 (m).  $^{31}\text{P}$  NMR [ $\text{d}_8$ -toluene]:  $\delta$  -102.4 (br. s), -111.1 (br. s) in an 11:1 ratio.

#### 11.9.11 Synthesis of $\text{CH}_2\{\text{CH}_2\text{CH}_2(\text{PHDipp})\}_2$ (**256**)

A solution of  $\text{PhCH}_2\text{K}$  (1.160 g, 8.90 mmol) in THF (20 ml) was added to a solution of  $\text{DippPH}_2$  (**243**) (1.73 g, 8.90 mmol) in THF (20 ml). The resulting solution was stirred for 30 min and added, dropwise, to a solution of 1,5-dibromopentane (0.60 ml, 4.40 mmol) in THF (20 ml) and the resulting mixture was stirred for 30 min. The solvent was removed from the resulting mixture *in vacuo* and the product was extracted into light petroleum (30 ml). The

resulting mixture was filtered and the solvent was removed from the filtrate *in vacuo* to give **256** as a colourless oil. Yield: 1.75 g, 87%.

$^1\text{H}$  NMR [ $\text{CDCl}_3$ ]:  $\delta$  1.21 (d,  $J_{\text{HH}} = 6.8$  Hz, 12H,  $\text{CHMeMe}$ ), 1.28 (d,  $J_{\text{HH}} = 6.8$  Hz, 12H,  $\text{CHMeMe}$ ), 1.38-1.88 (m, 10H,  $\text{PCH}_2\text{CH}_2\text{CH}_2$ ), 3.63 (m, 4H,  $\text{CHMeMe}$ ), 4.27 (dm,  $J_{\text{PH}} = 215$  Hz, 2H, PH), 7.14-7.17 (m, 4H, ArH), 7.29 (m, 2H, ArH).  $^{13}\text{C}\{^1\text{H}\}$  [ $\text{CDCl}_3$ ]:  $\delta$  23.86 (d,  $J_{\text{PC}} = 11.1$  Hz,  $\text{PCH}_2\text{CH}_2\text{CH}_2$ ), 24.42 ( $\text{CHMeMe}$ ), 24.95 ( $\text{CHMeMe}$ ), 28.35 (d,  $J_{\text{PC}} = 10.8$  Hz,  $\text{PCH}_2\text{CH}_2\text{CH}_2$ ), 32.56 ( $\text{PCH}_2\text{CH}_2\text{CH}_2$ ), 32.75 (d,  $J_{\text{PC}} = 13.9$  Hz,  $\text{CHMeMe}$ ), 123.21 (d,  $J_{\text{PC}} = 3.3$  Hz, ArH), 129.11 (ArH), 131.52 (d,  $J_{\text{PC}} = 16.2$  Hz), 152.88 (d,  $J_{\text{PC}} = 10.6$  Hz).  $^{31}\text{P}\{^1\text{H}\}$  NMR [ $\text{CDCl}_3$ ]: -94.4 (d,  $J_{\text{PH}} = 215$  Hz).

#### 11.9.12 Synthesis of $[\text{CH}_2\{\text{CH}_2\text{CH}_2\text{P}(\text{Dipp})\}_2]\text{Li}_2(\text{THF})_6(\text{C}_7\text{H}_8)$ (**261b**)

To a solution of  $\text{CH}_2\{\text{CH}_2\text{CH}_2(\text{PHDipp})\}_2$  (**256**) (1.08 g, 2.38 mmol) in THF (15 ml) was added a solution of *n*BuLi (2.3 M, 2.1 ml, 4.8 mmol) in hexanes and the resulting red solution was stirred for 1 h. The solvent was removed from the resulting solution *in vacuo* and the sticky orange solid was extracted into toluene (10 ml) and left to stand overnight. The resulting large yellow crystals of  $[\text{CH}_2\{\text{CH}_2\text{CH}_2\text{P}(\text{Dipp})\}_2]\text{Li}_2(\text{THF})_6(\text{C}_7\text{H}_8)$  (**261a**), which were characterised by X-ray crystallography, were washed with cold (0 °C) light petroleum (2 x 5 ml) and the residual solvent was removed under vacuum to give the alternative solvate  $[\text{CH}_2\{\text{CH}_2\text{CH}_2(\text{PLiDipp})\}_2](\text{THF})_{2.5}$  (**261b**). Yield: 0.867 g, 56%.

$^1\text{H}$  NMR [ $\text{d}_8$ -toluene, 353 K]: 1.32 (d,  $J_{\text{HH}} = 6.8$  Hz, 24H,  $\text{CHMe}_2$ ), 1.40 (m, 10H, THF), 1.76 (br. s, 6H,  $\text{PCH}_2\text{CH}_2\text{CH}_2$ ), 2.26 (br. s, 4H,  $\text{PCH}_2\text{CH}_2\text{CH}_2$ ), 3.47 (m, 10H, THF), 4.37 (br. s, 4H,  $\text{CHMe}_2$ ), 7.06 (s, 6H, ArH).  $^{13}\text{C}\{^1\text{H}\}$  NMR [ $\text{d}_8$ -toluene, 353 K]: 25.36 ( $\text{CHMe}_2$ ), 25.76 (THF), 34.08 ( $\text{CHMe}_2$ ), 68.80 (THF), 122.67 (ArH), 152.93 (br. s, Ar).  $^7\text{Li}$  NMR [ $\text{d}_8$ -toluene, 353 K]: 3.10 (br. s)  $^{31}\text{P}\{^1\text{H}\}$  NMR [ $\text{d}_8$ -toluene, 353 K]: -105.8 (br. s), -114.7 (br. s) in a 1:0.7 ratio respectively.

#### 11.10 References

- [1] (a) K. Issleib, *Zeitschrift für Chemie*, **1960**, 2, 163-173; (b) K. Issleib, W. Bttcher, *Z. Anorg. Allg. Chem.*, **1974**, 406, 178-184; (c) K. Issleib, G. Döll, *Chem. Ber.*, **1961**, 94, 2664-2669; (d) K. Issleib, H.-J. Deylig, *Chem. Ber.*, **1964**, 97, 946-951.
- [2] (a) P. B. Hitchcock, M. F. Lappert, P. P. Power, S. J. Smith, *J. Chem. Soc., Chem. Commun.*, **1984**, 1669-1670; (b) P. Brooks, D. C. Craig, M. J. Gallagher, A. D. Rae, A. Sarroff, *J. Organomet. Chem.*, **1987**, 323, C1-C4.
- [3] J. S. Ritch, D. Julienne, S. R. Rybchinski, K. S. Brockman, K. R. Johnson, P. G. Hayes, *Dalton Trans*, **2014**, 43, 267-276.
- [4] F. Gol, G. Hasselkuß, P. C. Knüppel, O. Stelzer, *Z. Naturforsch., B*, **1988**, 43.



- [5] F. Dornhaus, M. Bolte, H.-W. Lerner, M. Wagner, *J. Organomet. Chem.*, **2007**, 692, 2949-2955.
- [6] (a) A. M. Arif, R. A. Jones, M. H. Seeberger, B. R. Whittlesey, T. C. Wright, *Inorg. Chem.*, **1986**, 25, 3943-3949; (b) E. M. Lane, T. W. Chapp, R. P. Hughes, D. S. Glueck, B. C. Feland, G. M. Bernard, R. E. Wasylshen, A. L. Rheingold, *Inorg. Chem.*, **2010**, 49, 3950-3957; (c) R. Zaffaroni, T. B. Rauchfuss, A. Fuller, L. De Gioia, G. Zampella, *Organometallics*, **2012**, 32, 232-238; (d) A. L. Rheingold, *Acta Crystallogr. C*, **1985**, 41, 1043-1045; (e) L. Chen, D. J. Kountz, D. W. Meek, *Organometallics*, **1985**, 4, 598-601.
- [7] (a) P. B. Hitchcock, M. F. Lappert, W.-P. Leung, P. Yin, *J. Chem. Soc., Dalton Trans.*, **1995**; (b) E. P. Kyba, M. C. Kerby, R. P. Kashyap, K. L. Hassett, R. E. Davis, *J. Organomet. Chem.*, **1988**, 346, C19-C23; (c) R. Edge, R. J. Less, V. Naseri, E. J. McInnes, R. E. Mulvey, D. S. Wright, *Dalton Trans.*, **2008**, 6454-6460; (d) E. P. Kyba, M. C. Kerby, R. P. Kashyap, J. A. Mountzouris, R. E. Davis, *Organometallics*, **1989**, 8, 852-855; (e) M. D. Soucek, C. C. Clubb, E. P. Kyba, D. S. Price, V. G. Scheuler, H. O. Aldaz-Palacios, R. E. Davis, *Organometallics*, **1994**, 13, 1120-1128; (f) D. A. Atwood, A. H. Cowley, R. A. Jones, R. J. Powell, C. M. Nunn, *Organometallics*, **1996**, 15, 2657-2659; (g) R. L. Wells, H. Rahbarnoohi, P. B. Glaser, L. M. Liable-Sands, A. L. Rheingold, *Organometallics*, **1996**, 15, 3204-3209; (h) K. S. A. Motolko, D. J. H. Emslie, H. A. Jenkins, J. F. Britten, *Eur. J. Inorg. Chem.*, **2017**, 2017, 2920-2927; (i) M. S. Winston, J. E. Bercaw, *Organometallics*, **2010**, 29, 6408-6416; (j) A. Moores, N. Mézailles, L. Ricard, F. Mathey, P. Le Floch, *Chem. Commun.*, **2003**, 1914-1915.
- [8] (a) K. Issleib, R. Kümmel, H. Oehme, I. Meißner, *Chem. Ber.*, **1968**, 101, 3612-3618; (b) K. Issleib, G. Döll, *Chem. Ber.*, **1963**, 96, 1544-1550.
- [9] R. T. Boéré, J. D. Masuda, *Can. J. Chem.*, **2002**, 80, 1607-1617.
- [10] H. A. Tallis, P. D. Newman, P. G. Edwards, L. Ooi, A. Stasch, *Dalton Trans.*, **2008**, 47-53.
- [11] K. Izod, *Adv. Inorg. Chem.*, **2000**, 50, 33-107.
- [12] D. M. Anderson, P. B. Hitchcock, M. F. Lappert, I. Moss, *Inorg. Chim. Acta*, **1988**, 141, 157-159.
- [13] W. Clegg, K. Izod, W. McFarlane, P. O'Shaughnessy, *Organometallics*, **1999**, 18, 3950-3952.
- [14] H. J. Reich, B. Ö. Gudmundsson, *J. Am. Chem. Soc.*, **1996**, 118, 6074-6075.
- [15] M. A. Beswick, J. M. Goodman, A. D. Hopkins, M. A. Paver, P. R. Raithby, A. E. H. Wheatley, D. S. Wright, *Chem. Commun.*, **1997**, 1879.
- [16] S. Hietkamp, H. Sommer, O. Stelzer, A. L. Balch, J. C. Linehan, D. E. Oram, **1989**, 25, 120-122.
- [17] T. Shimidzu, K. Yamana, S. Maikuma, *Tetrahedron Lett.*, **1984**, 25, 4237-4240.

## Chapter 12. *P*-Heterocyclic stannylenes

In Chapter 4, we studied the effect of modifying the sterics at the phosphorus centres in diphosphatetrylenes and observed that a high degree of steric crowding is required to invoke planarity at one of the phosphorus centres. An alternative strategy to lowering the energy of planarization is the incorporation of the phosphorus centre into a ring.<sup>[1]</sup> There are only four examples reported of monomeric tetrylenes utilising *P*-heterocyclic ligand systems (Fig. 131).<sup>[2]</sup> Compound **77** is the only example of such a system that has a planar geometry at the phosphorus centres.<sup>[2b]</sup> The *P*-heterocyclic tetrylenes **172Ge** and **172Sn** have previously been synthesised using the 1,2-ethylenebis(phenylphosphide) ligand and are assumed to be oligomeric in solution.<sup>[3]</sup> We sought to use the previously prepared diphosphides (Chapter 11) as ligands for *P*-heterocyclic stannylenes, which feature the more sterically demanding Dipp substituents compared **172Ge** and **172Sn**.

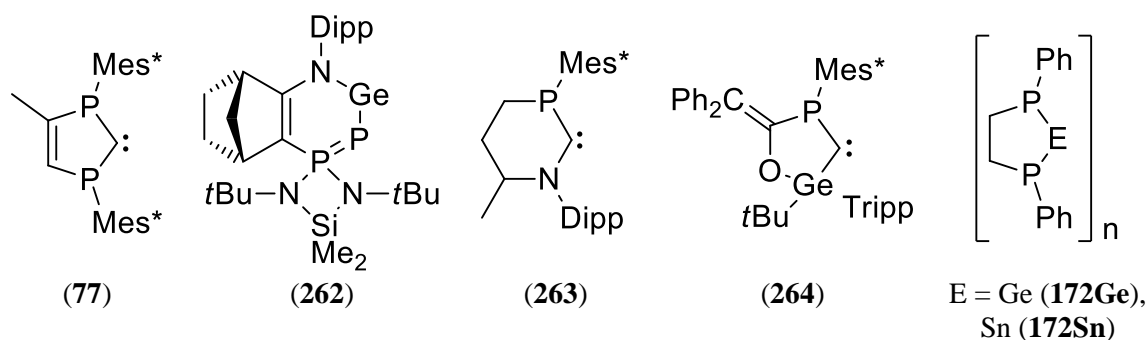
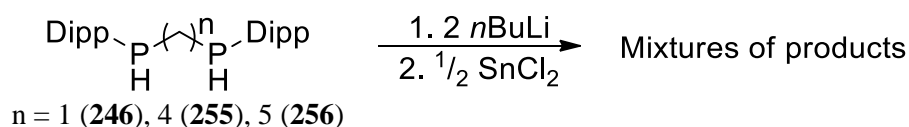


Figure 131: Previously reported *P*-heterocyclic tetrylenes

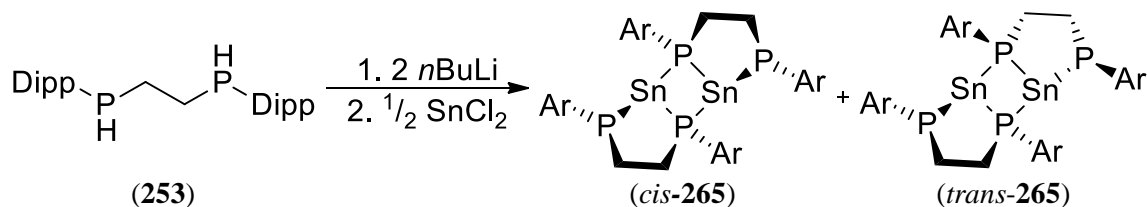
### 12.1 Synthesis of the *P*-Heterocyclic stannylenes

The reactions between **246**, **255** or **256** and two equivalents of *n*BuLi, followed by the addition of the respective dilithium diphosphides to SnCl<sub>2</sub> gave yellow solutions (Scheme 61), which exhibited multiple very broad, low intensity signals in their <sup>31</sup>P NMR spectra. Unfortunately, it was not possible to isolate clean products from these solutions for further analysis.



Scheme 61: Attempted synthesis of diphosphastannylenes

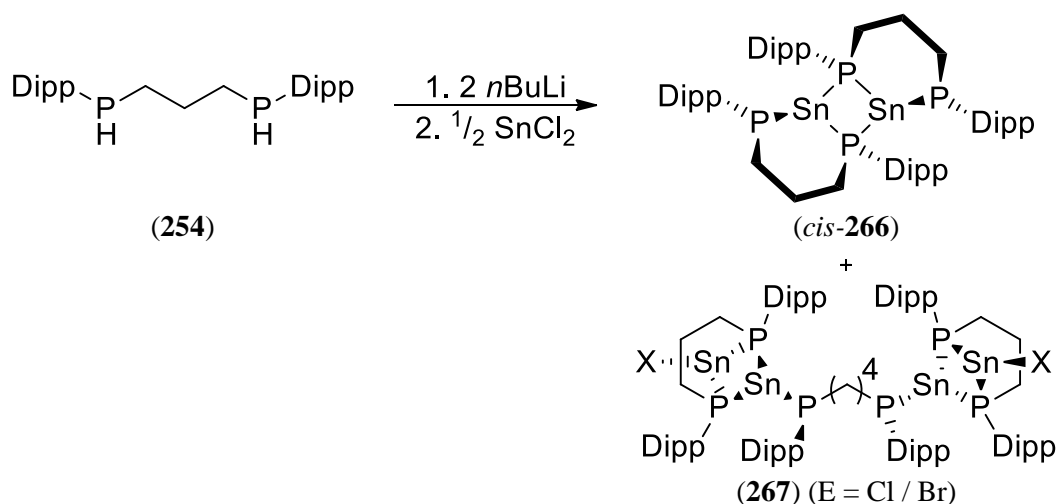
Treatment of **253** with two equivalents of *n*BuLi, followed by the addition of the resulting dilithium diphosphide to a solution of SnCl<sub>2</sub> in cold THF gave a yellow solution containing a mixture of two stereoisomers of [{CH<sub>2</sub>(PDipp)}<sub>2</sub>Sn]<sub>2</sub> (**265**), as observed by <sup>31</sup>P NMR spectroscopy (Scheme 62). A crystal of [{CH<sub>2</sub>(PDipp)}<sub>2</sub>Sn]<sub>2</sub>.Et<sub>2</sub>O (*trans*-**265a**) suitable for characterisation by X-ray crystallography was obtained by standing a solution of **265** in Et<sub>2</sub>O. Crystallisation from a mixture of Et<sub>2</sub>O and light petroleum gave [{CH<sub>2</sub>(PDipp)}<sub>2</sub>Sn]<sub>2</sub> (*cis/trans*-**265b**) in a moderate yield as a mixture of two stereoisomers in a 5:1 ratio.



**Scheme 62:** Synthesis of the diphosphastannylenes *cis/trans*-**265** (Ar = Dipp)

In a similar reaction, treatment of **254** with two equivalents of *n*BuLi, followed by the addition of the resulting dilithium diphosphide to a solution SnCl<sub>2</sub> in cold THF gave [CH<sub>2</sub>{CH<sub>2</sub>(PDipp)}<sub>2</sub>Sn]<sub>2</sub>.(*n*-hexane)(THF)<sub>0.5</sub> (**266a**) in low yield after crystallisation from *n*-hexane. Single crystals of [CH<sub>2</sub>{CH<sub>2</sub>(PDipp)}<sub>2</sub>Sn]<sub>2</sub>.(THF)<sub>2</sub> (*cis*-**266b**) suitable for X-ray crystallography were obtained from a mixture of THF and benzene, while crystals of the alternate solvate [CH<sub>2</sub>{CH<sub>2</sub>(PDipp)}<sub>2</sub>Sn]<sub>2</sub>.(THF)<sub>3</sub> (*cis*-**266c**) were obtained from THF.

In a single instance, a very small number of pale yellow crystals were obtained from the filtrate of **266a**, which were shown by X-ray crystallography to be heteroleptic species ([CH<sub>2</sub>{CH<sub>2</sub>(PDipp)}<sub>2</sub>SnX]Sn)<sub>2</sub>{(PDipp)CH<sub>2</sub>}<sub>2</sub>CH<sub>2</sub> [X = Cl/Br] (**267**); unfortunately, we were not able to isolate bulk samples of **267**.



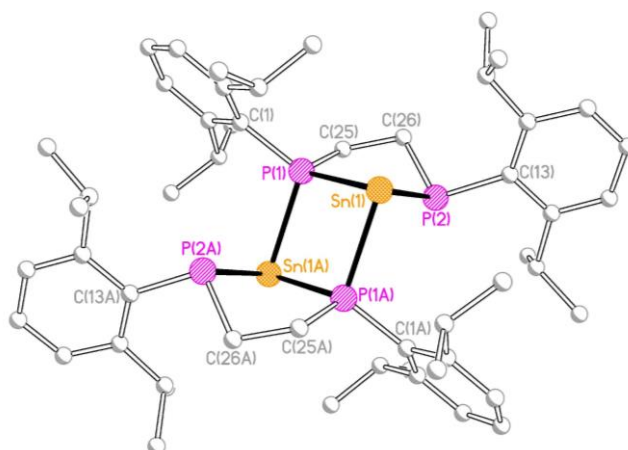
**Scheme 63:** Synthesis of the diphosphastannylene *cis*-**266** and the minor side-product **267**

**12.2 Solid-state structures of  $[\{\text{CH}_2(\text{PDipp})\}_2\text{Sn}]_2\cdot\text{Et}_2\text{O}$  (*trans*-**265a**),  $[\text{CH}_2\{\text{CH}_2(\text{PDipp})\}_2\text{Sn}]_2(\text{THF})_2$  (*cis*-**266b**) and  $([\text{CH}_2\{\text{CH}_2(\text{PDipp})\}_2\text{SnX}]\text{Sn})_2\{(\text{PDipp})\text{CH}_2\}_2\text{CH}_2\}$  [ $\text{X} = \text{Cl/Br}$ ] (**267**)**

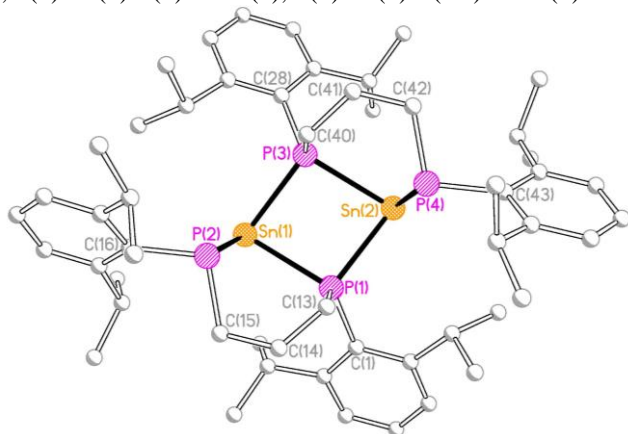
The molecular structures of *trans*-**265a**, *cis*-**266b** and **267** are shown in Figures 132, 133 and 134, respectively, along with selected bond lengths and angles. Compound *trans*-**265a** crystallises as a phosphorus-bridged dimer with inversion symmetry, with planar, rhombus-shaped  $\text{P}_2\text{Sn}_2$  core, and with one molecule of  $\text{Et}_2\text{O}$  in the lattice. The tin and terminal phosphorus atoms have distorted trigonal pyramidal geometries [sum of angles at  $\text{Sn}(1) = 244.26^\circ$  and  $\text{P}(2) = 308.13^\circ$ ] and a stereochemically active lone pair. The terminal phosphorus centres have a *trans*-arrangement and are chiral; both  $\text{P}^t_R\text{P}^t_S$  and  $\text{P}^t_S\text{P}^t_R$  stereoisomers are present as a racemic mixture in the crystal (where  $\text{P}^t$  and  $\text{P}^{\text{br}}$  refer to the bridging and terminal phosphorus atoms, respectively).

Compounds *cis*-**266b** and *cis*-**266c** are pseudo-polymorphs, which only differ in the number of THF molecules present in the asymmetric unit. Only the structure of *cis*-**266b** will be discussed in detail as it has the highest quality dataset. Compound *cis*-**266b** crystallises as a phosphorus-bridged dimer with two molecules of THF in the asymmetric unit. The  $\text{P}_2\text{Sn}_2$  core has a butterfly-shaped geometry and the two terminal phosphorus centres have a *cis*-arrangement. The  $\text{P}^t_R\text{P}^t_R$  and  $\text{P}^t_S\text{P}^t_S$  stereoisomers are present as a racemic mixture in the crystal.

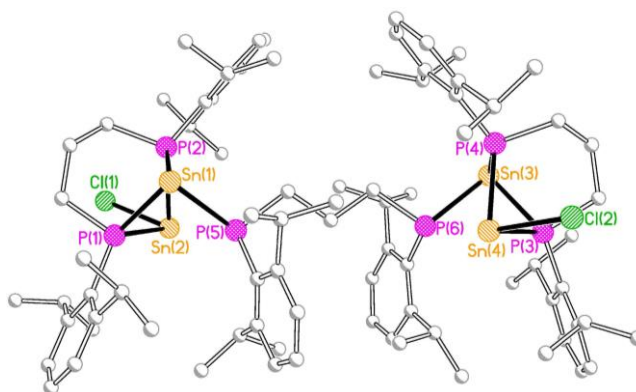
Compound **267** crystallises with minor disorder of the Dipp groups and with solvent-accessible voids that appear to contain both  $\text{Et}_2\text{O}$  and THF molecules in multiple, partially occupied sites, which could not be modelled. There are two distinct types of diphosphide ligand, one of which adopts a linear configuration that bridges two tin atoms [ $\text{Sn}(1)$  and  $\text{Sn}(3)$ ]. The two remaining diphosphide ligands each chelate  $\text{Sn}(1)$  or  $\text{Sn}(3)$  to generate six-membered rings. Each of these latter two ligands is further coordinated to a  $\text{SnX}$  unit, via both of the phosphorus centres. The halogen site on the tin atom has substitutional disorder where chlorine and bromine atoms are present in an approximate 60:40 ratio.



**Figure 132:** Molecular structure of *trans*-**265a** with solvent of crystallisation and H atoms omitted for clarity. Selected bond lengths (Å) and angles (°): Sn(1)-P(1) 2.6600(7), Sn(1)-P(1A) 2.6282(7), Sn(1)-P(2) 2.5949(7), P(1A)-Sn(1)-P(1) 80.01(2), P(2)-Sn(1)-P(1) 76.94(2), P(2)-Sn(1)-P(1A) 87.31(2).



**Figure 133:** Molecular structure of *cis*-**266b** with solvent of crystallisation and H atoms omitted for clarity. Selected bond lengths (Å) and angles (°): Sn(1)-P(1) 2.6616(6), Sn(1)-P(2) 2.5986(6), Sn(1)-P(3) 2.6216(6), Sn(2)-P(1) 2.6322(6), Sn(2)-P(3) 2.6662(6), Sn(2)-P(4) 2.6013(6), P(2)-Sn(2)-P(1) 83.548(18), P(2)-Sn(1)-P(3) 93.756(18), P(3)-Sn(1)-P(1) 79.723(18), P(1)-Sn(2)-P(3) 79.451(18), P(4)-Sn(2)-P(1) 93.856(18), P(4)-Sn(2)-P(3) 83.376(17).



**Figure 134:** Molecular structure of **267** with minor disorder components and H atoms omitted for clarity [N.B only Cl atoms shown for the disordered Cl/Br atoms]. Selected bond lengths (Å) and angles (°): Sn(1)-P(1) 2.6536(8), Sn(1)-P(2) 2.6474(8), Sn(1)-P(5) 2.5959(8), Sn(2)-P(1) 2.6642(7), Sn(2)-P(2) 2.6748(8), Sn(2)-Cl(1) 2.634(12), Sn(2)-Br(1) 2.723(7), Sn(3)-P(3) 2.6688(7), Sn(3)-P(4) 2.6418(8), Sn(3)-P(6) 2.5957(7), Sn(4)-P(3) 2.6771(7), Sn(4)-P(4) 2.6777(8), Sn(4)-Cl(2) 2.634(14), Sn(4)-Br(2) 2.715(7), P(2)-Sn(1)-P(1) 71.03(2), P(5)-Sn(1)-P(1) 82.35(2), P(5)-Sn(1)-P(2) 79.32(2), P(1)-Sn(2)-P(2) 70.45(2), P(1)-Sn(2)-Br(1) 92.79(16), P(2)-Sn(2)-Br(1) 93.07(15), Cl(1)-Sn(2)-P(1) 94.0(3), Cl(1)-Sn(2)-P(2) 88.8(3), P(4)-Sn(3)-P(3) 70.14(2), P(6)-Sn(3)-P(3) 80.43(2), P(6)-Sn(3)-P(4) 80.79(2), P(3)-Sn(4)-P(4) 69.48(2), P(3)-Sn(4)-Br(2) 93.1(2), P(4)-Sn(4)-Br(2) 94.4(2), Cl(2)-Sn(4)-P(3) 89.3(4), Cl(2)-Sn(4)-P(4) 93.0(4).

The Sn-P distances at the four-coordinate phosphorus centres [2.6282(7), 2.6600(7) (*trans*-**265a**); 2.6616(6), 2.6662(6) (*cis*-**266b**) and 2.6418(8)-2.6748(8) Å] are similar to the distances in [Li(THF){Sn(P*t*Bu<sub>2</sub>)<sub>3</sub>}], which range from 2.671(4) to 2.702(3) Å,<sup>[4]</sup> while the Sn-P distances at the three-coordinate phosphorus centres are slightly shorter [2.5949(7) (*trans*-**265a**); 2.5986(6), 2.6322(6) (*cis*-**266b**) and 2.5957(7)-2.5959(8) Å]. These distances are still similar to typical Sn(II)-P distances; for example, the Sn-P distances in [{(Me<sub>3</sub>Si)<sub>2</sub>CH}(C<sub>6</sub>H<sub>4</sub>-2-NMe<sub>2</sub>)P]<sub>2</sub>Sn range are 2.5995(10) and 2.61110(1) Å.<sup>[5]</sup> The dimeric structures of *trans*-**265a** and *cis*-**266b** demonstrate that the combination of Dipp and alkyl substituents in the diphosphide ligands are insufficiently bulky to prevent dimerization. In contrast, the diamido analogues {CH<sub>2</sub>(NDipp)}<sub>2</sub>Sn (**268**) and CH<sub>2</sub>{CH<sub>2</sub>(NDipp)}<sub>2</sub>Sn (**269**) are monomeric in the solid-state and are stabilised by pπ-pπ interactions from two planar nitrogen centres, while the less sterically hindered derivative [{CH<sub>2</sub>(NMe<sub>3</sub>)}<sub>2</sub>Sn]<sub>2</sub> (**270**) is dimeric and has a similar structure to *trans*-**265a**.<sup>[6]</sup> The difference in aggregation of the congeners *trans*-**265a**/**268** and *cis*-**266b**/**269** is most likely attributed to the ligand system not sufficiently lowering the energy of planarization of phosphorus. Therefore, the phosphorus centres in *trans*-**265a** and *cis*-**266b** adopt a pyramidal geometry, in which lone pairs can interact intermolecularly with the unstabilized tin centres, whereas nitrogen centres in **268** and **269** readily adopt a planar geometry that ties up the lone pairs by the stabilizing pπ-pπ interactions to the tin centres.

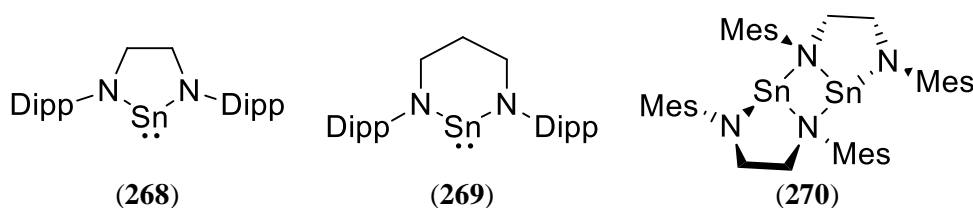


Figure 135: N-heterocyclic stannylene analogues of *trans*-**265a** and *cis*-**266b**

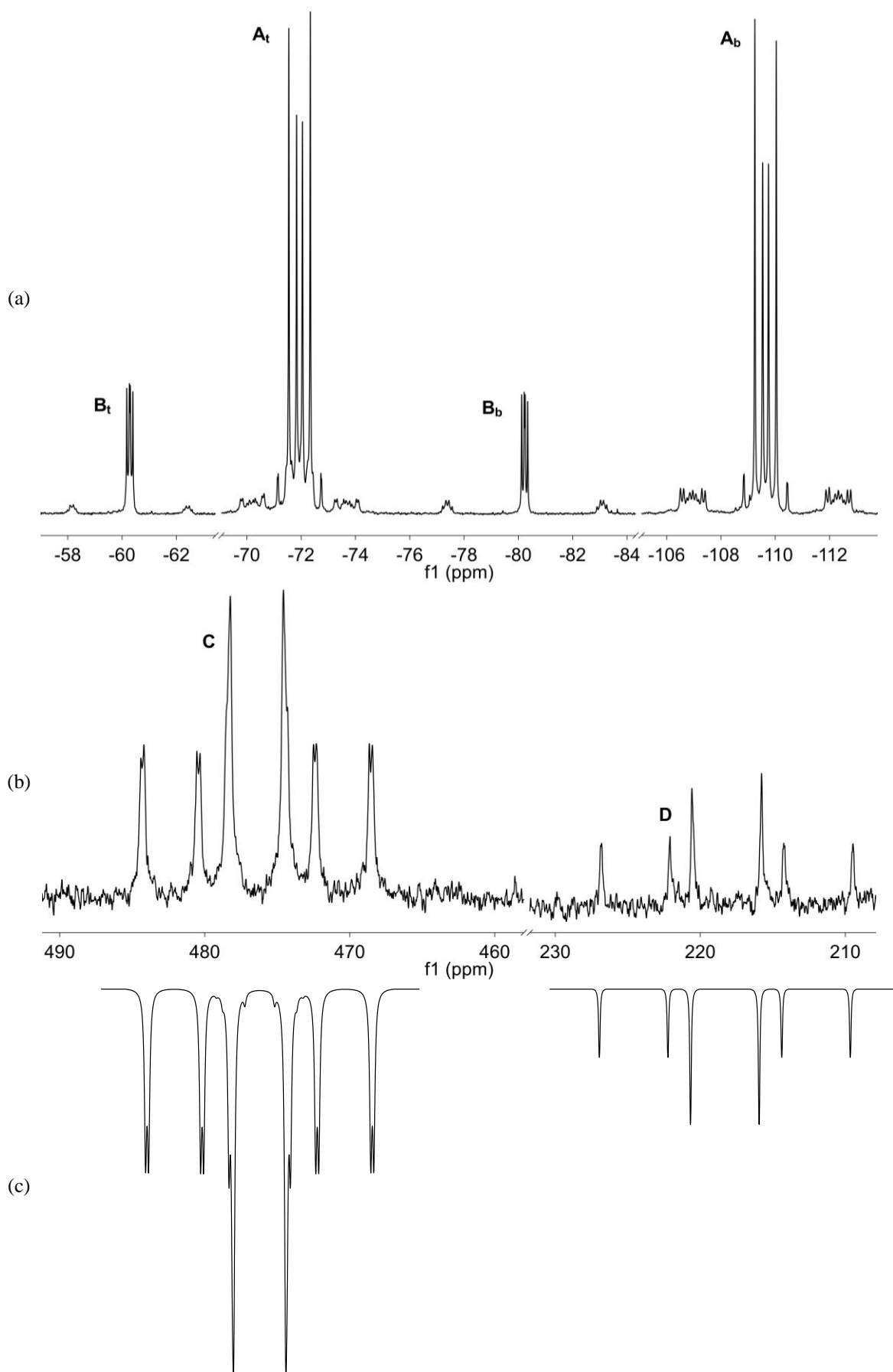
The *cis/trans* arrangement of the terminal phosphides in *cis*-**265a** and *trans*-**266b** does not appear to be influenced by the sterics at the phosphorus centres. Previous examples of X-ray crystallographically characterised diphosphatetrylenes dimers also show no correlation between the substituents and the relative stereochemistry of the terminal phosphides. For example, [{(Me<sub>3</sub>Si)<sub>2</sub>P}<sub>2</sub>Pb]<sub>2</sub> (**271**) and ([{(Me<sub>3</sub>Si)<sub>2</sub>CH}(Ph)P]<sub>2</sub>Ge)<sub>2</sub> (**272**) have a *cis*-arrangement while the diphosphatetrylenes {(*t*Bu<sub>2</sub>P)<sub>2</sub>Pb}<sub>2</sub> (**273**) and {(*i*Pr<sub>2</sub>P)<sub>2</sub>Ge}<sub>2</sub> (**274**) and the heteroleptic (phospha)(chloro)germylene {(μ<sub>2</sub>-*t*Bu<sub>2</sub>P)GeCl]<sub>2</sub> (**275**) have a *trans*-arrangement. The phosphastannylene dimers {(*t*Bu<sub>2</sub>P)<sub>2</sub>Sn]<sub>2</sub> (**276**)<sup>[7]</sup>, {(μ<sub>2</sub>-*t*Bu<sub>2</sub>P)SnCl]<sub>2</sub> (**277**)<sup>[7]</sup> and [{(Me<sub>3</sub>Si)<sub>2</sub>P]<sub>2</sub>Sn]<sub>2</sub> (**278**)<sup>[8]</sup> have only been characterised by NMR spectroscopy.

### 12.3 NMR spectra of $[\{\text{CH}_2(\text{PDipp})\}_2\text{Sn}]_2$ (*cis/trans*-**265b**) and $[\text{CH}_2\{\text{CH}_2(\text{PDipp})\}_2\text{Sn}]_2(n\text{-hexane})(\text{THF})_{0.5}$ (*cis*-**266c**)

As *cis/trans*-**265b** consists of a mixture of stereoisomers it was not possible to confidently assign the peaks in its  $^1\text{H}$  and  $^{13}\text{C}\{^1\text{H}\}$  NMR spectra to the individual stereoisomers as the broad, complex signals had significant overlap. The  $^{31}\text{P}\{^1\text{H}\}$  NMR spectrum of *cis/trans*-**265b** consists of two pairs of multiplets at -109.6 (**A<sub>b</sub>**,  $J_{\text{PSn}} = 1085$  Hz) and -71.9 (**A<sub>t</sub>**,  $J_{\text{PSn}} = 700$  Hz) for the major stereoisomer and at -80.2 (**B<sub>b</sub>**,  $J_{\text{PSn}} = 1150$  Hz) and -60.3 ppm (**B<sub>t</sub>**,  $J_{\text{SnP}} = 870$  Hz) for the minor stereoisomer, in an approximate 5:1 ratio (Fig. 136). A distribution of *cis/trans* isomers has been observed in **278**, as judged by  $^{31}\text{P}\{^1\text{H}\}$  NMR spectroscopy.<sup>[8]</sup> The identities of the bridging (**A<sub>b</sub>/B<sub>b</sub>**) and terminal phosphorus centres (**A<sub>t</sub>/B<sub>t</sub>**) were assigned by the relative intensities of tin satellites, with the satellites on the bridging centres having approximately twice the intensity. Peaks **A<sub>b</sub>/A<sub>t</sub>** exhibit significantly larger  $^{31}\text{P}$ - $^{31}\text{P}$  coupling than **B<sub>b</sub>/B<sub>t</sub>**. The  $^{119}\text{Sn}\{^1\text{H}\}$  NMR spectrum of *cis/trans*-**265b** consists of two complex multiplets at 218.2 (**C**) and 476.4 (**D**) in an approximate 4:1 ratio (Fig. 136a).

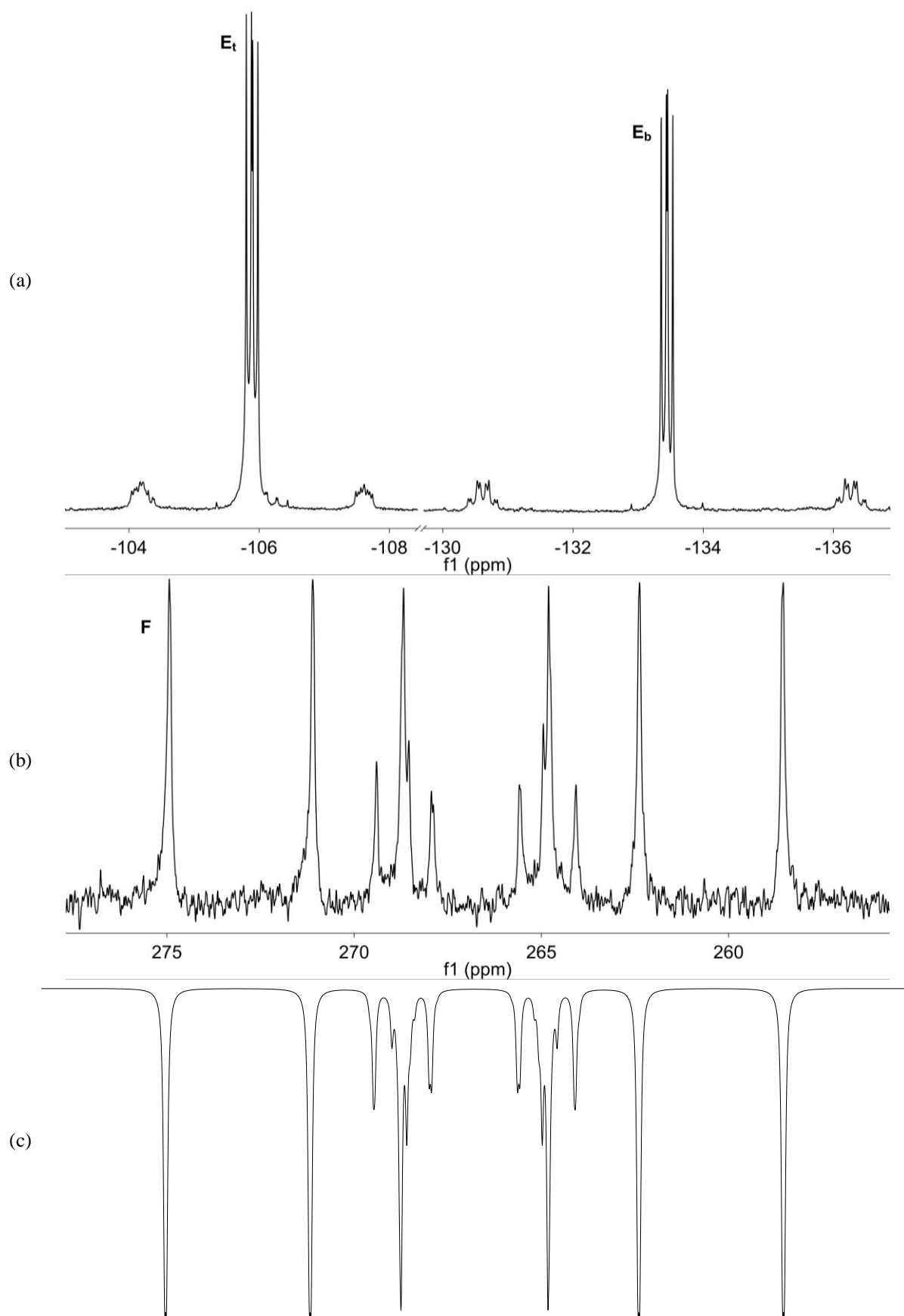
The  $^{31}\text{P}\{^1\text{H}\}$  NMR spectrum of **266c** consists of a pair of multiplets at -133.4 ppm (**E<sub>b</sub>**,  $J_{\text{PSn}} = 1140$  Hz) and -105.9 (**E<sub>t</sub>**,  $J_{\text{PSn}} = 700$  Hz) while the  $^{119}\text{Sn}$  NMR  $\{^1\text{H}\}$  spectrum of **266c** exhibits a complex multiplet at 266.8 ppm (**F**) (Fig. 137a). Once again, the identity of the bridging (**E<sub>b</sub>**) and terminal (**E<sub>t</sub>**) phosphorus centres were assigned by the relative intensities of the tin satellites.

The complex signals exhibited by *cis/trans*-**265b** and **266c** in their  $^{31}\text{P}\{^1\text{H}\}$  and  $^{119}\text{Sn}\{^1\text{H}\}$  NMR spectra are the result of strong second order effects and were closely replicated in the simulations generated by Professor William McFarlane, with the simulated  $^{119}\text{Sn}$  spectra displayed in Figures 136c and 137c, respectively. It is not possible to assign the peaks in the  $^{31}\text{P}\{^1\text{H}\}$  and  $^{119}\text{Sn}\{^1\text{H}\}$  NMR spectra of *cis/trans*-**265b** to either the *cis* or *trans* stereoisomers, as there appears to be no correlation between either the chemical shifts or coupling constants and those of **266c** (see Table 10).



**Figure 136:** (a)  $^{31}\text{P}\{^1\text{H}\}$  and (b)  $^{119}\text{Sn}\{^1\text{H}\}$  NMR spectra of *cis/trans*-**265b** in  $d_8$ -THF and (c) simulated  $^{119}\text{Sn}\{^1\text{H}\}$  spectra





**Figure 137:** (a)  $^{31}\text{P}\{^1\text{H}\}$  and (b)  $^{119}\text{Sn}\{^1\text{H}\}$  NMR spectra of *cis*-**266c** in  $d_8$ -THF and (c) simulated  $^{119}\text{Sn}\{^1\text{H}\}$  spectra

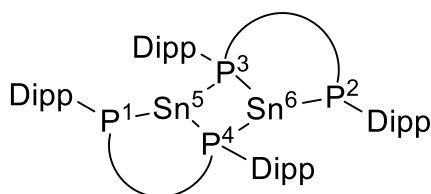


Figure 138: Numbering scheme for the NMR simulations

	<b>265b<sub>maj</sub></b>	<b>265b<sub>min</sub></b>	<b>266c</b>
P <sup>1</sup> /P <sup>2</sup>	-71.9	-60.3	-105.9
P <sup>3</sup> /P <sup>4</sup>	-109.6	-80.2	-133.4
Sn <sup>5</sup> /Sn <sup>6</sup>	476	218	262
P <sup>1</sup> -P <sup>2</sup>	3.0 ± 0.5	0 ± 1	0.0 ± 1
P <sup>2</sup> -P <sup>4</sup> / P <sup>1</sup> -P <sup>3</sup>	19.0 ± 0.5	-1.6 ± 0.5	3.5 ± 0.5
P <sup>2</sup> -P <sup>3</sup> / P <sup>1</sup> -P <sup>4</sup>	141 ± 0.5	47.0 ± 0.5	32.6 ± 0.5
P <sup>3</sup> -P <sup>4</sup>	140 ± 1	159.6 ± 0.5	108.5 ± 0.5
P <sup>1</sup> -Sn <sup>5</sup> / P <sup>2</sup> -Sn <sup>6</sup>	717.6 ± 0.5	883 ± 1	715 ± 1
P <sup>1</sup> -Sn <sup>6</sup> / P <sup>2</sup> -Sn <sup>5</sup>	-40 ± 0.5	8 ± 4	10 ± 2
P <sup>3</sup> -Sn <sup>5</sup> / P <sup>4</sup> -Sn <sup>6</sup>	1075 ± 2	1167 ± 3	1085 ± 2
P <sup>3</sup> -Sn <sup>6</sup> / P <sup>4</sup> -Sn <sup>5</sup>	1143 ± 2	1182 ± 3	1255 ± 2

**Table 10:** <sup>31</sup>P and <sup>119</sup>Sn chemical shifts (ppm) and <sup>31</sup>P-<sup>31</sup>P and <sup>31</sup>P-<sup>119</sup>Sn coupling constants (Hz) for **265b** and **266c** (coupling constants derived from simulations of the experimental <sup>31</sup>P{<sup>1</sup>H} and <sup>119</sup>Sn{<sup>1</sup>H} NMR spectra).

## 12.4 Conclusions

The reactions between **246**, **255** or **256** and two equivalents of *n*BuLi, followed by the addition of the respective dilithium diphosphides to SnCl<sub>2</sub> gave yellow solutions from which no products could be isolated. The dimeric diphosphastannylenes *cis/trans*-**265b** and *trans*-**266b** were prepared from the diphosphines **253** and **254**, respectively, which, to the best of our knowledge, are the first examples of heavier *P*-heterocyclic tetrylenes. These structures demonstrate that the ligand systems are insufficiently sterically bulky to prevent dimerization and invoke planarization of a phosphorus centre. The steric crowding at the tin centres may be increased in future *P*-heterocyclic stannylenes by using a bulkier aryl or alkyl substituent or by increasing the steric bulk on the backbone.

## 12.5 Experimental

### 12.5.1 Synthesis of $[\{\text{CH}_2(\text{PDipp})\}_2\text{Sn}]_2$ (*cis/trans*-**265b**)

To a solution of  $\{(\text{DippPH})\text{CH}_2\}_2$  (**253**) (0.44 g, 1.06 mmol) in THF (15 ml) was added a solution of *n*BuLi in hexanes (2.45 M, 0.9 ml, 2.21 mmol). The resulting orange solution was stirred for 30 min and added, dropwise, to a cold (-78 °C) solution of  $\text{SnCl}_2$  (0.200 g, 10.5 mmol) in THF (15 ml). The resulting yellow solution was allowed to warm to room temperature. The solvent was removed *in vacuo* to give a sticky yellow solid. The product was extracted into  $\text{Et}_2\text{O}$  (30 ml) to give a yellow solution with pale solids. The mixture was filtered and the yellow filtrate spontaneously formed yellow crystals of  $[\{\text{CH}_2(\text{PDipp})\}_2\text{Sn}]_2 \cdot \text{Et}_2\text{O}$  (*trans*-**265a**). Further material was obtained by storage of this mixture at 4 °C overnight. The supernatant solution was removed by filtration and the residual solvent was removed from the remaining solid under vacuum to give a yellow powder (0.08 g, 14% yield). Further material was obtained by adding light petroleum (15 ml) to the filtrate and reducing the solution in volume to 20 ml. Storage at -25 °C overnight formed yellow microcrystalline material. The supernatant solution was removed by filtration and the residual solvent was removed from the remaining solid under vacuum to give a yellow powder of *cis/trans*-**265b** (0.17 g, 30% yield). Combined yield: 0.25 g, 44%.

The  $^1\text{H}$  and  $^{13}\text{C}\{^1\text{H}\}$  NMR spectra of *cis/trans*-**265b** exhibit multiple overlapping signals from two stereoisomers (A = major stereoisomer, B = minor stereoisomer) and for a small amount of  $\text{Et}_2\text{O}$ .

$^1\text{H}$  NMR [ $d_8$ -THF]:  $\delta$  0.74 (br. m, 6.3H,  $^A\text{CHMe}_2$ ), 0.89 (d,  $J_{\text{HH}} = 6.8$  Hz, 12.6H,  $^A\text{CHMe}_2$ ), 1.13 (d,  $J_{\text{HH}} = 6.8$  Hz, 12.4H,  $^A\text{CHMe}_2 + \text{Et}_2\text{O}$ ), 1.19 (m, 2.8H,  $^B\text{CHMe}_2$ ), 1.24 (br. m, 11.7H,  $^A\text{CHMe}_2$ ), 1.31-1.33 (m, 4.8H,  $^B\text{CHMe}_2$ ), 1.35 (d,  $J_{\text{HH}} = 6.6$  Hz, 2.4H,  $^B\text{CHMe}_2$ ), 1.63 (br. m, 5.7H,  $^A\text{CHMe}_2$ ), 2.40-2.60 (m, 3.1H,  $^A\text{PCH}_2 + ^B\text{PCH}_2$ ), 2.66 (br. m, 2.1H,  $^A\text{PCH}_2$ ), 2.90 (m, 2.6H,  $^A\text{PCH}_2$ ), 3.08 (br. s, 2.0H,  $^A\text{CHMe}_2$ ), 3.35-3.43 (m, 3.1H,  $^A\text{PCH}_2 + \text{Et}_2\text{O}$ ), 3.52 (m, 4.0H,  $^A\text{CHMe}_2$ ), 3.76 (br. m, 1.3H,  $^B\text{CHMe}_2 + ^B\text{PCH}_2$ ), 4.05 (m, 0.9H,  $^B\text{CHMe}_2$ ), 4.57 (br. s, 2.0H,  $^A\text{CHMe}_2$ ), 6.96 (m, 3.9H, ArH), 7.04 (br. m, 1.9H, ArH), 7.10 (m, 2.6H, ArH), 7.15 (m, 2.0H, ArH), 7.22-7.30 (m, 4.7H, ArH).  $^{13}\text{C}\{^1\text{H}\}$  NMR [ $d_8$ -THF]:  $\delta$  24.74 ( $^A\text{CHMe}_2$ ), 26.16 ( $^A\text{CHMe}_2$ ), 26.89 ( $^B\text{CHMe}_2$ ), 27.45 ( $^A\text{CHMe}_2$ ), 30.28 (m,  $^A\text{PCH}_2$ ), 30.49 (m,  $^A\text{PCH}_2$ ), 33.26 (br. m,  $^A\text{PCH}_2 + ^B\text{PCH}_2 + ^A\text{CHMe}_2$ ), 34.01 (d,  $J_{\text{PC}} = 17.6$  Hz,  $^A\text{CHMe}_2$ ), 34.58-34.78 ( $^A\text{CHMe}_2 + ^B\text{CHMe}_2$ ), 123.85 (ArH), 124.16 (d,  $J_{\text{PC}} = 2.4$  Hz, ArH),

124.41, 125.71, 128.96, 129.51, 130.38, 130.49 (ArH), 135.82 (m, Ar), 136.17 (m, Ar), 153.61 (br. m, Ar), 154.48 (br. m, Ar), 154.72 (br. m, Ar), 156.08 (d,  $J_{PC} = 11.5$  Hz), 156.26 (d,  $J_{PC} = 10.8$  Hz).  $^{31}\text{P}\{^1\text{H}\}$  NMR [ $d_8$ -THF]:  $\delta$  -109.6 (m,  $J_{\text{PSn}} = 1085$  Hz,  $^A\text{P}_{\text{bridging}}$ ), -80.2 (m,  $J_{\text{PSn}} = 1150$  Hz,  $^B\text{P}_{\text{bridging}}$ ), -71.9 (m,  $J_{\text{PSn}} = 700$  Hz,  $^A\text{P}_{\text{terminal}}$ ), -60.3 (m,  $J_{\text{SnP}} = 870$  Hz,  $^B\text{P}_{\text{terminal}}$ ). The stereoisomers A and B are in a 5:1 ratio.  $^{119}\text{Sn}\{^1\text{H}\}$  NMR [ $d_8$ -THF]:  $\delta$  218.17 (m,  $^B\text{Sn}$ ), 476.41 (m,  $^A\text{Sn}$ ) in a 1:4 ratio

### 12.5.2 Synthesis of $[\text{CH}_2\{\text{CH}_2(\text{PDipp})\}_2\text{Sn}]_2 \cdot (n\text{-hexane})(\text{THF})_{0.5}$ (**266c**)

To a solution of  $\{\text{CH}_2\text{CH}_2(\text{PHDipp})\}_2$  (0.86 g, 2.01 mmol) in THF (20 ml) was added a solution of  $n\text{BuLi}$  in hexanes (2.45 M, 1.6 ml, 3.92 mmol). The resulting orange solution was stirred for 30 min and added, dropwise, to a cold ( $-78^\circ\text{C}$ ) solution of  $\text{SnCl}_2$  (0.377 g, 1.99 mmol) in THF (15 ml). The resulting solution was allowed to warm to room temperature to give an orange solution. The solvent was removed *in vacuo* to give a sticky orange solid. The product was extracted into  $\text{Et}_2\text{O}$  (20 ml) and the orange solution with pale solids was filtered. The solvent was removed from the filtrate *in vacuo* and  $n$ -hexane (10 ml) was added. A yellow solid immediately precipitated and the mixture was stored at  $4^\circ\text{C}$  for 2 days. The supernatant solution was removed by filtration and the residual solvent was removed from the remaining solid under vacuum to give  $[\text{CH}_2\{\text{CH}_2(\text{PDipp})\}_2\text{Sn}]_2 \cdot (n\text{-hexane})(\text{THF})_{0.5}$  (**266c**) as a yellow powder. Yield: 0.33 g, 27%.

Single crystals suitable for characterisation by X-ray crystallography of  $[\text{CH}_2\{\text{CH}_2(\text{PDipp})\}_2\text{Sn}]_2(\text{THF})_2$  (**266a**) were obtained by standing a solution of  $[\text{CH}_2\{\text{CH}_2(\text{PDipp})\}_2\text{Sn}]_2$  in a mixture of THF and benzene at room temperature for 1 week. Single crystals of the alternative solvate  $[\text{CH}_2\{\text{CH}_2(\text{PDipp})\}_2\text{Sn}]_2(\text{THF})_3$  (**266b**) were obtained by storage of a solution of  $[\text{CH}_2\{\text{CH}_2(\text{PDipp})\}_2\text{Sn}]_2$  in THF at  $-25^\circ\text{C}$  for 3 days.

The following NMR data are for **266c**. The  $^{31}\text{P}\{^1\text{H}\}$  and  $^{119}\text{Sn}\{^1\text{H}\}$  NMR spectra were collected at 298 K while the  $^1\text{H}$  and  $^{13}\text{C}\{^1\text{H}\}$  spectra were collected at 233 K in order to reduce motion of the alkyl and aryl groups to give sharp signals.

$^1\text{H}$  NMR [ $d_8$ -THF, 233 K]:  $\delta$  0.40 (d,  $J_{\text{HH}} = 6.4$  Hz, 6H,  $\text{CHMe}_2$ ), 0.88 (t,  $J_{\text{HH}} = 6.4$  Hz, 6H,  $n$ -hexane), 0.93 (d,  $J_{\text{HH}} = 6.3$  Hz, 6H,  $\text{CHMe}_2$ ), 1.23-1.27 (m, 20H,  $\text{CHMe}_2$  +  $n$ -hexane), 1.30 (d,  $J_{\text{HH}} = 6.2$  Hz,  $\text{CHMe}_2$ ), 1.34 (d,  $J_{\text{HH}} = 6.6$  Hz,  $\text{CHMe}_2$ ), 1.38 (d,  $J_{\text{HH}} = 6.5$  Hz,  $\text{CHMe}_2$ ), 1.42 (d,  $J_{\text{HH}} = 6.8$  Hz,  $\text{CHMe}_2$ ), 1.77 (s, 2H, THF), 1.80-1.85 (m, 2H,  $\text{PCH}_2\text{CH}_2$ ), 2.15 (m, 2H,  $\text{PCH}_2\text{CH}_2$ ), 2.50-2.66 (br. m, 4H,  $\text{CHMe}_2$  +  $\text{PCH}_2\text{CH}_2$ ), 2.95 (br. m,

2H,  $PCH_2CH_2$ ), 3.35 (br. m, 2H,  $PCH_2CH_2$ ), 3.61 (s, 2H, THF), 3.77 (br. m,  $PCH_2CH_2$ ), 4.04 (m, 2H,  $CHMe_2$ ), 4.12 (m, 2H,  $CHMe_2$ ), 4.61 (m, 2H,  $CHMe_2$ ), 7.02 (d,  $J_{HH} = 7.7$  Hz, 2H, ArH), 7.13 (d,  $J_{HH} = 7.7$  Hz, 2H, ArH), 7.18-7.20 (m, 4H, ArH), 7.25-7.30 (m, 4H, ArH).  $^{13}C\{^1H\}$  NMR [ $d_8$ -THF, 233 K]:  $\delta$  14.22 (*n*-hexane), 21.37 (br. m,  $PCH_2CH_2$ ), 21.61 (br. m,  $PCH_2CH_2$ ), 22.24 ( $CHMe_2$ ), 22.40 (br. m,  $PCH_2CH_2$ ), 22.68 (br. m,  $PCH_2CH_2$ ), 23.28 (*n*-hexane), 23.84, 24.00, 24.51, 24.71, 24.94, 25.05, 25.25 ( $CHMe_2$ ), 25.31 ( $PCH_2CH_2$ ), 25.25 ( $PCH_2CH_2$ ), 25.85 (THF), 26.66, 26.88, 27.04 ( $CHMe_2$ ), 27.18 (d,  $J_{PC} = 4.0$  Hz), 32.31 (*n*-hexane), 33.10 ( $J_{PC} = 37.8$  Hz,  $CHMe_2$ ), 33.72 ( $CHMe_2$ ), 34.56 (2  $CHMe_2$ ), 67.68 (THF), 122.2 (d,  $J_{PC} = 5.6$  Hz, ArH), 124.49, 124.59, 125.33, 128.91, 130.31 (ArH), 153.23 (m, Ar), 154.55, 155.70, 157.04, 157.09 (Ar).  $^{31}P\{^1H\}$  NMR [ $d_8$ -THF, 298 K]:  $\delta$  -105.89 (m,  $J_{PSn} = 700$  Hz,  $P^l$ ), -133.4 (m,  $J_{PSn} = 1140$  Hz,  $P^b$ ).  $^{119}Sn\{^1H\}$  NMR [ $d_8$ -THF, 298 K]:  $\delta$  266.8 (m).

## 12.6 References

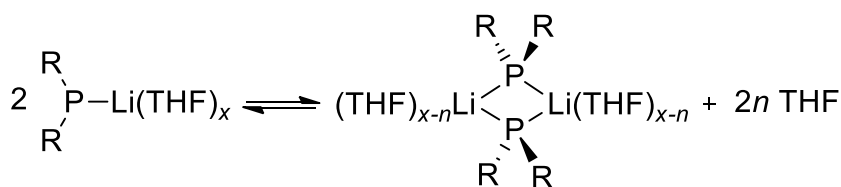
- [1] (a) G. Bouhadir, D. Bourissou, *Chem. Soc. Rev.*, **2004**, 33, 210-217; (b) M. Driess, K. Merz, C. Monsé, *Z. Anorg. Allg. Chem.*, **2000**, 626, 2264-2268; (c) F. G. N. Cloke, P. B. Hitchcock, P. Hunnab, J. F. Nixon, L. Nyulászi, E. Niecke, V. Thelen, *Angew. Chem. Int. Ed.*, **1998**, 37, 1083-1086.
- [2] (a) N. Del Rio, A. Baceiredo, N. Saffon-Merceron, D. Hashizume, D. Lutters, T. Muller, T. Kato, *Angew. Chem. Int. Ed. Engl.*, **2016**, 55, 4753-4758; (b) D. Martin, A. Baceiredo, H. Gornitzka, W. W. Schoeller, G. Bertrand, *Angew. Chem. Int. Ed. Engl.*, **2005**, 44, 1700-1703; (c) G. D. Frey, M. Song, J. B. Bourg, B. Donnadiou, M. Soleilhavoup, G. Bertrand, *Chem. Commun.*, **2008**, 4711-4713; (d) D. Ghereg, S. Ladeira, N. Saffon, J. Escudie, H. Gornitzka, *Angew. Chem. Int. Ed. Engl.*, **2011**, 50, 7607-7610.
- [3] (a) C. Couret, J. Satge, J. Escudie, J. D. Andriamizaka, *J. Organomet. Chem.*, **1977**, 132, C5-C8; (b) D. M. Anderson, P. B. Hitchcock, M. F. Lappert, I. Moss, *Inorg. Chim. Acta*, **1988**, 141, 157-159.
- [4] A. M. Arif, A. H. Cowley, R. A. Jones, J. M. Power, *J. Chem. Soc., Chem. Commun.*, **1986**, 1446.
- [5] K. Izod, J. Stewart, W. Clegg, R. W. Harrington, *Organometallics*, **2010**, 29, 108-116.
- [6] S. M. Mansell, C. A. Russell, D. F. Wass, *Inorg. Chem.*, **2008**, 47, 11367-11375.
- [7] A. H. Cowley, D. M. Giolando, R. A. Jones, C. M. Nunn, J. M. Power, W.-W. du Mont, *Polyhedron*, **1988**, 7, 1317-1319.
- [8] S. C. Goel, M. Y. Chiang, D. J. Rauscher, W. E. Buhro, *J. Am. Chem. Soc.*, **1993**, 115, 160-169.

## Chapter 13. Conclusions

The effects of modifying the steric demands of the phosphide ligands and the electronics and size of the tetrel centre (or two-coordinate pnictogen centre) in heavier main group carbene analogues with two phosphide substituents have been investigated. Prior to this work, only five monomeric diphosphatetrylenes had been reported, excluding base-stabilised systems, of which only two are stabilised by  $\pi$  interactions. The work presented here has greatly expanded on this and highlights new reactivity of such compounds.

### 13.1 Solid-state and solution behaviour of alkali metal phosphides

The alkali metal phosphides [(Dipp)<sub>2</sub>P]Li(THF)<sub>3</sub> (**128a**), {[(Dipp)<sub>2</sub>P]Na(THF)<sub>2</sub>}<sub>2</sub> (**129a**), [(Dipp)<sub>2</sub>P]Na(TMEDA) (**129c**), [(Dipp)<sub>2</sub>P]K(THF)<sub>4</sub> (**130a**), [(Dipp)(Mes)P]Li(THF)<sub>3</sub> (**131a**), [{(Mes)<sub>2</sub>P}Li(THF)<sub>3</sub>] (**132a**), [(Mes)<sub>2</sub>P]<sub>2</sub>Li<sub>2</sub>(THF)<sub>2</sub>(OEt<sub>2</sub>) (**132b**) and [(Dipp){(Me<sub>3</sub>Si)<sub>2</sub>CH}P]Li(THF)<sub>3</sub> (**134**) were prepared as potential ligand transfer reagents and were characterised by X-ray crystallography, with the THF solvates of the lithium phosphides adopting monomeric structures of the form [R<sub>2</sub>P]Li(THF)<sub>3</sub>. Compounds **128b**, **131a** and **134** are subject to a monomer/dimer equilibrium in solution (Scheme 64), with the monomeric species being highly favoured at low temperatures (<-80°C), demonstrating the considerable steric demands on these ligands. However, the variable-temperature NMR spectra of **132b** suggest the operation of a dynamic equilibrium between a dimer, a cyclic trimer and further unidentified species. The observation of these larger aggregates in solution shows that the (Mes)<sub>2</sub>P ligand is significantly less bulky than (Dipp)<sub>2</sub>P, as expected.



Scheme 64: Dynamic behaviour of **128**, **131a** and **134** in solution

The alkyl-bridged dilithium diphosphides [CH<sub>2</sub>(PLiDipp)<sub>2</sub>](TMEDA)<sub>2</sub> (**257**), {CH<sub>2</sub>(PLiDipp)}<sub>2</sub>(THF)(OEt<sub>2</sub>)<sub>1.5</sub> (**258a**), [CH<sub>2</sub>{CH<sub>2</sub>(PLiDipp)}<sub>2</sub>(THF)<sub>4</sub>] (**259**), {CH<sub>2</sub>CH<sub>2</sub>(PLiDipp)}<sub>2</sub>(THF)<sub>6</sub> (**260**) and [CH<sub>2</sub>{CH<sub>2</sub>CH<sub>2</sub>P(Dipp)}<sub>2</sub>]Li<sub>2</sub>(THF)<sub>6</sub>(C<sub>7</sub>H<sub>8</sub>) (**261a**) display a range of structural motifs in the solid-state, based on monomeric and dimeric species (Chart 3). Compounds **258a**, **259**, **260** and **261a** exhibit complex solution behaviour; the variable-temperature <sup>7</sup>Li and <sup>31</sup>P{<sup>1</sup>H} NMR spectra of these compounds suggest dynamic equilibria between monomeric and oligomeric species. There appears to be no correlation

between the length of the alkyl bridge in these dilithium diphosphides and their solid-state structures or solution behaviour.

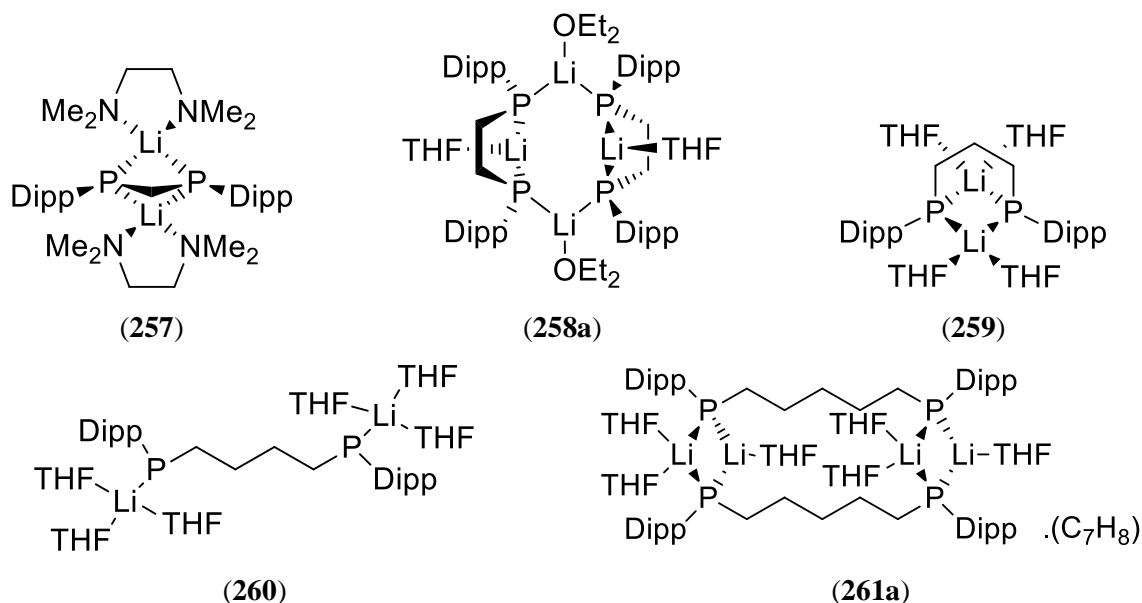


Chart 3: Structures of 257, 258, 259, 260 and 261a

### 13.2 Effect of modifying the steric demands of the phosphide ligands on the structure of diphosphatetrylenes

A series of diphosphagermylenes and –stannylenes were synthesised and characterised by X-ray crystallography. In the solid-state,  $\{(\text{Dipp})_2\text{P}\}_2\text{Sn}$  (**104Sn**),  $\{(\text{Tripp})_2\text{P}\}_2\text{Ge}\cdot\text{C}_7\text{H}_{14}$  (**145Ge}\cdot\text{C}\_7\text{H}\_{14}**) and  $\{[(\text{Me}_3\text{Si})_2\text{CH}]_2\text{P}\}_2\text{Sn}$  (**148Sn**) adopt a configuration with one planar and one pyramidal phosphorus centre (Fig. 139). A DFT study of these structures revealed that, in addition to the  $\pi$  interaction from the planar phosphorus, the tetrel centres are further stabilised (by up to  $61.9 \text{ kJ mol}^{-1}$ ) through delocalisation of the tetrel lone pair into a P-C  $\sigma^*$ -orbital of the planar phosphorus centre. Therefore, the diphosphatetrylenes **104Sn**, **145Ge}\cdot\text{C}\_7\text{H}\_{14}** and **148Sn** may be regarded as *push-pull* stabilised systems.



Figure 139: Configurations of diphosphatetrylenes

The diphosphatetrylenes  $\{(\text{Tripp})_2\text{P}\}_2\text{Sn}$  (**145Sn**),  $\{(\text{Dipp})(\text{Mes})\text{P}\}_2\text{Ge}\cdot(\text{C}_6\text{H}_{14})_{0.5}$  (**146Ge}\cdot(\text{C}\_6\text{H}\_{14})\_{0.5}**),  $\{(\text{Dipp})(\text{Mes})\text{P}\}_2\text{Sn}$  (**146Sn**) and  $[(\text{Dipp})\{(\text{Me}_3\text{Si})_2\text{CH}\}\text{P}]_2\text{Sn}$  (**147Sn**) adopt an alternative configuration in the solid-state with two pyramidal phosphorus centres. These compounds are each stabilised by two short Ge/Sn $\cdots\text{C}_{\text{ipso}}$  contacts, which DFT

calculations suggest may be providing up to 206 kJ mol<sup>-1</sup> of stabilisation. Compounds **146Ge**·(C<sub>6</sub>H<sub>14</sub>)<sub>0.5</sub>, **146Sn** and **147Sn** show little to no contribution of the planar configuration in solution, as judged by variable-temperature <sup>31</sup>P{<sup>1</sup>H} NMR spectroscopy; however, in solution **145Sn** has a significant proportion of the planar form in dynamic equilibrium with the pyramidal form.

From the solid-state structures and variable-temperature <sup>31</sup>P{<sup>1</sup>H} NMR data of the diphosphatetrylenes discussed above, we have determined that the (Dipp)<sub>2</sub>P, (Tripp)<sub>2</sub>P and {(Me<sub>3</sub>Si)<sub>2</sub>CH}<sub>2</sub>P ligands systems are sufficiently bulky to invoke planarization of phosphorus in these systems to provide stabilisation by  $\pi$  interactions. The (Dipp)(Mes)P and (Dipp){(Me<sub>3</sub>Si)<sub>2</sub>CH}P ligands are too small to sufficiently lower the energy barrier for the planarization of phosphorus, and so adopt a pyramidal configuration.

In marked contrast to the diphosphagermylenes discussed above and reported previously, the putative diphosphagermylene {(Mes)<sub>2</sub>P}<sub>2</sub>Ge (**160Ge**) decomposes to (Mes)<sub>2</sub>P-P(Mes)<sub>2</sub> (**161**) and the tetranuclear cluster [{(Mes)<sub>2</sub>P}Ge]<sub>4</sub>·(C<sub>7</sub>H<sub>14</sub>) (**162**), which was characterised by X-ray crystallography (Fig. 140). The inherent instability of **160Ge** must be a consequence of the low steric demands of the (Mes)<sub>2</sub>P ligand. Nevertheless, this allows synthetic access to the unique Ge(I) cluster **162**.

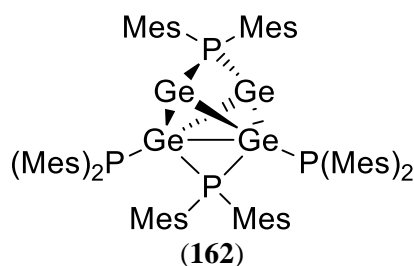


Figure 140: Tetranuclear Ge(I) cluster **162**

The isolation of the *P*-heterocyclic stannylenes [CH<sub>2</sub>{CH<sub>2</sub>(PDipp)}<sub>2</sub>Sn]<sub>2</sub>·(THF)<sub>2</sub> (**266b**) and [CH<sub>2</sub>{CH<sub>2</sub>(PDipp)}<sub>2</sub>Sn]<sub>2</sub>·(THF)<sub>3</sub> (*cis*-**266c**) as phosphorus-bridged dimers is clearly a result of the low steric demands of the ligand system (Fig. 141). The substitution, and so steric bulk, of the alkyl bridge would need to be dramatically increased to access monomeric tetrylenes of this class.

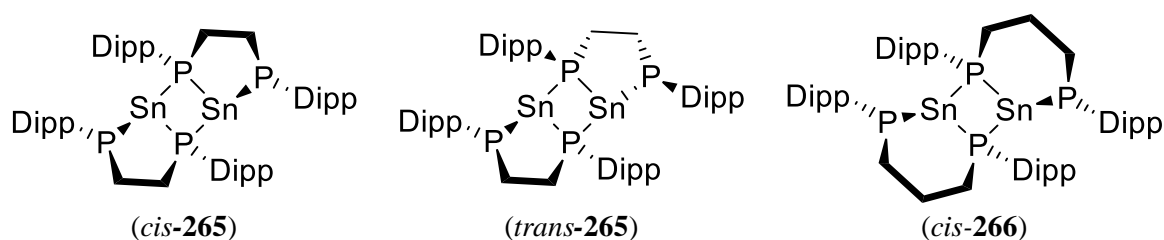


Figure 141: *P*-heterocyclic stannylenes *cis/trans*-**265** and *cis*-**266**



### 13.3 Effect of modifying the tetrel/pnictogen centre ( $R_2E$ ; $E = \text{Ge, Sn, As, Si, P}$ )

The variable-temperature  $^{31}\text{P}\{^1\text{H}\}$  NMR spectra of the diphosphatetrylenes **104Ge**, **104Sn**, **145Ge**, and **145Sn** show these compounds are subject to a dynamic equilibrium between the planar and pyramidal configurations in solution, although the solution behaviour of the diphosphagermylenes **104Ge** and **145Ge** is different to that of the diphosphastannylenes **104Sn** and **145Sn**. The broad signal exhibited by **145Ge** in its  $^{31}\text{P}\{^1\text{H}\}$  NMR spectra at room temperature decoalesces as the temperature at low temperatures into four signals, corresponding to the planar and pyramidal phosphorus environments in the solid-state structure and two configurations with two pyramidal phosphorus centres. The previously reported **104Ge** follows an almost identical pattern in its variable-temperature  $^{31}\text{P}\{^1\text{H}\}$  NMR spectra.

While we do observe decalescence of the signals exhibited by **145Sn** and **146Sn** in their  $^{31}\text{P}\{^1\text{H}\}$  NMR spectra into two signals corresponding to the two configurations, the concentration of the planar configuration rapidly diminishes as the temperature is reduced, until, at  $-80\text{ }^\circ\text{C}$ , the spectrum essentially consists of just the pyramidal configuration.

We associate this difference in solution behaviour between the diphosphagermylenes **104Ge** and **145Ge** and the diphosphastannylenes **104Sn** and **145Sn** to the planar configuration of the latter species being less stable, because of the reduced orbital overlap between the phosphorus centres and the tin centre, compared to the corresponding overlap with germanium. This is supported by the DFT calculations of **104Ge/Sn**, **145Ge/Sn** and **146Ge/Sn**, which show the planar configurations for the stannylenes are consistently less stable than in the respective germylene analogue. For comparison, the planar configuration of **104Ge** is calculated to be  $13.8\text{ kJ mol}^{-1}$  more stable than the pyramidal configuration, while the two configurations of **104Sn** are almost isoenergetic, with the pyramidal form more stable by  $2.5\text{ kJ mol}^{-1}$ .

The diphosphaarsenium cation  $[(\text{Dipp})_2\text{P}]_2\text{As}[\text{Al}\{\text{OC}(\text{CF}_3)_3\}_4]\cdot(\text{PhMe})_{1.5}$  (**208**) not only adopts an almost identical configuration to **104Ge** (with which it is isoelectronic) in the solid-state (Fig. 142), but also exhibits similar variable temperature  $^{31}\text{P}\{^1\text{H}\}$  NMR behaviour. The cationic nature of the two-coordinate arsenic centre further stabilises the planar configuration, which is calculated to be  $25.7\text{ kJ mol}^{-1}$  more stable than the pyramidal configuration.

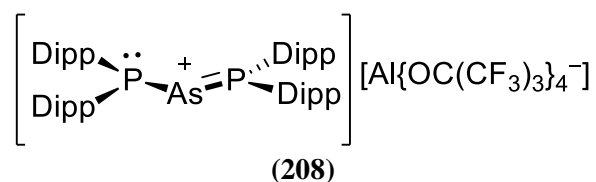


Figure 142: Diphosphaarsenium cation **208**

Although the putative diphosphasilylenes  $\{(\text{Dipp})_2\text{P}\}_2\text{Si}$  (**188**) and  $\{(\text{Mes})_2\text{P}\}_2\text{Si}$  (**173**) are valence isoelectronic and isostructural analogues of the diphosphagermylenes **104Ge** and **160Ge**, respectively, they exhibit unexpected and differing instability. While compound **160Ge** appears to be stable towards a decomposition process similar to that observed for **173**, we instead isolate the tetraphosphadisilene  $\{(\text{Mes})_2\text{P}\}_2\text{Si}=\text{Si}\{\text{P}(\text{Mes})_2\}$  (**181**) as a result of the limited steric demands of the ligand system (Fig. 143). The more sterically encumbered diphosphasilylene A undergoes a 1,2-aryl migration to give the phosphasilene **192** (Fig. 143). Similarly, the instability of the putative diphosphaphosphenium cation  $\{[(\text{Mes})_2\text{P}]_2\text{P}\}[\text{BArF}_{24}]$  (**220**) to rearrangement to give the diphosphaphosphonium  $[\{\mu\text{-(Mes)P}\}_2\text{P}(\text{Mes})_2][\text{BArF}_{24}]$  (**216**) contrasts with the remarkable stability of the related diphosphaarsenium cation **208** (Fig. 143).

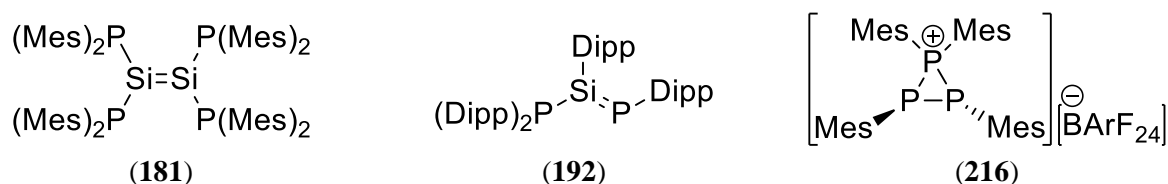
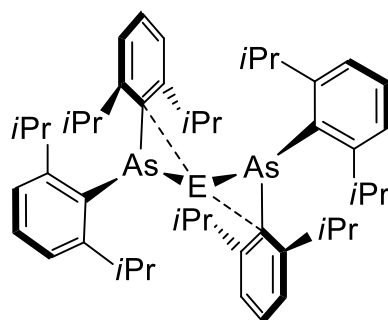


Figure 143: Isolated compounds from the attempted synthesis of **173**, **188** and **220**

The instability of the diphosphasilylenes **188** and **173** and the diphosphaphosphenium **220** may be associated with the increased Lewis acidity of the relatively small electron-deficient centres in these compounds and their affinity to achieve a stable orbital octet of electrons.

### 13.4 Effect of modifying the pnictogen of the ligand system

The solid-state structures of the diarsatetrylenes  $\{(\text{Dipp})_2\text{As}\}_2\text{Ge}\cdot\text{C}_7\text{H}_8$  (**234Ge**) and  $\{(\text{Dipp})_2\text{As}\}_2\text{Sn}\cdot\text{C}_7\text{H}_8$  (**234Sn**) further illustrate that aryl-substituted pnictide ligands may stabilise the tetrel centres with short  $\text{Ge/Sn}\cdots\text{C}_{ipso}$  contacts in systems where the planar configuration, required for  $\pi$ -interactions, is energetically inaccessible. DFT calculations suggest the short  $\text{Ge/Sn}\cdots\text{C}_{ipso}$  contacts from the arsenide ligands in **234Ge** and **234Sn** may be providing stabilisation by up to  $285.5 \text{ kJ mol}^{-1}$ , which is significantly greater than calculated for the diphosphatetrylenes previously discussed.



E = Ge (**234Ge**) / Sn (**234Sn**)

**Figure 144:** Diarsaatetrylenes **234Ge** and **234Sn**

### 13.5 Possible future work

The work presented in this thesis demonstrates how the stabilisation mode of diphosphatetrylenes can be influenced by subtle modification of the phosphide ligands or tetrel centre. An investigation of the small molecule activation of the diphosphatetrylenes **104Ge/Sn**, **145Ge/Sn**, **146Ge/Sn** and **147Sn** may reveal the influence of the  $\pi$ -interactions on the reactivity of these systems. Furthermore, the tetraphosphadisilene **181** and the tetranuclear Ge(I) cluster **162** are potential candidates for small molecule activation.

The instability of the putative diphosphasilylene **188** and diphosphaphosphenium cation **220** towards rearrangement demonstrates the need for a more robust phosphide ligand. A dialkylphosphide, such as  $\{(\text{Me}_3\text{Si})_2\text{CH}\}_2\text{P}$ , should be more stable towards substituent migration and potentially allow access to the first example of a diphosphasilylene and diphosphaphosphenium cation.

## Chapter 14. Appendix (on attached CD)

	Compound	Data	
		NMR spectra	Crystal structure
<b>109</b>	(Dipp)(Mes)PH	<input checked="" type="checkbox"/>	<input type="checkbox"/>
<b>110</b>	(Dep) <sub>2</sub> PH	<input checked="" type="checkbox"/>	<input type="checkbox"/>
<b>111</b>	(Dipp) <sub>2</sub> PH	<input checked="" type="checkbox"/>	<input checked="" type="checkbox"/>
<b>112</b>	(Tripp) <sub>2</sub> PH	<input checked="" type="checkbox"/>	<input type="checkbox"/>
<b>113</b>	(Dipp){(Me <sub>3</sub> Si) <sub>2</sub> CH}PH	<input checked="" type="checkbox"/>	<input type="checkbox"/>
<b>114</b>	{(Me <sub>3</sub> Si) <sub>2</sub> CH} <sub>2</sub> PH	<input checked="" type="checkbox"/>	<input type="checkbox"/>
<b>128a</b>	[(Dipp) <sub>2</sub> P]Li(THF) <sub>3</sub>	<input checked="" type="checkbox"/>	<input checked="" type="checkbox"/>
<b>129a</b>	{[(Dipp) <sub>2</sub> P]Na(THF) <sub>2</sub> } <sub>2</sub>	<input checked="" type="checkbox"/>	<input checked="" type="checkbox"/>
<b>129c</b>	[(Dipp) <sub>2</sub> P]Na(PMDETA)	<input checked="" type="checkbox"/>	<input checked="" type="checkbox"/>
<b>130a</b>	[(Dipp) <sub>2</sub> P]K(THF) <sub>4</sub>	<input checked="" type="checkbox"/>	<input checked="" type="checkbox"/>
<b>131a</b>	[(Dipp)(Mes)P]Li(THF) <sub>3</sub>	<input checked="" type="checkbox"/>	<input checked="" type="checkbox"/>
<b>132a</b>	[(Mes) <sub>2</sub> P]Li(THF) <sub>3</sub>	<input checked="" type="checkbox"/>	<input checked="" type="checkbox"/>
<b>132b</b>	[(Mes) <sub>2</sub> P] <sub>2</sub> Li <sub>2</sub> (THF) <sub>2</sub> (OEt <sub>2</sub> )	(see above)	<input checked="" type="checkbox"/>
<b>134</b>	[(Dipp){(Me <sub>3</sub> Si) <sub>2</sub> CH}P]Li(THF) <sub>3</sub>	<input checked="" type="checkbox"/>	<input checked="" type="checkbox"/>
<b>139</b>	[{(Me <sub>3</sub> Si) <sub>2</sub> CH} <sub>2</sub> P]Li <sup>1</sup> / <sub>3</sub> (OEt <sub>2</sub> )	<input checked="" type="checkbox"/>	<input type="checkbox"/>
<b>143</b>	{(Me <sub>2</sub> PhSi) <sub>2</sub> CH} <sub>2</sub> PCl	<input checked="" type="checkbox"/>	<input type="checkbox"/>
<b>144</b>	[K[μ-P(CH(SiMe <sub>2</sub> Ph) <sub>2</sub> )] <sub>2</sub> ] <sub>2</sub> ·C <sub>6</sub> H <sub>14</sub>	<input type="checkbox"/>	<input checked="" type="checkbox"/>
<b>104Sn</b>	{(Dipp) <sub>2</sub> P} <sub>2</sub> Sn	<input checked="" type="checkbox"/>	<input checked="" type="checkbox"/>
<b>145Ge</b> ·(C <sub>7</sub> H <sub>14</sub> )	{(Tripp) <sub>2</sub> P} <sub>2</sub> Ge·(C <sub>7</sub> H <sub>14</sub> )	<input checked="" type="checkbox"/>	<input checked="" type="checkbox"/>
<b>145Sn</b>	{(Tripp) <sub>2</sub> P} <sub>2</sub> Sn	<input checked="" type="checkbox"/>	<input checked="" type="checkbox"/>
<b>146Ge</b> ·(C <sub>6</sub> H <sub>14</sub> ) <sub>0.5</sub>	{(Dipp)(Mes)P} <sub>2</sub> Ge·(C <sub>6</sub> H <sub>14</sub> ) <sub>0.5</sub>	<input checked="" type="checkbox"/>	<input checked="" type="checkbox"/>
<b>146Sn</b>	{(Dipp)(Mes)P} <sub>2</sub> Sn	<input checked="" type="checkbox"/>	<input checked="" type="checkbox"/>
<b>147Sn</b>	[(Dipp){(Me <sub>3</sub> Si) <sub>2</sub> CH}P] <sub>2</sub> Sn	<input checked="" type="checkbox"/>	<input checked="" type="checkbox"/>
<b>148Sn</b>	[{(Me <sub>3</sub> Si) <sub>2</sub> CH} <sub>2</sub> P] <sub>2</sub> Sn	<input checked="" type="checkbox"/>	<input checked="" type="checkbox"/> *
<b>150</b>	(Dipp) <sub>2</sub> P-P(Dipp) <sub>2</sub>	<input checked="" type="checkbox"/>	<input checked="" type="checkbox"/>
<b>162</b>	[{(Mes) <sub>2</sub> P}Ge] <sub>4</sub> ·(C <sub>7</sub> H <sub>14</sub> )	<input checked="" type="checkbox"/>	<input checked="" type="checkbox"/> *
<b>174</b>	{(Mes) <sub>2</sub> P} <sub>2</sub> SiHCl	<input checked="" type="checkbox"/>	<input type="checkbox"/>
<b>175</b>	{(Mes) <sub>2</sub> P} <sub>2</sub> SiCl <sub>2</sub>	<input checked="" type="checkbox"/>	<input type="checkbox"/>
<b>176</b>	[{(Mes) <sub>2</sub> P} <sub>3</sub> Si]Li(THF)	<input checked="" type="checkbox"/>	<input type="checkbox"/>
<b>177</b> ·THF	[{(Mes) <sub>2</sub> P} <sub>3</sub> Si]K(THF) <sub>3</sub>	<input type="checkbox"/>	<input checked="" type="checkbox"/>

<b>181</b>	$\{(\text{Mes})_2\text{P}\}_2\text{Si}=\text{Si}\{\text{P}(\text{Mes})_2\}_2$	<input type="checkbox"/>	<input checked="" type="checkbox"/>
<b>190</b>	$\{(\text{Dipp})_2\text{P}\}_2\text{SiCl}_2$	<input type="checkbox"/>	<input checked="" type="checkbox"/>
<b>192</b>	$\{(\text{Dipp})_2\text{P}\}\text{Si}(\text{Dipp})\{\text{P}(\text{Dipp})\}$	<input checked="" type="checkbox"/>	<input checked="" type="checkbox"/>
<b>205</b>	$\{(\text{Dipp})_2\text{P}\}_2\text{AsCl}$	<input checked="" type="checkbox"/>	<input checked="" type="checkbox"/> <sup>a</sup>
<b>208</b>	$[\{(\text{Dipp})_2\text{P}\}_2\text{As}][\text{Al}\{\text{OC}(\text{CF}_3)_3\}_4]\cdot(\text{C}_7\text{H}_8)_{1.5}$	<input checked="" type="checkbox"/>	<input checked="" type="checkbox"/>
<b>213</b>	$\{(\text{Mes})_2\text{P}\}_2\text{PCl}$	<input checked="" type="checkbox"/>	<input checked="" type="checkbox"/>
<b>216</b>	$[\{\mu\text{-(Mes)P}\}_2\text{P}(\text{Mes})_2][\text{B}\{3,5\text{-(CF}_3)_2\text{C}_6\text{H}_3\}_4]$	<input checked="" type="checkbox"/>	<input checked="" type="checkbox"/>
<b>231</b>	$(\text{Dipp})_2\text{As}(\text{NiPr}_2)$	<input checked="" type="checkbox"/>	<input type="checkbox"/>
<b>232</b>	$(\text{Dipp})_2\text{AsCl}$	<input checked="" type="checkbox"/>	<input type="checkbox"/>
<b>226</b>	$(\text{Dipp})_2\text{AsH}$	<input checked="" type="checkbox"/>	<input type="checkbox"/>
<b>233</b>	$[(\text{Dipp})_2\text{P}]\text{Li}(\text{THF})_{2.75}(\text{Et}_2\text{O})$	<input checked="" type="checkbox"/>	<input checked="" type="checkbox"/>
<b>234Ge</b>	$\{(\text{Dipp})_2\text{As}\}_2\text{Ge}\cdot\text{C}_7\text{H}_8$	<input checked="" type="checkbox"/>	<input checked="" type="checkbox"/>
<b>234Sn</b>	$\{(\text{Dipp})_2\text{As}\}_2\text{Sn}\cdot\text{C}_7\text{H}_8$	<input checked="" type="checkbox"/>	<input checked="" type="checkbox"/>
<b>246</b>	$\text{CH}_2(\text{PHDipp})_2$	<input checked="" type="checkbox"/>	<input type="checkbox"/>
<b>253</b>	$\{\text{CH}_2(\text{PHDipp})\}_2$	<input checked="" type="checkbox"/>	<input type="checkbox"/>
<b>254</b>	$\text{CH}_2\{\text{CH}_2(\text{PHDipp})\}_2$	<input checked="" type="checkbox"/>	<input type="checkbox"/>
<b>255</b>	$\{\text{CH}_2\text{CH}_2(\text{PH}(\text{Dipp}))\}_2$	<input checked="" type="checkbox"/>	<input type="checkbox"/>
<b>256</b>	$\text{CH}_2\{\text{CH}_2\text{CH}_2(\text{PH}(\text{Dipp}))\}_2$	<input checked="" type="checkbox"/>	<input type="checkbox"/>
<b>257</b>	$[\text{CH}_2(\text{PLiDipp})_2](\text{TMEDA})_2$	<input checked="" type="checkbox"/>	<input checked="" type="checkbox"/>
<b>258a</b>	$\{\text{CH}_2(\text{PLiDipp})\}_2(\text{THF})(\text{OEt}_2)$	<input checked="" type="checkbox"/>	<input checked="" type="checkbox"/>
<b>259</b>	$[\text{CH}_2\{\text{CH}_2(\text{PLiDipp})\}_2(\text{THF})_4]$	<input checked="" type="checkbox"/>	<input checked="" type="checkbox"/>
<b>260</b>	$\{\text{CH}_2\text{CH}_2(\text{PLiDipp})\}_2(\text{THF})_6$	<input checked="" type="checkbox"/>	<input checked="" type="checkbox"/>
<b>261a</b>	$[\text{CH}_2\{\text{CH}_2\text{CH}_2\text{P}(\text{Dipp})\}_2]\text{Li}_2(\text{THF})_6(\text{C}_7\text{H}_8)$	<input checked="" type="checkbox"/>	<input checked="" type="checkbox"/>
<i>cis/trans</i> - <b>265a</b>	$[\{\text{CH}_2(\text{PDipp})\}_2\text{Sn}]_2\cdot\text{Et}_2\text{O}$	<input checked="" type="checkbox"/>	<input checked="" type="checkbox"/> <sup>b</sup>
<i>cis</i> - <b>266b</b>	$[\text{CH}_2\{\text{CH}_2(\text{PDipp})\}_2\text{Sn}]_2\cdot(\text{THF})_2$	<input checked="" type="checkbox"/>	<input checked="" type="checkbox"/>
<i>cis</i> - <b>266c</b>	$[\text{CH}_2\{\text{CH}_2(\text{PDipp})\}_2\text{Sn}]_2\cdot(\text{THF})_3$	(see above)	<input checked="" type="checkbox"/>
<b>267</b>	$([\text{CH}_2\{\text{CH}_2(\text{PDipp})\}_2\text{SnX}]\text{Sn})_2\{(\text{PDipp})\text{CH}_2\}_2\text{CH}_2\}$	<input type="checkbox"/>	<input checked="" type="checkbox"/>

**Table 11:** Contents located in the self-titled folders for the compounds prepared in this thesis, in which the NMR spectra may correspond to the alternative solvates described in the relevant section.

$[\text{*}^{31}\text{P}\{\text{}^1\text{H}\}]$  NMR spectra correspond to the crude reaction mixtures. <sup>a</sup>Crystal data is for the cocrystal **205-150**.

<sup>b</sup>Crystal data corresponds to the *trans* stereoisomer]